Molecular Characterization and Formation of Novel Reversible Boronic Acid Complexations

by

Karin Reznikov

Submitted in partial fulfilment of the requirements
for the degree of Master of Science

at

Dalhousie University
Halifax, Nova Scotia
November 2023

Dalhousie University is located in Mi'kma'ki, the ancestral and unceded territory of the Mi'kmaq. We are all Treaty people.

"You cannot hope to build a better world without improving the individuals. To that end each of us must work for his own improvement, and at the same time share a general responsibility for all humanity, our particular duty being to aid those to whom we think we can be most useful."

- A quote by Marie Curie whose life as a scientist was one which flourished because of her ability to observe, deduce and predict.

Table of Contents

List of Tables

List of Figures

List of Schemes

Abstract

Boronic acids have an impact on various applications in drug discovery and medicinal chemistry. Therefore, an understanding of their structure and reactivity is essential. Determining the pK_a of novel synthesized boronic acids was conducted to investigate the structural changes of the boron center. We estimated one pK_a value for each compound and showed reversibility to a select boronic acid derivatives. Next, we demonstrated and quantified a series of binding experiments at physiological pH. The iminoboronate formation between Boc-Lysine and carbonyl boronic acid derivative was successfully quantified. We found that compound DT14 had the highest binding affinity across the carbonyl derivatives. Diazaborine formation between Boc-Lysine and aldehyde derivatives did not demonstrate significant binding. Finally, diol binding between common saccharides and boronic acids was successfully quantified. We found that glucuronic acid bound tight to carboxylic acid derivatives. UV-Visible, NMR and Fluorescence spectroscopy were used to quantify the physicochemical properties and binding interactions.

List of Abbreviations Used

A	absorbance
A^-	sp^3-hybridized form of boronic acid
A_0	initial absorbance
A_c	absorbance of the complex
ARS	alizarin red S
BA	boronic acid
BNCT	boron neutron capture therapy
Boc	tert-Butyloxycarbonyl
D_2O	Deuterium oxide
e.g.	for example
F	fluorescence
F_0	initial fluorescence
F_c	fluorescence of the complex
FDA	Food and Drug Administration
H	hydrogen
HA	the sp^2-hybridized form of boronic acid
HCl	Hydrochloric acid
HEPES	4-(2-hydroxyethyl)-1-piperazineethanesulphonic acid
HMBC	heteronuclear multiple bond correlation
HSQC	heteronuclear single quantum coherence
K_a	Association constant
K_d	Dissociation constant
Lys	Lysine
NaOH	Sodium hydroxide
N-B	nitrogen-boron bond
NMR	nuclear magnetic resonance
Nu	nucleophile

O-B	oxygen-boron bond
PBA	phenylboronic acid
pD	potential of deuterium
pH	potential of hydrogen
pK_a	acid-base equilibrium constant
ppm	parts per million
Ser	serine residue
Thr	threonine
TLC	thin-layer chromatography
tRNA	transfer ribonucleic acid
UV-Vis	Ultraviolet–visible
2D	two-dimensional
2FPBA	2-Formylphenylboronic acid
3D	three-dimensional
3D-QSAR	three-dimensional quantitative structure-activity relationships
α	alpha
δ	chemical shift
ε	epsilon

Acknowledgements

I would first like to acknowledge my supervisor, Dr. David Jakeman, for providing guidance as I began independent research, and always being willing and available to offer advice. I would like to thank the members of the Jakeman group: thanks particularly to past members: Dr. Ebrahim Soleimani and Cyril O'Brian for synthesizing the compounds and welcoming me into the group and always being these for any question. I would also like to thank present members Elisa Ospanow and Bronwyn Rowland who all contributed in various ways during this path. I would also like to acknowledge past undergraduate students Tomer Reznikov, Jack McBeath and Sibi Aloshious who taught me as much as I hopefully taught them.

I would like to thank my supervisory committee, Dr. Alan Doucette and Dr. Fran Cozens, for providing guidance, support, and helpful advice throughout the course of this thesis.

Additionally, I would like to thank the incredible staff in the Dalhousie Department of Chemistry. Thanks especially to Dr. Mike Lumsden of the NMR facility for providing any help I needed in acquiring or interpreting NMR data. Also, thank you to the Goralski laboratory who allowed me to use their Fluorescence spectroscopy and provided me with guidance of the instrumentation. Thank you also to Lea Gawne, for helping me stay on track and always providing prompt and helpful information whenever I needed it. Additionally, I would like to thank Dr. Katherine Robertson of the Saint Mary's University Chemistry Department, who performed all X-ray crystallography experiments.

I would like to thank the various sources who contributed to funding this thesis, specifically the Natural Sciences and Engineering Research Council, the Canadian Institutes of Health Research, and the CREATE BioActives program.

Finally, I would like to thank my family, who has always supported me, and my friends.

Chapter 1. Introduction

1.1 General Boronic Acid Chemistry

Boronic acid compounds play an important role in medicinal chemistry and drug discovery; however, they have not been widely studied until recently due to toxicity concerns.[1] More recently, the boron toxicity belief has been disproven and the interest for in boronic acid chemistry has been growing especially after the FDA approval of Bortezomib (**Figure 1.1.1**), a boronic acid containing pharmaceutical which is used in multiple myeloma therapy in 2003.[2–4]

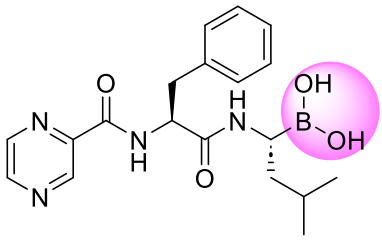

Figure 1.1.1: Structure of Bortezomib, a boronic acid containing pharmaceutical.

Boronic acids were first synthetized in 1860 by Edward Frankland and were used as building blocks and synthetic intermediates.[5,6] Boronic acids were found to have versatile reactivity, good stability, and have low toxicity.[1,7] Since their discovery and synthesis, boronic acids have become one of the most prevalent classes of reagents in modern synthesis, enabling the effective construction of different types of C-C and C-heteroatom bonds. The boron centre in boronic acids contain an empty p-orbital, making them mildly Lewis acidic, and react as good electrophiles.

At the boron centre, boronic acids are susceptible to nucleophilic attack, from Lewis bases such as hydroxide anions and electro-donating nitrogen or oxygen functionalities[1,5,7,8] This Lewis acid-base reaction results in the central interconversion between uncharged trigonal planar to anionic tetravalent borate species, with a geometry that is sp^3-hybridized.[9,10] Due to their Lewis acidic nature, boronic acids form a reversible dative covalent bond with nucleophilic compounds such as ammonium ions and diol moieties in carbohydrates as shown in **Scheme 1.1.1**.[1] These reversible non-ionic interactions are the basis for research on boronic acids compounds as therapeutics and sensors.

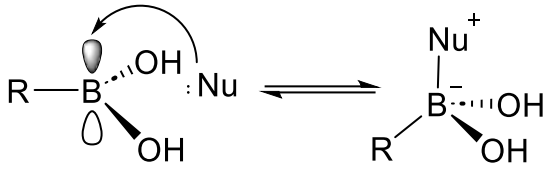

Scheme 1.1.1: Formation of a dative covalent bond between the nucleophile and a boronic acid.

The acid-base equilibrium constant (pK_a) of a molecule or a functional group is the quantitative measure of the strength of an acid in solution.[11] Many chemical, physical and biological properties of natural and synthetic compounds are governed by the interactions of acidic and basic groups.[12,13] The pK_a is a key physicochemical parameter influencing many biopharmaceutical characteristics.[11,13] Moreover, the pK_a is an important parameter that indicates the formal charge of molecules in solution at different pH values.[11–13]

Boronic acids typically have pK_a values between 4 and 10.[5] These values vary depending on the substituents on the boronic acid derivatives, with aryl boronic acids being more acidic than alkyl boronic acids.[7] If an electron withdrawing group, such as fluorine, is attached to an aromatic boronic acid, the pK_a value decreases, while an electron donating group, such as an alkoxy group, increases the pK_a values.[7] For example, if a fluorine is substituted to an aryl boronic acid, the electron-withdrawing fluorine will make the boron more electron deficient, resulting in the boron center to become more Lewis acidic; therefore, the pK_a of the boronic acid will decrease because the pH in which the boron readily accepts a lone-pair from a Lewis base will decrease.[7] The ionization equilibrium (pK_a) for a boronic acid is shown in **Scheme 1.1.2**.

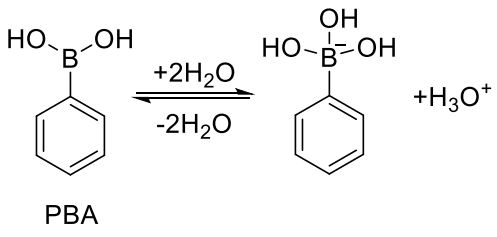

Scheme 1.1.2: Ionization equilibrium of boronic acid in aqueous solutions. Phenylboronic acid acting as Lewis acid. The pK_a for phenyl boronic acid is 8.8.[14]

At physiological pH (pH 7.4), boronic acids with lower pK_a values than physiological pH remain at their neutral trigonal form, but in aqueous solutions with pH values higher than pK_a, they would be gradually converted to their anionic tetrahedral forms as a function of pH.[2,7,8] This provides the information of the ionization state of the boronic acid center. Ionization is the process by which ions are formed by gain or loss of an electron from an atom or molecule.[15] In the boronic acid case, the gain of electron causes the boronic acid functionality to become negatively charged.[15] The equilibrium between the negatively charged and the neutral form depends on the differences between pH levels and pK_a values of the boronic acid.[1,7,8]

1.2 Boronic Acid Applications

Boronic acids have been widely used in many applications such drug design, which explores its functional diversity beyond conventional organic framework sensor applications, biomaterials preparation and bioconjugation[1,5] The appearance of many publications related to boronic acids in the last two decades demonstrates their relevance. Fundamental studies on boronic acid chemistry and their interactions with physiological systems underpin the different applications. As mentioned above, a boron atom has a vacant p orbital that makes boronic acid Lewis Acidic in nature.[1,16] Therefore, boronic acid interconverts sp^2 to sp^3 rapidly and also exchange two hydroxyl groups with water, alcohols, or amines at physiological pH.[16] In addition, cyclic boronate ester formation between boronic acid and cis-(1,2)-diol is a widely known reaction that showcases that affinity towards sugar recognition. Boronic acids are also used for anticancer, antibacterial and antiviral activities.[1]

An important consideration of boronic acid is also its degradation to boric acid which is a “clean compound” that is essential for bacterial treatment (such as bacterial vaginosis), wound healing and it is in phase IV clinical trials for a combination with probiotics to treat yeast infections.[17] Boric acid is easily and non-toxically eliminated by the body, which is the reason why it is acceptable to release into the body.[5,8]

Boronic acid, as well, have been used in different already approved drugs with more drugs in the process of clinical trials, which is why it is interesting to continue investigating boronic acid containing compounds.[8] Boronic acids serve as excellent covalent ligands, and have been used in reactive oxygen species (ROS)-triggered prodrugs.[17] Prodrugs are medications that turn into an active form once they enter the body. They help improve a medication's effectiveness and may also be designed to avoid certain side effects or toxicities.[18] **Figure 1.2.1** shows examples of prodrugs that were approved by the FDA and Health Canada and are being used for cancer and bacterial treatments. Boronic acid-based prodrugs have also been used to improve the pharmacokinetic properties of anti-estrogens based on their glycan-binding capability.[1]

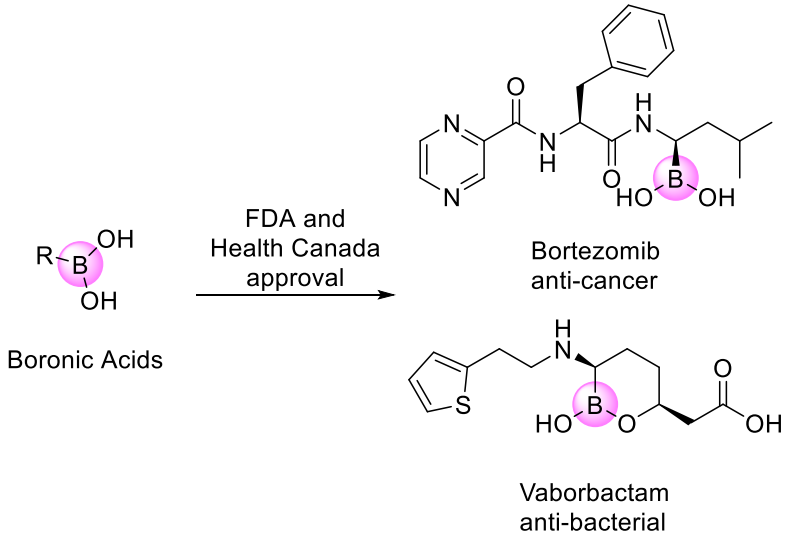

Figure 1.2.1: Boronic acids used in drug discovery and approved by the FDA and Health Canada to treat cancer and bacterial infections.[1]

Also, when a drug candidate is being carried through the body, transition between the outside and inside a cell is a function of the drug physico-chemical parameters.[19] Acid–base (pK_a) features have a vital importance for boronic acids not only for physiologic characteristics but also for being used as a ligand or for changing their physico-chemical features by turning them into salts.[20] pK_a values play an important role in many research fields such as the stereochemical and conformational structure determination, orientation of nucleophilic and electrophilic attacks, the stabilities of intermediates, and

the magnitude of activation energy in organic reactions and the detection of active centers of biochemical enzymes.[20] Besides these, pK_a values are important thermodynamic parameters for biochemical interactions, industrial processes or the environmental fate of polyprotic molecules.[20]

1.3 How Boronic Acid-Containing Drugs Interact With Their Targets?

The presence of boron is central to the reactivity of many of the drugs that contain boronic acids. They can adopt a broad spectrum of covalent binding modes in diverse target microenvironments. These binding modes were revealed from the crystal structure of different protein-boronic acid drug interactions.[21] There are currently more than 40 covalent drugs on the market, and more are in clinical trials. Covalent drugs bind via a covalent bond to the target protein, which results in slow rates and sustained inhibition.[22] Incorporating reversibility into covalent drugs would lead to less off-target toxicity by forming reversible adducts with off-target proteins and, thus, reduce the risk of toxicities caused by the permanent modification of proteins, which leads to higher levels of potential haptens.[22]

Boronic acids play a dual role with high-affinity target engagement. Covalent bond formation through B-sp^2 and H-bonds by two hydroxyl groups. For instance, the newly developed beta-lactamase boron-inhibitors, Vaborbactam. It is a cyclic boronic acid beta-lactamase inhibitor drug that is added to the therapy of infection related symptoms of urinary tract infections to reduce the resistance by inhibiting the serine beta-lactamases expressed by the microorganism of target.[4] Studies have found that it elicits strong inhibition of classes A and C enzymes. A covalent bond is formed between the boron of Vaborbactam and catalytic serine residues in the active site as shown in **Scheme 1.3.1**. This covalent bond contributes towards the binding affinity, but it is not enough for high affinity to the beta-lactamase. The rest of the functional groups can also impact binding affinity, making hydrogen bonding interactions within the active sites, which are observed classes A and C enzymes in complex with boronic acids.[17,23–25]

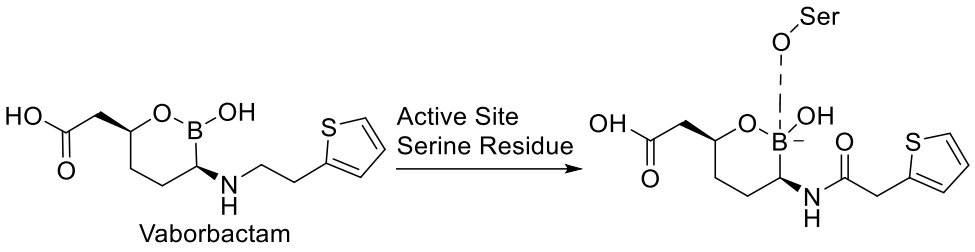

Scheme 1.3.1: Covalent bond formation between the boron of Vaborbactam and catalytic serine residues in the active site.[4]

As mentioned before, Bortezomib (**Figure 1.3.1**) was the first boronic acid-containing drug. This drug is a proteasome inhibitor, used for treatment of multiple myeloma. The boronic acid moiety of Bortezomib covalently forms a complex with the nucleophilic N-terminal threonine hydroxyl group, present in the active site of the proteasome, leading to the disruption of the protein complex, and promoting growth inhibition and apoptosis of cancer cells.[26] The proteasome inhibitor bortezomib is a dipeptide boronic acid analog that reversibly inhibits the activity of the 20S subunit of the proteasome.[27] 3D-QSAR studies revealed that there are three important regions for the interaction between Bortezomib and proteasome: (i) A covalent site to allow the bonding between Bortezomib and proteasome Thr1 residue; (ii) an aromatic ring; (iii) a pyrazinyl as an acceptor and hydrophobic group.[1,28] The reason why boronic acid was added in the drug design of this compound was due to the known high selectivity and low dissociation rates of this group towards the active site of proteasome.[1]

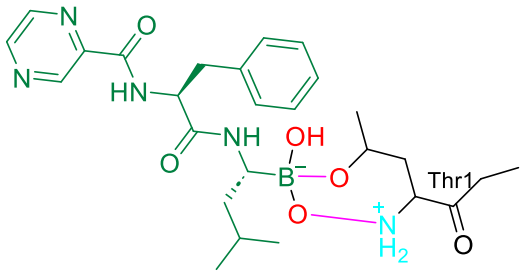

Figure 1.3.1: Interactions of Bortezomib with Active Site Residue Thr1.[29]

Another known drug that was approved by the FDA in 2014 is Tavaborole (**Figure 1.3.2**). It is being used for antifungal benzoxaborole drug and due to its low molecular weight (151.93 g/mol), it permits optimal nail plate penetration.[30] Tavaborole interferes with

protein synthesis in fungal cells by acting on cytoplasmic aminoacyl-transfer RNA (tRNA) synthetases.[30] It specifically binds to the diol tRNA 3'-terminal adenosine in the editing site, resulting tetravalent cyclic boronic ester and thus preventing fungal protein synthesis and ultimately suppressing fungal cell activity.[4]

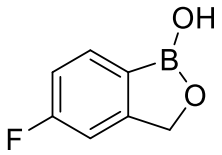

Figure 1.3.2: Chemical structure of the benzoxaborole containing drug Tavaborole.

Over the past decade the interest in the area of covalent inhibition has increased and new therapeutics that use a covalent linkage to site specific target residues are now being investigated and used.[31] The ability to target a desired protein for covalent inhibition under physiological conditions is often limited to reaction with cysteine residues.[31]

Recently, it has been reported that carbonyl boronic acid can enable rapid and reversible modification of the ε-amino group of lysine residues.[31,32] Carbonyl boronic acids can bind covalently to the hydroxy group of the N-terminal of the lysine residue by forming reversible trigonal covalent bond iminoboronate.[32] This unique reactivity of boronic acids can be generalized to other nucleophiles. Thus, boronic acids are useful as high-affinity ligands with low molecular mass.[32,33] The reversibility minimizes off-target reactions and helps avoid permanent modification of the target protein.[33]

Lysine is an amino acid that is involved in many post-translational modifications with essential roles in cell physiology and pathology such as methylation, acetylation, and glycation.[32] Lysine is a known nucleophile that interacts preferentially with electrophiles such as sulfonyl chlorides or isothiocyanates.[34] Lysine is basic (pK_a ~10.5), and is thus usually protonated under physiological conditions.[34] It is only nucleophilic when neutral, as in an enzyme binding pocket where bulk water may be excluded; therefore, electrophiles targeting lysine may be less likely to experience off-target binding events, as covalent modification is more likely to occur within the site of interest.[21] All the

covalent bonding approaches are reversible, making them more attractive in drug design because they defeat unwanted off-target modifications.[2,34]

The lysine residue can be selectively modified during the formation of imines. The reaction between aldehydes and the N-terminus on the lysine residue to form an imine has been widely employed to modify proteins, however, the use of aldehyde that forms an imine that is stabilized through intermolecular interactions has been less employed.[35] Recently, iminoboronate chemistry has been proven extremely useful for bioconjugation and reversibly targeting biological amines.[35] Iminoboronate refers to forming a thermodynamically stable Schiff base with 2FPBA derivatives via additional coordination between boron and nitrogen as shown in **Scheme 1.3.2** at a pH range of 6-10.[11] In the practice of covalent based drug design, the ligand (C, N, O, S framework) primarily assures the selectivity of target binding. At the same time, boron provides better affinity by a covalent connection along with H-bond with the target.[11]

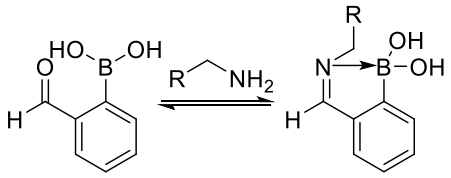

2FPBA

Scheme 1.3.2: Iminoboronate formation between 2FPBA and an amine nucleophile. The presence of the boronic acid stabilizes the imine formation by 4 -5 kcal/mol giving rise to a species that is substantially more stable under aqueous conditions.[9]

Because boron is a strong electrophile, it can either direct coordinate the lone pair of the electrons on the nitrogen atom to the boron atom (i.e, an N-B interaction) or cause a solvent-inserted zwitterionic species observed in protic solvents. Hence, initial nucleophilic attack by the amine is facilitated by the O-B interaction in the carbonyl functionality of the 2FPBA derivatives. The formation of a stable imine in aqueous media would allow a direct, selective, and potentially reversible strategy to modify the lysine residues which showcases the potential use of boronic acids for the site-selective functionalization with lysine.[9,32,33,35]

1.4 Boronic Acid Chemistry with Diols

Cyclic boronate ester formation between boronic acids and cis-1,2 diol has been widely explored, showing the potential affinity towards sugar recognition.[36] The ability for the boronic acids to selectively bind with 1,2-cis-diols was found to be a valuable interaction for the early detection of diseases such as cancer and diabetes.[36] The search for stable, selective, sensitive and non-enzymatic sensors towards glucose has been going on in recently.[37] Boronic acid derivatives binding to glucose relying on their dynamic covalent binding and could potentially offer continuous glucose monitoring devices. The lack of selectivity to glucose was a big obstacle to practical application.[37] Boronic acid-diol binding motifs have been also used in hydrogels, nanomaterials and was even used as building block for creating dynamic assemblies composed of gold nanoparticles.[2,38] Although boronic acid and diol binding has been used in such wide range of applications, there is still a need for simple characterization tools to study binding, to monitor the effects of structural changes that contribute to binding at different pH values, or the selectivity towards different saccharides.[38] The thermodynamic stability of a boronate ester and the kinetic association to form a boronate ester relies on different factors, including the nature of the diols, substitution of the boronic acid derivatives, solvent systems, and other factors.[2]

Saccharides with a free reducing end usually exist as mixtures of anomers and in either furanose (5-membered ring) or pyranose (6-membered ring) forms. Several esters of saccharides are known where the boron atom is bound to three hydroxyl functions. For example, glucose preferentially forms a boronic acid-ligand ester between the furanose anomer with the boronate group at 1,2-position.[36,39] This way of binding positions 3,5,6-OH-functions in a geometry that is pre-organized to bind a second boronate group, in a tridentate fashion.[36,39] Since cis-diol functions in furanose anomers have the greatest affinity for boronate ester formation, the anomeric equilibria in many sugars shift to these anomers after the addition of a boronic acid. Consequently, the anomeric equilibria shift

causes less available pre-organized pyranose anomer diol functions for binding to boronate, which have considerably weaker affinity toward the boronate.[36]

Formation of trigonal and tetrahedral boron-containing esters is very fast, usually almost instantaneous. However, the measuring of sugar affinity may suffer from the slow establishment of the mutarotation equilibrium, which may take many minutes for free sugars. It was found that after mixing of boronic acid and an equilibrated D-glucose sample, initially a rapid conversion of the boronate ester of the α-D-glucopyranose anomer to the corresponding furanose takes place, in approximately 3 minutes. After that, the reaction continues for more than an hour at about the rate of the mutarotation of glucose until the final equilibrium of boronate esters has been attained. A mechanism has been proposed in which the boronate remains bound to the 1,2-diol group of glucose during the conversion of pyranose to furanose.[36,40]

The association constants (K_a) between the boronic acids and diols are determined by titrating boronic acid-Alizarin Red S. (ARS) solutions with target diols.[41] ARS is a hydrophilic dye that binds to a boronic acid emitting a fluorescence signal (**Scheme 1.4.1**). The titration of boronic acid to ARS perturbs the first equilibrium and therefore results in a change of the fluorescence intensity of the solution.[41] The extent to which the diol moiety changes the fluorescence intensity depends on the binding affinity between boronic acid and diol rather than the concentrations and the pH of the ester formation.[41] This method offers high sensitivity, general applicability, reproducibility and flexibility regarding the pH and the buffer used.[41]

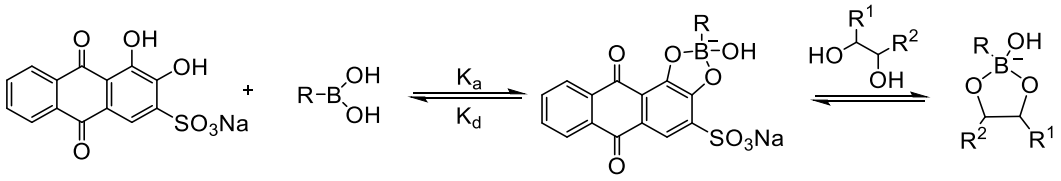

Scheme 1.4.1: Cis-diol complex formation using a competitive boronic acid (BA) receptor.

Another known method for detecting boronate ester is the ^{11}B NMR method which offers a direct and excellent approach to the determination of the binding constants.[42] This method, however, is limited by low sensitivity, difficulty with peak resolution and requires high concentration of the sensor compound. These limitations make this method less useful in the development of boronic acid sensors.[42] ^{1}H NMR and ^{13}C NMR methods were also used under neutral nonaqueous and alkaline aqueous conditions between aromatic boronic acids and glucose complex.[39] The titration of boronic acid and ARS and using fluorescence is advantageous over NMR methods due to the small quantities of material needed for study.[41]

1.5 Mechanistic Pathway for Boronic Acid-Diol Binding

The mechanistic pathway for boronic acid-diol binding exemplify the importance of an understanding of boronic acid acidity and electronic effects from both the diol and the boronic acid. A sp^2-hybridized boronic acid possessing an empty p-orbital, which undergoes hydroxylation with water and generating hydronium (1, boronic acid, **Scheme 1.5.1**).[1,10] This generates a sp^3 borate anion (2). In the presence of 1,2-diols, the borate anion is in equilibrium with boronate ester (2').[1,10] In the second pathway, the 1,2-diol binds with the boronic acid which creates a boronic ester (1'). Once that boronic ester (1') is formed, it can act as an acid (hydroxylation) and releasing hydronium.[1] These reactions combined with the accompanying change in electronic properties have been important in the development of boronic acid-based fluorescent and other sensors for these anions.[2,38]

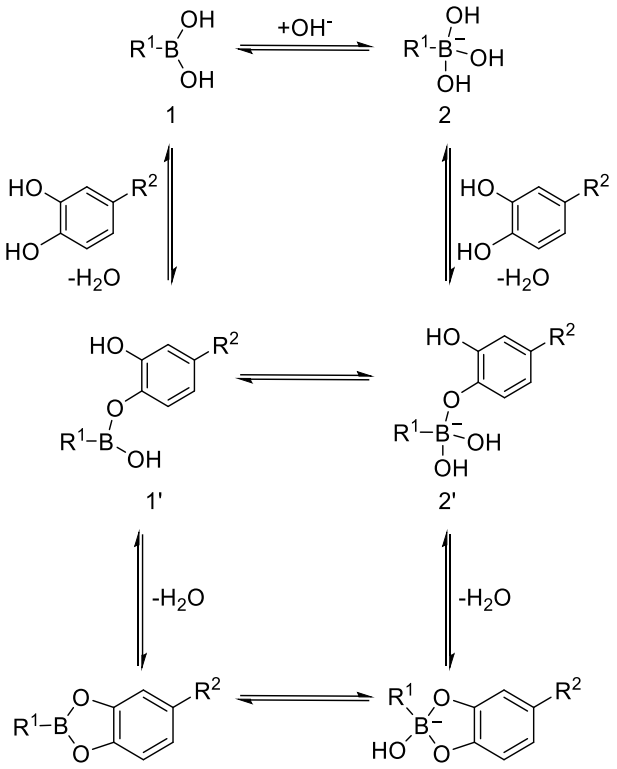

Scheme 1.5.1: Two proposed mechanistic pathways of boronic acid and 1,2-diol binding.

Both pathways create a diol binding, however, pathway 1 leading directly to boronic ester 1' is more thermodynamically stable than the other. Arguably, it is dependent on the pH of the solution and the pK_a of the boronic acid. According to literature, a five-membered boron-containing ring is less strained with an sp^3 boron (2') than an sp^2 boron (1').[2,43] Thus, forming the more stable five-membered ring of the boronate ester (2') should be used with a pH that is exceeding the pK_a of the boronic ester.[4,41] From that, the binding affinity is dependent on the boronic acid and the diol.[2,7,43]

The use of boronic acid and its derivatives in chemical biology and medicinal chemistry has increased dramatically in the recent years. These moieties have many advantages such as formation of strong, reversible covalent bonds to target amino acids and diols. These processes are being extensively studied and characterised, however, there is still a need to search and understand their behavior more extensively to increase their usage in therapeutic applications. Their chemistry is extremely versatile, and their small size

means it can be incorporated into small molecules, inhibitors and receptors while also permitting selectivity for those inhibitors and receptors. Those functionalities also depend on the additional functional groups of the designed compounds.

1.6 Research Aims

Novel compounds were synthesized in the Jakeman lab and were categorized into five groups based on the chemical functionality proximal to the boronic acid: carbonyl boronic acid derivatives, phenylboronic acid derivatives, carboxylic acid derivatives, aldehyde derivatives, and benzoxaborole derivatives, as shown in **Figure 1.6.1**. The synthesis of DT9, DT14 and DT22 has been reported in the literature.[38]. The synthesis of remaining compounds that were prepared by Dr. E. Soleimani and Cyril O'Brian will be reported together with the results presented herein.

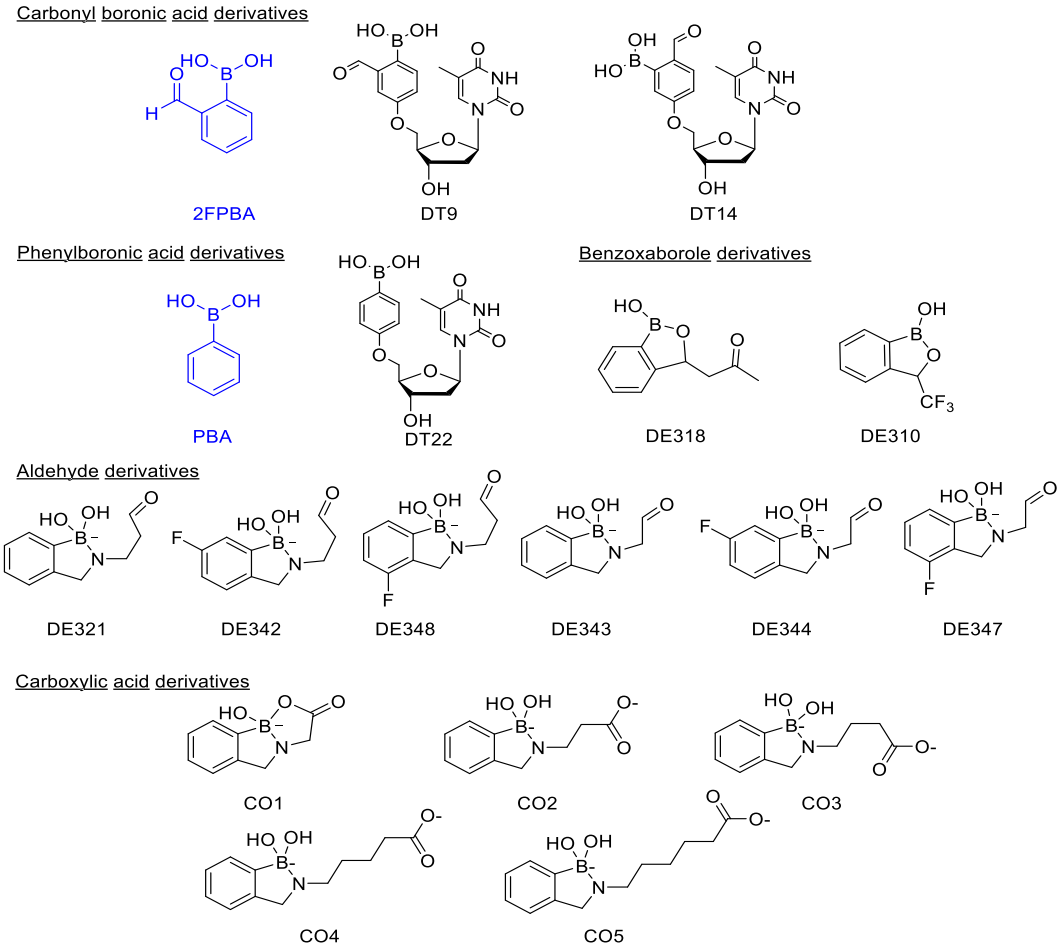

Figure 1.6.1: Novel Boronic acid derivatives synthesized in the Jakeman lab.

In this thesis, we aim to:

1. Determine the pK_a values of the novel synthesised compounds using UV-Vis and ^{11}B, ^{19}F and ^{1}H NMR spectroscopy. These values are measured to see the structural changes that could contribute to binding.[38]
2. Evaluate and quantify iminoboronate formation of carbonyl boronic acid compounds with Boc-Lysine-OH using UV-Vis and ^{1}H NMR spectroscopy.
3. Evaluate and quantify diazaborine formation of aldehyde derivatives with Boc-Lysine-OH using UV-Vis and ^{1}H NMR spectroscopy.
4. Evaluate and quantify the diol binding affinity of our novel boronic acids to ARS and demonstrate the changes in affinity depending on the presence of boron and the additional functionalities.
5. Evaluate and quantify a competitive diol binding affinity of our novel boronic acids to different saccharides that are mostly found and used in mammalians.

Chapter 2. Experimental Procedures

2.1 General Methodology

2-formylphenylboronic acid (2FPBA), phenylboronic acid (PBA), Boc-Lys-OH, Alizarin Red S. (ARS) were purchased from Aldrich and used as received. Sugars and buffers were bought from Aldrich or Astatech and were used as received. The remaining compounds evaluated were synthesized in our lab. The synthesis and characteristic data will be reported elsewhere.[38] Deionized water used for preparation of the buffer and for the binding studies. pH measurements were recorded using a Sentron SI series pH meter (SI600 7600-010), which was attached to a Sentron SI series pH probe (pH 0-14). All UV-Vis spectroscopy samples were measured using a Molecular Devices SpectraMax Plus 384 Microplate Reader. Falcon® 96-well Clear Flat Bottom TC-treated Culture Microplates were used in all studies. Absorbance and fluorescence data were collected using a Bio-Tek Synergy™ HT multi-detection microplate reader for all the studies. The excitation filter used was 485/20 nm and the emission filter used was 590/35 nm. 1 cm quartz cuvette was used instead of a glass cuvette since quartz excels at transmitting UV-Vis light and has a higher durability. The measured UV-Vis spectra were plotted using Microsoft Excel. All NMR spectroscopy samples were measured using a Bruker AV-500 MHz spectrometer at the NMR-3 facility at Dalhousie University. Quartz NMR tubes were used instead of borosilicate tubes to produce a smooth baseline on the ^{11}B NMR spectrum. The measured NMR spectra were analysed using Bruker's Topspin 4.0.8 software.

2.2 Procedure of pK_a Determination of Boronic Acids Using UV-Vis Spectroscopy

2.2.1 Preparation of solutions for UV-Vis pH titrations

For each compound a working stock solution (10 mM) was prepared by dissolving each boronic acid derivative in 10 mL aqueous phosphate buffer (100 mM, pH 7.4). In case of solubility limitations 10% acetonitrile/ 90% phosphate buffer or 10% methanol/ 90% phosphate buffer were used. 1.0 mL of the stock solution was diluted with 9 mL of phosphate buffer (10 fold dilution- 1.0 mM), from which 1.4 mL solution was taken and

further dissolved in 12.6 mL of phosphate buffer (100 fold dilution-0.1 mM). From the final solution, 3.0 mL of the aliquot were transferred to a glass vial. The pH of the solution of these aliquots was then adjusted using 0.1 M HCl, 1.0 M HCl, 0.1 M NaOH, 1.0 M NaOH, and 5.0 M NaOH and measured using a pH meter. The sample was first adjusted to the most acidic desired pH value of 1 with HCl and then NaOH was used to slowly raise the pH to each desired pH value in approximately one pH unit increments. After the pH was adjusted, each aliquot was transferred to a cuvette and then analyzed using UV-Vis spectroscopy in the wavelengths between 190 nm to 350 nm. 100% phosphate buffer, 1% acetonitrile/ 99% phosphate buffer or 1% methanol/ 99% phosphate buffer solution was used as the blank, depending on the solution used to dissolve the boronic acid derivative. Experiments were performed in duplicate and the average pK_a was reported.

2.2.2 Determination of pK_a values using UV-Vis Spectroscopy

The same methodology was used for all UV-Vis spectra recorded. The absorbance was measured between 190 nm to 350 nm. The wavelength where the maximum absorbance change was observed was plotted as a function of the solution pH. To calculate the pK_a, a plot was constructed of pH as a function of *log*(difference) using **Equation 2.2.2** to fit for one pK_a value.[44]

$$\log(\text{difference}) = \log\frac{(\text{highest } A\text{-pH } A)}{(\text{pH } A\text{-lowest } A)} \qquad (\mathbf{2.2.2})$$

The absorbance measured using UV-Vis spectroscopy is represented by the function *A*. The (highest *A*) is the maximum absorption observed by UV-Vis spectroscopy during the titration, (lowest *A*) is the minimum absorption observed by UV-Vis spectroscopy during the titration, and (pH *A*) is the observed absorbance by UV-Vis spectroscopy at a particular pH. The pK_a was determined by the y-intercept of this plot. Calculations were performed using the changes in absorbance at wavelengths 200 nm, 230 nm, and 260 nm since these wavelengths showed high absorbance change as the pH increased. The pK_a's determined at each of these wavelengths receive similar results.

2.3 Procedure of pK_a Determination of Boronic Acids Using NMR Spectroscopy

2.3.1 Preparation of solutions for NMR spectroscopy pH titrations

Samples of boronic acid derivatives (15 mM) were prepared in D_2O. In case of solubility limitations 10% acetonitrile-d_3/ 90% D_2O or 10% methanol-d_3/ 90% D_2O were used. The samples were adjusted to an initial pH value of 1 and NMR spectra recorded. ^{11}B NMR, ^{1}H NMR, and ^{19}F NMR for the boronic acid derivatives that contained fluorine, were collected at that initial pH. Then, the pH was adjusted using NaOH to the next pH, the pH was measured and NMR spectroscopy was measured again. This procedure was repeated until the desired end pH value was recorded and measured by NMR spectroscopy. The sample adjusted to exhibit the desired pH values within the NMR tube using 0.1 M HCl, 1.0 M HCl, 0.1 M NaOH, 1.0 M NaOH, and 5.0 M NaOH. Since D_2O was used to prepare the solutions, the conversion of pH into pD is then accomplished by adding a constant of 0.4 to the measured pH value.[45] Samples were taken back to pH 1 after the higher pH values to demonstrate reversibility.

2.3.2 Determination of pK_a Values from NMR Spectra

The same NMR methodology was used for all types of NMR spectra recorded (^{1}H, ^{11}B, or ^{19}F), resulting in pK_a values associated with different functional groups. The chemical shift versus pH data were plotted. The inflection point represents the pK_a value and was determined by non-linear fit using equation for a two-state pK_a system.[46] Different methods of analysis were compared as described below.[36]

2.3.3 ^{11}B NMR pK_a Dependence Analysis

Three methods of calculation were tested in this experiment.[2-4] The boronic acid derivative's chemical shift from the ^{11}B NMR titration data versus pH, mole fraction versus pH, and integration of peaks at those chemical shifts versus pH. Those methods determined equivalent pK_a values and using chemical shift as a method of determination of pK_a was decided to be used based on simplicity of the method and less error of determination of the chemical shift versus the possibility of error when calculating mole fraction or determination of integration. **Figure 2.3.3** examines all three methods. Inflection points (pK_a) were determined using the midpoint calculation of the pH versus

chemical shift plot using its average between the two points (the half equivalence point) to fit the estimate of the pK_a value. Each pK_a was estimated to two significant figures.

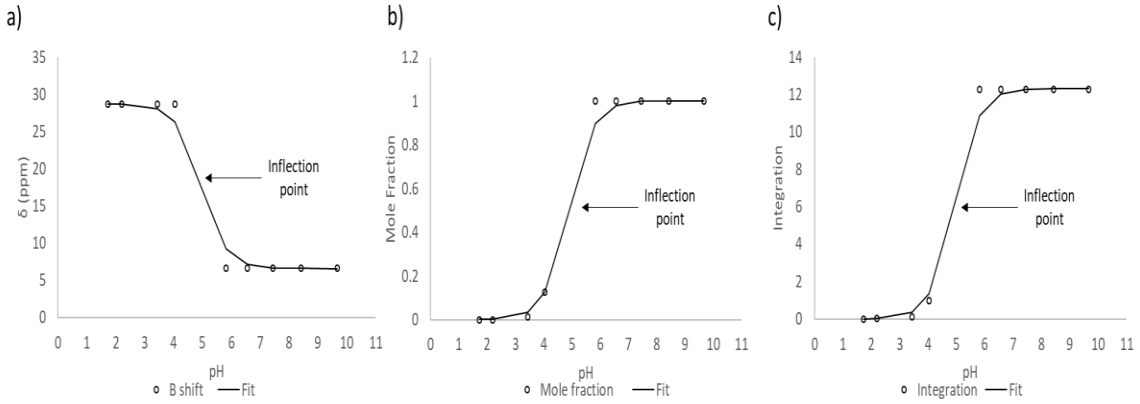

Figure 2.3.3: Examination of three pK_a calculation methods of compound DE348. a) Method using chemical shift of boron peaks. b) Method using mole fraction of boron peaks. c) Method using integration of boron peaks.

The chemical shift was used also due to the fact that the signal to noise was poor due to the need to increase the number of scans. The baseline is not quite determined which is why the best method to estimate the p*K*a values of the compound is by using the chemical shifts.

The pK_a was determined from a non-linear fit of **Equation 2.3.3** of the chemical shift (δ) data versus pH, where pK_a represents the ionization constant of the free respective boronic acid, δ_{HA} is the chemical shift for the sp^2-hybridized form of the respective boronic acid, and δ_{A^-} is the chemical shift for the sp^3-hybridized form of the respective boronic acid.[47]

$$\delta = \left(\frac{\delta_{HA} - \delta_{A^-}}{10^{pH-pK_a+1}}\right) + \delta_{A^-} \qquad (\mathbf{2.3.3})$$

2.4 Procedure for Iminoboronate Formation of Boronic Acids and Boc-Lys-OH Using UV-Vis Spectroscopy

2.4.1 Preparation of solutions for iminoboronate formation using UV-Vis spectroscopy

A UV-Vis spectrum was recorded in a 1 cm quartz cuvette of a solution of each boronic acid (1.0 mM, HEPES buffer (1.0 M, pH 7.4)). To this solution, aliquots of BocLys-OH (1.0 M, HEPES buffer (1.0 M, pH 7.4) were added and mixed to give final BocLys-OH concentrations of 5 – 80 mM. The pH value of HEPES buffer solution was adjusted to 7.4 (if required) using 0.1 M HCl, 1.0 M HCl, 0.1 M NaOH, 1.0 M NaOH, and 5.0 M NaOH. Samples were incubated for 2.5 minutes prior to recording each spectrum and the pH monitored to ensure no change occurred. UV-Vis spectrum were recorded in the wavelengths between 190 nm to 350 nm and the pH value was monitored throughout the experiment.

2.4.2 Iminoboronate formation analysis

The observed equilibrium constant for Schiff-base formation (K_a) was determined by fitting **Equation 2.4.2**.[35]

$$A = \frac{A_0 + A_c K_a [ligand]_T}{1 + K_a [ligand]_T} \qquad (\mathbf{2.4.2})$$

The absorbance vs. concentration of total Boc-Lys-OH was plotted. (A_0) is the initial absorbance of boronic acid derivatives measured without Boc-Lys-OH, and (A_c) is the absorbance of the complex. Ka represents the association constant of the iminoboronate binding formation.[35]

2.5 Procedure for Iminoboronate Formation of Boronic Acids and Boc-Lys-OH Using ^{1}H NMR Spectroscopy

2.5.1 Preparation of solutions for iminoboronate formation using NMR spectroscopy

Samples of boronic acid derivatives (5.0 mM) were prepared in 10% phosphate buffer (D_2O, pH 7.4)/ 90% D_2O. In case of solubility limitations 10% acetonitrile-d3/10% phosphate buffer/ 80% D_2O or 10% methanol-d3/ 10% phosphate buffer/ 80% D_2O were

used. To the boronic acid solutions, Boc-Lys-OH (500 mM, 10% phosphate buffer/ 90% D_2O, pH 7.4) was added to have equivalent concentration of the boronic acid derivative in the solution. The samples were adjusted to pH of 7.4, if necessary, and ^1H NMR spectra recorded.

2.5.2 Iminoboronate formation analysis

Conversions based on the comparison of the signal from α-protons to the Boc-Lys-OH, which converts from ~4.0 ppm to ~3.4 ppm, respectively. In addition, the disappearance of the aldehyde peak of the boronic acid derivative was converted to the iminoboronate peak at 8.5 ppm.[33]

2.6 Procedure for Diazaborine Formation of Boronic Acids and Boc-Lys-OH Using UV-Vis Spectroscopy

The same methodology and analysis as for the iminoboronate formation (**2.4**) was used for diazaborine formation.

2.7 Procedure for Diazaborine Formation of Boronic Acids and Boc-Lys-OH Using NMR Spectroscopy

The same methodology and analysis as for the iminoboronate formation (**2.5**) was used for to potentially observe diazaborine formation.

2.8 Procedure for Diol Binding of Boronic Acids with ARS

2.8.1 Measurement of diol binding dissociation constants of boronic acid derivatives and ARS

The association constant for the ARS-BA complex (K_a) was measured. A HEPES buffer solution (100 mM, pH 7.4) was added to a well plate. A solution of ARS (0.1 mM in HEPES buffer (100 mM, pH 7.4)), made within the last 7 days and stored in the refrigerator (solution A). This concentration of ARS was chosen because it was found to give a strong fluorescence profile. Boronic acid (BA) derivatives were added to the portion of solution A to make 0.10 mM ARS, 2 mM BA derivative solution (Solution B). The pH values of the

solutions were checked and corrected, if necessary. Solution B was titrated into solution A in order to make mixtures with a constant concentration of ARS and a range of concentrations of BA derivatives. All solutions in the well plate gave a final volume of 360 µL. Different final concentrations of boronic acid between the ranges of 0.05 and 2 mM were prepared in order to cover as much of the binding curve as possible. The rapid changes in absorbance and fluorescence showed that equilibrium was reached within seconds. Experiments were carried out in duplicate.

2.8.2 Data collection

The data was collected at room temperature and without delay. Absorbance data in the range of 300-600 nm was also collected using the same instrument and the same set- up for comparison between the data collection methods and absorbing the change of wavelength. The absorbance of the compounds did not show a shift in wavelength other than 520 nm to 480 nm which allows the detection only at the 485 nm and 520 nm by fluorescence which is within the limits of the measured absorbance.

2.8.3 Theory of diol binding of boronic acid derivatives and ARS

The spectroscopic change in the ARS following diol binding allows the binding coefficient between the ARS and the boronic acid to be measured directly using UV-Vis spectroscopy and fluorescence spectroscopy. This relationship was fitted using non-linear fit of **Equation 2.4.2** where the recorded intensity was plotted against the boronic acid concentration.[41]

It was determined that this equation can also fit diol binding with boronic acid derivatives (See Appendix C). The same form of equation was used for fluorescence spectroscopy system with (F_0), F_c and (K_a) for association and dissociation constants (**Equation 2.8.3).**

$$F = \frac{F_0 + F_c K_a [Ligand]_T}{1 + K_a [Ligand]_T} \qquad (\mathbf{2.8.3})$$

The Fluorescence of the system (F) to the initial fluorescence (F_0) the fluorescence of the free ARS (F_c), the association constant of the boronic acid to the monosaccharide (K_a), and the concentration of the saccharide $[ligand]_T$.

2.9 Procedure for Diol Displacement Assay to Measure Sugar K_a Values

2.9.1 Measurement of diol binding dissociation constants of boronic acid derivatives and saccharides

The method of Wang and Springsteen was used.[41] The displacement assay dissociation constant of sugar-boronic acid complex (K_a) was measured. A HEPES buffer solution (100 mM, pH 7.4) was added to a well plate. A solution of ARS (0.1 mM in HEPES buffer (100 mM, pH 7.4)), made within the last 7 days and stored in the refrigerator (solution A). Boronic acid (BA) derivatives were added to the portion of solution A to make 0.10 mM ARS, 2 mM BA derivative solution (Solution B). A range of saccharide solutions were prepared in varying concentrations (0.01-2 mM in HEPES buffer (100 mM, pH 7.4)) depending on the solubility of each saccharide (Solution C). The pH values of the solutions were monitored throughout the experiment. Solutions B and C were titrated into solution A in order to make mixtures with constant concentrations of ARS and BA and an increasing concentrations of saccharide. All solutions in the well plate gave a final volume of 360 µL .The rapid changes in absorbance and fluorescence showed that equilibrium was reached within seconds. Experiments were carried out in duplicate.

2.9.2 Data collection

The data was collected at room temperature (25°C) and without delay. Fluorescence data at wavelength of 485 nm was collected using the same instrument and same set-up as for the binding of ARS to the boronic acid derivatives.

2.9.3 Theory of diol binding of boronic acid derivatives and saccharides

The spectroscopic change in the ARS following the dissociation of a bond diol allows the binding coefficient between the saccharide and the boronic acid to be measured directly using fluorescence spectroscopy. This relationship was fitted using **Equation 2.8.3** where the recorded fluorescence intensity was plotted against the saccharide concentration. The association constant of the boronic acid to the saccharide is (K_a) and the concentration of the saccharide ($[ligand]_T$).[41]

Chapter 3. Results and Discussion of pK_a Determination Using UV-Vis and NMR Spectroscopy

3.1 Introduction

The pK_a of a boronic acid is defined as the pH at which 50% of the boronic acid exists as the hydroxyboronate anion species.[1] It is often dictated by the transition from hydrophobic neutral boronic acid to the anionic hydroxyboronate or boronate ester.[1] Various pK_a values of boronic acid containing compounds are known in literature. A few examples of pK_a values are 3-acetamidophenylboronic acid (3AcPBA) has a pK_a of 8.5, while the electron-withdrawing inductive and resonance effects for both 4-methylcarbamoyl-phenylboronic (4MCPBA) acid and 4-formylphenylboronic acid (4FPBA) result in a decrease of pK_a for both boronic acids with pK_a values of 7.9 and 7.8, respectively.[36] Benzoxaborole is a heterocycle boronic acid, with a pK_a lower than 3AcPBA, 4MCPBA, or 4FPBA. The lower pK_a is driven by the release of ring strain in the five-membered ring as the boron center transitions from a trigonal planar geometry to a tetrahedral geometry in the boronate anion form, with the heterocycle being retained. [36]

The boronic acid derivatives that were synthesized in the Jakeman group contain different functionalities which vary in their boronic acid pK_a values and as a result change the overall pK_a of the compounds.[1] **Scheme 3.1.1** shows pK_a dissociation for three types of chemical functionality found in our synthesized compounds. i. Boronic acid ii. Carboxylic acid and iii. Ammonium ion.

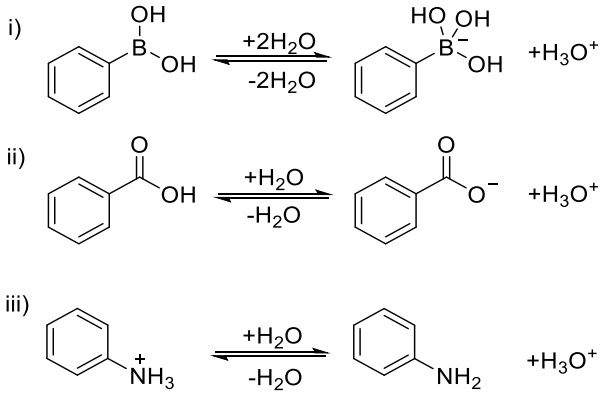

Scheme 3.1.1: pK_a dissociation of i. Boronic acid ii. Carboxylic acid and iii. Ammonium ion.

Boronic acids have been shown to be effective sensors for various saccharides (**Scheme 3.1.2**).[2,3] Initially, it was shown that the binding affinity of a boronic acid to diols and saccharides was often related to the pK_a of the boronic acid, the higher the pH, the higher binding constant between a boronic acid and a diol. However, Springsteen and peers discovered that the binding is dependent on the pK_a values of the boronic acid and the diol.[3] Moreover, the belief that boronic acids with lower pK_a values have greater binding affinities at neutral pH is not always true.[3] In this work, the determination of pK_a values for a series of boronic acids will be measured.

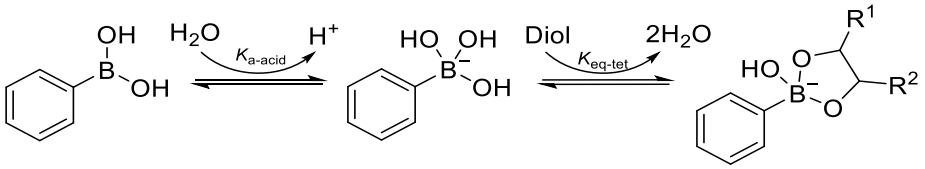

Scheme 3.1.2: The relationships between phenylboronic acid and its diol ester. K_{eq-tet} is the equilibrium constant of the tetrahedral form of boronic acid.[3]

3.2 pK_a determination of novel boronic acid derivatives using UV-Vis spectroscopy

UV-Vis spectroscopy was used to determine the pK_a of the novel synthesized boronic acid derivatives. pK_a values were obtained by monitoring changes in absorbance as the boronic acid derivatives were titrated with sodium hydroxide.[1] As the boronic acid compound transitions from the neutral trigonal planar species to the tetrahedral boronate center, the absorbance at wavelengths ranging from 200-260 nm changes, allowing for facile pK_a determinations.[1] The wavelength where there is maximal change between the two states was chosen for a linear regression calculation.

The conjugate base of the boronic acid derivative has an additional hydroxyl group from the base added to the solution which forms a tetravalent hydroxyboronate structure carrying a negative charge. This Lewis acidic behavior is well established for boronic acid derivatives and, although, they can engage in hydrogen-bonding interaction in solution, boronic acids form a tetravalent trihydroxyborate anion as their conjugate base in water.[9] To validate the pK_a determination method, the pK_a value of 2FPBA, which is a commercially available compound and its pK_a value has been reported, was used has a

control. The pK_a of 2FPBA was measured in 90% phosphate buffer at room temperature (7.6) and was in agreement with the reported value (7.5).[1] Also, PBA was used and its results were in agreement with the reported values (pK_a measured was 8.8 while the reported value was approximately 8.8).[1,4] To observe the spectral changes in the synthesized boronic acid derivatives as a function of pH, absorbance measurements were recorded. The measurements were taken in duplicates and the average pK_a was calculated. It is important to mention that the pK_a determination using UV-Vis spectroscopy is of the whole environmental pK_a in the solutions rather than the pK_a values of the different functional groups on the molecule. The different functionalities attached to the boronic acid derivatives have shown different trends on the changes in absorbance. An ideal result of the one pK_a module calculation is the carbonyl boronic acid derivative, compound DT14, is shown in **Figure 3.2.1**.

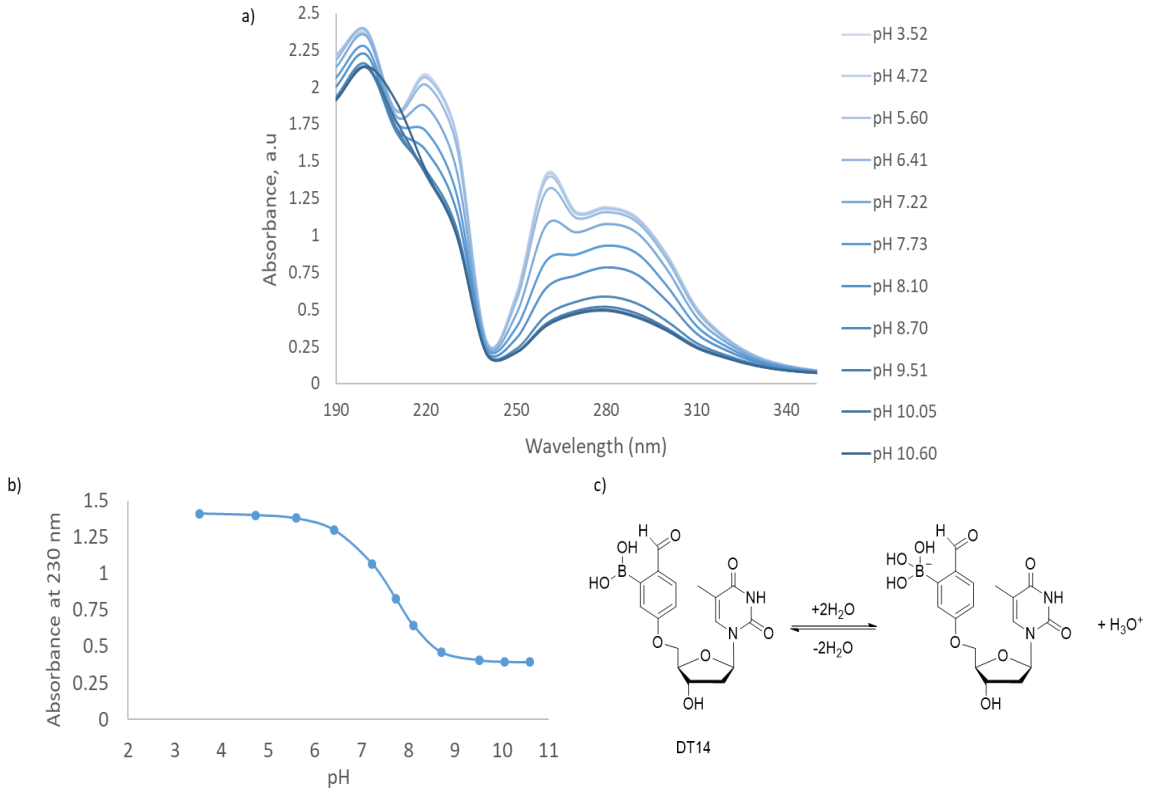

Figure 3.2.1: Absorbance changes with increases in pH and pK_a determination of compound DT14. a) UV-Vis Spectrum (λ= 190-350 nm) with pH values from 3.5 to 10.6. b) Plot of absorbance (λ= 230 nm) versus pH to determine pK_a. c) Reversible transition from the neutral trigonal planar form of the carbonyl boronic acid derivative DT14 to the tetrahedral boronate center as the pH of solution increases.

The changes observed in the UV-Vis spectrum depending on the equilibrium species present in solution are clearly seen in **Figure 3.2.1**. At pH 3, the boronic acid functionality was neutral with a maximum absorption difference shown at 230 nm, whereas at pH 10, only the tetrahedral species is likely present. It is expected that the tetrahedral geometry of the boronic acid will result in lower absorbance signal.[9] From **Figures 3.2.1(b)** and **(c)**, there is a decrease to the absorption signal observed at 230 nm as pH increases. This decrease in absorption is likely due to a transition from the trigonal planar to tetrahedral geometry of the boronic acid.

An isosbestic point can be observed at 210 and 240 nm. An isosbestic point is the wavelength in which the absorbance of two species is the same which indicates that the starting material and the product have an equal extinction coefficients at this wavelength. This gives the information that one species is transitioning to another and in this case, transitioning from its neutral trigonal planar geometry to the tetrahedral geometry. A lack of such point indicates the existence of multiple species in solution. For compound DT14, the decrease in absorbance signal near the isosbestic point at 240 nm was used to determine the pK_a of the boronic acid by using pH as a function of log(difference), which was calculated using **Equation 2.2.3** and using a linear regression as a one pK_a module (**See Appendix A**). From this spectral analysis, the pK_a of DT14 was calculated to be 7.5.

Not all compounds fit the one pK_a fitting model, presumably due to the presence of multiple chemical functionalities such as the amine. The lack of the isosbestic point indicated that there were multiple species present in the solution and the boronic acid did not transform solely from a trigonal planar to the tetrahedral species. More changes to the absorbance were shown, however, calculating additional pK_a values requires a multiple pK_a fitting model. As a result, these boronic acid derivatives will not be discussed in this thesis. An example of this were the aldehyde derivatives. **Figure 3.2.2** presents the aldehyde derivative DE344.

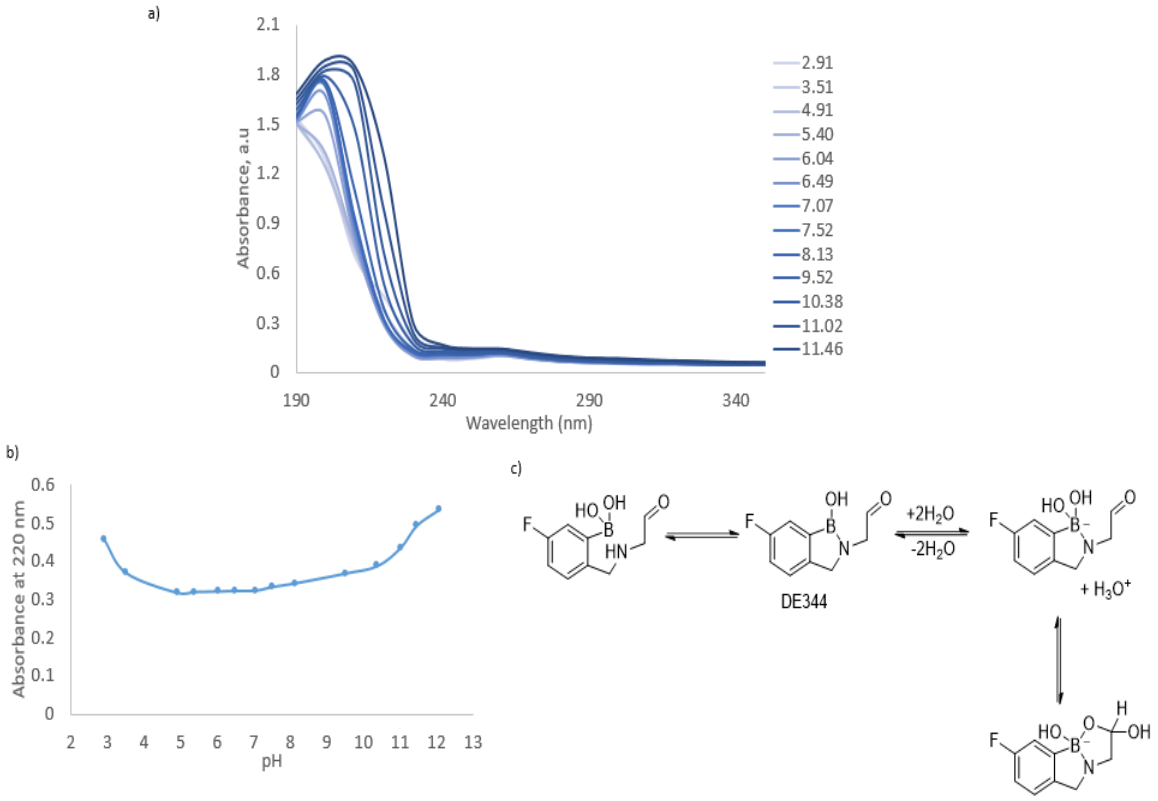

Figure 3.2.2: Absorbance changes with pH increases and pK_a determination of compound DE344. a) UV-Vis Spectrum (λ= 190-330 nm) with ranging pH values. b) Plot of total absorbance at the wavelength of 220 nm versus pH to determine pK_a. c) Reversible transition from the neutral trigonal planar form of the aldehyde derivative DE344 to the tetrahedral boronate center and to the hemiacetal cyclized form as the pH of solution increases.

The changes observed in the UV-Vis spectrum depend on the species present in solution, which is seen in **Figure 3.2.2**. The plot of absorbance (220 nm) versus pH (**3.2.2b**) shows an increase in absorbance. One scheme of reactivity that may account for these changes is shown in **Figure 3.2.2c**, where the secondary amine directly coordinates to the boronic acid, and the aldehyde potentially cyclizes with the boronic acid and forms a hemiacetal (**Scheme 3.2.1**). The conformation causes the aldehyde derivative to be closer to the boronic acid and, thus, form a hemiacetal cyclized form, which prevents optimal B-O conjugation reactions and, as a result, increases the boron atom's electronic deficiency.[2,4] Amines have a pK_a value of 9-10 and aldehydes have a pK_a value of 17 which effects the multiple pK_a values of the aldehyde derivatives.[4]

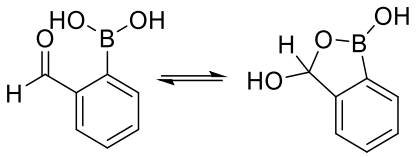

Scheme 3.2.1: Cyclisation between the aldehyde and the boronic acid to form a hemiacetal.

However, it is difficult to prescribe the precise functionality in solution of DE344 given these potential equilibria. This led us to record changes in the ^{1}H, ^{11}B and ^{19}F NMR against pH to gain insight. **Table 3.2.1** shows the compounds that were able to fit the one pK_a fitting model versus the compounds that did not. This data represents a case where it is unknown what and how the functionalities of the compound contributes to the change in intensity.

Table 3.2.1: Compounds that fit the one pK_a fitting model versus compounds that require a multiple pK_a fitting model.

Single pK_a Value	Structure	Multiple pK_a Values	Structure
2FPBA		DE343	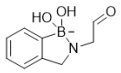
PBA		DE344	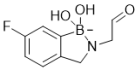
DT9	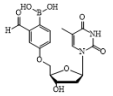	DE347	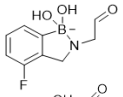
DT14	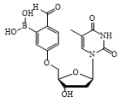	DE321	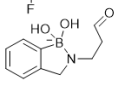
DT22	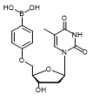	DE342	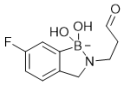
DE310		DE348	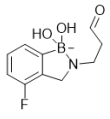
DE318	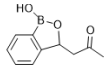	CO2	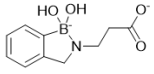
CO1	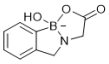	CO3	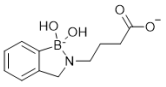
		CO4	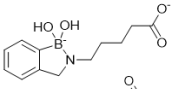
		CO5	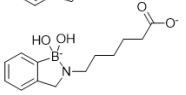

The pK_a values of the synthesized compounds that fit the one pKa fitting model was determined using UV-Vis spectroscopy are shown in **Table 3.2.2**. Each pK_a value represents the transition from neutral trigonal planar to anionic tetrahedral boron center.

Table 3.2.2: Calculated pK_a Values for boronic acid derivatives using UV-Vis spectroscopy. pK_a values were measured in duplicate and average reported. In brackets: wavelength used for pK_a fit.

Compound	Structure	pK_a using UV-Vis	Compound	Structure	pK_a using UV-Vis
2FPBA	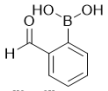	7.6 (260 nm)	DE310	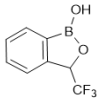	6.9 (220 nm)
DT9	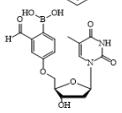	7.5 (260 nm)	DE318	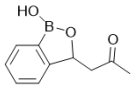	7.3 (220 nm)
DT14	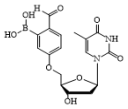	7.5 (260 nm)	CO1	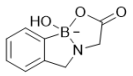	9.3 (220 nm)
PBA		8.8 (260 nm)			
DT22	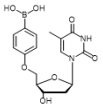	7.9 (230 nm)			

Boronic acid derivatives are Lewis acids and therefore, they can bind OH^- ion from the solution.[5] In the case of carbonyl boronic acid derivatives and phenyl boronic acid derivatives that contain thymidine, the absorbance decreases as the pH increases. Carbonyl boronic acids have lower pK_a values than phenylboronic acid derivatives because the aldehyde group is an electron withdrawing group. Aldehydes tend to withdraw electrons from electron rich systems because of the presence of the electronegative oxygen atom in its carbonyl structure, which, in turn, leads to inductive effects. Comparing to their control compounds, 2FPBA and PBA, the pK_a values of DT9 and DT14 are not significantly lower than 2FPBA, while DT22 has a 0.9 pK_a value difference with PBA which is considered more significant.

The carboxylic acid functionality is an electron withdrawing group with a pK_a value of ~5, which could affect the overall pK_a of compounds that were shown to have multiple pKa values. However, CO1 fits the one pK_a fitting model while CO2-CO5 do not. It was demonstrated that CO1 is in its cyclic form by comparison to a related derivative that was characterized by x-ray analysis shown in **Figure 3.2.3** while compounds CO2 to CO5 have not been proven to be cyclized yet which could be the reason for the differences in the fitting of one pK_a model.

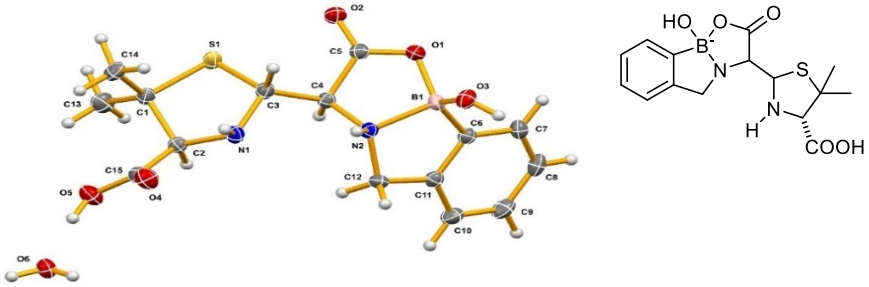

Figure 3.2.3: X-ray crystallography of a boronic acid derivative giving an insight to the structure of compound CO1.

3.3 pK_a determination of novel boronic acid derivatives using ^{1}H, ^{11}B and ^{19}F NMR spectroscopy

Acid-base properties of the synthesized compounds are an important issue in living systems due to many molecules having different properties at certain pH values. NMR spectroscopy can be used to determine pK_a values by comparing the signal integration and chemical shifts.[6] In the determination of pK_a of our novel boronic acid derivatives, special approaches based on ^{11}B, ^{15}N, ^{31}P, or ^{19}F NMR spectroscopy being used alongside ^{1}H NMR spectroscopy have been adapted to successfully determine pK_a values.[6] The pK_a determination with ^{11}B NMR spectroscopy is based on the effect of the ionization and structural changes to the boron center with changing pH. The hybridization of the boron center is monitored by observing the chemical shift changes, as the structure of the molecule is altered due to the increasing or decreasing solution pH. NMR titration, in contrast to UV-Vis spectroscopy, the direct structural change to the functionality of interest is specified.[6]

In this study, the chemical shifts obtained with ^{11}B NMR spectrum were analyzed with inflection-point graphical analysis, using a plot of chemical shift against the pH of the solution to estimate the pK_a values of the boronic acid compounds.[1] The signal-to-noise of the NMR spectroscopy did not allow us to obtain a proper baseline due to the lower number of scans that was used. Therefore, the chemical shifts were used to estimate the pK_a, instead of the integration of the peaks or the mole fraction. This was done to observe information regarding the structural changes in the synthesized boronic acid derivatives as shown in **Figure 3.3.1**. ^{1}H and ^{19}F NMR spectra were measured to observe the complexity of the compounds and gain more understanding on the structural changes to the entire molecule. The carbonyl boronic acid DT14 was used as an example to demonstrate the ability of the compound to form a tetrahedral species (sp^3) from a trigonal planar species (sp^2) and determine whether it is reversible.

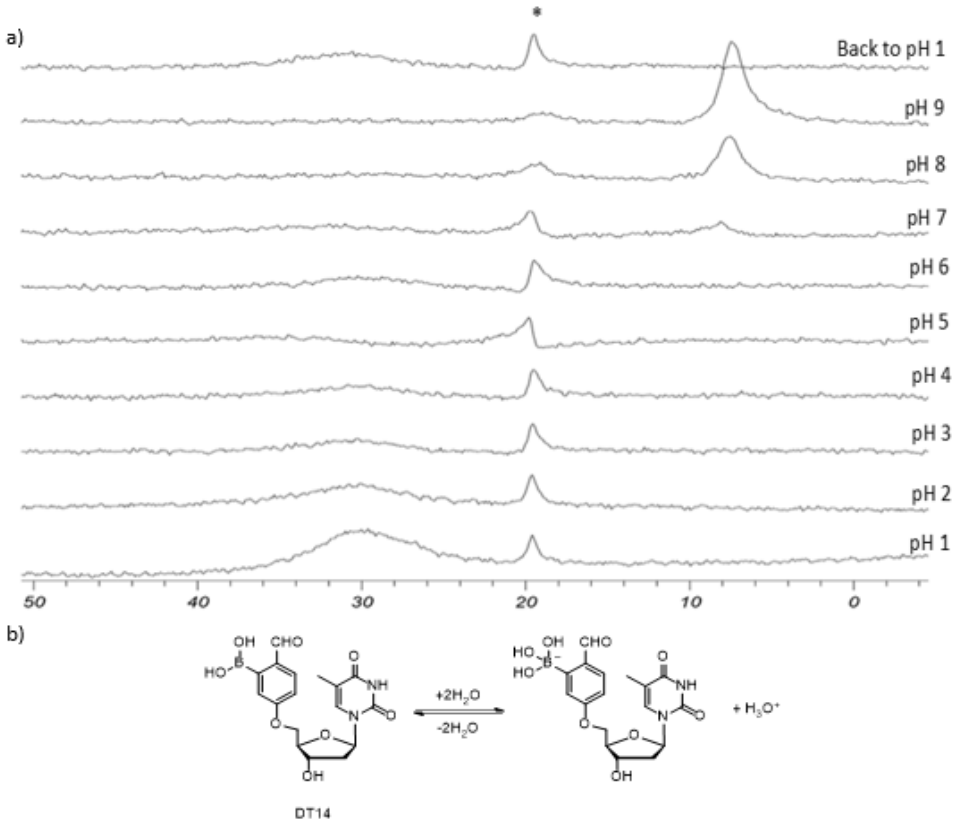

Figure 3.3.1: a) ^{11}B NMR data versus pH of DT14; b) Boronic acid ionization showing trigonal planar to tetrahedral gradually change of the boron center. *Peak at 19.5 ppm represents boric acid (pK_a of boric acid is 9.2).

The carbonyl boronic acid derivative DT14 has shown that as the pH of the solution increases, there is a chemical shift change from 29.9 ppm to 7.5 ppm, which provides information that the boron environment has changed, and the boronic acid is transforming from a trigonal planar form to a tetrahedral coordination as the chemical shift moves upfield. When the pH was brought back from pH 9 to 1, reversibility was observed since the peak shifts back to 29.9 ppm while the peak at 7.5 disappears and the boric acid peak at 19.5 ppm reappears. To calculate the pK_a using ^{11}B NMR data, the chemical shift was plotted against pH as shown in **Figure 3.3.2**. Integration of the peaks was used to determine which peak represents the majority coordination of the compound.

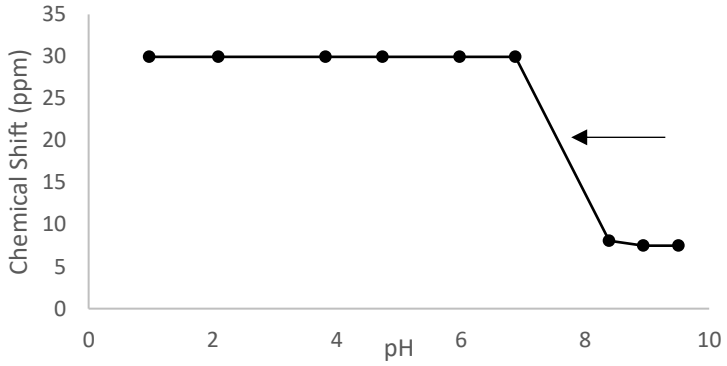

Figure 3.3.2: The curve to determine pK_a of DT14, forming a tetrahedral center. The chemical shift was determined using the ^{11}B NMR from **Figure 3.3.1**. Solid line represents the fitted pK_a calculation. The pK_a was experimentally determined to be 7.6.

The inflection point in this case is the half equivalence point to where the compound converts from a trigonal planar form to the tetrahedral coordination, which defines the pK_a. Using this method, the pK_a can be calculated and determined. Comparing this result with the UV-Vis spectroscopy (pK_a=7.5), the differences in pK_a are not significant. To observe structural changes of DT14 at different pH values, ^{1}H NMR spectra were recorded and reversibility was determined as shown in **Figure 3.3.3**.

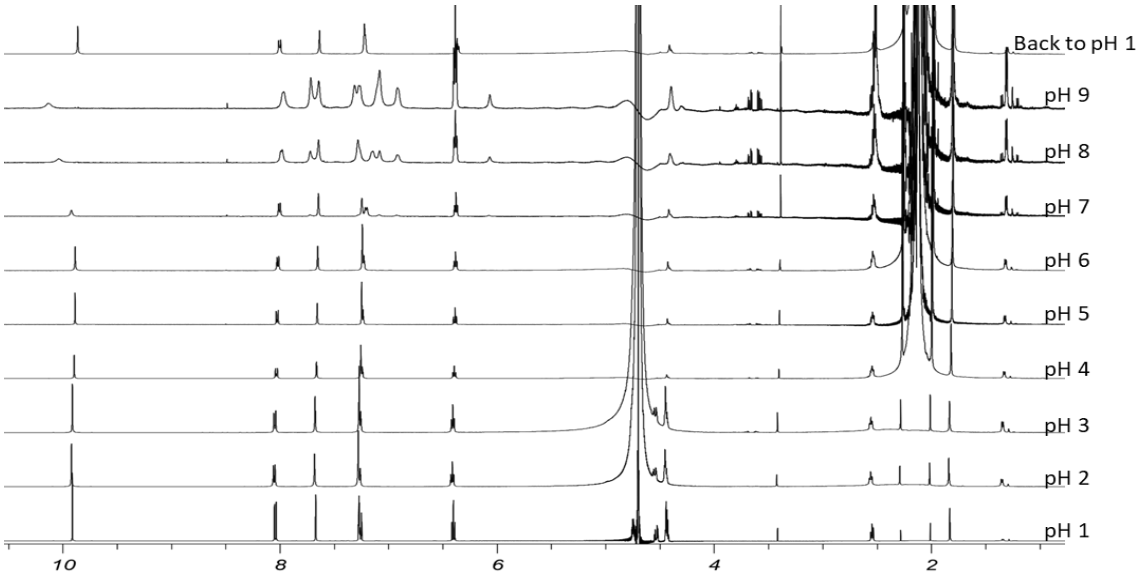

Figure 3.3.3: ^{1}H NMR spectra of DT14 with increasing pH. The reversibility of the structural changes was observed by returning the pH to 1.

The ^{1}H NMR spectrum of DT14 shows that the aldehyde peak at 9.9 ppm decreases in intensity and shifts to 10.3 ppm as the pH of the solution increases. This could be due cyclization of the compound with the boronic acid at higher pH values of the solution. Also, there are additional signals in the aromatic region that could be consistent with cyclisation between the aldehyde and the boronic acid. In addition, a peak at 6 ppm appears as the pH increases and a series of enantiotopic peaks also appeared at 3.6 ppm that are clearly observable by pH 7. The shifts at 3.6 ppm potentially correspond to methylene protons that increase in intensity as the pH of the solution increases. When pH was reversed back to pH 1, the aldehyde peak appeared at 9.9 ppm and the additional peaks that were observed at higher pH values disappeared, which demonstrates the hypothesis that those compounds are reversible. Similar additional peaks in the ^{1}H NMR and peaks shifting in the ^{11}B NMR were found for phenylboronic acid, carboxylic acid derivatives and benzoxaborole derivatives as only one chemical shift was observed which indicates that one chemical species was determined.

It is important to note that the ^{1}H NMR spectra is complex, and it is difficult to observe the structural changes as the pH of the solution increases. In addition, DT14 showed reversibility when the pH of the solution was brought back to pH 1. This reversibility was

observed in multiple compounds, however, not all compounds showed this reversibility and rather showed that the compounds decomposed. Irreversibility is observed as there are new peaks shown after titrating back to pH 1, that were not observed previously. Increased complexity of the spectrum informs us that irreversible structural changes occurred as a result of changing the compounds conditions to the extreme. **Table 3.3.1** shows the compounds in which reversibility was observed and the compounds that did not show reversibility. Moreover, the same compounds that did not fit the 1 pK_a fitting model using UV-Vis did not fit this method of estimation. Therefore, their pKa values were not reported in this thesis.

Table 3.3.1: Reversible compounds versus irreversible compounds based on reversibility experiment using ^{1}H NMR.

Reversible	Structure	Irreversible	Structure
DT9	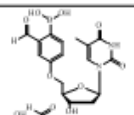	DE321	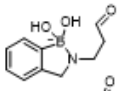
DT14	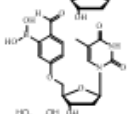	DE342	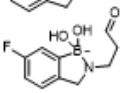
DT22	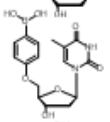	DE348	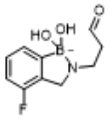
DE310		CO2	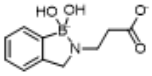
DE318	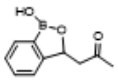	CO3	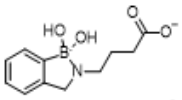
DE343	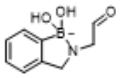	CO4	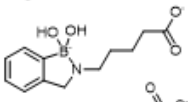
DE344	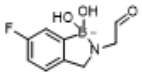	CO5	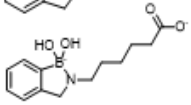
DE347	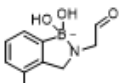		
CO1	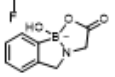		

Looking at the compounds that were found to be reversible, it is interesting to see that the aldehyde derivatives that contains one methylene group between the amine and the

aldehyde, was found to be reversible while the aldehyde derivatives that were contain two methylene groups were found irreversible when the pH of the solution was reversed back to 1.

Another example of pK_a estimation using ^{11}B NMR is of the aldehyde derivative DE344. The chemical shift from 29.2 to 12.1 ppm in **Figure 3.3.4** indicates the transition of the boronic acid center from its neutral trigonal planar species to the anionic tetrahedral species.

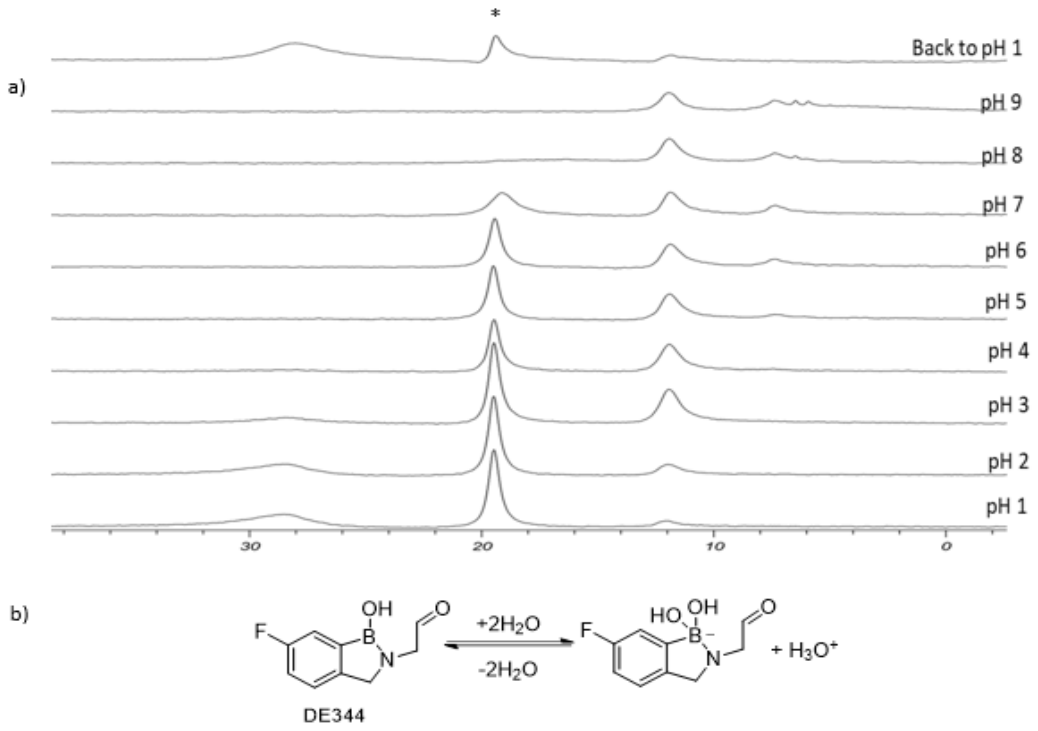

Figure 3.3.4: a) ^{11}B NMR data versus pH of DE344; b) Boronic acid ionization showing trigonal planar to tetrahedral gradually changes of the boron center. *Peak at 19.5 ppm represents boric acid (pK_a of boric acid is 9.2).

The aldehyde derivative DE344 has shown that as the pH of the solution increases, the boron environment changes, since the boronic acid is transforming from a trigonal planar form to tetrahedral coordination. This can be seen at the chemical shift of the peak. Between pH 1 to 2, a peak at 28.5 ppm is observed as the major peak (when looking at integration of those peaks), then between the pH values of 3 until 9, this peak shifts to

11.9 ppm. When the pH was brought to pH 1, reversibility was observed since the peak shifts from 11.9 ppm back to 28.5 ppm. To calculate the pK_a using ^{11}B NMR, the chemical shift was plotted against pH as shown in **Figure 3.3.5**.

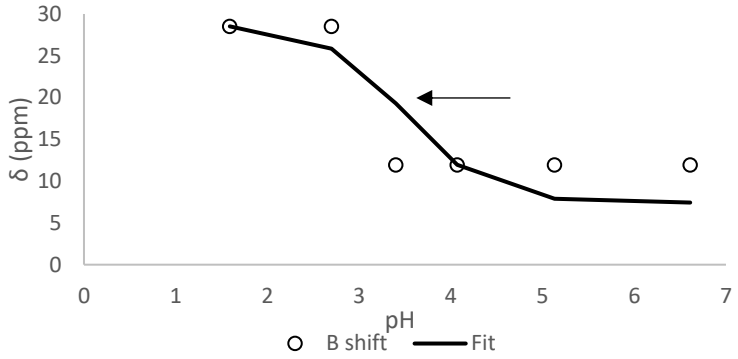

Figure 3.3.5: The curve to determine pK_a of DE344, forming a tetrahedral boron center. The chemical shift was determined using the ^{11}B NMR from **Figure 3.3.4**. The pK_a value was fitted and determined to be 3.5.

Integration of the peaks was performed to determine the shifting of the peaks. This method of calculation incorporates the Henderson-Hasselbach equation and the assumption that the observed chemical shift is a result of the proportions of sp^2 and sp^3 hybridized boronic acid in solution. Fitting the final equation (**Equation 2.3.2**) to the data also provides estimates of the true (pH-independent) chemical shifts of the sp^2 and sp^3 hybridized forms, in addition to the pK_a value. The inflection point shown in **Figure 3.3.5** represent the pK_a value surrounding the boron of the boronic acid compound.

However, it is important to mention that some compounds have multiple pK_a values due to the different organic functionalities bound to the compounds, but ^{11}B NMR represents the boronic acid pK_a rather than the different pK_a values of each compound. Our main focus was to determine the pK_a value of the boronic acid when it transitions from trigonal planar to the tetrahedral species which is why one pK_a value was estimated. The two species are in equilibrium throughout all the pH values of the solution until the

tetrahedral species is favored at pH 4. Reversibility of the compound is also presented by decreasing the pH back to value of 1.

Since compound DE344 contains a fluorine substitute on the ring, ^{19}F NMR was also measured in order to investigate the structural changes around the fluorine as shown in **Figure 3.3.6**.

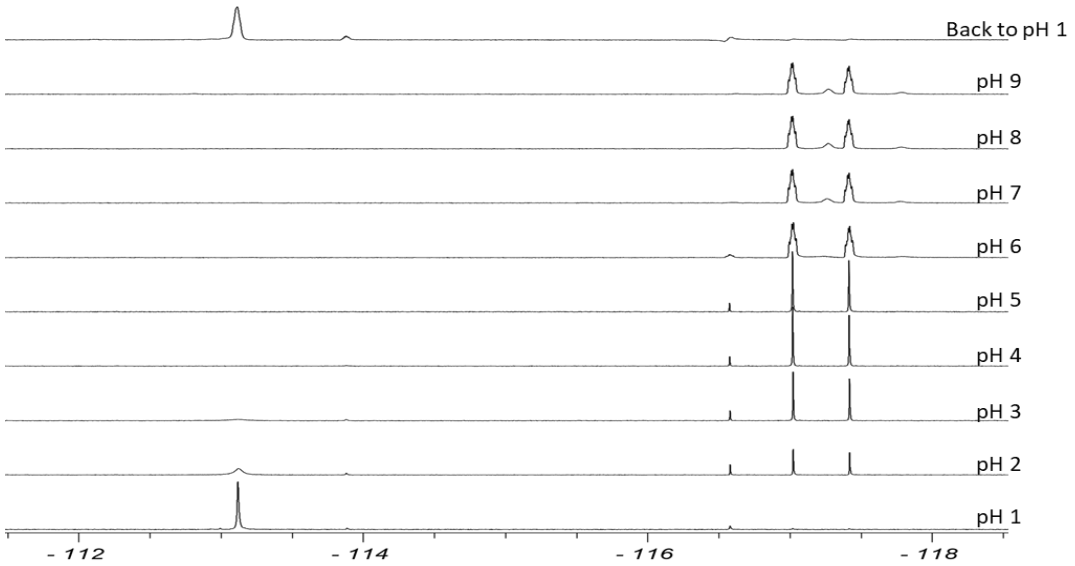

Figure 3.3.6: ^{19}F NMR spectra of DE344 with increasing pH. Reversibility of the compound is also presented by decreasing the pH back to value of 1.

As the pH of the solution of DE344 increases a distinct chemical shift change from -113.1 ppm to three species was observed. These three peaks corresponded to a minor peak at -116.6 and two larger intensity signals of equal intensity at -117.2 and -117.4 ppm. Reversibility of the compound was also observed in the ^{19}F data after decreasing the pH to 1. To determine the structural changes of DE344 at the different pH values, ^{1}H NMR was measured, and its reversibility was determined shown in **Figure 3.3.7**.

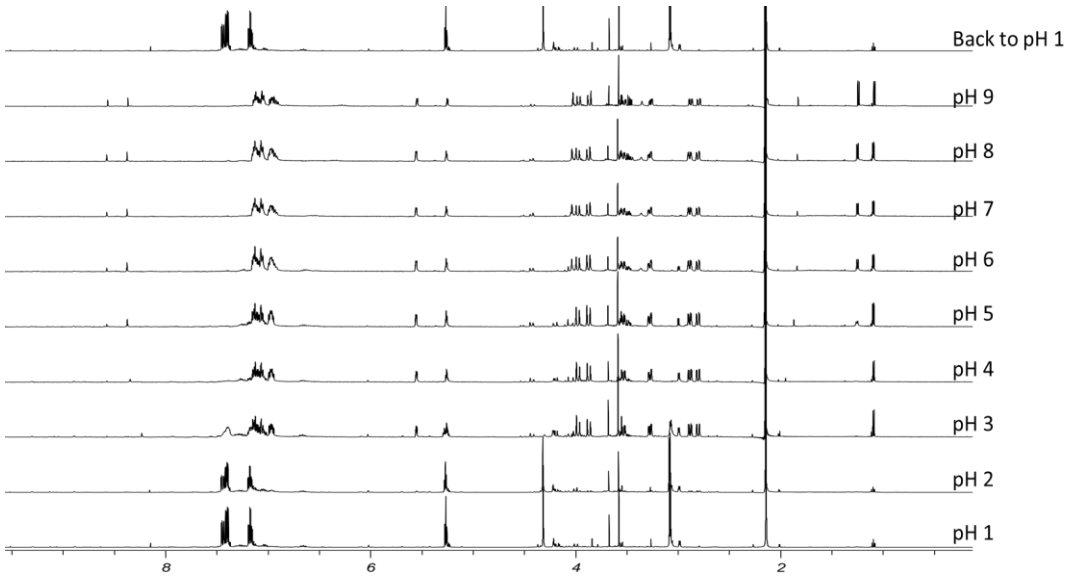

Figure 3.3.7: Changes to the ^{1}H NMR spectra of DE344 with increasing pH. Reversibility of the compound is also presented by returning the pH to 1.

Looking at the ^{1}H NMR, different structures are being observed as the pH of the solution increases. The aldehyde peak at 8.5 ppm is shifted even further and split. Also the chemical shift of the protons on the aromatic ring and the methylene groups shift upfield. The new peak at the aldehyde region that appears as a result of a split increases while the original peak decreases. Peaks at 1.5 ppm, 3 ppm and 4 ppm appear as well. When pH of the solution was brought back to pH 1, the spectrum returned to its original spectra and all peaks that appear at higher pH values disappear.

There are various structural changes between the pH of the solution between 1 and 2 in the ^{19}F NMR, and then the peak at -117.2 disappears at pH 6. However, in the ^{1}H NMR, there are different changes in the spectrum between pH 2 to 3, where the enantiotopic peaks appear, a peak at 5.5 ppm appears and additional unknown peaks. Also between pH 5 and 6, peaks at 1.5 and 1.8 ppm appear while the aldehyde peak splits as well at 8.5 ppm. All these peaks in both ^{19}F and ^{1}H NMR represents the different structural changes that occur as the pH of the solution increases.

There are similarities and differences between carbonyl boronic acid derivative DT14 and the aldehyde derivative DE344. Both compounds were observed to have a distinct chemical shift change in ^{11}B NMR spectra. The ^{1}H NMR of DE344 showed a enantiotopic proton peak at 2.6 ppm is observed, similar to DT14, indicating hemiacetal formation (**Scheme 3.2.1**). In addition, the appearance of an aldehyde peak in DE344 at higher pH values than as in DT14 and it shifts downfield as the solution pH increases. The observed aldehyde peak at higher pH suggests that at low pH DE344 exists as a hydrate (**Scheme 3.3.1**). Furthermore, the aromatic ring signals of both DT14 and DE344 shift upfield as the pH of the solution increases. These subtle similarities and differences in the ^{1}H NMR between DT14 and DE344 show that there are different structural changes to the compounds that are not to the boron center. Different structural changes to the entire molecule illustrates the importance of ^{11}B NMR in accurately estimating pK_a values for only the boron center. The site-specific pK_a determined by NMR cannot be achieved by UV-Vis spectroscopy. **Table 3.3.2** shows the pK_a values estimated both by UV-Vis spectroscopy and ^{11}B NMR.

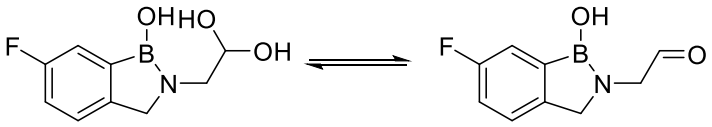

Scheme 3.3.1: Compound DE344 exists in equilibrium between the hydrate and the aldehyde forms as the pH of the solution increases.

Table 3.3.2: Comparison of pK_a measurements of synthesized boronic acid derivatives using UV-Vis spectroscopy shown in **Table 3.2.2** and ^{11}B NMR.

Compound	Structure	pK$_a$ using UV-Vis	pK$_a$ using ^{11}B NMR
DT9	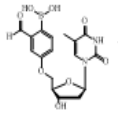	7.5 (260 nm)	7.8
DT14	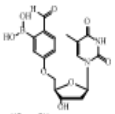	7.5 (260 nm)	7.7
DT22	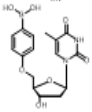	7.9 (230 nm)	8.5
DE310		6.9 (220 nm)	5.2
DE318	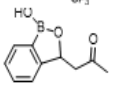	7.3 (220 nm)	6.9
CO1	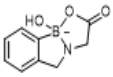	9.3 (220 nm)	7.8

Compound	Structure	pK$_a$ using ^{11}B NMR
DE343	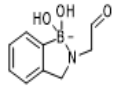	4.1
DE344	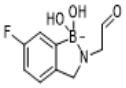	3.5
DE347	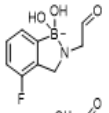	3.3
DE321	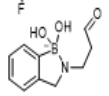	3.4
DE342	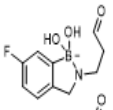	4.4
DE348	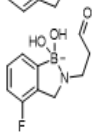	3.9

Compound	Structure	pK$_a$ using ^{11}B NMR
CO2	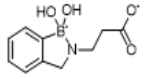	5.4
CO3	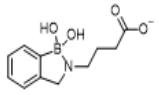	6.6
CO4	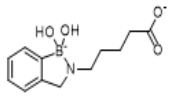	6.6
CO5	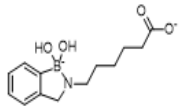	5.7

In this study, ^{1}H, ^{11}B and ^{19}F NMR of the compounds as a function of increasing pH were monitored. The pK_a values were determined primarily from the ^{11}B NMR data, where the boronic acid transitions between a neutral trigonal planar species to a tetrahedral boronate entity. The determined pK_a values are shown in **Table 3.3.2** and compared to the pK_a values determined from the UV-vis spectroscopy data in **Table 3.2.2**. Carbonyl boronic acid, phenylboronic acid, benzoxaborole and the carboxylic acid derivative CO1 have shown to have similar pK_a values to determined using UV-Vis and ^{11}B NMR spectroscopy. Moreover, some of these compounds are comparable to their control compounds 2FPBA (pK_a = 7.5), and PBA (pK_a = 8.8), for the carbonyl and phenylboronic acid derivatives, respectively. Furthermore, both the carbonyl boronic acid and the phenylboronic acid derivatives have shown that thymidine or the surrounding substituents do not affect the pK_a values of boronic acid.

The benzoxaborole derivatives have shown similar or lower pK_a values than the literature value of benzoxaborole with pK_a of 7.3. DE318 has a pK_a value of 6.9, which is comparable

to its literature value.[4] However, DE310 has a pK_a value of 5.2 which is significantly lower than benzoxaborole. These pK_a values are consistent with the idea that the ring strain in the 5-membered oxaborole ring distorts the geometry about the boron atom leading to a more favorable ionization and a lowered pK_a.[4] A lower pK_a value of the benzoxaborole group may be explained by the reduced flexibility of the intramolecular monoboronic ester, which prevents optimal B-O (lone pair) conjugation in DE318 and consequently increases the boron atom's electronic deficiency. Comparing between the two benzoxaborole derivatives, DE310 had a low pK_a as a consequence of the inductively electron withdrawing trifluoromethyl substituent.

The aldehyde derivatives, however, have shown a pKa value using the 11B NMR and was able to fit the one pKa model using **Equation 2.3.2**. Those compounds have shown multiple pK_a values using UV-Vis spectroscopy. All the aldehyde compounds have a chemical shift that goes upfield as the pH of the solution increases. The fluorinated compounds that contain one methylene group such as compounds DE344 and DE347 on the meta position relative to the boronic acid and ortho position relative to the amine group, have pK_a values of 3.3 and 3.5, respectively. They have shown to have a lower pK_a value than the non-fluorinated compound DE343 (pK_a=4.1), which is in agreement with the fluorine being an electron withdrawing group. However, the fluorinated compounds DE342 and DE348 have shown slightly higher pK_a values that the non-fluorinated compounds DE321 with a pK_a value of 3.4 compared to 4.4 and 3.9 of compounds DE342 and DE348, respectively.

CO1 and DE343 have structural similarities with the difference that CO1 was determined to be cyclized and contains a carboxylic acid rather than an aldehyde functionality. DE343 have different pK_a values compared to CO1. The only reason that could cause this significant difference in pK_a is that CO1 is cyclized making a 5 membered ring of oxygen-boron-nitrogen while DE343 only has a nitrogen-boron bond and an open chain and an aldehyde functionality. CO2 is also structurally similar to DE321, with the only difference

of an aldehyde functionality rather than a carboxylic acid. There are pK_a differences in these two compounds as well with CO2 having a higher pK_a value. This pK_a value is slightly higher than those of DE321 which could possibly be due to the carbonyl functionality. They are both electron withdrawing groups which bring the pK_a lower. However, carboxylic acid is much stronger electron withdrawing and the expectation was for CO2 to have a lower pK_a.

3.4 Summary

We have measured UV-Vis spectroscopy data together with ^{11}B, ^{1}H and ^{19}F (where appropriate) 1D NMR data for a series of novel boronic acid-containing compounds as a function of pH. The changes observed were likely more complex than the observations of ionizable groups (pK_a), particularly given the multiple additional signals observed in the ^{1}H and ^{19}F NMR spectra. The compounds prepared were grouped based on the type of boronic acid chemical functionality present in the molecule including boronic acids, formylphenylboronic acids, benzoxaboroles, and some additional aldehyde- and carboxylic acid-containing derivatives. Most of the compounds had additional ionizable chemical functionalities (e.g. secondary aliphatic amine, carboxylic acid, and aldehyde) in addition to a boronic acid. These additional chemical functionality contributed towards the overall pK_a determined for the compounds as measured by UV-Vis spectroscopy. UV-Vis spectroscopy represents the overall pK_a of the compound rather than for a specific functional group. Meanwhile, NMR observes the structural changes of the specific element of interest. For example, ^{11}B NMR demonstrate the structural changes of the boron when its hybridization changes. Some NMR spectra showed that structure changes are reversible for certain compounds, however not all compounds have shown this reversibility. The reversibility for certain compounds is useful to consider for the design of sensors.

Chapter 4. Results and Discussion of Iminoboronate and Diazaborine Formation of Boronic Acid Derivatives with Boc-Lysine-OH Using UV-Vis and ^{1}H NMR Spectroscopy

4.1 Introduction-Iminoboronate Formation

The reaction between an aldehyde and an amino group of the lysine residue or the amino terminus of a protein to form an imine has been widely employed to modify proteins.[48] However, the use of an aldehyde that forms an imine that is stabilized through intermolecular interactions has been less widely employed. More recently, carbonyl arylboronic acids such as 2FPBA have been used in biocompatible conjugation reactions which results in iminoboronate adduct stabilized by an intermediate nitrogen-boron interaction[35] They were used to modify the N-terminus of the protein (especially of cysteine), or ε-NH_2 group of Lysine residues in proteins, serving as the basis for several biocompatible conjugation reactions used in chemical biology.[32,35,49,50] Since boron has a vacant p orbital it is a Lewis acid and a strong electrophile. Hence, direct coordination of the lone pair of electrons on the imine nitrogen atom to the boron atom (dative covalent bond) stabilizes the enzyme-iminoboronate adduct.[32] In **Scheme 4.1.1**, the mechanism of iminobornate formation in aqueous solution is shown. The initial nucleophilic attack by an amine is facilitated by an oxygen-boron interaction in the carbonyl arylboronic acid reagent.[32,51] Iminoboronate formation has been unambiguously demonstrated with formyl- and acetylphenylboronic acids, where a stable, yet reversible iminoboronate is formed due to the N-B dative covalent interaction.[32,35] We hypothesized that the novel carbonyl boronic acids prepared in the Jakeman laboratory (**Figure 4.1.1**) would form iminoboronates.

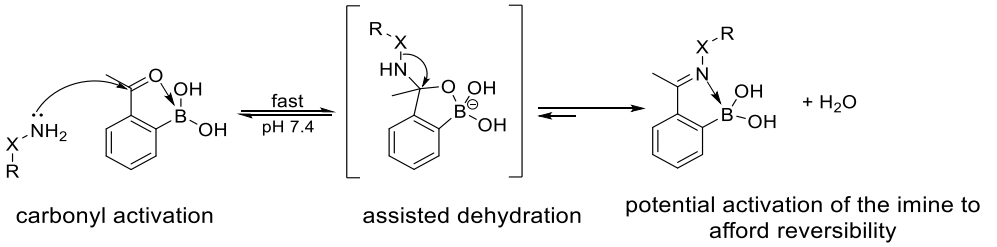

Scheme 4.1.1: Mechanistic illustration of the conjugation of 2FPBA with α nucleophile via the N-terminus in aqueous solution.[49]

Herein the focus was to examine the properties of a series of aldehyde or ketone-containing molecules previously synthesized in the Jakeman laboratory.

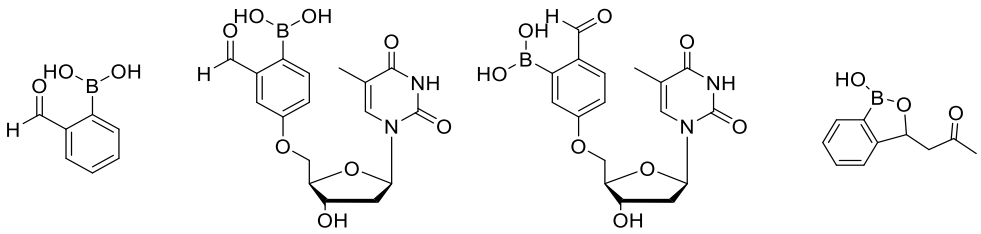

Figure 4.1.1: Aldehyde or ketone-containing molecules that were previously synthesized in the Jakeman laboratory and were used in the iminoboronate studies.

The experimental methods of Gois[32] and Douglas[35] were used to quantify iminoboronate formation. UV-Vis and NMR spectroscopy have been found to be informative methods to study iminoborante formation by tracking observed binding between aldehyde and amino functionalities. The spectrometric data was then used to determine affinity constants between lysine and our carbonyl boronic acid derivatives. The data of iminoboronate binding between 2FPBA and ethylamine was collected and compared to previously reported results for experimental validation purposes (85 ± 6 M^{-1} compared to 79 ± 2 M^{-1} from Douglas*)* using UV-Vis spectroscopy.[35] Additionally, affinity constants between 2FPBA and Lysine using ^{1}H NMR spectroscopy were determined and similar results to previously reported values were obtained (65% conversion compared to 61% from *Gois*).[32] Based on the results of these control experiments, the iminoboronate formation with a series of carbonyl boronic acid derivatives using UV-Vis and ^{1}H NMR spectroscopy was demonstrated and quantified.

4.2 Iminoboronate formation using UV-Vis Spectroscopy

The reaction between the synthesized carbonyl boronic acid derivatives and Boc-Lys-OH was taken under physiological environment in order to mimic its reaction in physiological conditions that include a pH of 7.4 and incubation under 37 °C. **Scheme 4.2.1** shows the iminoborante formation between DT14 and Boc-Lys-OH.

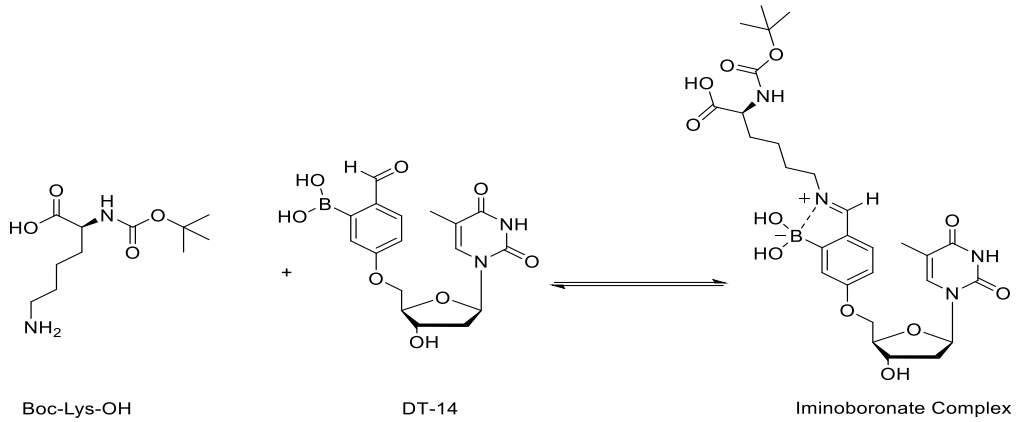

Scheme 4.2.1: Iminoboronate formation reaction between Boc-Lys-OH and DT14.

Using UV-Vis spectroscopy, the iminoboronate formation between our synthesized carbonyl boronic acid derivatives and Boc-Lys-OH was observed by increasing the concentration of Boc-Lys-OH titrated into our compounds. The results of our UV-Vis binding experiments using DT14 are shown in **Figure 4.2.1**.

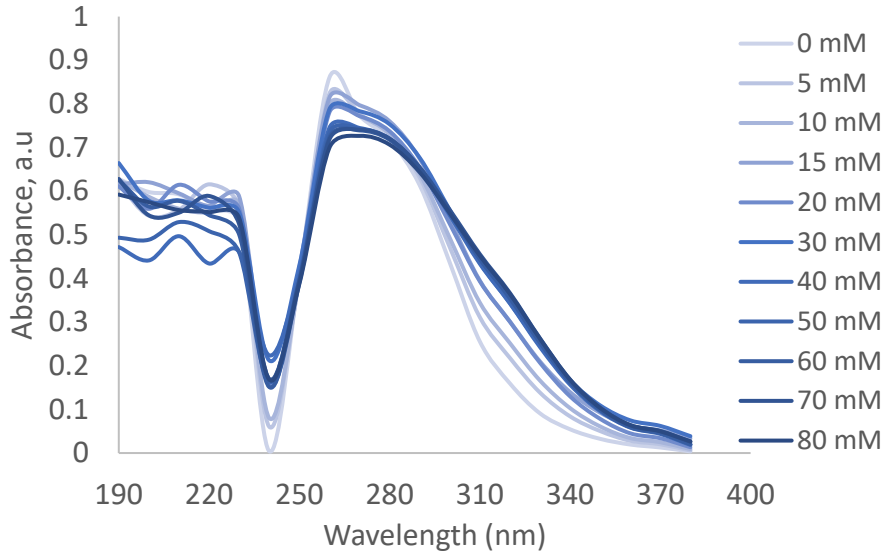

Figure 4.2.1: UV-Vis Spectroscopy changes of compound DT14 (1.0 mM) with increasing concentration of Boc-Lys-OH (0-80 mM) in HEPES buffer (1.0 M, pH 7.4).

The affinity of our synthesized compounds when binding to Boc-Lys-OH was measured by following the changes in absorbance at the maximum absorbance at 320 nm. From **Figure 4.2.1**, as the concentration of the Boc-Lys-OH increases, the absorbance increases above 320 nm illustrating that a reaction is occurring.

To obtain an indication of how favorable imine formation with DT14 was under our conditions, K_a value was determined following the approach described by Yatsimirsky and coworkers and **Equation 2.2.3** and a non-linear fit (**See Chapter 2**) and shown in **Figure 4.2.2**.[52]

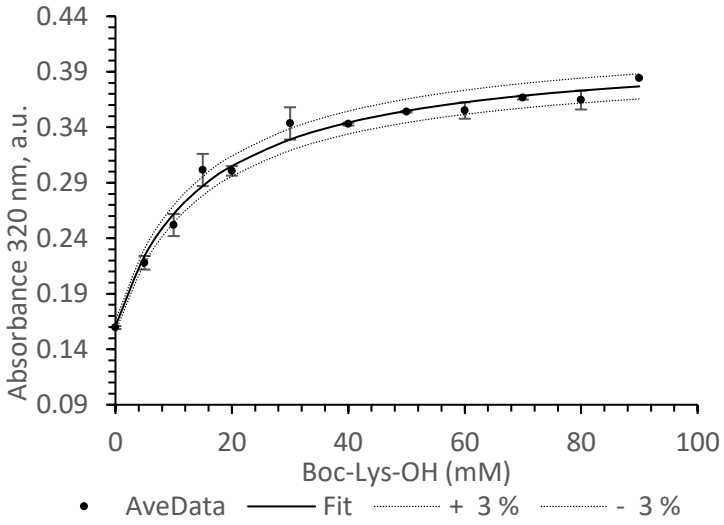

Figure 4.2.2: Plot of absorbance (320 nm) changes of DT14 (1 mM) with increasing of Boc-Lys-OH concentration (0-80 mM) in HEPES buffer (1.0 M, pH 7.4). (K_a was calculated to be 66.9 ± 0.7 M^{-1}). Value is the average of duplicate runs. Dotted lines represent 3% error calculated of the absorbance measured. Error bars represent the standard deviation of averaged absorbance measured that were used in **Equation 2.2.3.**

From **Figure 4.2.2**, we determined that as the concentration of Boc-Lys-OH increases, the absorbance at 320 nm increases until it reaches a plateau. This hyperbolic plot shows that between 5.0 mM and 30 mM of Boc-Lys-OH, the equilibrium is observed; however, from 40 mM until 80 mM the equilibrium favors iminoboronate formation. The error bars represent 3% error of the average of the duplicate runs.

These experiments and calculations were performed on the carbonyl boronic acid type of derivatives which includes DT9, DT14, and the benzoxaborole derivative DE318. 2FPBA was used as a control compound to monitor iminoboronate formation using Boc-Lys-OH. The iminoboronate formation results are presented in **Figure 4.2.3** and **Table 4.2.1**.

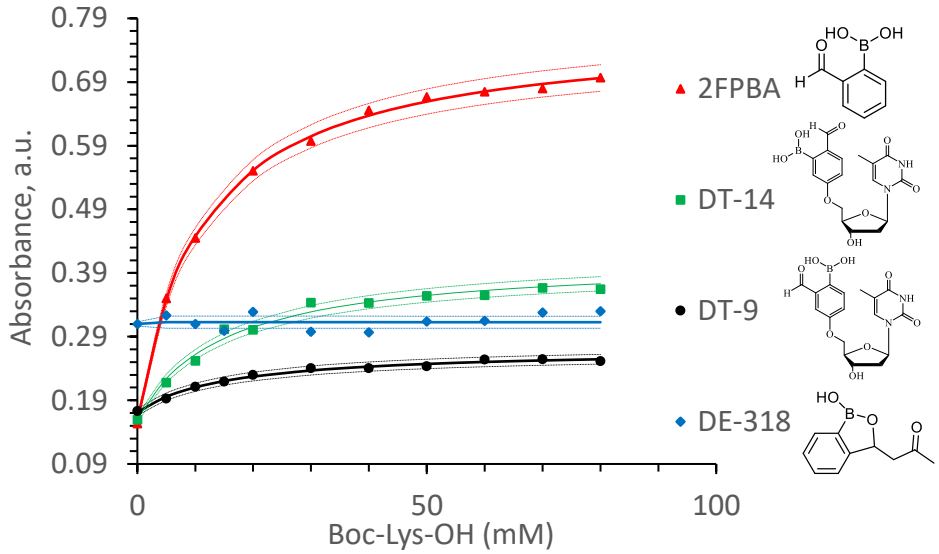

Figure 4.2.3: Plot of absorbance changes of carbonyl boronic acid derivatives 2FPBA as a control, DT9 and DT14 (1.0 mM) with increasing concentration of Boc-Lys-OH (0-80 mM) in HEPES buffer (1.0 M, pH 7.4). Values are the average of duplicate runs. Dotted lines represent 3% error calculated of absorbance measured.

2FPBA was observed to have the tightest binding out of the carbonyl boronic acids with hyperbolic plot that reaches plateau at 40 mM of Boc-Lys-OH. It means there is little to no change in the absorbance as the concentration of Boc-Lys-OH increases. However, DE318 showed the weakest N-B binding with a linear pot. DT9 and DT14 are analogous and no significant difference between the binding affinities was observed.

Table 4.2.1: Association constants (K_a) between carbonyl boronic acid derivatives and Boc-Lys-OH. Values are the average of duplicate runs.

Compounds	Structure	K_a (M^{-1})
2FPBA	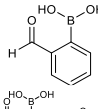	88.7 ± 0.4
DT9	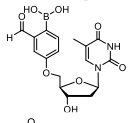	64.4 ± 0.3
DT14	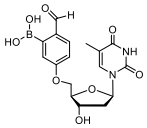	66.9 ± 0.7
DE318	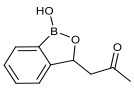	0.0 ± 0.2

From **Figure 4.2.3** and **Table 4.2.1**, it was observed that carbonyl boronic acid derivatives were found to rapidly conjugate with Boc-Lys-OH under physiological conditions with thymidine containing carbonyl boronic acid derivative bind well, while the benzoxaborole showed no reaction between the ketone on the benzoxaborole and the amino group on the Boc-Lys-OH. Comparing to the control compound 2FPBA, K_a of DT9 and DT14 are of comparable magnitude. DE318 did not show a change in absorbance when interacting with Boc-Lys-OH, which suggests that DE318 did not interact with Boc-Lys-OH.

This experiment was performed under the physiological pH of 7.4, while various sources performed similar iminoboronate formation experiments between pH values of 7.0-7.5.[32,35] The side chain of Lysin has a pK_a of 10.52 while the ethylamine that was used as a comparison has a pK_a of 10.6. At physiological pH, lysine is positively charged as shown in structure 1 of **Scheme 4.2.2**.[53] The pK_a of Boc-Lys-OH ε-NH_2 is likely similar to lysine (10.5), thus it is protonated at physiological pH.

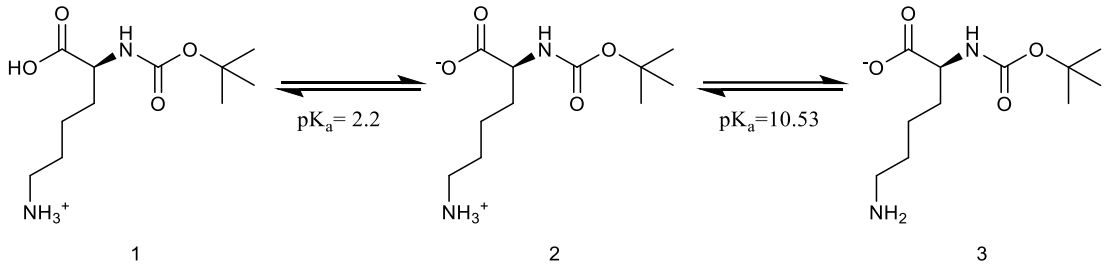

Scheme 4.2.2: Structure of Boc-lysine-OH at different pH values.

Due to Lysine's side chain being protonated, it affects the formation of iminoboronate since the protonated form would not have a lone pair to bind to the carbonyl substituent of the aryl boronic acid. However, since this reaction is in equilibrium, the reaction proceeds and iminoboronate formation in neutral environment gives low K_a values.

The thermodynamic stabilization of the iminoboronate can be potentially rationalized by the formation of an N-B dative bond. An iminoboronate complex associates rapidly, indicating that iminoboronate formation is under thermodynamic control at physiological

conditions. The rapid reversibility can be rationalized by the N-B coordination or imine protonation resulting from solvent insertion as shown in **Scheme 4.1.1**. Nevertheless, the ortho-boronyl substituent, while providing thermodynamic stabilization of the product, also accelerates the forward and the backward reaction of iminoboronates.[9]

The boronic acid derivatives used in the previous experiments were synthesized for the purpose of developing iminoboronate reversible covalent protein probes or inhibitors, with varying substituents around the aryl ring to potentially tune reactivity. From the results above, the reversible covalent binding between the aldehyde and the ε- amino functionality of the Lysine forms an iminoboronate.

4.3 Iminoboronate formation using ^{1}H NMR Spectroscopy

Iminoboronate formation between Boc-Lys-OH and our novel carbonyl boronic acid derivatives was also monitored using ^{1}H NMR to confirm whether the UV-Vis spectroscopy method showed that an N-B bond formed, rather than another reaction.

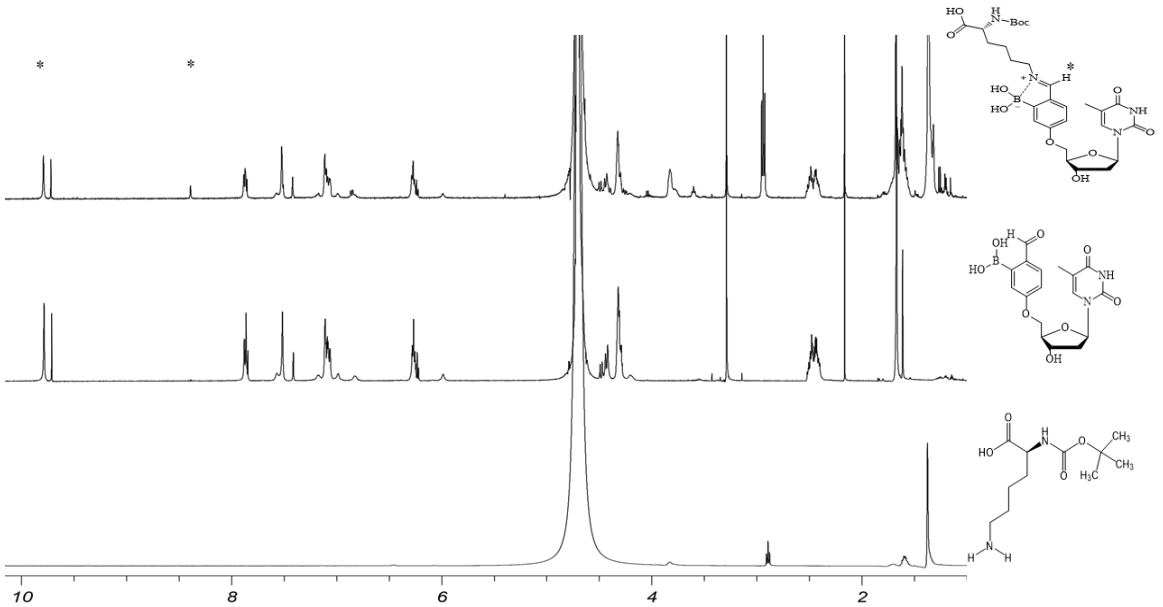

Figure 4.3.1: Iminoboronate formation between N_ε-Boc-Lys-OH and DT14. ^{1}H NMR (500 MHz): [ligand] 5.0 mM (1:1) in phosphate buffer (500 mM) pH 7.4, 90% D_2O. The peak at 9.8 ppm aldehyde, 9.75 ppm of NH (thymidine) and 8.5 ppm iminoboronate. The peak of the α-protons of Boc-Lys-OH from the imine which shifts from 4.2 to 3.8 also represents the change in the α-proton of the amine.

Figure 4.3.1 shows a new peak at 8.5 ppm which is consistent with iminoboronate formation, indicating that the NMR data supports the UV-Vis results.[32] Moreover, the NMR showed that the presence of thymidine did not affect iminoboronate formation with the carbonyl boronic acid derivatives. Compound DT14 (5.0 mM) was treated with increased concentrations of Boc-Lys-OH (0-80 mM) in phosphate buffer. In the NMR spectra in **Figure 4.3.1** the analysis of the region between 8 to 10 ppm in the ^{1}H NMR indicated that the aldehyde peak decreases as the concentration of Boc-Lys-OH increases. With the decrease of the aldehyde peak, a new peak at 8.5 ppm appeared, and is consistent with the chemical shift observed for the formation of an iminoboronate.[32] Moreover, analysis of the region between 3 and 4.6 ppm indicated conversion of the signal from the α-protons of Boc-Lys-OH. When the iminoboronate formation is observed, the peak at 4.3 ppm shifts to 3.7 ppm.

To quantify the iminoboronate formation by ^{1}H NMR spectroscopy from **Figure 4.3.1**, the conversion percentage was calculated of DT14 and Boc-Lys-OH at the 1:1 molar ratio and was found to be 26% conversion by integrating the aldehyde peak and the imine peak at 8.5 ppm. These results are comparable with other reported iminoboronates, indicating that neither the thymidine ring nor the deoxyribose functionalities disrupt iminoboronate formation.[32]

The presence of thymidine offers the opportunity to target those enzymes that bind thymidine (or uridine) where the hydrogen-bonding acceptor/donor/acceptor properties of the thymidine base enhance selectivity toward active sites that complement these interactions. Several existing therapeutic targets take advantage of this interaction, such as the cancer-implicated enzymes thymidine kinase 1 or bacterial thymidylyl transferases involved in bacterial cell wall formation.[38]

Similar to the UV-Vis results, DE318 did not show any reaction occurring by NMR. The NMR method would provide more insight of whether any sort of reaction occurring

between DE318 and Boc-Lys-OH because NMR more accurately tracks structural changes during iminoboronate formation (**Figure 4.3.2)**.

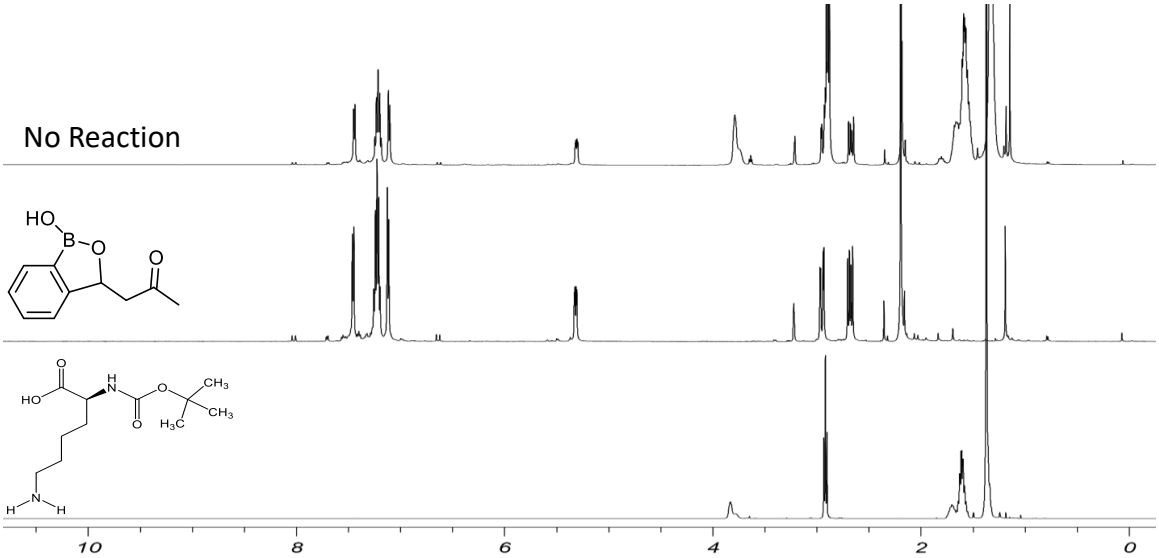

Figure 4.3.2: Mixing between N_a-Boc-Lys-OH and DE318. ^{1}H NMR (500 MHz): [ligand] 5.0 mM (1:3) in phosphate buffer (500 mM) pH 7.4, 80% D_2O. No iminoboronate formed.

The NMR in **Figure 4.3.2** has confirmed that no reaction between DE318 and Boc-Lys-OH occurred and it supports the UV-Vis spectroscopy results. A ratio of 1:3 between DE318 and Boc-Lys-OH is shown in the NMR and shows that at higher concentrations of Lysine, the formation of iminoboronate or any other reaction does not occur either. The NMR shows a mix of the two reactants, rather than a reaction because there are no new peaks. DE318 contains a boronic acid on a 5-membered ring. Comparing the geometries of DE318, when binding to Boc-Lys-OH, to a 6-membered ring benzoxaborole, we expect the formation of iminoboronate to occur on the 6-membered ring because amine attack, from Boc-Lys-OH, to the boron center is geometrically easier. In our 5-membered ring benzoxaborole, however, the amine would not approach the boron and no iminoboronate formation was be detected.

Finally, to confirm the importance of boronic acid in this reaction, a mixture of benzaldehyde (5.0 mM) and Boc-Lys-OH (15 mM) in phosphate buffer (500 mM, pH 7.4) was analyzed. Less than 10% conversion to the imine (Schiff base) was detected using ^{1}H NMR and conversion was calculated using integration of the aldehyde peak at 9.8 ppm

and the appearing peak at 8.5 ppm which is the imine proton (**Figure 4.3.3**). Such up-field shift is typically observed on transformation of the aldehyde group into an imine.[52]

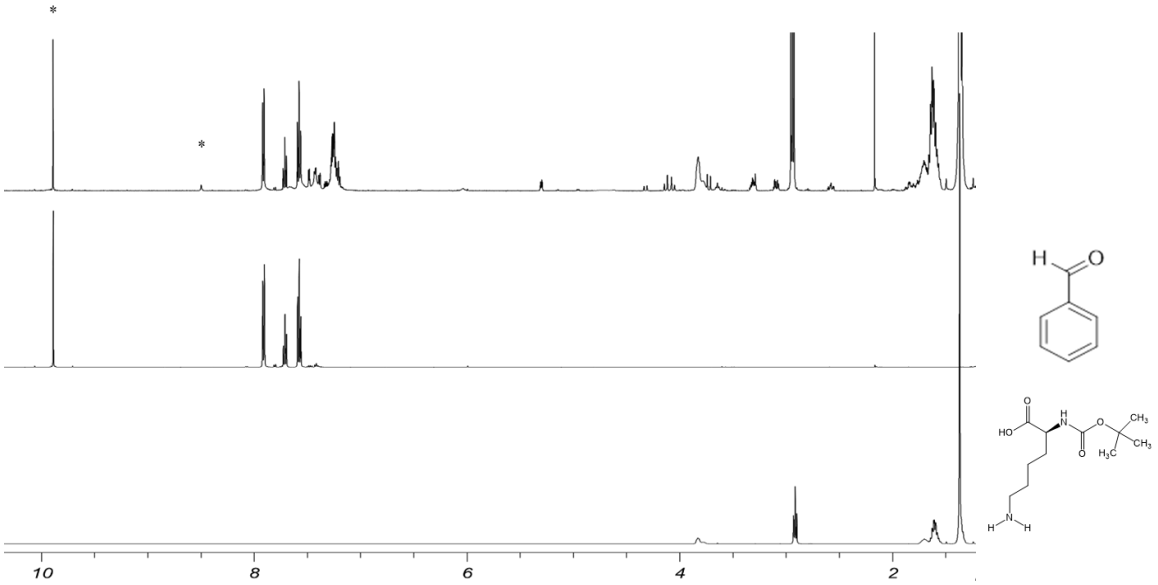

Figure 4.3.3: Imine formation between N_a-Boc-Lys-OH and Benzaldehyde. ^{1}H NMR (500 MHz): [ligand] 5.0 mM (1:3) in phosphate buffer (500 mM) pH 7.4, 90% D_2O. Less than 10% formation was detected based on the aldehyde peak at 9.8 ppm and the new peak at 8.5 ppm which is the proton of the imine (these peaks are marked with a star).

Literature also shows that formaldehyde, a simple aldehyde, does not react with lysine under these conditions, illustrating that a boronic acid is necessary for iminoboronate formation to occur.[54]

4.4 Introduction-Diazaborine Formation

Diazaborines and related B−N heterocycles have also been explored as enzyme inhibitors and as reversible linkers for drug delivery to cancer cells.[33] Diazaborine formation is interesting to explore since this reaction was reported to be more stable and showed a slowed dissociation kinetics in comparison to the iminoboronate chemistry.[33]

While some diazaborines exhibit a flat aromatic structure, others display a hydrated boron with a nonplanar tetrahedral form.[33] The first report of a reversible lysine-conjugation chemistry using diazaborines was reported by *Gao*, as shown in **Scheme 4.4.1**.[33] The properties of the formed diazaborine were significantly different from an

iminoboronate. The stability of the diazaborine adduct was much greater than an iminoboronate, as demonstrated by dilution experiments where the diazaborine remained formed for significantly longer periods of time whereas iminoboronates are hydrolysed within seconds. The diazaborine complexes comprise two nitrogen atoms, one internal, and one external, the amine, with only one hydroxyl substituent at boron. A series of aliphatic amine-containing arylboronic acids were synthesized in the Jakeman group previously (**Figure 4.4.1**). Herein are the reported investigations as to whether they were able to repeat the diazaborine formation as reported by *Gao* for the benzaldehyde derivative.[33] The only structural difference between RMR1 (*Gao* compound) and one of our analogues (DE321) was a benzaldehyde versus a propanal aldehyde. This proposed reaction should yield a hydrated diazaborine formation.

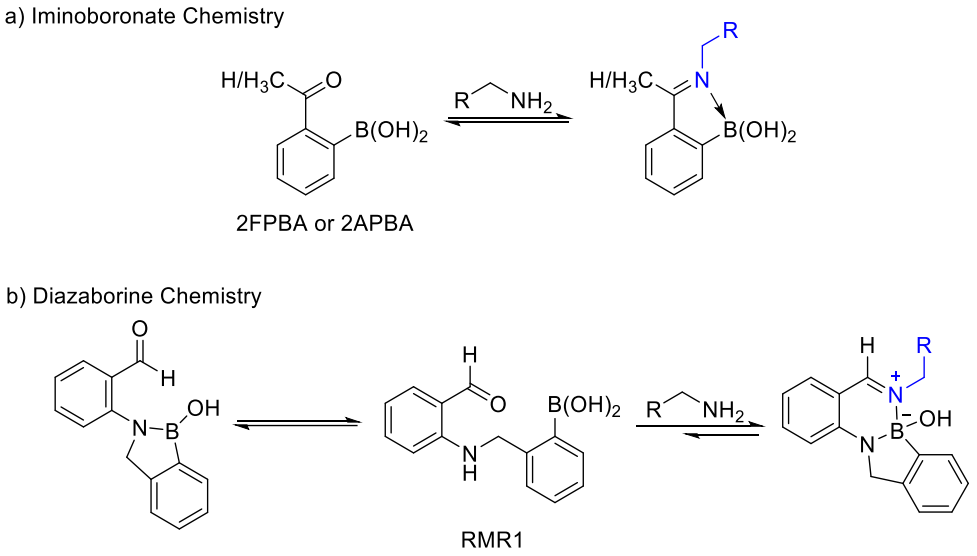

Scheme 4.4.1: Covalent lysine-conjugation reaction to form iminoboronate versus the diazaborine formation between aldehyde/ nitrogen containing compounds and amino acid.[33]

Both reactions shown in **Scheme 4.4.1** form an N-B bond through a covalent reversible bond, however, the nitrogen bound on the synthesized compound would form a reversible bond with the boron making it a cyclic form as shown in **Scheme 4.4.2** which then would proceed to the conjugation reaction similar to an iminoboronate formation.

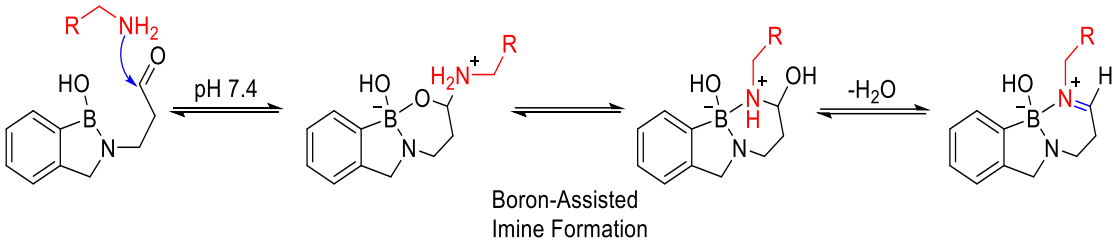

Scheme 4.4.2: Mechanism of the reversible reaction to form a diazaborine. A postulated reaction cascade for DE321-amine conjugation (as analogous to RMR1) to give a hydrated diazaborine.[33]

The aldehyde containing boronic acid DE321 was investigated for its potential to form diazaborine adducts under the same reaction conditions as used for iminoboronate formation (**Figure 4.4.2**). RMR1 and DE321 have similar functionalities, such as the aldehyde group and the amine functionality. However, the differences between our compounds and RMR1 is the aromatic ring near the amine and that our compounds were found to have a nitrogen-boron dative bond (See crystallography in Chapter 3), while RMR1 was not reported to have this dative bond. The literature diazaborine formation with RMR1 showed more significant changes to the UV-Vis spectrum,[33] however, RMR1 also contains an additional aromatic functionality that may contribute to the UV-Vis spectrum.[33] Nevertheless, these initial results were not considered promising.

We examined the ability of diazaborine formation of a series of aldehyde-containing molecules that contain an amine functionality that were previously synthesized in the Jakeman laboratory (**Figure 4.4.1**).

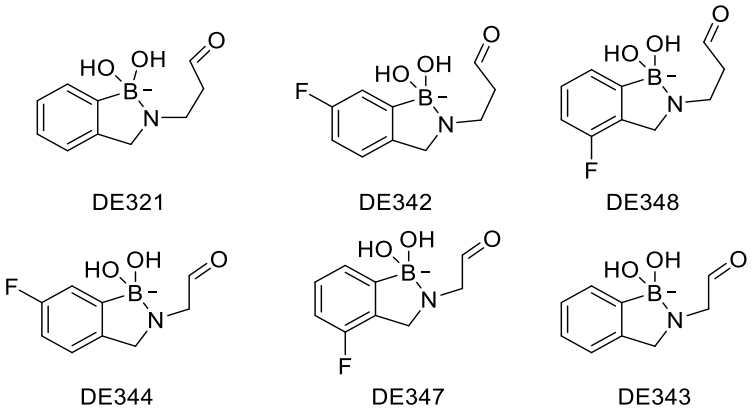

Figure 4.4.1: Aldehyde-containing molecules that contain an amine functionality that were synthesized in the Jakeman laboratory.

4.5 Diazaborine Formation using UV-Vis Spectroscopy

The synthesized compound DE321 from the category of the aldehyde derivatives contains an amine attached between the aldehyde functional group and the phenylboronic acid. Consulting the paper of Reja, the same reaction conditions were used, aqueous buffer at pH of 7.4.[33] UV-Vis spectroscopy measurements were recorded as a function of increasing concentration of Boc-Lys-OH into aldehyde derivatives such as DE321. **Figure 4.5.1** shows that as the concentration of Boc-Lys-OH increases in the reaction with DE321, and the absorbance does not change, which illustrates that a reaction likely does not occur.

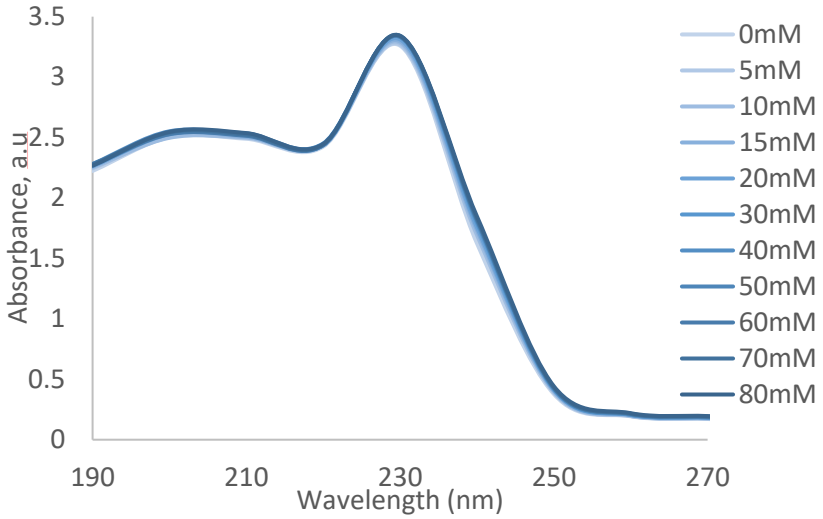

Figure 4.5.1: UV Spectroscopy changes of compound DE321 (1.0 mM) with increasing concentration of Boc-Lys-OH (0-80 mM) in HEPES buffer (1000 mM, pH 7.4).

To investigate whether an affinity constant (K_a) could be determined. The data was replotted using the maximum absorbance at 240 nm in a non-linear fit (**Figure 4.5.2**). This figure shows the binding affinity between an aldehyde derivative and Boc-Lys-OH and it shows that there is no significant binding event as the concentration of Boc-Lys-OH increases.

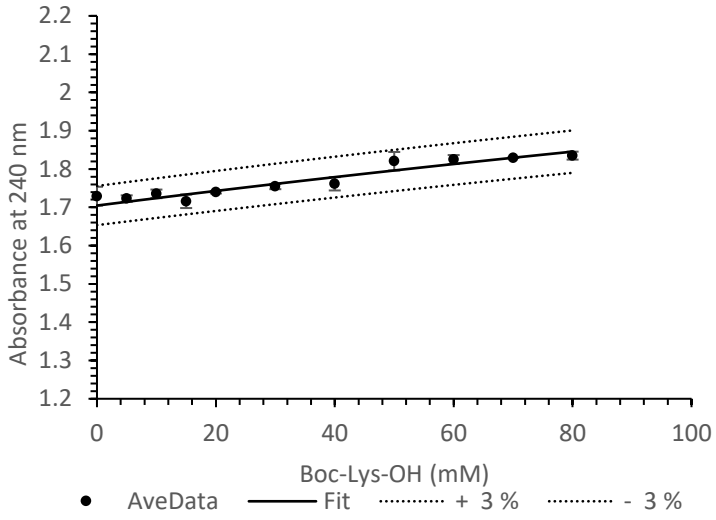

Figure 4.5.2: Plot of absorbance (at maximum intensity of 240 nm) changes of DE321 (1.0 mM) with increasing of Boc-Lys-OH concentration (0-80 mM) in HEPES buffer (1000 mM, pH 7.4). (K_a was calculated to be 0.027 M^{-1}). Value is the average of duplicate runs. Dotted lines represent 3% error calculated absorbance. Error bars represent the standard deviation of averaged absorbance.

4.6 Investigating Diazaborine Formation using NMR

To further investigate our results with the aldehyde derivatives. ^{1}H NMR analysis was performed in similar manner to iminoboronate formation.

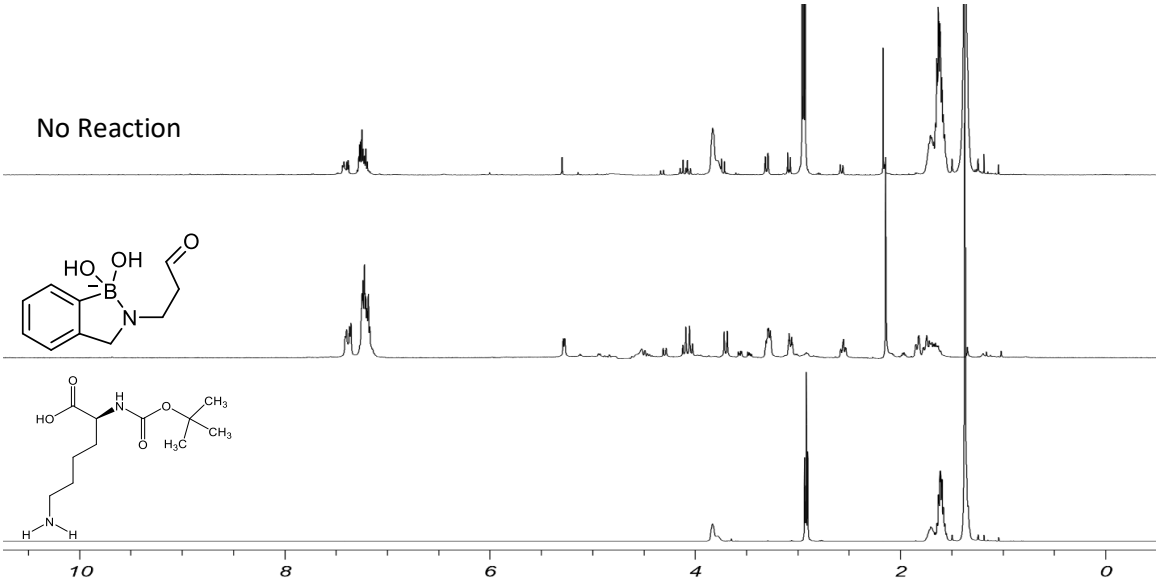

Figure 4.6.1: Diazaboronate formation between N_ε-BocLysOH and DE321. ^{1}H NMR (500 MHz): [DE321] 5.0 mM (1:3) in phosphate buffer (500 mM) pH 7.4, D_2O.

The first difference observed upon viewing the ^{1}H NMR spectrum of DE321 was the lack of a significant aldehyde peak at pH 7.4, in comparison to the compounds investigated for iminoboronate formation. From the ^{1}H NMR spectroscopy data collected between pH 1 to 9 in **Chapter 3**, there is no aldehyde group above pH 3. The structure shows that Boc-Lys-OH could not form a conjugative bond and thus form a diazaborine. The rest of the aldehyde derivatives were not further explored for the matter of saving the quantity of these compounds. DE321 was chosen since it is a simple non-fluorinated compound with 2 methylene groups which gives a flexibility to form a ring and a nitrogen-boron bond.

The ^{1}H spectrum of DE321 at pH 7.4 is significantly more complicated than at low pH. The pH reversible species formed at pH 7.4, as observed and discussed in Chapter 3, does not react with Boc-Lys-OH under these aqueous conditions. The effect of pH on the structure of DE321 is more fully explored in chapter 3. The ^{1}H NMR spectrum of DE321 was also significantly more complicated than the recorded spectrum in D_2O upon synthesis of the compound, *vide infra*.

To eliminate the option that Boc-Lys-OH is the reason for the lack of reactivity, DE321 was also tested with ethylamine as shown in **Figure 4.6.2**.

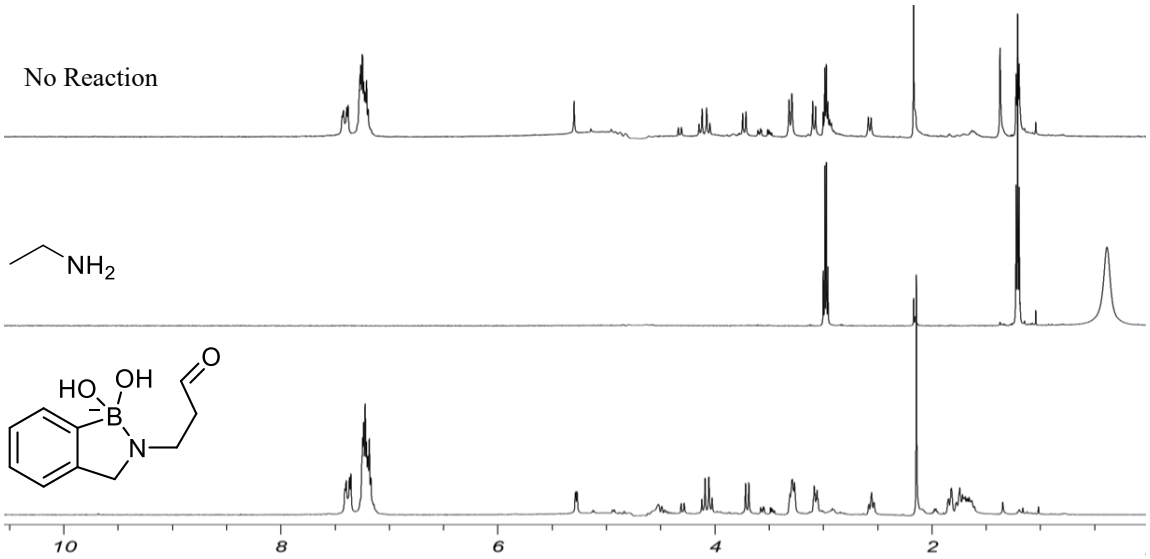

Figure 4.6.2: Imine formation between N_a-ethylamine and DE321. ^{1}H NMR (500 MHz): [ligand] 5.0 mM (1:3) in phosphate buffer (500 mM) pH 7.4, D_2O. No reaction formation detected.

Looking at both **Figures 4.6.1** and **4.6.2**, it is possible to see that reactions of DE321 with both Boc-Lys-OH and ethylamine show no formation and show a mixture of the reactants rather than a new product. There are no undesired reactions occurring either which rises a new question. What is the structure of DE321 at the physiological pH that could possibly interfere from the imine formation?

The ^{1}H NMR spectrum of DE321 that was recorded when it was prepared, was compared to the spectrum at pH 7.4 in phosphate buffer. The original spectrum was recorded in D_2O (pH 4) and is shown in **Figure 4.6.3**. There is an aldehyde peak at 9.8 ppm. The aldehyde may also exist in equilibrium as a hydrate, where the proton's chemical shift would be around 5 ppm (see **Scheme 4.6.1**). The equilibrium properties of the aldehyde were discussed in more detail in Chapter 3.

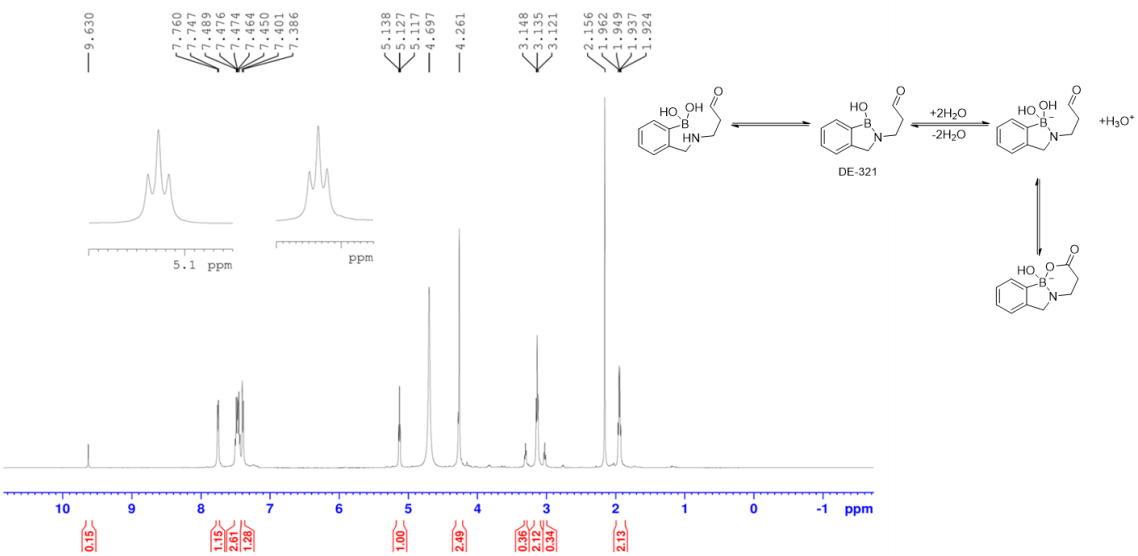

Figure 4.6.3: ^{1}H NMR spectrum (500 MHz, D_2O, pH 4) of DE321. This spectrum was recorded at the time of synthesis (April 2022), 4 months before the diazaborine experiment was conducted.

Also, as shown in chapter 3, as the pH of the solution increases, the aldehyde peak decreases which could be the reason for the reactivity with Boc-Lys-OH to be low. Based on **Scheme 4.4.2**, imine formation requires an aldehyde group and favours a trigonal planar boron atom which compound DE321 lacks at physiological pH based on the ^{1}H NMR spectrum data.

As mentioned above, the aldehyde functionality of the aldehyde derivative DE321 may also exist in equilibrium as a hydrate. Also, it could be in equilibrium with the cyclized form.

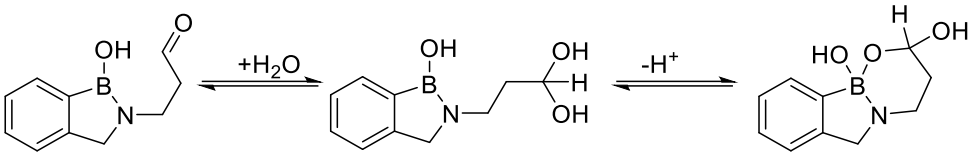

Scheme 4.6.1: Equilibrium between aldehyde and hydrate.

The examination of the rest of the aldehyde boronic acid derivatives was not continued in order to save the derivatives for future experiments. Compounds DE342 and DE348 are the fluorinated analogues of DE321 and according to the NMR data in chapter 3 (**Appendix B**), they likely cyclize at physiological pH and form a 6-membered ring intramolecular species. The same rational would apply for compounds DE344, DE347 and DE343 since they are likely form a 5-membered ring intramolecular species (**Appendix B**) and would not form a diazaborine.

4.7 Summary

We explored the iminoboronate formation between Boc-Lys-OH and our novel synthesized carbonyl boronic acids and the diazaborine formation between Boc-Lys-OH and related aldehyde derivatives. Boc-Lys-OH was used as a lysine probe component in aqueous solution under neutral conditions. The potential reaction was quantified using UV-Vis and ^{1}H NMR spectroscopy. The carbonyl boronic acid DT9 and DT14 showed promising iminoboronate formation results. DE318 that contains an aliphatic ketone, however, did not show iminoboronate formation. The formation of diazaborine using DE321 that contains an aliphatic aldehyde with Boc-Lys-OH was unsuccessful because the aldehyde may also exist in equilibrium as a hydrate which does not have the carbonyl functionality to perform a conjugation reaction and then form the N-B bonding through electrostatic interactions.

Chapter 5. Results and Discussion of Boronic Acid-Diol Binding

5.1 Introduction

Boronic acids have been employed for many different biomedical applications, for example, in sensors and drug delivery.[36] Boronic acids are known to bind with compounds containing diol moieties with high affinity through reversible ester formation (**Scheme 5.1.1**).[41] Such tight binding allows boronic acids to be used as the recognition moiety in the construction of sensors for saccharides, as nucleotide and carbohydrate transporters and as affinity ligands for the separation of carbohydrates.[10] Boronic acid compounds also have shown potential as antibody mimics targeted to cell-surface carbohydrates. Quantifying the interaction between boronic acid and diol by measuring association constants under aqueous conditions at physiological pH will assist in understanding the fundamental factors behind boronate-diol binding.

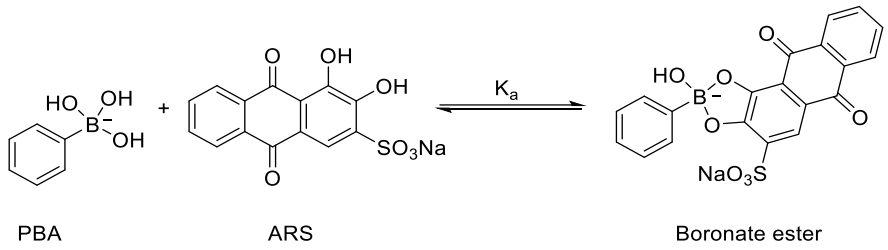

Scheme 5.1.1: Reversible boronate ester formation using the boronic acid PBA and the diol ARS. Both UV-Vis and Fluorescence changes occur because of this interaction.

There are numerous examples in which fluorescence or UV-Vis spectroscopy have quantified binding constants, often these cases are limited to compounds whose spectroscopic properties are sensitive to the binding event.[41] There is an interest in developing boronic acid-containing antibody mimics for cell surface carbohydrates.[41] However, often these boronic acid containing compounds are not fluorescent. Under such circumstances, spectroscopic determination of binding constants relying on the intrinsic spectroscopic property changes of absorbance and fluorescence upon binding becomes difficult.[41] Therefore, a method was developed by Springsteen and Wang that allows quantification of binding constants between sugar and boronic acids regardless of whether the boronic acid derivative is fluorescent.[41]

The method developed by Springsteen and Wang used an assay which utilized Alizarin Red S. (ARS) as a reporter tool for boronic acid binding. Changes observed in UV-Vis intensity and an increase in fluorescence are due to the catechol functionality in ARS interacting with the boronic acid (**Scheme 5.1.1**).[41] In this study, the method of Springsteen and Wang was used to measure and quantify the boronate ester formation of our novel synthesized compounds using either the UV-Vis or the fluorescence properties of ARS. The modification made from the Springsteen and Wang method were the use of HEPES buffer instead of a phosphate buffer, and a 96 well plate was used instead of a cuvette. Subsequently, a competitive experiment between common saccharides that are found in mammalian cells, boronic acid derivatives and ARS were conducted and quantified using the fluorescence or UV-Vis data.

It is known that the pH of a solution influences the BA-ARS interaction. The effect of pH on the BA-ARS interaction could interfere with the binding or cause much tighter binding.[41,55] Literature has reported that when investigating the optimal pH for the ARS system, pH profiling showed that maximum fluorescence intensity changes were observed at neutral pH.[41,55] This is an ideal situation since we are interested in searching for sensors that are functional at physiological pH. The reason for the optimal sensitivity at pH 7.4 could be due to pH-dependent binding strength of the BA-diol complex and ionization state changes.[55,56] It is known that the affinity of boronic acids with diols at low pH is small and the large increase in fluorescence while raising the pH from 4 to 7 is consistent with an increase in the binding constants in this pH range.

5.2 Boronic acid-diol binding between boronic acid derivatives and ARS

ARS, contains a catechol functionality. This demonstrates a high affinity for boronic acids[36] and is often used as a fluorescent reporter (i.e., an indicator), as it becomes fluorescent upon binding with a boronic acid.[36] This provides a direct method to determine of binding constants with ARS. The binding of ARS was found to follow a similar pattern for most of the boronic acids in question, with the highest association constant found near

physiological pH.[10,41] **Scheme 5.2.1** shows the binding interaction between ARS, and our novel, synthesized boronic acid derivative, compound DT14.

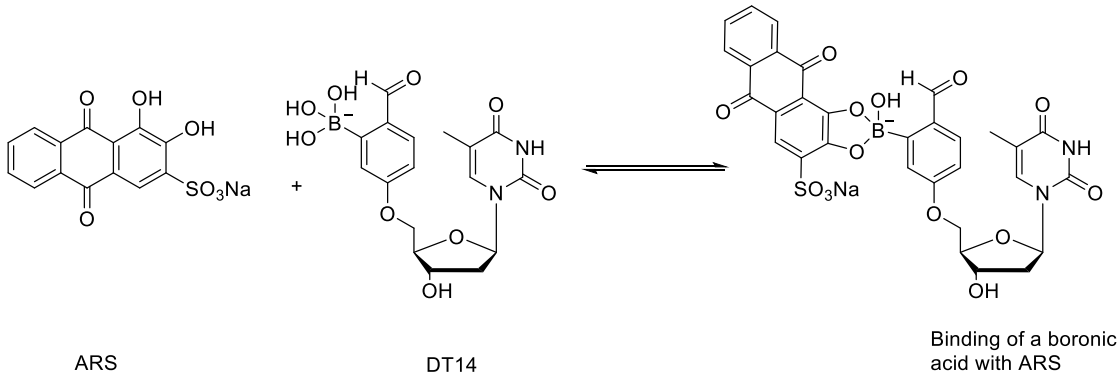

Scheme 5.2.1: Formation of boronate ester complex between the carbonyl boronic acid DT14 and Alizarin Red S. A change in UV and fluorescence was used to quantify binding.

The BA-diol complex formed between DT14 and ARS resulted in a change in the absorbance of the solution. The BA-diol complex solution showed a λ_{max} change and a visible color change from red to yellow upon addition of the boronic acid derivative. As an example, the UV-Vis Spectrum of the carbonyl boronic acid derivative DT14 was measured and a color change was observed. As the concentration of DT14 increased the color of the solution changes vividly from red to yellow as shown in **Figure 5.2.1**. This occurs as a consequence of the shift of λ_{max} from 520 nm (red) to 460 nm (yellow), as shown in **Figure 5.2.2**.

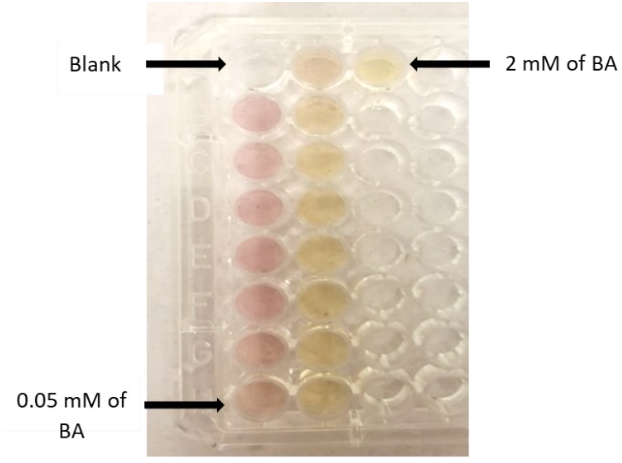

Figure 5.2.1: Example of color changes from red to yellow as the concentration of DT14 increases.

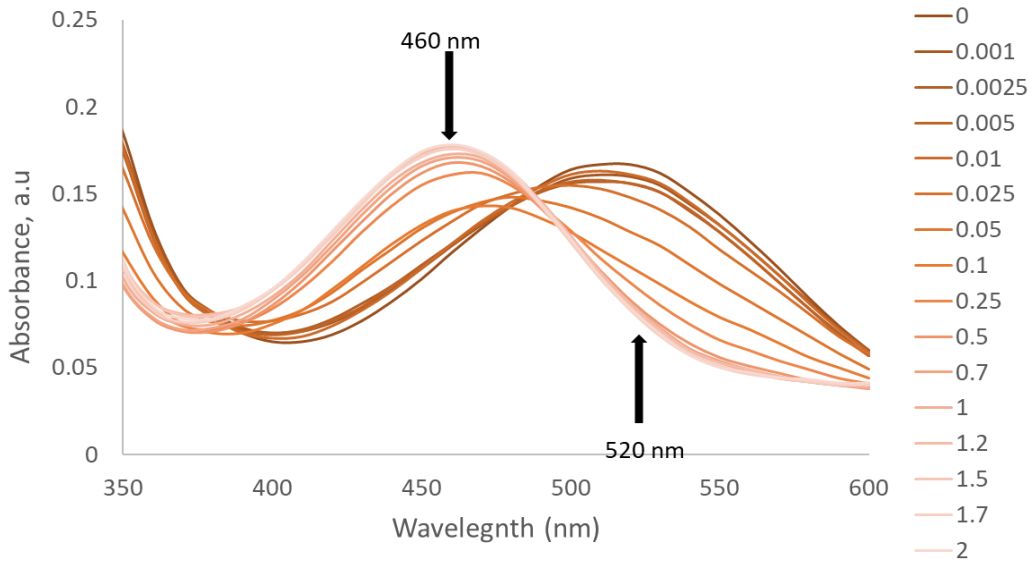

Figure 5.2.2: Absorption spectral changes of ARS (0.1 mM) with increasing concentration of DT14 (0-2 mM) in HEPES buffer (100 mM, pH 7.4).

Looking at the absorption spectra, an isosbestic point is observed at 480 nm, indicating the starting material and the product have an equal extinction coefficient. This indicates that the reaction between the reporter, ARS, and the boronic acid is proceeding.

To determine whether UV-Vis or fluorescence spectroscopy would be more sensitive in determining association constants, the above binding experiment between DT14 and ARS was repeated and monitored using fluorescence spectroscopy. **Figure 5.2.3** shows the comparison between the two spectroscopic methods used to determine the association constants between DT14 and ARS.

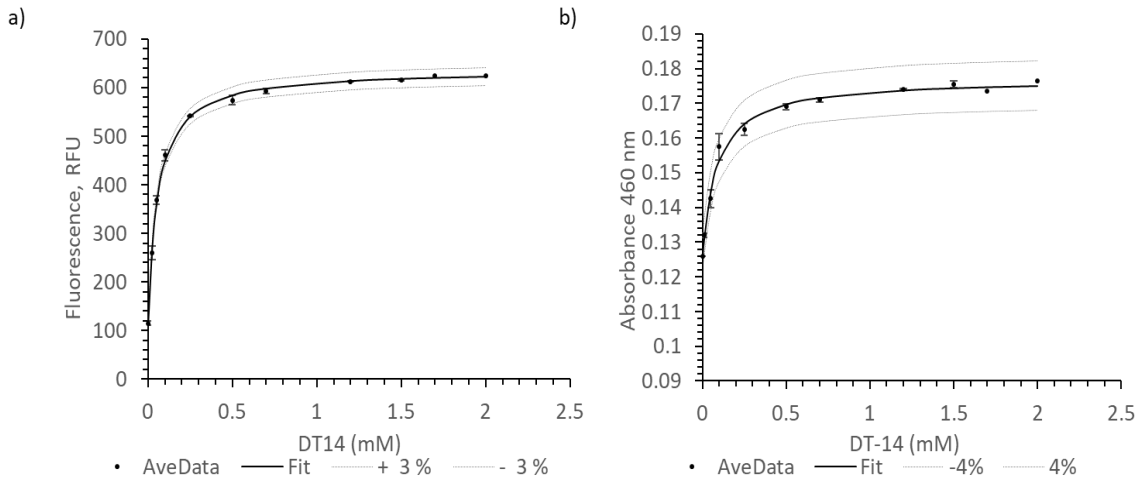

Figure 5.2.3: Comparison between UV-Vis and Fluorescence spectroscopy measurements of changes of ARS (0.1 mM) with increasing of boronic acid (DT14) concentration (0-2 mM) in HEPES buffer (100 mM, pH 7.4). a) Plot of fluorescence changes. K_a is 17,973.6 ± 1.6 M^{-1}. b) Plot of UV-Vis spectroscopy changes. K_a is 11,829.6 ± 2.8 M^{-1}. Value is the average of duplicate runs. Dotted lines represent 3% error for fluorescence changes and 4% error for absorbance/fluorescence changes. Error bars represent standard deviation of average absorbance across the duplicates.

From the results, comparing UV-Vis and fluorescence spectroscopy in **Figures 5.2.2** and **5.2.3** and from Wang's method, it was concluded that fluorescence was more sensitive than UV-Vis.[41] The binding affinity using fluorescence spectroscopy is significantly higher with a lower standard deviation then using UV-Vis spectroscopy. This can be explained with the argument that fluorescence spectroscopy is the most sensitive and selective over background reactions while UV-Vis spectroscopy is not.[10,56] When considering the quantification of this interaction, Thordarson's 2011 paper was consulted regarding the sensitivity and selectivity issues when carrying out supramolecular titrations.[56] Thordarson mentions that the primary concern when picking an instrument for the instrumental method, should be factors such as concentration vs. expected association strength or the potential influences of impurities.[56] Fluorescence is particularity useful in the case of when only one of the species in solution is fluorescent active (as in our case).[56] Fluorescence is more sensitive to impurities that give rise to fluorescence intensity.[56] UV-Vis spectroscopy, however, assumes a significant change in the molar absorptivity (ε) upon

complexation and is vulnerable to the presence of impurities in the boronic acid or the diol solutions.[56]

The addition of boronic acid to an ARS solution increases its fluorescence intensity, presumably through the removal of the fluorescence quenching mechanism.[41] This suggests that, in solution, an excited-state proton transfer between the catechol hydroxyl groups and the adjacent ketone results in quenching of the ARS fluorescence intensity (**Scheme 5.2.2**).[55] This boronate ester formation experiment was performed with all the synthesized boronic acid derivatives. An example of a typical set of fluorescence intensity seen in an ARS solution upon addition of a boronic acid, is shown in **Figure 5.2.4.**

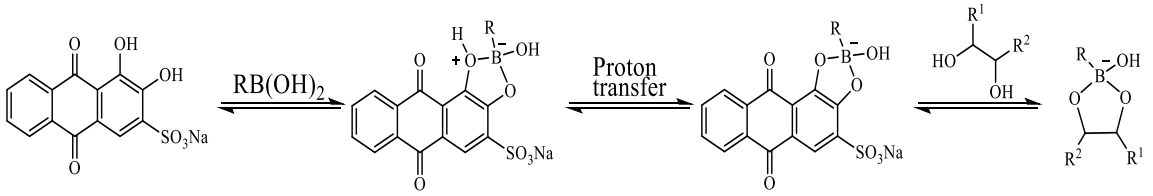

Scheme 5.2.2: Competitive binding of a boronic acid with Alizarin Red S. and a 1,2-diol. The addition of boronic acid to ARS increases the fluorescence intensity through the proton transfer to the quinone between the hydroxyl groups and the adjacent ketone.[41]

The association constant for the boronic acid-diol complex (K_a) was found by titrating boronic acid solution with the target diol compound. The extent to which the diol moiety changes the fluorescence intensity depends on the binding affinity between boronic acid and diol. Using the equation for association constant (**Equation 2.3.2**) where the association constant for the ARS-BA complex (K_a) was calculated using a non-linear fit and the boronic acid-diol interaction method (**see Chapter 2**),[41] the fluorescence at 460 nm was plotted against the concentration changes of the boronic acid compound. The wavelength of 460 nm was chosen because this is the λ_{max} at which we detect the BA-ARS complex formation at low concentrations of boronic acids and possible to monitor the intensity changes at that λ_{max}. The K_a of the BA-diol complex was then be calculated. Plots of fluorescence changes of ARS with increasing concentration of a boronic acid derivative of each category is shown in **Figure 5.2.4.**

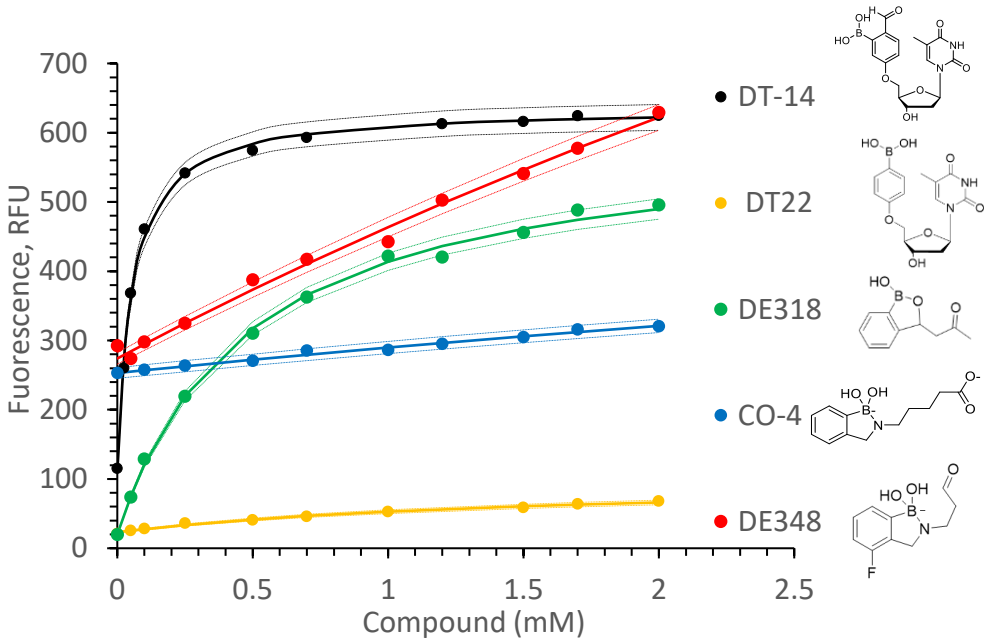

Figure 5.2.4: Plot of fluorescence changes of ARS 0.1 mM) with increasing concentration of synthesized boronic acid derivative of each category (0-2 mM) in HEPES buffer (100 mM, pH 7.4). Fluorescence versus concentration of the carbonyl boronic acid derivative DT14 (mM) at pH 7.4 in 0.1 mM HEPES buffer solution and ARS. (K_a is 17,973.7 ± 1.6 M^{-1}). Of phenylboronic acid derivative DT22 (K_a is 56.3 ± 0.044 M^{-1}), of aldehyde derivative DE348 (K_a is 139.7 ± 3.2 M^{-1}), of benzoxaborole derivative DE318 (K_a 2,053.2 ± 1.2 M^{-1}), and of carboxylic acid derivative CO4 (87.9 ± 0.23 M^{-1}). Values are the average of duplicate runs. Dotted lines represent 3% error for fluorescence changes.

The shape of the plot represents the tightness of the binding of ARS as the concentration of the boronic acid increases. **Figure 5.2.4** shows an example of boronic acid derivative from each category (Carbonyl boronic acids, phenylboronic acids, benzoxaborole derivatives, aldehyde derivatives and carboxylic acid derivatives). DT14 shows a sharp increase in intensity at lower concentrations and plateaus at 0.5 mM. The binding of DT14 is the tightest out of the compounds in **Figure 5.2.4**, with a K_a of 17,973.7 ± 1.6 M^{-1}. Thus, sharp increase in the fluorescence signal indicates tight binding. DE318 has a similar shape to DT14; however, the shape of DE318 is not as sharp, which suggests that DE318 exhibits weaker binding compared to DT14, with K_a 2,053.2 ± 1.2M^{-1}. DE348 has a slight curve at 0.1 mM of DE348, which indicates weak binding affinity to ARS with K_a of 139.7 ± 3.2 M^{-1}. The plots of DT22 and CO4 are essentially linear, suggesting that binding to ARS is weak.

In this case, the binding affinities of DT22 and CO4 are low with K_a of 56.3 ± 0.044 M^{-1} and 87.9 ± 0.23 M^{-1}, respectively. All the boronic acid derivatives were quantified based on their binding to ARS and their association constants are summarized in **Table 5.2.1**.

Table 5.2.1: Calculated K_a of binding of our synthesized compounds with ARS. Values are the average of duplicate runs. Errors represent the standard deviation of averaged absorbance measured that were used in **Equation 2.2.3.**

Category	Compound	K_a BA-ARS (M^{-1})
Reported control	2FPBA	1,024.6 ± 0.17
	PBA	1,553.1 ± 1.1
Thymidine derivatives	DT9	1,211.8 ± 2.9
	DT14	17,973.7 ± 1.6
	DT22	56.3 ± 0.044
Benzoxaborole derivatives	DE310	929.7 ± 0.78
	DE318	2,053.2 ± 1.2
Amino-aldehydes	DE321	165.3 ± 0.75
	DE342	166.7 ± 0.22
	DE348	139.7 ± 3.2
	DE343	117.9 ± 1.5
	DE344	120.7 ± 2.9
	DE347	130.7 ± 0.45
Carboxylic acid derivatives	CO1	387.4 ± 0.86
	CO2	295.6 ± 0.31
	CO3	113.6 ± 1.8
	CO4	87.9 ± 0.23
	CO5	38.8 ± 2.8

It is known that pK_a of boronic acids have an effect on the binding between boronic acids and the diol.[41] It was reported that: (1) higher pH favors the binding between boronic acid and a diol; (2) the pH needs to be above the pK_a of the boronic acid to see meaningful binding; and, (3) more acidic boronic acids bind more tightly with diols.[10,55] In our studies, we initially compared the pK_a values that were measured for each compound (**See Chapter 3**) to the binding affinity constants calculated in **Table 5.2.1** to test these three factors. **Figure 5.2.5** shows correlation scatter between the binding affinity constants and the pK_a values of our synthesized boronic acid derivatives.

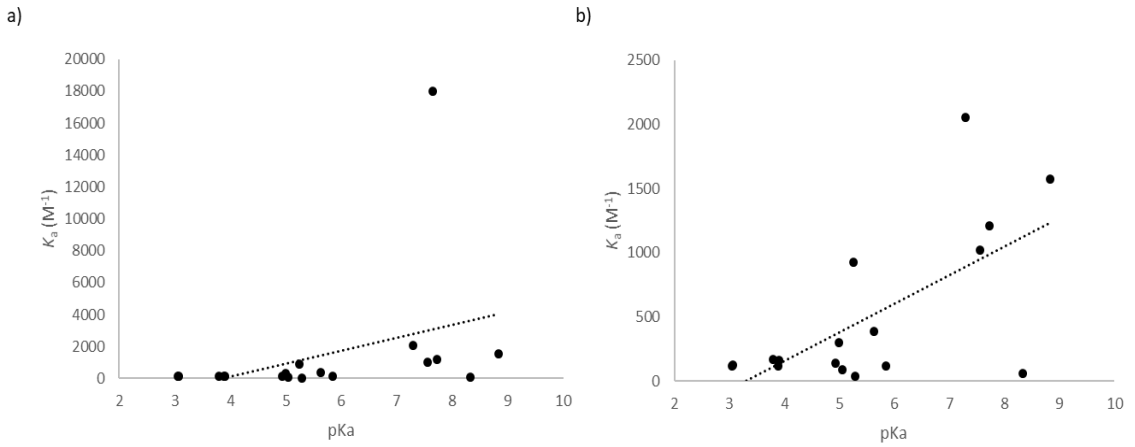

Figure 5.2.5: Relationship between pK_a values of our synthesized boronic acid containing compounds. pK_a used were determined by using ^{11}B NMR Spectroscopy (**Table 3.3.2**) and K_a values reported in **Table 5.2.1**. a) Including DT14. b) Excluding DT14.

Figure 5.2.5 shows the relationship between pK_a values of the boronic acid derivatives and their binding affinities to ASR. **Figure 5.2.5(b)** is shown excluding DT14 since the binding affinity is very high and is shown as an outlier. There is a small linear correlation between the pK_a and the binding affinity for any of our compounds within each category, however, the significance of the scatter in the data is much higher than the linear correlation. As shown in **Figure 5.2.5(b)** as the pK_a is higher, the binding affinity is also higher. The structure of boronic acid derivatives, with the different functionalities, at physiological pH does have more of an effect on the binding affinity than the pK_a alone. From **Table 5.2.1**, it was observed that the carbonyl boronic acid derivatives bind more tightly at physiological conditions. The thymidine containing carbonyl boronic acid derivatives bind the tightest to ARS. A reason that could affect the binding and give these significate and surprising differences between DT14 and DT9 would be the purity of these compounds. The carbonyl boronic acid and phenylboronic acid derivatives, illustrate that the structural functionalities in the boronic acid effects the magnitude of K_a. The magnitude threshold for our binding of the compounds with diols is >3 to be a significant difference between each other and between their controls. The structures of DT9, DT14 and 2FPBA each include an aldehyde functionality. The order of magnitude of binding affinity between DT14 and DT9 is 15, which is surprising given the structural similarity between the compounds. Thus, the proximity of the boronic acid group in DT9 to the

oxygen on the C5 of the ribose could explain the difference in ARS binding between DT14 and DT9. Moreover, the ARS binding affinity to DT22 is significantly weaker than to DT14 or DT9, while the only structural difference is the absence of an aldehyde. Comparing the order of magnitudes of DT22 to DT14, DT9, and the control compound PBA, DT22 was considered as an outlier because of its weak binding affinity to ARS. Based on the analysis of the differences in K_a values between DT14, DT9 and DT22, it is clear that the addition of an aldehyde at the meta position of the boronic acid to the oxygen on the C5 of the ribose increases the binding affinity to ARS.

The phenylboronic acid derivative DT22 bound weakly to ARS while PBA, which was used as a control, bound tightly. This could be due to decomposition of DT22, or environmental effects. DT22 was evaluated for purity by TLC analysis, however, a single spot was observed, with R_f value consistent with that reported,[38] suggesting that decomposition was not a factor for the binding affinity difference. Another possibility could be the absence of aldehyde and the addition of thymidine effecting the coordination of the molecule and not allowing the ARS to bind to DT22. The aldehyde derivatives have shown moderate binding; however, the binding affinity is not as tight as the carbonyl boronic acids, with DE321 binding tighter than the rest of the other compounds under this category with K_a of 165.3 ± 0.75 M^{-1} and DE343 and DE344 with weaker association constants of 117.9 ± 1.5 and 120.7 ± 2.9 M^{-1}, respectively. Altogether, the results show that the aldehyde containing compounds show good binding regardless of the presence of a thymidine group. However, a compound that contains thymidine and no aldehyde, such as DT22, does not bind well. Therefore, we can conclude that the aldehyde functionality might be responsible for good binding within our compounds, and that a thymidine group only promotes binding when an aldehyde functionality is present.

For the benzoxaborole boronic acid derivatives, no accurate control compound was tested to compare ARS binding association constants. However, literature binding affinity was compared to our synthesized benzoxaborole derivatives. According to *Tomsho,* the

binding affinity of benzoxaborole at pH 7 is 3,190 ± 110 M^{-1}.[57] This is within the range of binding of our benzoxaborole derivatives with ARS. DE318 binds tighter than DE310, with a K_a of 2,053.2 ± 1.2 M^{-1} and 929.7 ± 0.78 M^{-1}, respectively. The order of magnitude difference between the K_a values of DE318 and DE310 is 2.2, which is below the significance threshold of 3; therefore, the difference in binding affinity between DE318 and DE310 is insignificant. As was mentioned in Chapter 3, the pK_a of benzoxaborole is similar to the carbonyl boronic acid derivatives.[14] It is known that benzoxaboroles bind well to diols and form a boronate ester.[36] Although the benzoxaborole derivative, DE318, has a pK_a value similar to carbonyl boronic acid derivatives, it is less hindered by an electron-withdrawing carbonyl, which provides a tighter binding under physiological conditions. DE310 however, has a lower pK_a value than DE318, which would prefer the trigonal planar geometry and would bind slightly weaker with a diol than DE318. Moreover, the benzoxaborole derivatives contain a strong electron withdrawing group that might be much more hindered and provides a lower interaction under physiological pH compared to the carbonyl boronic acid derivatives.

Looking at the carboxylic acid derivatives (CO1-CO5), the only difference between each compound is the number of methylene groups between the amine and the carboxylic acid functionalities. As the number of methylene increases, the K_a decreases, and the binding is weaker. The order of magnitude of binding affinity between the K_a values CO1 (containing 1 methylene group) and CO2 (containing 2 methylene groups) is 1.3. As the compound gets more clustered, the order of magnitude increases to 2.5 between CO2 and CO3 (containing 3 methylene groups). The same trend is observed between all the carboxylic acid compounds. Thus, as the number of methylene groups increases, the binding affinity of ARS to the boronic acid decreases.

The amino-aldehyde series had K_a values between 166.7 ± 0.22 M^{-1} and 117.9 ± 1.5 M^{-1}, a tight distribution of values, indicating that the structural changes of the analogues did not significantly change diol binding. The two structural changes within the amino-

aldehyde series were the number of methylene units (between 1-2) and the presence or absence of fluorine on the aromatic ring. Considering the number of methylene units, going from DE321 (1 methylene unit) to DE343 (2 methylene units) the affinity decreases. Regarding the presence or absence of a fluorine atom on the ring, there was an insignificant decrease in binding affinity between the fluorinated and the non-fluorinated compounds. The carboxylic acid series had K_a values between 387.4 ± 0.86 and 38.8 ± 2.8 M^{-1}, a greater range of values and a clear trend was observed where the binding affinity decreased with increasing methylene units between the carboxylic acid and the amino functionality.

Moreover, the aldehyde derivatives and the carboxylic acid derivatives contain a secondary amine. Based on the X-ray crystallographic and mass spectrometry data **(See Chapter 3 for Crystallography results**), CO1 was found to have a boron-nitrogen dative bond between the boronic acid and the secondary amine. This results provides evidence that the compounds containing a secondary amine all likely contain a boron-nitrogen bond, forming a 5-membered ring. The pK_a of a secondary amine is between 9 and 10.[58] Solutions at lower pH that the amine's pK_a, the amine would exist as a protonated ammonium group, and the anionic sulfonate group on the ARS would interact with the ammonium through an electrostatic attraction.[55] The electrostatic interaction would result in lower BA-ARS binding affinity. For our aldehyde and carboxylic acid derivative, the association constants were much lower than those for the other boronic acids suggesting that significant electrostatic interactions may influence the binding affinities for these two groups of BA derivatives.[55]

To conclude, in this study, boronate ester formation association constants were determined for our synthesized boronic acid derivatives and ARS. K_a values were determined using the increased fluorescence intensity as ARS complexed to the boronic acid derivatives. It was found that the carbonyl boronic acid derivatives have the greatest binding affinity to ARS, while the carboxylic acid and aldehyde derivatives had the

weakest binding, relative to the two control compounds, PBA and 2FPBA. Specifically, DT14 had an exceptionally tight association constant, relative to all the other compounds analyzed. Benzoxaborole derivatives had tight binding to ARS and this is in agreement with the literature.[36] Phenyl boronic acid derivatives did not bind tightly to ARS, despite the control compound PBA exhibiting strong binding to ARS. Our results indicate that changing the structure of the boronic acid-containing compound varies the association constant over a range of 10 – 10^5. The design of a boronic acid-based sensor will require knowledge of the intrinsic binding affinities between boronic acid and diol moieties. The ARS system can be used to rapidly compare the affinities of many boronic acid derivatives. Furthermore, the method employed in this work provides a way to study boronate ester formation under physiological conditions.

5.3 Boronic acid-diol binding between boronic acid derivatives and various saccharides

Saccharides (or carbohydrates) are ubiquitous throughout the natural world. From simple monosaccharides consisting of a single unit, to complex polysaccharides composed of hundreds or thousands of individual monomers, these molecules form a diverse range of structures allowing them to perform a wide range of different roles such as metabolic fuel and cell-recognition events.[59] Compounds which complex to sugars can be useful for saccharide sensor applications such as chemosensors for blood-glucose monitoring. Therefore, we were interested in investigating the association constants of the boronic acids with different saccharides. The same method developed by the Wang group was used to quantify the association constant between our synthesized boronic acid derivatives and various saccharides that are present on mammalian cell surfaces.[10,41]

A three-component competitive reaction between the boronic acid, ARS and saccharide was developed by Springsteen and Wang was found to be a useful and straightforward method. [10,41] This method was used successfully (**See Chapter 2**), with the assumptions that the starting concentration of the saccharides must be 100 times higher than the concentration of the boronic acid containing compounds and of the ARS. Also, the rapid

equilibria between the boronic acid, the ARS and the saccharide allows us to measure the association constants. Various saccharides were used to determine the binding affinity between our previously synthesized boronic acid compounds and those saccharides. The saccharides used in this study are shown in **Figure 5.3.1**.

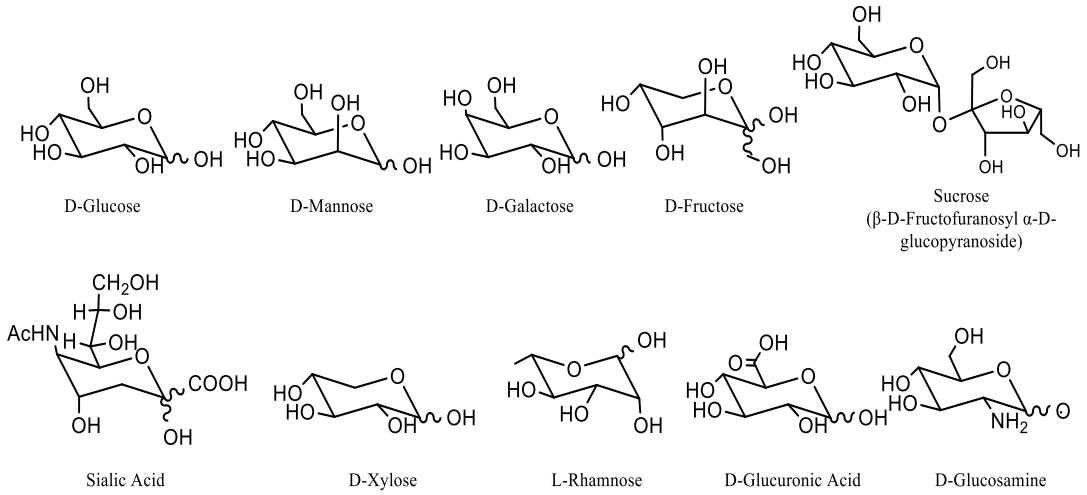

Figure 5.3.1: Saccharides used in the three-component competitive reaction between ARS and boronic acid derivatives.

Based on the work presented above and in **Chapter 3**, we expect that compounds with lower ARS binding affinity will have higher binding affinity to the saccharides because higher fraction of free boronic acids to bind with the sugars. Conversely, the compounds that bind with greater affinity to ARS would be expected to bind with weaker affinity to saccharides. **Scheme 5.3.1** illustrates one example of the three-component competitive reaction between ARS, one of our boronic acid derivatives, and fructose. The monosaccharide fructose, is often used in boronic acid binding studies since it was found to be have a high assosiation constant, as a consequance of the 1,2 cis-diol.[36,60]

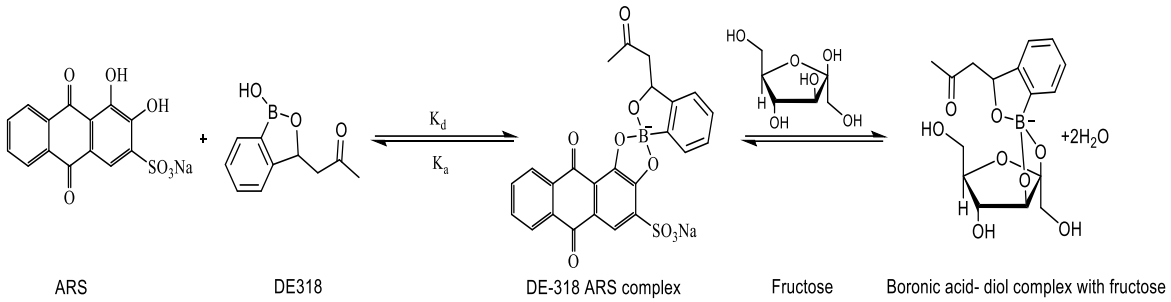

Scheme 5.3.1: Formation of a potential 1,2 cis-diol complex between the benzoxaborole derivative DE318, ARS and fructose. [ARS] 0.1 mM, [DE318] 10 mM, [fructose] 0-0.1 M, HEPES buffer (50 mM, pH 7.4).

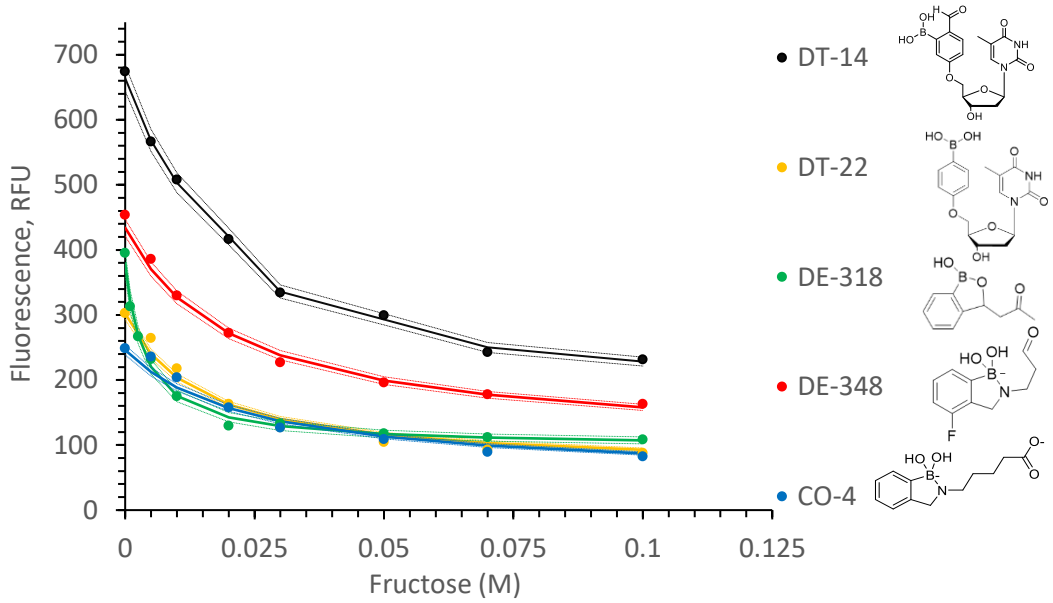

Figure 5.3.2: Plot of fluorescence changes of ARS- boronic acid complex with increasing fructose. ARS (0.1 mM), boronic acid (10 mM), fructose (0-0.1 M), HEPES buffer (100 mM, pH 7.4). For the carbonyl boronic acid derivative DT14, K_a is 94.4 ± 0.64 M^{-1}. For phenylboronic acid derivative DT22 (K_a is 70.1 ± 1.9 M^{-1}), of aldehyde derivative DE348 (Ka is 90.1 ± 2.4 M^{-1}), for benzoxaborole derivative DE318 (K_a 256.6 ± 1.5 M^{-1}), and for carboxylic acid derivative CO4 (41.1 ± 1.7 M^{-1}). Values are the average of duplicate runs. Dotted lines represent 3% error for fluorescence changes.

In this experiment there are two competing equilibria. The first system is between the boronic acid and the ARS, which has previously been measured, and the second system is between the boronic acid and the diol which gives a new BA-diol complex.[10,56] When boronic acid compounds bind to ARS, the fluorescence intensity increases. However,

when there is a competition between saccharide and ARS to bind with the boronic acid, the fluorescence intensity decreases. This correlates with the association constants of those compounds when binding to the saccharides. In **Figure 5.3.2**, a compound from each boronic acid series shows the decrease in fluorescence intensity as the concentration of fructose increases in the three-component assay between ARS and fructose and the boronic acid derivative. All plots are hyperbolic and decrease sharply at lower fructose concentrations (for example, 0.005 M), such as the plot of DE318, which correlates to a tighter binding to fructose and a higher K_a of 260 ± 1.5 M^{-1}. Next, DT14 shows a less hyperbolic shape which correlates to the slightly weaker binding and a K_a of 94 ± 0.64 M^{-1}. The rest of the compounds showed a small hyperbolic shape, but no linear shapes, which suggests that all compounds bind to fructose, with DT22 binding tighter than DE348 and CO4 with K_a of 70 ± 1.9 M^{-1}. DE348 and CO4 indicate a weak binding to fructose at any concentration. The calculated association constants (K_a) are shown in **Table 5.3.1** and **Table 5.3.2**. K_a was calculated in the same manner as the K_a of ARS binding.

Table 5.3.1: Saccharide association constants (K_a) with boronic acid derivatives using 3-component ARS assay. Values are the average of duplicate runs. N.b = no binding.

Compound	Fructose (M^{-1})	Glucuronic Acid (M^{-1})	Glucose (M^{-1})	Xylose (M^{-1})	Sialic Acid (M^{-1})
2FPBA	85.8 ± 21.4	n.b	10.6 ± 2.8	16.5 ± 1.2	4.0 ± 9.4
PBA	117.3 ± 1.1	27.4 ± 4.9	3.7 ± 1.1	4.8 ± 4.9	53.6 ± 27.9
DE310	24.7 ± 1.7	56.7 ± 0.43	6.9 ± 4.1	22.9 ± 4.0	19.1 ± 7.8
DE318	256.6 ± 1.5	143.1 ± 0.27	10.9 ± 21	34.6 ± 1.3	42.1 ± 1.4
DE321	71.3 ± 0.83	36.1 ± 2.2	66.6 ± 7.9	106.9 ± 2.5	22.9 ± 0.38
DE342	161.5 ± 1.6	28.1 ± 0.45	19.1 ± 1.3	15.5 ± 1.1	1.9 ± 8.1
DE343	84.7 ± 0.35	21.7 ± 0.55	40.2 ± 1.5	91.5 ± 5.2	n.b
DE344	105.3 ± 4.9	12.6 ± 2.1	n.b	n.b	n.b
DE347	116.3 ± 6.9	25.3 ± 0.61	n.b	3.4 ± 0.65	21.5 ± 3.8
DE348	91.1 ± 2.4	86.1 ± 1.5	21.2 ± 2.5	55.9 ± 14	17.7 ± 3.8
DT9	105.3 ± 0.66	n.b	15.3 ± 0.49	28.8 ± 0.30	n.b
DT14	94.4 ± 0.64	2.72 ± 5.1	16.1 ± 6.9	7.6 ± 4.6	61.3 ± 7.0
DT22	70.1 ± 1.9	n.b	n.b	n.b	n.b
CO1	30.8 ± 5.8	231.1 ± 0.52	2.4 ± 2.5	8.4 ± 4.2	84.3 ± 12.5
CO2	28.5 ± 2.2	134.9 ± 0.47	7.8 ± 0.98	7.5 ± 5.7	85.1 ± 3.9
CO3	30.2 ± 1.6	63.6 ± 1.1	1.9 ± 1.1	10.2 ± 1.1	7.0 ± 0.22
CO4	41.1 ± 1.7	39.4 ± 0.45	1.1 ± 2.1	4.2 ± 3.1	10.2 ± 5.7
CO5	71.6 ± 1.6	59.4 ± 2.2	2.7 ± 0.88	6.9 ± 2.5	3.3 ± 8.9

Table 5.3.2: Continued table of saccharide association constants (K_a) with boronic acid derivatives using 3-component ARS assay. Values are the average of duplicate runs. N.b = no binding.

Compound	Mannose (M^{-1})	Galactose (M^{-1})	Rhamnose (M^{-1})	Sucrose (M^{-1})	Glucosamine (M^{-1})
2FPBA	8.1 ± 1.3	4.8 ± 0.41	11.9 ± 2.1	n.b	n.b
PBA	9.4 ± 1.2	5.4 ± 0.43	n.b	n.b	n.b
DE310	6.8 ± 2.1	2.7 ± 2.6	1.5 ± 0.64	n.b	n.b
DE318	6.9 ± 1.6	18.6 ± 3.6	11.7 ± 2.4	n.b	n.b
DE321	3.1 ± 2.1	n.b	n.b	n.b	15.1 ± 0.98
DE342	41.6 ± 2.3	33.1 ± 0.49	7.6 ± 0.61	1.4 ± 6.4	n.b
DE343	n.b	n.b	n.b	n.b	n.b
DE344	6.1 ± 1.4	1.8 ± 1.6	n.b	n.b	1.9 ± 0.044
DE347	19.9 ± 1.3	2.2 ± 6.2	n.b	n.b	n.b
DE348	20.2 ± 0.85	2.4 ± 7.7	n.b	18.1 ± 9.1	n.b
DT9	8.1 ± 1.3	17.1 ± 4.6	39.9 ± 7.0	52.5 ± 2.5	1.4 ± 4.7
DT14	9.1 ± 4.5	5.7 ± 2.0	6.0 ± 0.77	n.b	1.0 ± 2.9
DT22	23.2 ± 0.97	n.b	n.b	n.b	n.b
CO1	27.2 ± 4.5	4.5 ± 2.3	n.b	n.b	n.b
CO2	1.2 ± 1.2	1.3 ± 1.4	n.b	n.b	n.b
CO3	1.1 ± 1.8	3.3 ± 1.6	n.b	n.b	n.b
CO4	5.8 ± 1.3	2.7 ± 4.0	n.b	n.b	n.b
CO5	2.1 ± 1.7	2.7 ± 1.8	n.b	n.b	n.b

From our results, we observed that different compounds had different affinities to saccharides, indicating that it is possible to create a more selective binder. Out of all the sugars investigated, fructose, glucuronic acid, and glucose exhibited the highest association constants across all boronic acid derivatives. Within this group of sugars, fructose bound most tightly. Fructose was found to bind tightly to many of the synthesized boronic acid derivatives and its tight binding is with agreement with control compounds and literature values.[10,55] Comparing all the boronic acid derivatives and their association constants with fructose, DE318 had the highest binding affinity at 256.6 ± 1.5 M^{-1}, greater than PBA or 2FPBA. The other benzoxaborale compound DE310, had a significantly lower association constant (order of magnitude is 3.4) with fructose compared to DE318, most likely due to induction effects from the trifluoromethyl group. The aldehyde derivatives showed a wide range of binding affinities from the weakest

binder DE321, with a K_a = 71.3 ± 0.83 M^{-1}, to the greatest binder DE342, with a K_a = 161.5 ± 1.6 M^{-1}. The higher binding affinity of DE342 compared to the other aldehyde derivatives could potentially be explained by the position of the fluorine and the number of methylene groups between the amine and the aldehyde. The carbonyl boronic acids, DT14 and DT9, showed moderate binding with fructose, slightly higher than 2FPBA. In general, the carboxylic acid derivatives exhibited the weakest binding to fructose, with the exception of CO5, which had an association constant of 71.6 ± 1.6 M^{-1}. Finally, DT22 showed slightly weaker binding than PBA, with an order of magnitude of 0.6, which is not significantly different. There were some compounds that bound more tightly to other sugars than fructose, notably CO1 bound to glucuronic acid, CO2 bound to glucuronic acid and DE321 bound to xylose.

The trends in binding affinity between glucuronic acid and the boronic acids were contrast with the trends observed for fructose binding. Overall, glucuronic acid was found to bind tightly to our synthesized derivatives. There have been few reports investigating the sugar binding of boronic acids to glucuronic acid in the literature.[61] For glucuronic acid, the carboxylic acid derivatives bound more tightly than the other boronic acid categories, compared to the aldehyde derivatives for fructose. CO1 and CO2 showed greater binding to glucuronic acid with K_a values of 231.1 ± 0.52 M^{-1} and 134.9 ± 0.47 M^{-1}, respectively. Furthermore, CO3, CO4, and CO5 bind weakly with K_a = 63.6 ± 1.1 M^{-1} for CO3, 39.4 ± 0.45 M^{-1} for CO4 and 59.4 ± 2.2 M^{-1} for CO5. The carbonyl derivatives DT9 and DT22 did not bind to glucuronic acid at all, and DT14 bound weakly with a K_a of 2.72 ± 5.1 M^{-1}. Weak binding to the carbonyl derivatives is unlike the binding with fructose, which bound strongly to these compounds. The carbonyl boronic acid control, 2FPBA, also did not bind to glucuronic acid, which suggests that there is a structural reason why these derivatives do not bind to glucuronic acid specifically. One structural feature of glucuronic acids is the presence of a carboxylic acid functionality at C6, which could result in glucuronic acid selectively binding to boronic acids without an aldehyde functionality. Comparing the binding affinities of the aldehyde derivatives between glucuronic acid and fructose, a

significant decrease in association constants is observed. Specifically, DE342, which bound fructose, did not bind to glucuronic acid. Alternatively, the increase in binding of the carboxylic acid derivatives with glucuronic acids could have resulted from proximity of the carboxylic acid in the boronic acid to the boron atom. Finally, the benzoxaborole derivatives show similar binding affinities to glucuronic acid compared with fructose, with DE318 more tightly binding than DE310, with association constants of 143.1 ± 0.27 and 56.7 ± 0.43 M^{-1}, respectively.

Following fructose and glucuronic acid, glucose was the next tightest binder to the boronic acid derivatives. Glucose is known to be a sugar of interest in biological applications and it was reported to have moderate binding to boronic acids.[10,55] Glucose binds with a similar trend across all boronic acids but with overall lower association constants compared to fructose. DE321 showed the highest binding affinity to glucose, with an association constant of 66.6 ± 7.9 M^{-1}, comparable to its binding with fructose. Across the rest of the aldehyde derivatives, glucose bound tightly relative to the aldehyde control 2FPBA, with the exception of DE344 and DE374, which did not bind to glucose. Comparing DE344 and DE374 to DE321, the former have a fluorine substituent and a lower number of methylene groups between the amine and the aldehyde. This suggests that the functionalities of the aldehyde boronic acid derivatives influenced the binding affinity to glucose. The benzoxaborole and carbonyl derivatives bind to glucose with similar affinities. For example, DE318 and DT14 were the tightest binders in their respective categories, with association constants of 10.9 ± 21 and 16.1 ± 6.9 M^{-1}, respectively. The phenylboronic and carboxylic acid derivatives bind with an equal or less order of magnitude to their control compounds PBA and 2FPBA, which had association constants of 3.7 ± 1.1 and 10.6 ± 2.8 M^{-1}, respectively. Based on our results, glucose is a weak to moderate binder to our boronic acid derivatives, relative to fructose and glucuronic acid.

Comparing the remaining saccharides, there are some similar and some unique trends in the association constants across all the boronic acid derivatives. Sialic acid shows similar trends in association constants to glucuronic acid. CO1 and CO2, which bind tightly to glucuronic acid also bind the tightest to sialic acid, with association constants of 84.3 ± 12.5 and 85.1 ± 3.9 M^{-1}, respectively. The boronic acids which did not bind to sialic acid, also showed low to no binding with glucuronic acid. For example, DE344 did not bind to either saccharide, and DE343 did not bind to sialic acid but bound to glucuronic acid with a weak binding. The trends in binding for sialic acid and glucuronic acid can both be attributed to their similar structure. Glucuronic acid and sialic acid both contain a carboxylic acid. As discussed previously, these sugars selectively bind to boronic acids with carboxylic acid functionalities. Rhamnose favors a cis-diol pyranose in solution; however, does not bind to most of the boronic acid derivatives. Rhamnose is an example where not all cis-diols bind boronic acids. Rhamnose is the only saccharide out of the tested saccharides to contain a methyl group on C5 and its binding affinity is mostly low. This could be due to a steric effect between the hydroxyl and methyl groups at C3 and C5 which would block the ability of the boronic acid to bind to rhamnose. Rhamnose is also a sugar that contains a 2,3-cis diol, which was expected to coordinate boronic acids with higher affinity than observed.

Xylose showed a significant binding to DE321, with a K_a of 106.9 ± 2.5 M^{-1}, and no binding to DT22 and DE344. The rest of the compounds were bound moderately to xylose, where DT9 has a K_a of 28.8 ± 0.30 M^{-1}, DT14 has a lower K_a of 7.6 ± 4.6 M^{-1} and DE318 has K_a of 34.6 ± 1.3 M^{-1}. Aldehyde derivatives have a moderate interaction with xylose except for DE343 binding tightly with K_a of 91.5 ± 5.2 M^{-1} and DE348 with K_a of 55.9 ± 14 M^{-1}. The carboxylic acid derivatives showed weak binding between 4-10 M^{-1} with CO3 having a K_a of 10.2 ± 1.1 M^{-1} and CO4 having K_a of 4.2 ± 3.1 M^{-1}. This could be because of a positively charged group that electrostatically interacts with the negatively charged group or by hydrogen bonds since xylose has multiple hydroxyl groups and the carboxylic acid on the C1.[36] Mannose and Galactose showed a similar binding affinity patterns to xylose, with

the tightest binder being DE342 binding with K_a of 41.6 ± 2.3 M^{-1} and 33.1 ± 0.49 M^{-1}, respectively.

Sucrose and glucosamine did not bind or bound weakly to the boronic acid derivatives with the exception of DT9 binding to sucrose and DE321 binding to glucosamine with a K_a of 52.5 ± 2.5 and 15.1 ± 0.98 M^{-1}, respectively. Sucrose is comprised of glucose and fructose linked through their anomeric centers. As a consequence of this structure, neither the glucose or fructose units in sucrose are able to present a cis diol for boronic acid binding. Boronic acids are well known to interact with the furanose form of glucose.[62] However, the formation of glucofuranose-boronic acid complexes is driven by the stability of the boronate ester of the 1,2-diol of the glucofuranose, which is not possible for glucosamine.[63] This is consistent with the lack of binding observed for glucosamine and our boronic acid derivatives.

Overall, our results show that there are binding similarities based on the boronic acid series. Boronic acids within a series bound similarly to the same saccharide. However, some compounds show more selective interactions, for example, DE342 binds tightly to fructose, but more weakly to all other saccharides. Selective binders will be helpful when designing compounds for a specific saccharide. However, some compounds bound tightly to many saccharides (Such as DE318, CO1, DE321, DE348), that could become universal saccharide binders. Thus, the structure and binding affinities need to be carefully considered when developing a sensor. Furthermore, future work based on this study, could determine the structure of complexes between specific boronic acids and a particular sugar by NMR. Such an analysis would help understand the trends in association constants across all saccharides and boronic acids evaluated in this work.

5.4 Summary

We explored the boronic ester formation between ARS as a reporter tool and our novel synthesized boronic acid compounds and later the binding of various saccharides to those boronic acid compounds. The complexation was quantified using fluorescence. We found that different functionalities within the structure effect the binding with ARS, and the different saccharides with each compound independently. The magnitude of the binding affinity represents the differences in binding of each compound with different functionalities and the different saccharides. This gives the possibility to create and synthesize selective binders depending on the functionalities and the saccharide of interest.

Chapter 6. Conclusion

The work reported in this thesis evaluated a library of boronic acid derivatives, by measuring a series of physicochemical properties to provide insight into the utility of the boronic acid derivatives to function as potential sensors. The sixteen different boronic acid containing compounds had additional functionalities including thymidine, benzoxaborole, aldehyde, amine, carboxylic acid and ortho-aldehydes. These compounds were characterized by measuring their pK_a values and their structural equilibria under aqueous conditions, their boronate ester formation when binding to diols and saccharides, and where appropriate, their reactivity towards Lysine.

In the pK_a determination study, all 16 boronic acid compounds were evaluated based on their structural changes at different solution pH values. Using UV-VIS and NMR spectroscopy, the pK_a values of each category of boronic acid derivatives were determined. NMR spectroscopy was found to be the most accurate technique used for pK_a determination because NMR can isolate signals for the boron center, rather than reporting the average pK_a for the entire structure. pK_a values were determined for the carbonyl boronic acids, the phenylboronic acids and the benzoxaborole derivatives, as they showed only one structural change across varied solution pH values using NMR spectroscopy. However, the aldehyde and the carboxylic acid derivatives showed multiple chemical changes that were not further explored in our one pK_a fitting methods. Potential future work would be to explore the hypothesis of having a ring cyclization by performing a full NMR analysis, which would collect and analyse the 1D ^{1}H, ^{11}B, ^{13}C, and 2D HMBC and HSQC NMR data. Conducting these measurements at appropriate pH values will provide greater insight to the structural changes of the compounds and the selectivity and binding of each derivative to diols. Moreover, developing a crystallographic method at high pH solutions to further explore its structure would complement our NMR characterization.

In the iminoboronate and diazaboronate formation study, Boc-Lys-OH was used as a potential binder. The carbonyl boronic acid derivatives DT9 and DT14 formed an iminoboronates successfully. However, our hypothesis that the aldehyde derivatives would form a diazaboronate was incorrect, despite their structural similarity to other diazaboronates in the literature. This could be due to the chemical structure of the compounds or of the amino acid at physiological pH. Future work repeating this experiment at different pH solutions would explore the structure-binding properties of our aldehyde derivatives further. Furthermore, testing a range of solution pH values would explore the effect of pK_a values of Boc-Lys-OH and of our compounds that were obtained from the pK_a determination study. Theoretically, we would want a high fraction of tetrahedral boronate center, which would exist at higher pH solutions. Moreover, this work would determine at what pH would yield the highest formation of the iminoboronate complex. Ultimately, we would want the highest formation of the iminoboronate complex at physiological pH to have any practical application.

In the final study, the binding of our boronic acid derivatives to different saccharides was quantified. Out of the different saccharides that were studied, there were novel interactions between the saccharides and the boronic acid derivatives such as the high affinity of the compound CO1 with glucuronic acid. We found that different functionalities within the boronic acid structure influenced the binding with each saccharide independently. The result of this finding is a good starting point for creating and synthesizing selective binders for saccharides of interest. It is known that diols bind to boronic acid via 1,2-cis diol binding, however, the structure of the complexes were not determined in our study. Future work could be to investigate the boronic acid-diol interactions using NMR spectroscopy. By using NMR spectroscopy, the structural factors influencing strong binding between a boronic acid derivative, and a particular saccharide could be determined.

References

(1) Silva, M. P.; Saraiva, L.; Pinto, M.; Sousa, M. E. Boronic Acids and Their Derivatives in Medicinal Chemistry: Synthesis and Biological Applications. *Molecules* **2020**, *25* (18), 4323. https://doi.org/10.3390/molecules25184323.

(2) Chatterjee, S.; Tripathi, N. M.; Bandyopadhyay, A. The Modern Role of Boron as a 'Magic Element' in Biomedical Science: Chemistry Perspective. *Chemical Communications* **2021**, *57* (100), 13629–13640. https://doi.org/10.1039/D1CC05481C.

(3) Raedler, L. Velcade (Bortezomib) Receives 2 New FDA Indications: For Retreatment of Patients with Multiple Myeloma and for First-Line Treatment of Patients with Mantle-Cell Lymphoma. *Am Health Drug Benefits* **2015**, *8* (Spec Feature), 135–140.

(4) Kazmi, M. Z. H.; Schneider, O. M.; Hall, D. G. Expanding the Role of Boron in New Drug Chemotypes: Properties, Chemistry, Pharmaceutical Potential of Hemiboronic Naphthoids. *J Med Chem* **2023**. https://doi.org/10.1021/acs.jmedchem.3c01194.

(5) Trippier, P. C.; McGuigan, C. Boronic Acids in Medicinal Chemistry: Anticancer, Antibacterial and Antiviral Applications. *Medchemcomm* **2010**, *1* (3), 183. https://doi.org/10.1039/c0md00119h.

(6) Frankland, E.; Duppa, B. F. Vorläufige Notiz Über Boräthyl. *Annalen der Chemie und Pharmacie* **1860**, *115* (3), 319–322. https://doi.org/10.1002/jlac.18601150324.

(7) Hall, D. G. Structure, Properties, and Preparation of Boronic Acid Derivatives. In *Boronic Acids*; Wiley, 2011; pp 1–99. https://doi.org/10.1002/9783527639328.ch1.

(8) Baker, S. J.; Ding, C. Z.; Akama, T.; Zhang, Y.-K.; Hernandez, V.; Xia, Y. Therapeutic Potential of Boron-Containing Compounds. *Future Med Chem* **2009**, *1* (7), 1275–1288. https://doi.org/10.4155/fmc.09.71.

(9) António, J. P. M.; Russo, R.; Carvalho, C. P.; Cal, P. M. S. D.; Gois, P. M. P. Boronic Acids as Building Blocks for the Construction of Therapeutically Useful Bioconjugates. *Chem Soc Rev* **2019**, *48* (13), 3513–3536. https://doi.org/10.1039/C9CS00184K.

(10) Peters, J. A. Interactions between Boric Acid Derivatives and Saccharides in Aqueous Media: Structures and Stabilities of Resulting Esters. *Coord Chem Rev* **2014**, *268*, 1–22. https://doi.org/10.1016/j.ccr.2014.01.016.

(11) Wallace, M.; Adams, D. J.; Iggo, J. A. Titrations without the Additions: The Efficient Determination of p K_a Values Using NMR Imaging Techniques. *Anal Chem* **2018**, *90* (6), 4160–4166. https://doi.org/10.1021/acs.analchem.8b00181.

(12) Zscherp, C.; Schlesinger, R.; Tittor, J.; Oesterhelt, D.; Heberle, J. *In Situ* Determination of Transient PK $_a$ Changes of Internal Amino Acids of Bacteriorhodopsin by Using Time-Resolved Attenuated Total Reflection Fourier-Transform Infrared Spectroscopy. *Proceedings of the National Academy of Sciences* **1999**, *96* (10), 5498–5503. https://doi.org/10.1073/pnas.96.10.5498.

(13) Manallack, D. T. The PK(a) Distribution of Drugs: Application to Drug Discovery. *Perspect Medicin Chem* **2007**, *1*, 25–38.

(14) Tomsho, J. W.; Pal, A.; Hall, D. G.; Benkovic, S. J. Ring Structure and Aromatic Substituent Effects on the p K_a of the Benzoxaborole Pharmacophore. *ACS Med Chem Lett* **2012**, *3* (1), 48–52. https://doi.org/10.1021/ml200215j.

(15) Ionization. In *The IUPAC Compendium of Chemical Terminology*; International Union of Pure and Applied Chemistry (IUPAC): Research Triangle Park, NC, 2014. https://doi.org/10.1351/goldbook.I03183.

(16) Sun, X.; Chapin, B. M.; Metola, P.; Collins, B.; Wang, B.; James, T. D.; Anslyn, E. V. The Mechanisms of Boronate Ester Formation and Fluorescent Turn-on in Ortho-Aminomethylphenylboronic Acids. *Nat Chem* **2019**, *11* (9), 768–778. https://doi.org/10.1038/s41557-019-0314-x.

(17) Werner, J. P.; Mitchell, J. M.; Taracila, M. A.; Bonomo, R. A.; Powers, R. A. Exploring the Potential of Boronic Acids as Inhibitors of OXA-24/40 B-lactamase. *Protein Science* **2017**, *26* (3), 515–526. https://doi.org/10.1002/pro.3100.

(18) Augeri, D. J.; Robl, J. A.; Betebenner, D. A.; Magnin, D. R.; Khanna, A.; Robertson, J. G.; Wang, A.; Simpkins, L. M.; Taunk, P.; Huang, Q.; Han, S.-P.; Abboa-Offei, B.; Cap, M.; Xin, L.; Tao, L.; Tozzo, E.; Welzel, G. E.; Egan, D. M.; Marcinkeviciene, J.; Chang, S. Y.; Biller, S. A.; Kirby, M. S.; Parker, R. A.; Hamann, L. G. Discovery and Preclinical Profile of Saxagliptin (BMS-477118): A Highly Potent, Long-Acting, Orally Active Dipeptidyl Peptidase IV Inhibitor for the Treatment of Type 2 Diabetes. *J Med Chem* **2005**, *48* (15), 5025–5037. https://doi.org/10.1021/jm050261p.

(19) Chandrashekar, N.; Shobha Rani, R. Physicochemical and Pharmacokinetic Parameters in Drug Selection and Loading for Transdermal Drug Delivery. *Indian J Pharm Sci* **2008**, *70* (1), 94. https://doi.org/10.4103/0250-474X.40340.

(20) Öğretir, C.; Yarlıgan, S.; Demirayak, Ş.; Arslan, T. A Theoretical Approach to Acidity–Basicity Behaviour of Some Biologically Active 6-Phenyl-4,5-Dihydro-3(2H)-Pyridazinone Derivatives. *Journal of Molecular Structure: THEOCHEM* **2003**, *666–667*, 609–615. https://doi.org/10.1016/j.theochem.2003.08.085.

(21) Cuesta, A.; Taunton, J. Lysine-Targeted Inhibitors and Chemoproteomic Probes. *Annu Rev Biochem* **2019**, *88* (1), 365–381. https://doi.org/10.1146/annurev-biochem-061516-044805.

(22) Faridoon; Ng, R.; Zhang, G.; Li, J. J. An Update on the Discovery and Development of Reversible Covalent Inhibitors. *Medicinal Chemistry Research* **2023**, *32* (6), 1039–1062. https://doi.org/10.1007/s00044-023-03065-3.

(23) Lomovskaya, O.; Sun, D.; Rubio-Aparicio, D.; Nelson, K.; Tsivkovski, R.; Griffith, D. C.; Dudley, M. N. Vaborbactam: Spectrum of Beta-Lactamase Inhibition and Impact of Resistance Mechanisms on Activity in Enterobacteriaceae. *Antimicrob Agents Chemother* **2017**, *61* (11). https://doi.org/10.1128/AAC.01443-17.

(24) Lomovskaya, O.; Tsivkovski, R.; Nelson, K.; Rubio-Aparicio, D.; Sun, D.; Totrov, M.; Dudley, M. N. Spectrum of Beta-Lactamase Inhibition by the Cyclic Boronate QPX7728, an Ultrabroad-Spectrum Beta-Lactamase Inhibitor of Serine and Metallo-Beta-Lactamases: Enhancement of Activity of Multiple Antibiotics against Isogenic Strains Expressing Single Beta-Lactamases. *Antimicrob Agents Chemother* **2020**, *64* (6). https://doi.org/10.1128/AAC.00212-20.

(25) Plescia, J.; Moitessier, N. Design and Discovery of Boronic Acid Drugs. *Eur J Med Chem* **2020**, *195*, 112270. https://doi.org/10.1016/j.ejmech.2020.112270.

(26) Albers, H. M. H. G.; van Meeteren, L. A.; Egan, D. A.; van Tilburg, E. W.; Moolenaar, W. H.; Ovaa, H. Discovery and Optimization of Boronic Acid Based Inhibitors of Autotaxin. *J Med Chem* **2010**, *53* (13), 4958–4967. https://doi.org/10.1021/jm1005012.

(27) LeBlanc, R.; Catley, L. P.; Hideshima, T.; Lentzsch, S.; Mitsiades, C. S.; Mitsiades, N.; Neuberg, D.; Goloubeva, O.; Pien, C. S.; Adams, J.; Gupta, D.; Richardson, P. G.; Munshi, N. C.; Anderson, K. C. Proteasome Inhibitor PS-341 Inhibits Human Myeloma Cell Growth in Vivo and Prolongs Survival in a Murine Model. *Cancer Res* **2002**, *62* (17), 4996–5000.

(28) Lei, M.; Feng, H.; Wang, C.; Li, H.; Shi, J.; Wang, J.; Liu, Z.; Chen, S.; Hu, S.; Zhu, Y. 3D-QSAR-Aided Design, Synthesis, in Vitro and in Vivo Evaluation of Dipeptidyl Boronic Acid Proteasome Inhibitors and Mechanism Studies. *Bioorg Med Chem* **2016**, *24* (11), 2576–2588. https://doi.org/10.1016/j.bmc.2016.04.025.

(29) Groll, M.; Berkers, C. R.; Ploegh, H. L.; Ovaa, H. Crystal Structure of the Boronic Acid-Based Proteasome Inhibitor Bortezomib in Complex with the Yeast 20S Proteasome. *Structure* **2006**, *14* (3), 451–456. https://doi.org/10.1016/j.str.2005.11.019.

(30) Rock, F. L.; Mao, W.; Yaremchuk, A.; Tukalo, M.; Crépin, T.; Zhou, H.; Zhang, Y.-K.; Hernandez, V.; Akama, T.; Baker, S. J.; Plattner, J. J.; Shapiro, L.; Martinis, S. A.; Benkovic, S. J.; Cusack, S.; Alley, M. R. K. An Antifungal Agent Inhibits an Aminoacyl-TRNA Synthetase by Trapping TRNA in the Editing Site. *Science* **2007**, *316* (5832), 1759–1761. https://doi.org/10.1126/science.1142189.

(31) Akçay, G.; Belmonte, M. A.; Aquila, B.; Chuaqui, C.; Hird, A. W.; Lamb, M. L.; Rawlins, P. B.; Su, N.; Tentarelli, S.; Grimster, N. P.; Su, Q. Inhibition of Mcl-1 through Covalent Modification of a Noncatalytic Lysine Side Chain. *Nat Chem Biol* **2016**, *12* (11), 931–936. https://doi.org/10.1038/nchembio.2174.

(32) Cal, P. M. S. D.; Vicente, J. B.; Pires, E.; Coelho, A. V.; Veiros, L. F.; Cordeiro, C.; Gois, P. M. P. Iminoboronates: A New Strategy for Reversible Protein Modification. *J Am Chem Soc* **2012**, *134* (24), 10299–10305. https://doi.org/10.1021/ja303436y.

(33) Reja, R. M.; Wang, W.; Lyu, Y.; Haeffner, F.; Gao, J. Lysine-Targeting Reversible Covalent Inhibitors with Long Residence Time. *J Am Chem Soc* **2022**, *144* (3), 1152–1157. https://doi.org/10.1021/jacs.1c12702.

(34) Lonsdale, R.; Ward, R. A. Structure-Based Design of Targeted Covalent Inhibitors. *Chem Soc Rev* **2018**, *47* (11), 3816–3830. https://doi.org/10.1039/C7CS00220C.

(35) Douglas, C. D.; Grandinetti, L.; Easton, N. M.; Kuehm, O. P.; Hayden, J. A.; Hamilton, M. C.; St. Maurice, M.; Bearne, S. L. Slow-Onset, Potent Inhibition of Mandelate Racemase by 2-Formylphenylboronic Acid. An Unexpected Adduct Clasps the Catalytic Machinery. *Biochemistry* **2021**, *60* (32), 2508–2518. https://doi.org/10.1021/acs.biochem.1c00374.

(36) Brooks, W. L. A.; Deng, C. C.; Sumerlin, B. S. Structure–Reactivity Relationships in Boronic Acid–Diol Complexation. *ACS Omega* **2018**, *3* (12), 17863–17870. https://doi.org/10.1021/acsomega.8b02999.

(37) Nan, K.; Jiang, Y.-N.; Li, M.; Wang, B. Recent Progress in Diboronic-Acid-Based Glucose Sensors. *Biosensors (Basel)* **2023**, *13* (6), 618. https://doi.org/10.3390/bios13060618.

(38) Rangaswamy, A. M. M.; Beh, M. H. R.; Soleimani, E.; Sequeira, S.; Cormier, J.; Robertson, K. N.; Jakeman, D. L. Synthesis of 5'-Thymidine-Conjugated Formylphenylboronic Acids as Potential Lysine Targeting Iminoboronate Reversible Covalent Enzyme Probes. *J Org Chem* **2022**, *87* (21), 13542–13555. https://doi.org/10.1021/acs.joc.2c01000.

(39) Norrild, J. C.; Eggert, H. Evidence for Mono- and Bisdentate Boronate Complexes of Glucose in the Furanose Form. Application of 1JC-C Coupling Constants as a Structural Probe. *J Am Chem Soc* **1995**, *117* (5), 1479–1484. https://doi.org/10.1021/ja00110a003.

(40) Gao, Y.; Chachadi, V. B.; Cheng, P.-W.; Brockhausen, I. Glycosylation Potential of Human Prostate Cancer Cell Lines. *Glycoconj J* **2012**, *29* (7), 525–537. https://doi.org/10.1007/s10719-012-9428-8.

(41) Springsteen, G.; Wang, B. A Detailed Examination of Boronic Acid–Diol Complexation. *Tetrahedron* **2002**, *58* (26), 5291–5300. https://doi.org/10.1016/S0040-4020(02)00489-1.

(42) Whyte, G. F.; Vilar, R.; Woscholski, R. Molecular Recognition with Boronic Acids—Applications in Chemical Biology. *J Chem Biol* **2013**, *6* (4), 161–174. https://doi.org/10.1007/s12154-013-0099-0.

(43) Groleau, R. R.; James, T. D.; Bull, S. D. The Bull-James Assembly: Efficient Iminoboronate Complex Formation for Chiral Derivatization and Supramolecular Assembly. *Coord Chem Rev* **2021**, *428*, 213599. https://doi.org/10.1016/j.ccr.2020.213599.

(44) Kazmi, M. Z. H.; Rygus, J. P. G.; Ang, H. T.; Paladino, M.; Johnson, M. A.; Ferguson, M. J.; Hall, D. G. Lewis or Brønsted? A Rectification of the Acidic and Aromatic Nature of Boranol-Containing Naphthoid Heterocycles. *J Am Chem Soc* **2021**, *143* (27), 10143–10156. https://doi.org/10.1021/jacs.1c02462.

(45) Krężel, A.; Bal, W. A Formula for Correlating p K a Values Determined in D 2 O and H 2 O. *J Inorg Biochem* **2004**, *98* (1), 161–166. https://doi.org/10.1016/j.jinorgbio.2003.10.001.

(46) Matsumoto, A.; Stephenson-Brown, A. J.; Khan, T.; Miyazawa, T.; Cabral, H.; Kataoka, K.; Miyahara, Y. Heterocyclic Boronic Acids Display Sialic Acid Selective Binding in a Hypoxic Tumor Relevant Acidic Environment. *Chem Sci* **2017**, *8* (9), 6165–6170. https://doi.org/10.1039/C7SC01905J.

(47) Graham, B. J.; Windsor, I. W.; Gold, B.; Raines, R. T. Boronic Acid with High Oxidative Stability and Utility in Biological Contexts. *Proceedings of the National Academy of Sciences* **2021**, *118* (10). https://doi.org/10.1073/pnas.2013691118.

(48) Means, G. E.; Feeney, R. E. Reductive Alkylation of Amino Groups in Proteins. *Biochemistry* **1968**, *7* (6), 2192–2201. https://doi.org/10.1021/bi00846a023.

(49) Faustino, H.; Silva, M. J. S. A.; Veiros, L. F.; Bernardes, G. J. L.; Gois, P. M. P. Iminoboronates Are Efficient Intermediates for Selective, Rapid and Reversible N-Terminal Cysteine Functionalisation. *Chem Sci* **2016**, *7* (8), 5052–5058. https://doi.org/10.1039/C6SC01520D.

(50) Cambray, S.; Gao, J. Versatile Bioconjugation Chemistries of *Ortho* -Boronyl Aryl Ketones and Aldehydes. *Acc Chem Res* **2018**, *51* (9), 2198–2206. https://doi.org/10.1021/acs.accounts.8b00154.

(51) Akgun, B.; Hall, D. G. Boronic Acids as Bioorthogonal Probes for Site-Selective Labeling of Proteins. *Angewandte Chemie International Edition* **2018**, *57* (40), 13028–13044. https://doi.org/10.1002/anie.201712611.

(52) Gutiérrez-Moreno, N. J.; Medrano, F.; Yatsimirsky, A. K. Schiff Base Formation and Recognition of Amino Sugars, Aminoglycosides and Biological Polyamines by 2-Formyl Phenylboronic Acid in Aqueous Solution. *Org Biomol Chem* **2012**, *10* (34), 6960–6972. https://doi.org/10.1039/c2ob26290h.

(53) Bandyopadhyay, A.; Cambray, S.; Gao, J. Fast and Selective Labeling of N-Terminal Cysteines at Neutral PH via Thiazolidino Boronate Formation. *Chem Sci* **2016**, *7* (7), 4589–4593. https://doi.org/10.1039/C6SC00172F.

(54) Sýkora, D.; Jindřich, J.; Král, V.; Jakubek, M.; Tatar, A.; Kejík, Z.; Martásek, P.; Zakharov, S. Formaldehyde Reacts with Amino Acids and Peptides with a Potential Role in Acute Methanol Intoxication. *J Anal Toxicol* **2020**, *44* (8), 880–885. https://doi.org/10.1093/jat/bkaa039.

(55) Thordarson, P. Determining Association Constants from Titration Experiments in Supramolecular Chemistry. *Chem. Soc. Rev.* **2011**, *40* (3), 1305–1323. https://doi.org/10.1039/C0CS00062K.

(56) Yan, J.; Springsteen, G.; Deeter, S.; Wang, B. The Relationship among PKa, PH, and Binding Constants in the Interactions between Boronic Acids and Diols—It Is Not as Simple as It Appears. *Tetrahedron* **2004**, *60* (49), 11205–11209. https://doi.org/10.1016/j.tet.2004.08.051.

(57) Tomsho, J. W.; Benkovic, S. J. Examination of the Reactivity of Benzoxaboroles and Related Compounds with a *Cis* -Diol. *J Org Chem* **2012**, *77* (24), 11200–11209. https://doi.org/10.1021/jo302264g.

(58) Wiskur, S. L.; Lavigne, J. J.; Ait-Haddou, H.; Lynch, V.; Chiu, Y. H.; Canary, J. W.; Anslyn, E. V. P K_a Values and Geometries of Secondary and Tertiary Amines Complexed to Boronic AcidsImplications for Sensor Design. *Org Lett* **2001**, *3* (9), 1311–1314. https://doi.org/10.1021/ol0156805.

(59) Williams, G. T.; Kedge, J. L.; Fossey, J. S. Molecular Boronic Acid-Based Saccharide Sensors. *ACS Sens* **2021**, *6* (4), 1508–1528. https://doi.org/10.1021/acssensors.1c00462.

(60) James, T. D.; Sandanayake, K. R. A. S.; Iguchi, R.; Shinkai, S. Novel Saccharide-Photoinduced Electron Transfer Sensors Based on the Interaction of Boronic Acid and Amine. *J Am Chem Soc* **1995**, *117* (35), 8982–8987. https://doi.org/10.1021/ja00140a013.

(61) Di Pasquale, A.; Tommasone, S.; Xu, L.; Ma, J.; Mendes, P. M. Cooperative Multipoint Recognition of Sialic Acid by Benzoboroxole-Based Receptors Bearing Cationic Hydrogen-Bond Donors. *J Org Chem* **2020**, *85* (13), 8330–8338. https://doi.org/10.1021/acs.joc.0c00173.

(62) Melavanki, R.; Kusanur, R.; Sadasivuni, K. K.; Singh, D.; Patil, N. R. Investigation of Interaction between Boronic Acids and Sugar: Effect of Structural Change of Sugars on Binding Affinity Using Steady State and Time Resolved Fluorescence Spectroscopy and Molecular Docking. *Heliyon* **2020**, *6* (10), e05081. https://doi.org/10.1016/j.heliyon.2020.e05081.

(63) Tran, T. M.; Alan, Y.; Glass, T. E. A Highly Selective Fluorescent Sensor for Glucosamine. *Chemical Communications* **2015**, *51* (37), 7915–7918. https://doi.org/10.1039/C5CC00415B.

Appendix A. pK_a Using UV-Vis Spectroscopy Absorbance Plots and Calculations

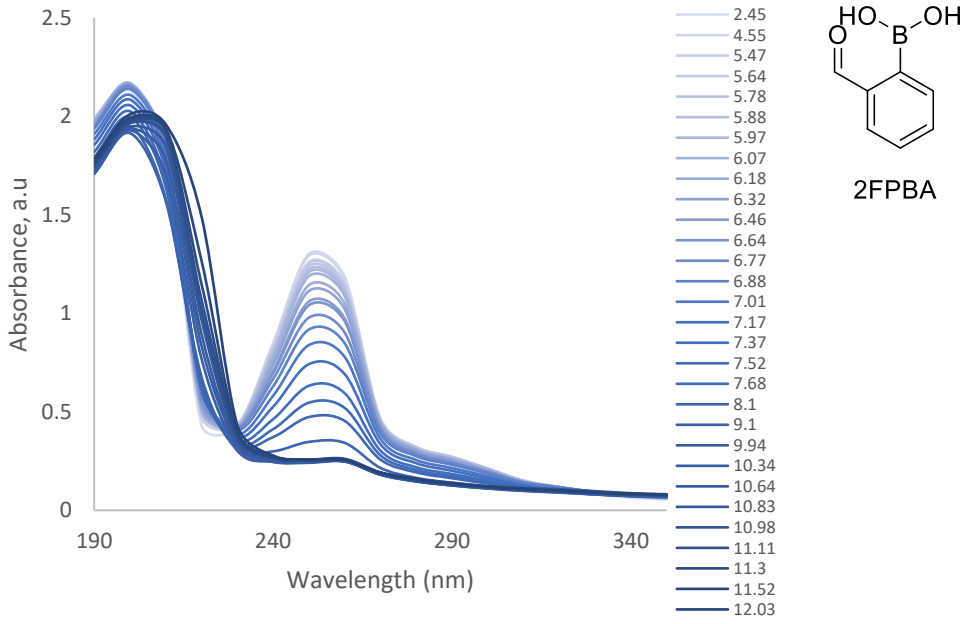

Spectroscopy changes of compound 2FPBA with increasing pH values.

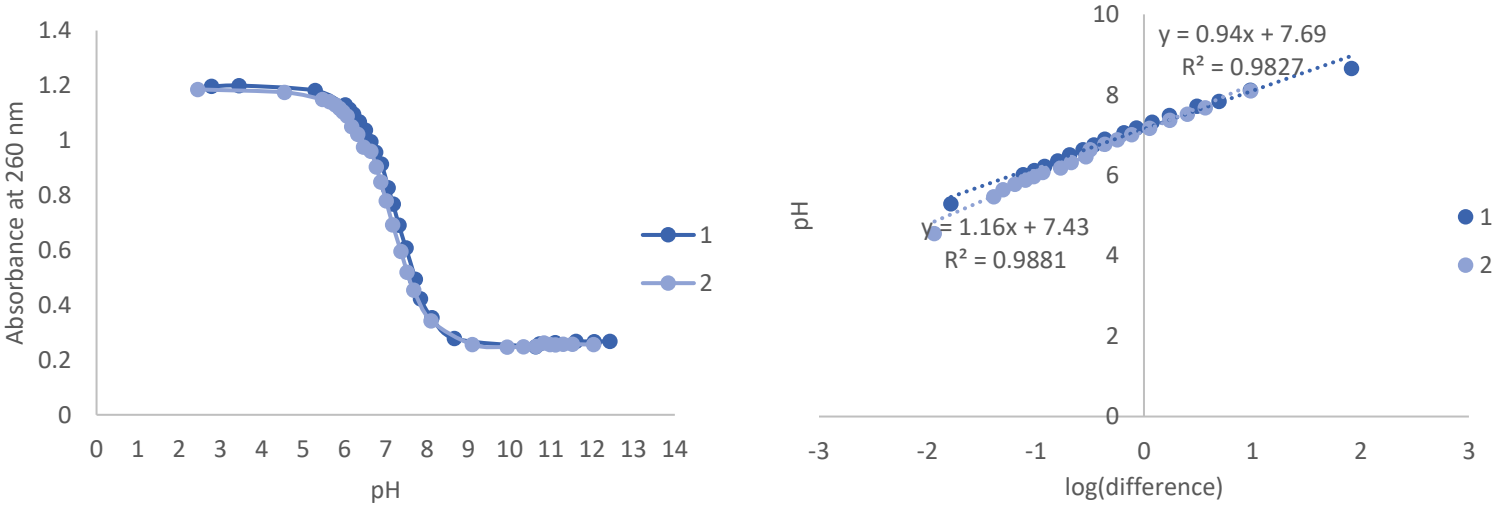

pK_a calculations of 2FPBA. Left: pH versus maximum absorbance at 260 nm. Right: log(difference) using equation 2.2.3 versus pH. The y-intercept is the calculated pK_a. Average pK_a is 7.6.

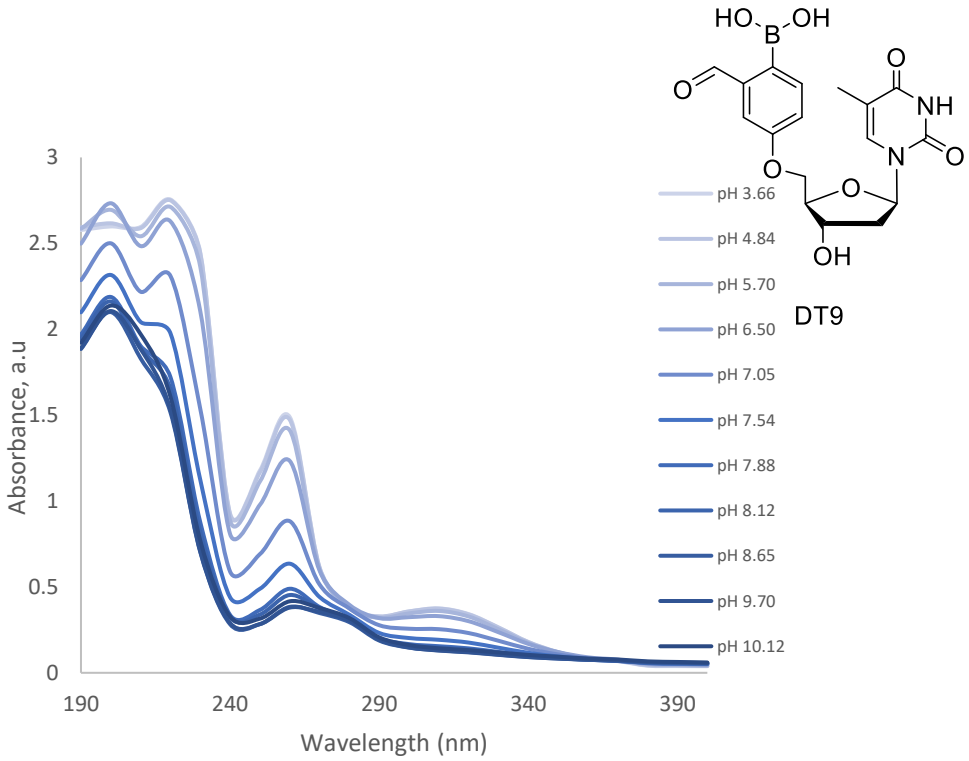

Spectroscopy changes of compound DT9 with increasing pH values.

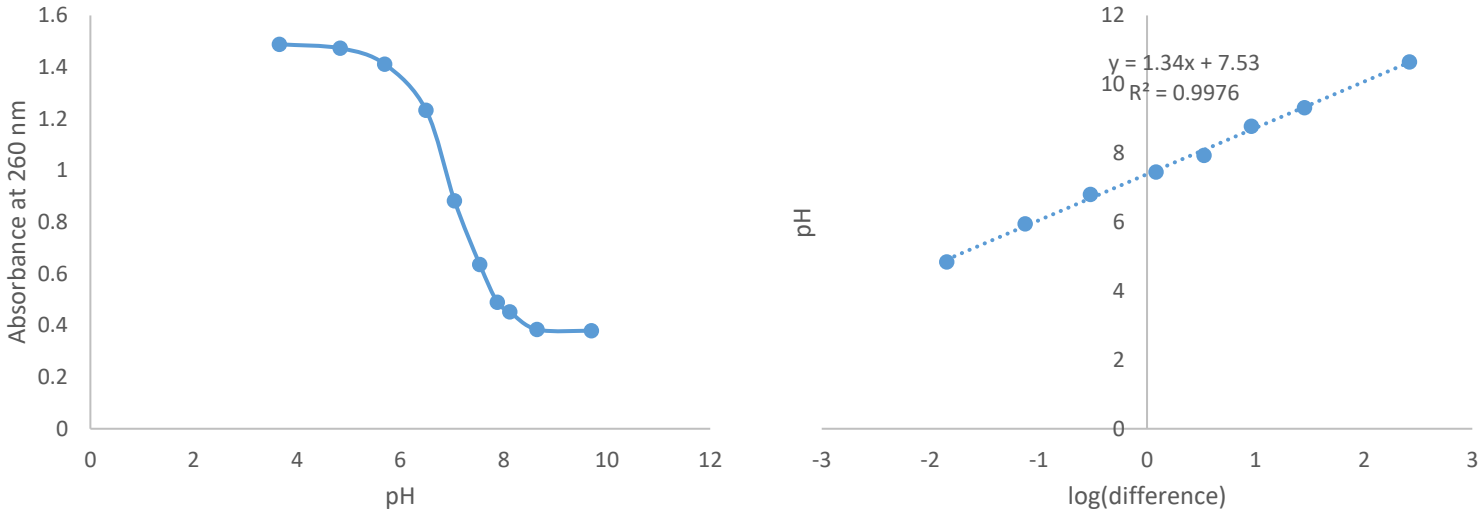

pK_a calculations of DT9. Left: pH versus maximum absorbance at 260 nm. Right: log(difference) using equation 2.2.3 versus pH. The y-intercept is the calculated pK_a. Average pK_a is 7.5.

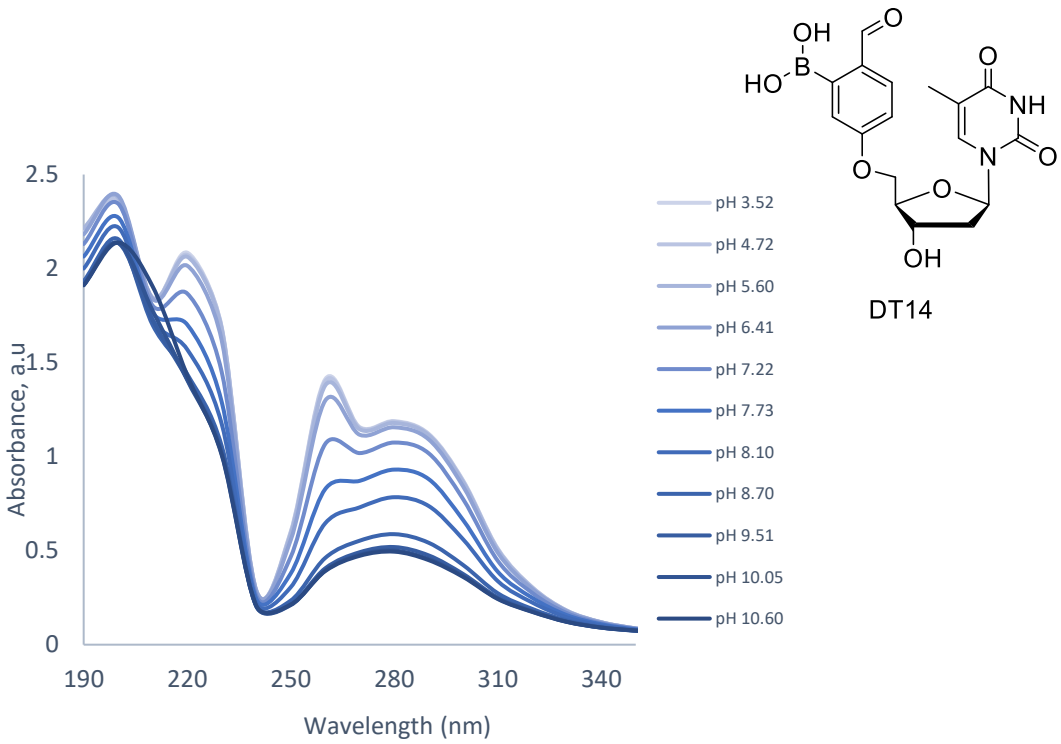

Spectroscopy changes of compound DT14 with increasing pH values.

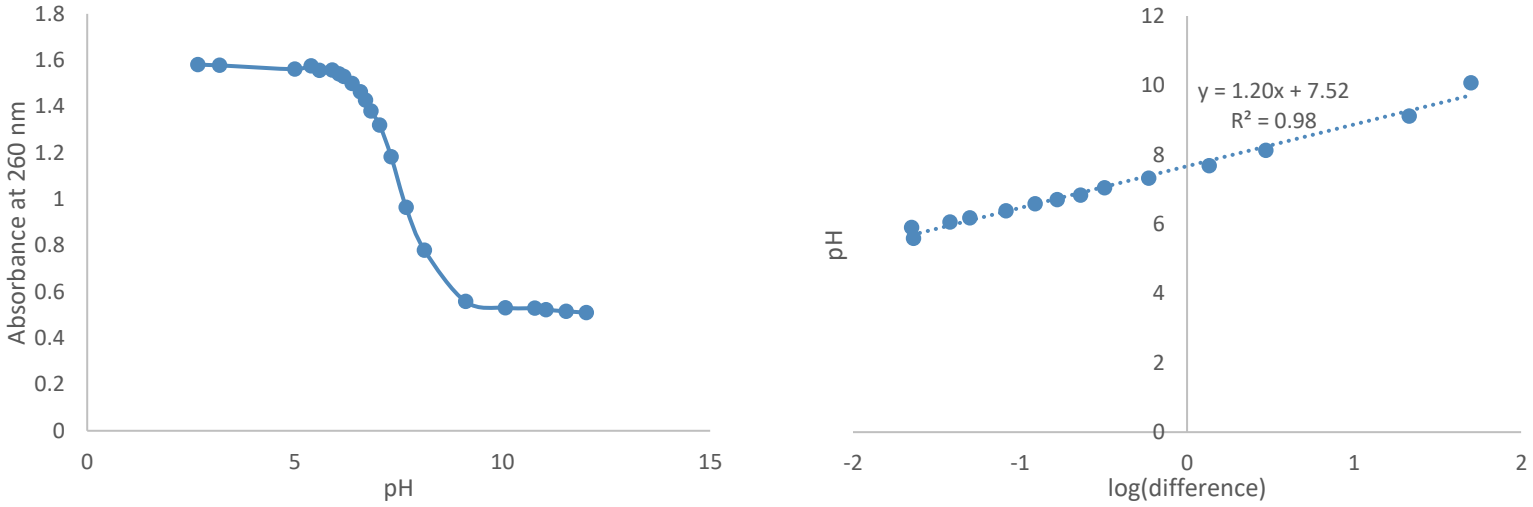

pK_a calculations of DT14. Left: pH versus maximum absorbance at 260 nm. Right: log(difference) using equation 2.2.3 versus pH. The y-intercept is the calculated pK_a. Average pK_a is 7.5.

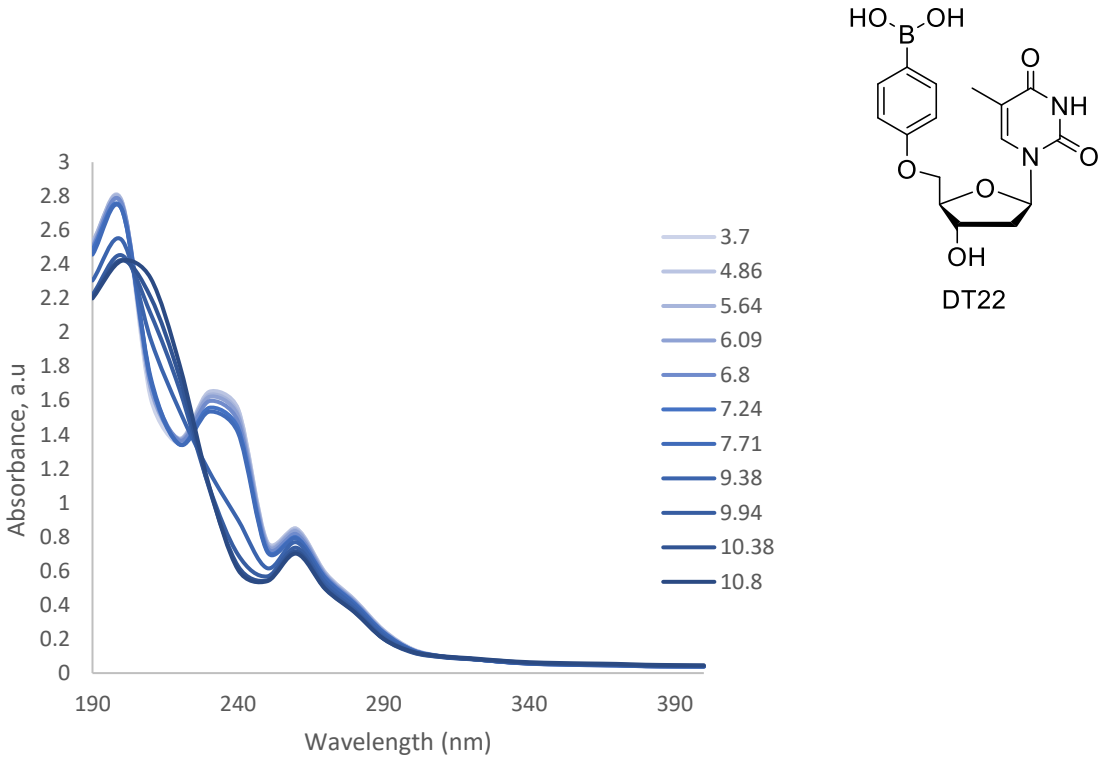

Spectroscopy changes of compound DT22 with increasing pH values.

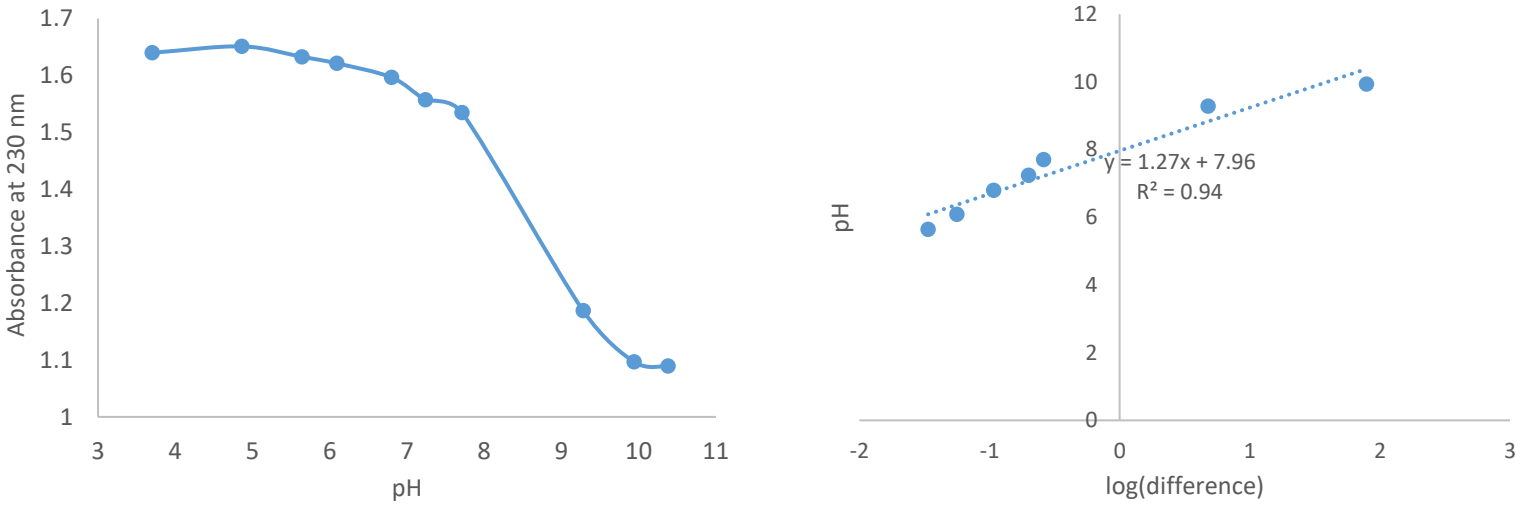

pK_a calculations of DT22. Left: pH versus maximum absorbance at 230 nm. Right: log(difference) using equation 2.2.3 versus pH. The y-intercept is the calculated pK_a. Average pK_a is 7.9.

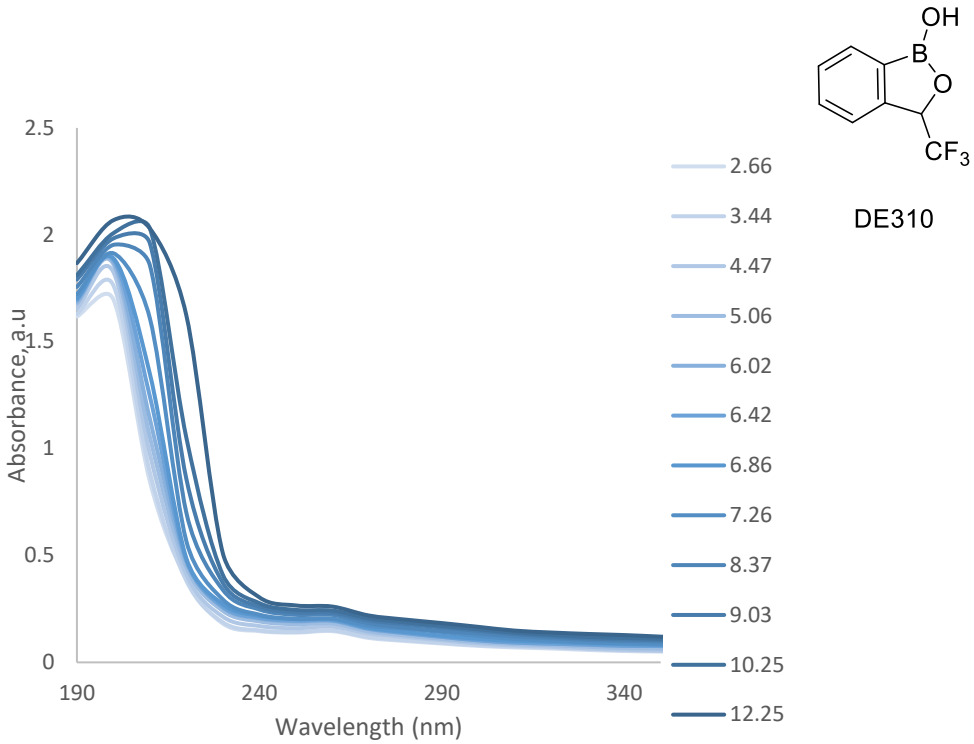

Spectroscopy changes of compound DE310 with increasing pH values.

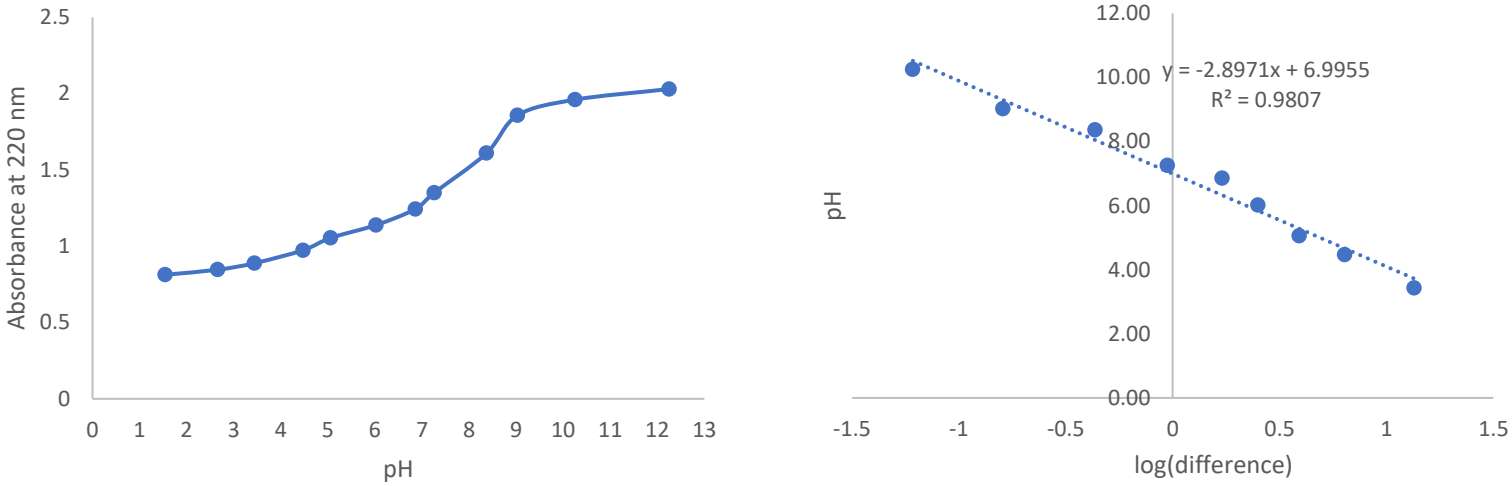

pK_a calculations of DE310. Left: pH versus maximum absorbance at 220 nm. Right: log(difference) using equation 2.2.3 versus pH. The y-intercept is the calculated pK_a. Average pK_a is 6.9.

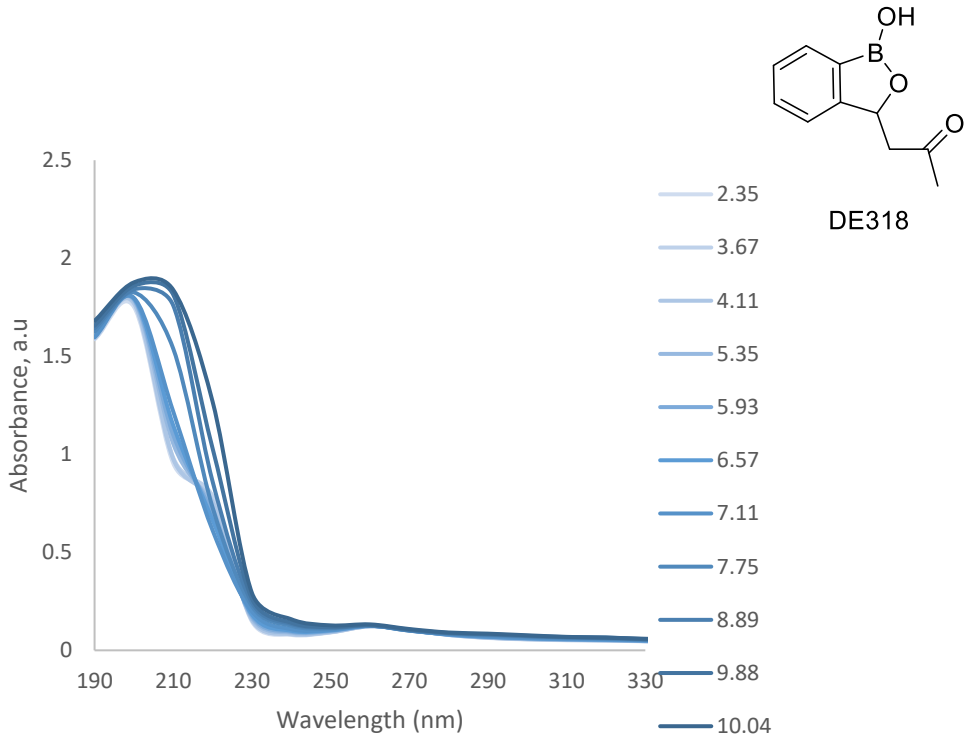

Spectroscopy changes of compound DE318 with increasing pH values.

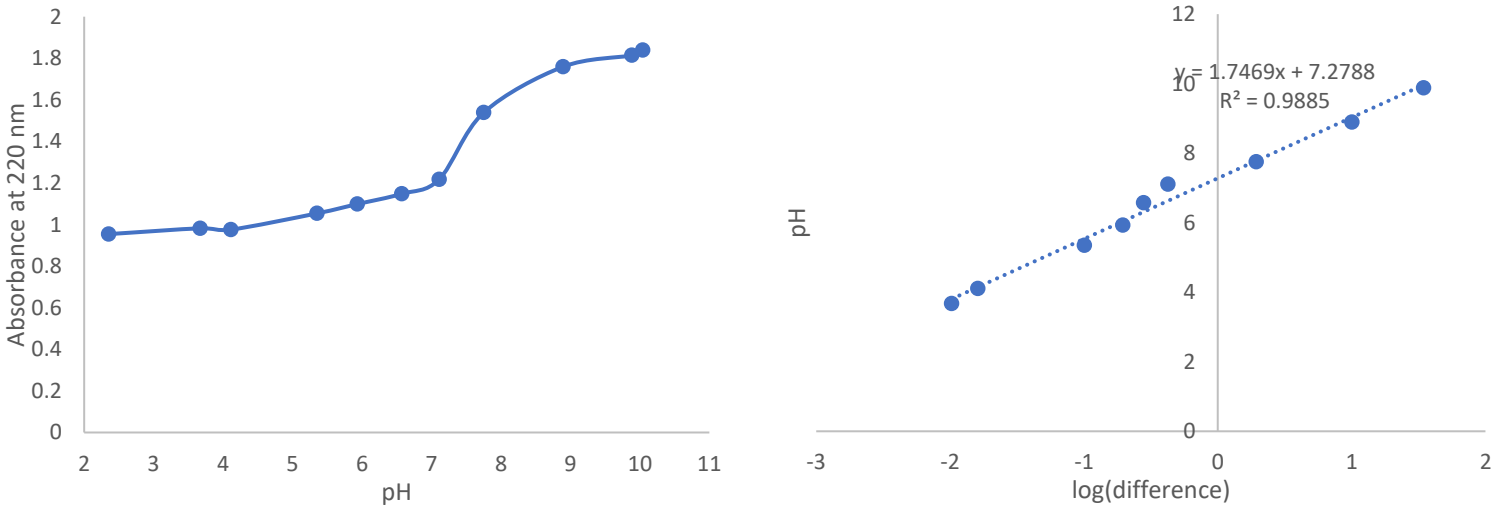

pK_a calculations of DE318. Left: pH versus maximum absorbance at 220 nm. Right: log(difference) using equation 2.2.3 versus pH. The y-intercept is the calculated pK_a. Average pK_a is 7.3.

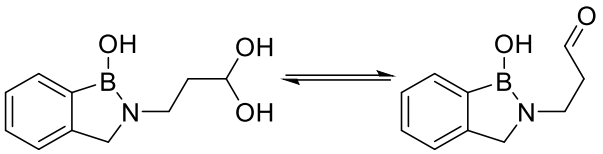

DE321

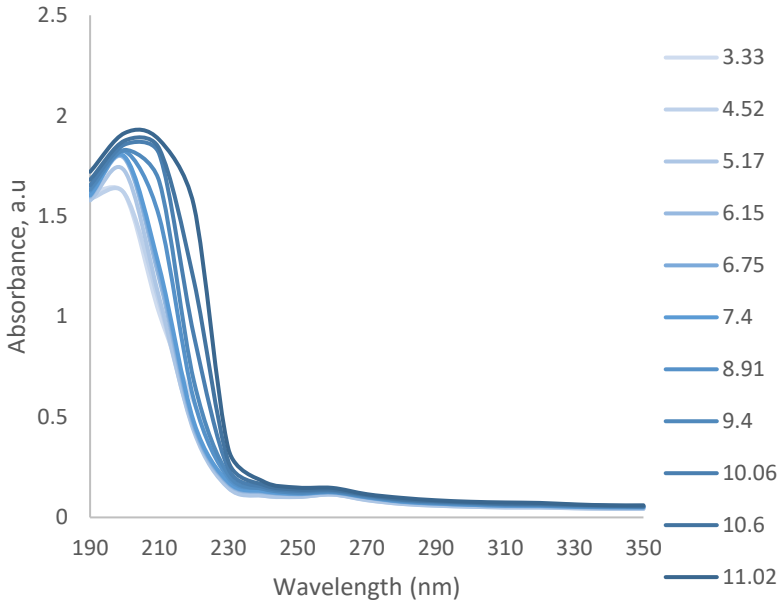

Spectroscopic changes of compound DE321 with increasing pH values.

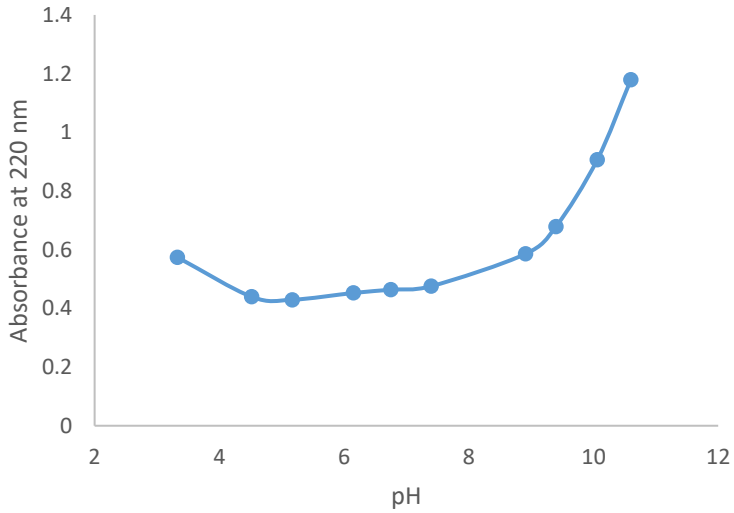

pH versus maximum absorbance at 220 nm showing multiple pK_a values.

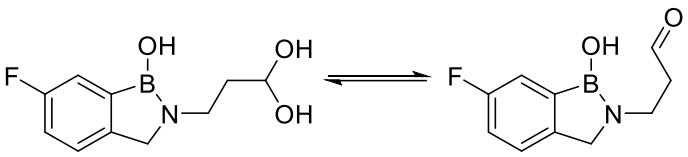

DE342

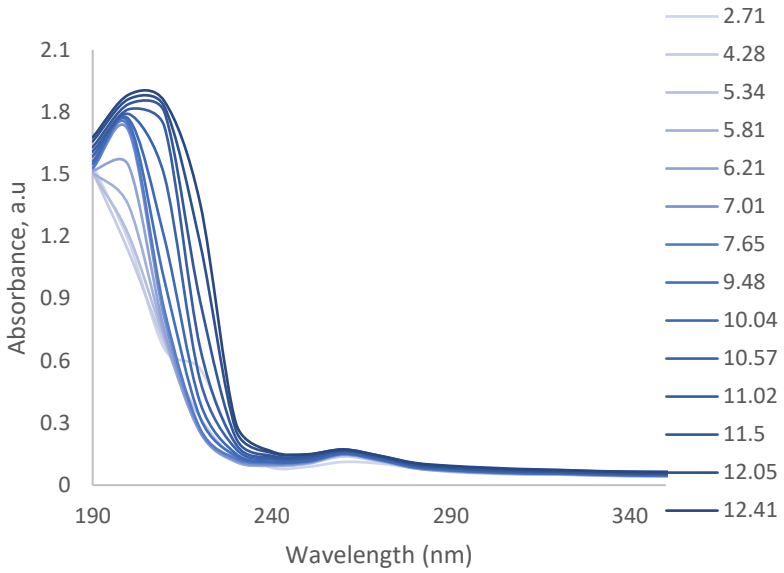

Spectroscopy changes of compound DE342 with increasing pH values.

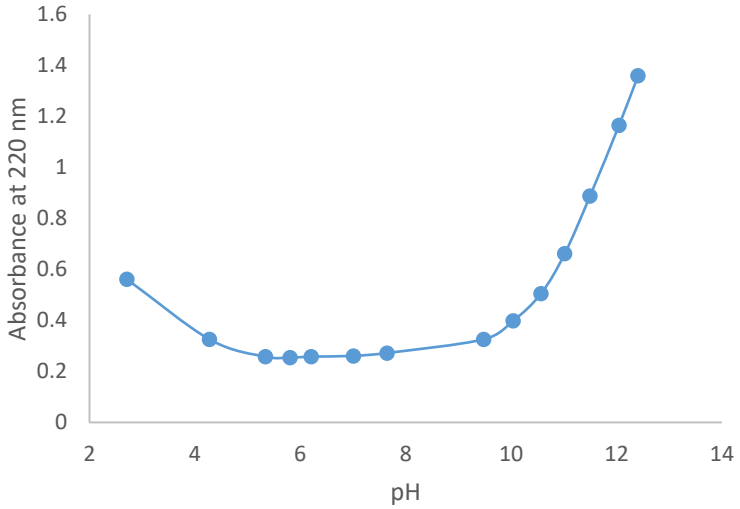

pH versus maximum absorbance at 220 nm showing multiple pK_a values.

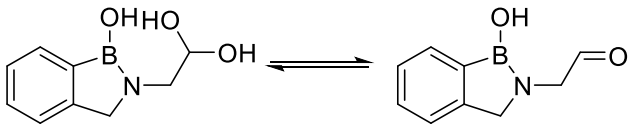

DE343

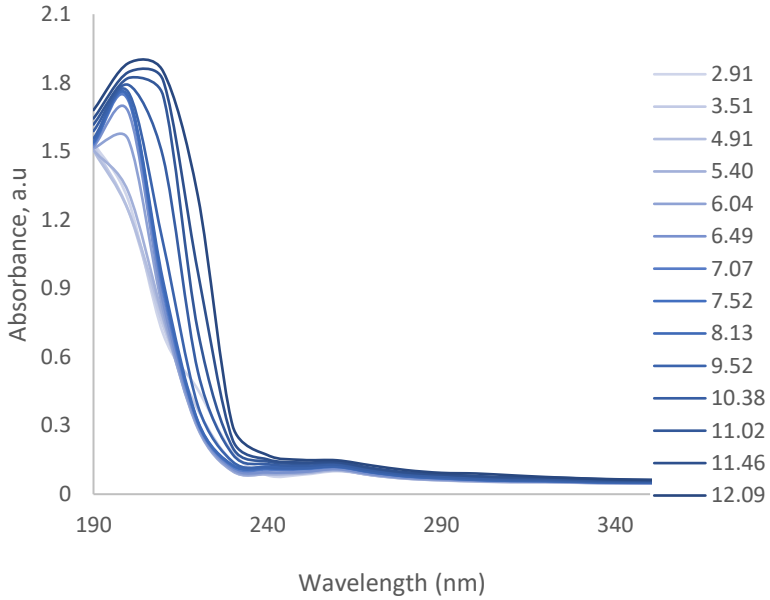

Spectroscopy changes of compound DE343 with increasing pH values.

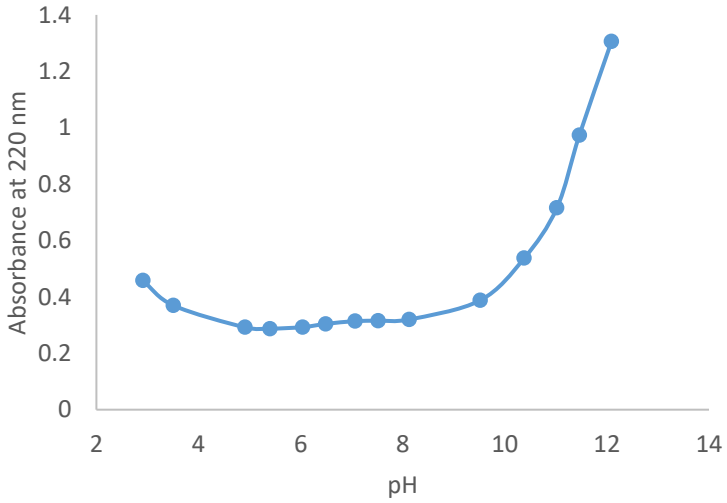

pH versus maximum absorbance at 220 nm showing multiple pK_a values.

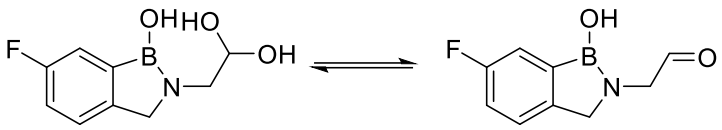

DE344

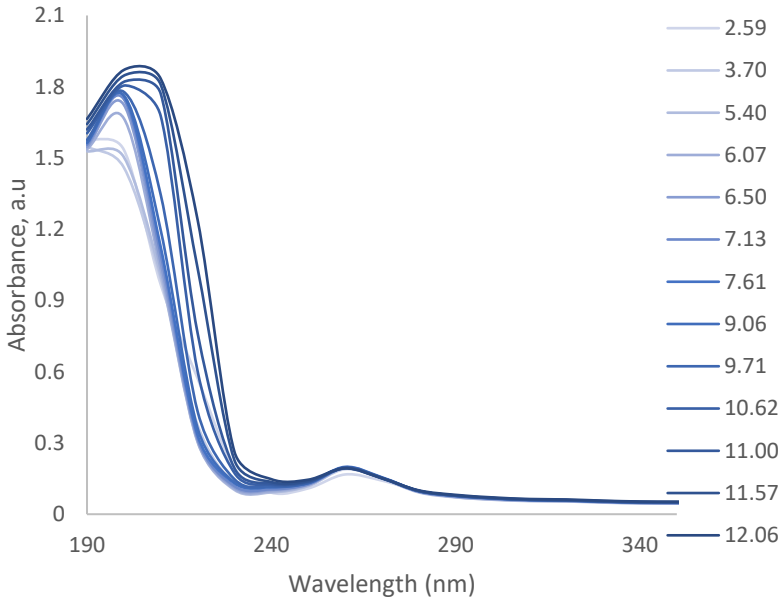

Spectroscopy changes of compound DE344 with increasing pH values.

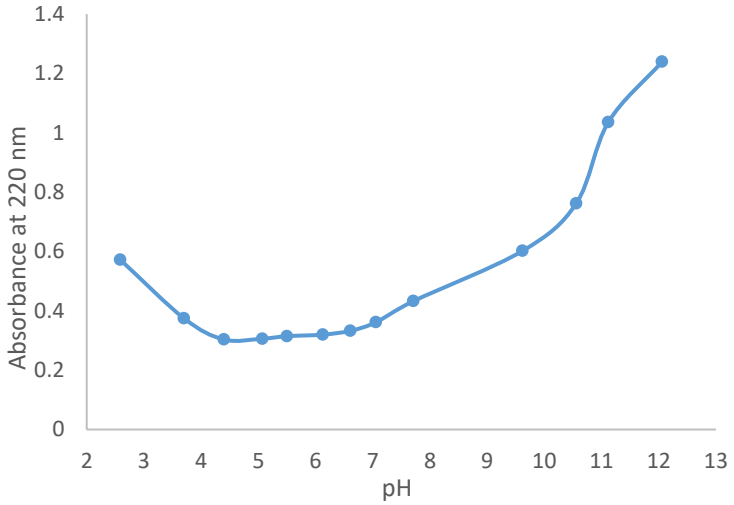

pH versus maximum absorbance at 210 nm showing multiple pK_a values.

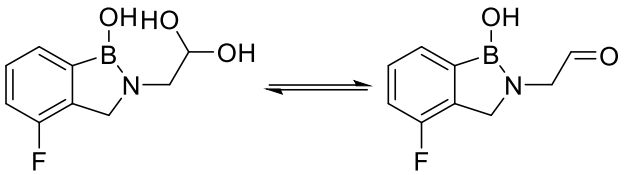

DE347

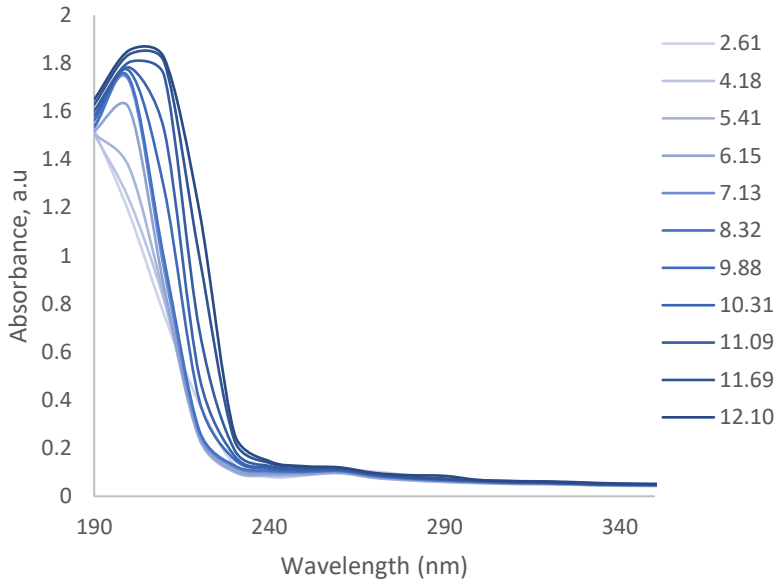

Spectroscopy changes of compound DE347 with increasing pH values.

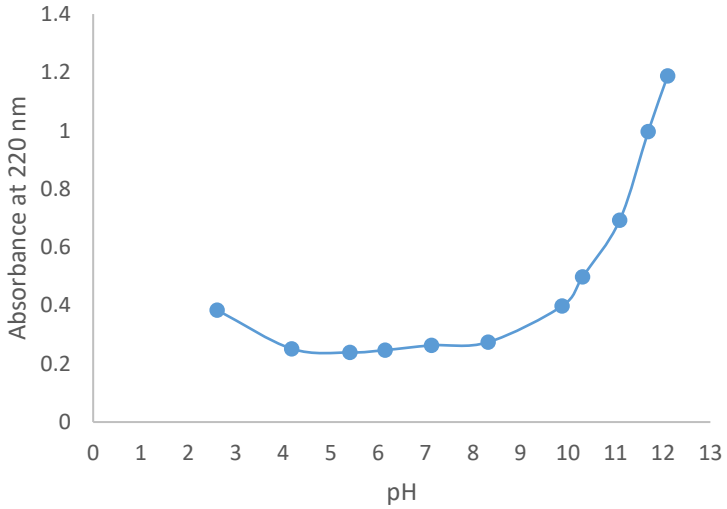

pH versus maximum absorbance at 220 nm showing multiple pK_a values.

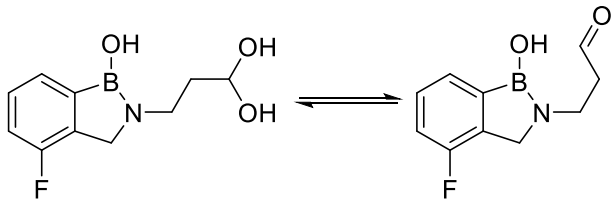

DE348

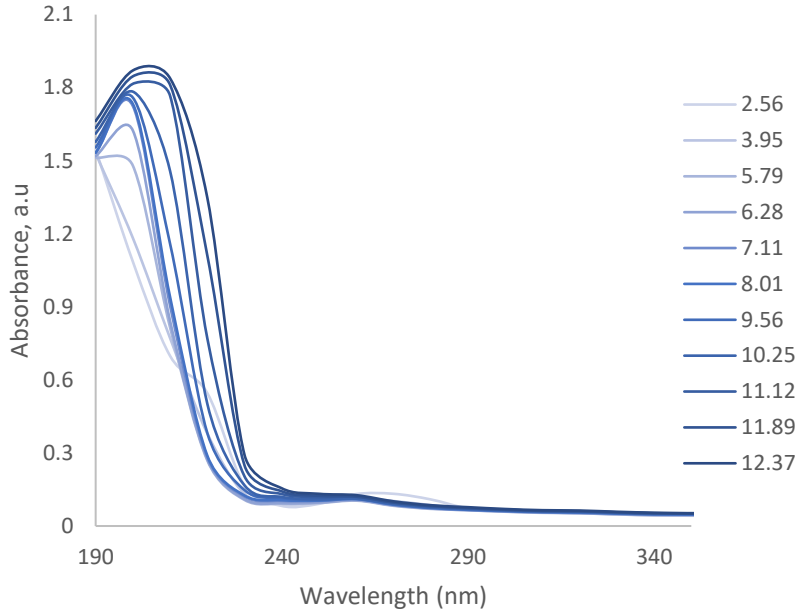

Spectroscopy changes of compound DE348 with increasing pH values.

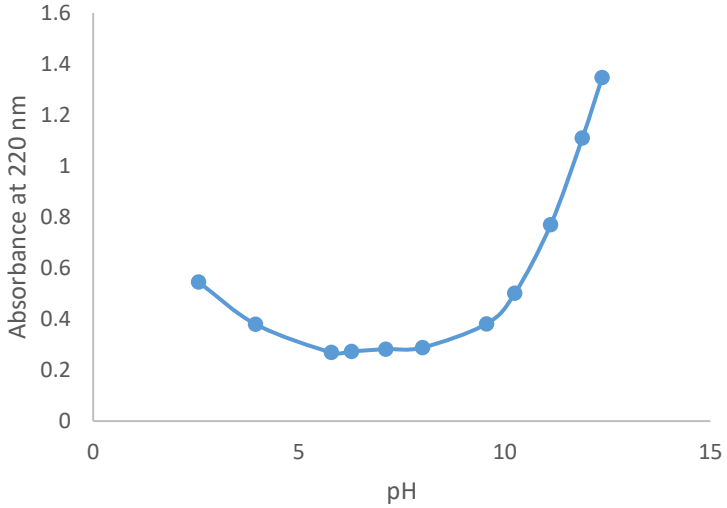

pH versus maximum absorbance at 220 nm showing multiple pK_a values.

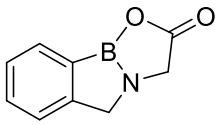

CO1

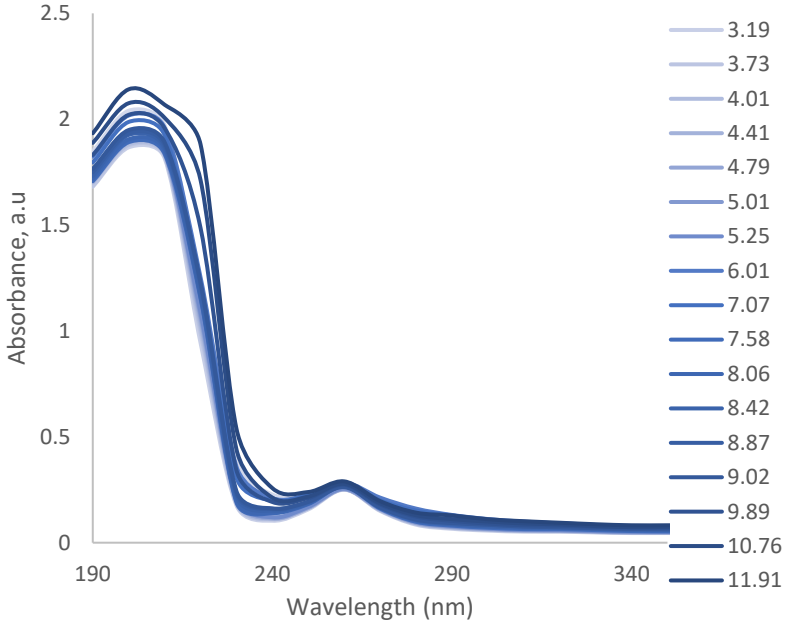

Spectroscopy changes of compound CO1 with increasing pH values.

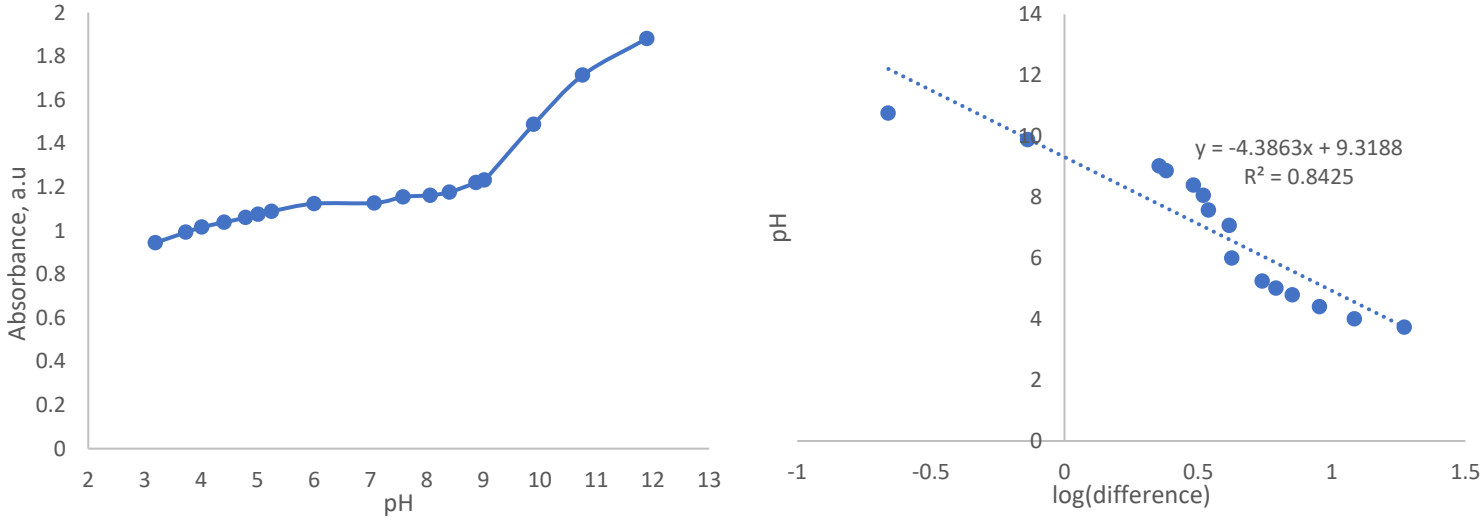

pK_a calculations of CO1. Left: pH versus maximum absorbance at 220 nm. Right: log(difference) using equation 2.2.3 versus pH. The y-intercept is the calculated pK_a. Average pK_a value is 9.3.

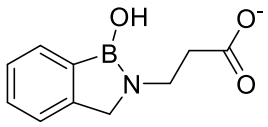

CO2

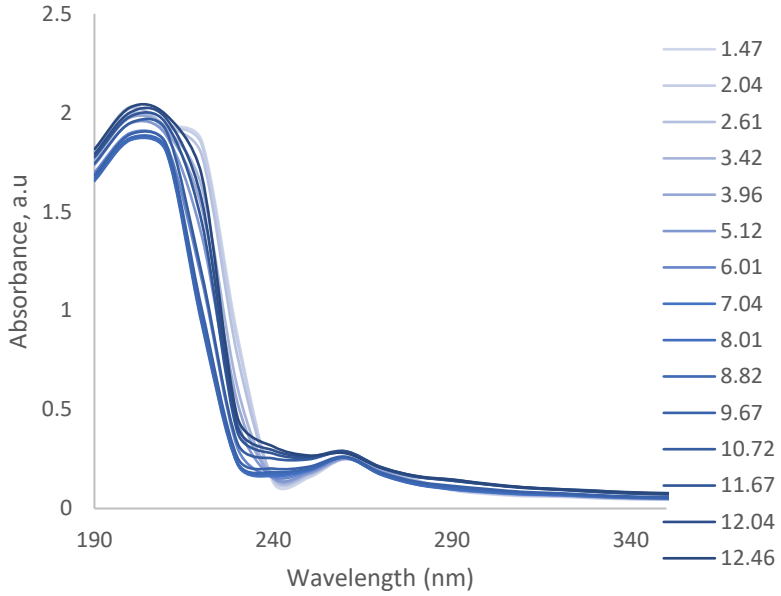

Spectroscopy changes of compound CO2 with increasing pH values.

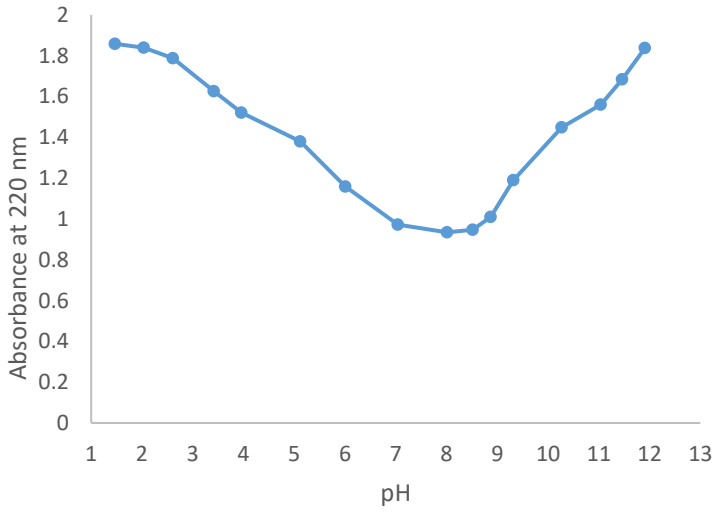

pH versus maximum absorbance at 220 nm showing multiple pK_a values.

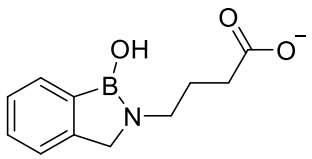

CO3

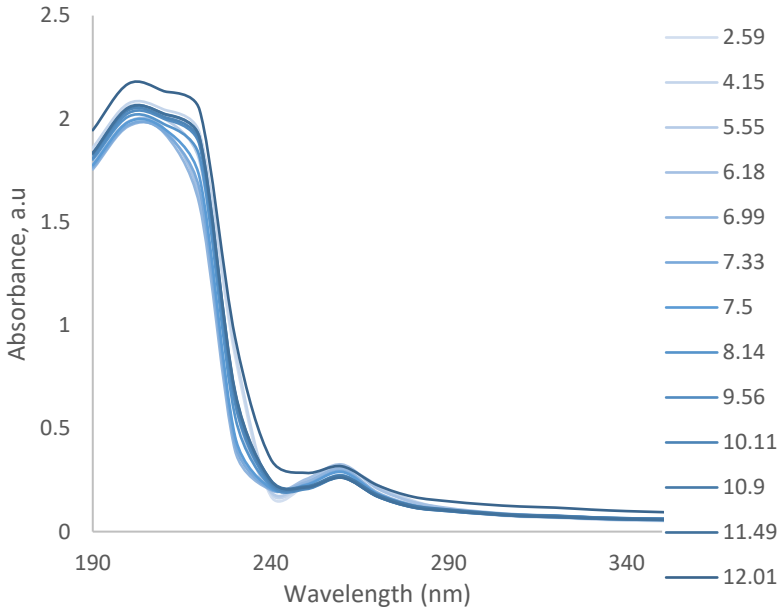

Spectroscopy changes of compound CO3 with increasing pH values.

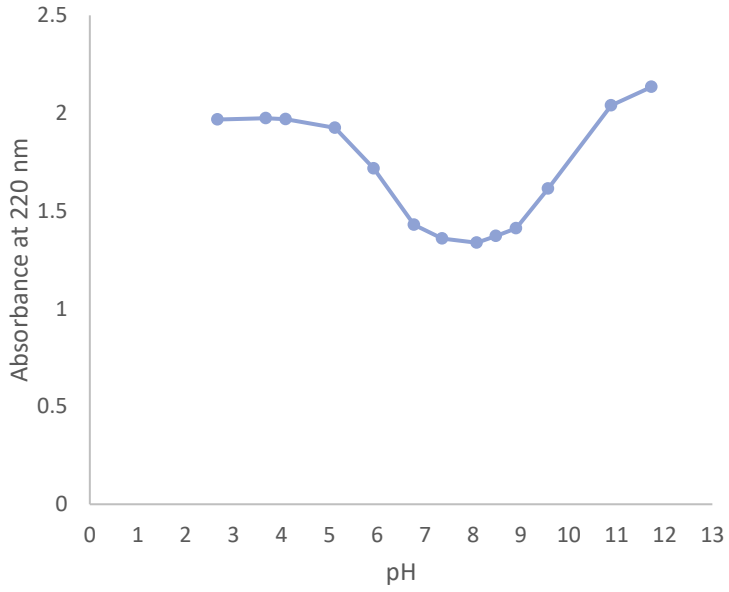

pH versus maximum absorbance at 220 nm showing multiple pK_a values.

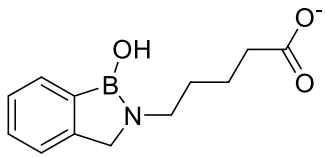

CO4

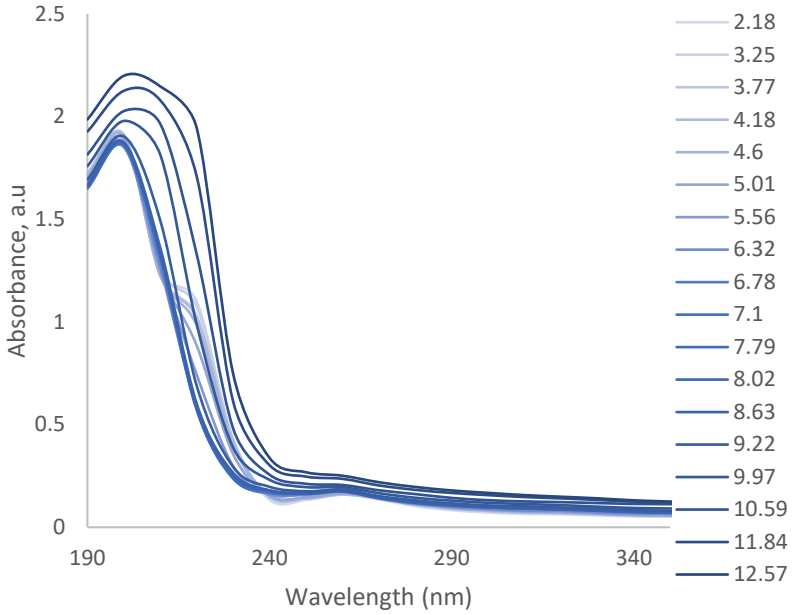

Spectroscopy changes of compound CO4 with increasing pH values.

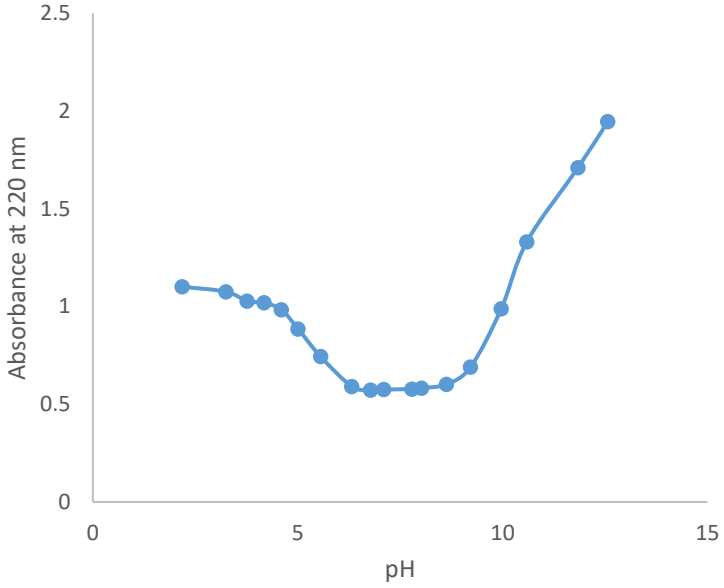

pH versus maximum absorbance at 220 nm showing multiple pK_a values.

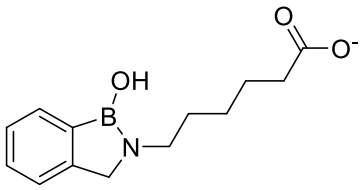

CO5

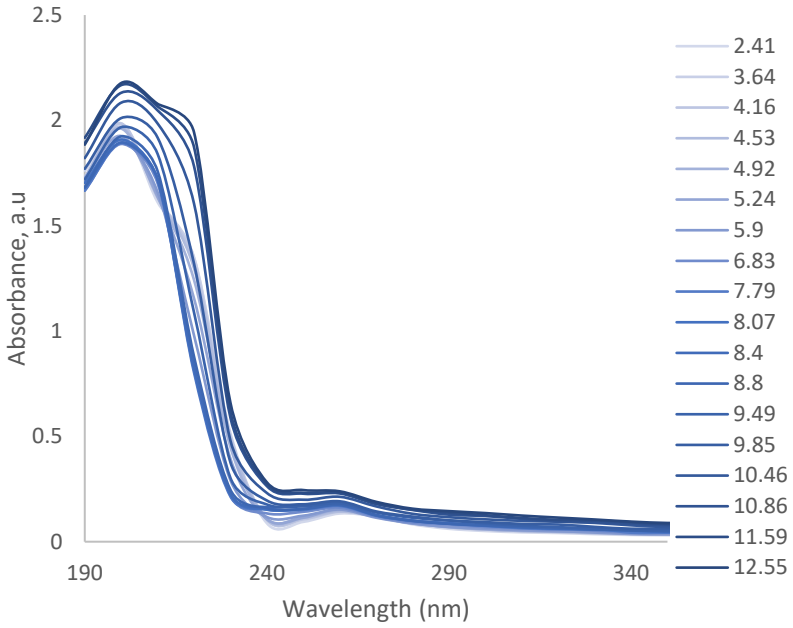

Spectroscopy changes of compound CO5 with increasing pH values.

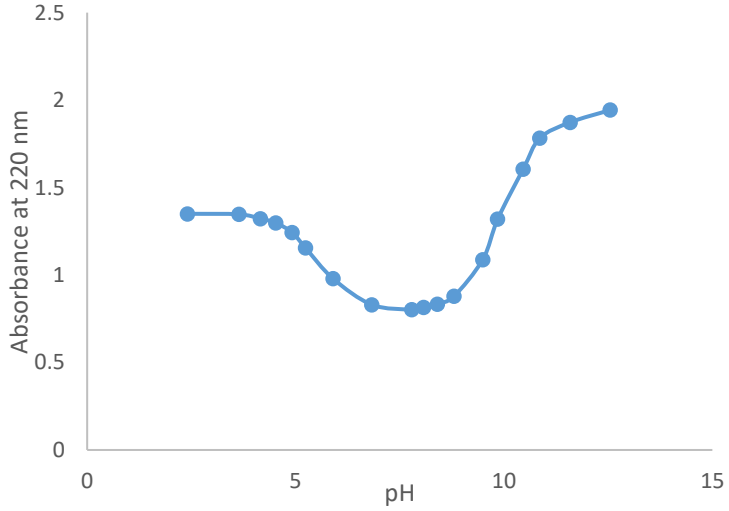

pH versus maximum absorbance at 220 nm showing multiple pK_a values.

Appendix B. P*K*$_a$ Using ^{1}H, ^{11}B and ^{19}F NMR Spectroscopy Plots And Calculations

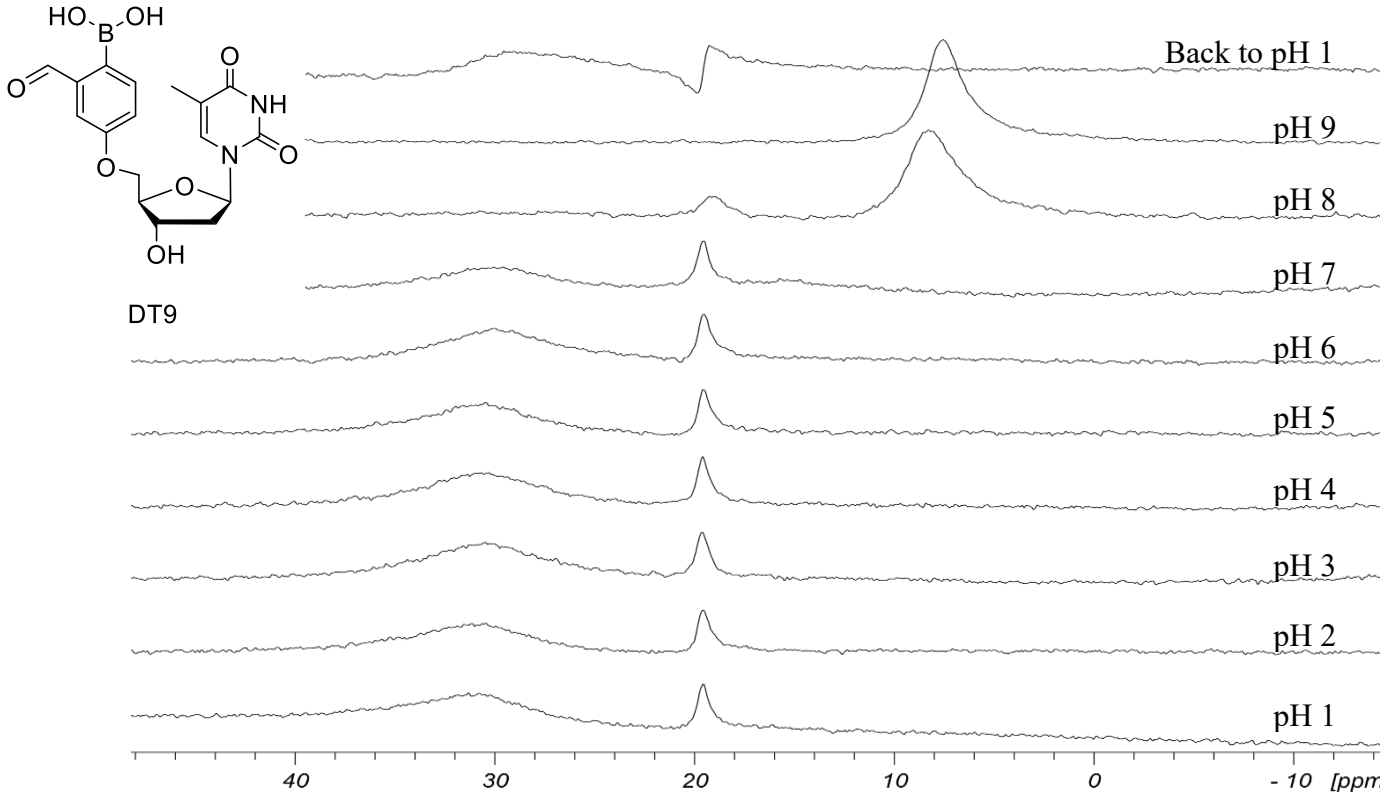

^{11}B NMR Spectrum (500 MHz, D_2O) of DT9 with increasing pH values.

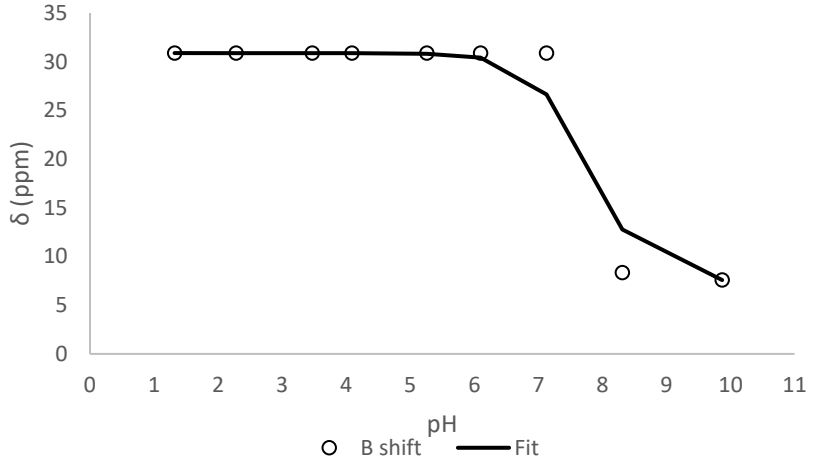

pK_a calculations of DT9 using the non-linear equation 2.3.3. pK_a is 7.8.

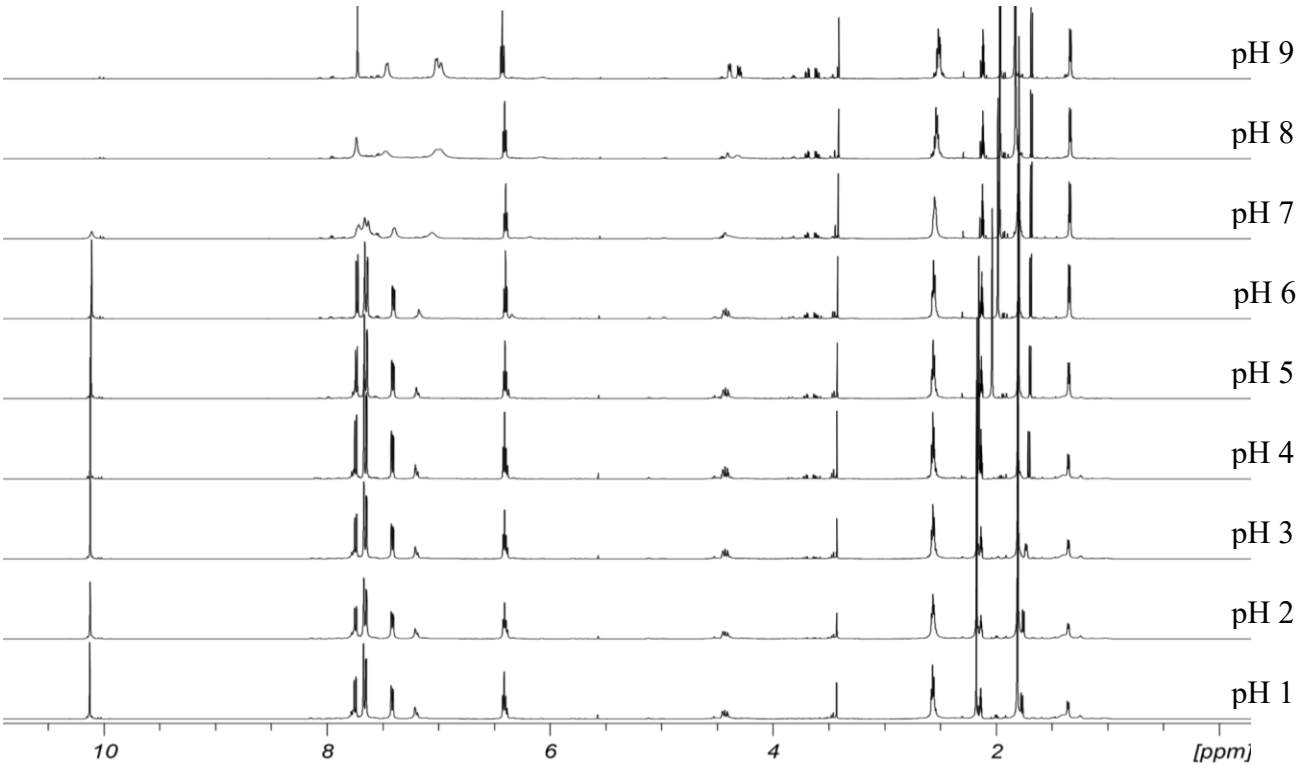

^{1}H NMR Spectrum (500 MHz, D_2O) of DT9 in different pH values.

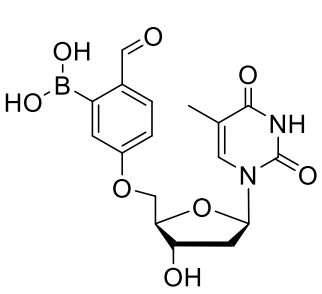

DT14

^{11}B NMR Spectrum (500 MHz, D_2O) of DT14 with increasing pH values.

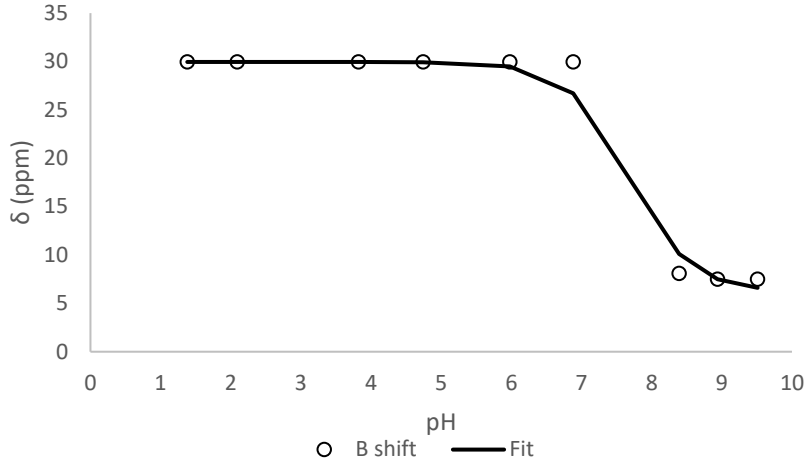

pK_a calculations of DT14 using the non-linear equation 2.3.3. pK_a is 7.7.

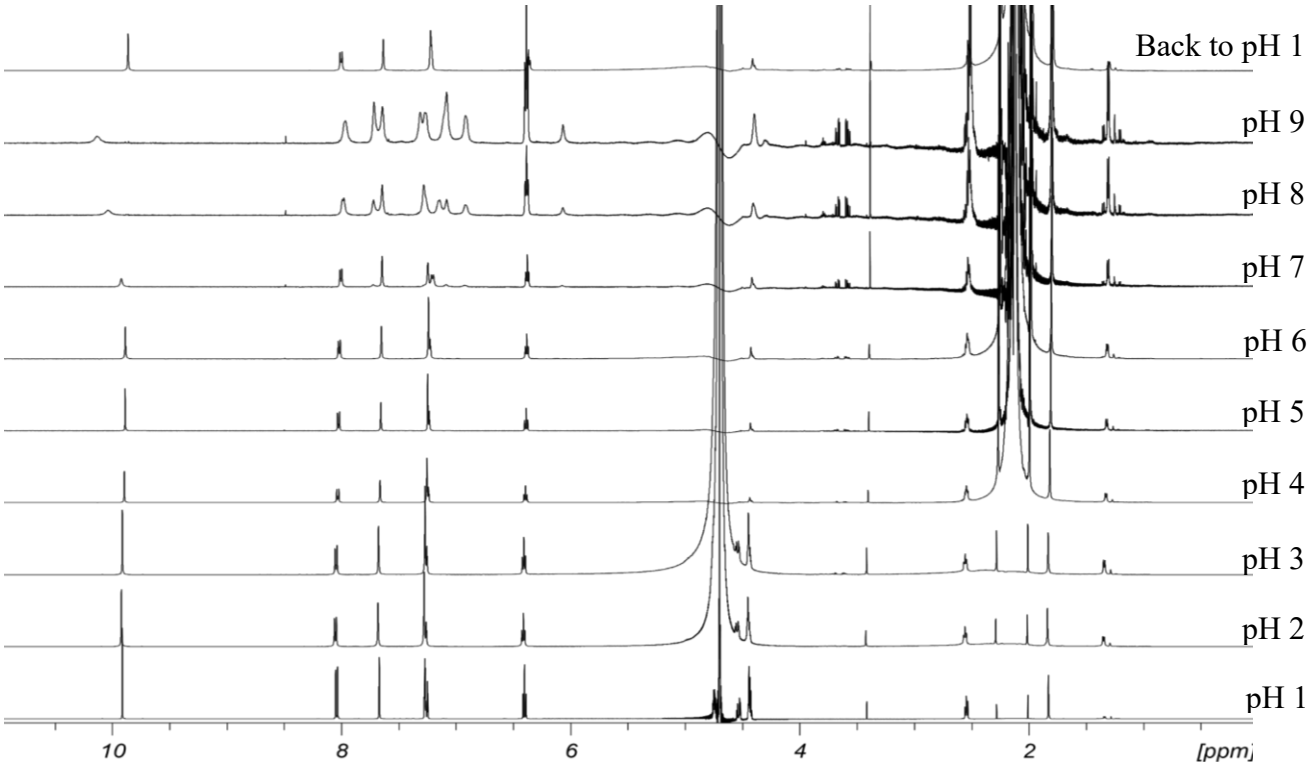

^1H NMR Spectrum (500 MHz, D_2O) of DT14 with increasing pH values.

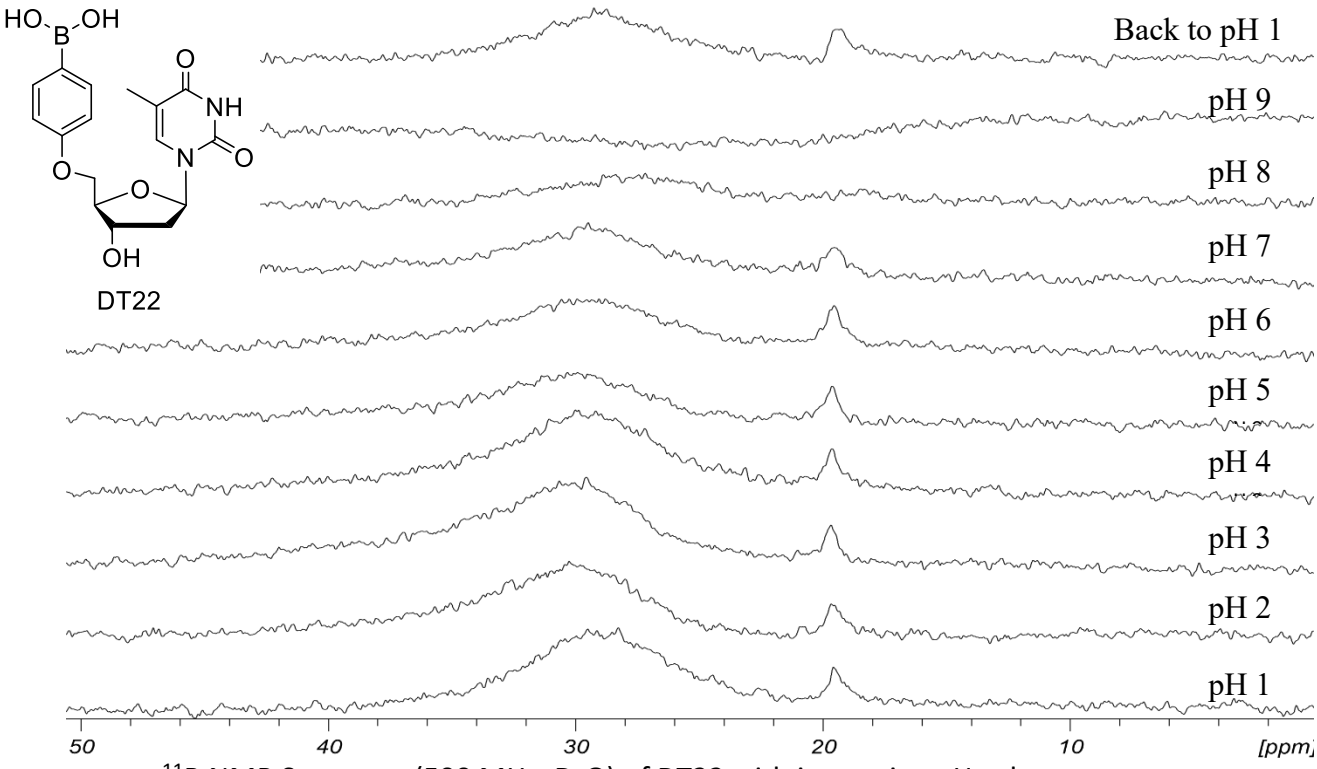

^{11}B NMR Spectrum (500 MHz, D_2O) of DT22 with increasing pH values.

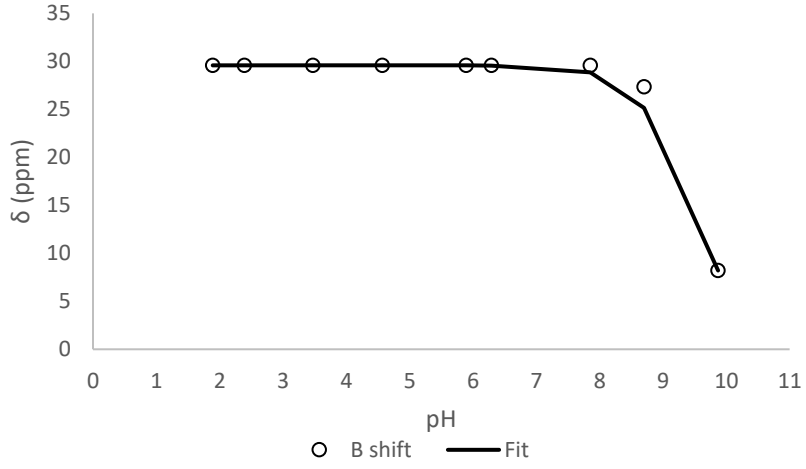

pK_a calculations of DT22 using the non-linear equation 2.3.3. pK_a is 8.5.

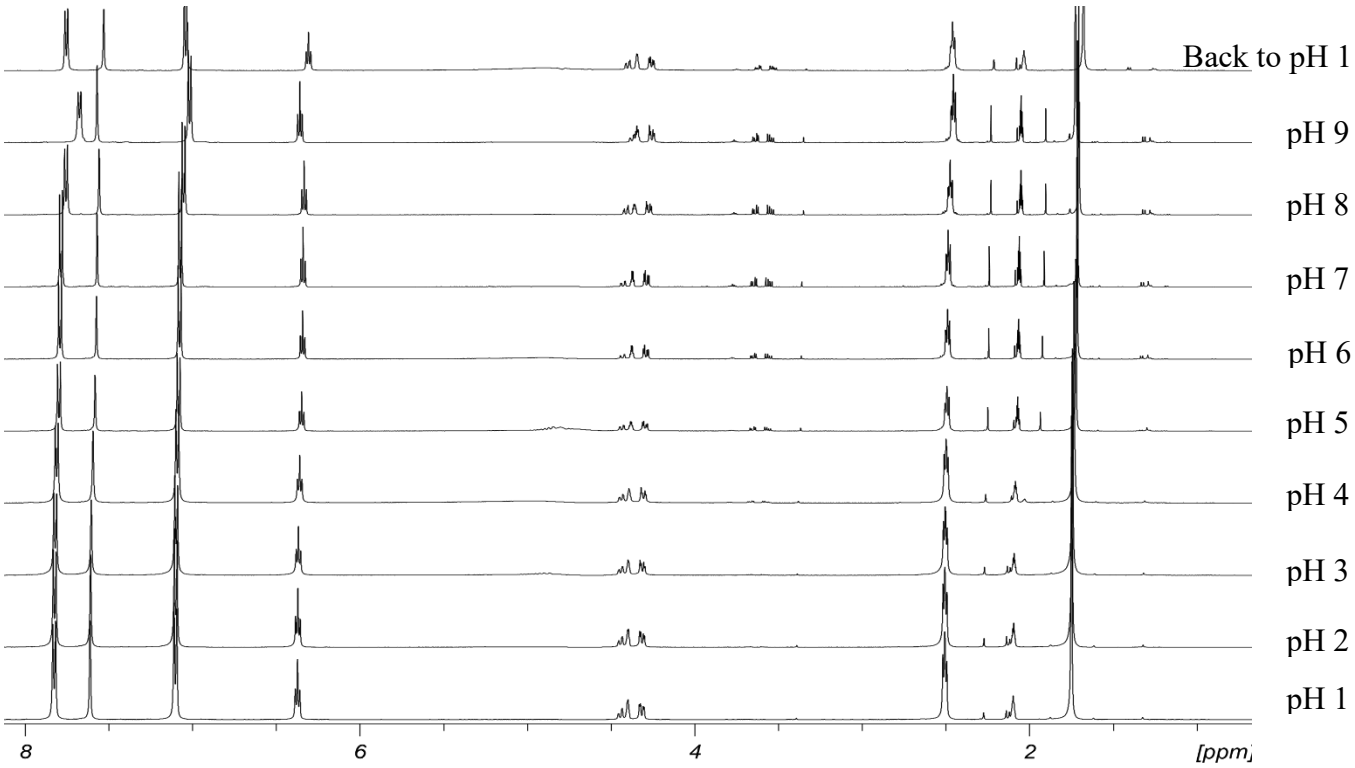

^{1}H NMR Spectrum (500 MHz, D_2O) of DT22 with increasing pH values.

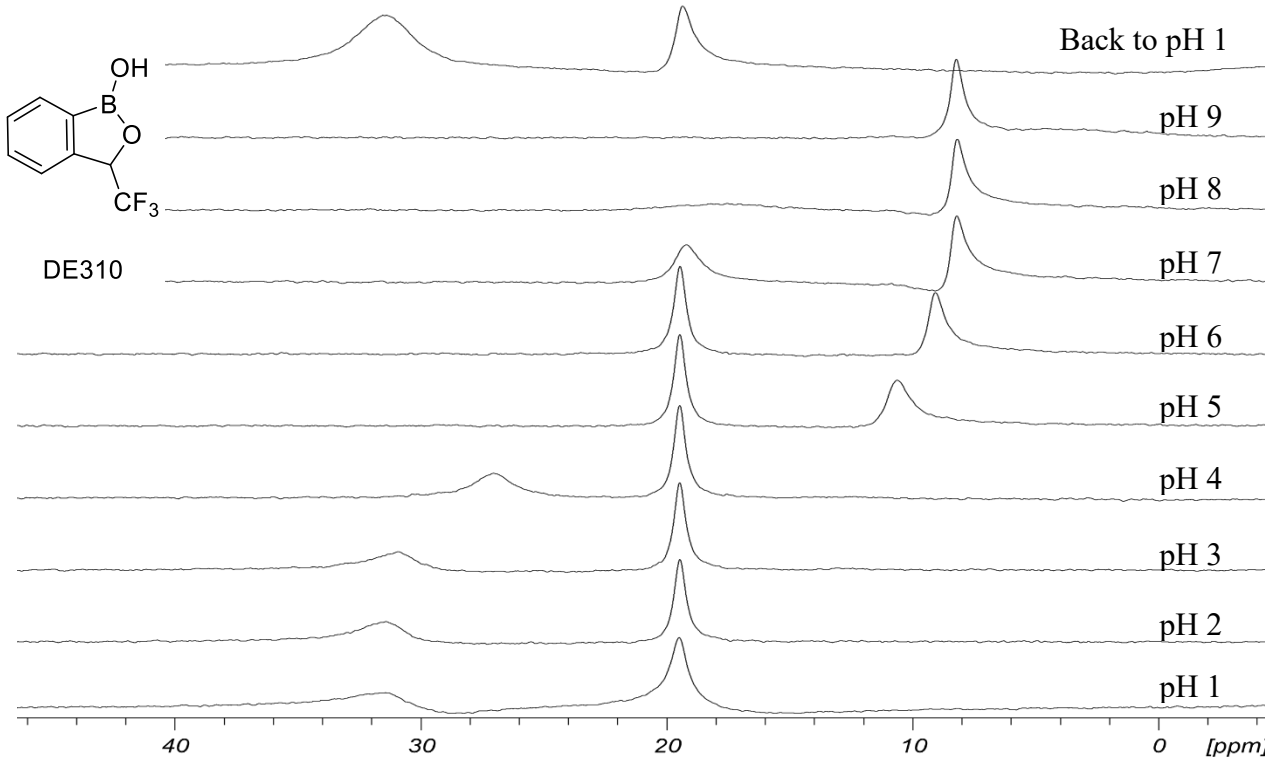

^{11}B NMR Spectrum (500 MHz, D_2O) of DE310 with increasing pH values.

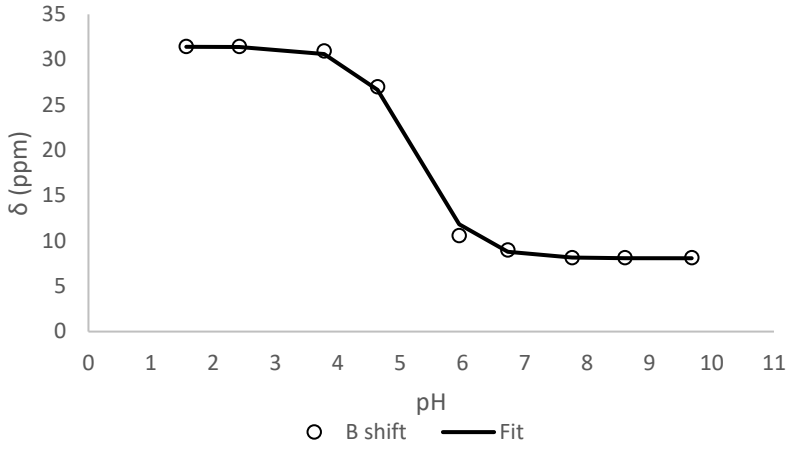

pK_a calculations of DE310 using the non-linear equation 2.3.3. pK_a is 5.2.

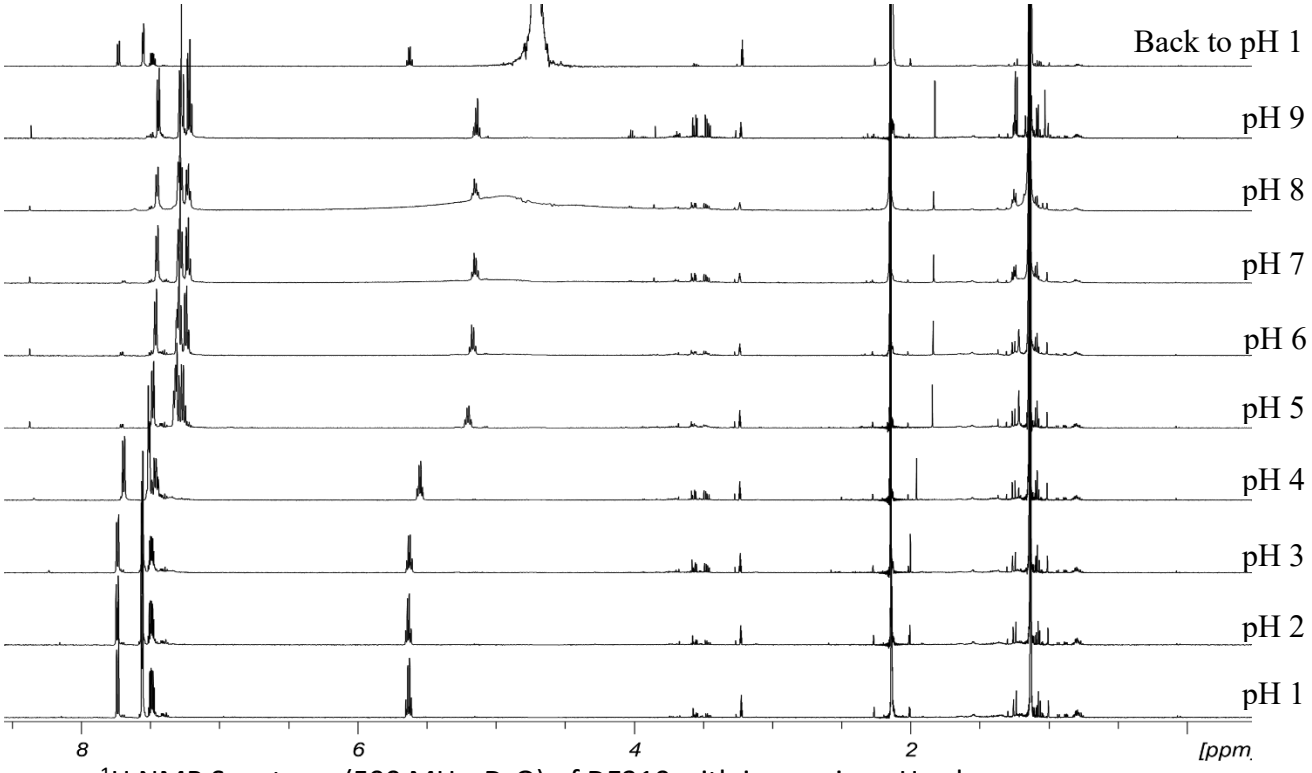

^1H NMR Spectrum (500 MHz, D_2O) of DE310 with increasing pH values.

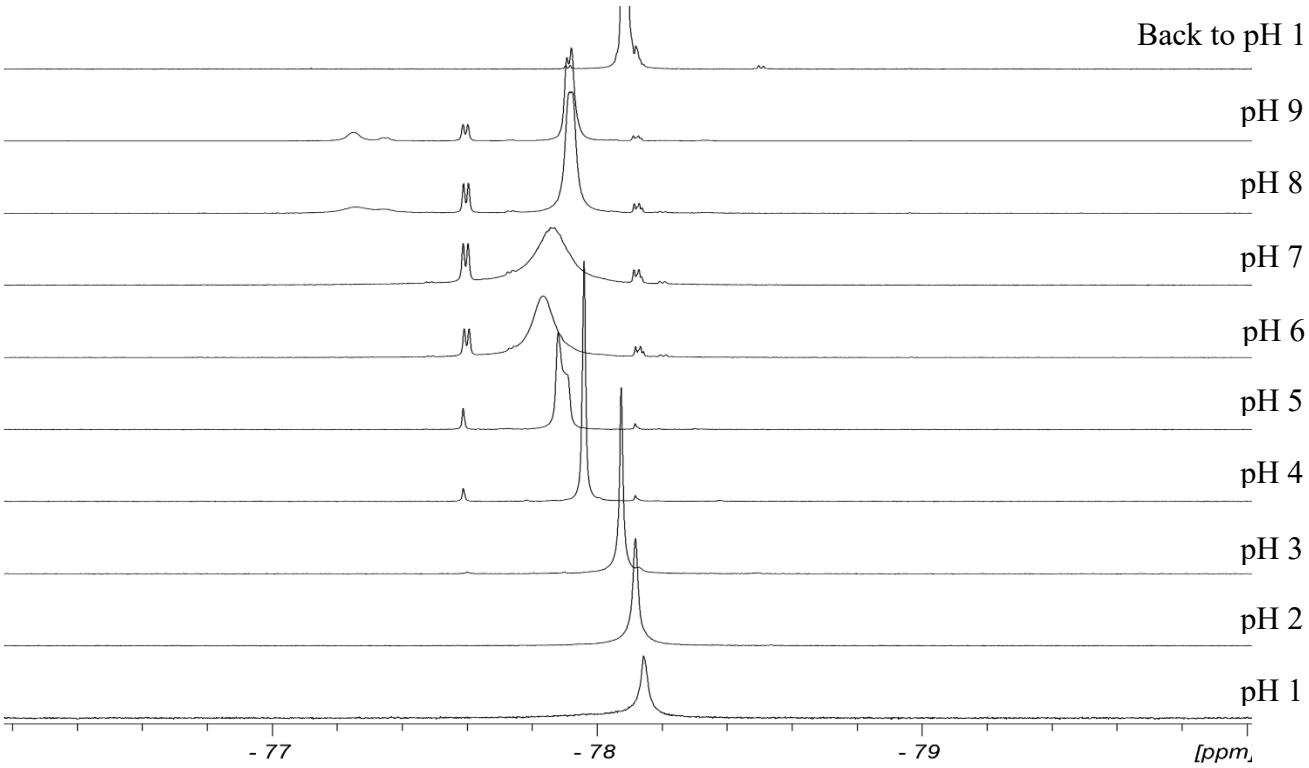

^{19}F NMR Spectrum (500 MHz, D_2O) of DE310 with increasing pH values.

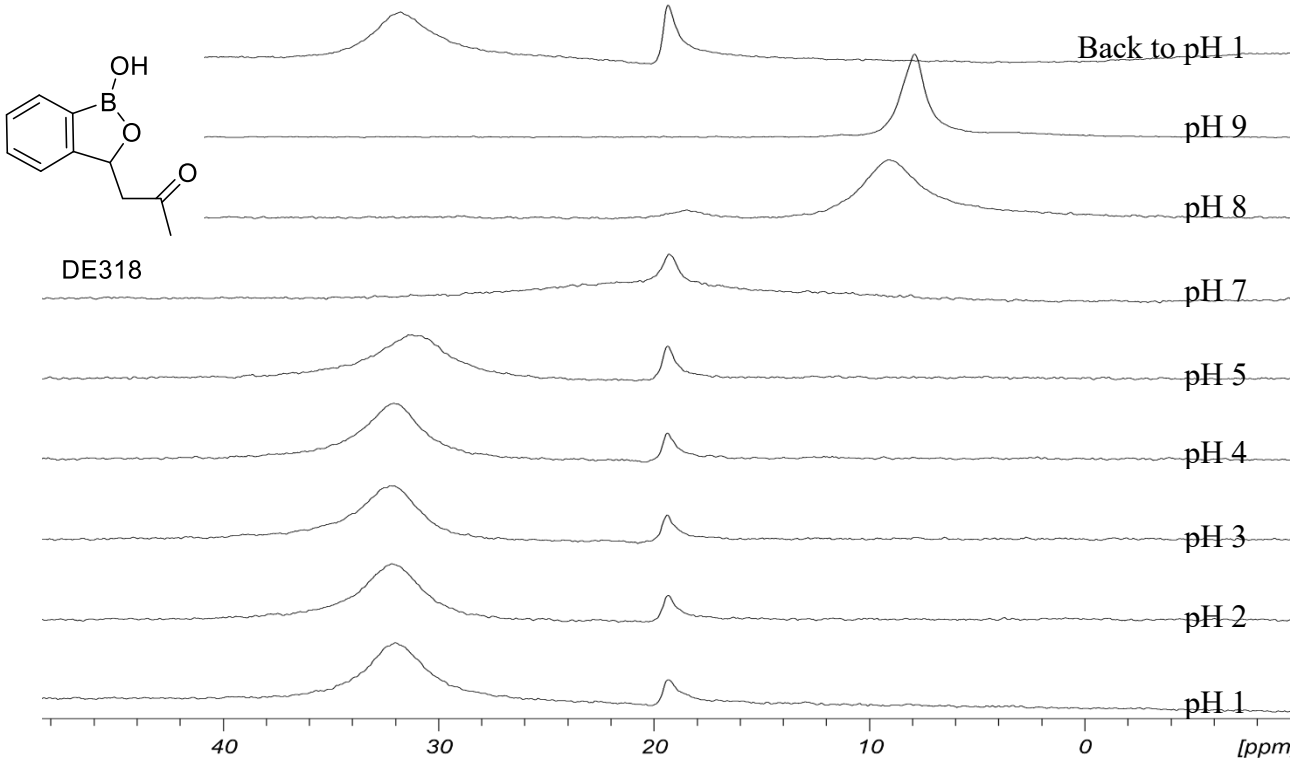

^{11}B NMR Spectrum (500 MHz, D_2O) of DE318 with increasing pH values.

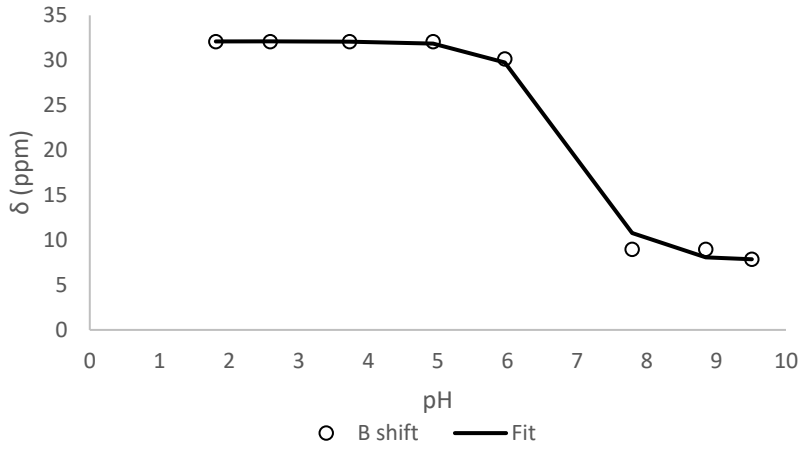

pK_a calculations of DE318 using the non-linear equation 2.3.3. pK_a is 6.9.

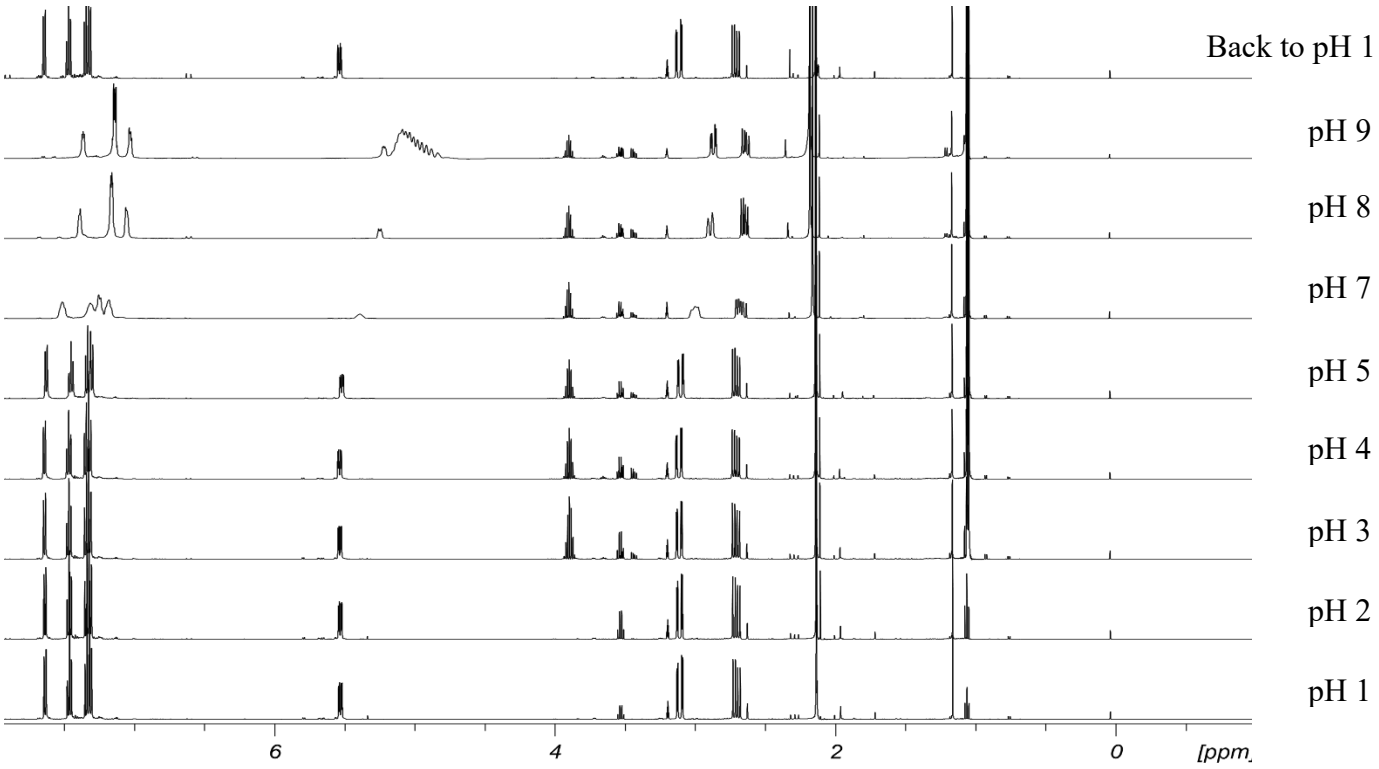

^1H NMR Spectrum (500 MHz, D_2O) of DE318 with increasing pH values.

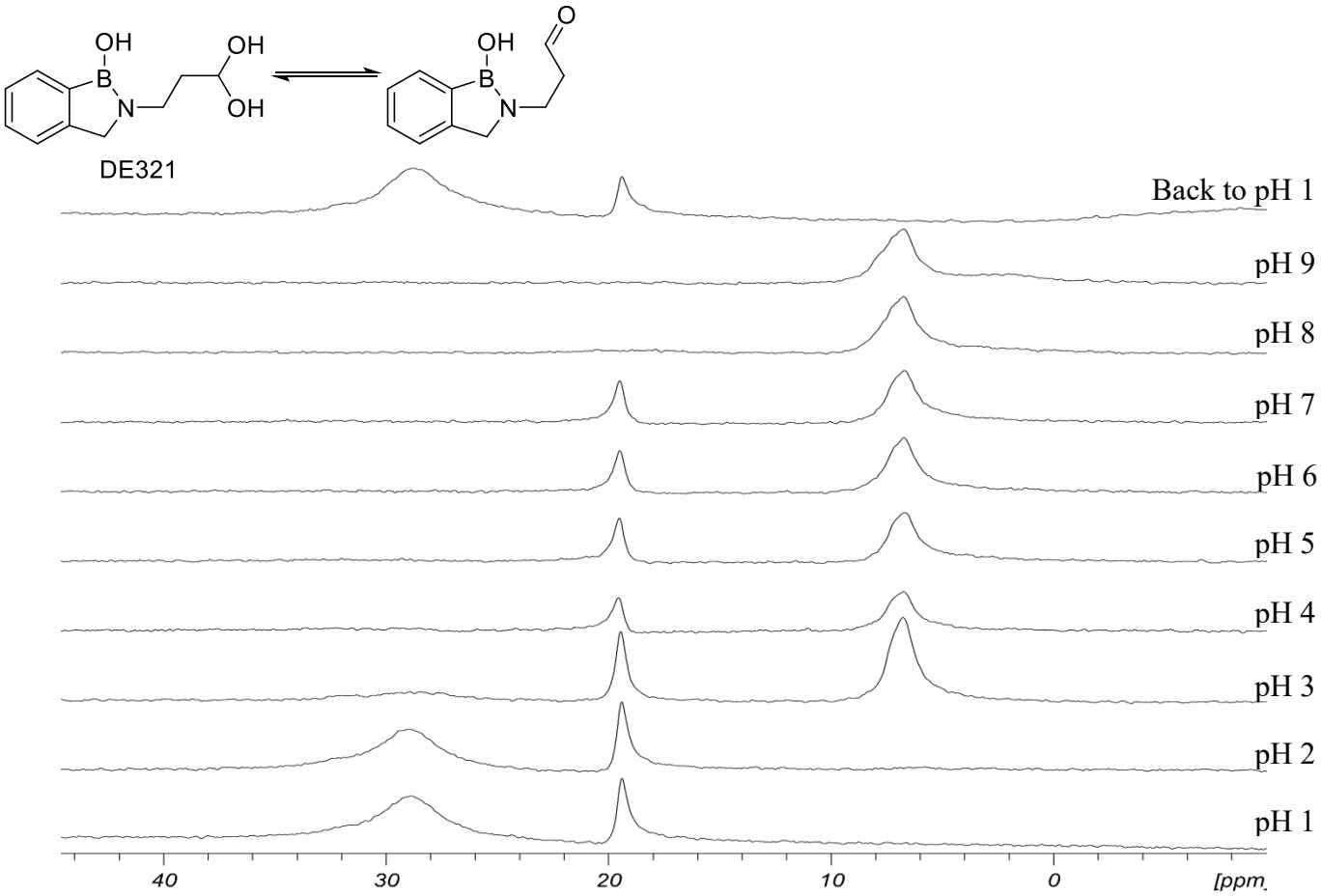

^{11}B NMR Spectrum (500 MHz, D_2O) of DE321 with increasing pH values.

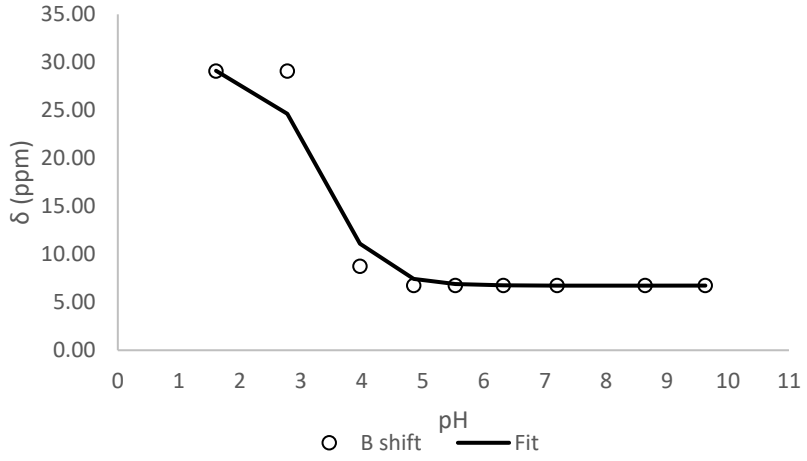

pK_a calculations of DE321 using the non-linear equation 2.3.3. pK_a is 3.3.

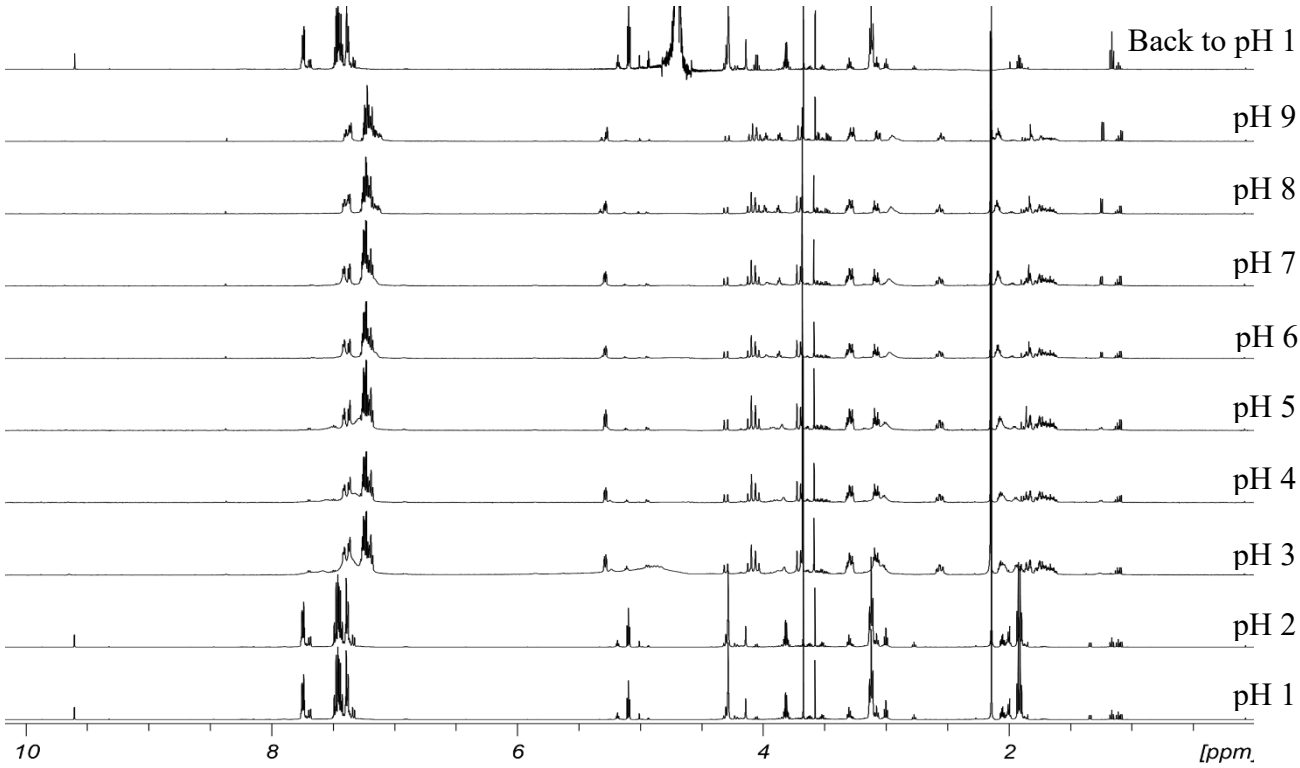

^{1}H NMR Spectrum (500 MHz, D_2O) of DE321 with increasing pH values.

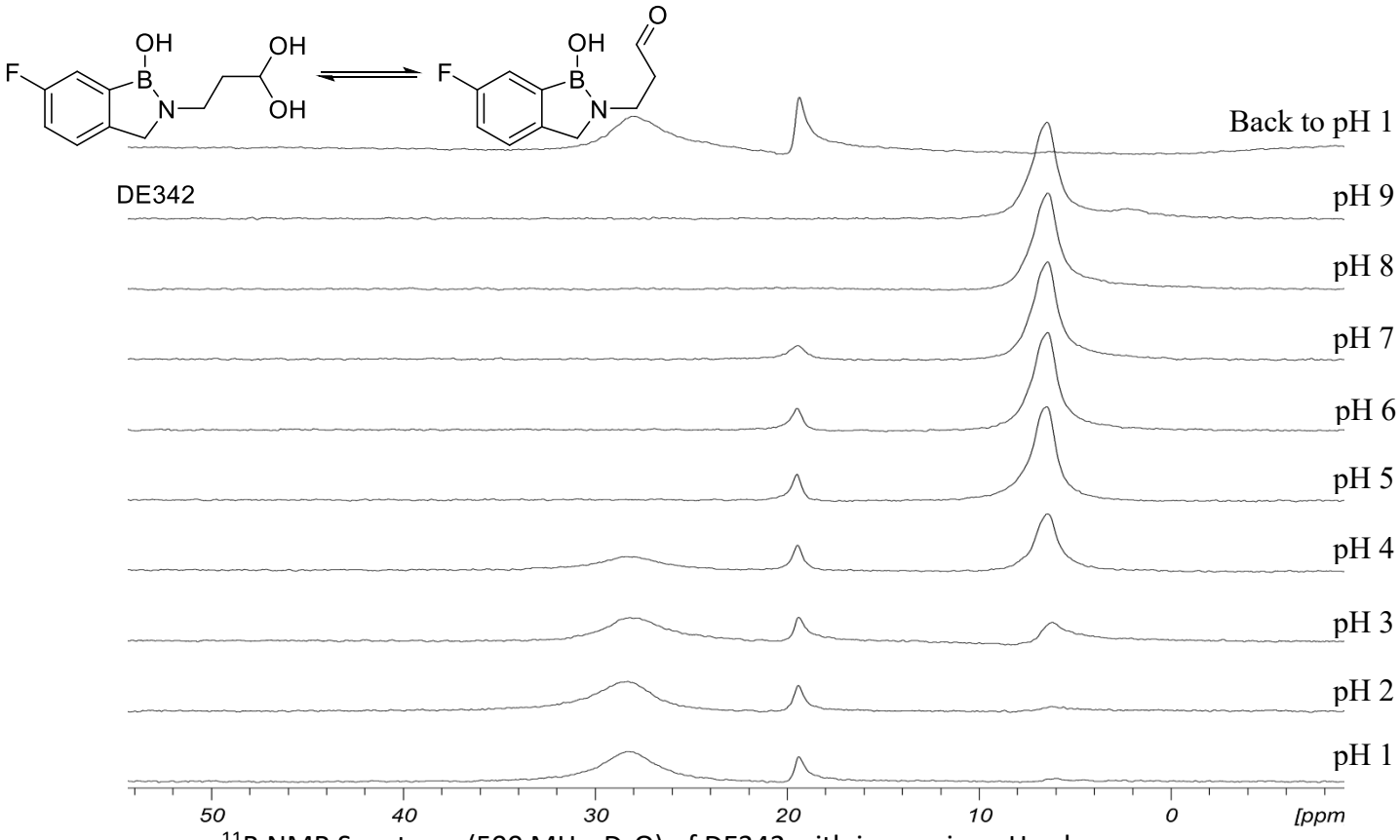

^{11}B NMR Spectrum (500 MHz, D_2O) of DE342 with increasing pH values.

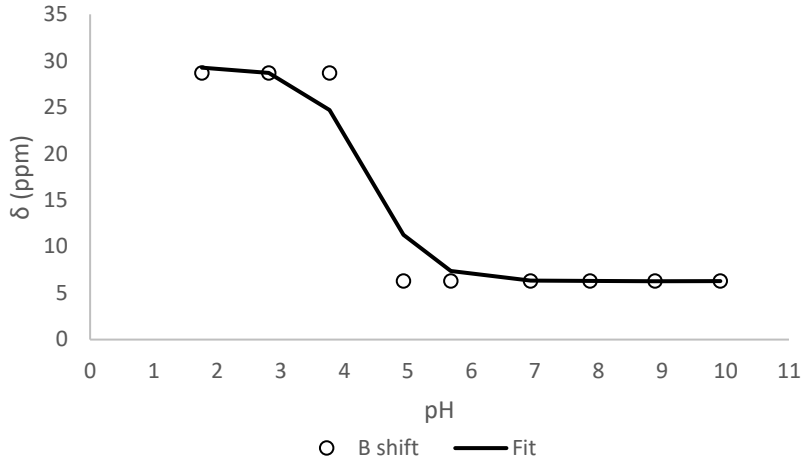

pK_a calculations of DE342 using the non-linear equation 2.3.3. pK_a is 4.4.

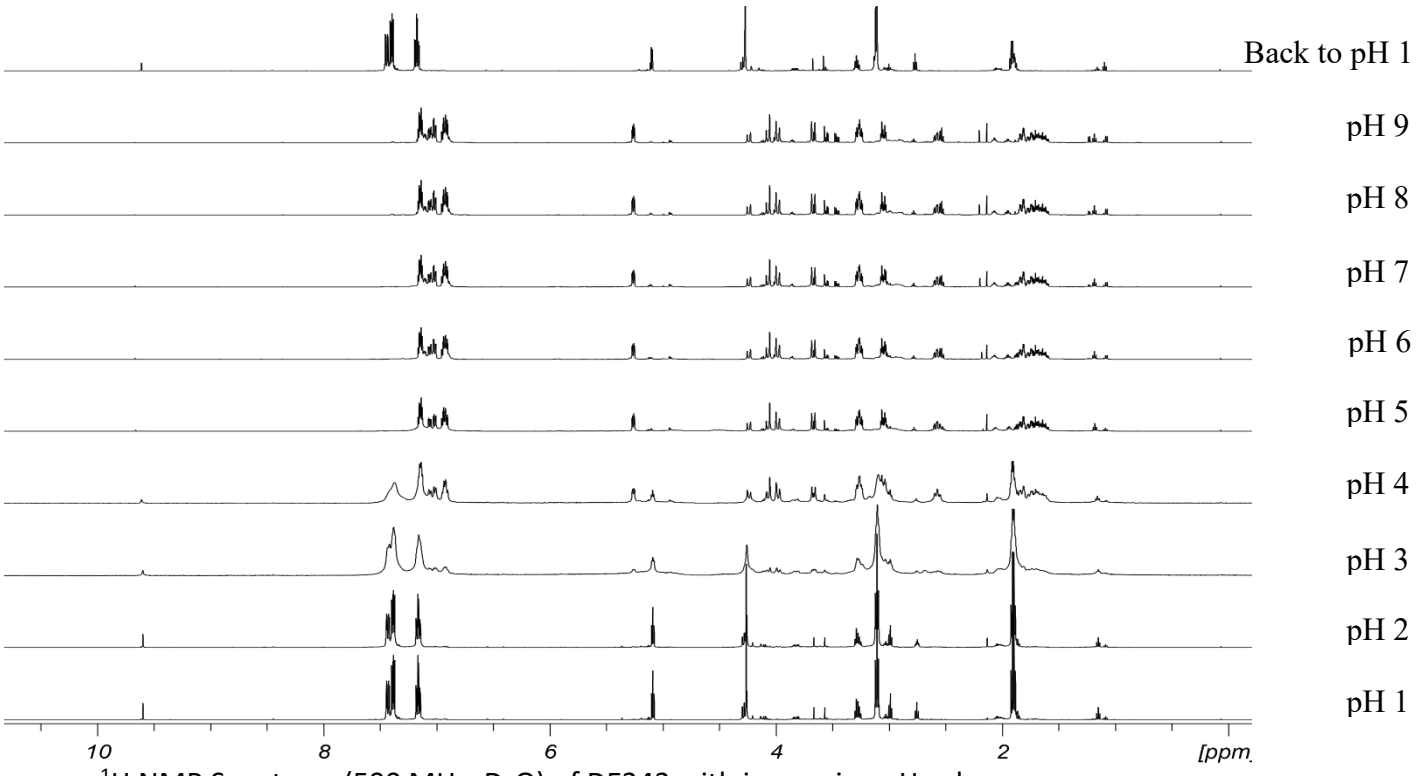

^1H NMR Spectrum (500 MHz, D_2O) of DE342 with increasing pH values.

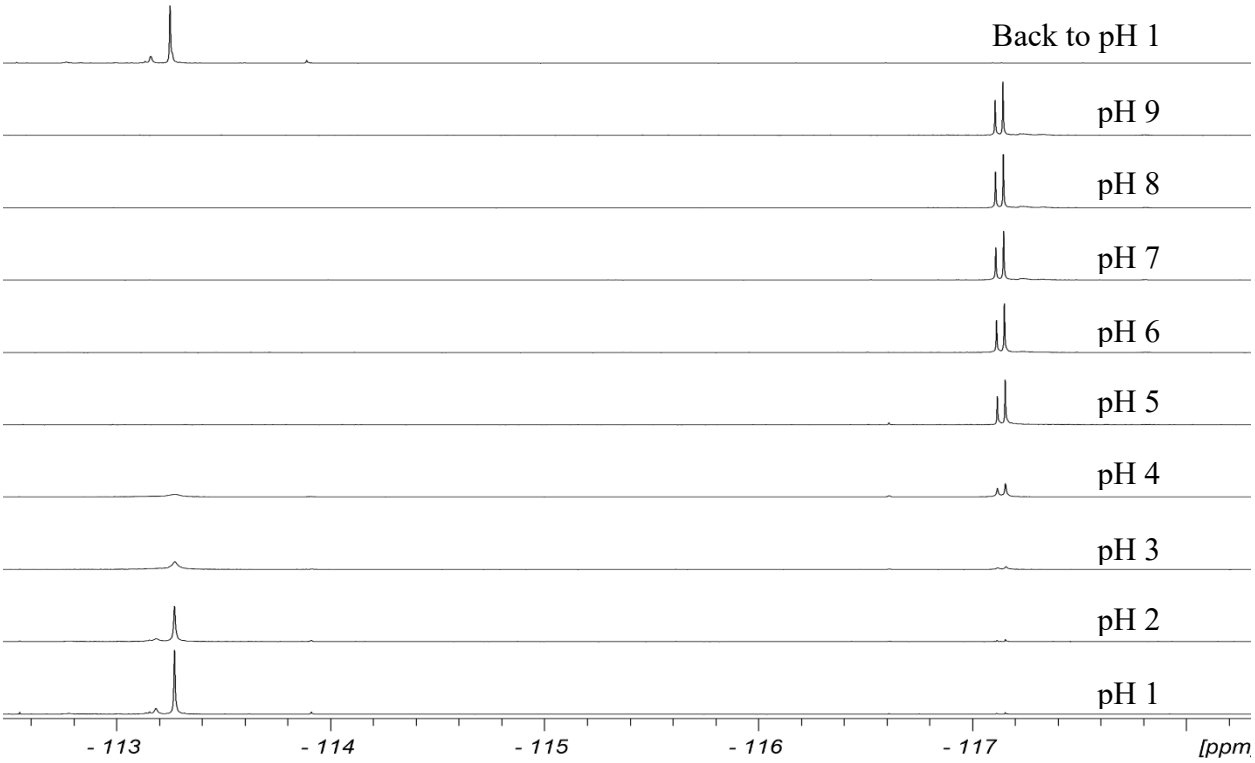

^{19}F NMR Spectrum (500 MHz, D_2O) of DE342 with increasing pH values.

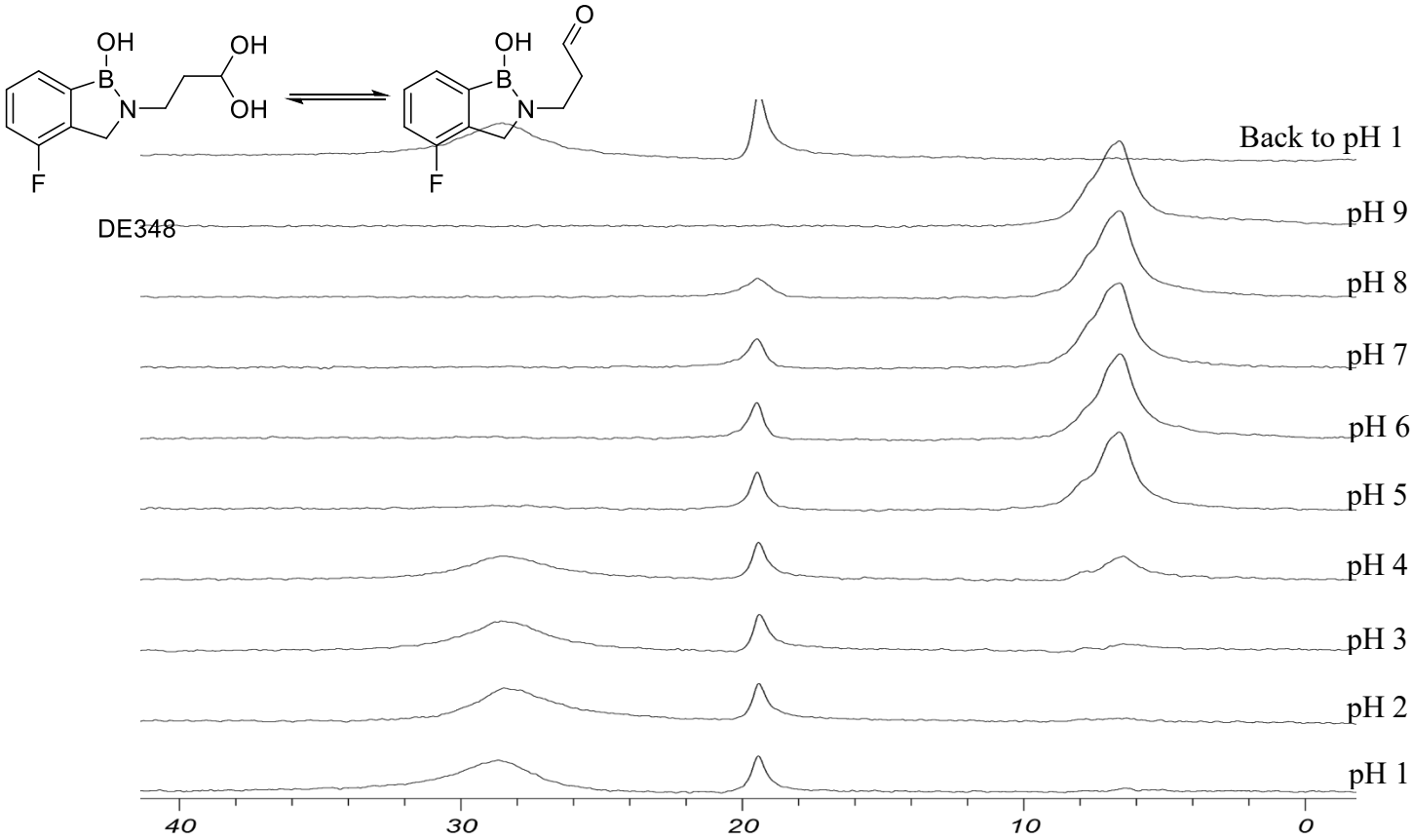

^{11}B NMR Spectrum (500 MHz, D_2O) of DE348 with increasing pH values.

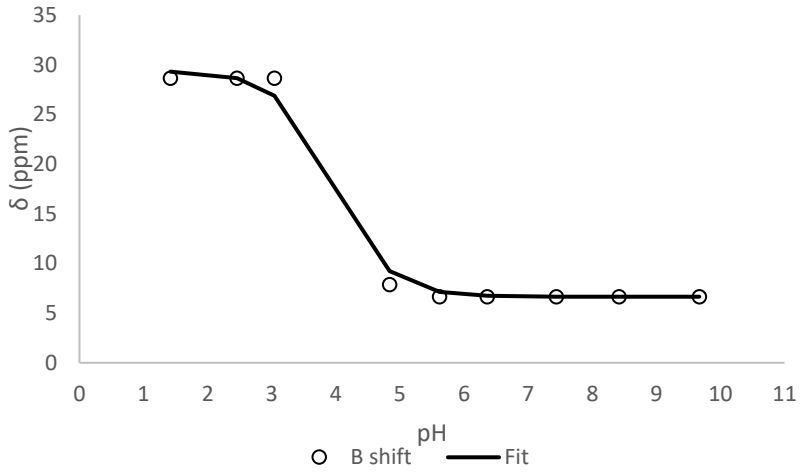

pK_a calculations of DE348 using the non-linear equation 2.3.3. pK_a is 3.9.

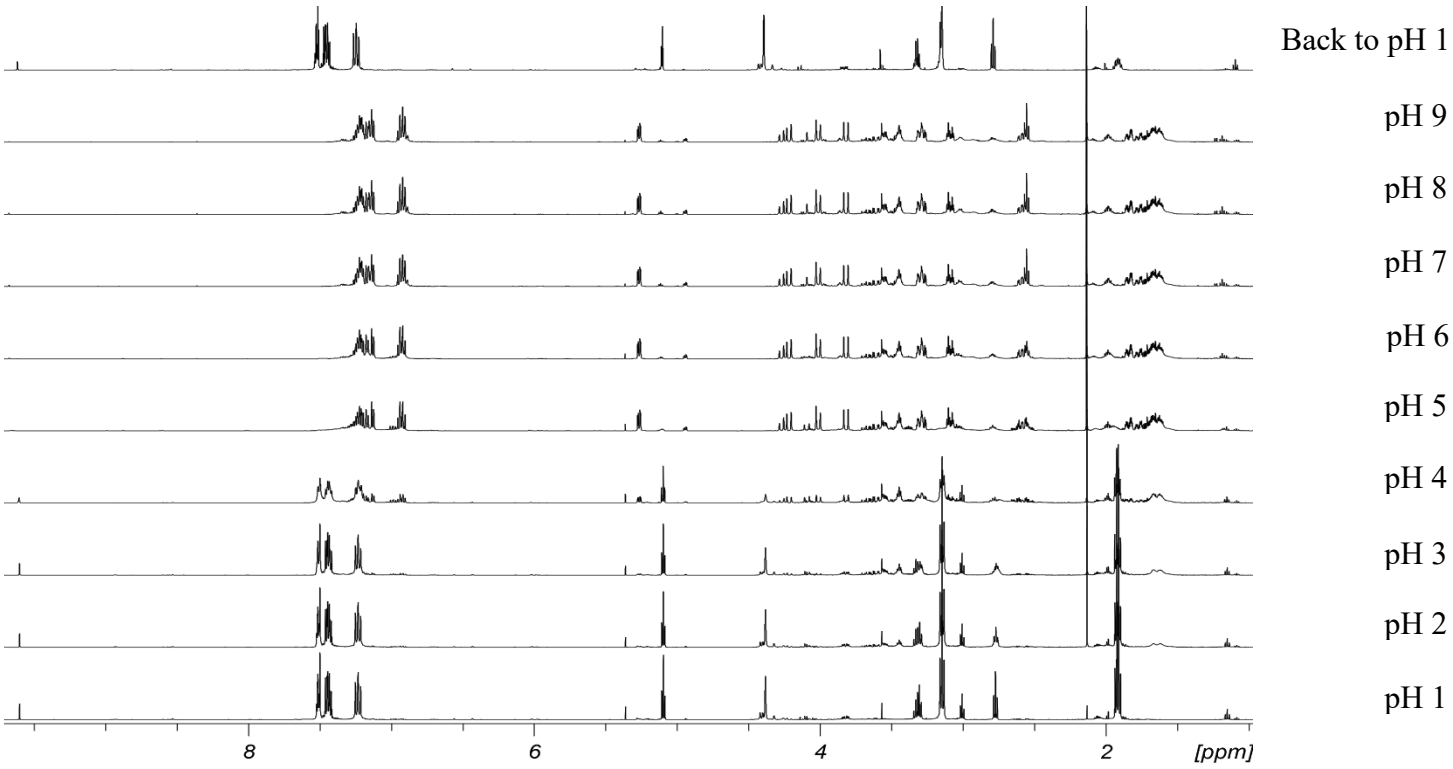

^1H NMR Spectrum (500 MHz, D_2O) of DE348 with increasing pH values.

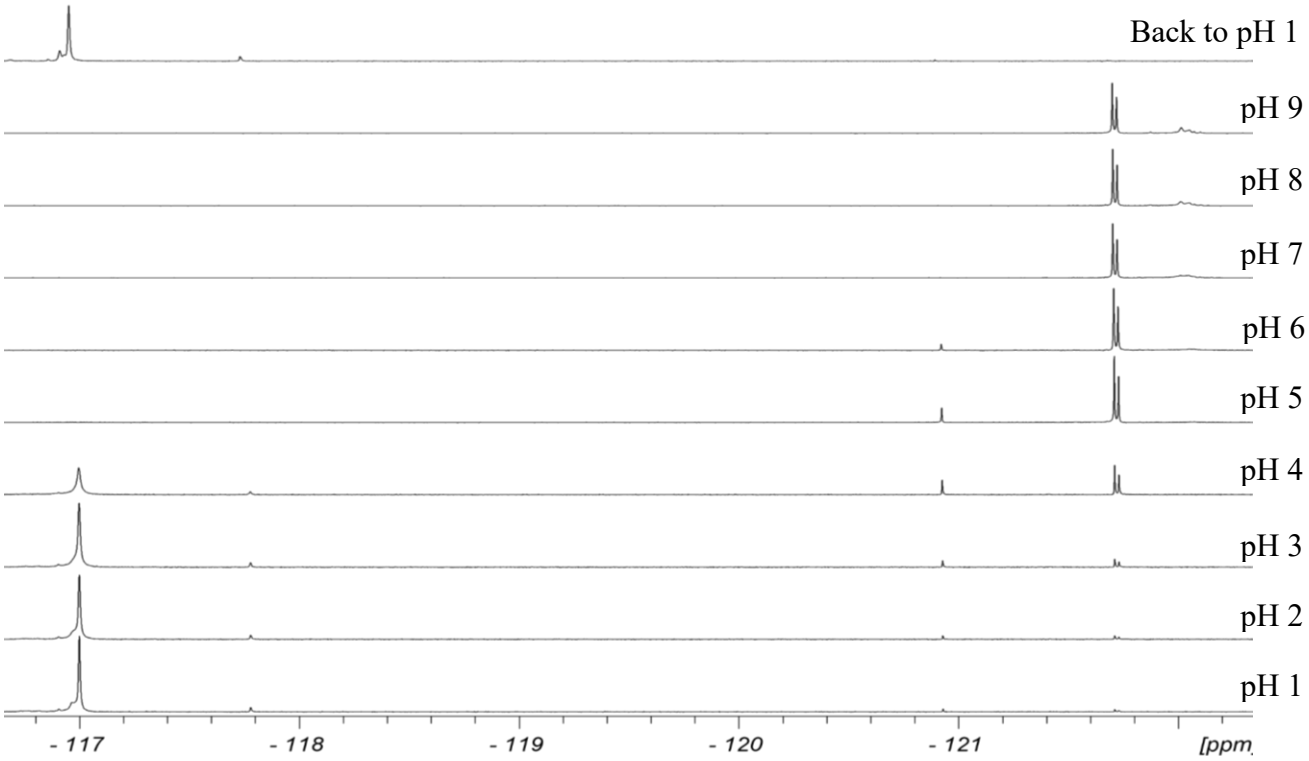

^{19}F NMR Spectrum (500 MHz, D_2O) of DE348 with increasing pH values.

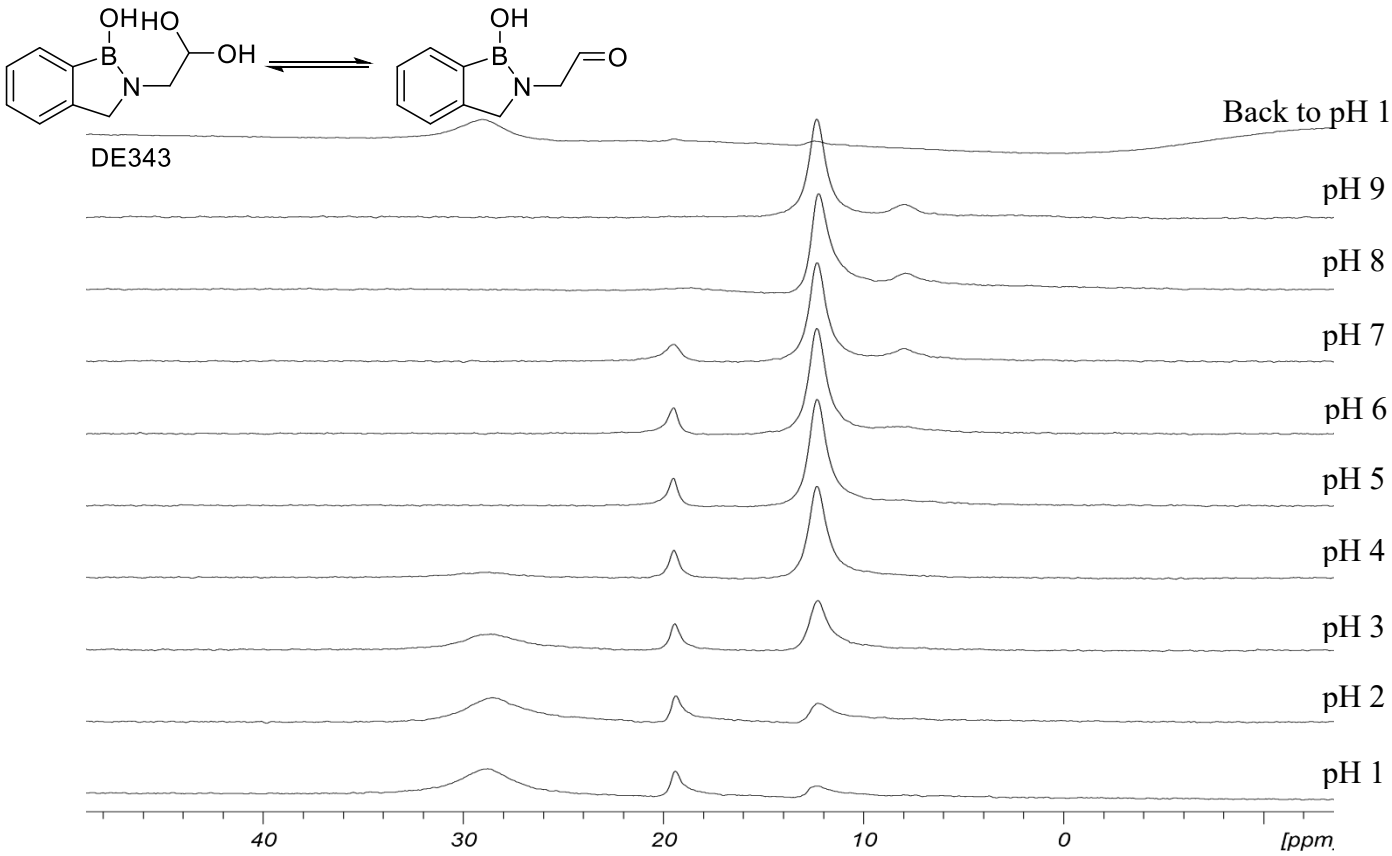

^{11}B NMR Spectrum (500 MHz, D_2O) of DE343 with increasing pH values.

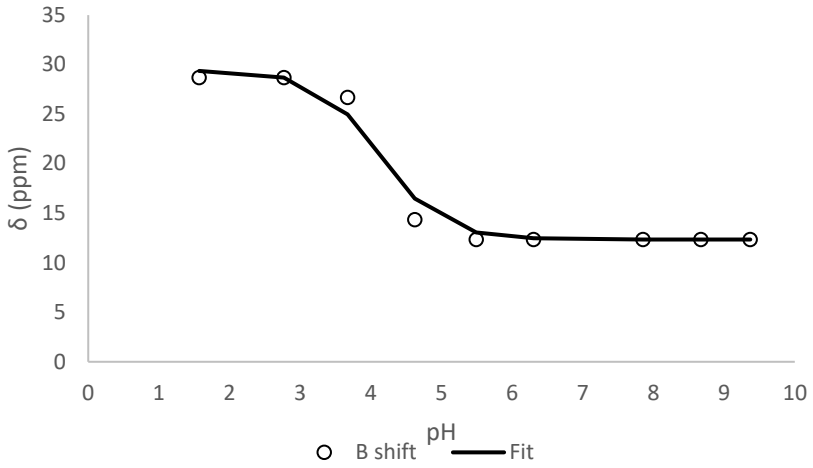

pK_a calculations of DE343 using the non-linear equation 2.3.3. pK_a value is 4.1.

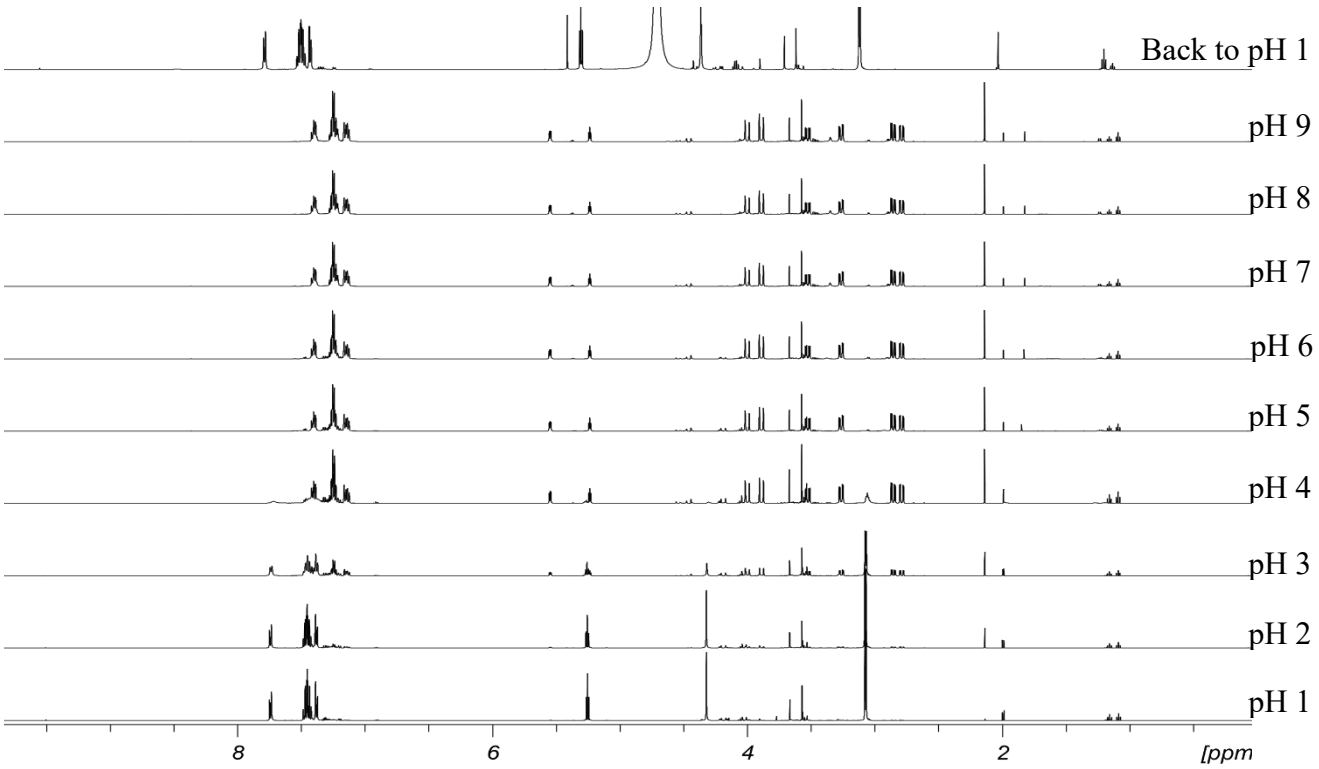

^1H NMR Spectrum (500 MHz, D_2O) of DE343 with increasing pH values.

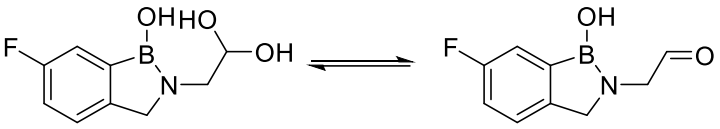

DE344

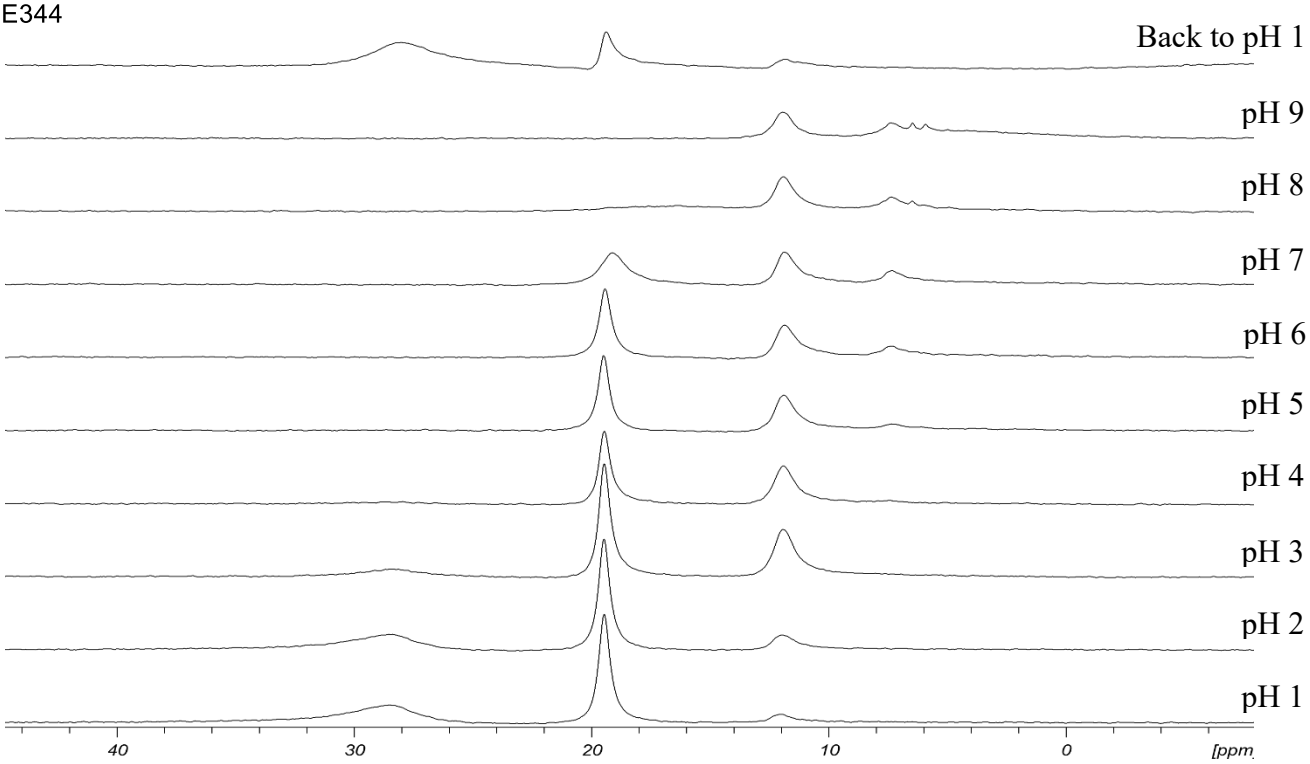

^{11}B NMR Spectrum (500 MHz, D_2O) of DE344 with increasing pH values.

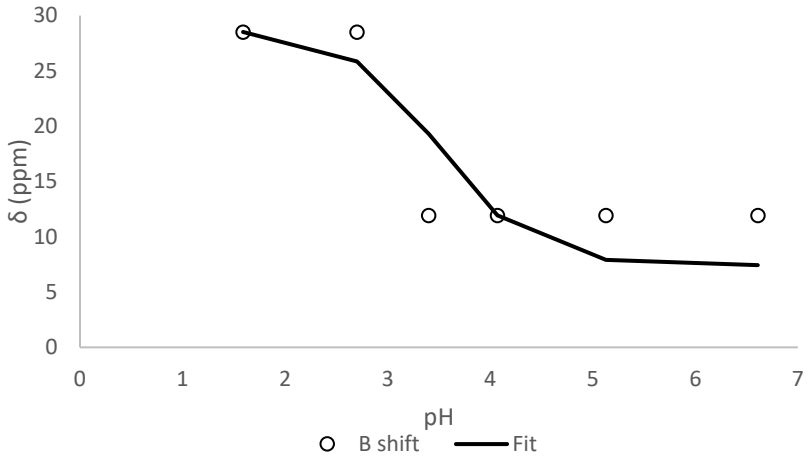

pK_a calculations of DE344 using the non-linear equation 2.3.3. pK_a value is 3.5.

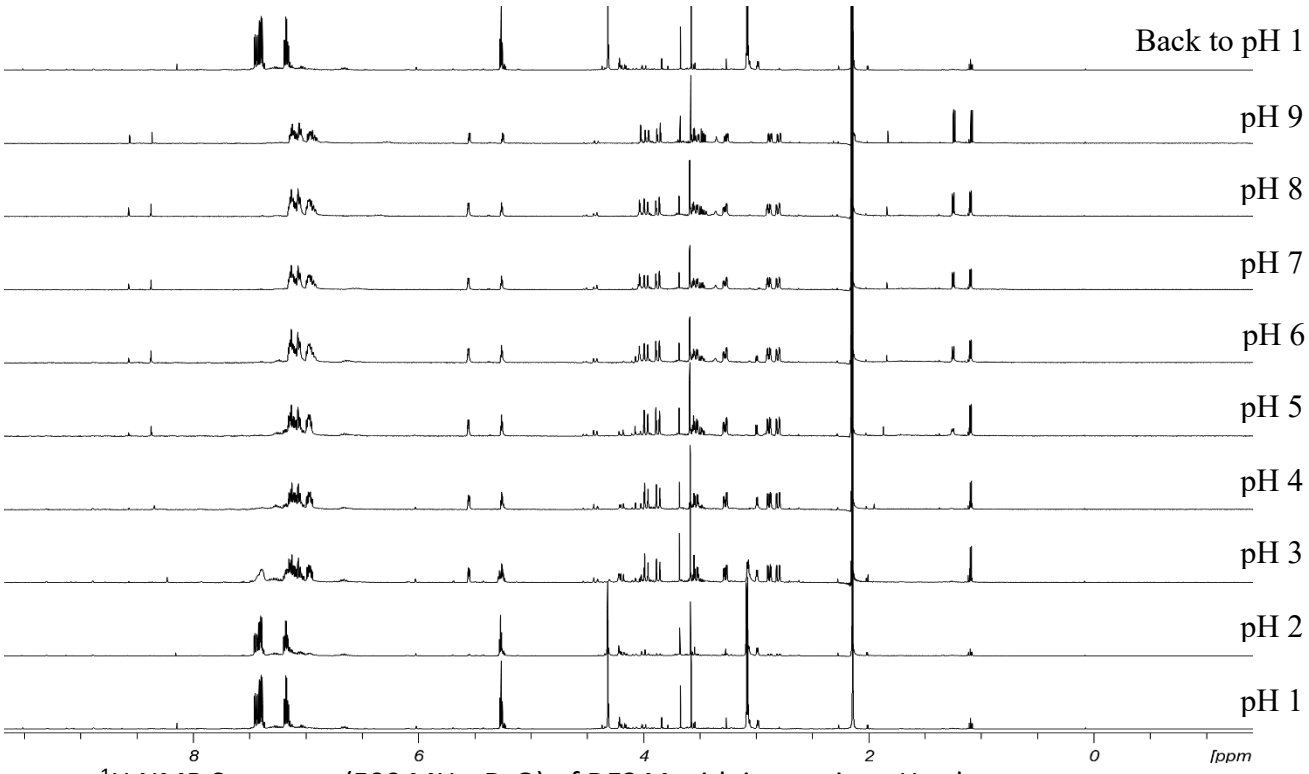

^{1}H NMR Spectrum (500 MHz, D_2O) of DE344 with increasing pH values.

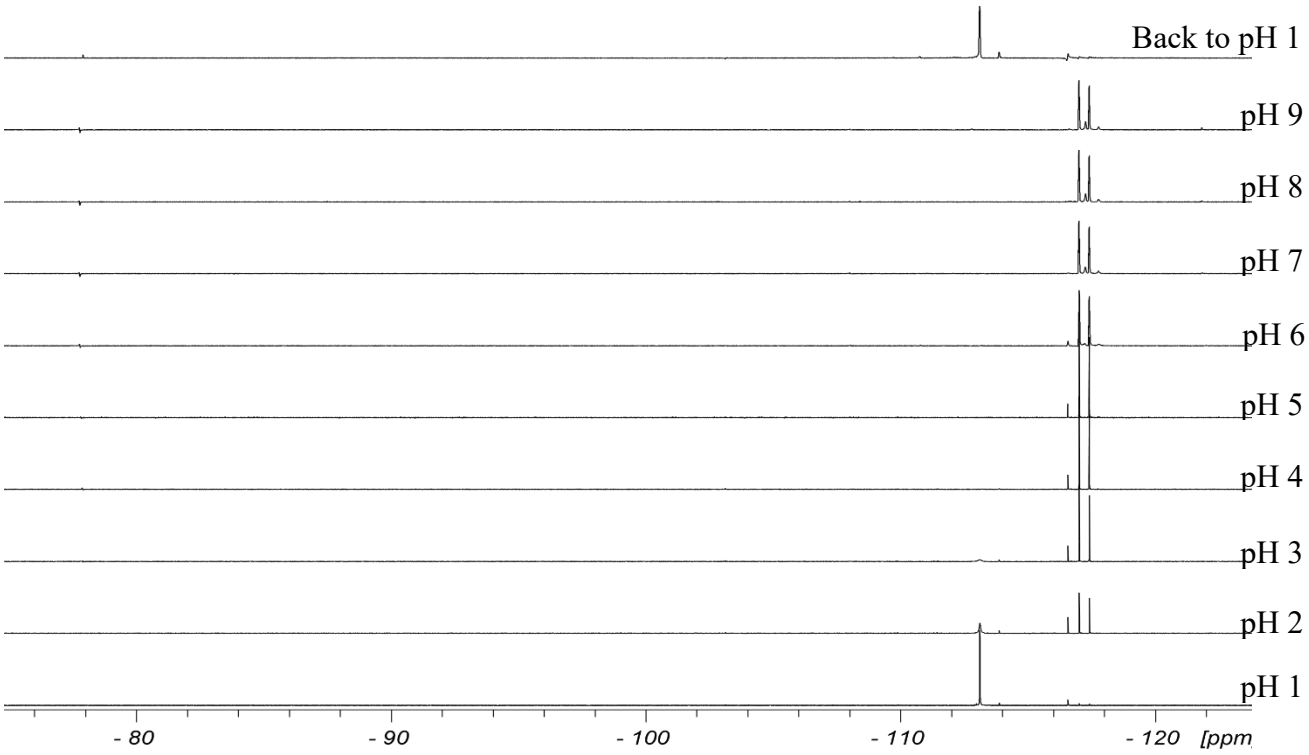

^{19}F NMR Spectrum (500 MHz, D_2O) of DE344 with increasing pH values.

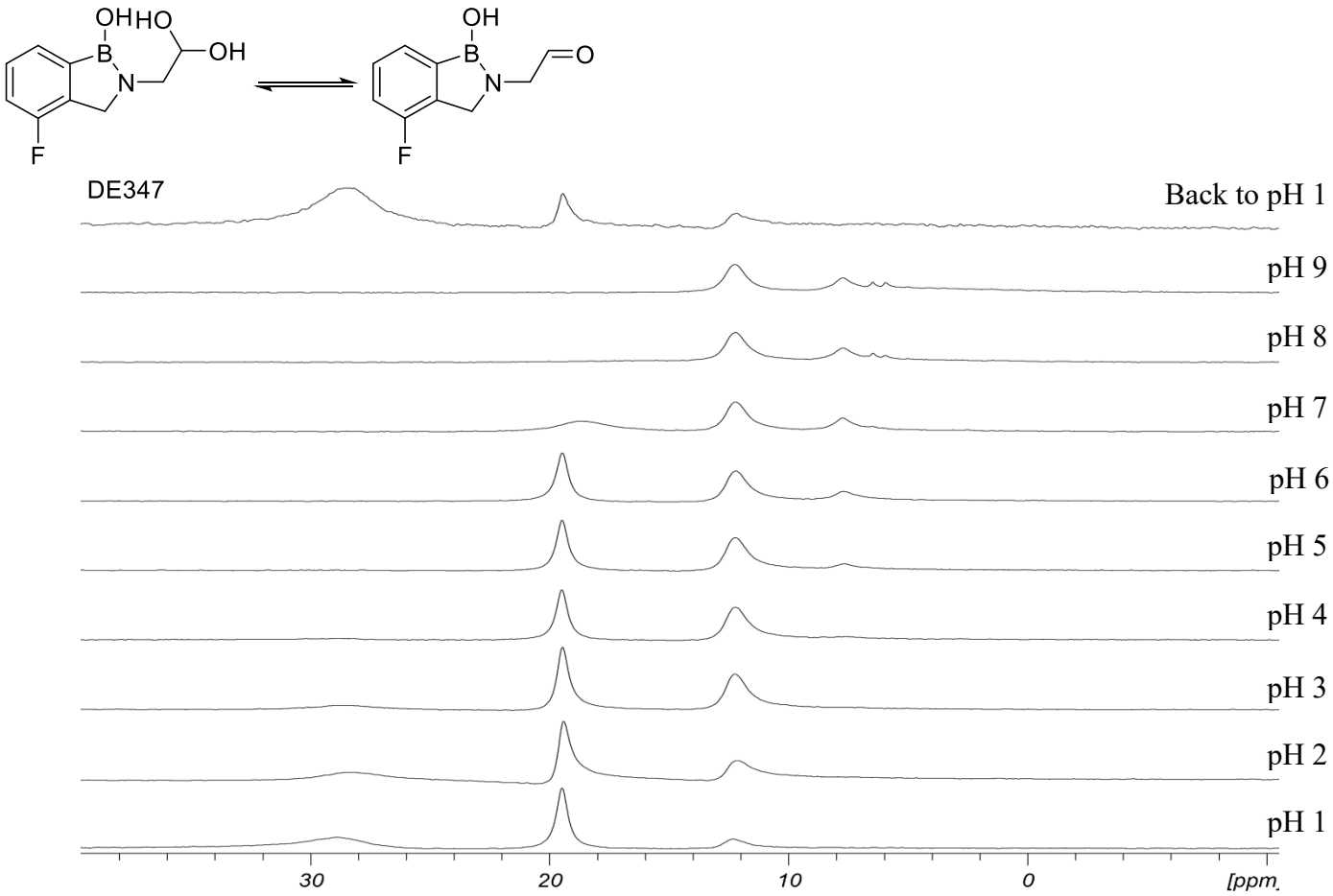

^{11}B NMR Spectrum (500 MHz, D_2O) of DE347 with increasing pH values.

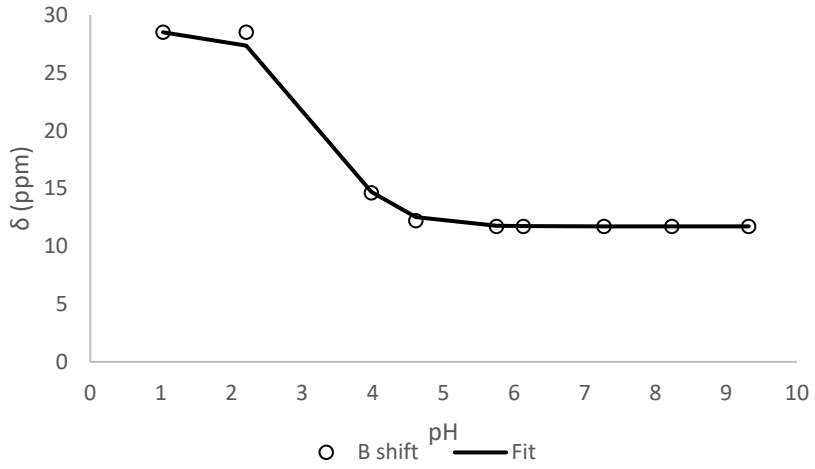

pK_a calculations of DE347 using the non-linear equation 2.3.3. pK_a value is 3.3.

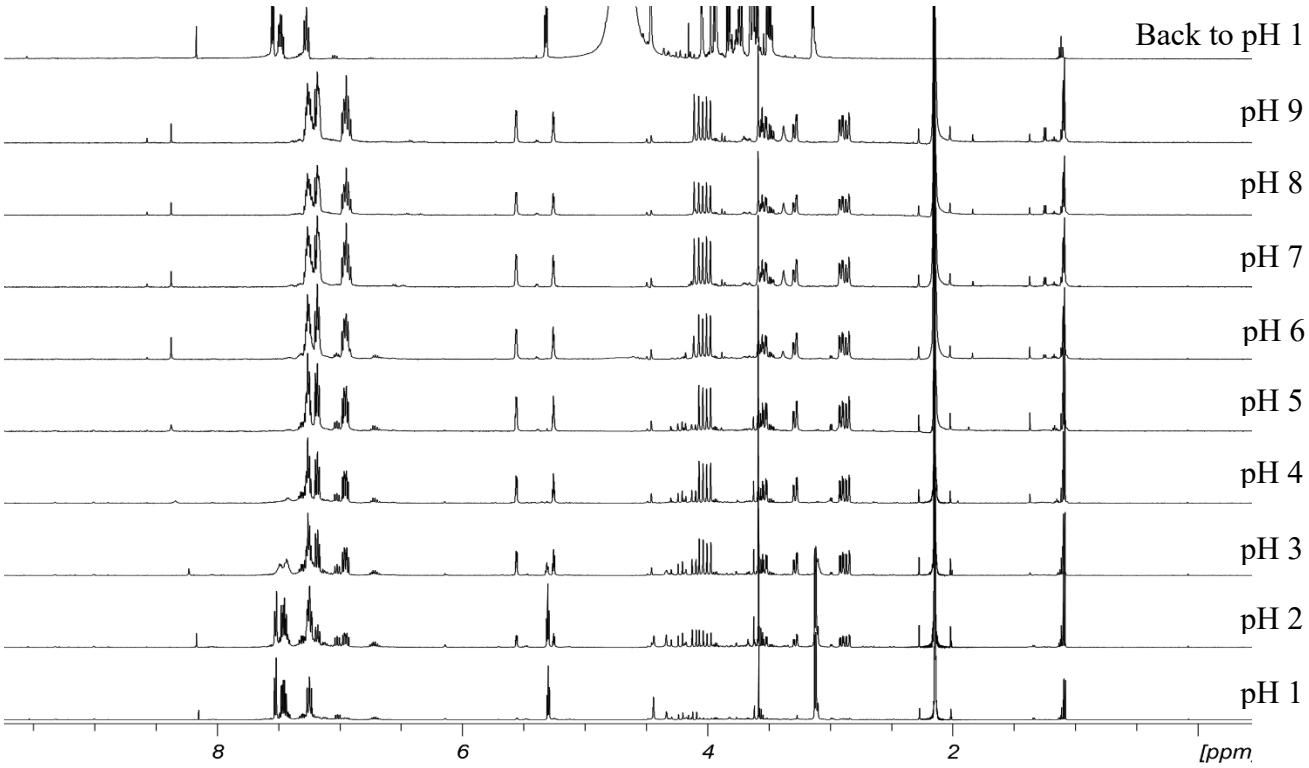

^{1}H NMR Spectrum (500 MHz, D_2O) of DE347 with increasing pH values.

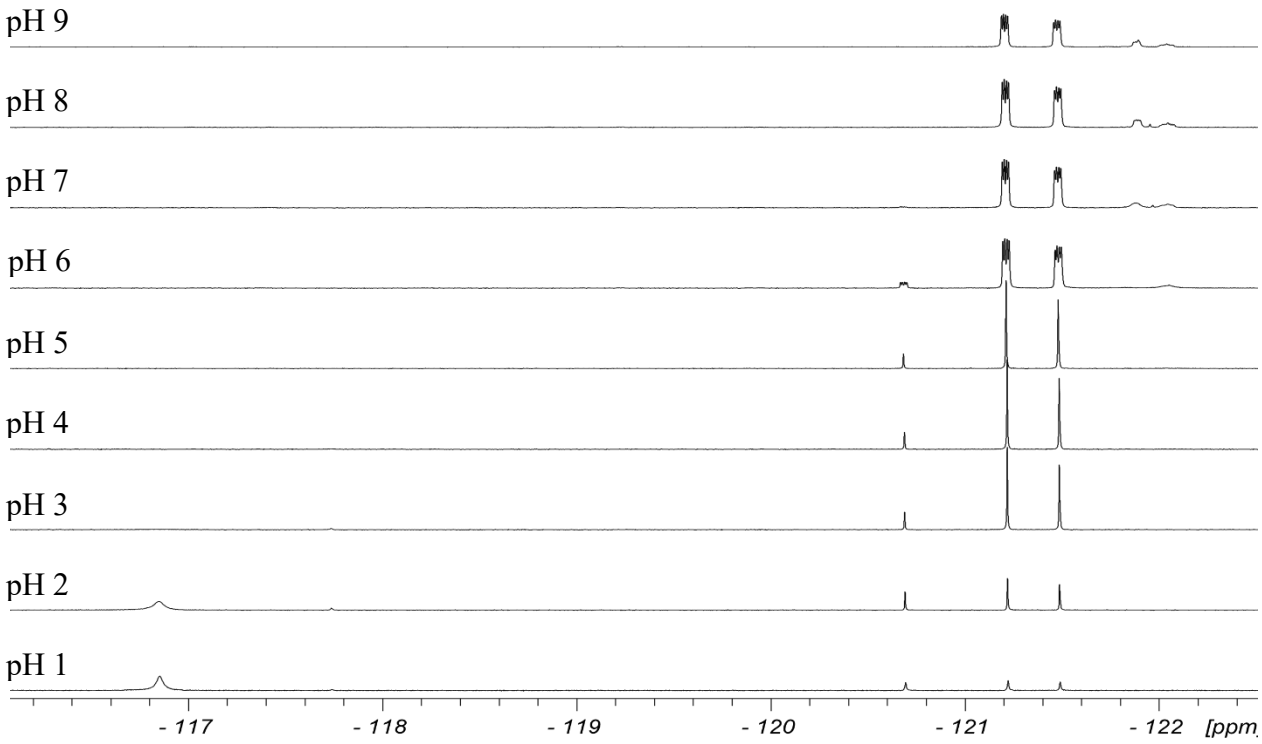

^{19}F NMR Spectrum (500 MHz, D_2O) of DE347 with increasing pH values.

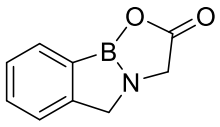

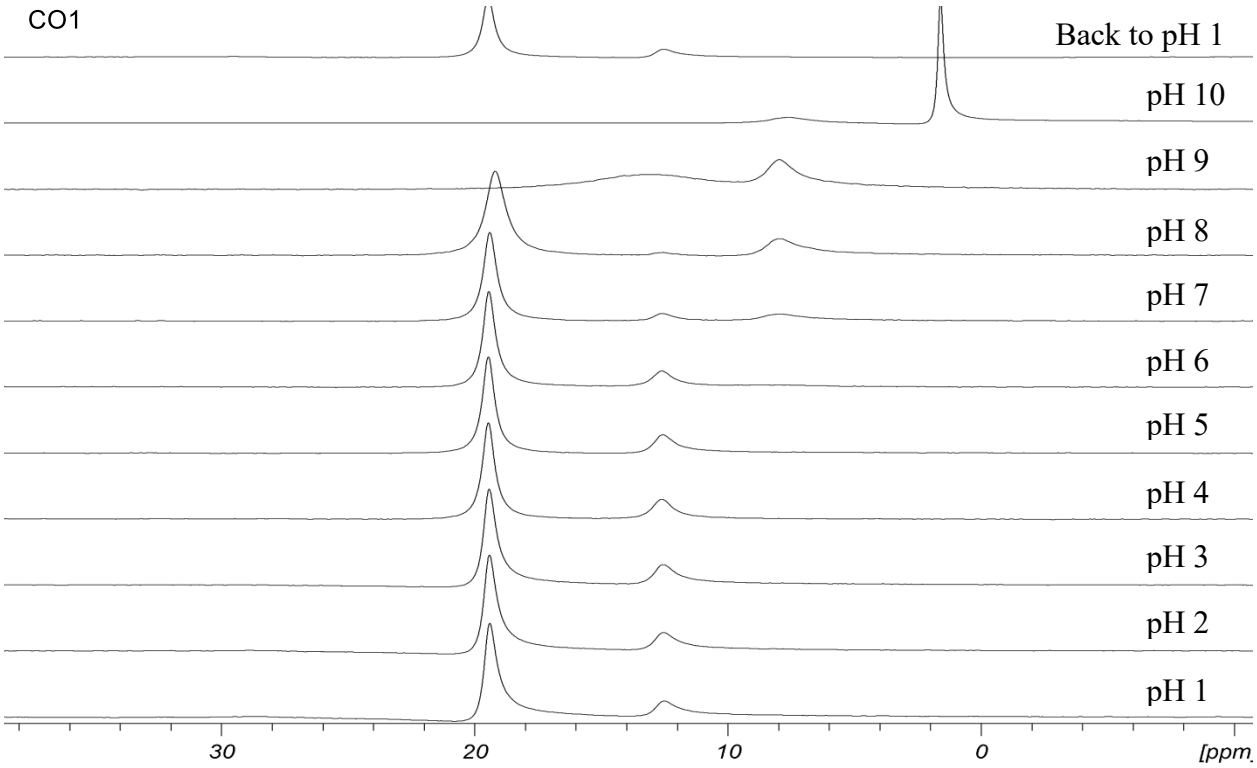

^{11}B NMR Spectrum (500 MHz, D_2O) of CO1 with increasing pH values.

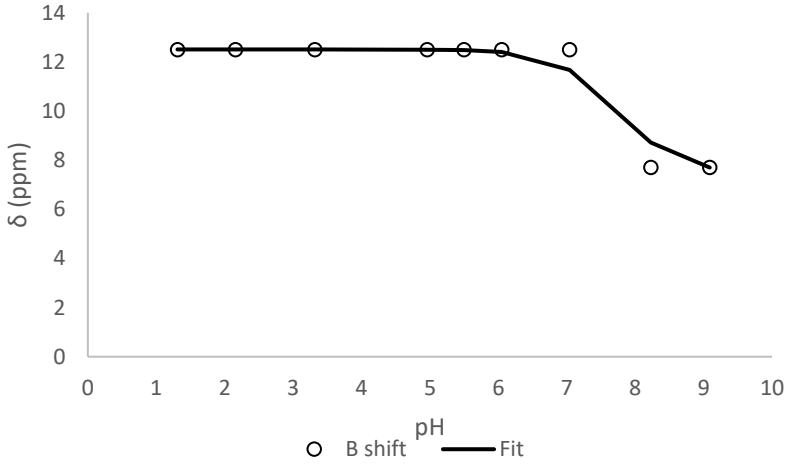

pK_a calculations of CO1 using the non-linear equation 2.3.3. pK_a is 7.8.

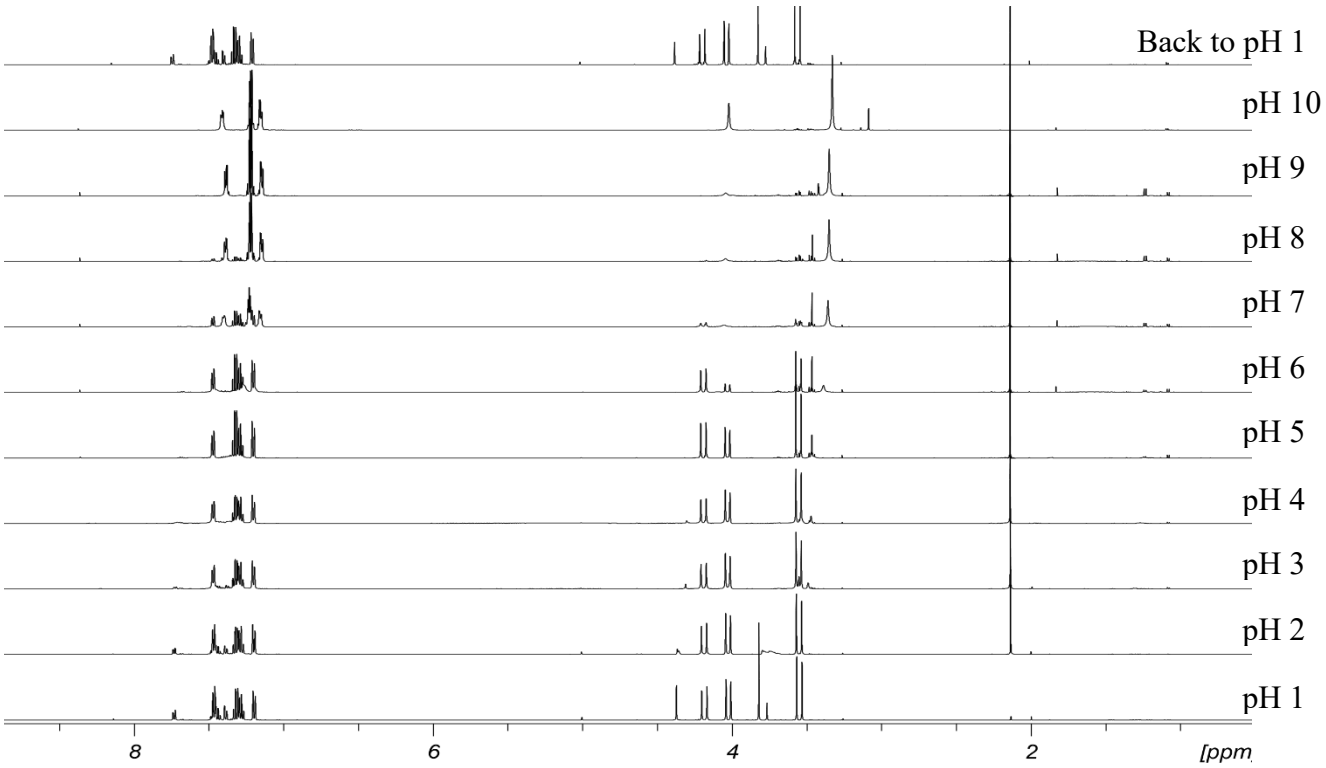

^{1}H NMR Spectrum (500 MHz, D_2O) of CO1 with increasing pH values.

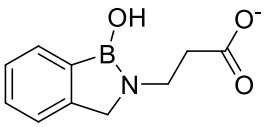

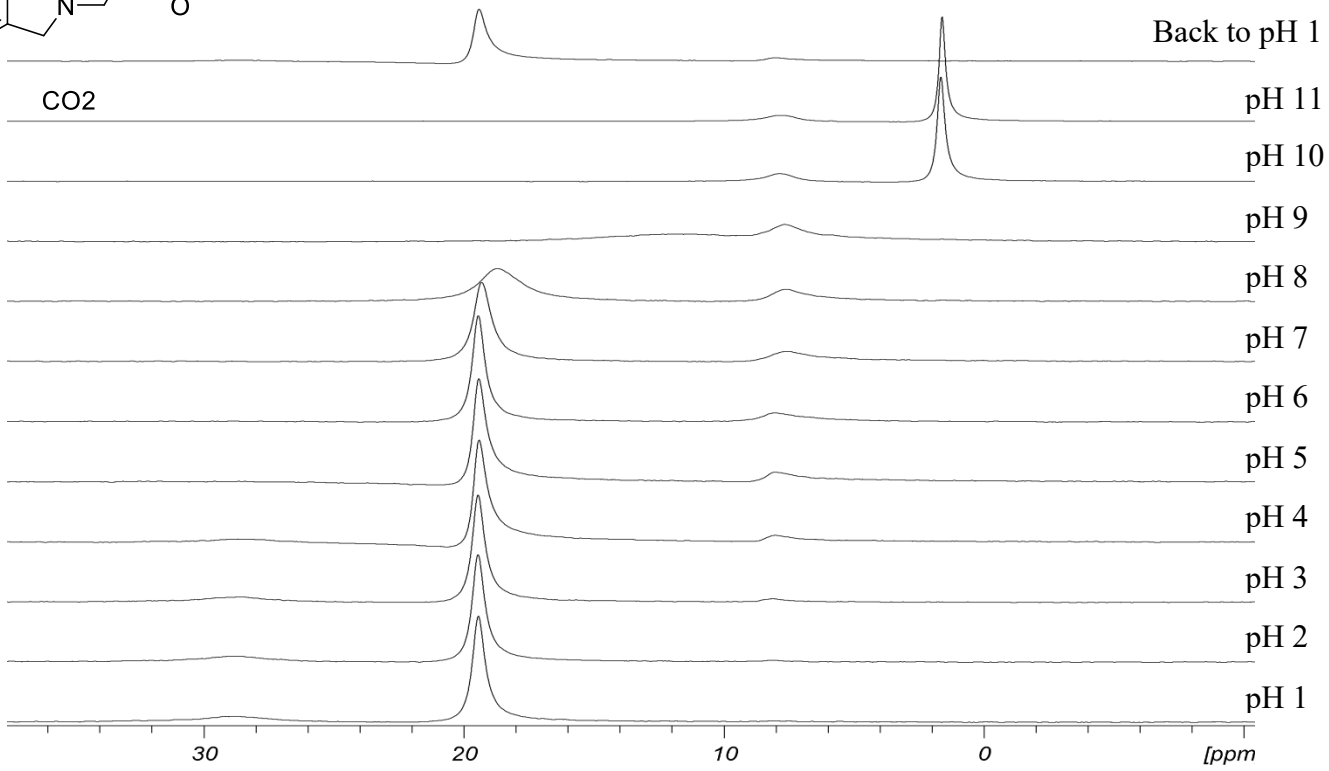

^{11}B NMR Spectrum (500 MHz, D_2O) of CO2 with increasing pH values.

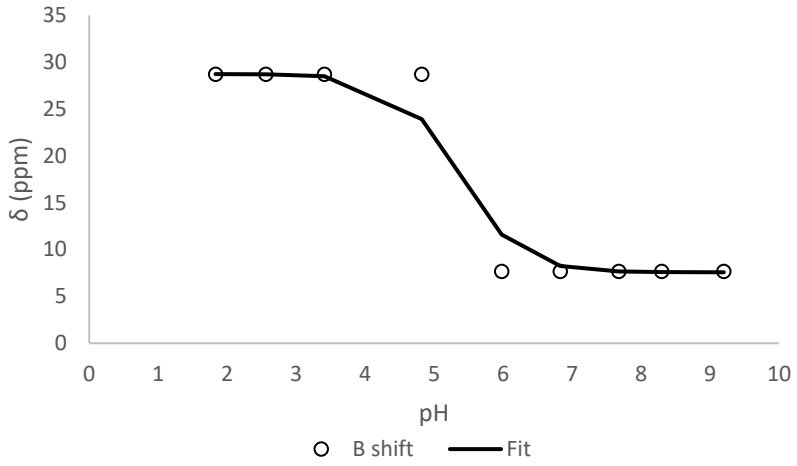

pK_a calculations of CO2 using the non-linear equation 2.3.3. pK_a is 5.4.

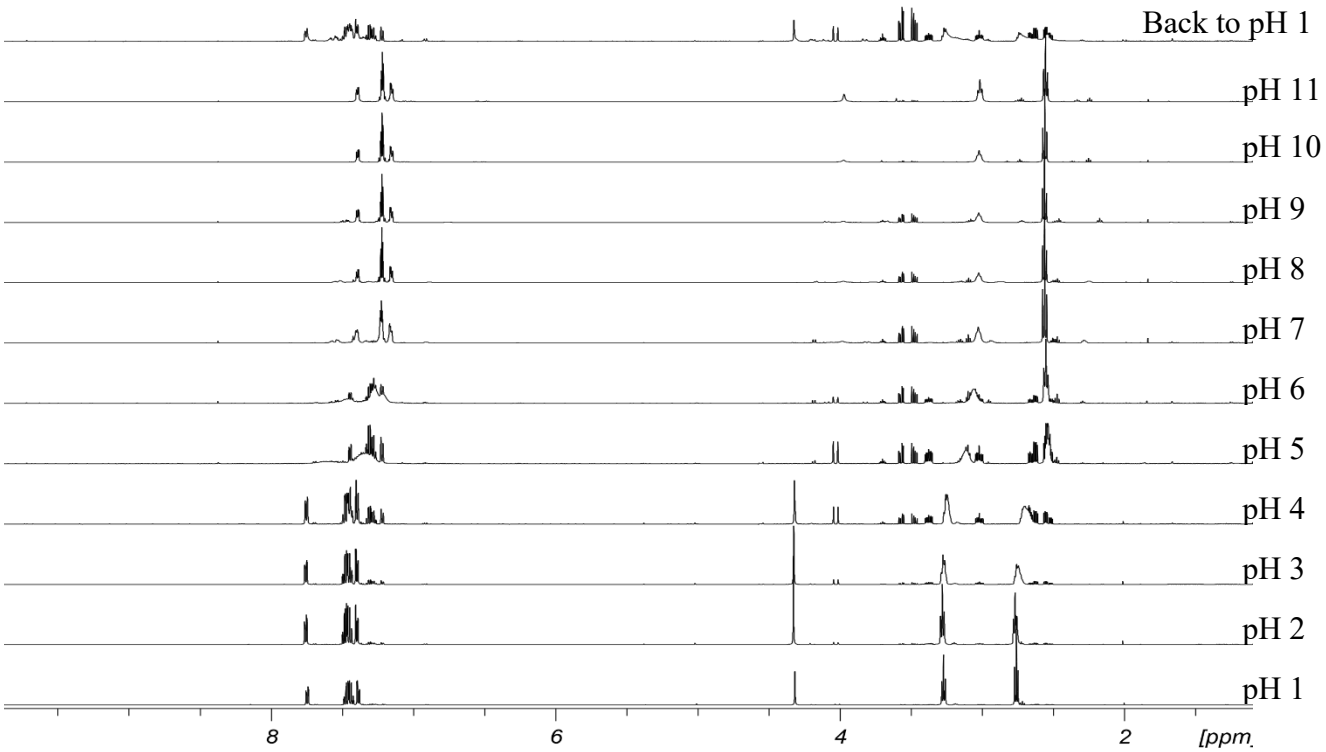

^1H NMR Spectrum (500 MHz, D_2O) of CO2 with increasing pH values.

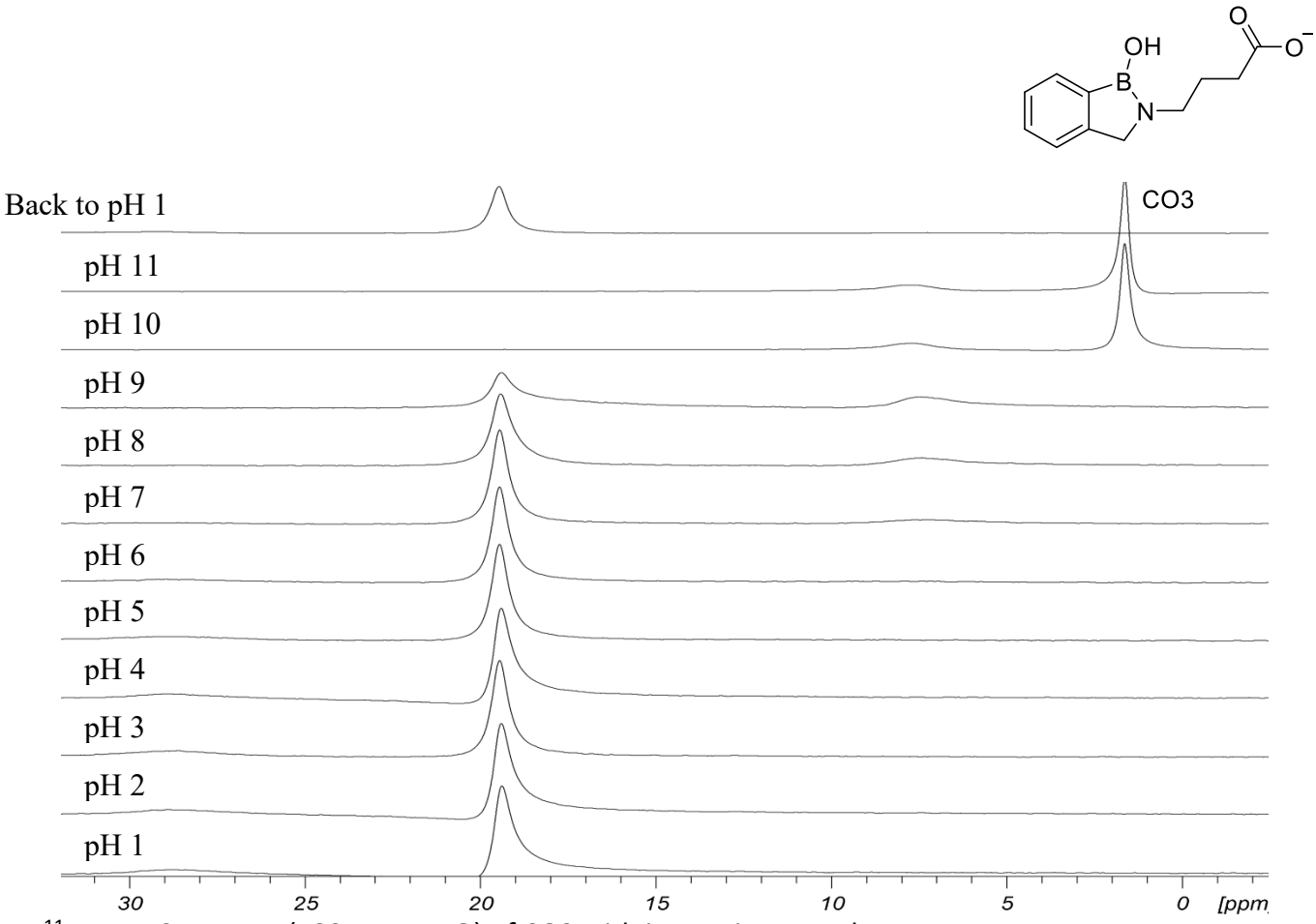

^{11}B NMR Spectrum (500 MHz, D_2O) of CO3 with increasing pH values.

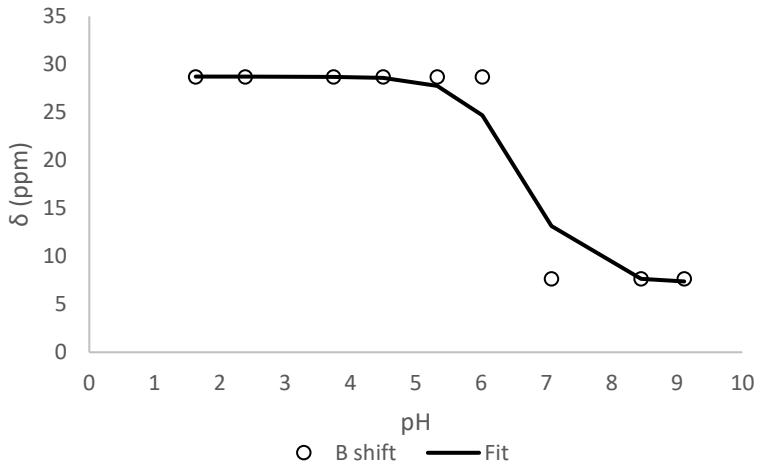

pK_a calculations of CO3 using the non-linear equation 2.3.3. pK_a is 6.7.

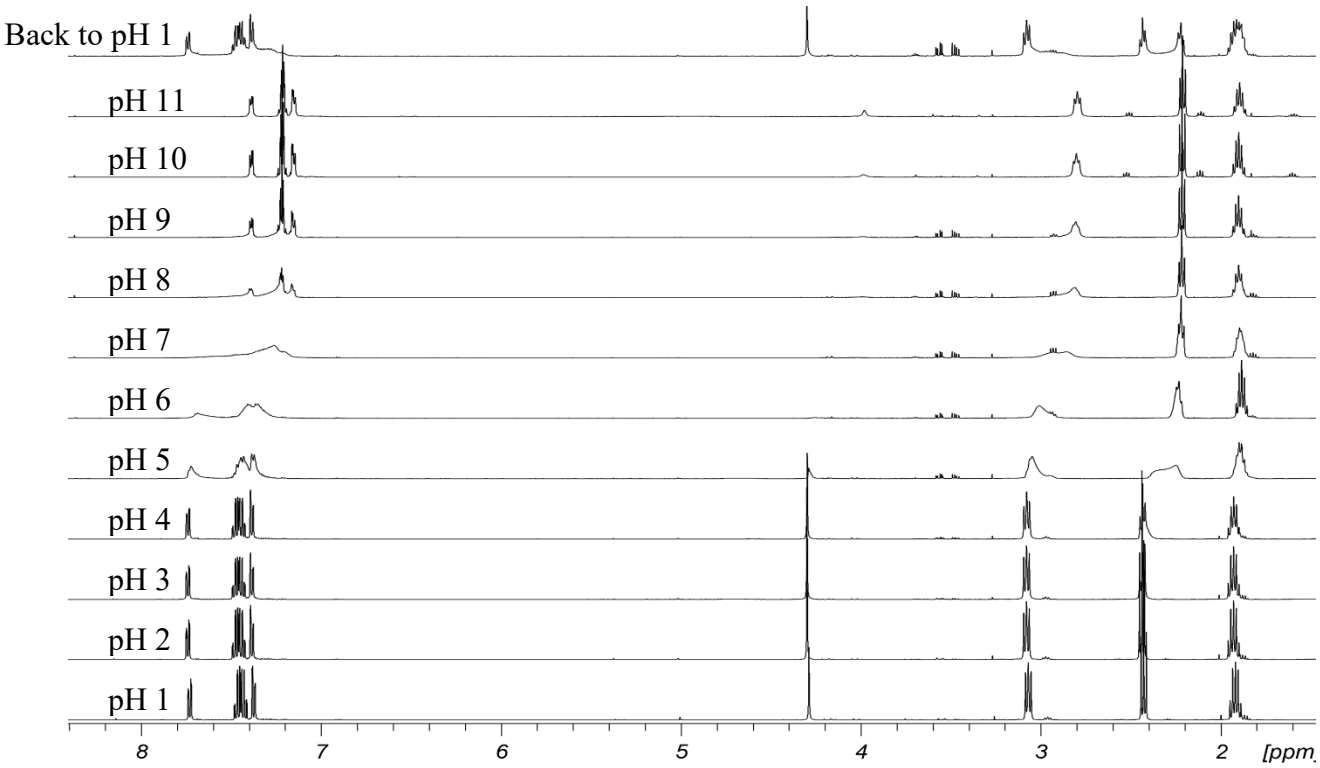

^{1}H NMR Spectrum (500 MHz, D_2O) of CO3 with increasing pH values.

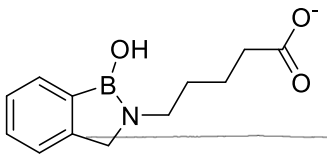

CO4

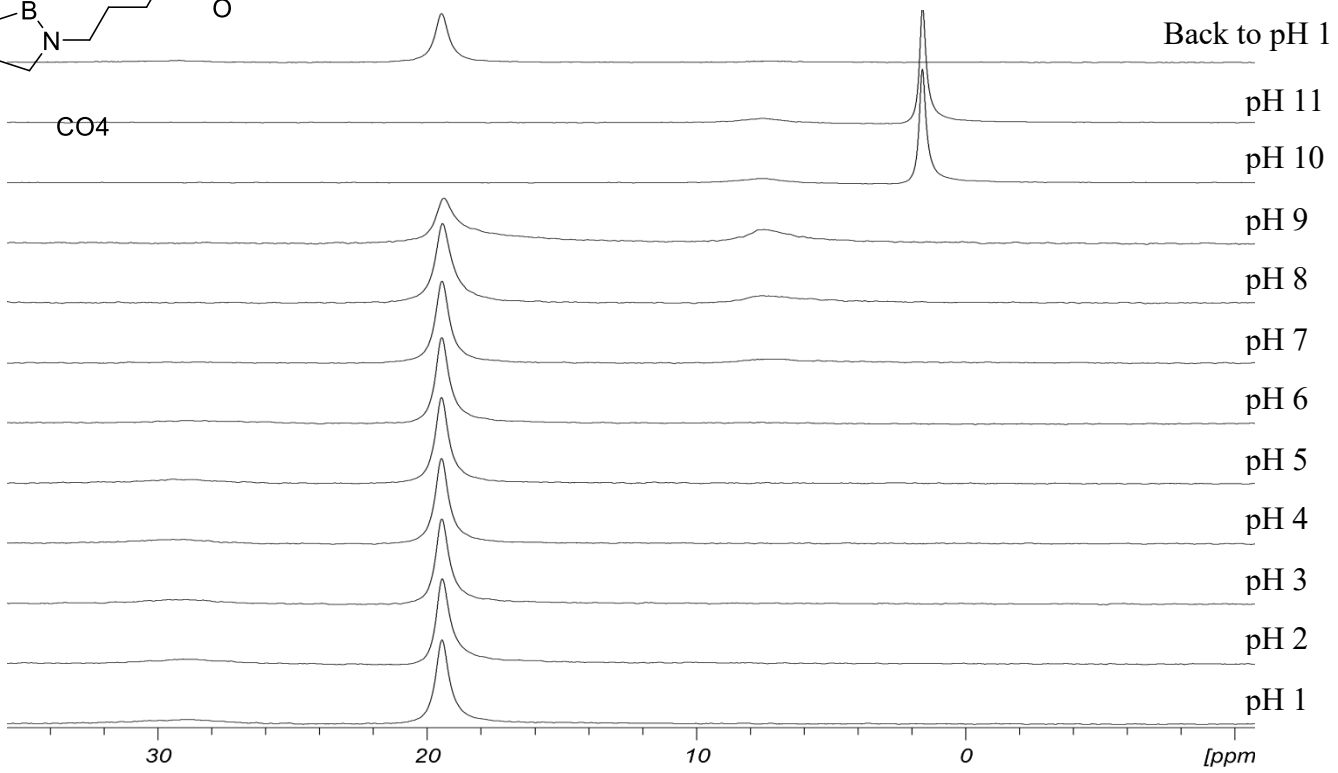

^{11}B NMR Spectrum (500 MHz, D_2O) of CO4 with increasing pH values.

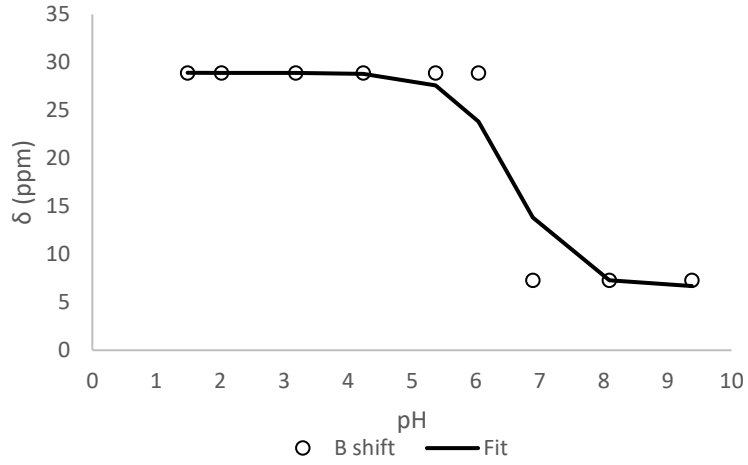

pK_a calculations of CO4 using the non-linear equation 2.3.3. pK_a is 6.6.

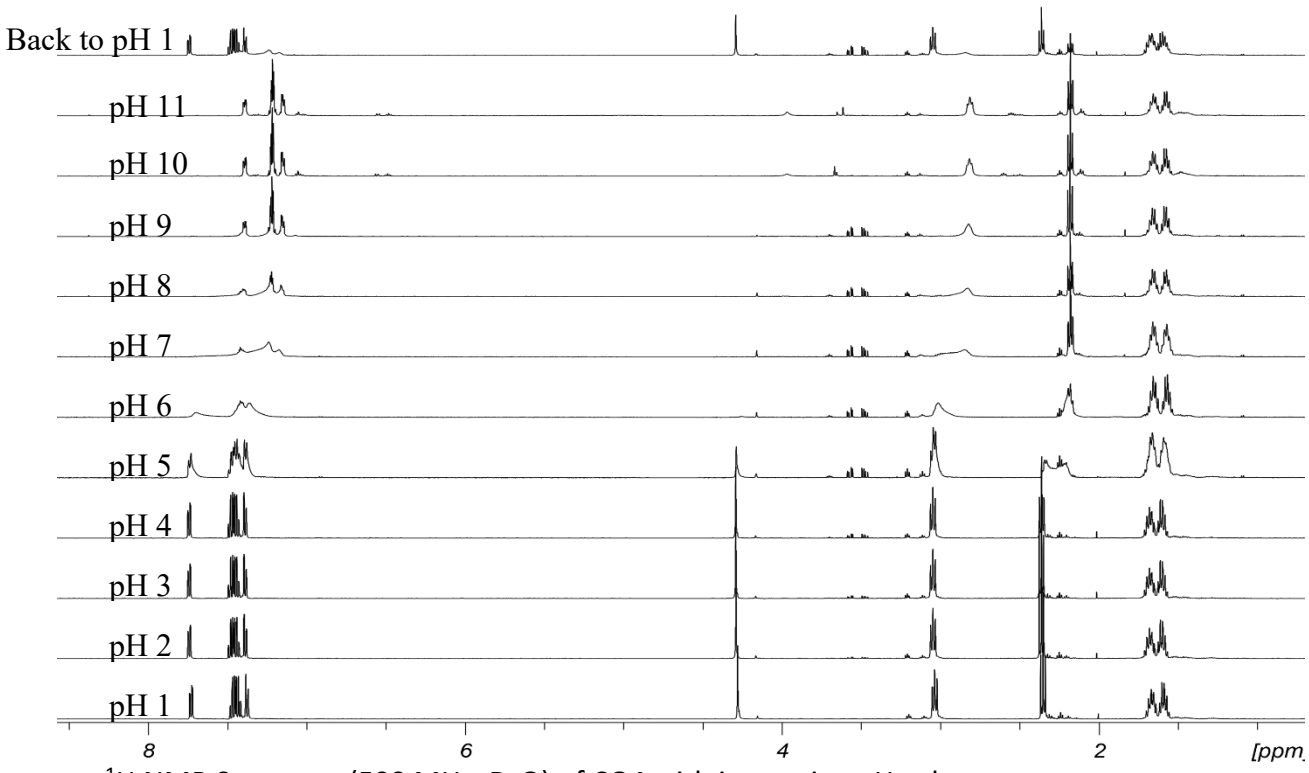

^1H NMR Spectrum (500 MHz, D_2O) of CO4 with increasing pH values.

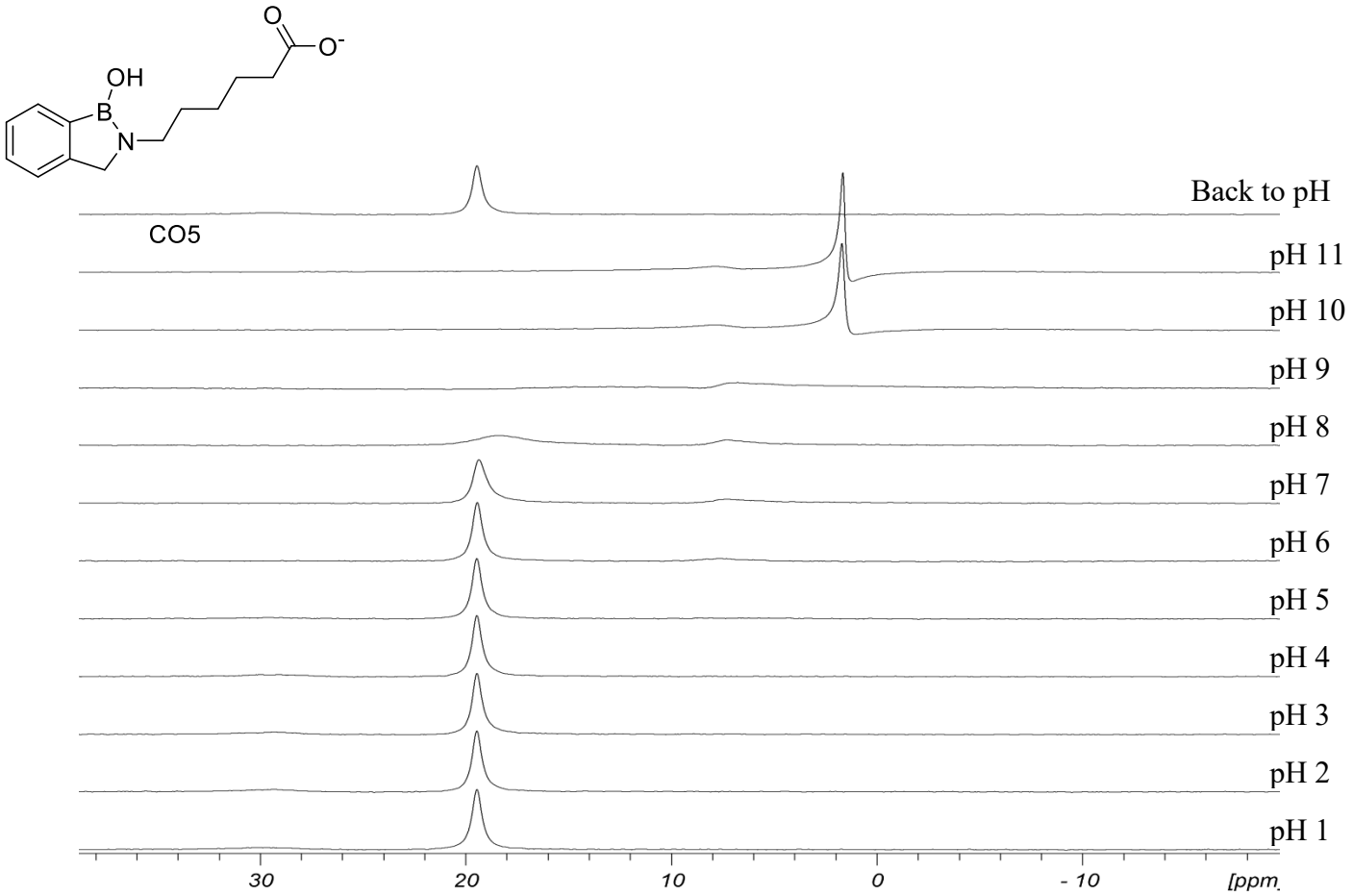

^{11}B NMR Spectrum (500 MHz, D_2O) of CO5 with increasing pH values.

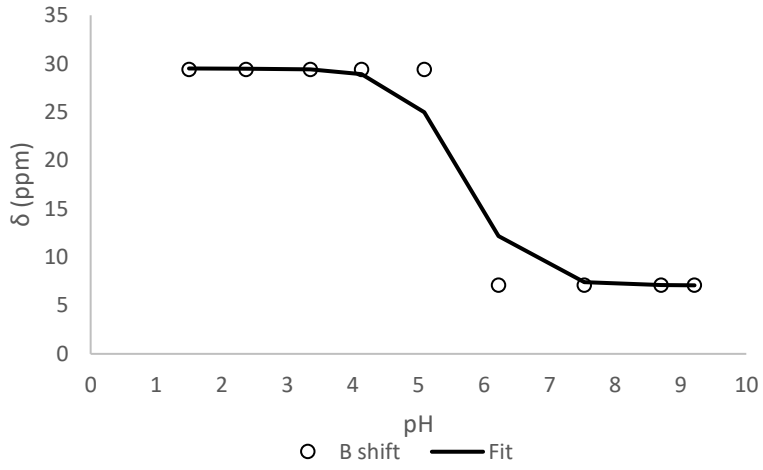

pK_a calculations of CO5 using the non-linear equation 2.3.3. pK_a is 5.7.

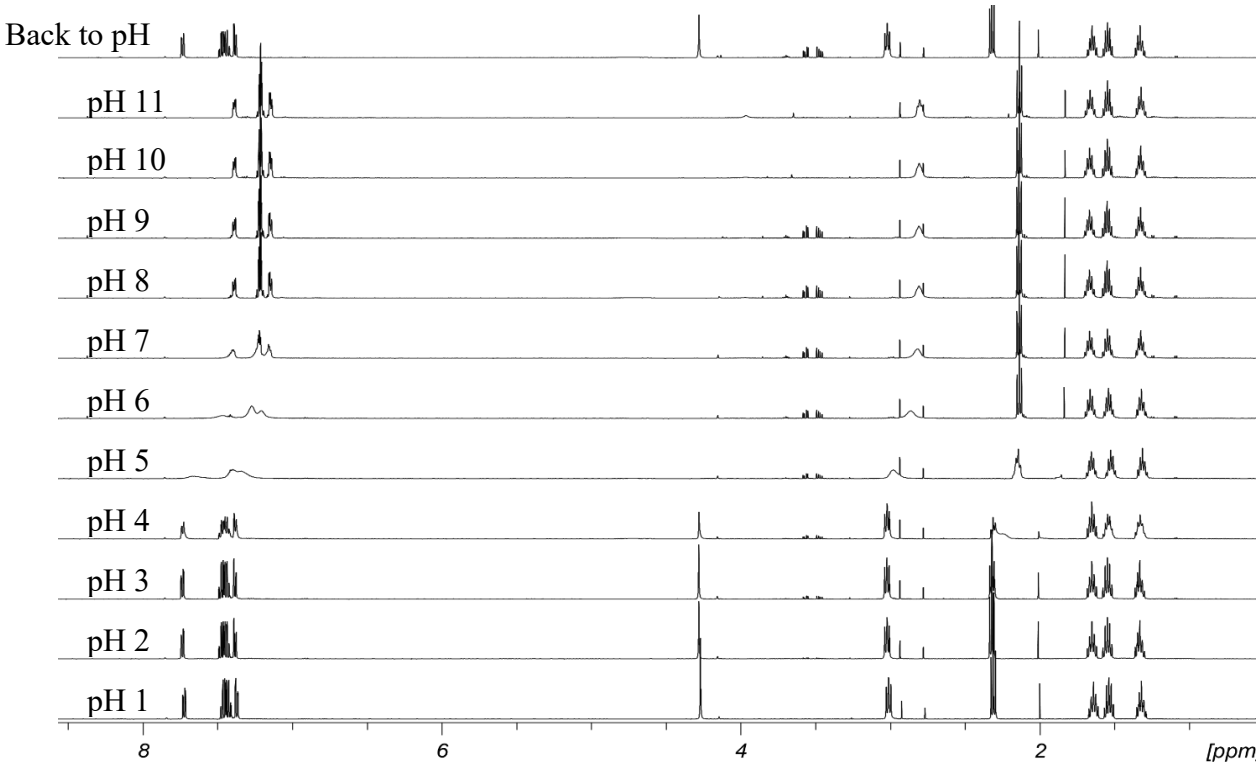

^{1}H NMR Spectrum (500 MHz, D_2O) of CO5 with increasing pH values.

Appendix C. Derivation of Equation 2.4.2

The spectroscopic change in the ARS following diol binding allows the binding coefficient between the ARS and the boronic acid to be measured directly using fluorescence spectroscopy. This relationship was modeled using Equation 1 where the recorded intensity was plotted against the boronic acid concentration.

$$A = \frac{A_0 + A_c K_d [Ligand]_T}{1 + K_d [Ligand]_T}$$

The derivation of equation 1 is as follows. The basic equilibrium for the diol binding of ARS and boronic acid to form an ARS- BA complex is defined in equation 2. ARS= A, boronic acid= $[ligand]_T$, and ARSBA= A_c leading to equation 3. Using the equilibrium defined with equation 3, the thermodynamic association constant K_d is defined in equation 4. Equations 4 and 5 are defined by the relation between the initial concentration of the ligand and the initial concentration of A to the concentration of the free ARS [A], free boronic acid $[ligand]_T$ and the complex forming between ARS and the boronic acid [A_c]. Equation 6 is rearranged into equation 7. Substituting equation 4 into equation 7 gives equation 8. Inversing equation 8 gives a ratio between the concentration of the free ARS [A] and the initial concentration of ARS $[A]_0$ in equation 9. The ratio between the concentration of the ARS- BA complex and the initial concentration of ARS is first introduced in equation 10, using equation 6 to define the denominator. Substituting equation 4 into equation 10 yields equation 11, which is repeated to yield equation 12. Equations 12-14 are simplified which brings to the final form of the ratio. This experiment is performed with about a 1000 times more concentrated boronic acid than the initial concentration of ARS, which is shown in equation 15. This allows the assumption that the high majority of ARS in the equilibrium exists in the ARS- boronic acid complex, instead of being free in the solution. This is shown in equation 16 and 17. The Absorbance of a compound Ax can be defined in equation 18, and it is the product of the initial intensity I_o, the absorbance quantum yields Φ, the extinction coefficient ε, the path length b, and the concentration of the absorbent [X]. These intrinsic properties of the absorbent and the instrument are simplified to a term k_x.

The initial absorbance can be modeled with equation 19, as there is no ARS- boronic acid complex formed. The only Absorbent compound is the initial ARS. The Absorbance of the system at equilibrium A can be modeled with equation 20 with both the free ARS and the ARS- boronic acid complex add to the overall absorbance of the system. The ratio between the absorbance of the system at equilibrium A and the initial absorbance A_0 is defined in equation 21. Rearranging equation 21, substituting in equation 4, and simplifying is shown in equations 21-24. At this point, a second assumption is made about the system. There is no self-quenching observed and it is being expressed in equation 25. When equation 25 is substituted into equation 24, equation 26 is derived and rearranging it yields to equation 27. Substituting equation 19 into equation 27 yields equation 28 which is then being simplified into equation 29. Equation 17 is then substituted into equation 29, which yields equation 30. Finally equation 18 is used to transform equation 30 into the final relationship defined by equation 1.

$$ARS + BA \rightleftarrows ARS\ BA \tag{2}$$

$$A + [Ligand]_T \rightleftarrows A_c \tag{3}$$

$$K_d = \frac{[A_c]}{[A][[Ligand]_T]} \tag{4}$$

$$[[Ligand]_T]_o = [[Ligand]_T] + [A_c] \tag{5}$$

$$[A]_o = [A] + [A_c] \tag{6}$$

$$\frac{[A]_o}{[A]} = 1 + \frac{[A_c]}{[A]} \tag{7}$$

$$\frac{[A]_o}{[A]} = 1 + K_d[[Ligand]_T] \tag{8}$$

$$\frac{[A]}{[A]_o} = \frac{1}{1 + K_d[[Ligand]_T]} \tag{9}$$

$$\frac{[A_c]}{[A]_o} = \frac{[A_c]}{[A] + [A_c]} \tag{10}$$

$$\frac{[A_c]}{[A]_o} = \frac{K_d[A][[Ligand]_T]}{\frac{[A_c]}{K_d[[Ligand]_T]} + K_d[A][[Ligand]_T]} \tag{11}$$

$$\frac{[A_c]}{[A]_o} = \frac{K_d[A][[Ligand]_T]}{\frac{K_d[A][[Ligand]_T]}{K_d[[Ligand]_T]} + K_d[A][[Ligand]_T]} \tag{12}$$

$$\frac{[A_c]}{[A]_o} = \frac{1}{\frac{1}{K_d[[Ligand]_T]} + 1} \tag{13}$$

$$\frac{[A_c]}{[A]_o} = \frac{K_d[[Ligand]_T]}{K_d[[Ligand]_T] + 1} \tag{14}$$

$$[[Ligand]_T]_o \gg [A]_o \tag{15}$$

$$\therefore [A_c] \gg [A] \tag{16}$$

$$\therefore [A]_o \approx [A_c] \tag{17}$$

$$A_x = I_o \Phi \varepsilon b[X] = k_X[X] \tag{18}$$

$$A_o = A_{A_o} + A_{[Ligand]_{T_o}} + A_{c_o} = A_{A_o} = k_{A_o}[A]_o \tag{19}$$

(20)

$$A = A_A + A_{[Ligand]_T} + A_c = A_A + A_c = k_A[A] + k_{A_c}[A_c]$$

$$\frac{A}{A_o} = \frac{k_A[A] + k_{A_c}[A_c]}{k_{A_o}[A]_o} \tag{21}$$

(22)

$$\frac{A}{A_o} = \frac{k_A[A]}{k_{A_o}[A]_o} + \frac{k_{A_c}[A_c]}{k_{A_o}[A]_o}$$

(23)

$$\frac{A}{A_o} = \frac{k_A}{k_{A_o}}\left(\frac{1}{1 + K_d[[Ligand]_T]}\right) + \frac{k_{A_c}}{k_{A_o}}\left(\frac{K_d[[Ligand]_T]}{1 + K_d[[Ligand]_T]}\right)$$

(24)

$$\frac{A}{A_o} = \frac{{k_A}/{k_{A_o}} + {k_{A_c}}/{k_{A_o}} K_d[[Ligand]_T]}{1 + K_d[[Ligand]_T]}$$

(25)

$$k_A = k_{A_o}$$

(26)

$$\frac{A}{A_o} = \frac{1 + {k_{A_c}}/{k_{A_o}} K_d[[Ligand]_T]}{1 + K_d[[Ligand]_T]}$$

(27)

$$A = \frac{A_o + {k_{A_c}}/{k_{A_o}} A_o K_d[[Ligand]_T]}{1 + K_d[[Ligand]_T]}$$

(28)

$$A = \frac{A_o + {k_{A_c}}/{k_{A_o}} k_{A_o}[A]_o K_d[[Ligand]_T]}{1 + K_d[[Ligand]_T]}$$

(29)

$$A = \frac{A_o + [A]_o k_{A_c} K_d [[Ligand]_T]}{1 + K_d [[Ligand]_T]}$$

(30)

$$A = \frac{A_o + [A_c] k_{A_c} K_d [[Ligand]_T]}{1 + K_d [[Ligand]_T]}$$

(1)

$$A = \frac{A_0 + A_c K_d [Ligand]_T}{1 + K_d [Ligand]_T}$$

This equation relates the absorbance of the system A to the initial absorbance A_0 the absorbance of the free ARS A_c, the association constant of the boronic acid to the monosaccharide K_d, and the concentration of the monosaccharide $[ligand]_T$. Same form of equation was used for fluorescence spectroscopy system.

Appendix D. Iminoboronate and Diazaborine Using UV-Vis Spectroscopy

Iminoboronate Formation

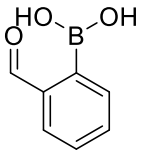

2FPBA

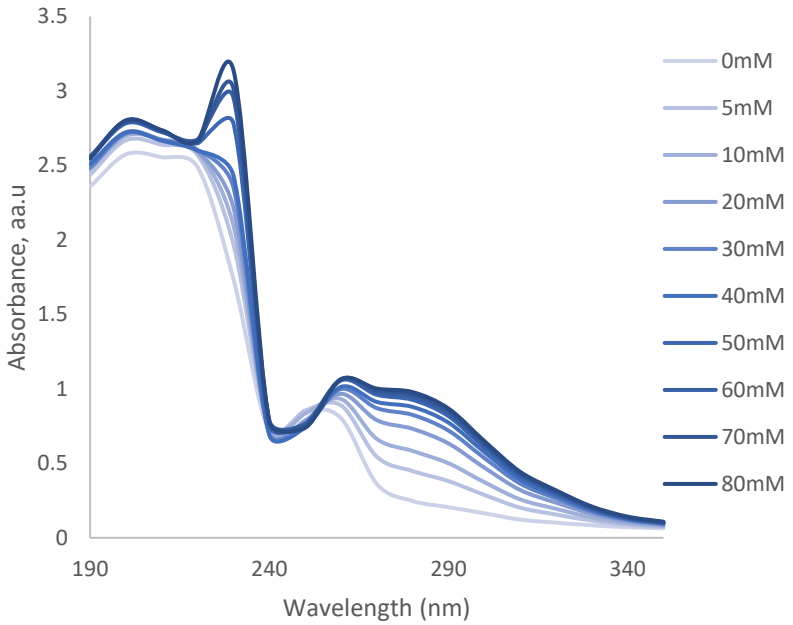

UV Spectroscopy of 2FPBA with increasing concentration of Boc-Lys-OH.

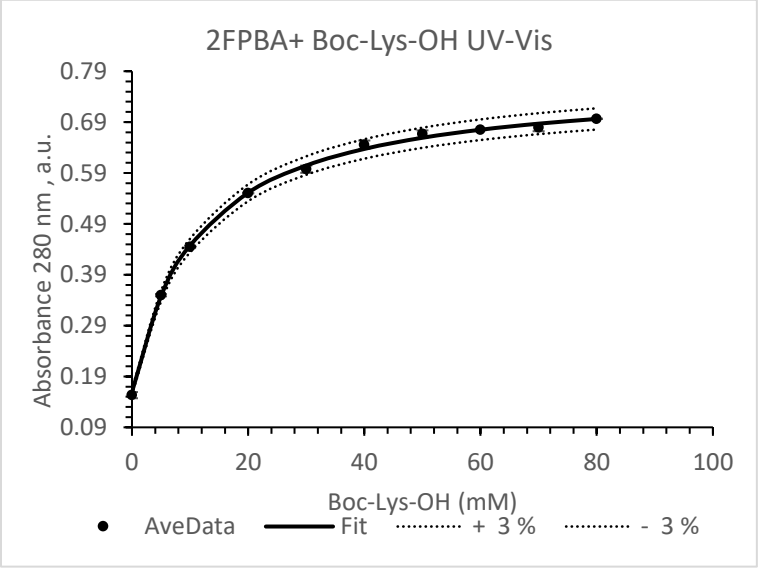

Plot of absorbance (280 nm) changes of 2FPBA (1.0 mM) with increasing of Boc-Lys-OH concentration (0-80 mM) in HEPES buffer (1000 mM, pH 7.4). (K_a was calculated to be 88.7 ± 0.04 M^{-1}). Values are the average of duplicate runs. Dotted lines represent 3% error calculated of absorbance.

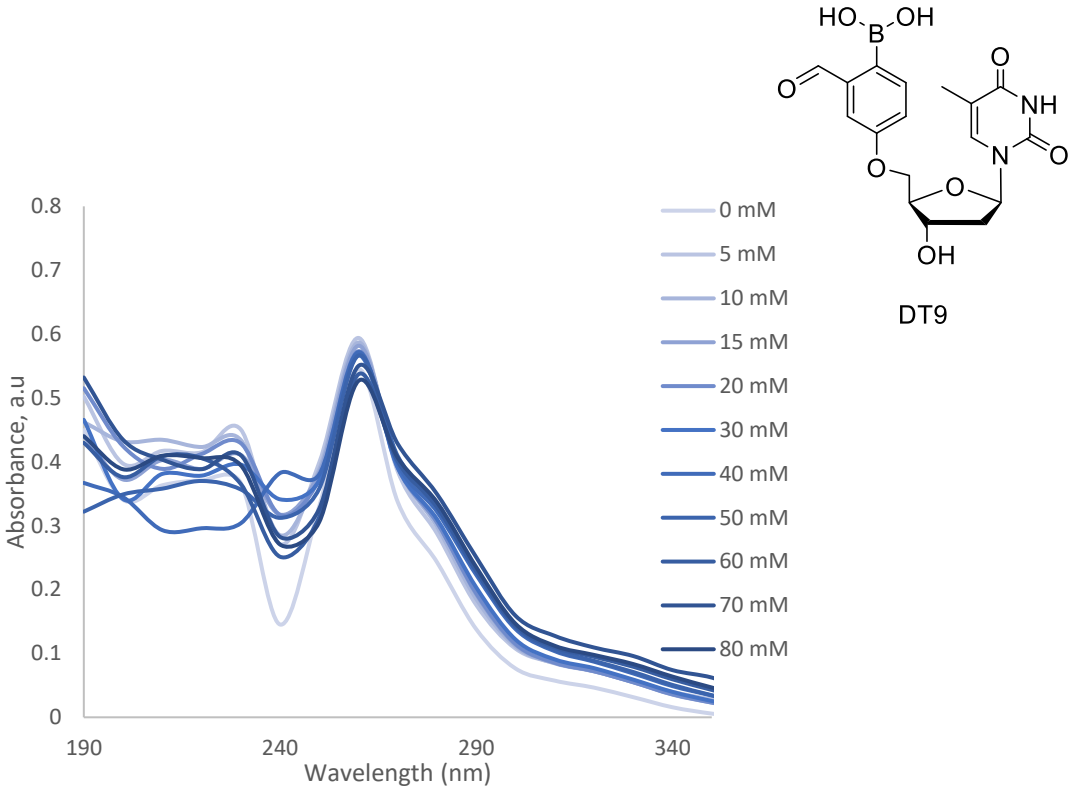

UV Spectroscopy of DT9 with increasing concentration of Boc-Lys-OH.

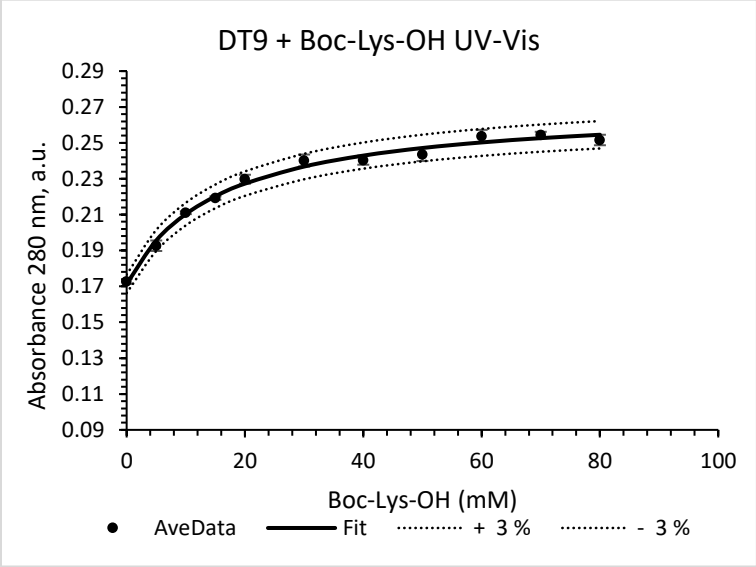

Plot of absorbance (280 nm) changes of DT9 (1.0 mM) with increasing of Boc-Lys-OH concentration (0-80 mM) in HEPES buffer (1000 mM, pH 7.4). (K_a was calculated to be 64.4 ± 0.03 M^{-1}). Values are the average of duplicate runs. Dotted lines represent 3% error calculated of absorbance.

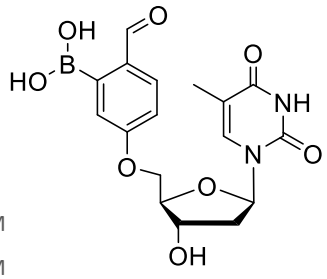

DT14

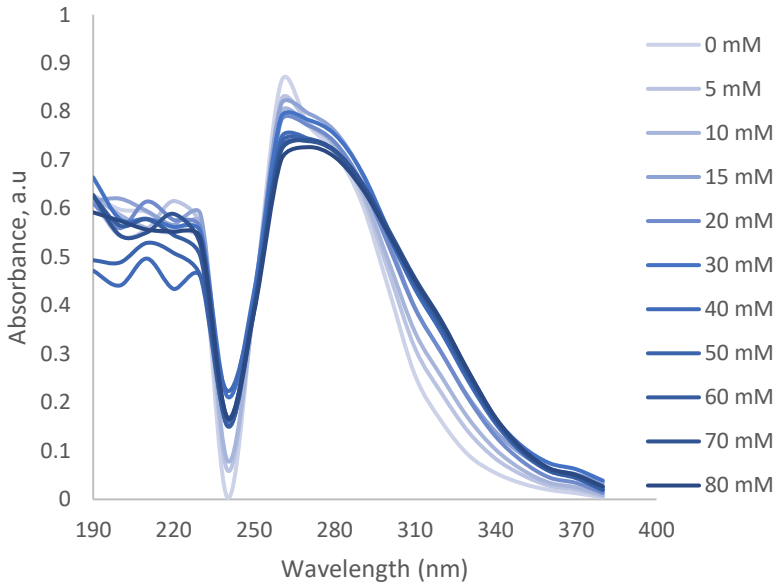

UV-Vis Spectroscopy of DT14 with increasing concentration of Boc-Lys-OH.

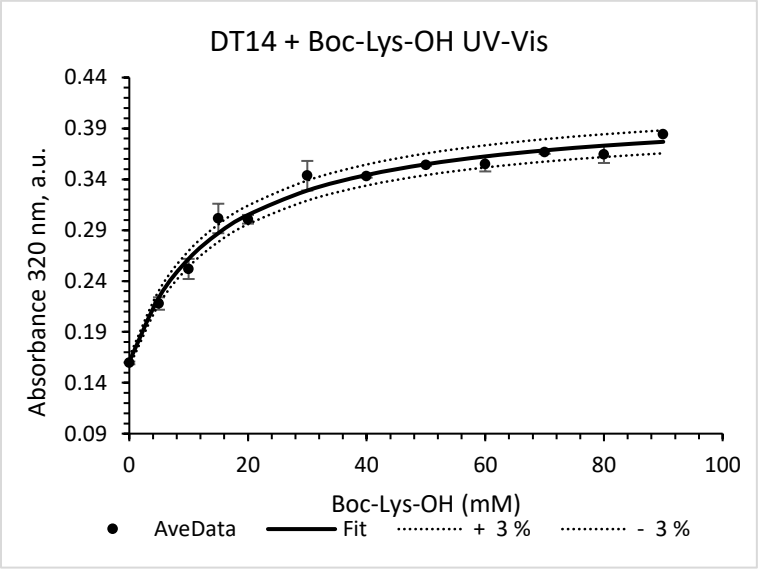

Plot of absorbance (320 nm) changes of DT14 (1.0 mM) with increasing of Boc-Lys-OH concentration (0-80 mM) in HEPES buffer (1000 mM, pH 7.4). (K_{abs} was calculated to be 66.9 ± 0.07 M^{-1}). Values are the average of duplicate runs. Dotted lines represent 3% error calculated of absorbance.

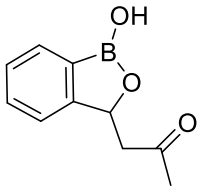

DE318

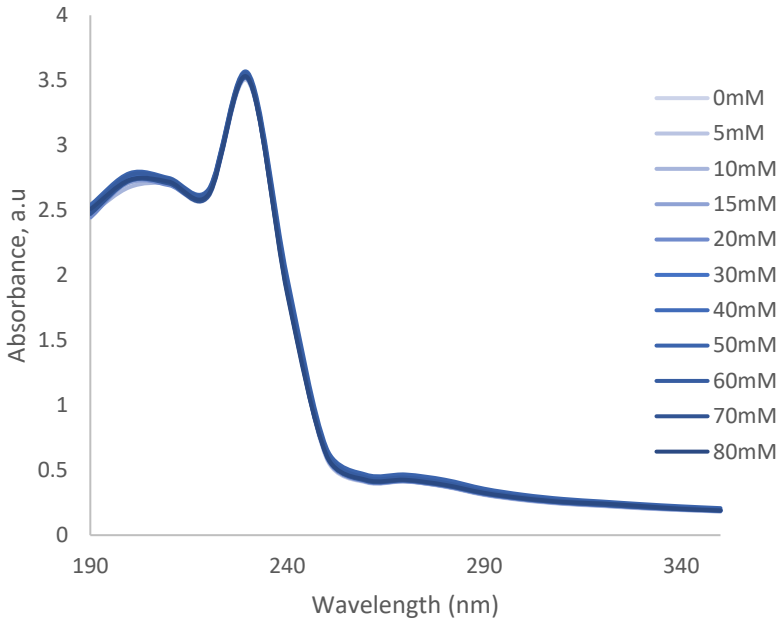

UV Spectroscopy of DE318 with increasing concentration of Boc-Lys-OH.

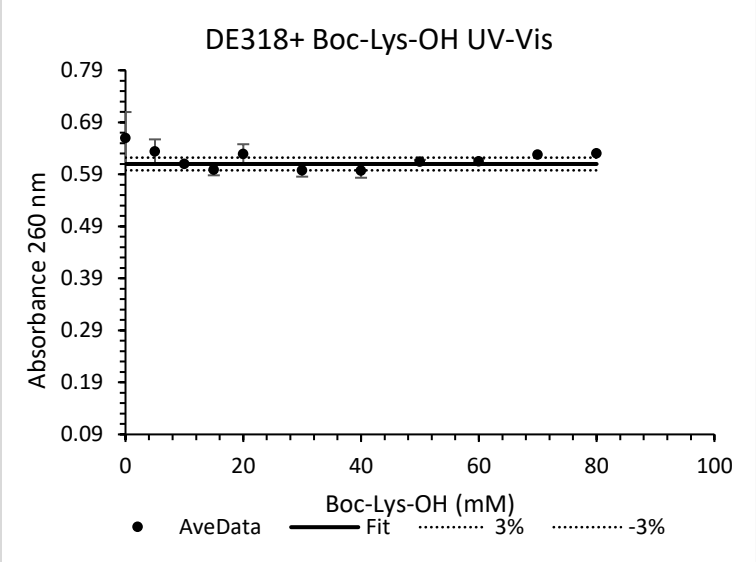

Plot of absorbance (260 nm) changes of DE318 (1.0 mM) with increasing of Boc-Lys-OH concentration (0-80 mM) in HEPES buffer (1000 mM, pH 7.4). (K_a was calculated to be 0.00±0.2 M^{-1}). Values are the average of duplicate runs. Dotted lines represent 3% error calculated of absorbance.

Diazaborine Formation

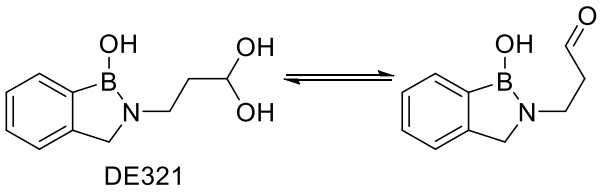

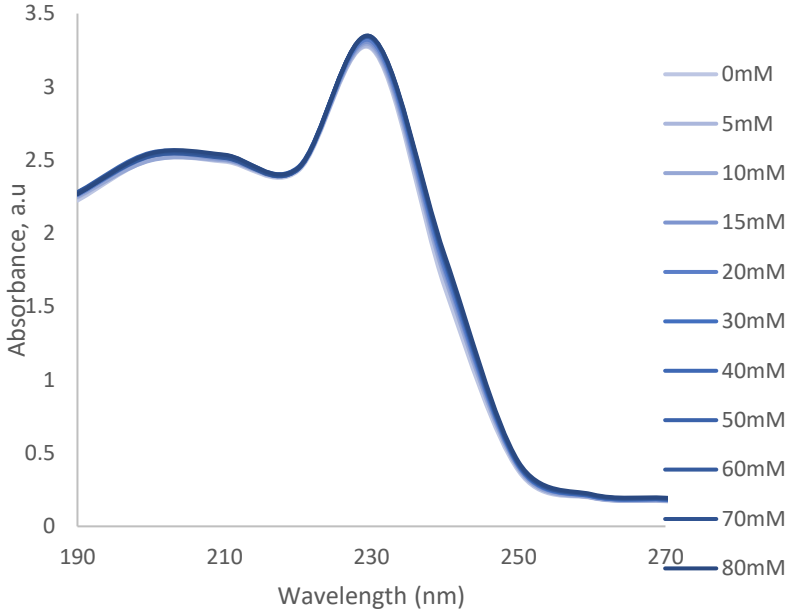

UV Spectroscopy of DE321 with increasing concentration of Boc-Lys-OH.

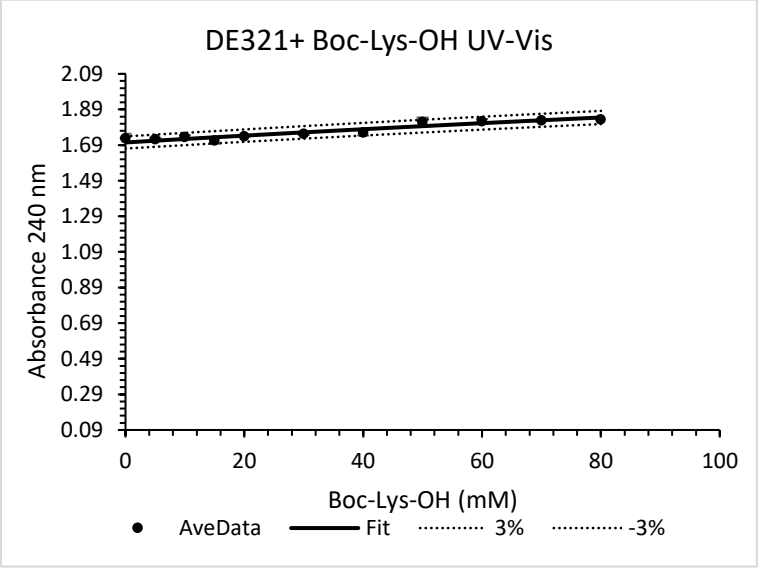

Plot of absorbance (240 nm) changes of DE321 (1.0 mM) with increasing of Boc-Lys-OH concentration (0-80 mM) in HEPES buffer (1000 mM, pH 7.4). (K_a was calculated to be 0.00±0.001 M^{-1}). Values are the average of duplicate runs. Dotted lines represent 3% error calculated of absorbance.

Iminoboronate Formation with Ethylamine

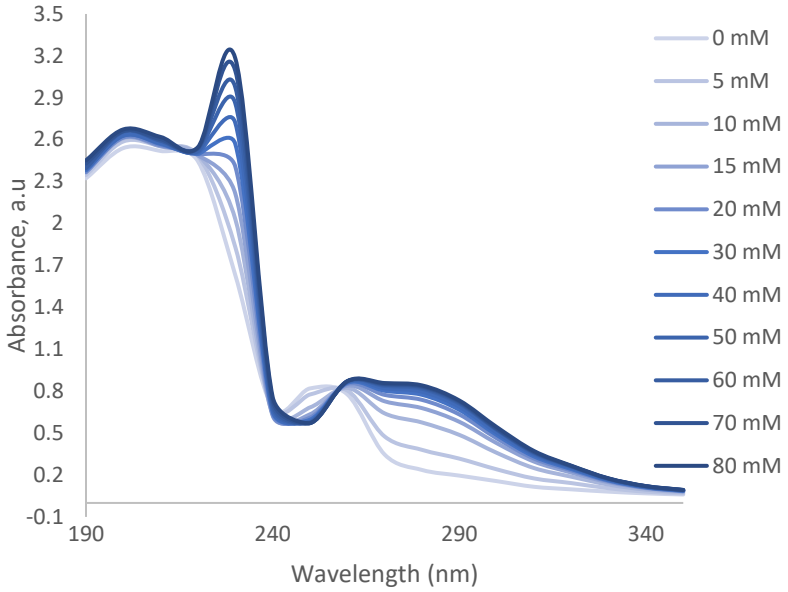

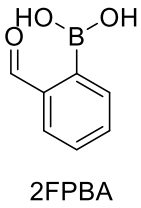

2FPBA

UV Spectroscopy of 2FPBA with increasing concentration of ethylamine.

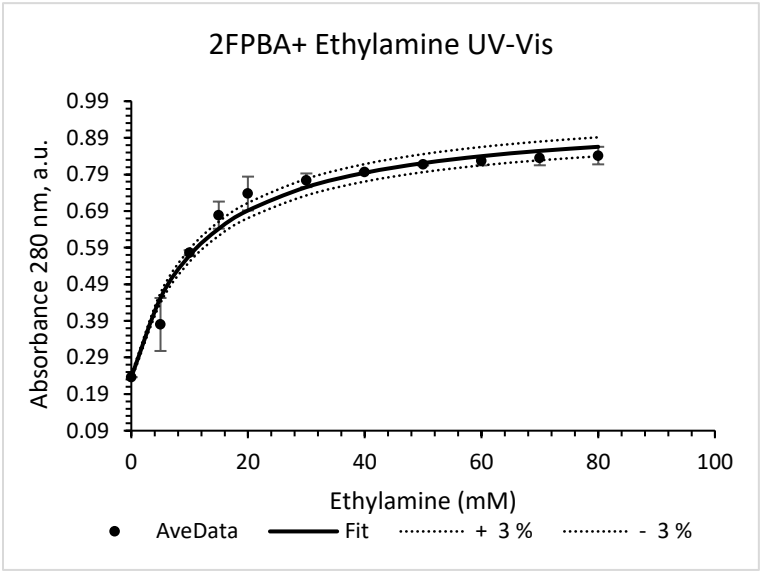

Plot of absorbance (280 nm) changes of 2FPBA (1.0 mM) with increasing of ethylamine concentration (0-80 mM) in HEPES buffer (1000 mM, pH 7.4). (K_a was calculated to be 86.4 ± 0.01 M^{-1}). Values are the average of duplicate runs. Dotted lines represent 3% error calculated of absorbance.

Appendix E. Iminoboronate and Diazaborine using NMR Spectroscopy

Iminoboronate Formation

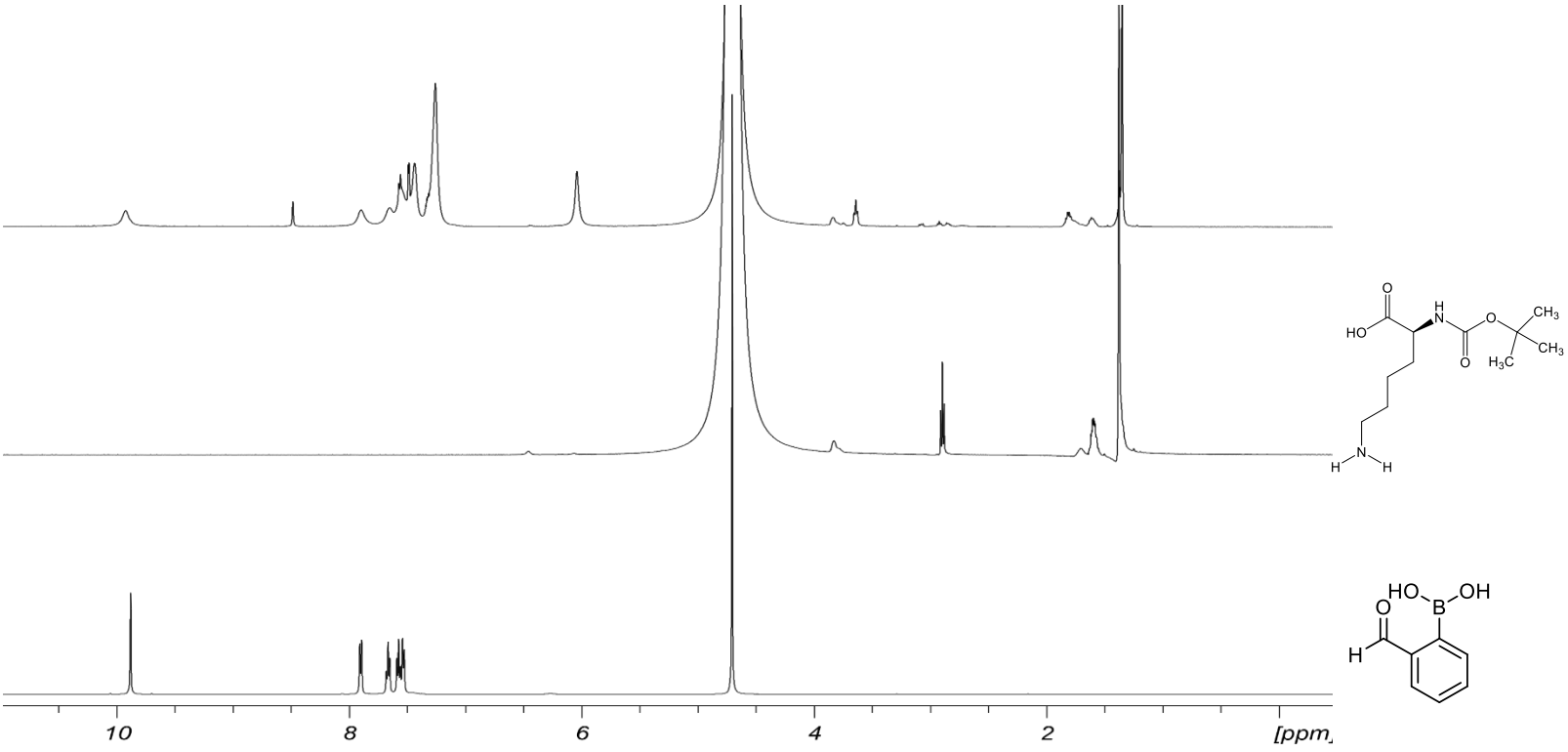

^{1}H NMR Spectrum (500 MHz, phosphate buffer) of 2FPBA added with Boc-Lys-OH.

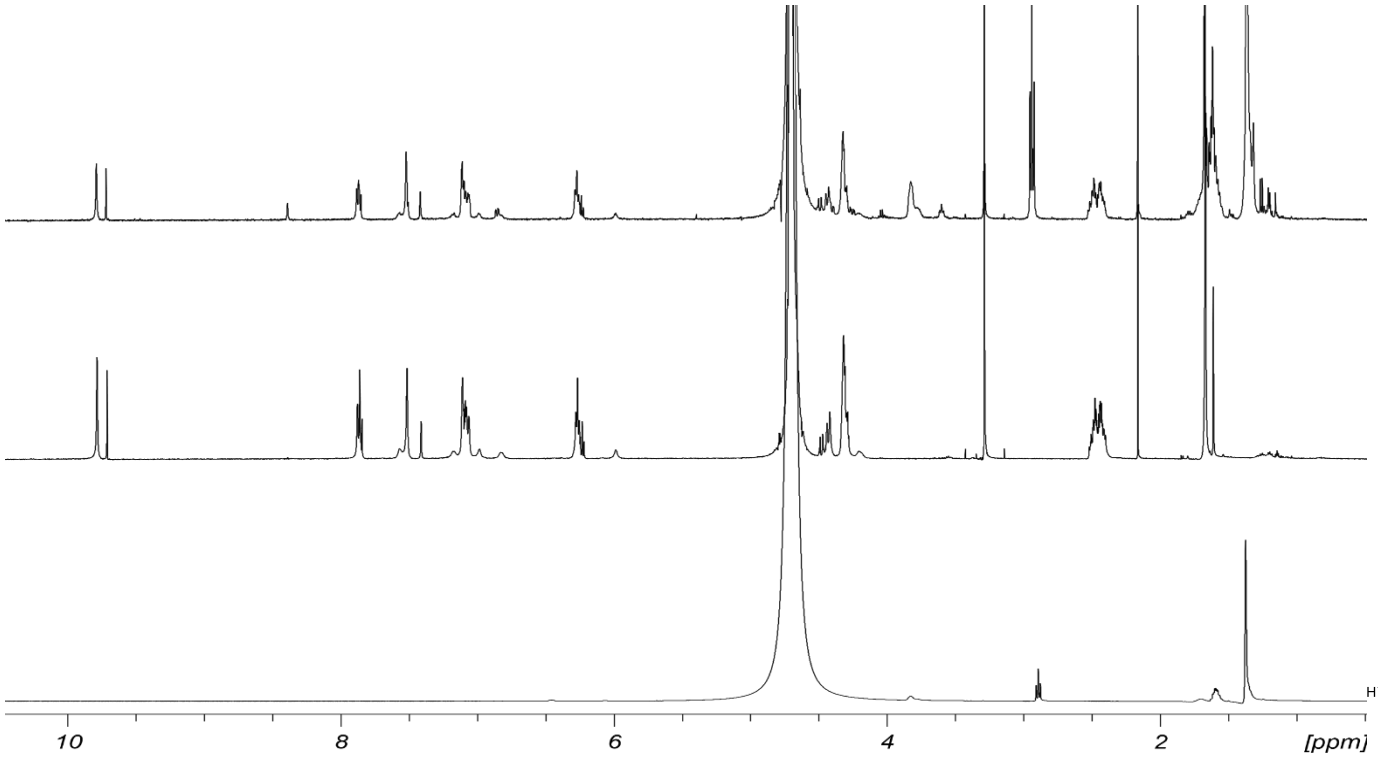

^{1}H NMR Spectrum (500 MHz, phosphate buffer) of DT9 added with Boc-Lys-OH.

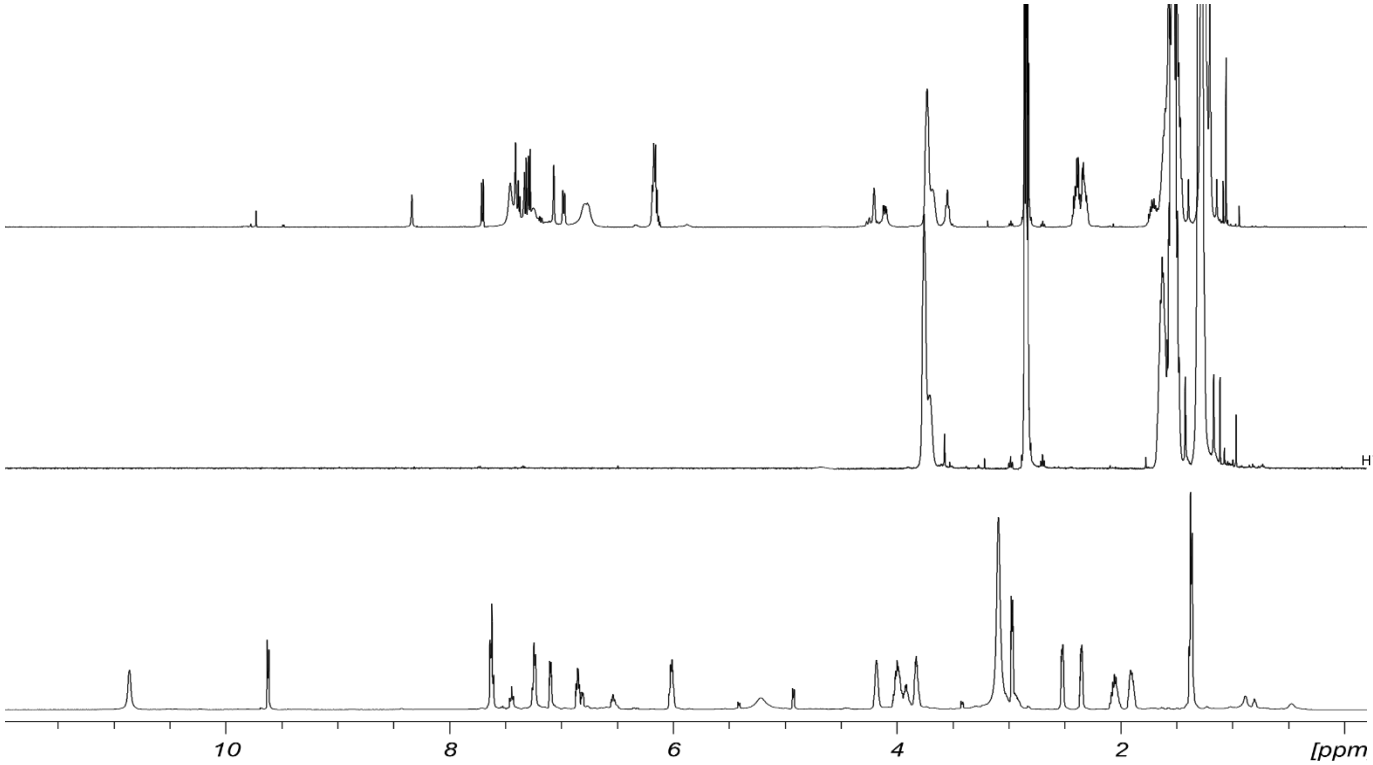

^{1}H NMR Spectrum (500 MHz, phosphate buffer) of DT14 added with Boc-Lys-OH.

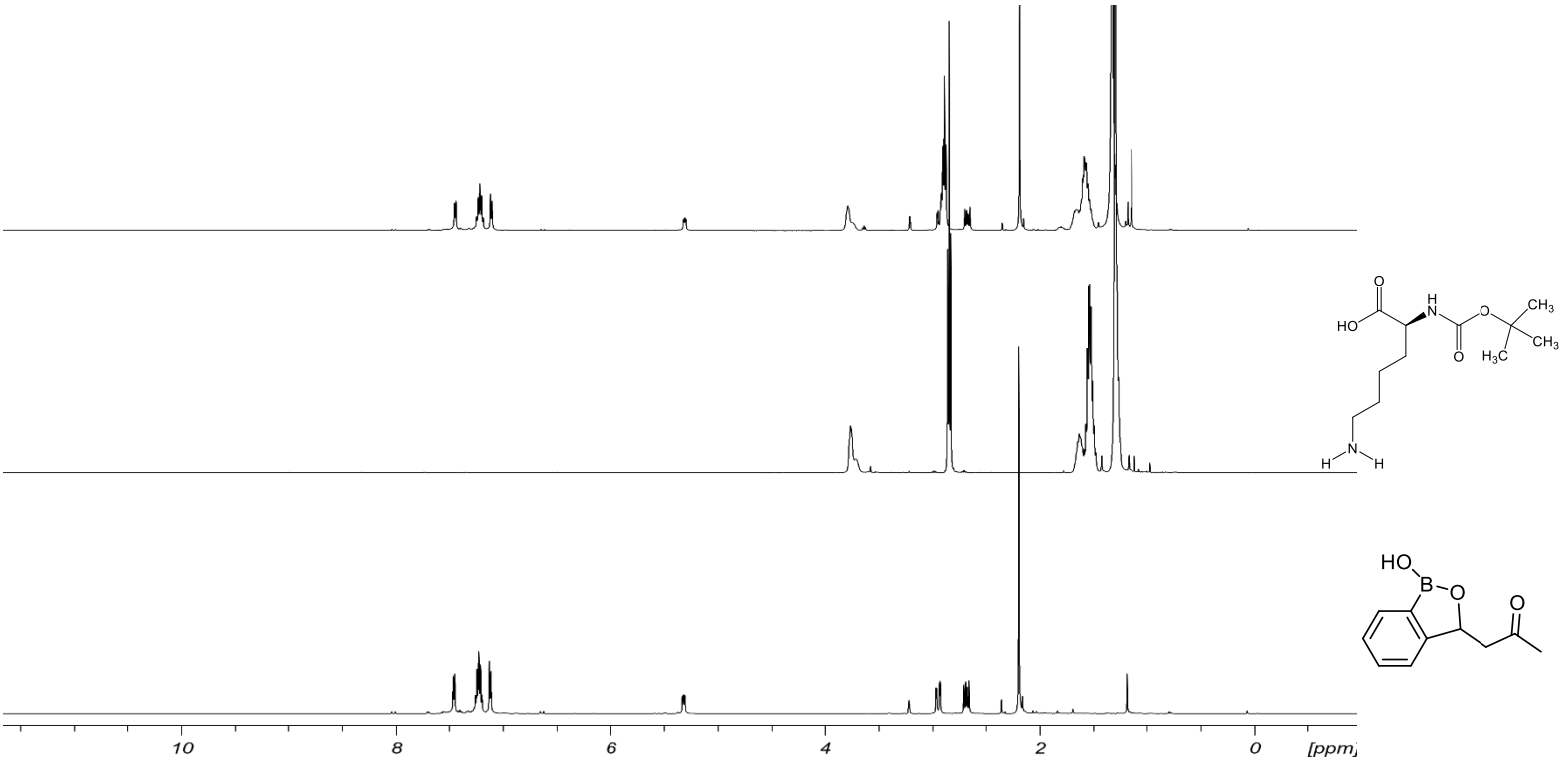

^{1}H NMR Spectrum (500 MHz, phosphate buffer) of DE318 added with Boc-Lys-OH.

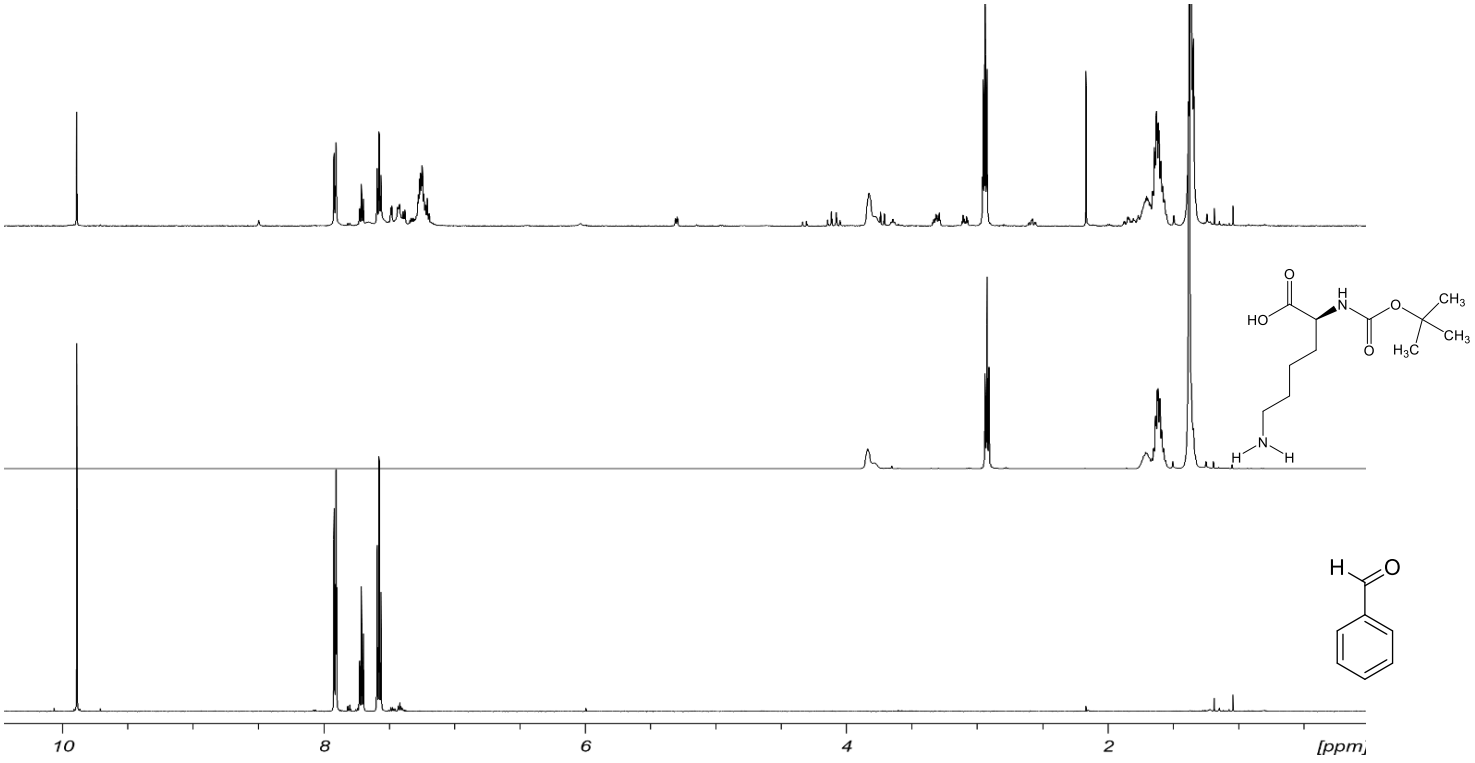

^{1}H NMR Spectrum (500 MHz, phosphate buffer) of Benzaldehyde added with Boc-Lys-OH.

Diazaborine Formation

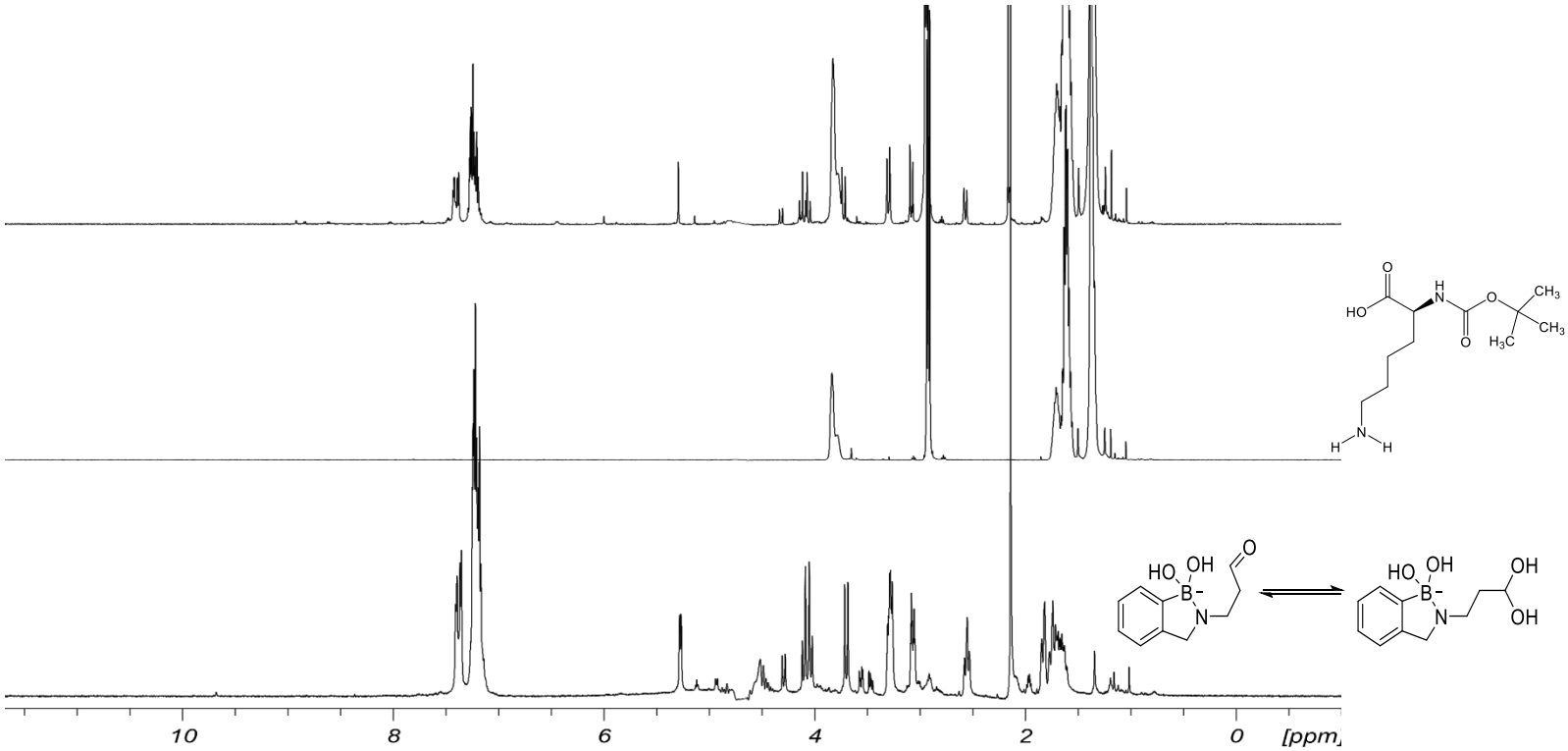

^{1}H NMR Spectrum (500 MHz, phosphate buffer) of DE321 added with Boc-Lys-OH.

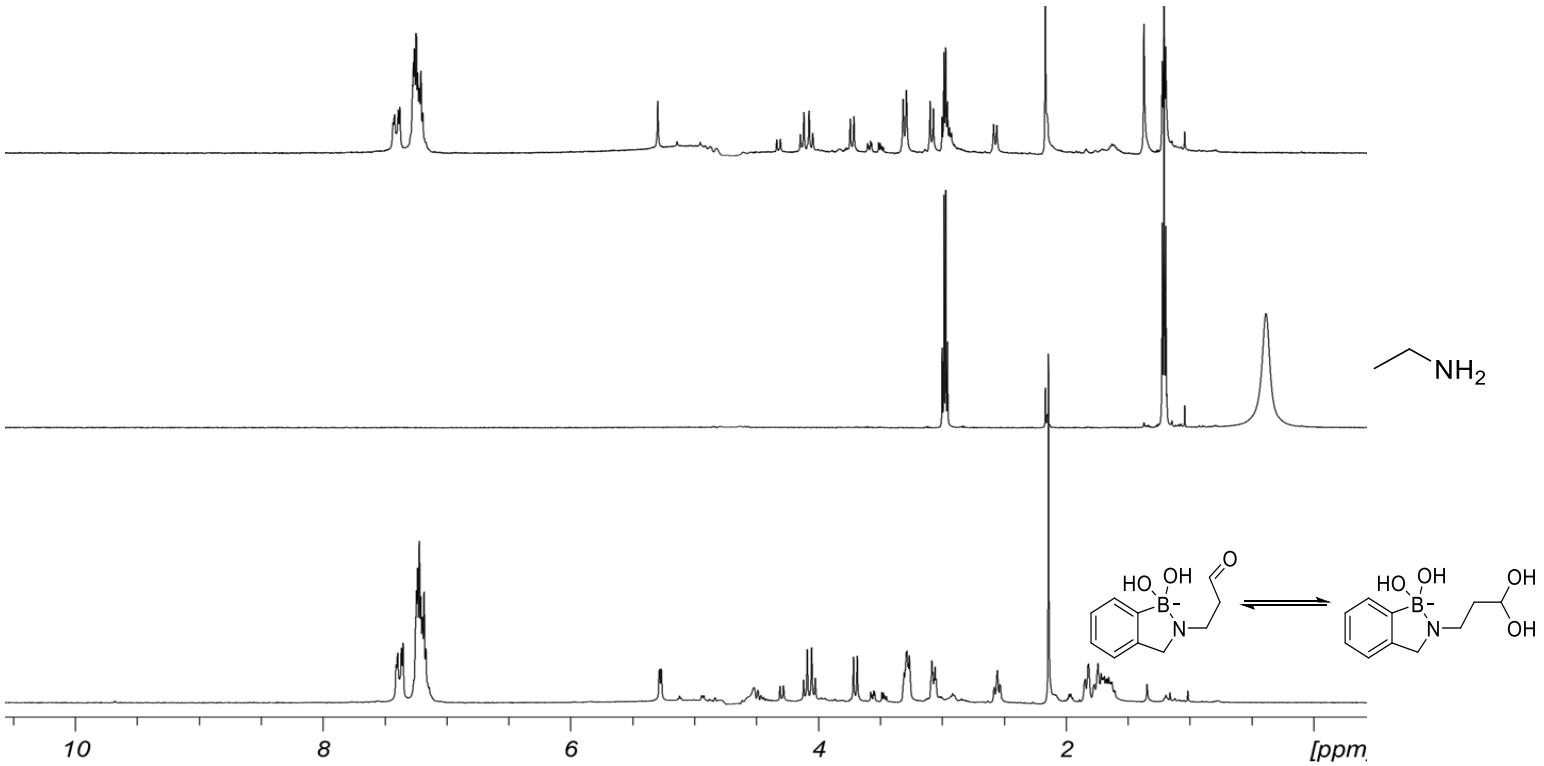

^{1}H NMR Spectrum (500 MHz, phosphate buffer) of DE321 added with ethylamine.

Appendix F. Diol Binding to Boronic Acids UV-Vis Spectroscopy Data

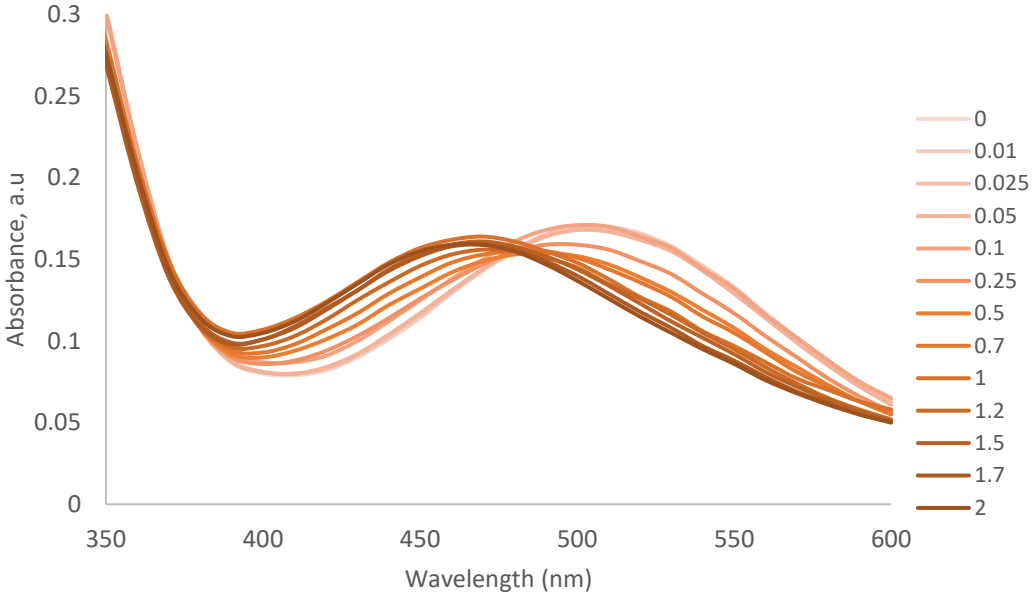

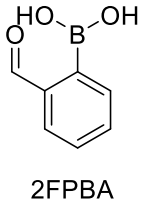

UV Spectroscopy of 2FPBA with increasing concentration of ARS.

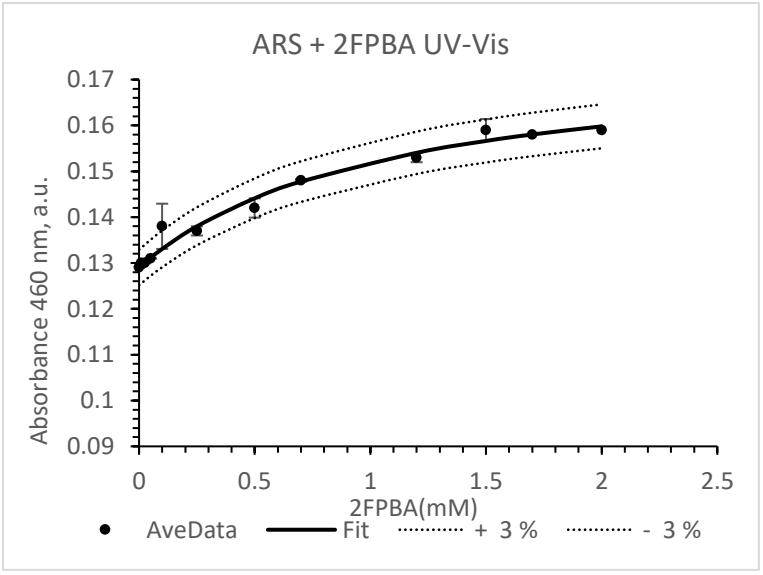

Plot of absorbance (460 nm) changes of 2FPBA (0.1 mM) with increasing of ARS concentration (0-2 mM) in HEPES buffer (100 mM, pH 7.4). (K_a was calculated to be 944.6 ± 0.003 M^{-1}). Value is the average of duplicate runs. Dotted lines represent 3% error.

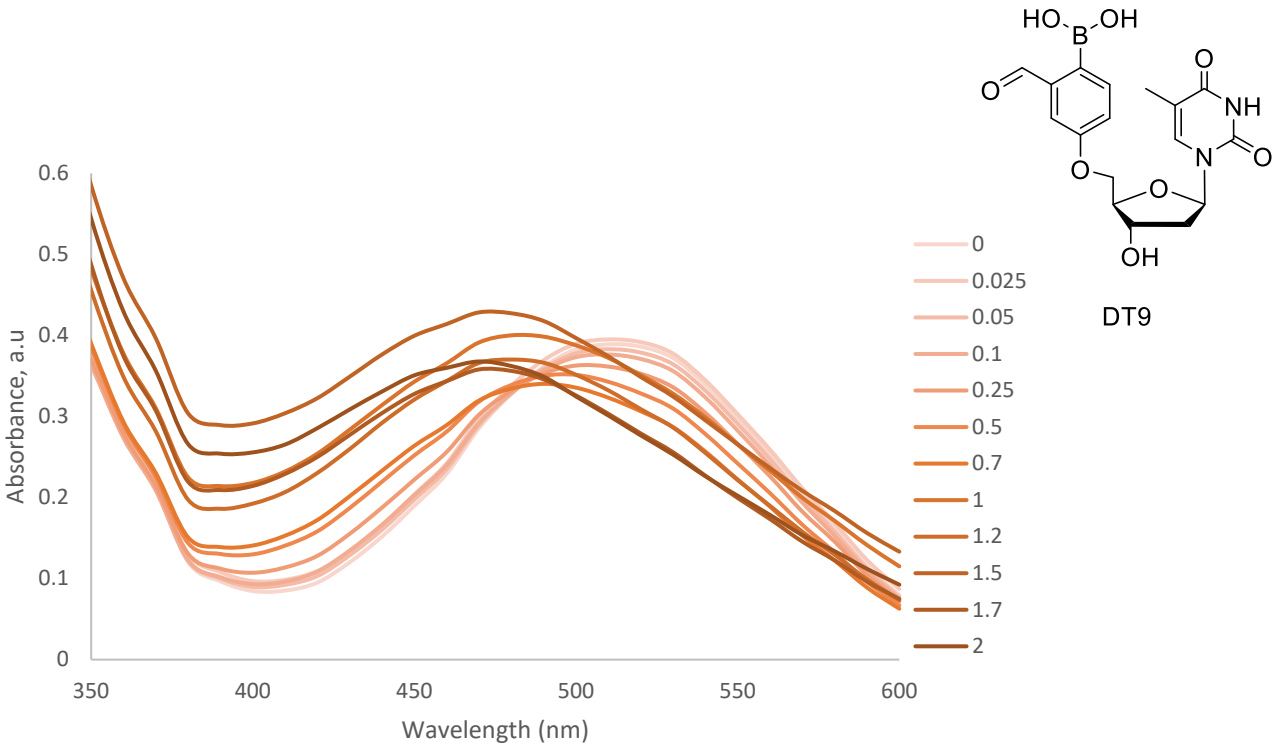

UV Spectroscopy of DT9 with increasing concentration of ARS.

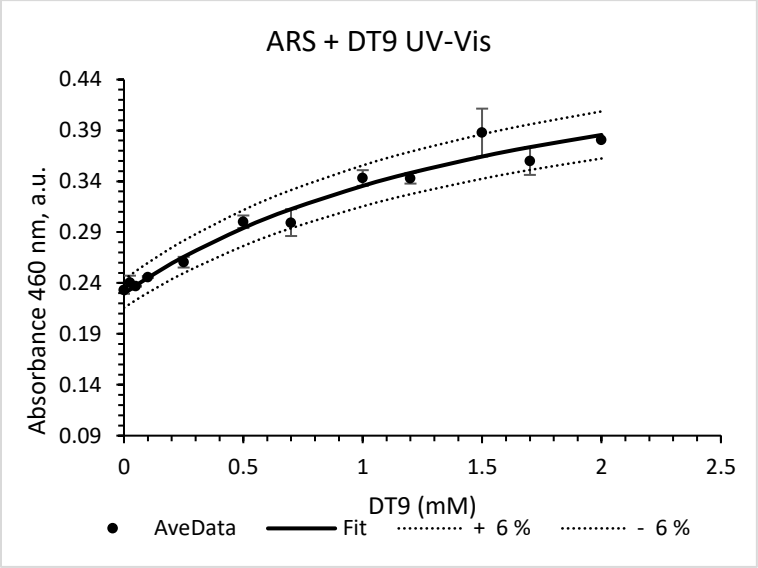

Plot of absorbance (460 nm) changes of DT9 (0.1 mM) with increasing of ARS concentration (0-2 mM) in HEPES buffer (100 mM, pH 7.4). (K_a was calculated to be 558.8 ± 0.003 M^{-1}). Value is the average of duplicate runs. Dotted lines represent 6% error.

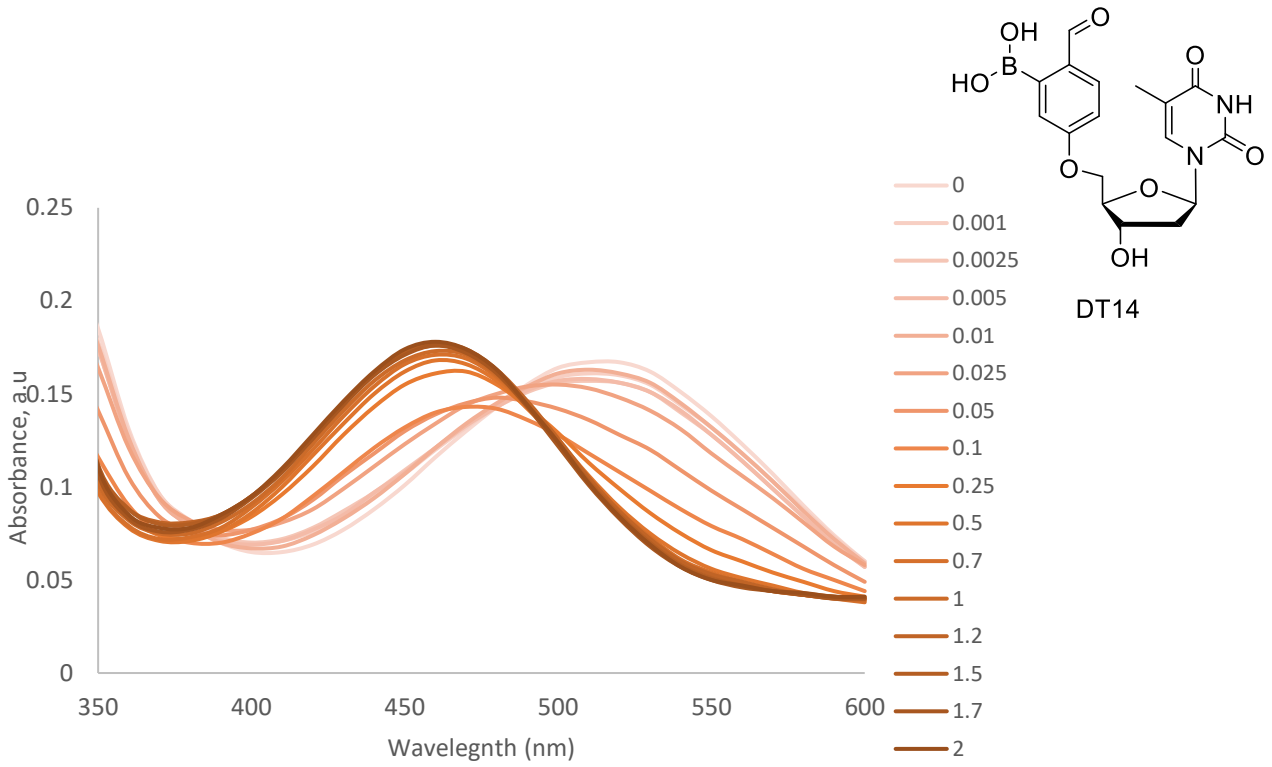

UV Spectroscopy of DT14 with increasing concentration of ARS.

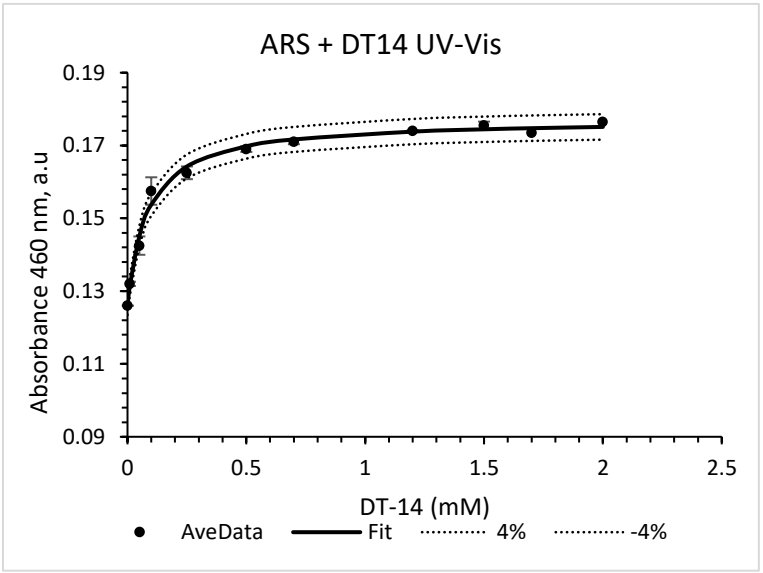

Plot of absorbance (460 nm) changes of DT14 (0.1 mM) with increasing of ARS concentration (0-2 mM) in HEPES buffer (100 mM, pH 7.4). (K_a was calculated to be 11,829.6 ± 0.0002 M^{-1}). Value is the average of duplicate runs. Dotted lines represent 3% error.

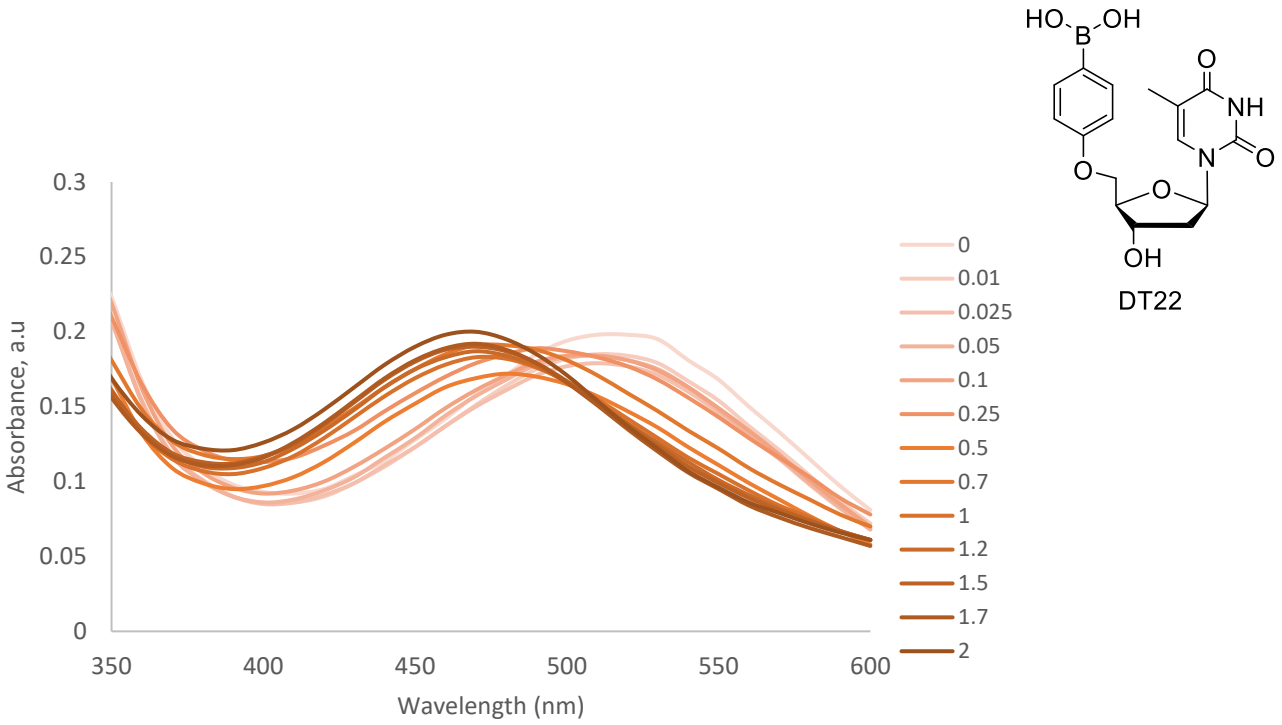

UV Spectroscopy of DT22 with increasing concentration of ARS.

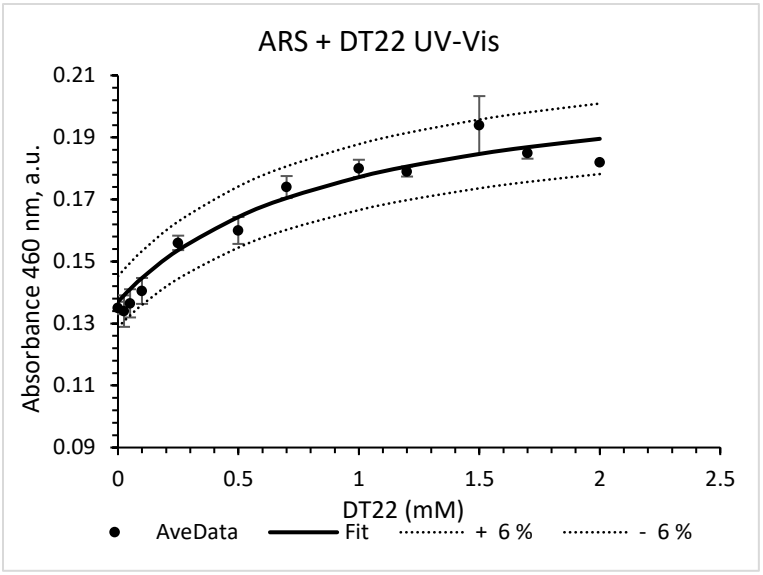

Plot of absorbance (460 nm) changes of DT22 (0.1 mM) with increasing of ARS concentration (0-2 mM) in HEPES buffer (100 mM, pH 7.4). (K_a was calculated to be 1,126.1 ± 0.002 M^{-1}). Value is the average of duplicate runs. Dotted lines represent 6% error.

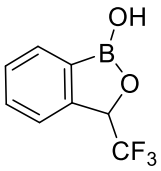

DE310

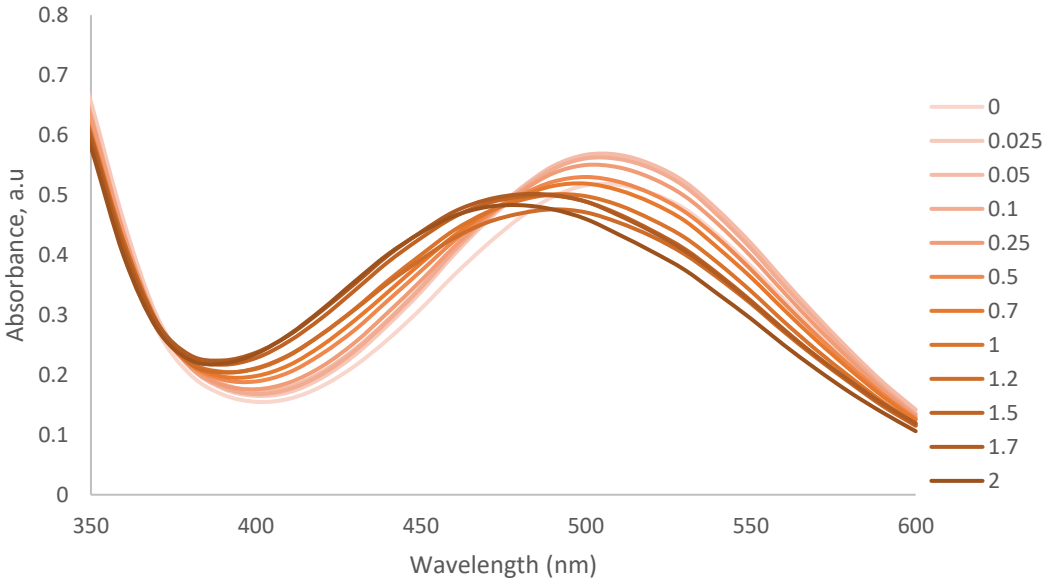

UV Spectroscopy of DE310 with increasing concentration of ARS.

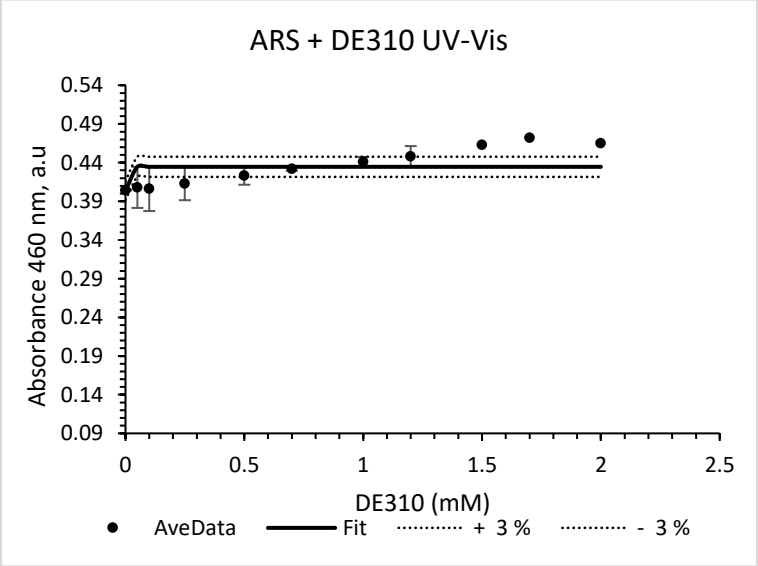

Plot of absorbance (460 nm) changes of DE310 (0.1 mM) with increasing of ARS concentration (0-2 mM) in HEPES buffer (100 mM, pH 7.4). (K_a was calculated to be 89.3 ± 0.1 M^{-1}). Value is the average of duplicate runs. Dotted lines represent 3% error.

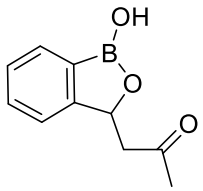

DE318

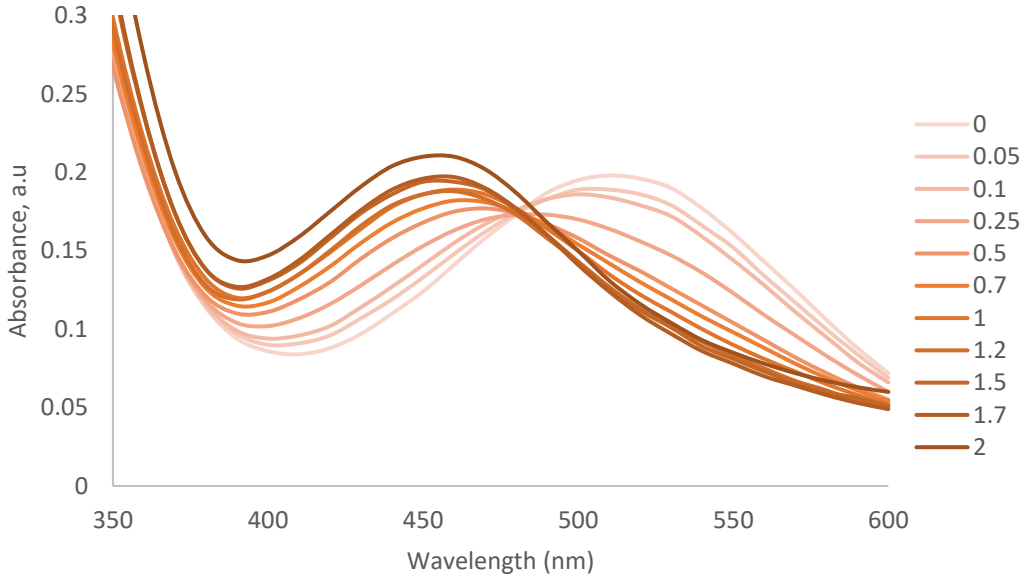

UV Spectroscopy of DE318 with increasing concentration of ARS.

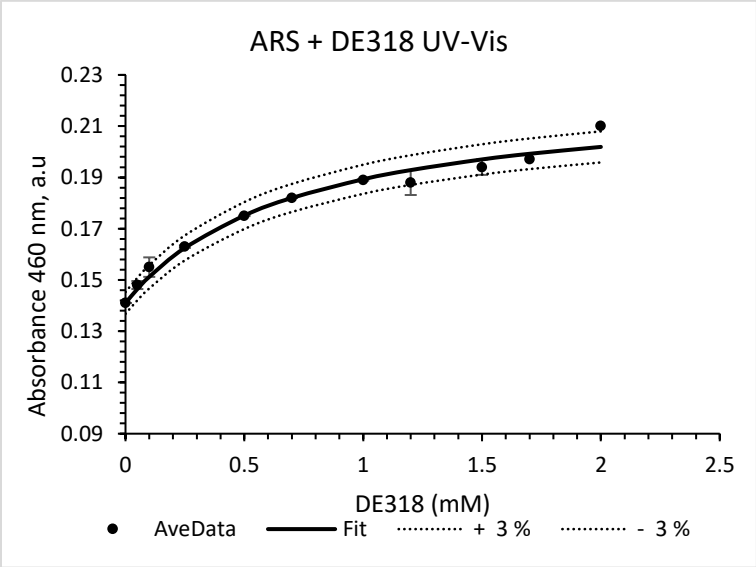

Plot of absorbance (460 nm) changes of DE318 (0.1 mM) with increasing of ARS concentration (0-2 mM) in HEPES buffer (100 mM, pH 7.4). (K_a was calculated to be 1,411.2 ± 0.0006 M^{-1}). Value is the average of duplicate runs. Dotted lines represent 3% error.

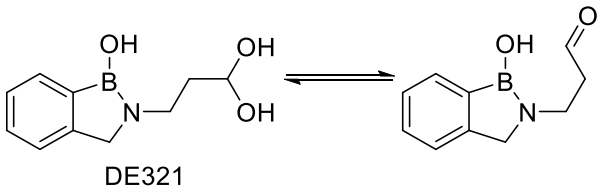

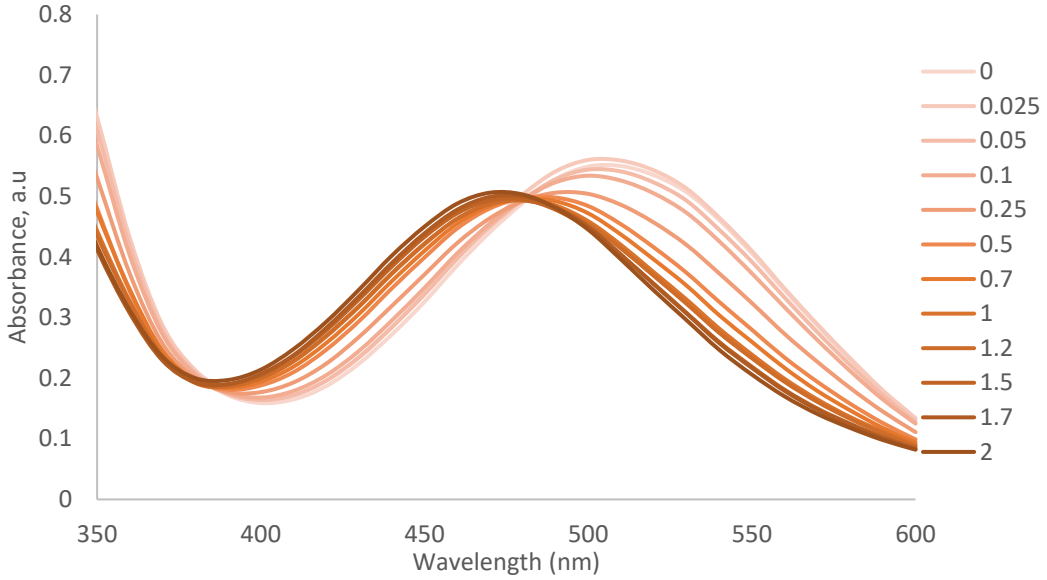

UV Spectroscopy of DE321 with increasing concentration of ARS.

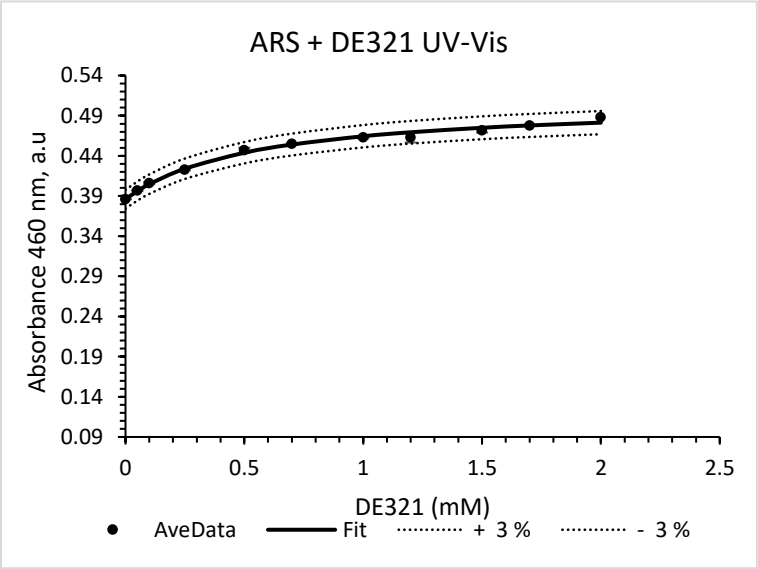

Plot of absorbance (460 nm) changes of DE321 (0.1 mM) with increasing of ARS concentration (0-2 mM) in HEPES buffer (100 mM, pH 7.4). (K_a was calculated to be 1,816.2 ± 0.0002 M^{-1}). Value is the average of duplicate runs. Dotted lines represent 3% error.

Appendix G. Diol Binding to Boronic Acid Fluorescence Data

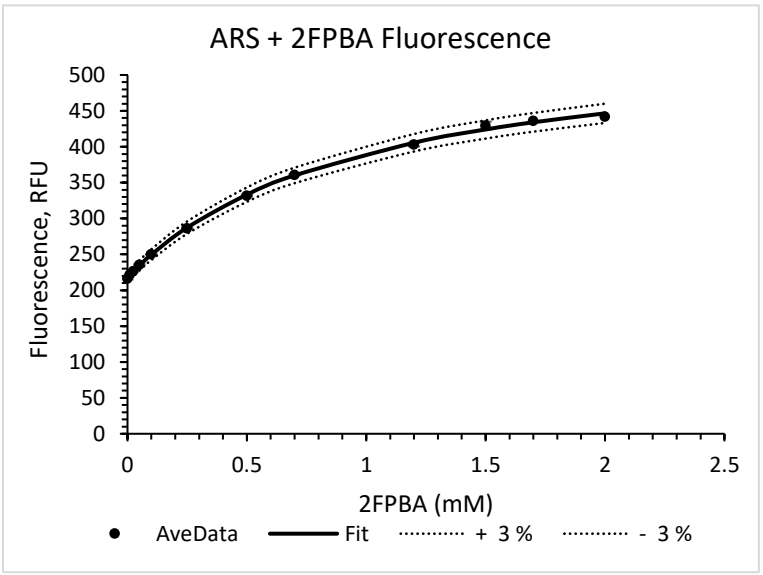

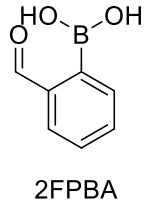

2FPBA

Plot of fluorescence (460 nm) changes of ARS (0.1 mM) with increasing of 2FPBA concentration (0-2 mM) in HEPES buffer (100 mM, pH 7.4). (K_a was calculated to be 1024.6 ± 0.17 M^{-1}). Value is the average of duplicate runs. Dotted lines represent 3% error.

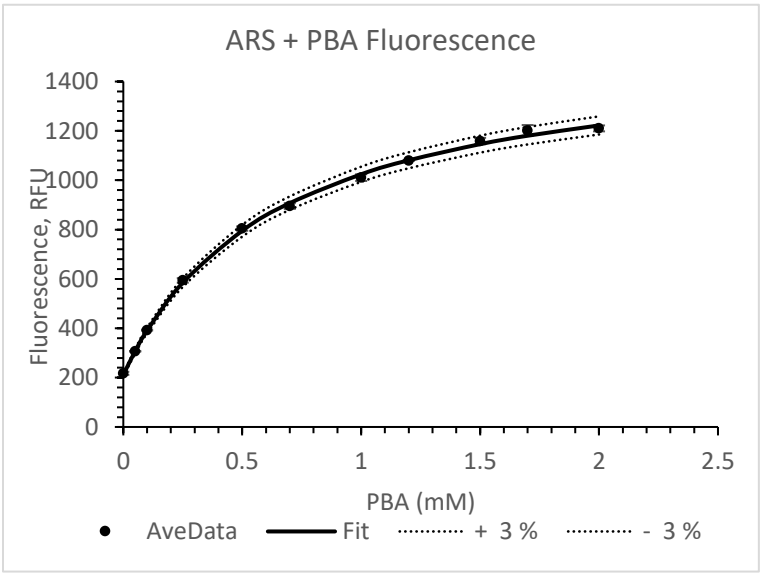

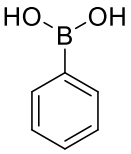

PBA

Plot of fluorescence (460 nm) changes of ARS (0.1 mM) with increasing of PBA concentration (0-2 mM) in HEPES buffer (100 mM, pH 7.4). (K_a was calculated to be 1553.1 ± 1.1 M^{-1}). Value is the average of duplicate runs. Dotted lines represent 3% error.

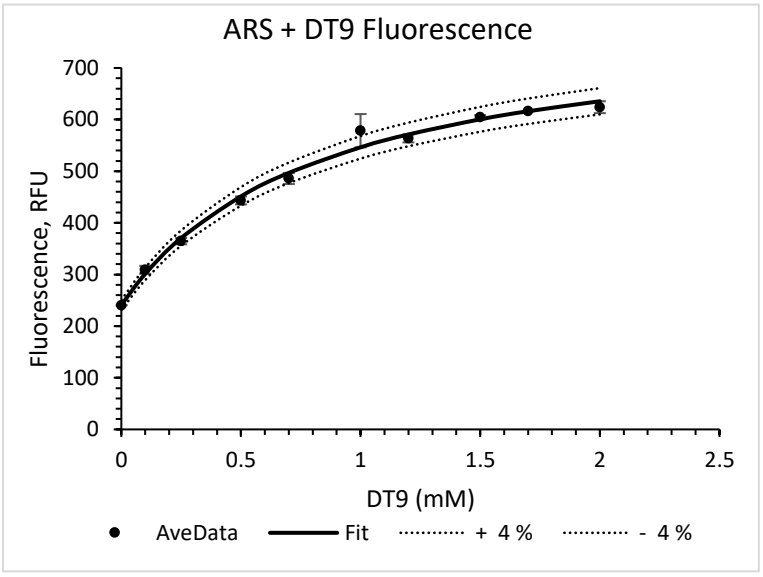

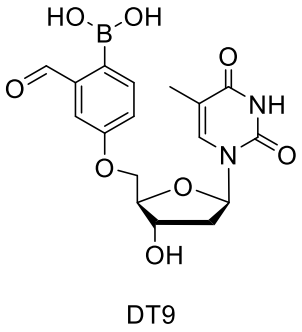

DT9

Plot of fluorescence (460 nm) changes of ARS (0.1 mM) with increasing of DT9 concentration (0-2 mM) in HEPES buffer (100 mM, pH 7.4). (K_a was calculated to be 1211.8 ± 2.9 M^{-1}). Value is the average of duplicate runs. Dotted lines represent 4% error.

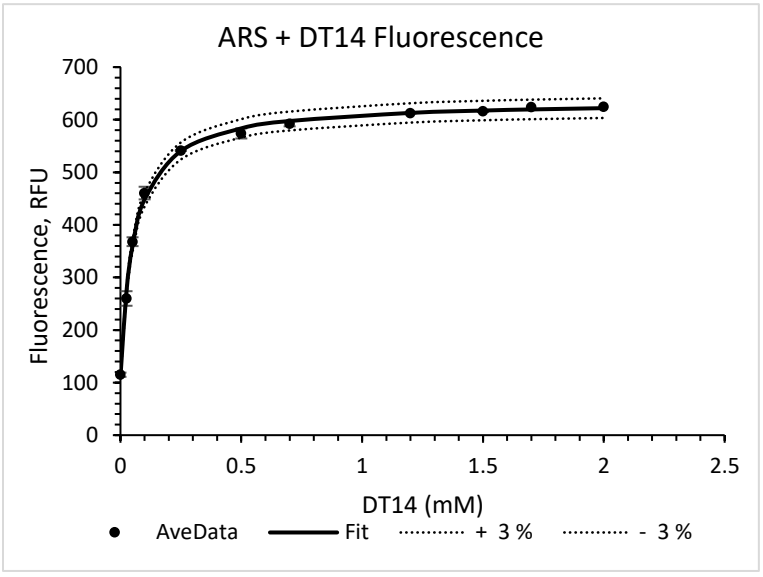

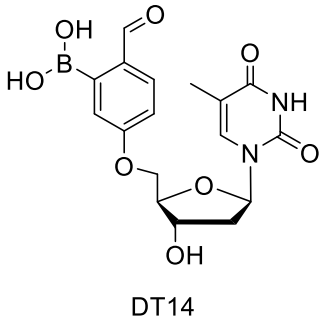

DT14

Plot of fluorescence (460 nm) changes of ARS (0.1 mM) with increasing of DT14 concentration (0-2 mM) in HEPES buffer (100 mM, pH 7.4). (K_a was calculated to be 17,973.7 ± 1.6 M^{-1}). Value is the average of duplicate runs. Dotted lines represent 3% error.

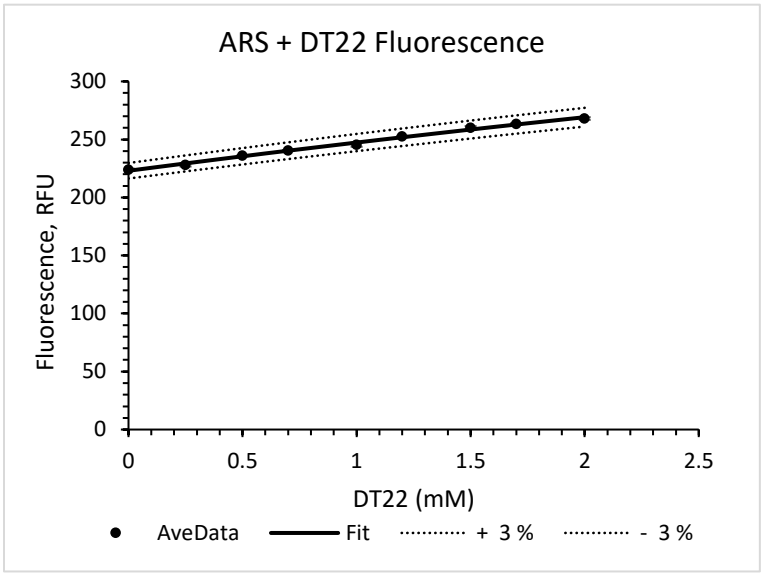

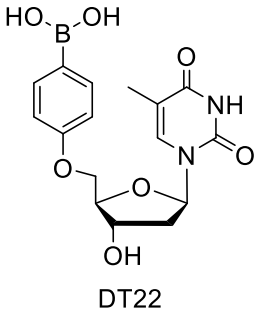

DT22

Plot of fluorescence (460 nm) changes of ARS (0.1 mM) with increasing of DT22 concentration (0-2 mM) in HEPES buffer (100 mM, pH 7.4). (K_a was calculated to be 56.3 ± 0.044 M^{-1}). Value is the average of duplicate runs. Dotted lines represent 3% error.

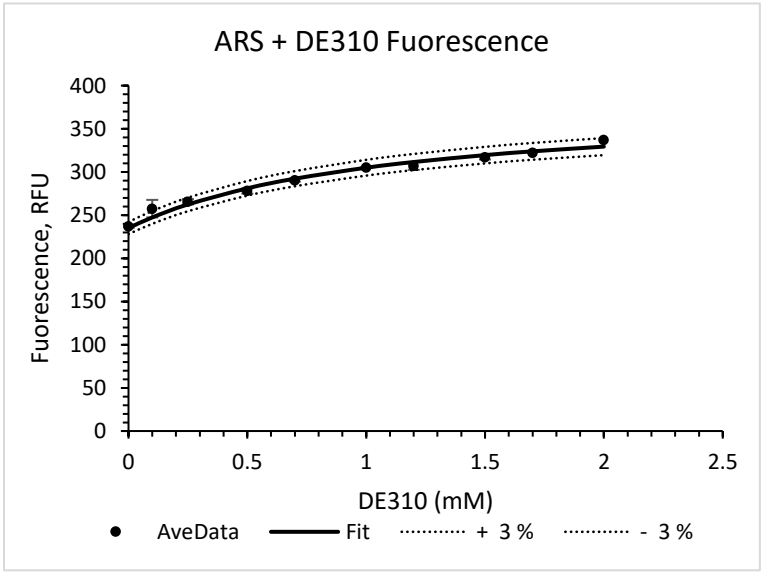

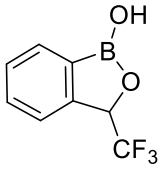

DE310

Plot of fluorescence (460 nm) changes of ARS (0.1 mM) with increasing of DE310 concentration (0-2 mM) in HEPES buffer (100 mM, pH 7.4). (K_a was calculated to be 929.7 ± 0.78 M^{-1}). Value is the average of duplicate runs. Dotted lines represent 3% error.

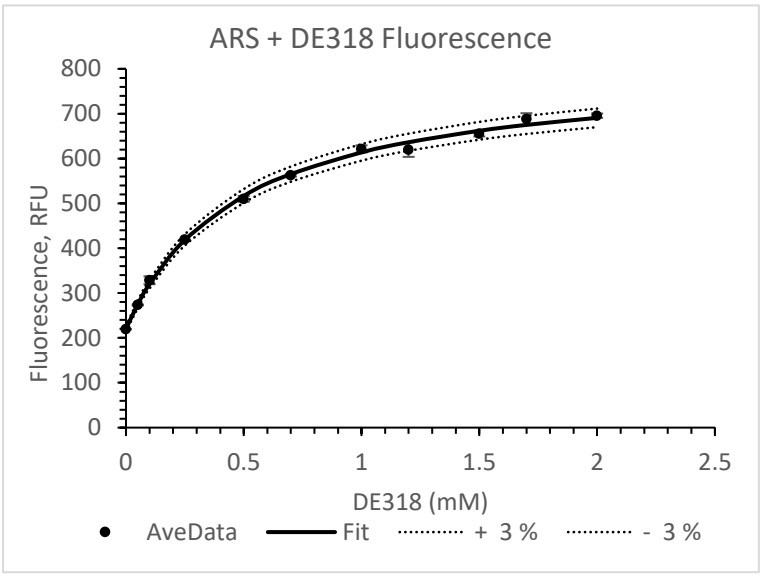

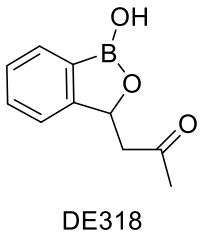

DE318

Plot of fluorescence (460 nm) changes of ARS (0.1 mM) with increasing of DE318 concentration (0-2 mM) in HEPES buffer (100 mM, pH 7.4). (K_a was calculated to be 2053.2 ± 1.2 M^{-1}). Value is the average of duplicate runs. Dotted lines represent 3% error.

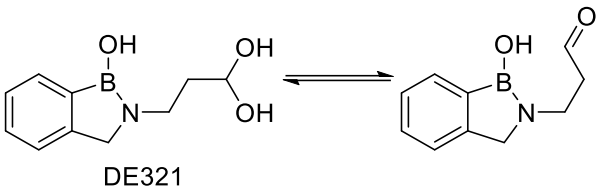

DE321

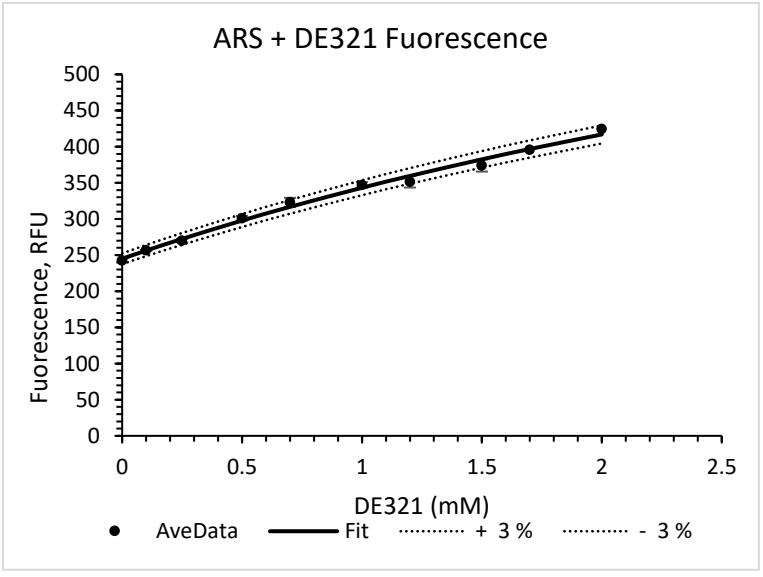

Plot of fluorescence (460 nm) changes of ARS (0.1 mM) with increasing of DE321 concentration (0-2 mM) in HEPES buffer (100 mM, pH 7.4). (K_a was calculated to be 165.3 ± 0.75 M^{-1}). Value is the average of duplicate runs. Dotted lines represent 3% error.

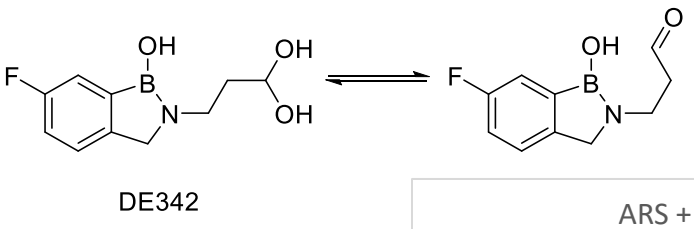

DE342

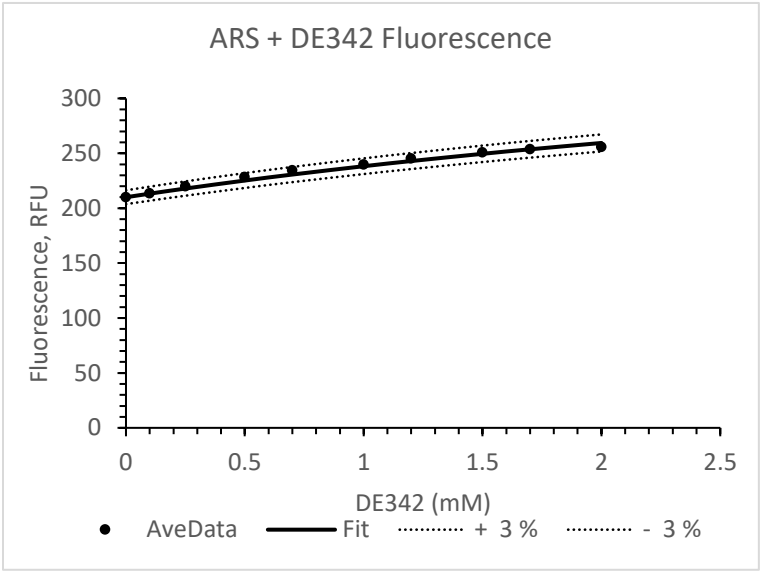

Plot of fluorescence (460 nm) changes of ARS (0.1 mM) with increasing of DE342 concentration (0-2 mM) in HEPES buffer (100 mM, pH 7.4). (K_a was calculated to be 166.7 ± 0.22 M^{-1}). Value is the average of duplicate runs. Dotted lines represent 3% error.

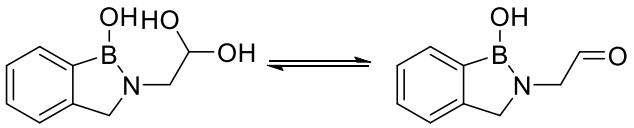

DE343

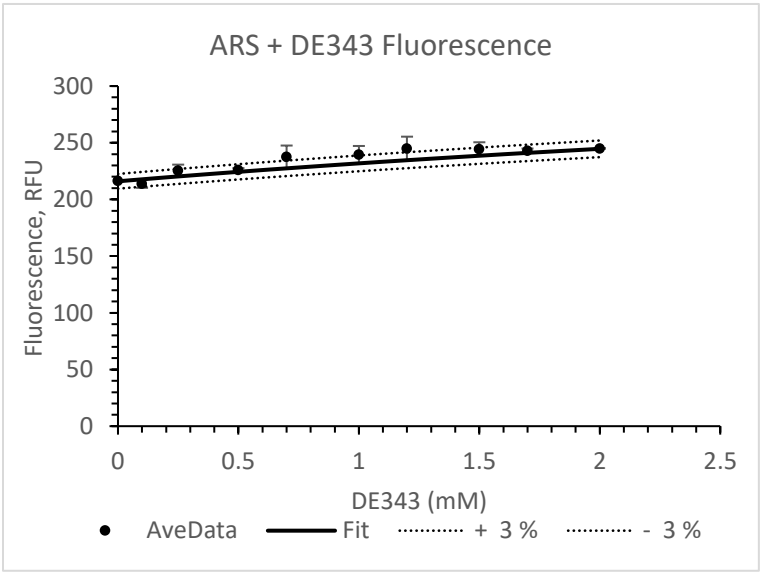

Plot of fluorescence (460 nm) changes of ARS (0.1 mM) with increasing of DE343 concentration (0-2 mM) in HEPES buffer (100 mM, pH 7.4). (K_a was calculated to be 117.9 ± 1.5 M^{-1}). Value is the average of duplicate runs. Dotted lines represent 3% error.

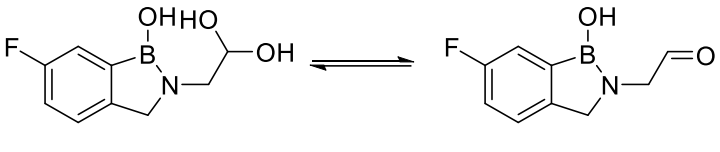

DE344

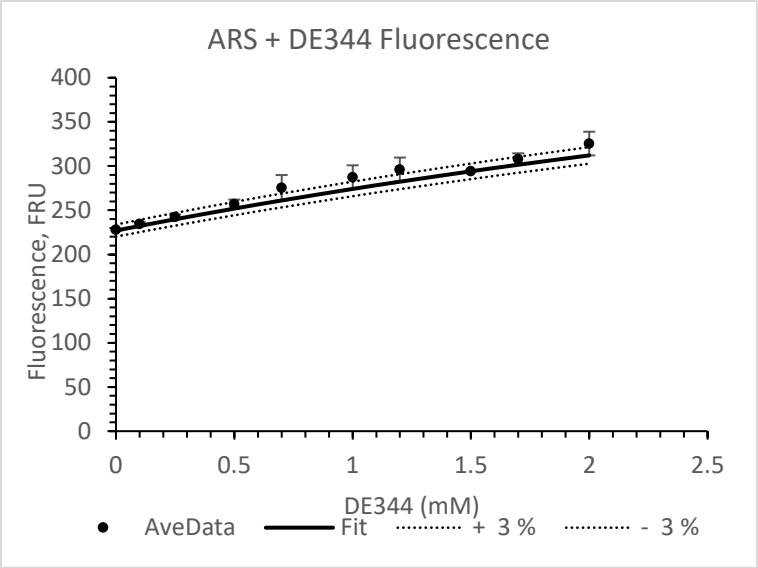

Plot of fluorescence (460 nm) changes of ARS (0.1 mM) with increasing of DE344 concentration (0-2 mM) in HEPES buffer (100 mM, pH 7.4). (K_a was calculated to be 120.7 ± 2.9 M^{-1}). Value is the average of duplicate runs. Dotted lines represent 3% error.

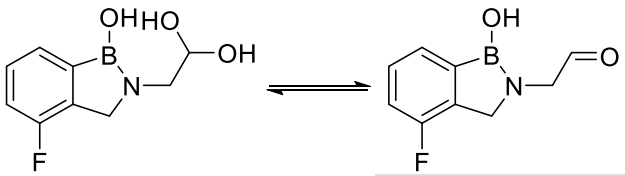

DE347

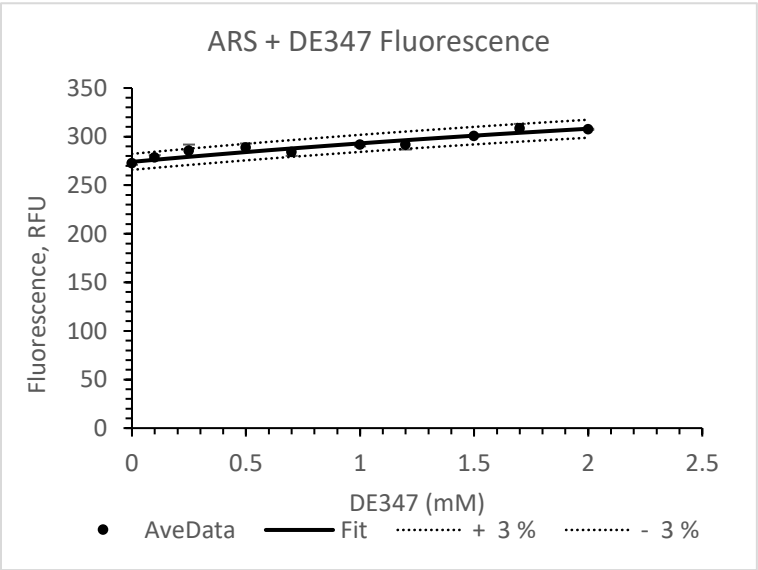

Plot of fluorescence (460 nm) changes of ARS (0.1 mM) with increasing of DE347 concentration (0-2 mM) in HEPES buffer (100 mM, pH 7.4). (K_a was calculated to be 130.7 ± 0.45 M^{-1}). Value is the average of duplicate runs. Dotted lines represent 3% error.

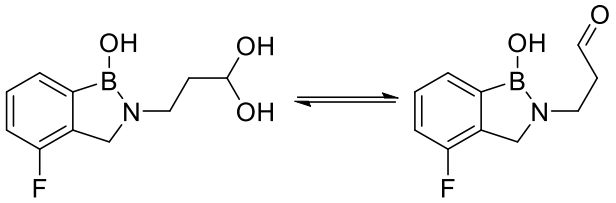

DE348

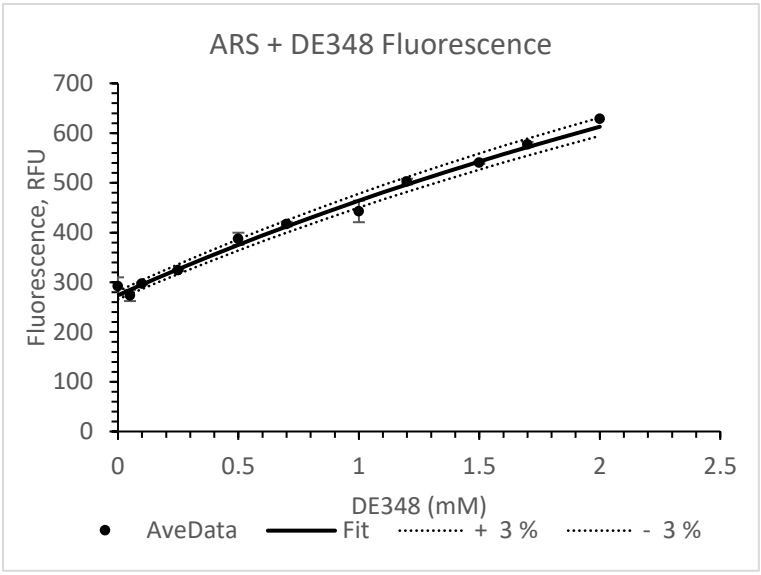

Plot of fluorescence (460 nm) changes of ARS (0.1 mM) with increasing of DE348 concentration (0-2 mM) in HEPES buffer (100 mM, pH 7.4). (K_a was calculated to be 139.7 ± 3.2 M^{-1}). Value is the average of duplicate runs. Dotted lines represent 3% error.

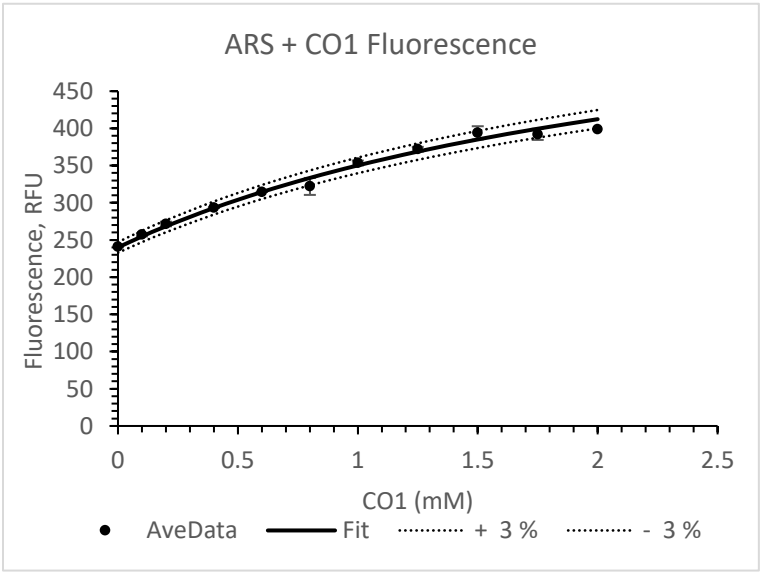

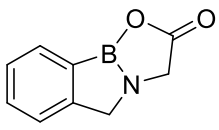

CO1

Plot of fluorescence (460 nm) changes of ARS (0.1 mM) with increasing of CO1 concentration (0-2 mM) in HEPES buffer (100 mM, pH 7.4). (K_a was calculated to be 387.4 ± 0.86 M^{-1}). Value is the average of duplicate runs. Dotted lines represent 3% error.

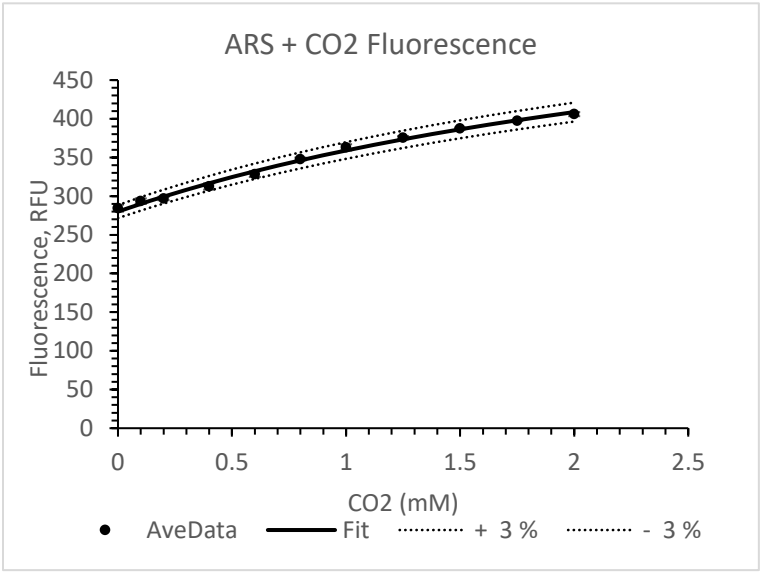

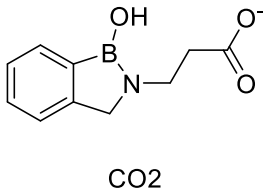

CO2

Plot of fluorescence (460 nm) changes of ARS (0.1 mM) with increasing of CO2 concentration (0-2 mM) in HEPES buffer (100 mM, pH 7.4). (K_a was calculated to be 295.6 ± 0.31 M^{-1}). Value is the average of duplicate runs. Dotted lines represent 3% error.

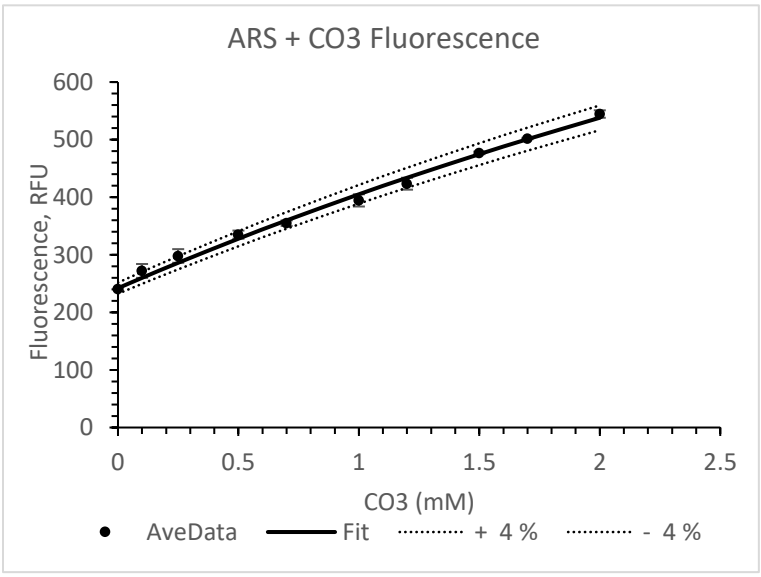

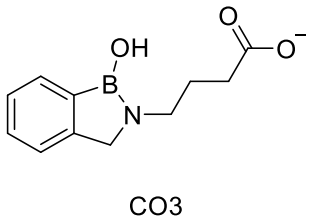

CO3

Plot of fluorescence (460 nm) changes of ARS (0.1 mM) with increasing of CO3 concentration (0-2 mM) in HEPES buffer (100 mM, pH 7.4). (K_a was calculated to be 113.6 ± 1.8 M^{-1}). Value is the average of duplicate runs. Dotted lines represent 4% error.

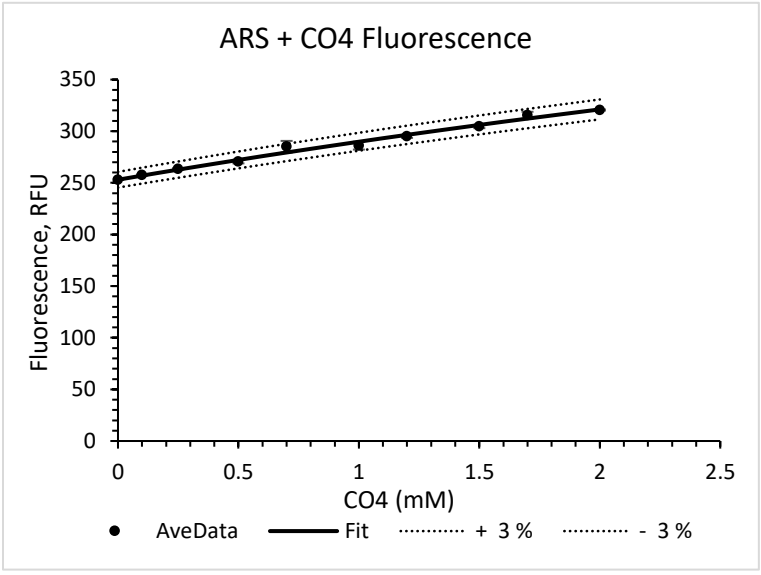

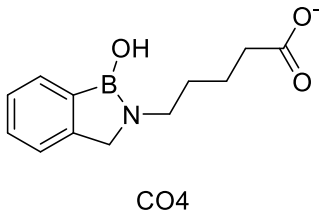

CO4

Plot of fluorescence (460 nm) changes of ARS (0.1 mM) with increasing of CO4 concentration (0-2 mM) in HEPES buffer (100 mM, pH 7.4). (K_a was calculated to be 87.9 ± 0.23 M^{-1}). Value is the average of duplicate runs. Dotted lines represent 3% error.

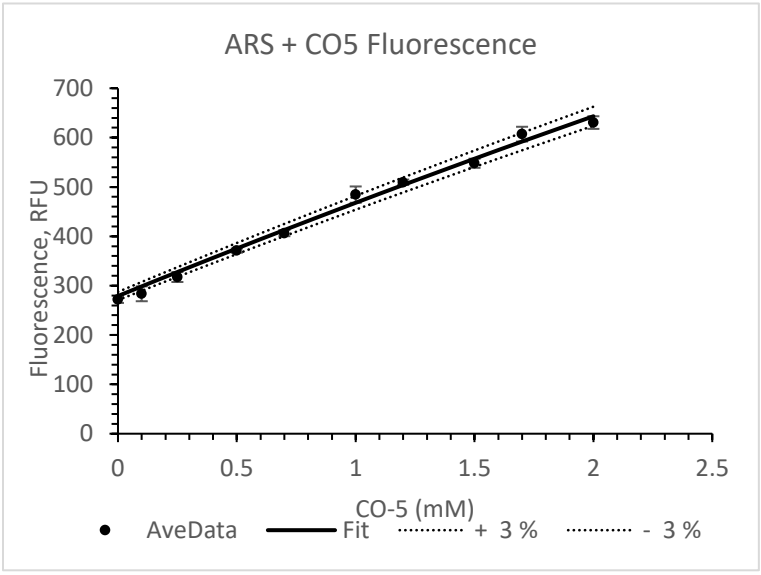

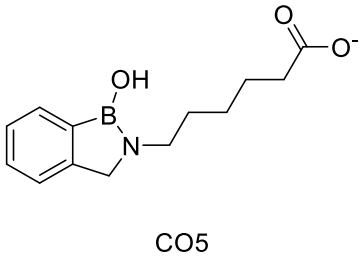

CO5

Plot of fluorescence (460 nm) changes of ARS (0.1 mM) with increasing of CO5 concentration (0-2 mM) in HEPES buffer (100 mM, pH 7.4). (K_a was calculated to be 38.8 ± 2.8 M^{-1}). Value is the average of duplicate runs. Dotted lines represent 3% error.

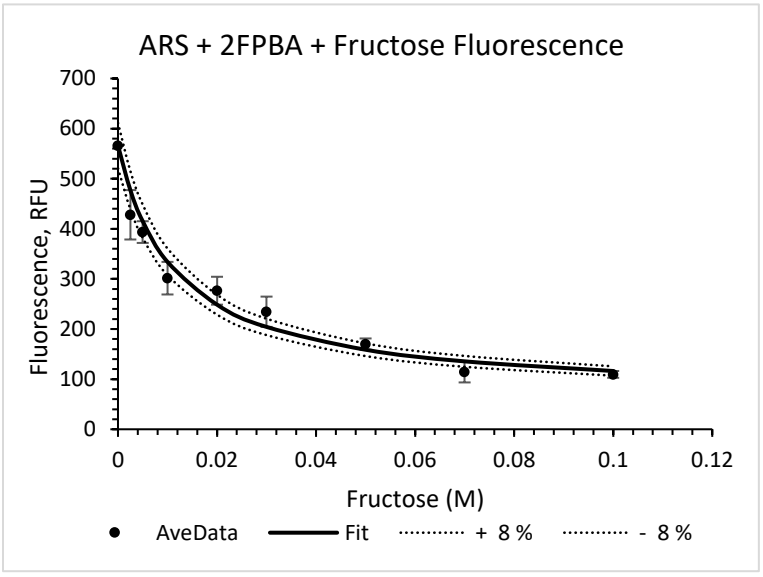

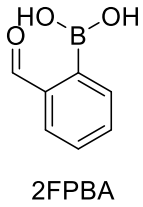

Plot of fluorescence changes of ARS-2FPBA complex with increasing concentration of fructose. ARS (0.1 mM), 2FPBA (10 mM), fructose (0-0.1 M), HEPES buffer (100 mM, pH 7.4). (K_a was calculated to be 85.8 ± 21.4 M^{-1}). Value is the average of duplicate runs. Dotted lines represent 8% error.

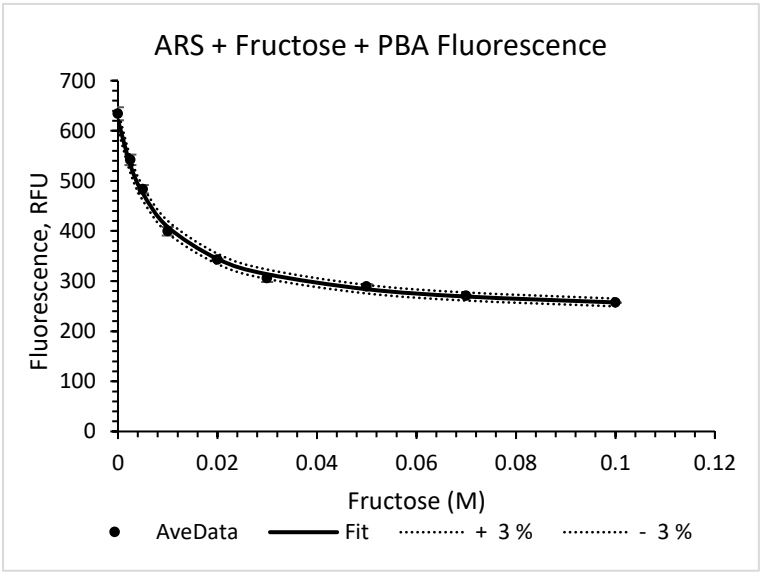

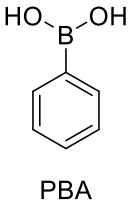

Plot of fluorescence changes of ARS-PBA complex with increasing concentration of fructose. ARS (0.1 mM), PBA (10 mM), fructose (0-0.1 M), HEPES buffer (100 mM, pH 7.4). (K_a was calculated to be 117.7 ± 1.1 M^{-1}). Value is the average of duplicate runs. Dotted lines represent 3% error.

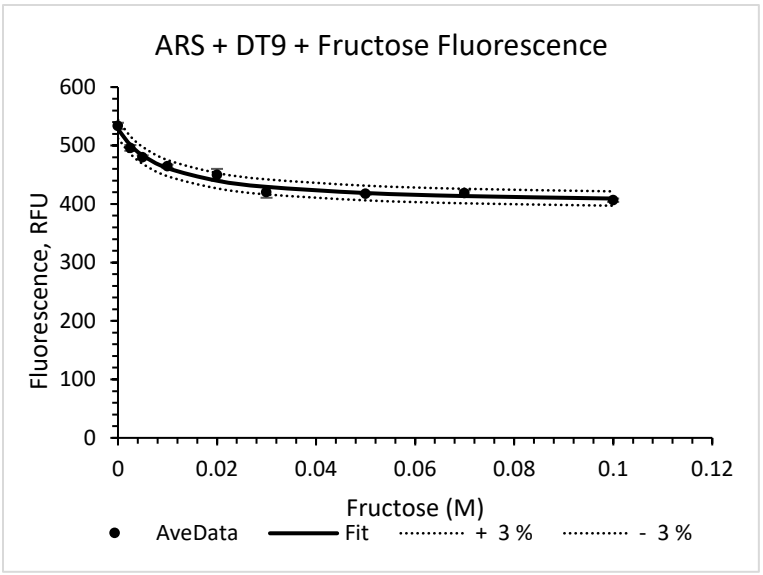

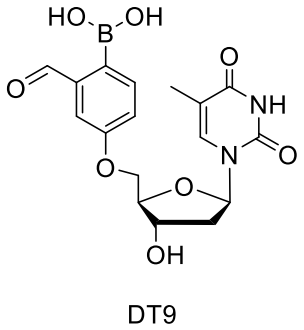

DT9

Plot of fluorescence changes of ARS-DT9 complex with increasing concentration of fructose. ARS (0.1 mM), DT9 (10 mM), fructose (0-0.1 M), HEPES buffer (100 mM, pH 7.4). (K_a was calculated to be 105.3 ± 0.66 M^{-1}). Value is the average of duplicate runs. Dotted lines represent 3% error.

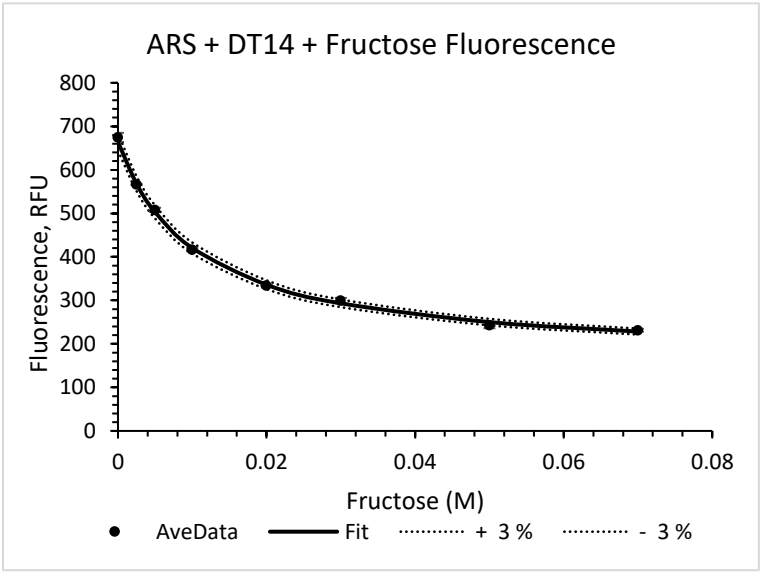

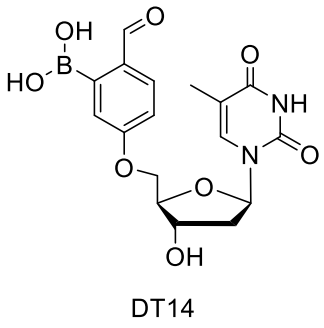

DT14

Plot of fluorescence changes of ARS-DT14 complex with increasing concentration of fructose. ARS (0.1 mM), DT14 (10 mM), fructose (0-0.1 M), HEPES buffer (100 mM, pH 7.4). (K_a was calculated to be 94.4 ± 0.64 M^{-1}). Value is the average of duplicate runs. Dotted lines represent 3% error.

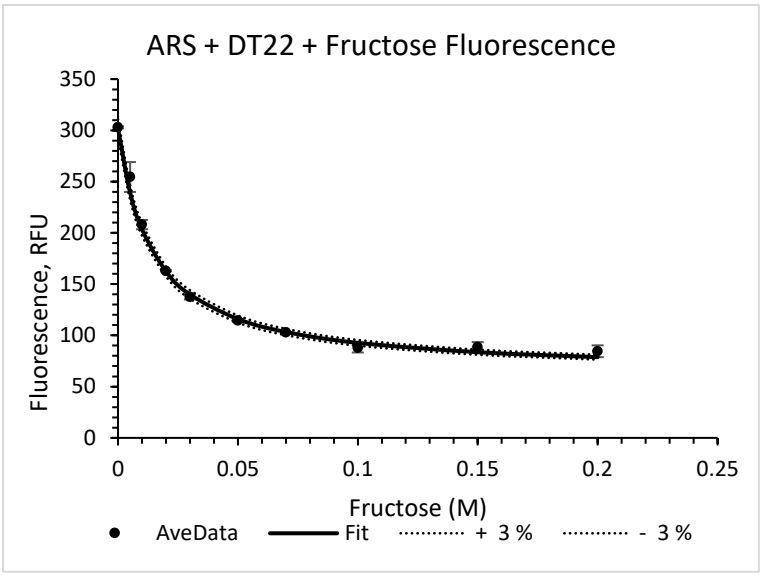

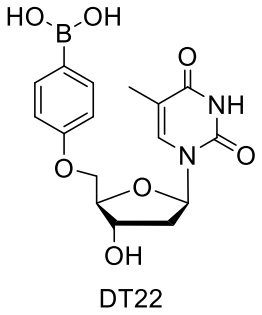

DT22

Plot of fluorescence changes of ARS-DT22 complex with increasing concentration of fructose. ARS (0.1 mM), DT22 (10 mM), fructose (0-0.1 M), HEPES buffer (100 mM, pH 7.4). (K_a was calculated to be 70.1 ± 1.9 M^{-1}). Value is the average of duplicate runs. Dotted lines represent 3% error.

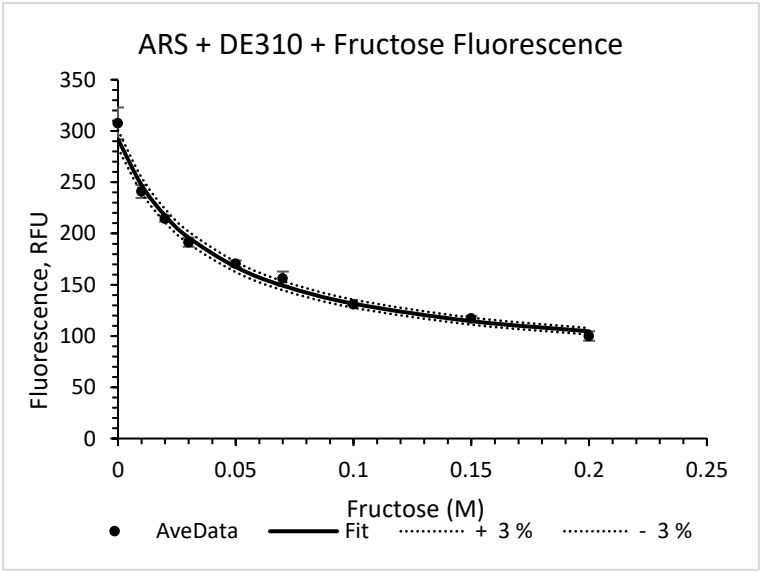

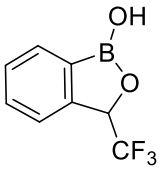

DE310

Plot of fluorescence changes of ARS-DE310 complex with increasing concentration of fructose. ARS (0.1 mM), DE310 (10 mM), fructose (0-0.1 M), HEPES buffer (100 mM, pH 7.4). (K_a was calculated to be 24.7 ± 1.7 M^{-1}). Value is the average of duplicate runs. Dotted lines represent 3% error.

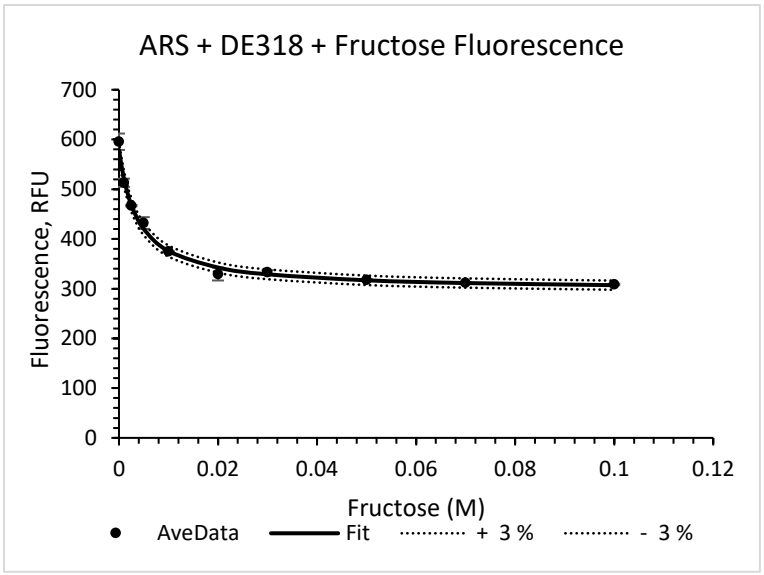

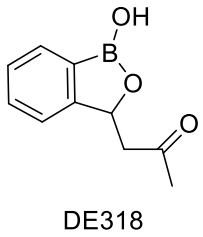

DE318

Plot of fluorescence changes of ARS-DE318 complex with increasing concentration of fructose. ARS (0.1 mM), DE318 (10 mM), fructose (0-0.1 M), HEPES buffer (100 mM, pH 7.4). (K_a was calculated to be 256.6 ± 1.5 M^{-1}). Value is the average of duplicate runs. Dotted lines represent 3% error.

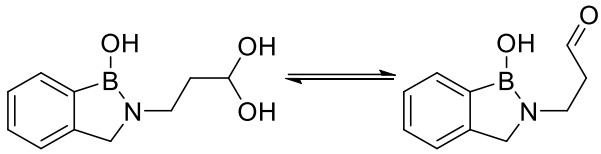

DE321

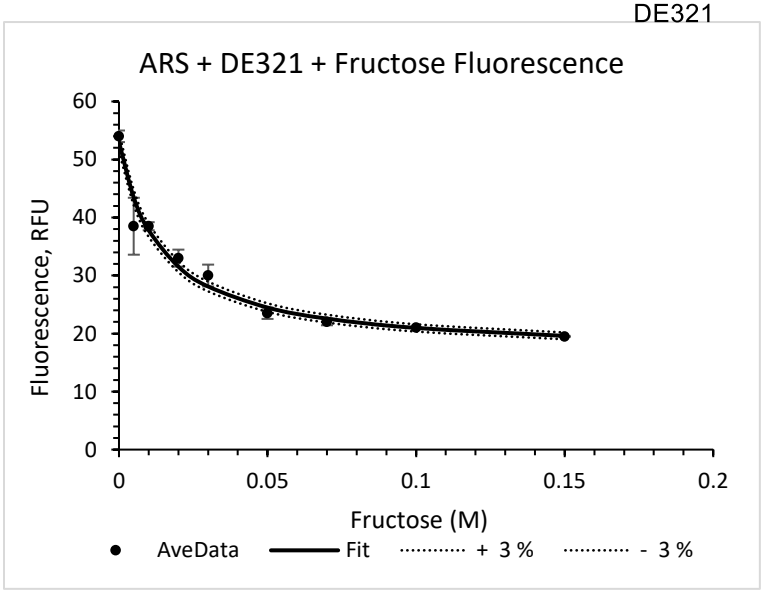

Plot of fluorescence changes of ARS-DE321 complex with increasing concentration of fructose. ARS (0.1 mM), DE321 (10 mM), fructose (0-0.1 M), HEPES buffer (100 mM, pH 7.4). (K_a was calculated to be 71.3 ± 0.83 M^{-1}). Value is the average of duplicate runs. Dotted lines represent 3% error.

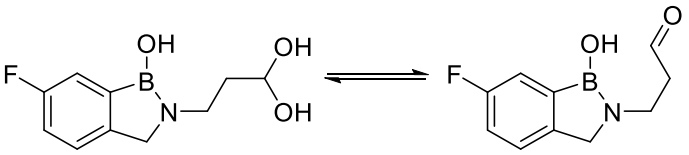

DE342

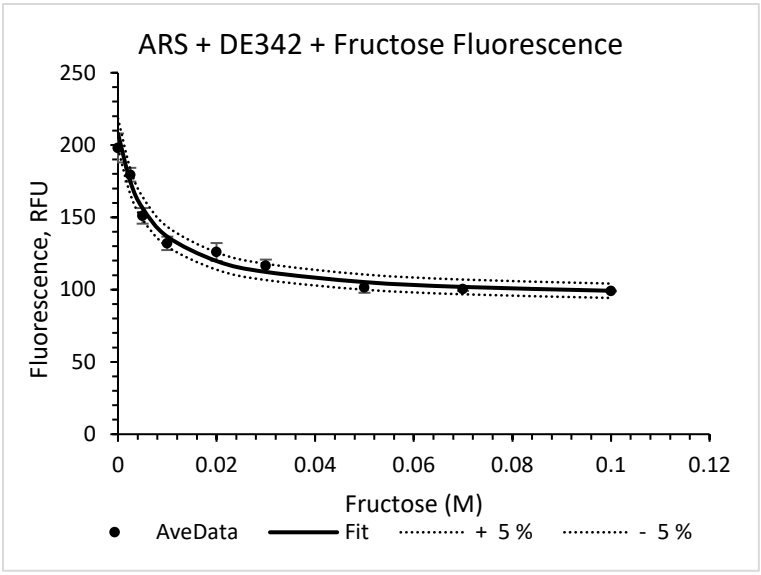

Plot of fluorescence changes of ARS-DE342 complex with increasing concentration of fructose. ARS (0.1 mM), DE342 (10 mM), fructose (0-0.1 M), HEPES buffer (100 mM, pH 7.4). (K_a was calculated to be 161.5 ± 1.6 M^{-1}). Value is the average of duplicate runs. Dotted lines represent 5% error.

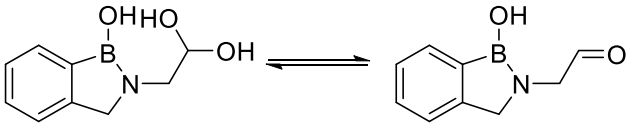

DE343

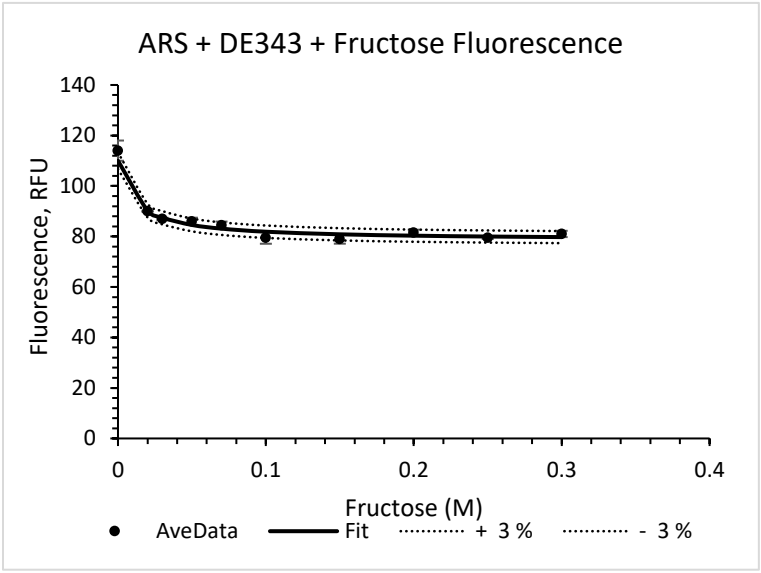

Plot of fluorescence changes of ARS-DE343 complex with increasing concentration of fructose. ARS (0.1 mM), DE343 (10 mM), fructose (0-0.1 M), HEPES buffer (100 mM, pH 7.4). (K_a was calculated to be 84.7 ± 0.35 M^{-1}). Value is the average of duplicate runs. Dotted lines represent 3% error.

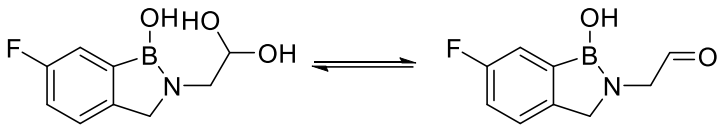

DE344

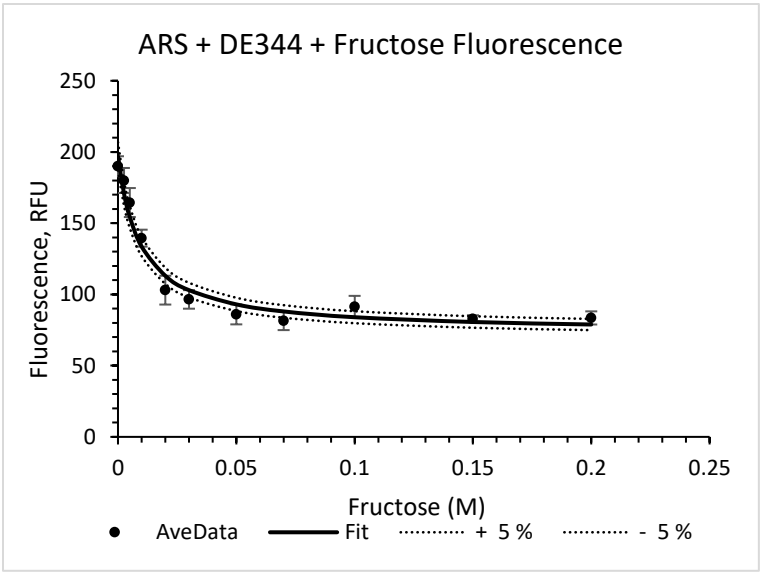

Plot of fluorescence changes of ARS-DE344 complex with increasing concentration of fructose. ARS (0.1 mM), DE344 (10 mM), fructose (0-0.1 M), HEPES buffer (100 mM, pH 7.4). (K_a was calculated to be 105.3 ± 4.9 M^{-1}). Value is the average of duplicate runs. Dotted lines represent 5% error.

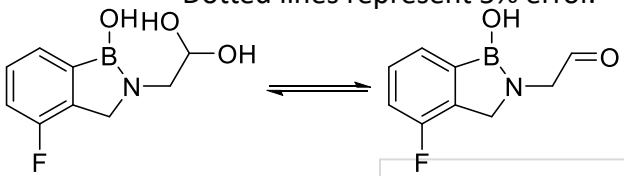

DE347

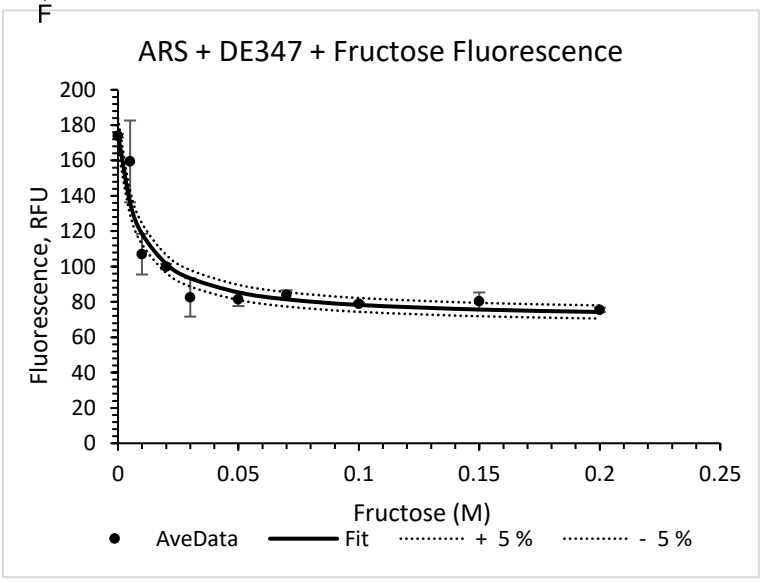

Plot of fluorescence changes of ARS-DE347 complex with increasing concentration of fructose. ARS (0.1 mM), DE347 (10 mM), fructose (0-0.1 M), HEPES buffer (100 mM, pH 7.4). (K_a was calculated to be 116.3 ± 6.9 M^{-1}). Value is the average of duplicate runs. Dotted lines represent 5% error.

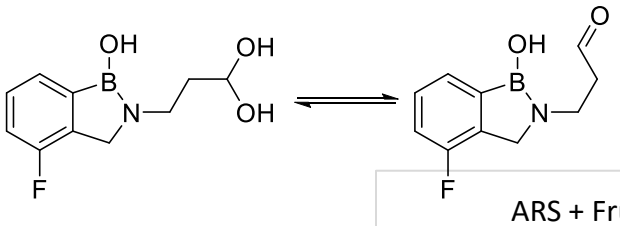

DE348

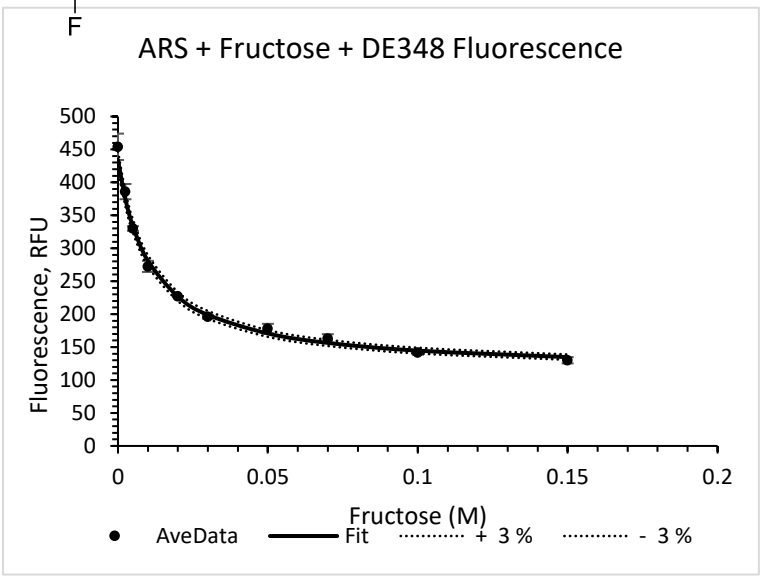

Plot of fluorescence changes of ARS-DE348 complex with increasing concentration of fructose. ARS (0.1 mM), DE348 (10 mM), fructose (0-0.1 M), HEPES buffer (100 mM, pH 7.4). (K_a was calculated to be 91.2 ± 2.4 M^{-1}). Value is the average of duplicate runs. Dotted lines represent 3% error.

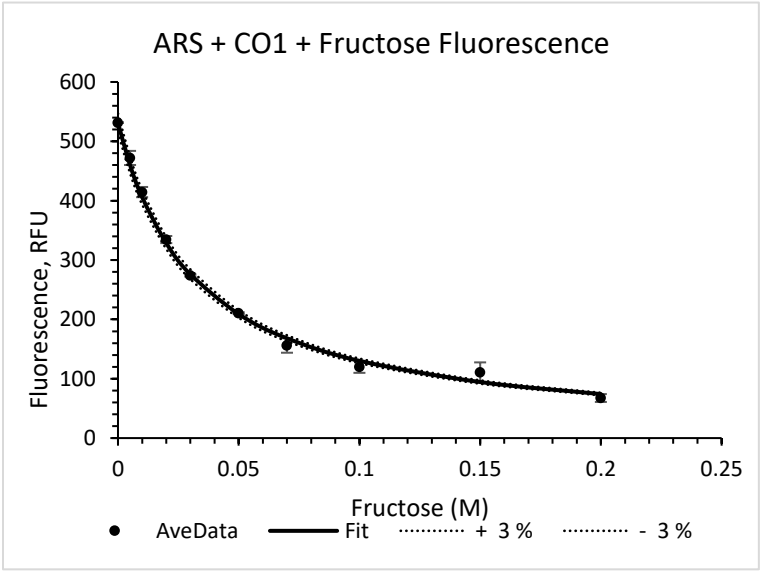

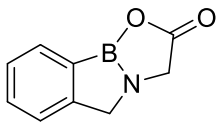

CO1

Plot of fluorescence changes of ARS-CO1 complex with increasing concentration of fructose. ARS (0.1 mM), CO1 (10 mM), fructose (0-0.1 M), HEPES buffer (100 mM, pH 7.4). (K_a was calculated to be 30.8 ± 5.8 M^{-1}). Value is the average of duplicate runs. Dotted lines represent 3% error.

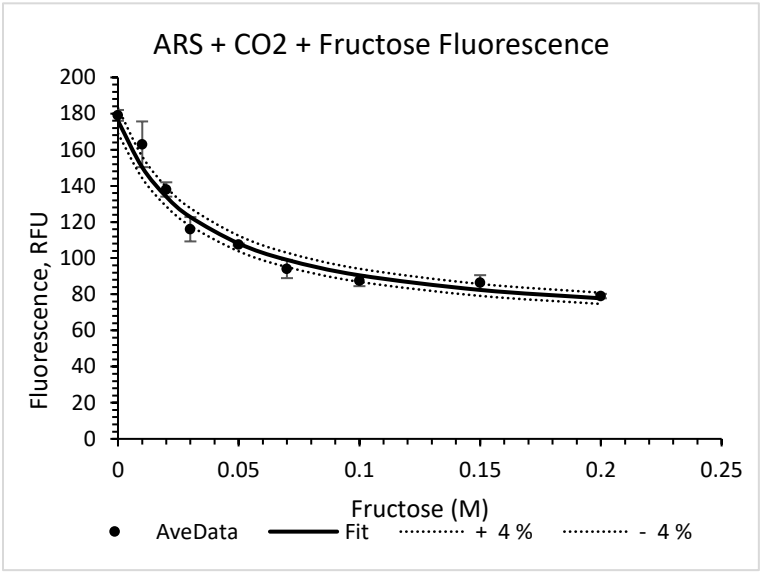

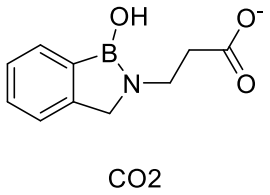

CO2

Plot of fluorescence changes of ARS-CO2 complex with increasing concentration of fructose. ARS (0.1 mM), CO2 (10 mM), fructose (0-0.1 M), HEPES buffer (100 mM, pH 7.4). (K_a was calculated to be 28.5 ± 2.2 M^{-1}). Value is the average of duplicate runs. Dotted lines represent 4% error.

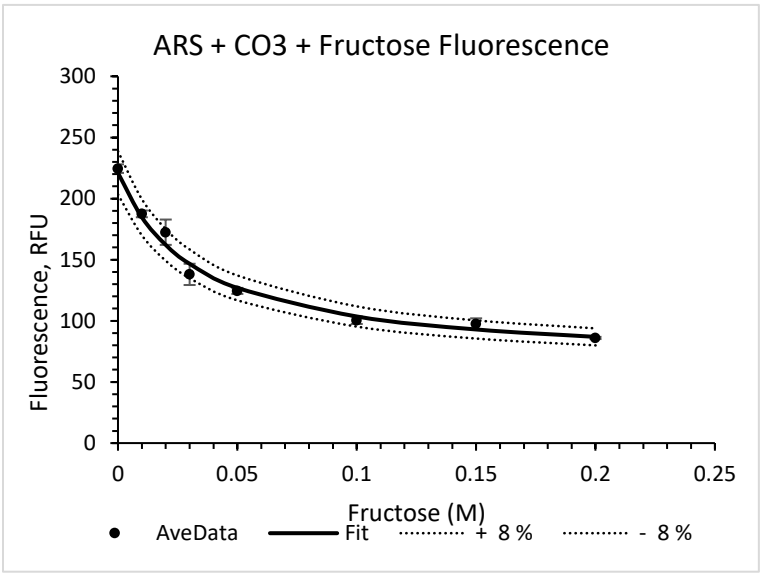

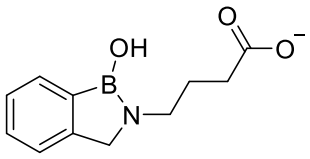

CO3

Plot of fluorescence changes of ARS-CO3 complex with increasing concentration of fructose. ARS (0.1 mM), CO3 (10 mM), fructose (0-0.1 M), HEPES buffer (100 mM, pH 7.4). (K_a was calculated to be 30.2 ± 1.6 M^{-1}). Value is the average of duplicate runs. Dotted lines represent 8% error.

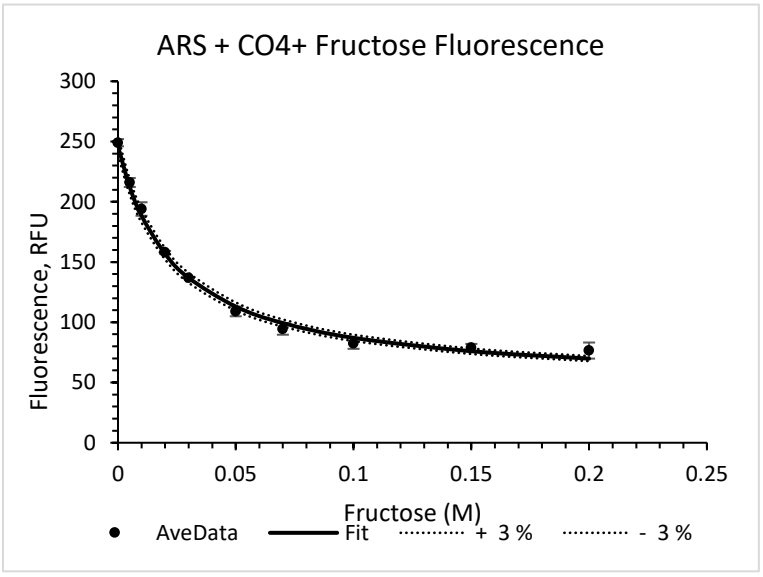

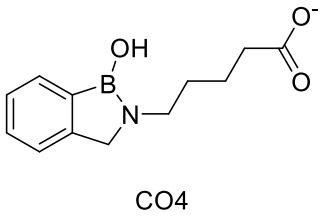

CO4

Plot of fluorescence changes of ARS-CO4 complex with increasing concentration of fructose. ARS (0.1 mM), CO4 (10 mM), fructose (0-0.1 M), HEPES buffer (100 mM, pH 7.4). (K_a was calculated to be 41.1 ± 1.7 M^{-1}). Value is the average of duplicate runs. Dotted lines represent 3% error.

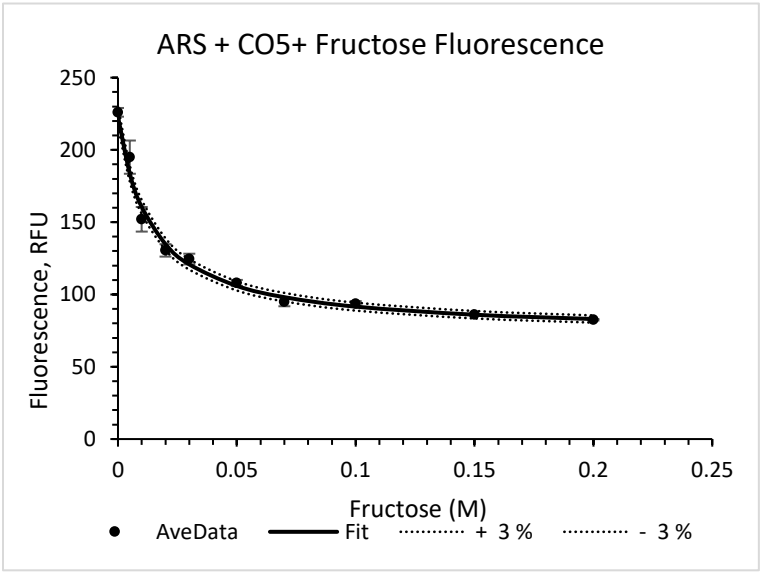

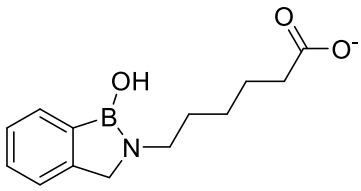

CO5

Plot of fluorescence changes of ARS-CO5 complex with increasing concentration of fructose. ARS (0.1 mM), CO5 (10 mM), fructose (0-0.1 M), HEPES buffer (100 mM, pH 7.4). (K_a was calculated to be 71.6 ± 1.6 M^{-1}). Value is the average of duplicate runs. Dotted lines represent 3% error.

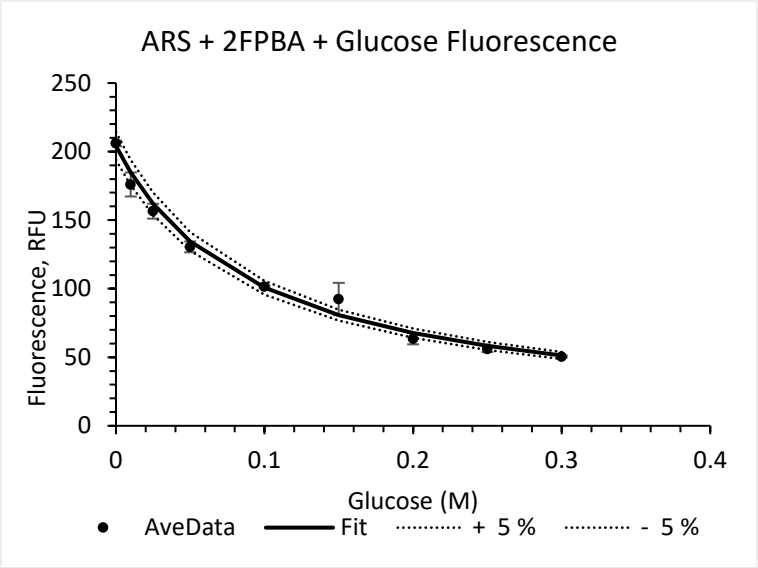

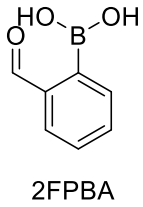

2FPBA

Plot of fluorescence changes of ARS-2FPBA complex with increasing concentration of glucose. ARS (0.1 mM), 2FPBA (10 mM), glucose (0-0.1 M), HEPES buffer (100 mM, pH 7.4). (K_a was calculated to be 10.6 ± 2.8 M^{-1}). Value is the average of duplicate runs. Dotted lines represent 5% error.

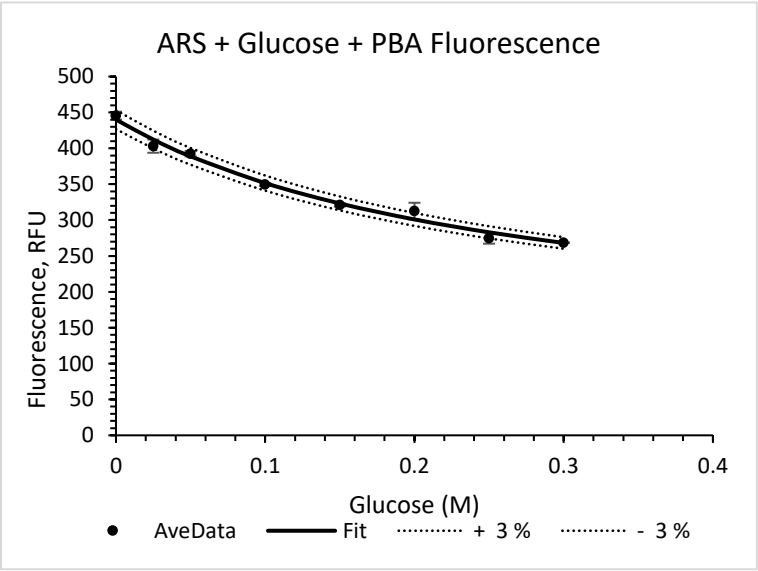

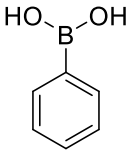

PBA

Plot of fluorescence changes of ARS-PBA complex with increasing concentration of glucose. ARS (0.1 mM), PBA (10 mM), glucose (0-0.1 M), HEPES buffer (100 mM, pH 7.4). (K_a was calculated to be 3.7 ± 1.1 M^{-1}). Value is the average of duplicate runs. Dotted lines represent 3% error.

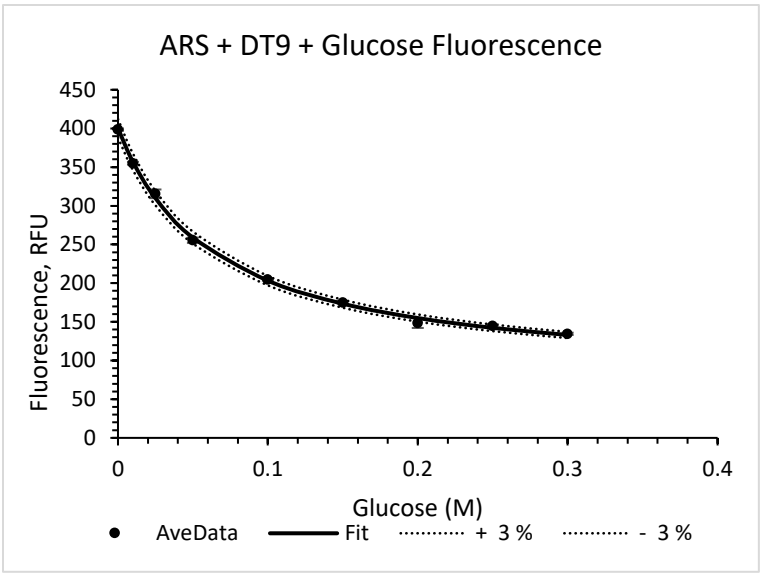

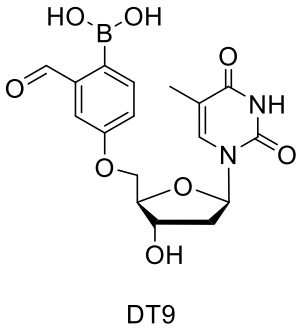

DT9

Plot of fluorescence changes of ARS-DT9 complex with increasing concentration of glucose. ARS (0.1 mM), DT9 (10 mM), glucose (0-0.1 M), HEPES buffer (100 mM, pH 7.4). (K_a was calculated to be 15.3 ± 0.49 M^{-1}). Value is the average of duplicate runs. Dotted lines represent 3% error.

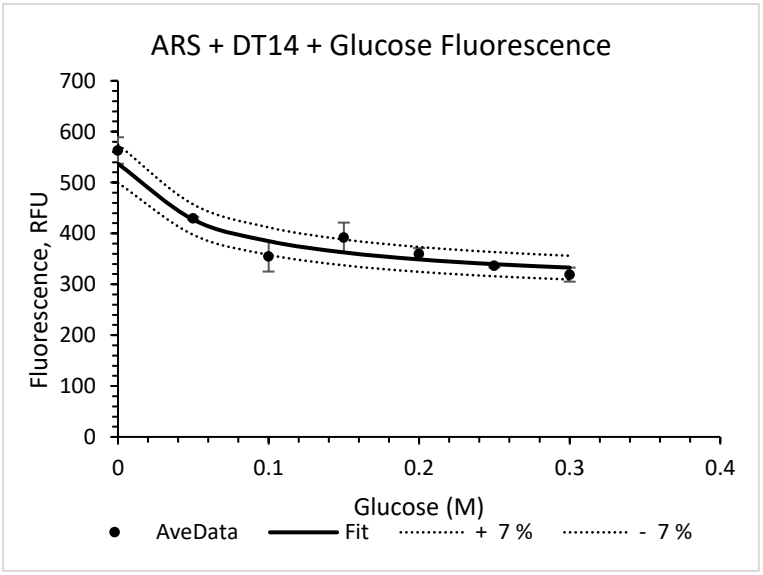

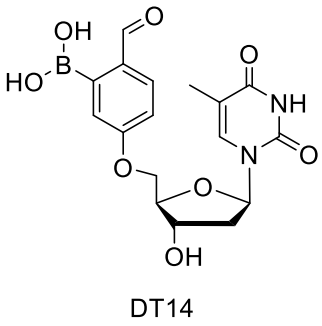

DT14

Plot of fluorescence changes of ARS-DT14 complex with increasing concentration of glucose. ARS (0.1 mM), DT14 (10 mM), glucose (0-0.1 M), HEPES buffer (100 mM, pH 7.4). (K_a was calculated to be 16.1 ± 6.9 M^{-1}). Value is the average of duplicate runs. Dotted lines represent 7% error.

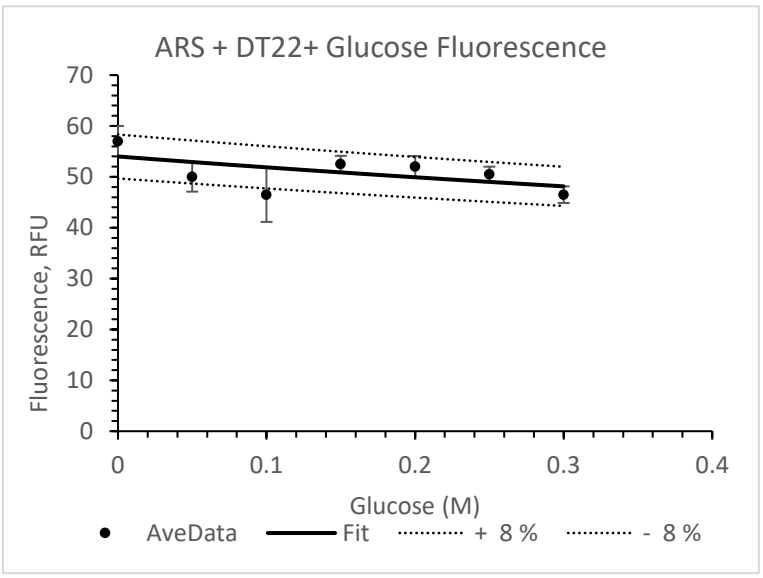

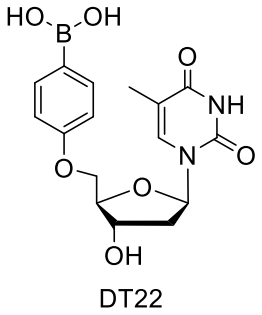

DT22

Plot of fluorescence changes of ARS-DT22 complex with increasing concentration of glucose. ARS (0.1 mM), DT22 (10 mM), glucose (0-0.1 M), HEPES buffer (100 mM, pH 7.4). (K_a was calculated to be 0.47 ± 1.1 M^{-1}). Value is the average of duplicate runs. Dotted lines represent 8% error.

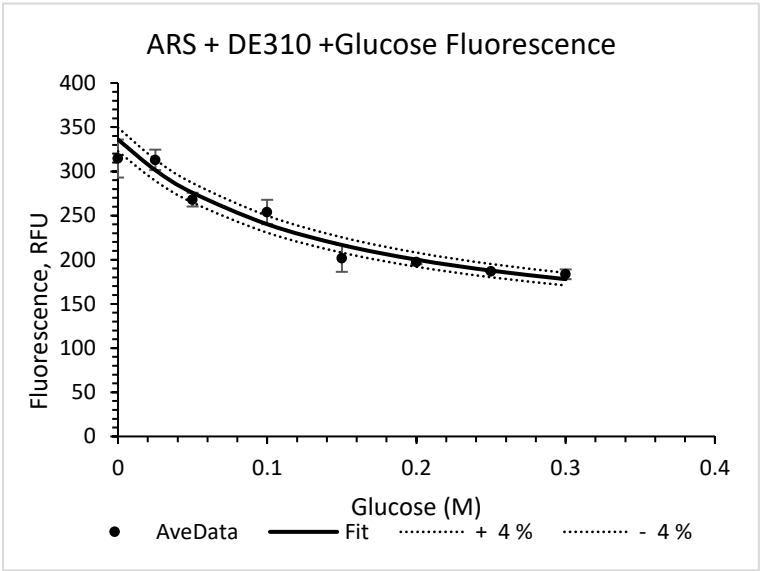

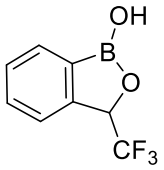

DE310

Plot of fluorescence changes of ARS-DE310 complex with increasing concentration of glucose. ARS (0.1 mM), DE310 (10 mM), glucose (0-0.1 M), HEPES buffer (100 mM, pH 7.4). (K_a was calculated to be 6.9 ± 4.1 M^{-1}). Value is the average of duplicate runs. Dotted lines represent 4% error.

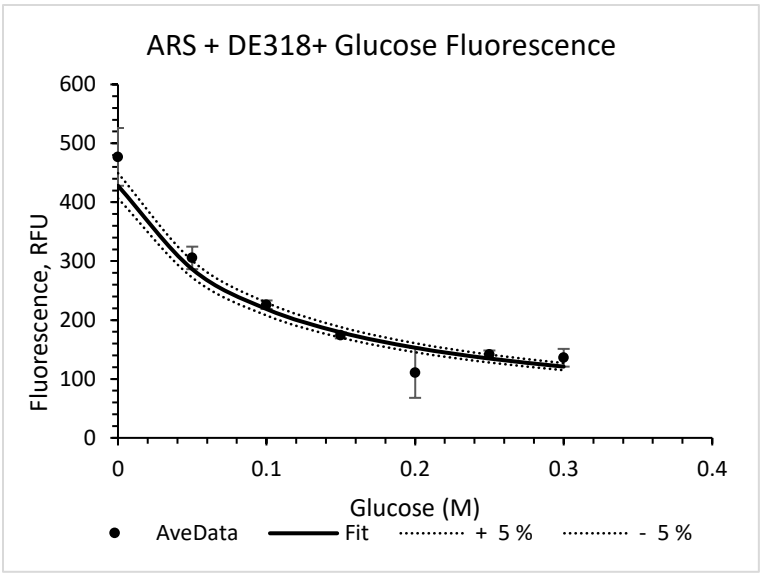

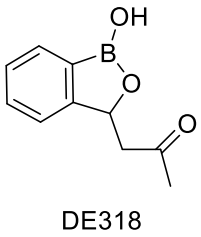

DE318

Plot of fluorescence changes of ARS-DE318 complex with increasing concentration of glucose. ARS (0.1 mM), DE318 (10 mM), glucose (0-0.1 M), HEPES buffer (100 mM, pH 7.4). (K_a was calculated to be 10.9 ± 21 M^{-1}). Value is the average of duplicate runs. Dotted lines represent 5% error.

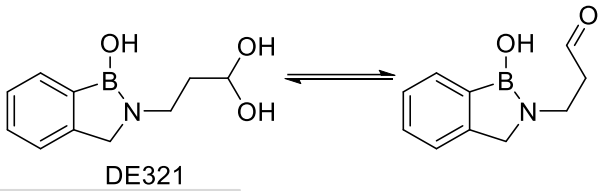

DE321

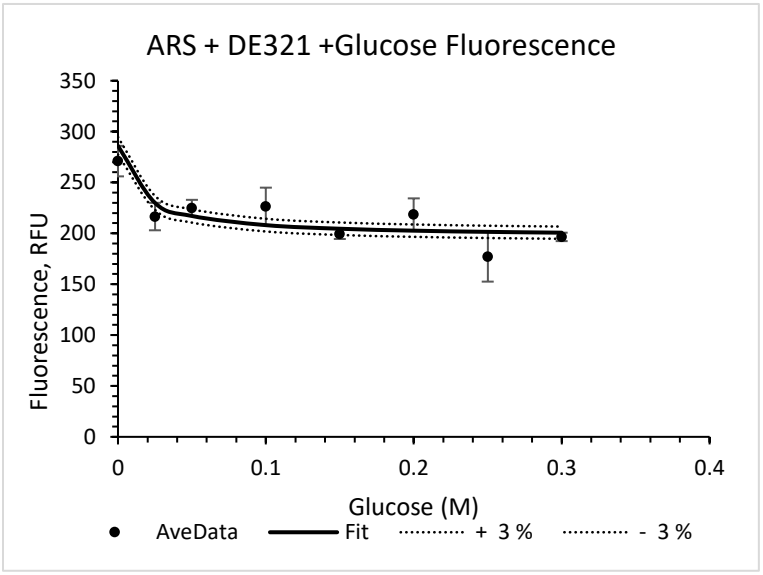

Plot of fluorescence changes of ARS-DE321 complex with increasing concentration of glucose. ARS (0.1 mM), DE321 (10 mM), glucose (0-0.1 M), HEPES buffer (100 mM, pH 7.4). (K_a was calculated to be 66.6 ± 7.9 M^{-1}). Value is the average of duplicate runs. Dotted lines represent 3% error.

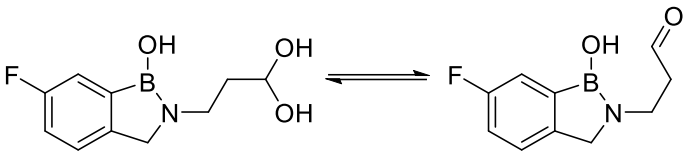

DE342

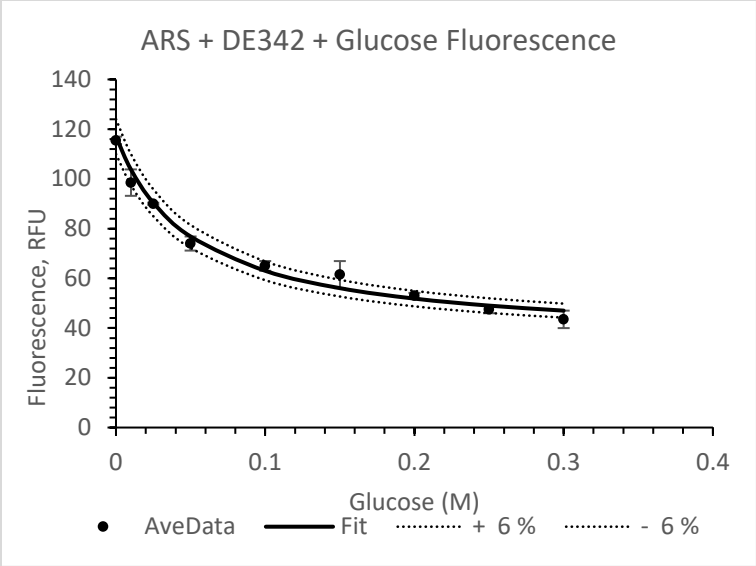

Plot of fluorescence changes of ARS-DE342 complex with increasing concentration of glucose. ARS (0.1 mM), DE342 (10 mM), glucose (0-0.1 M), HEPES buffer (100 mM, pH 7.4). (K_a was calculated to be 19.1 ± 1.3 M^{-1}). Value is the average of duplicate runs. Dotted lines represent 6% error.

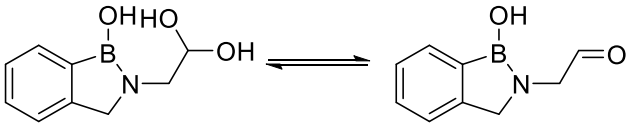

DE343

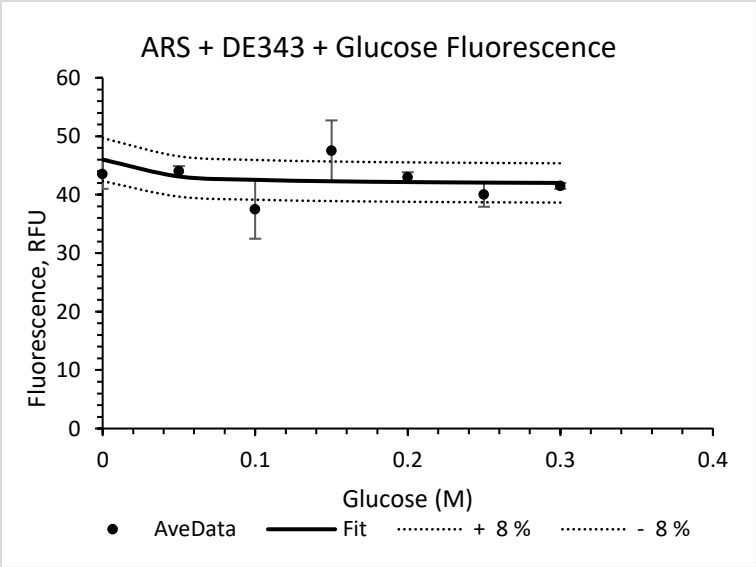

Plot of fluorescence changes of ARS-DE343 complex with increasing concentration of glucose. ARS (0.1 mM), DE343 (10 mM), glucose (0-0.1 M), HEPES buffer (100 mM, pH 7.4). (K_a was calculated to be 40.2 ± 1.5 M^{-1}). Value is the average of duplicate runs. Dotted lines represent 8% error.

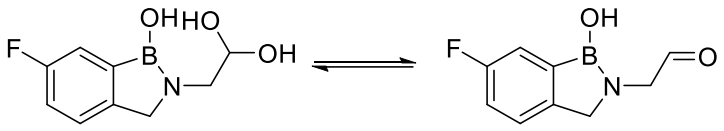

DE344

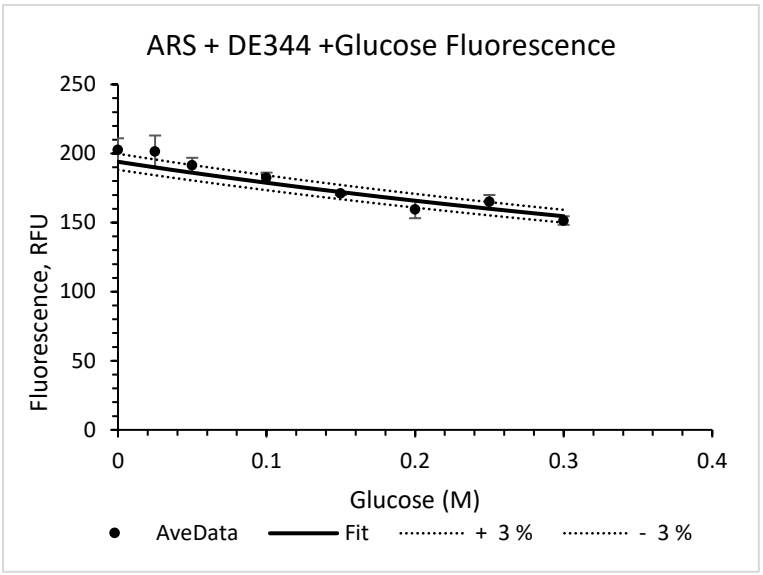

Plot of fluorescence changes of ARS-DE344 complex with increasing concentration of glucose. ARS (0.1 mM), DE344 (10 mM), glucose (0-0.1 M), HEPES buffer (100 mM, pH 7.4). (K_a was calculated to be 0.85 ± 1.7 M^{-1}). Value is the average of duplicate runs. Dotted lines represent 3% error.

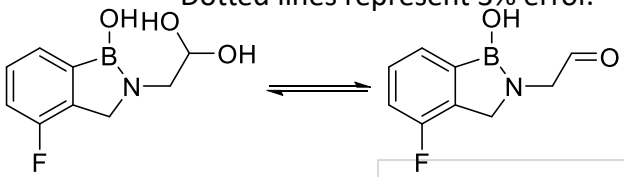

DE347

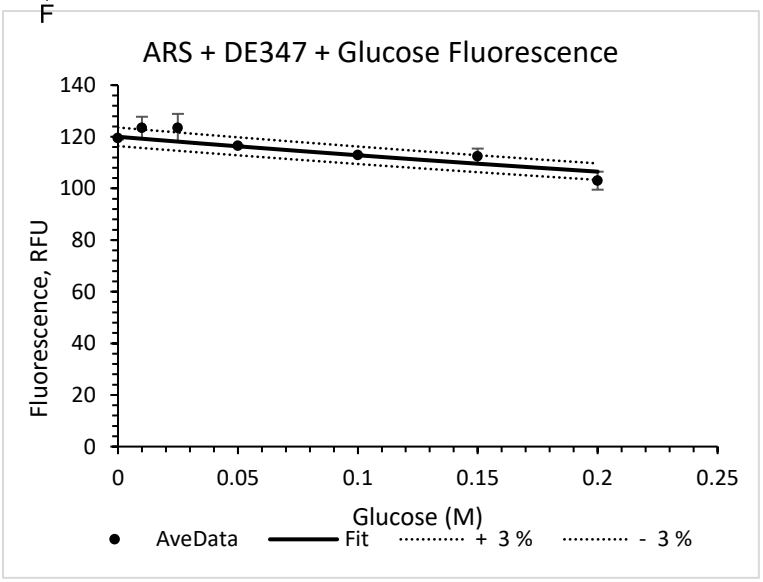

Plot of fluorescence changes of ARS-DE347 complex with increasing concentration of glucose. ARS (0.1 mM), DE347 (10 mM), glucose (0-0.1 M), HEPES buffer (100 mM, pH 7.4). (K_a was calculated to be 0.63 ± 0.58 M^{-1}). Value is the average of duplicate runs. Dotted lines represent 3% error.

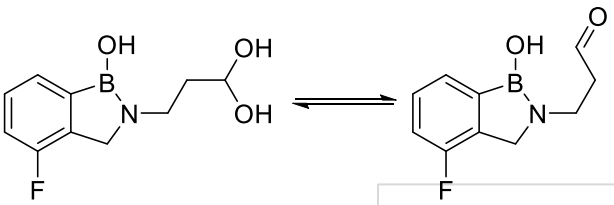

DE348

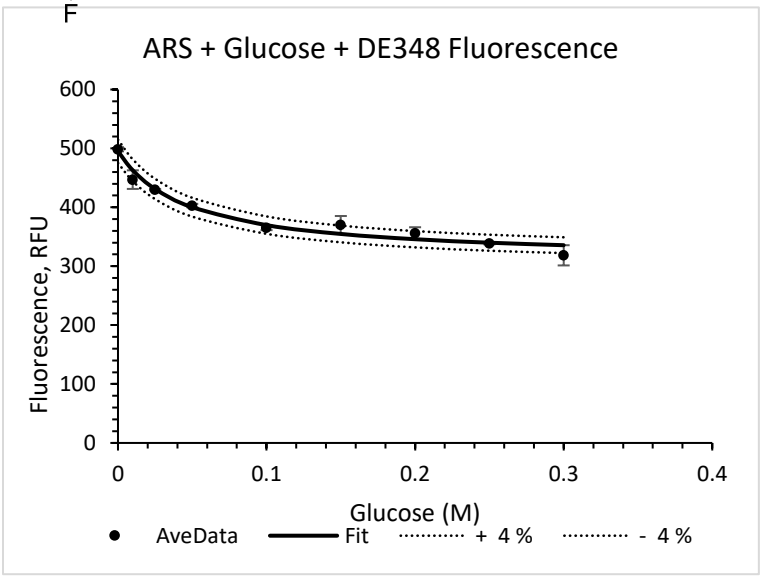

Plot of fluorescence changes of ARS-DE348 complex with increasing concentration of glucose. ARS (0.1 mM), DE348 (10 mM), glucose (0-0.1 M), HEPES buffer (100 mM, pH 7.4). (K_a was calculated to be 21.2 ± 2.5 M^{-1}). Value is the average of duplicate runs. Dotted lines represent 4% error.

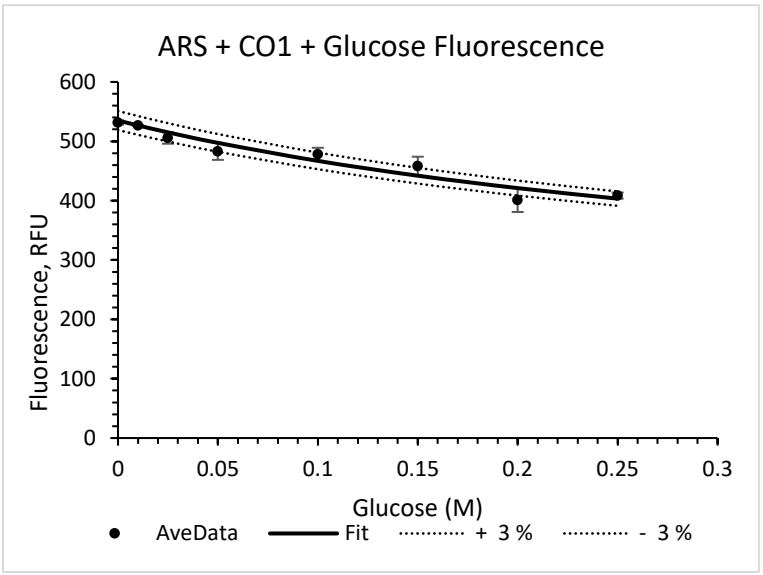

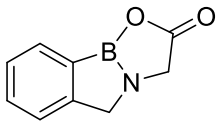

CO1

Plot of fluorescence changes of ARS-CO1 complex with increasing concentration of glucose. ARS (0.1 mM), CO1 (10 mM), glucose (0-0.1 M), HEPES buffer (100 mM, pH 7.4). (K_a was calculated to be 2.4 ± 2.5 M^{-1}). Value is the average of duplicate runs. Dotted lines represent 3% error.

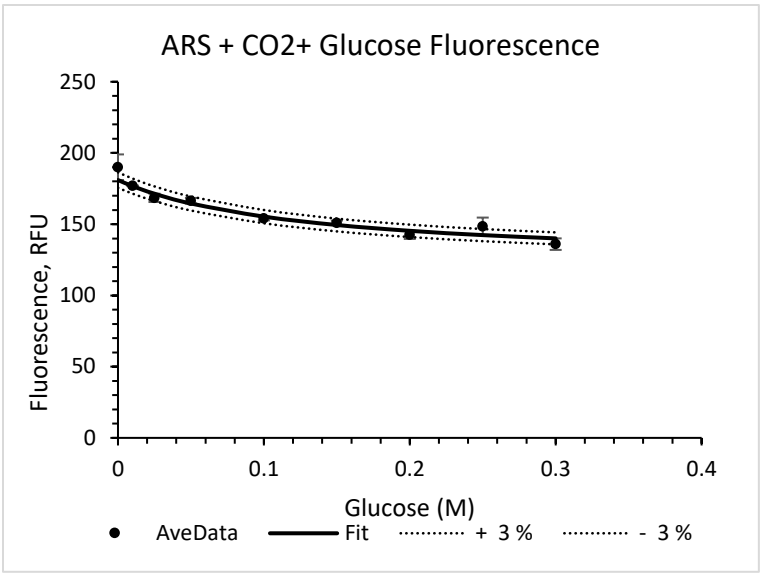

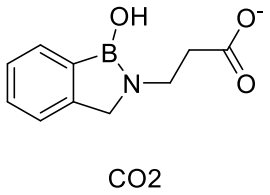

CO2

Plot of fluorescence changes of ARS-CO2 complex with increasing concentration of glucose. ARS (0.1 mM), CO2 (10 mM), glucose (0-0.1 M), HEPES buffer (100 mM, pH 7.4). (K_a was calculated to be 7.8 ± 0.98 M^{-1}). Value is the average of duplicate runs. Dotted lines represent 3% error.

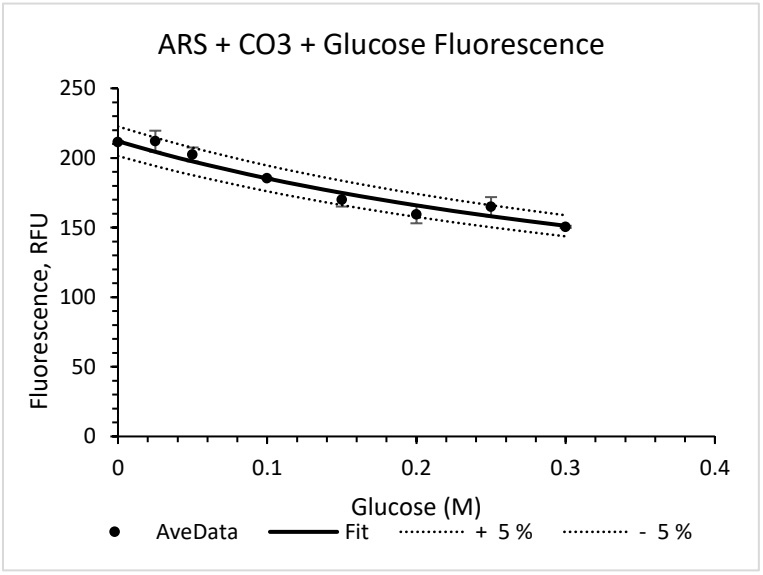

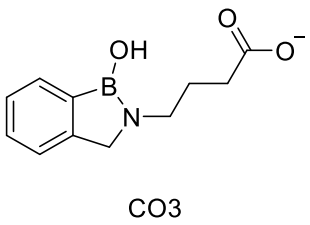

CO3

Plot of fluorescence changes of ARS-CO3 complex with increasing concentration of glucose. ARS (0.1 mM), CO3 (10 mM), glucose (0-0.1 M), HEPES buffer (100 mM, pH 7.4). (K_a was calculated to be 1.9 ± 1.1 M^{-1}). Value is the average of duplicate runs. Dotted lines represent 5% error.

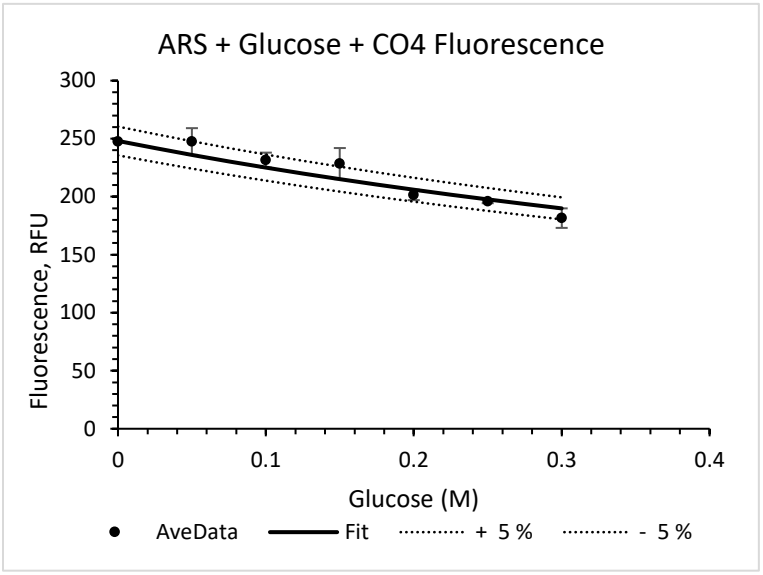

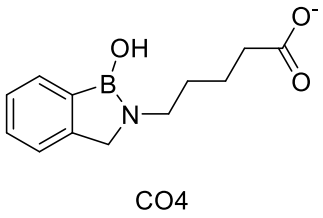

CO4

Plot of fluorescence changes of ARS-CO4 complex with increasing concentration of glucose. ARS (0.1 mM), CO4 (10 mM), glucose (0-0.1 M), HEPES buffer (100 mM, pH 7.4). (K_a was calculated to be 1.1 ± 2.1 M^{-1}). Value is the average of duplicate runs. Dotted lines represent 5% error.

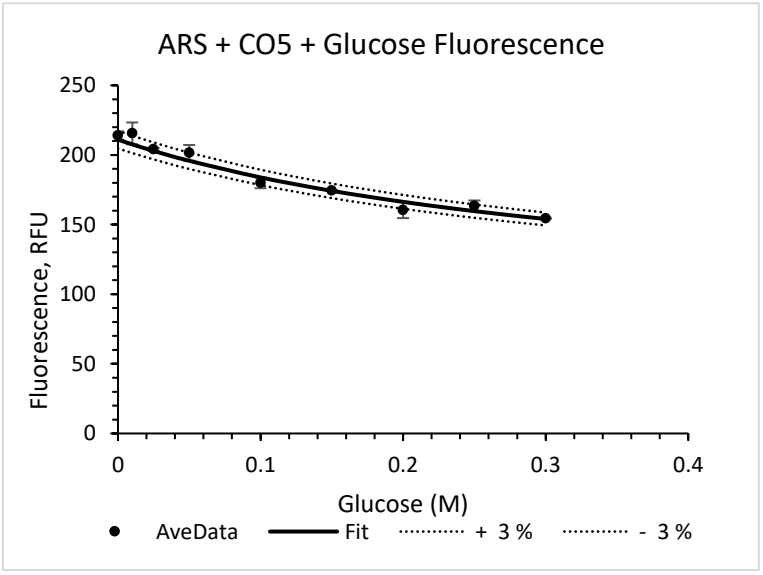

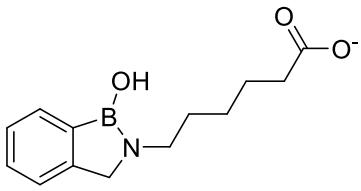

CO5

Plot of fluorescence changes of ARS-CO5 complex with increasing concentration of glucose. ARS (0.1 mM), CO5 (10 mM), glucose (0-0.1 M), HEPES buffer (100 mM, pH 7.4). (K_a was calculated to be 2.7 ± 0.88 M^{-1}). Value is the average of duplicate runs. Dotted lines represent 3% error.

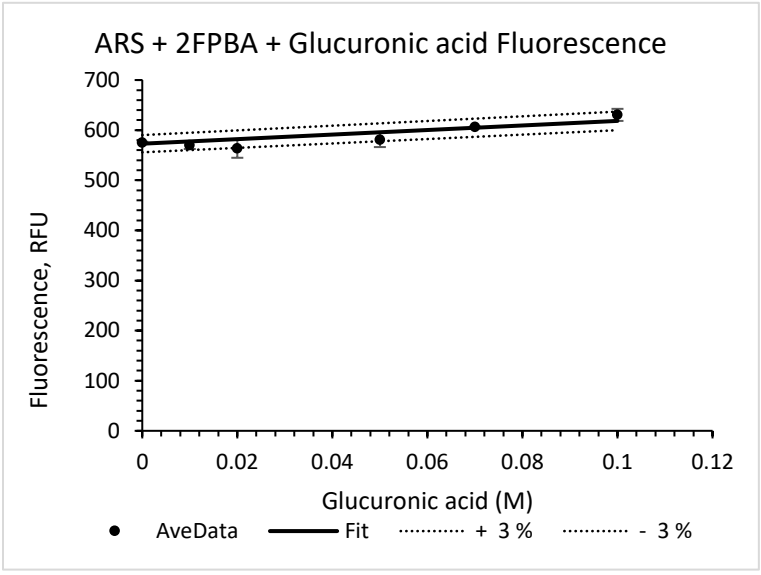

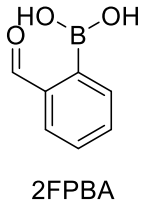

2FPBA

Plot of fluorescence changes of ARS-2FPBA complex with increasing concentration of glucuronic acid. ARS (0.1 mM), 2FPBA (10 mM), glucuronic acid (0-0.1 M), HEPES buffer (100 mM, pH 7.4). (K_a was calculated to be 0.0034 ± 1.3 M^{-1}). Value is the average of duplicate runs. Dotted lines represent 3% error.

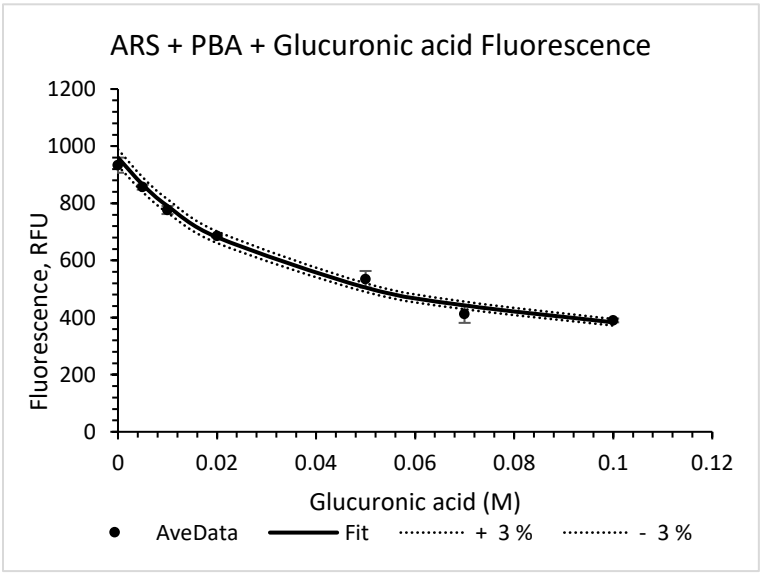

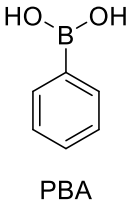

PBA

Plot of fluorescence changes of ARS-PBA complex with increasing concentration of glucuronic acid. ARS (0.1 mM), PBA (10 mM), glucuronic acid (0-0.1 M), HEPES buffer (100 mM, pH 7.4). (K_a was calculated to be 27.4 ± 4.9 M^{-1}). Value is the average of duplicate runs. Dotted lines represent 3% error.

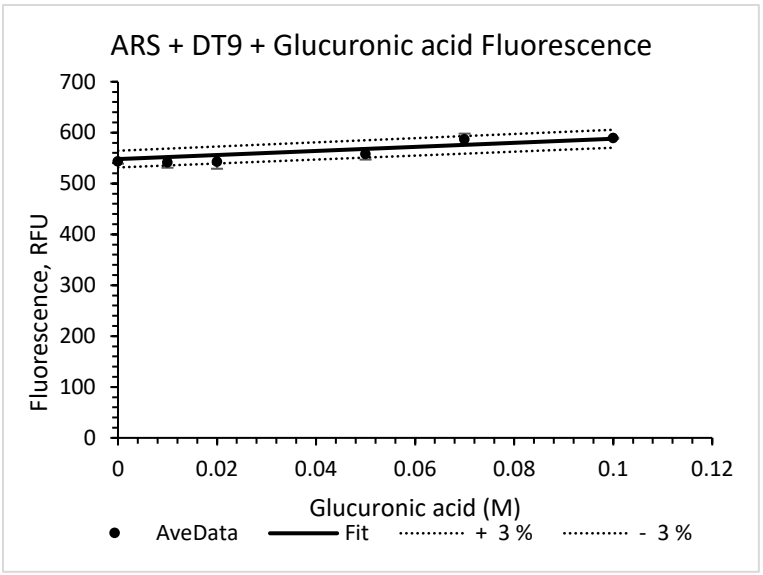

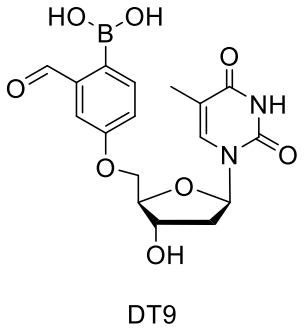

DT9

Plot of fluorescence changes of ARS-DT9 complex with increasing concentration of glucuronic acid. ARS (0.1 mM), DT9 (10 mM), glucuronic acid (0-0.1 M), HEPES buffer (100 mM, pH 7.4). (K_a was calculated to be 0.0071 ± 0.92 M^{-1}). Value is the average of duplicate runs. Dotted lines represent 3% error.

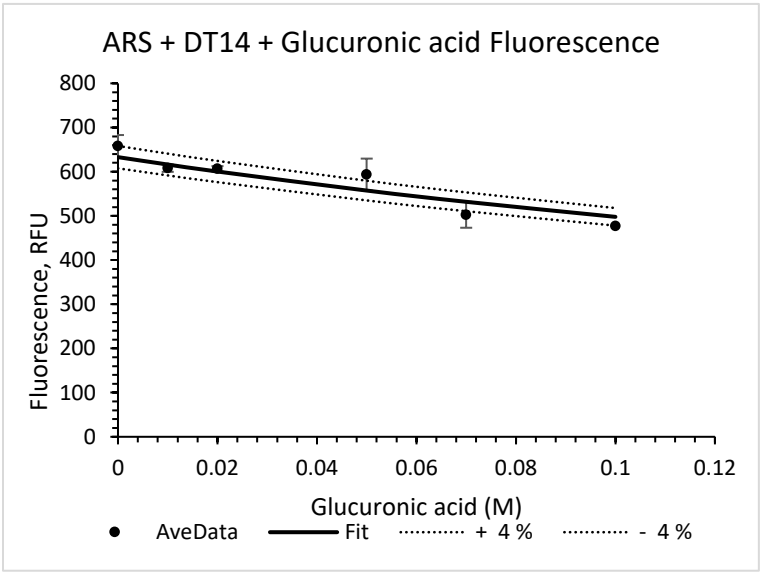

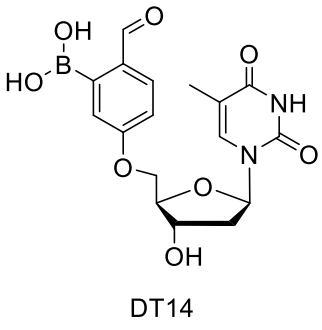

DT14

Plot of fluorescence changes of ARS-DT14 complex with increasing concentration of glucuronic acid. ARS (0.1 mM), DT14 (10 mM), glucuronic acid (0-0.1 M), HEPES buffer (100 mM, pH 7.4). (K_a was calculated to be 2.7 ± 5.1 M^{-1}). Value is the average of duplicate runs. Dotted lines represent 4% error.

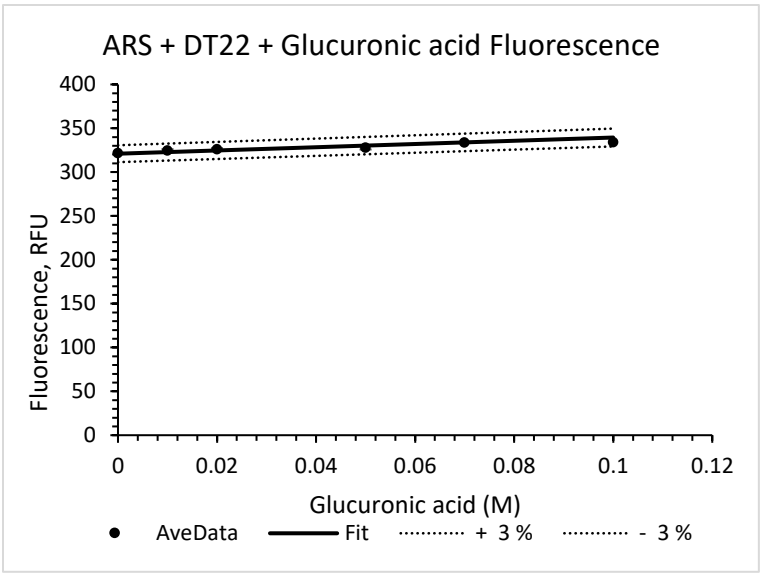

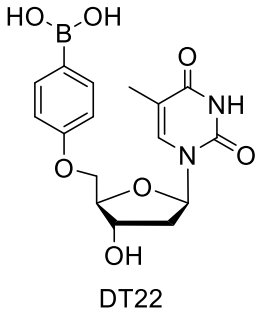

DT22

Plot of fluorescence changes of ARS-DT22 complex with increasing concentration of glucuronic acid. ARS (0.1 mM), DT22 (10 mM), glucuronic acid (0-0.1 M), HEPES buffer (100 mM, pH 7.4). (K_a was calculated to be 0.0044 ± 0.033 M^{-1}). Value is the average of duplicate runs. Dotted lines represent 3% error.

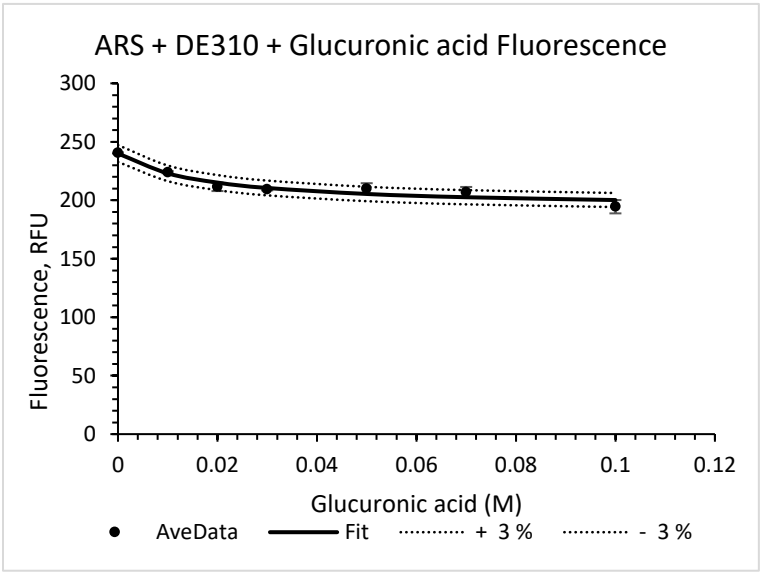

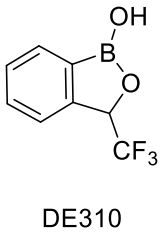

DE310

Plot of fluorescence changes of ARS-DE310 complex with increasing concentration of glucuronic acid. ARS (0.1 mM), DE310 (10 mM), glucuronic acid (0-0.1 M), HEPES buffer (100 mM, pH 7.4). (K_a was calculated to be 56.7 ± 0.43 M^{-1}). Value is the average of duplicate runs. Dotted lines represent 3% error.

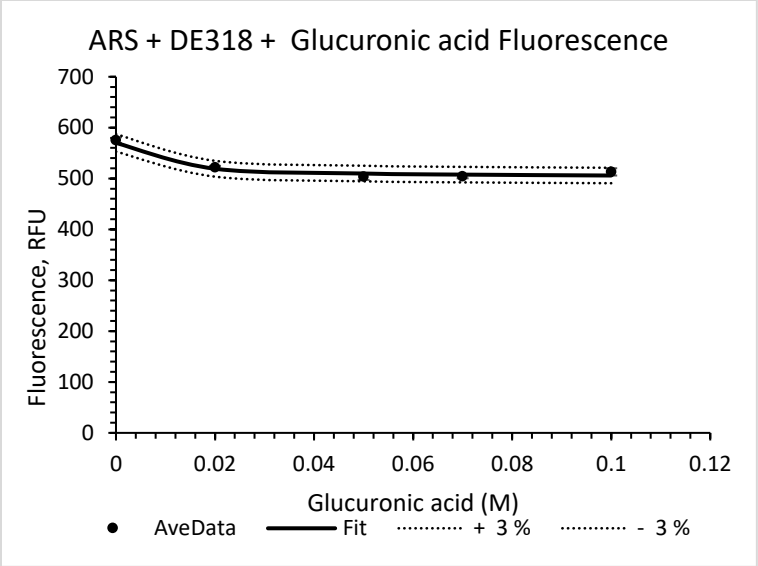

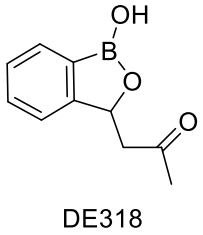

DE318

Plot of fluorescence changes of ARS-DE318 complex with increasing concentration of glucuronic acid. ARS (0.1 mM), DE318 (10 mM), glucuronic acid (0-0.1 M), HEPES buffer (100 mM, pH 7.4). (K_a was calculated to be 143.1 ± 0.27 M^{-1}). Value is the average of duplicate runs. Dotted lines represent 3% error.

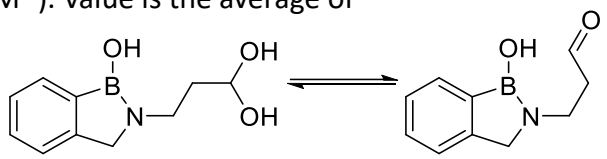

DE321

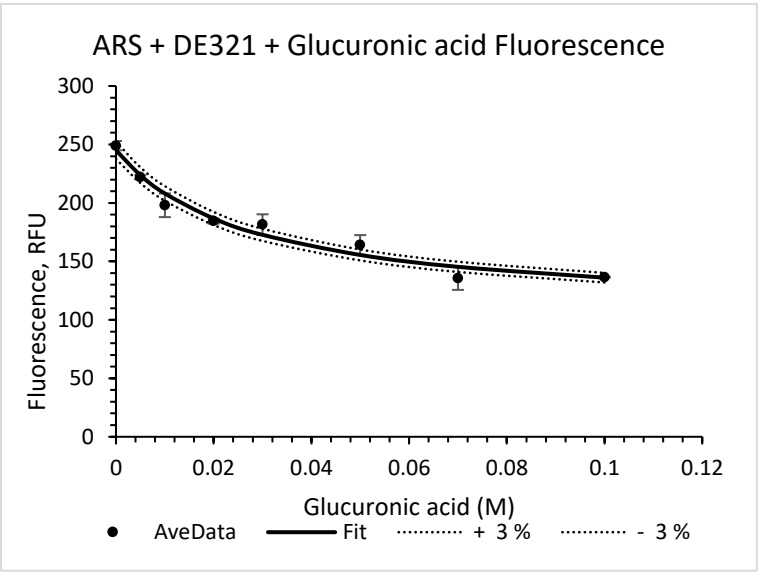

Plot of fluorescence changes of ARS-DE321 complex with increasing concentration of glucuronic acid. ARS (0.1 mM), DE321 (10 mM), glucuronic acid (0-0.1 M), HEPES buffer (100 mM, pH 7.4). (K_a was calculated to be 36.1 ± 2.2 M^{-1}). Value is the average of duplicate runs. Dotted lines represent 3% error.

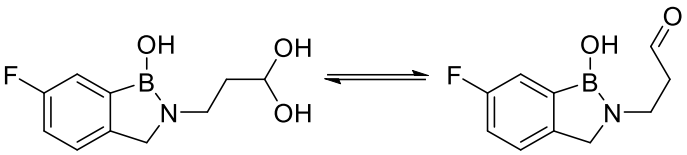

DE342

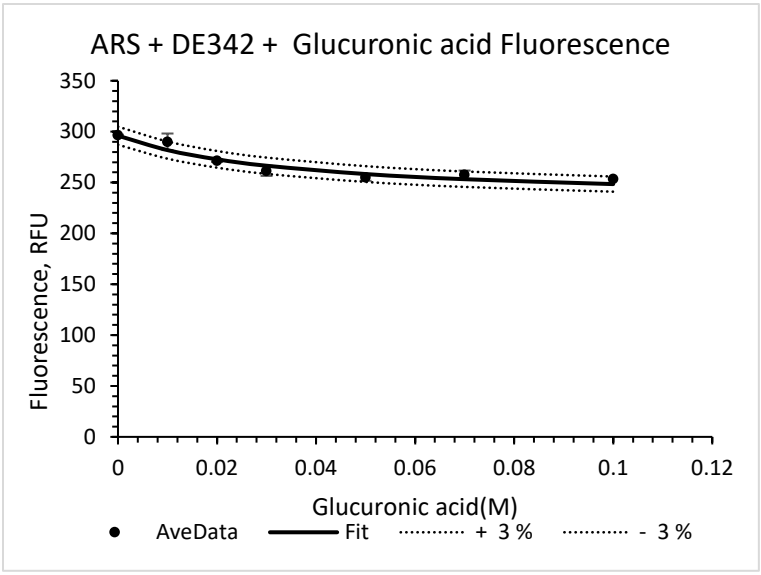

Plot of fluorescence changes of ARS-DE342 complex with increasing concentration of glucuronic acid. ARS (0.1 mM), DE342 (10 mM), glucuronic acid (0-0.1 M), HEPES buffer (100 mM, pH 7.4). (K_a was calculated to be 28.1 ± 0.45 M^{-1}). Value is the average of duplicate runs. Dotted lines represent 3% error.

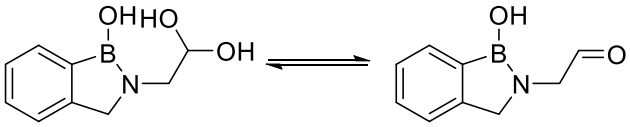

DE343

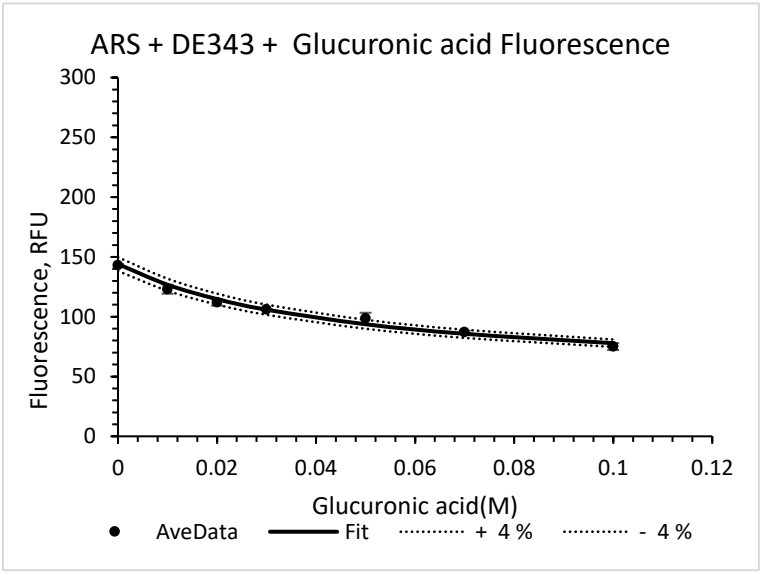

Plot of fluorescence changes of ARS-DE343 complex with increasing concentration of glucuronic acid. ARS (0.1 mM), DE343 (10 mM), glucuronic acid (0-0.1 M), HEPES buffer (100 mM, pH 7.4). (K_a was calculated to be 21.7 ± 0.55 M^{-1}). Value is the average of duplicate runs. Dotted lines represent 4% error.

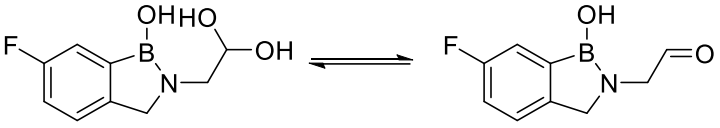

DE344

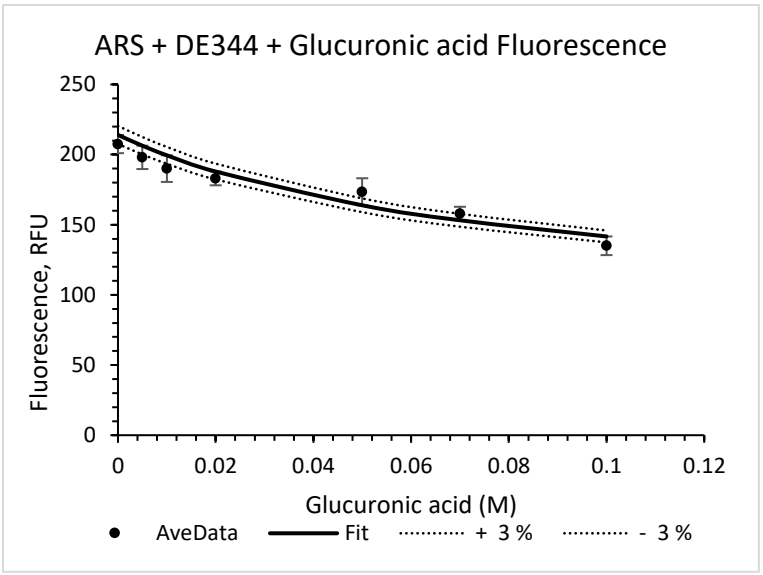

Plot of fluorescence changes of ARS-DE344 complex with increasing concentration of glucuronic acid. ARS (0.1 mM), DE344 (10 mM), glucuronic acid (0-0.1 M), HEPES buffer (100 mM, pH 7.4). (K_a was calculated to be 12.6 ± 2.1 M^{-1}). Value is the average of duplicate runs. Dotted lines represent 3% error.

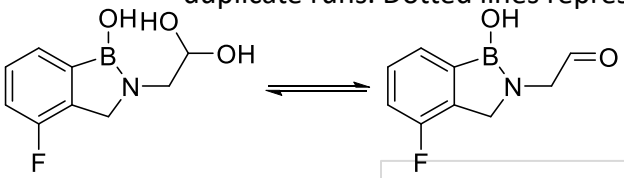

DE347

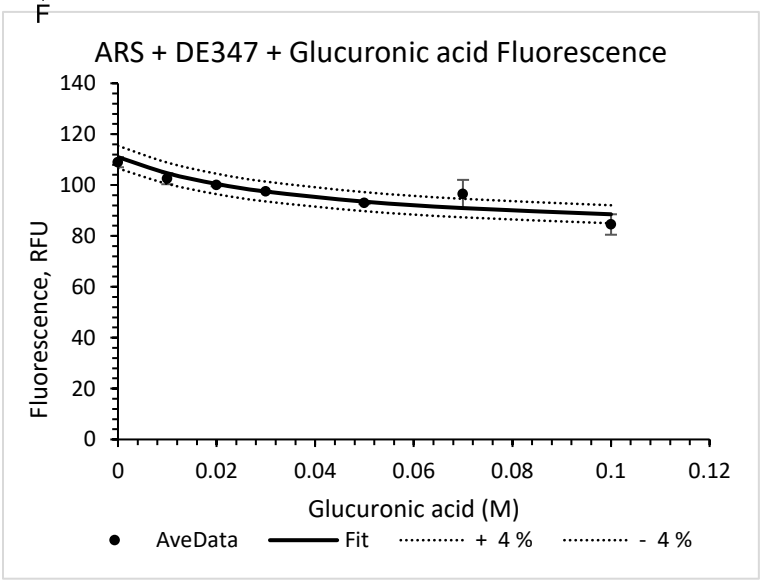

Plot of fluorescence changes of ARS-DE347 complex with increasing concentration of glucuronic acid. ARS (0.1 mM), DE347 (10 mM), glucuronic acid (0-0.1 M), HEPES buffer (100 mM, pH 7.4). (K_a was calculated to be 25.3 ± 0.61 M^{-1}). Value is the average of duplicate runs. Dotted lines represent 4% error.

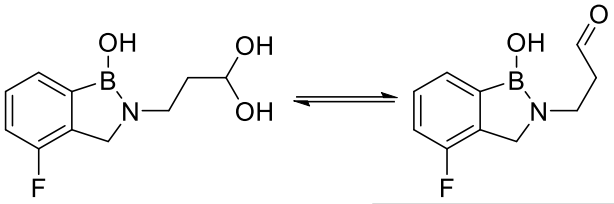

DE348

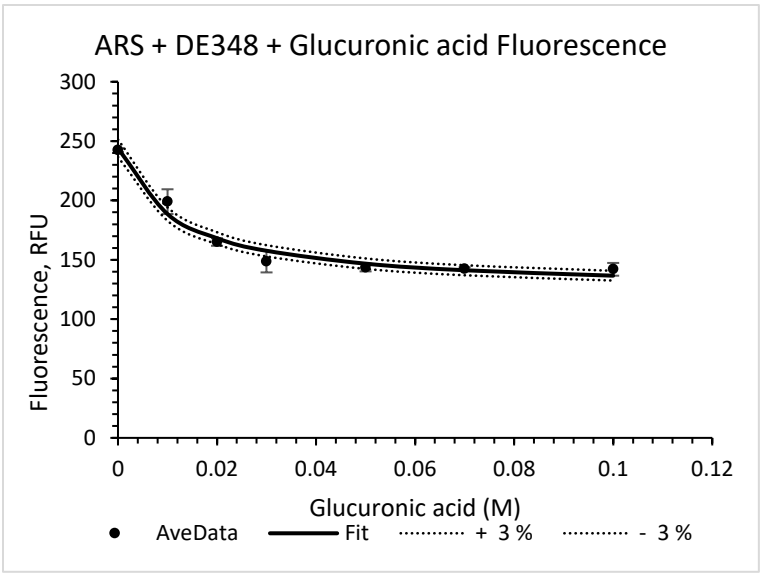

Plot of fluorescence changes of ARS-DE348 complex with increasing concentration of glucuronic acid. ARS (0.1 mM), DE348 (10 mM), glucuronic acid (0-0.1 M), HEPES buffer (100 mM, pH 7.4). (K_a was calculated to be 86.1 ± 1.5 M^{-1}). Value is the average of duplicate runs. Dotted lines represent 3% error.

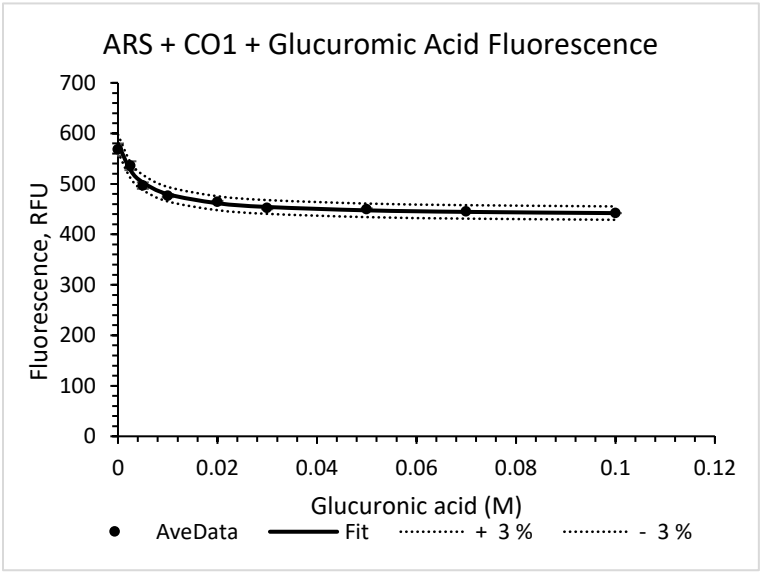

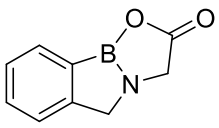

CO1

Plot of fluorescence changes of ARS-CO1 complex with increasing concentration of glucuronic acid. ARS (0.1 mM), CO1 (10 mM), glucuronic acid (0-0.1 M), HEPES buffer (100 mM, pH 7.4). (K_a was calculated to be 231.1 ± 0.52 M^{-1}). Value is the average of duplicate runs. Dotted lines represent 3% error.

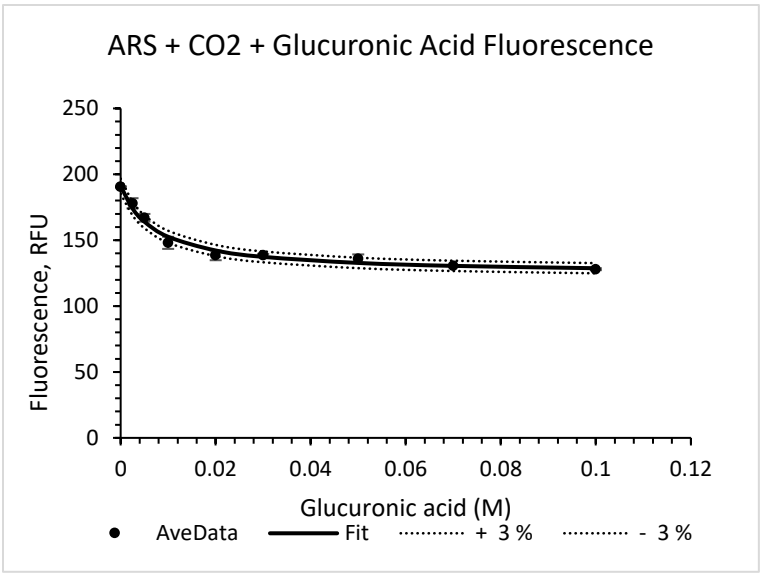

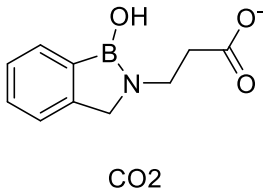

CO2

Plot of fluorescence changes of ARS-CO2 complex with increasing concentration of glucuronic acid. ARS (0.1 mM), CO2 (10 mM), glucuronic acid (0-0.1 M), HEPES buffer (100 mM, pH 7.4). (K_a was calculated to be 134.9 ± 0.47 M^{-1}). Value is the average of duplicate runs. Dotted lines represent 3% error.

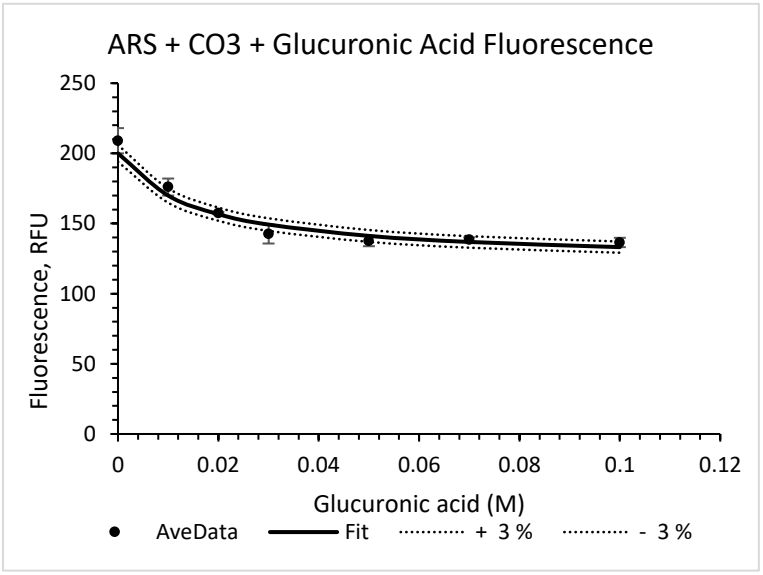

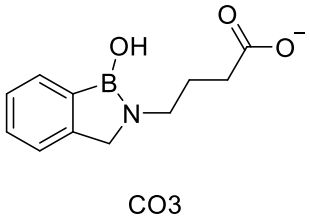

CO3

Plot of fluorescence changes of ARS-CO3 complex with increasing concentration of glucuronic acid. ARS (0.1 mM), CO3 (10 mM), glucuronic acid (0-0.1 M), HEPES buffer (100 mM, pH 7.4). (K_a was calculated to be 63.6 ± 1.1 M^{-1}). Value is the average of duplicate runs. Dotted lines represent 3% error.

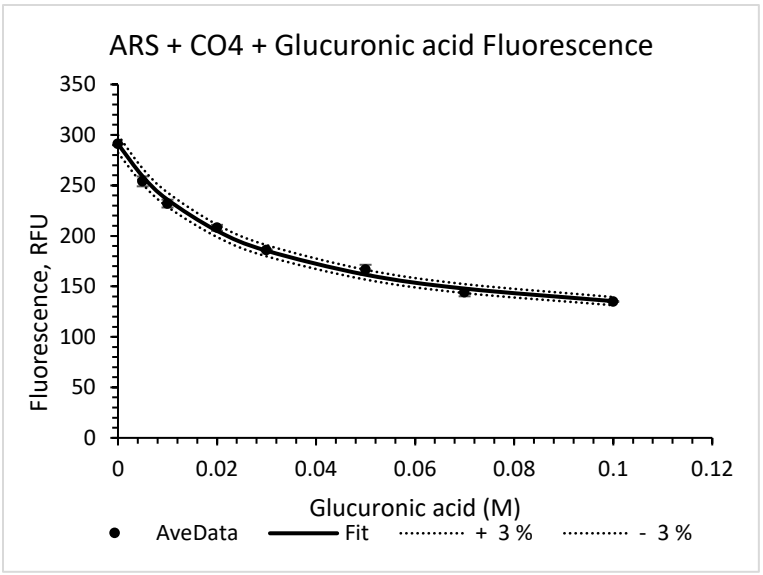

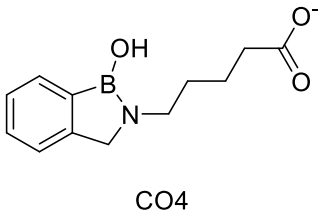

CO4

Plot of fluorescence changes of ARS-CO4 complex with increasing concentration of glucuronic acid. ARS (0.1 mM), CO4 (10 mM), glucuronic acid (0-0.1 M), HEPES buffer (100 mM, pH 7.4). (K_a was calculated to be 39.4 ± 0.45 M^{-1}). Value is the average of duplicate runs. Dotted lines represent 3% error.

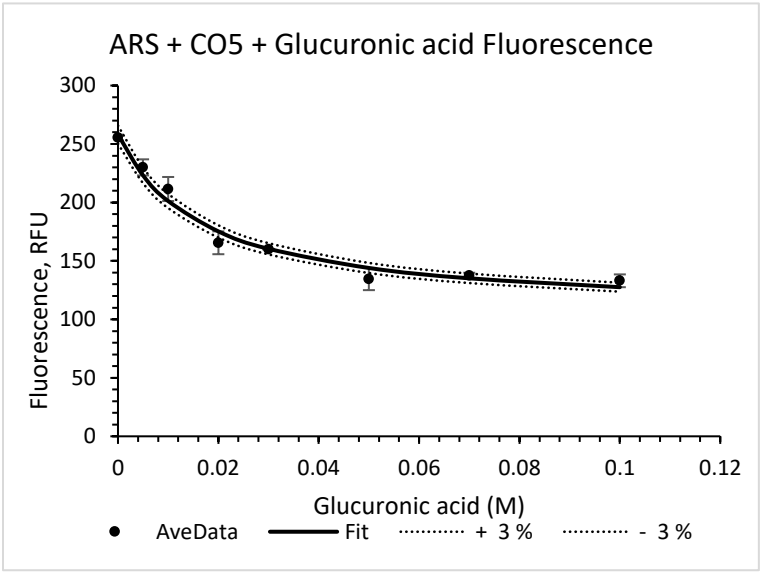

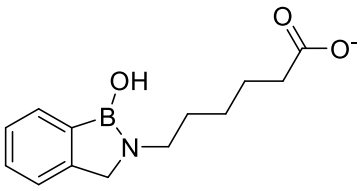

CO5

Plot of fluorescence changes of ARS-CO5 complex with increasing concentration of glucuronic acid. ARS (0.1 mM), CO5 (10 mM), glucuronic acid (0-0.1 M), HEPES buffer (100 mM, pH 7.4). (K_a was calculated to be 59.4 ± 2.2 M^{-1}). Value is the average of duplicate runs. Dotted lines represent 3% error.

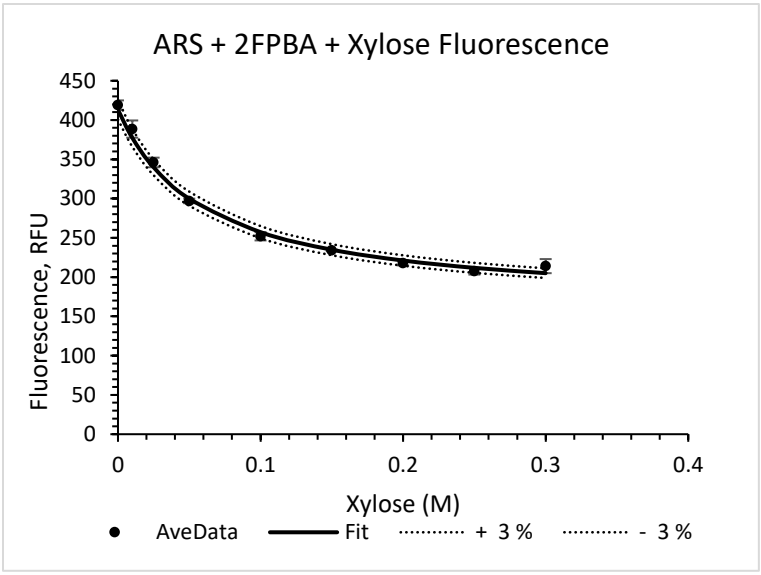

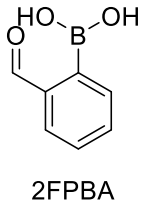

2FPBA

Plot of fluorescence changes of ARS-2FPBA complex with increasing concentration of xylose. ARS (0.1 mM), 2FPBA (10 mM), xylose (0-0.1 M), HEPES buffer (100 mM, pH 7.4). (K_a was calculated to be 16.5 ± 1.2 M^{-1}). Value is the average of duplicate runs. Dotted lines represent 3% error.

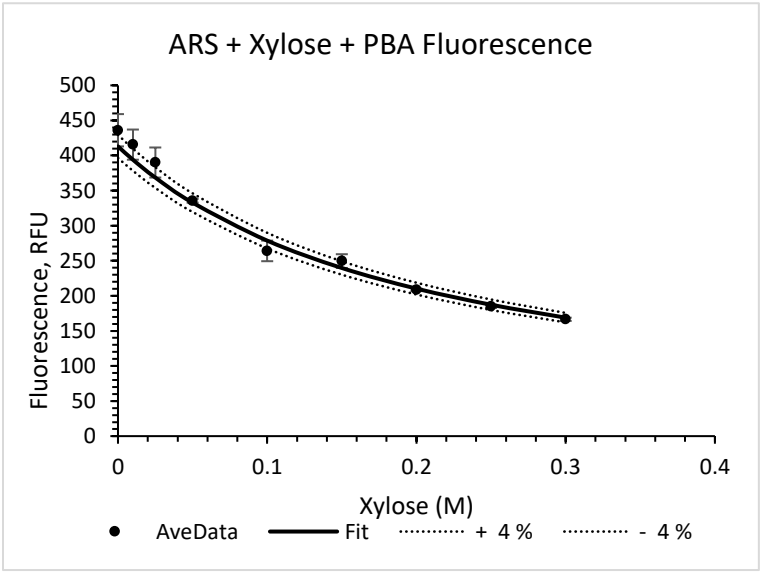

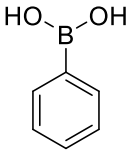

PBA

Plot of fluorescence changes of ARS-PBA complex with increasing concentration of xylose. ARS (0.1 mM), PBA (10 mM), xylose (0-0.1 M), HEPES buffer (100 mM, pH 7.4). (K_a was calculated to be 4.8 ± 4.9 M^{-1}). Value is the average of duplicate runs. Dotted lines represent 4% error.

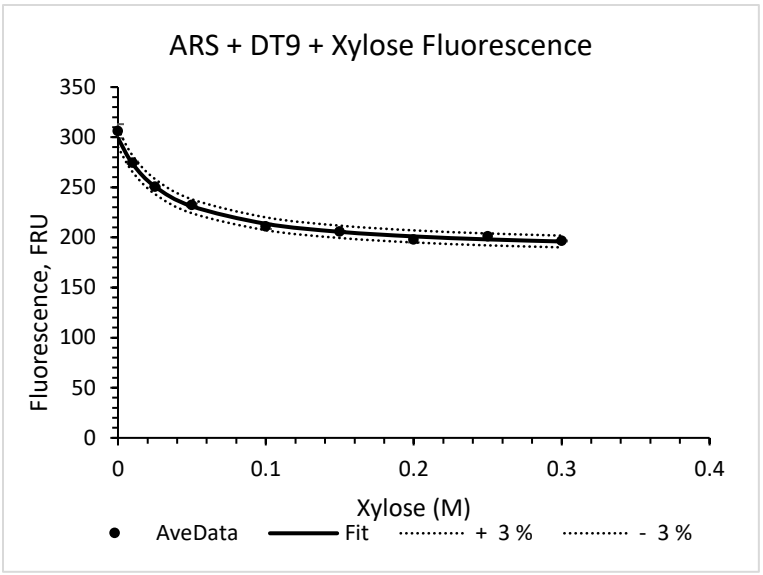

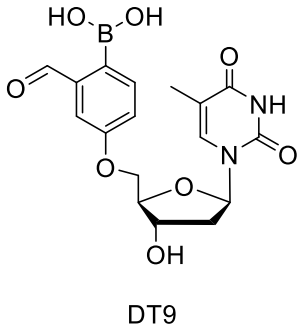

DT9

Plot of fluorescence changes of ARS-DT9 complex with increasing concentration of xylose. ARS (0.1 mM), DT9 (10 mM), xylose (0-0.1 M), HEPES buffer (100 mM, pH 7.4). (K_a was calculated to be 28.8 ± 0.30 M^{-1}). Value is the average of duplicate runs. Dotted lines represent 3% error.

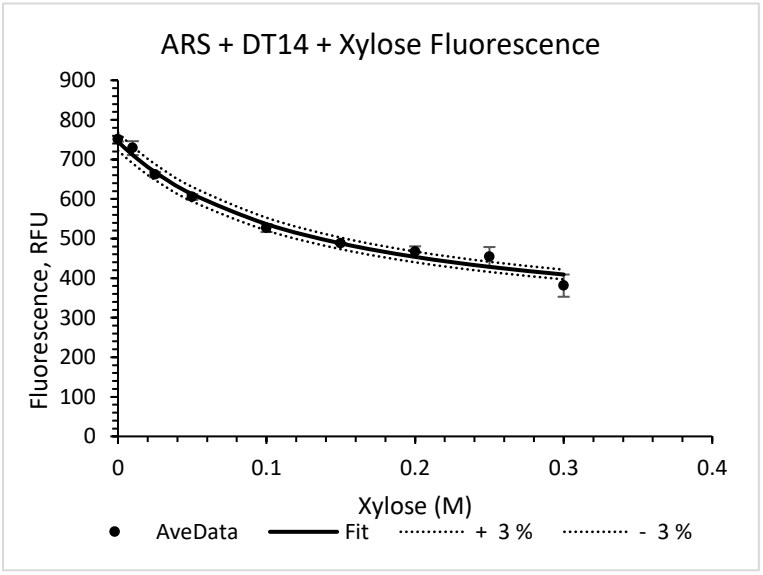

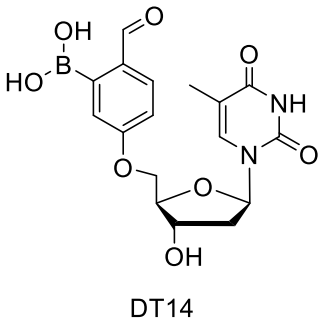

DT14

Plot of fluorescence changes of ARS-DT14 complex with increasing concentration of xylose. ARS (0.1 mM), DT14 (10 mM), xylose (0-0.1 M), HEPES buffer (100 mM, pH 7.4). (K_a was calculated to be 7.6 ± 4.6 M^{-1}). Value is the average of duplicate runs. Dotted lines represent 3% error.

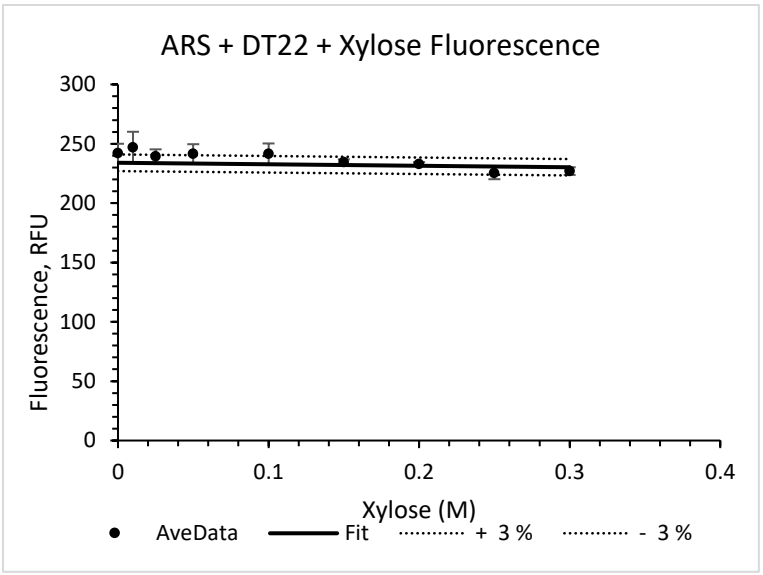

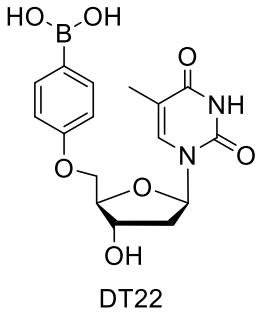

DT22

Plot of fluorescence changes of ARS-DT22 complex with increasing concentration of xylose. ARS (0.1 mM), DT22 (10 mM), xylose (0-0.1 M), HEPES buffer (100 mM, pH 7.4). (K_a was calculated to be 0.055 ± 1.9 M^{-1}). Value is the average of duplicate runs. Dotted lines represent 3% error.

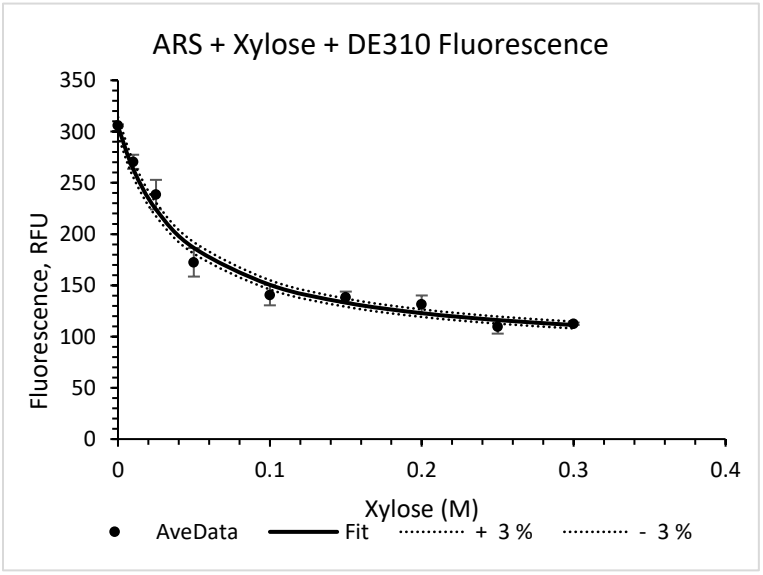

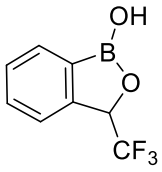

DE310

Plot of fluorescence changes of ARS-DE310 complex with increasing concentration of xylose. ARS (0.1 mM), DE310 (10 mM), xylose (0-0.1 M), HEPES buffer (100 mM, pH 7.4). (K_a was calculated to be 22.9 ± 4.0 M^{-1}). Value is the average of duplicate runs. Dotted lines represent 3% error.

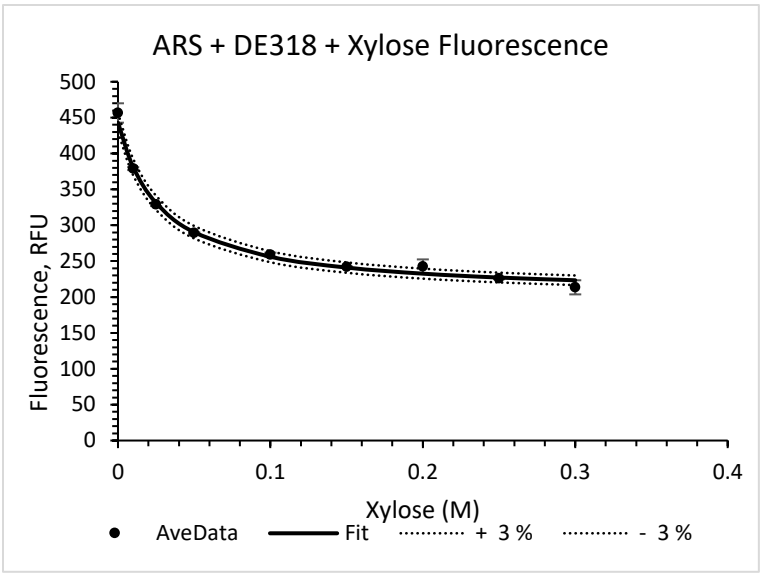

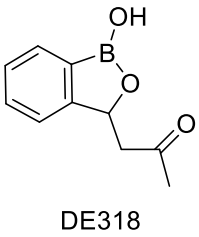

DE318

Plot of fluorescence changes of ARS-DE318 complex with increasing concentration of xylose. ARS (0.1 mM), DE318 (10 mM), xylose (0-0.1 M), HEPES buffer (100 mM, pH 7.4). (K_a was calculated to be 34.6 ± 1.3 M^{-1}). Value is the average of duplicate runs. Dotted lines represent 3% error.

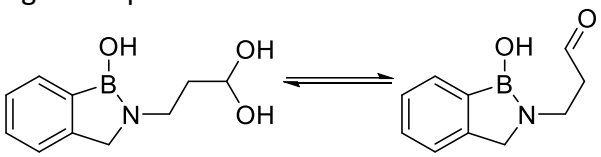

DE321

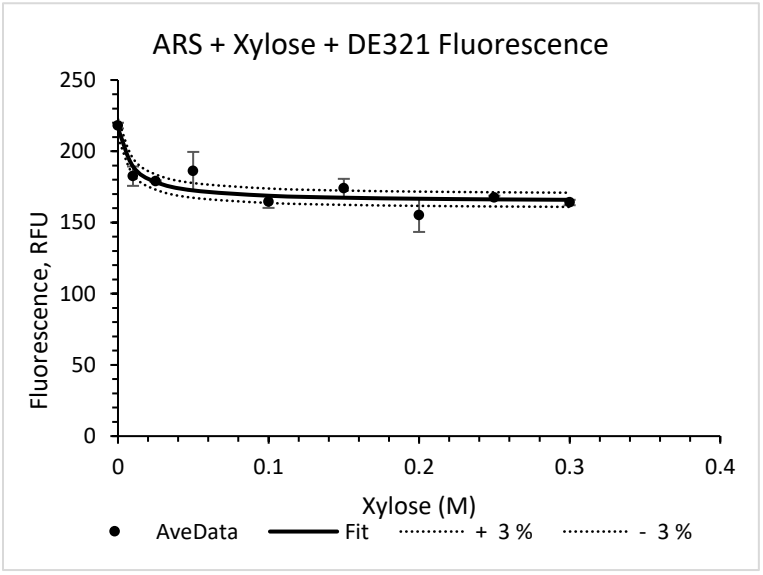

Plot of fluorescence changes of ARS-DE321 complex with increasing concentration of xylose. ARS (0.1 mM), DE321 (10 mM), xylose (0-0.1 M), HEPES buffer (100 mM, pH 7.4). (K_a was calculated to be 106.9 ± 2.5 M^{-1}). Value is the average of duplicate runs. Dotted lines represent 3% error.

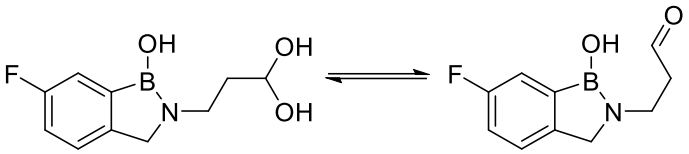

DE342

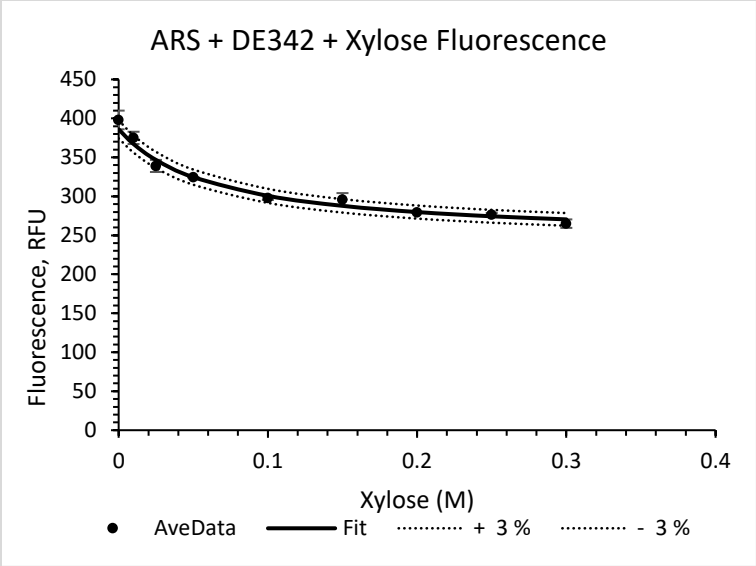

Plot of fluorescence changes of ARS-DE342 complex with increasing concentration of xylose. ARS (0.1 mM), DE342 (10 mM), xylose (0-0.1 M), HEPES buffer (100 mM, pH 7.4). (K_a was calculated to be 15.5 ± 1.1 M^{-1}). Value is the average of duplicate runs. Dotted lines represent 3% error.

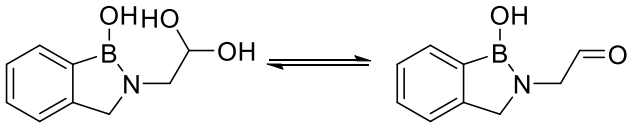

DE343

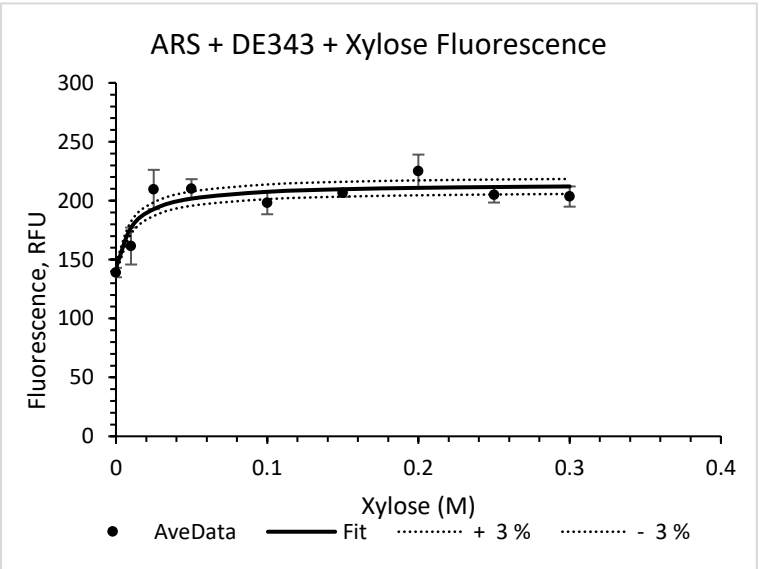

Plot of fluorescence changes of ARS-DE343 complex with increasing concentration of xylose. ARS (0.1 mM), DE343 (10 mM), xylose (0-0.1 M), HEPES buffer (100 mM, pH 7.4). (K_a was calculated to be 91.5 ± 5.2 M^{-1}). Value is the average of duplicate runs. Dotted lines represent 3% error.

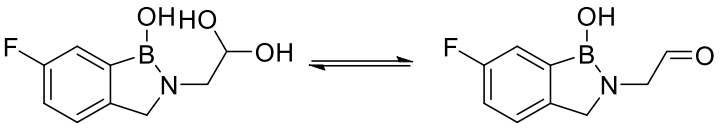

DE344

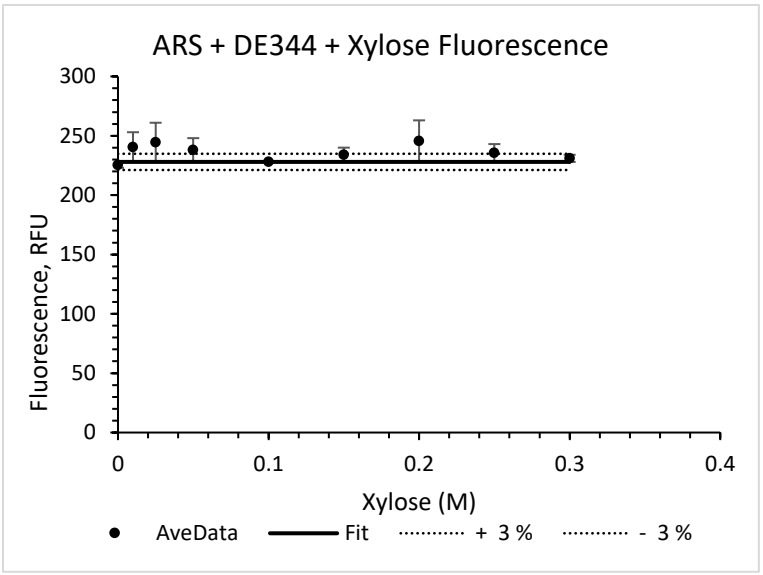

Plot of fluorescence changes of ARS-DE344 complex with increasing concentration of xylose. ARS (0.1 mM), DE344 (10 mM), xylose (0-0.1 M), HEPES buffer (100 mM, pH 7.4). (K_a was calculated to be 0.0 ± 4.1 M^{-1}). Value is the average of duplicate runs. Dotted lines represent 3% error.

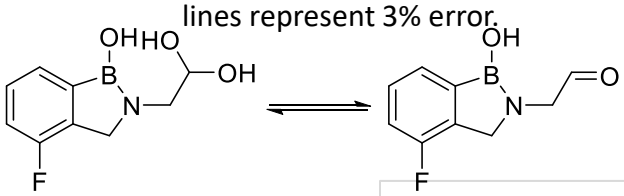

DE347

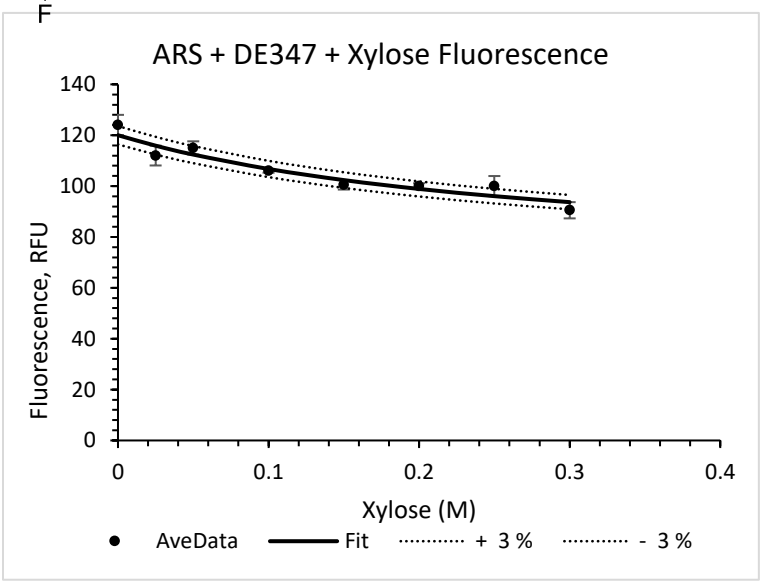

Plot of fluorescence changes of ARS-DE347 complex with increasing concentration of xylose. ARS (0.1 mM), DE347 (10 mM), xylose (0-0.1 M), HEPES buffer (100 mM, pH 7.4). (K_a was calculated to be 3.4 ± 0.65 M^{-1}). Value is the average of duplicate runs. Dotted lines represent 3% error.

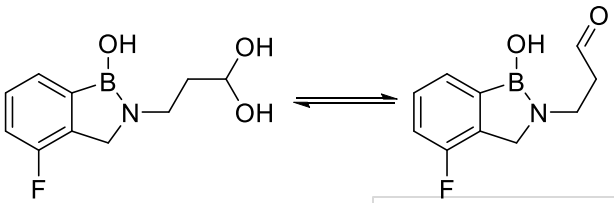

DE348

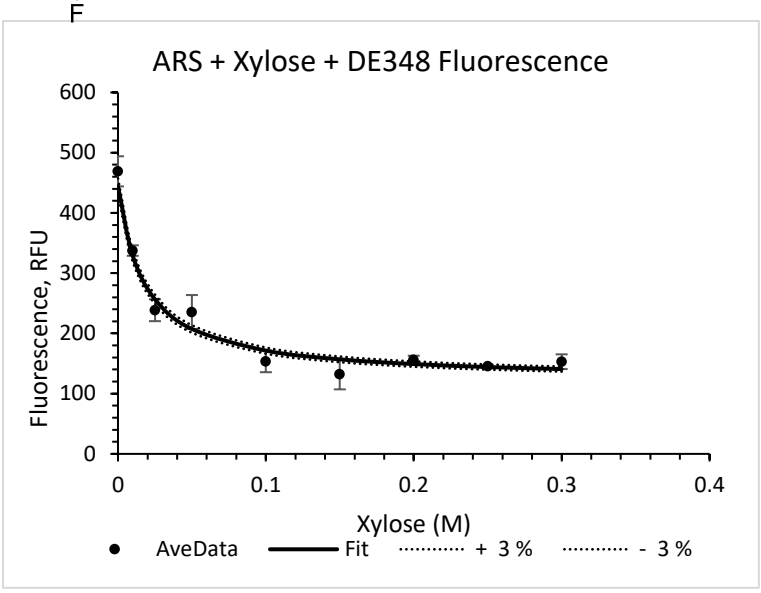

Plot of fluorescence changes of ARS-DE348 complex with increasing concentration of xylose. ARS (0.1 mM), DE348 (10 mM), xylose (0-0.1 M), HEPES buffer (100 mM, pH 7.4). (K_a was calculated to be 55.9 ± 14.1 M^{-1}). Value is the average of duplicate runs. Dotted lines represent 3% error.

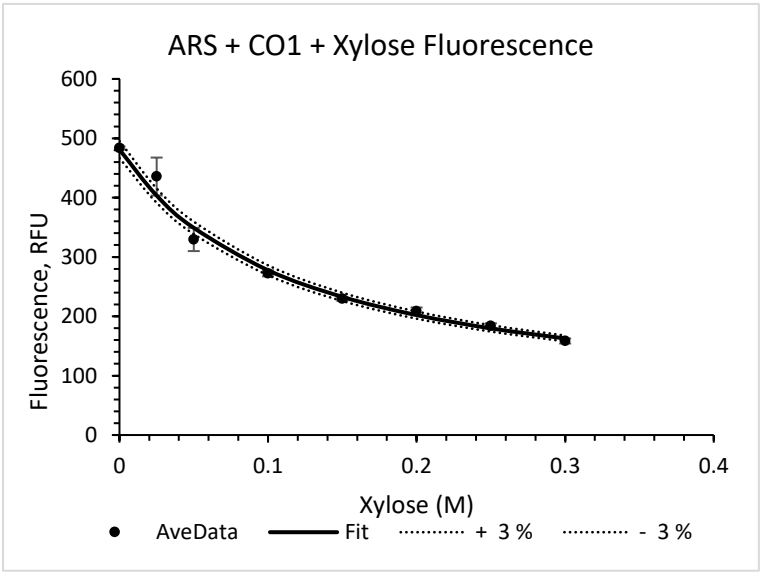

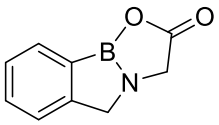

CO1

Plot of fluorescence changes of ARS-CO1 complex with increasing concentration of xylose. ARS (0.1 mM), CO1 (10 mM), xylose (0-0.1 M), HEPES buffer (100 mM, pH 7.4). (K_a was calculated to be 8.4 ± 4.2 M^{-1}). Value is the average of duplicate runs. Dotted lines represent 3% error.

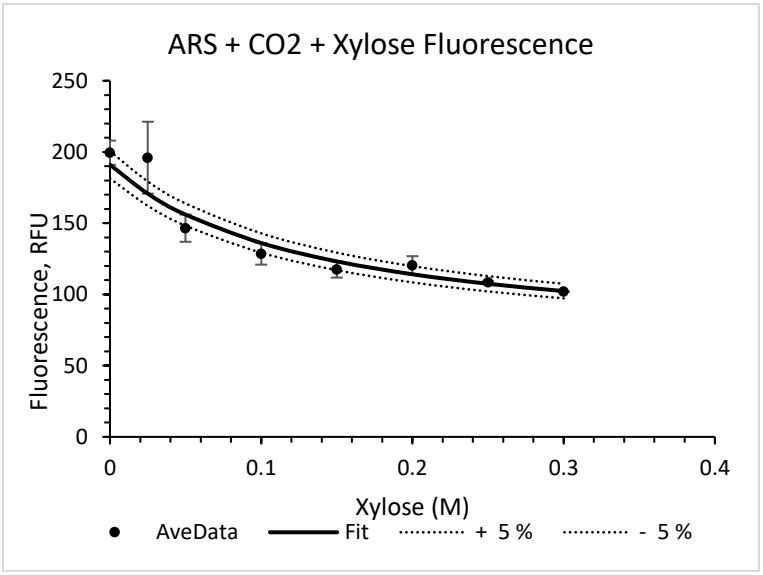

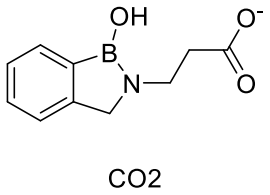

Plot of fluorescence changes of ARS-CO2 complex with increasing concentration of xylose. ARS (0.1 mM), CO2 (10 mM), xylose (0-0.1 M), HEPES buffer (100 mM, pH 7.4). (K_a was calculated to be 7.5 ± 5.7 M^{-1}). Value is the average of duplicate runs. Dotted lines represent 5% error.

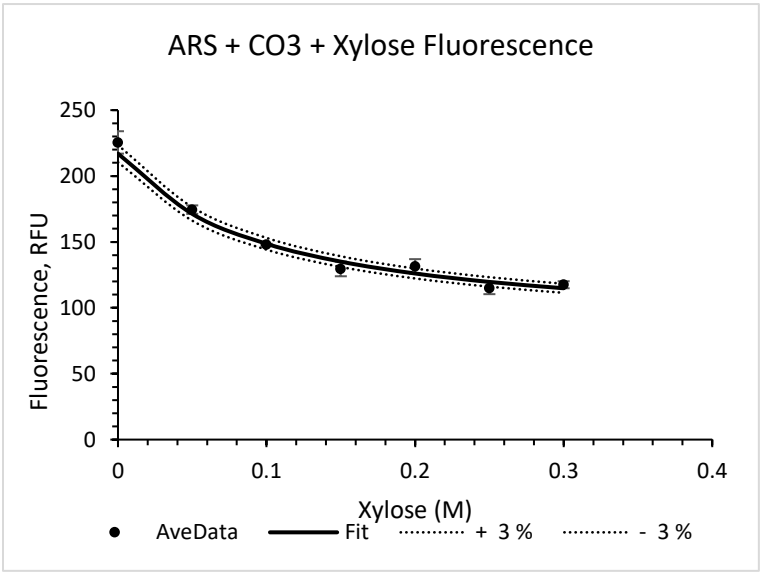

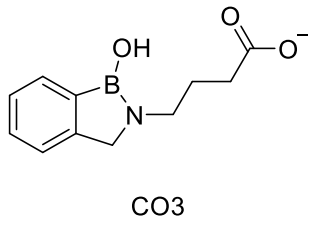

Plot of fluorescence changes of ARS-CO3 complex with increasing concentration of xylose. ARS (0.1 mM), CO3 (10 mM), xylose (0-0.1 M), HEPES buffer (100 mM, pH 7.4). (K_a was calculated to be 10.2 ± 1.1 M^{-1}). Value is the average of duplicate runs. Dotted lines represent 3% error.

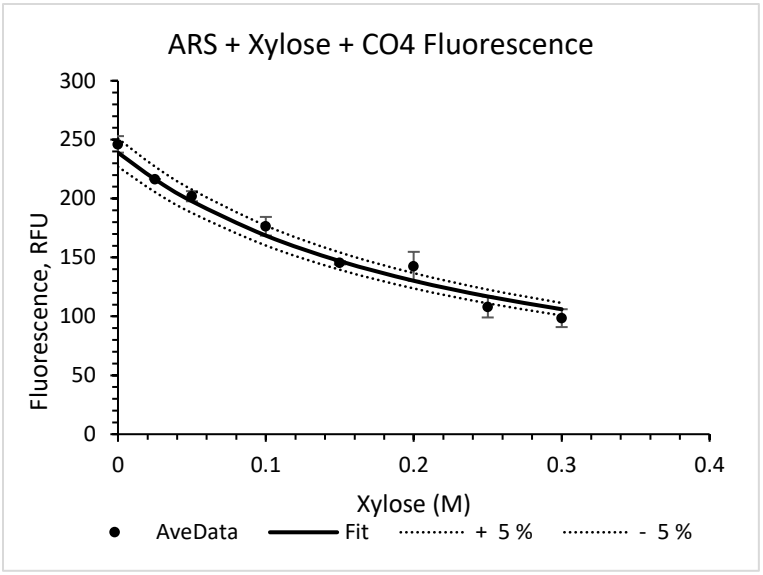

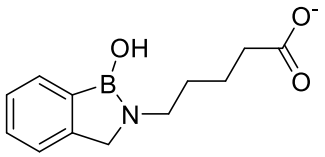

CO4

Plot of fluorescence changes of ARS-CO4 complex with increasing concentration of xylose. ARS (0.1 mM), CO4 (10 mM), xylose (0-0.1 M), HEPES buffer (100 mM, pH 7.4). (K_a was calculated to be 4.2 ± 3.1 M^{-1}). Value is the average of duplicate runs. Dotted lines represent 5% error.

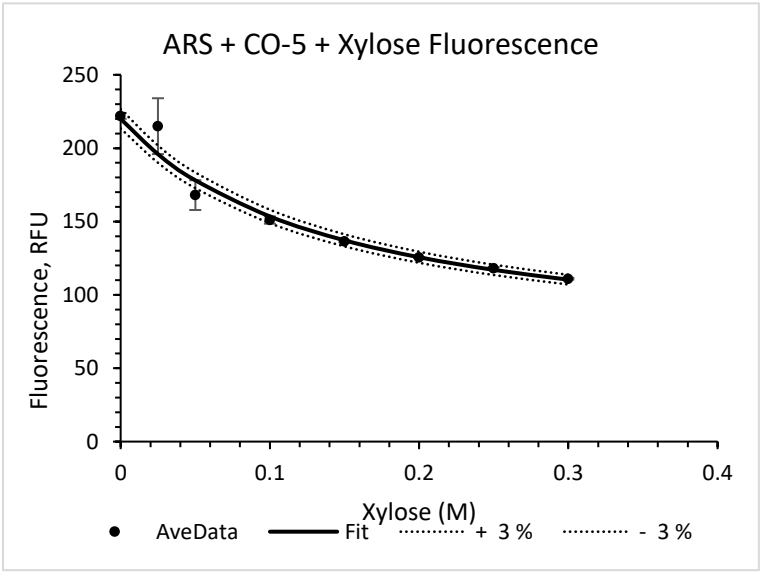

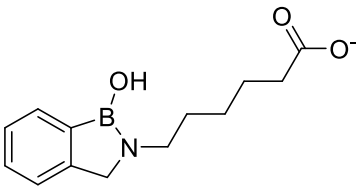

CO5

Plot of fluorescence changes of ARS-CO5 complex with increasing concentration of xylose. ARS (0.1 mM), CO5 (10 mM), xylose (0-0.1 M), HEPES buffer (100 mM, pH 7.4). (K_a was calculated to be 6.9 ± 2.5 M^{-1}). Value is the average of duplicate runs. Dotted lines represent 3% error.

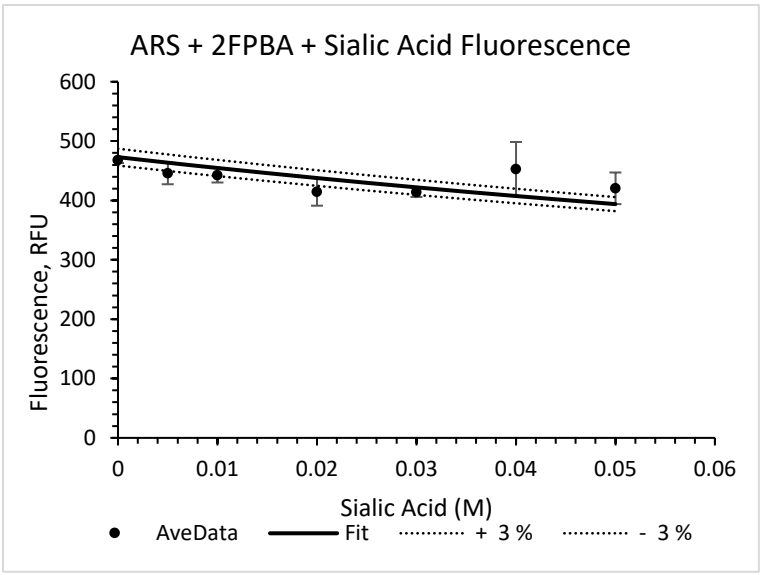

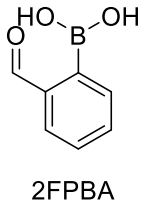

2FPBA

Plot of fluorescence changes of ARS-2FPBA complex with increasing concentration of sialic acid. ARS (0.1 mM), 2FPBA (10 mM), sialic acid (0-0.1 M), HEPES buffer (100 mM, pH 7.4). (K_a was calculated to be 4.0 ± 9.4 M^{-1}). Value is the average of duplicate runs. Dotted lines represent 3% error.

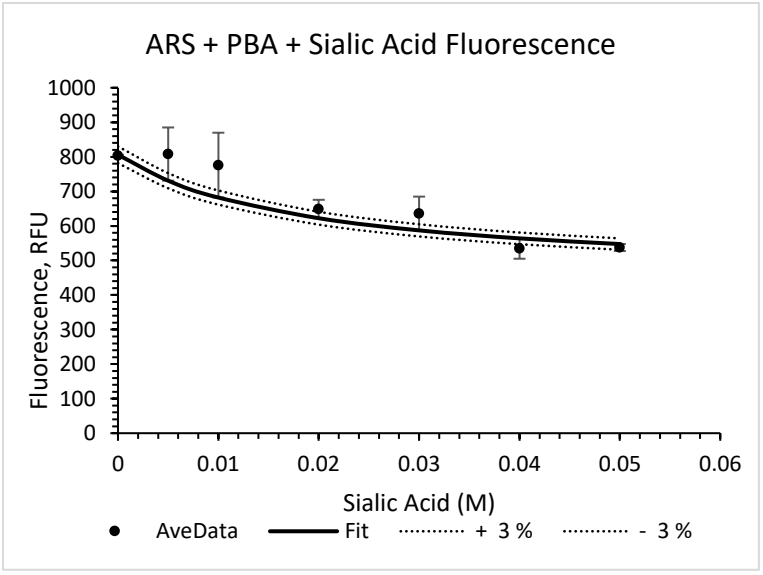

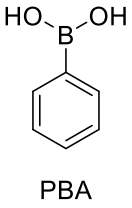

PBA

Plot of fluorescence changes of ARS-PBA complex with increasing concentration of sialic acid. ARS (0.1 mM), PBA (10 mM), sialic acid (0-0.1 M), HEPES buffer (100 mM, pH 7.4). (K_a was calculated to be 53.6 ± 27.9 M^{-1}). Value is the average of duplicate runs. Dotted lines represent 3% error.

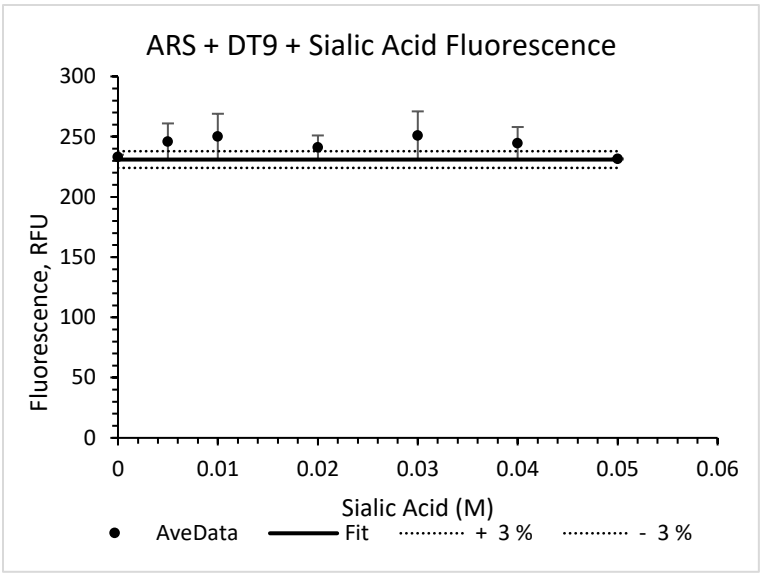

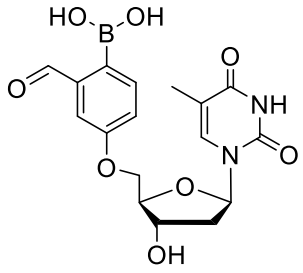

DT9

Plot of fluorescence changes of ARS-DT9 complex with increasing concentration of sialic acid. ARS (0.1 mM), DT9 (10 mM), sialic acid (0-0.1 M), HEPES buffer (100 mM, pH 7.4). (K_a was calculated to be 0.0 ± 5.5 M^{-1}). Value is the average of duplicate runs. Dotted lines represent 3% error.

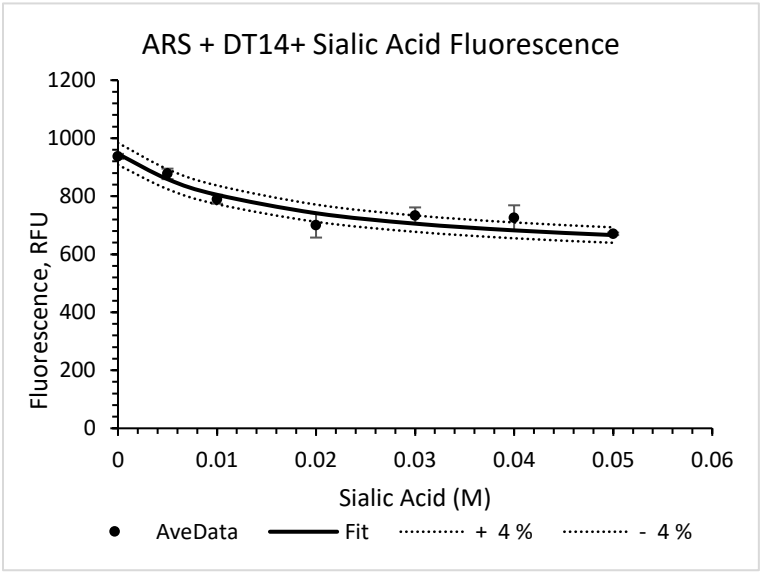

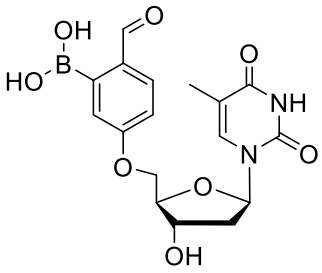

DT14

Plot of fluorescence changes of ARS-DT14 complex with increasing concentration of sialic acid. ARS (0.1 mM), DT14 (10 mM), sialic acid (0-0.1 M), HEPES buffer (100 mM, pH 7.4). (K_a was calculated to be 61.3 ± 7.0 M^{-1}). Value is the average of duplicate runs. Dotted lines represent 4% error.

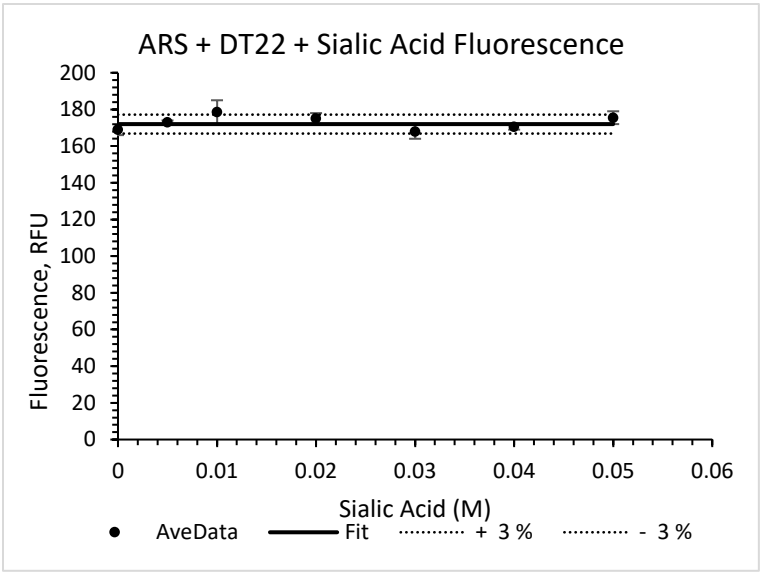

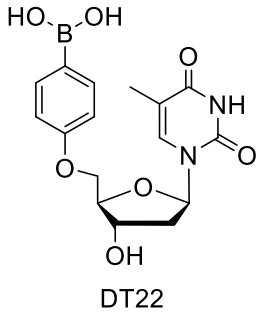

DT22

Plot of fluorescence changes of ARS-DT22 complex with increasing concentration of sialic acid. ARS (0.1 mM), DT22 (10 mM), sialic acid (0-0.1 M), HEPES buffer (100 mM, pH 7.4). (K_a was calculated to be 0.0 ± 0.53 M^{-1}). Value is the average of duplicate runs. Dotted lines represent 3% error.

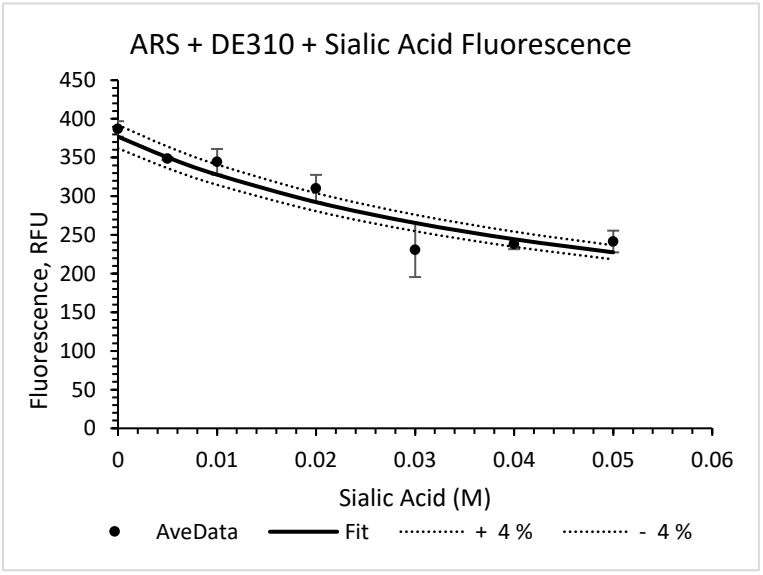

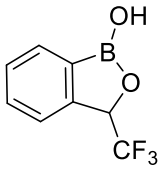

DE310

Plot of fluorescence changes of ARS-DE310 complex with increasing concentration of sialic acid. ARS (0.1 mM), DE310 (10 mM), sialic acid (0-0.1 M), HEPES buffer (100 mM, pH 7.4). (K_a was calculated to be 19.1 ± 7.8 M^{-1}). Value is the average of duplicate runs. Dotted lines represent 4% error.

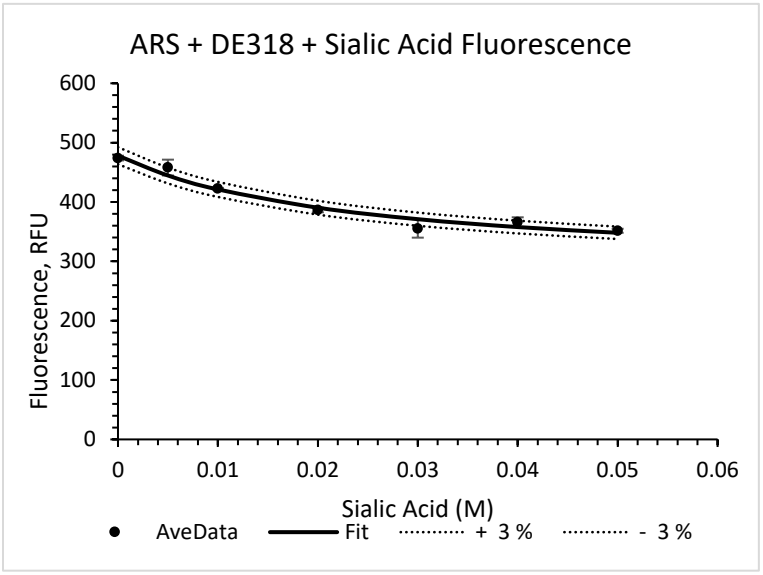

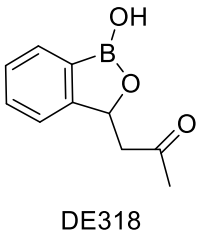

DE318

Plot of fluorescence changes of ARS-DE318 complex with increasing concentration of sialic acid. ARS (0.1 mM), DE318 (10 mM), sialic acid (0-0.1 M), HEPES buffer (100 mM, pH 7.4). (K_a was calculated to be 42.1 ± 1.4 M^{-1}). Value is the average of duplicate runs. Dotted lines represent 3% error.

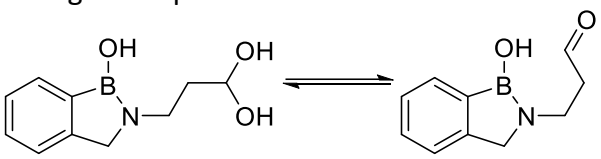

DE321

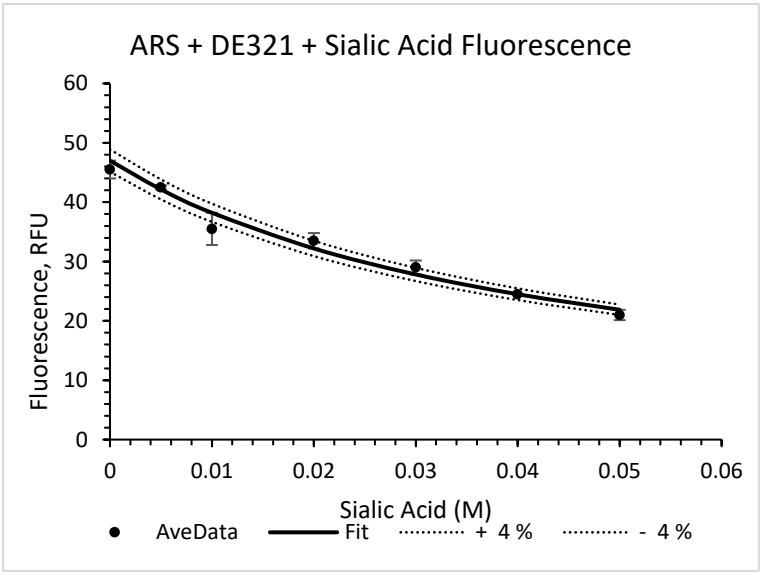

Plot of fluorescence changes of ARS-DE321 complex with increasing concentration of sialic acid. ARS (0.1 mM), DE321 (10 mM), sialic acid (0-0.1 M), HEPES buffer (100 mM, pH 7.4). (K_a was calculated to be 22.9 ± 0.38 M^{-1}). Value is the average of duplicate runs. Dotted lines represent 4% error.

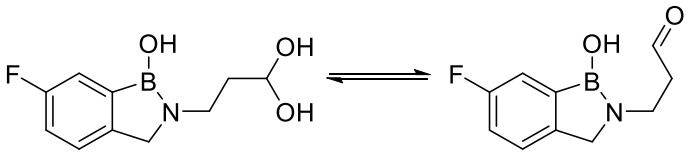

DE342

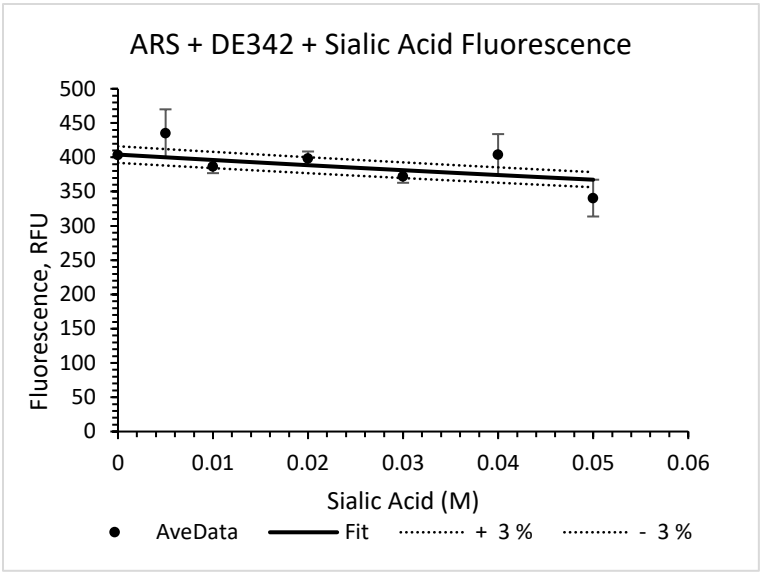

Plot of fluorescence changes of ARS-DE342 complex with increasing concentration of sialic acid. ARS (0.1 mM), DE342 (10 mM), sialic acid (0-0.1 M), HEPES buffer (100 mM, pH 7.4). (K_a was calculated to be 1.9 ± 8.1 M^{-1}). Value is the average of duplicate runs. Dotted lines represent 3% error.

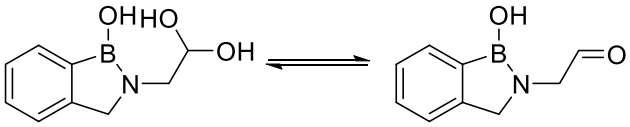

DE343

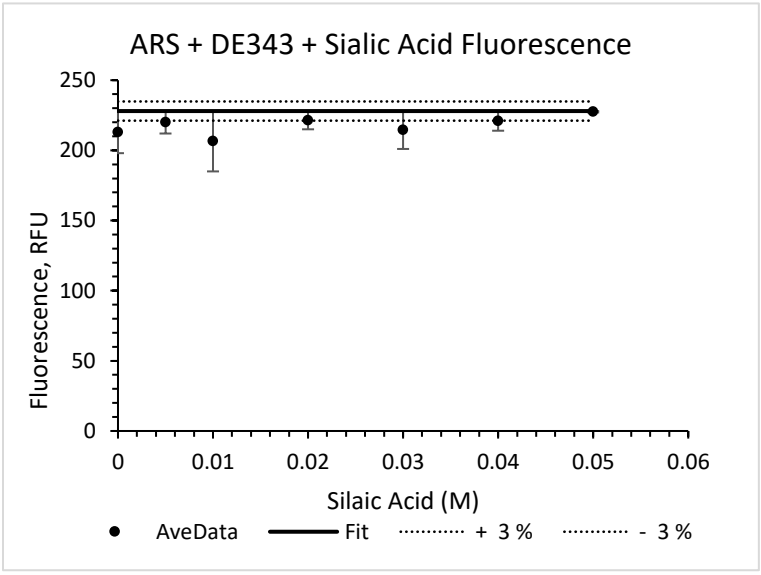

Plot of fluorescence changes of ARS-DE343 complex with increasing concentration of sialic acid. ARS (0.1 mM), DE343 (10 mM), sialic acid (0-0.1 M), HEPES buffer (100 mM, pH 7.4). (K_a was calculated to be 0.0 ± 4.5 M^{-1}). Value is the average of duplicate runs. Dotted lines represent 3% error.

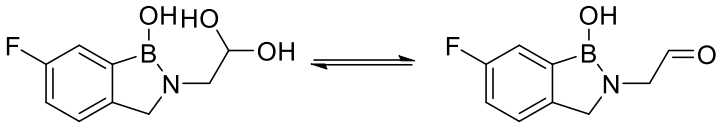

DE344

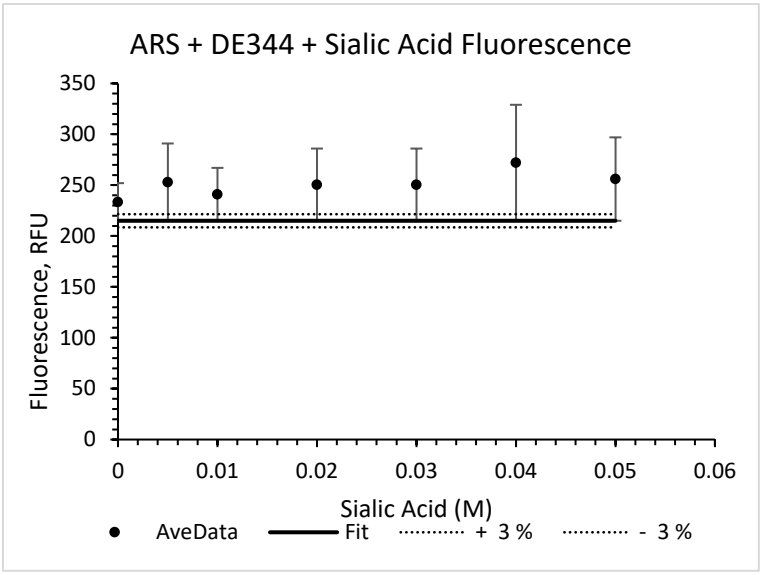

Plot of fluorescence changes of ARS-DE344 complex with increasing concentration of sialic acid. ARS (0.1 mM), DE344 (10 mM), sialic acid (0-0.1 M), HEPES buffer (100 mM, pH 7.4). (K_a was calculated to be 0.0 ± 46.2 M^{-1}). Value is the average of duplicate runs. Dotted lines represent 3% error.

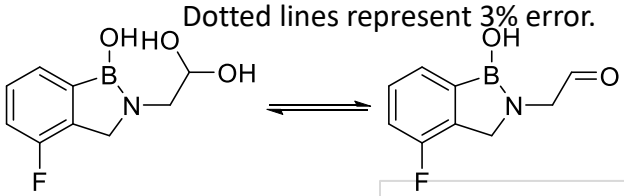

DE347

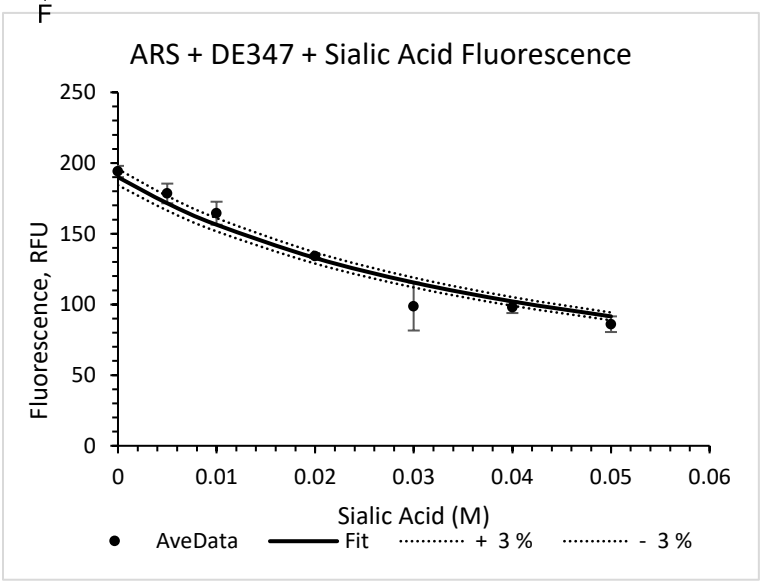

Plot of fluorescence changes of ARS-DE347 complex with increasing concentration of sialic acid. ARS (0.1 mM), DE347 (10 mM), sialic acid (0-0.1 M), HEPES buffer (100 mM, pH 7.4). (K_a was calculated to be 21.5 ± 3.8 M^{-1}). Value is the average of duplicate runs. Dotted lines represent 3% error.

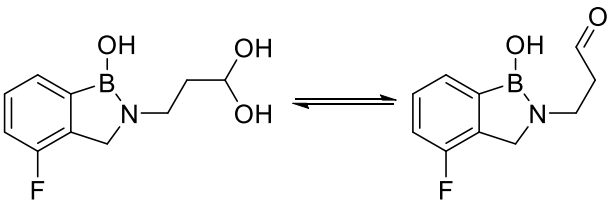

DE348

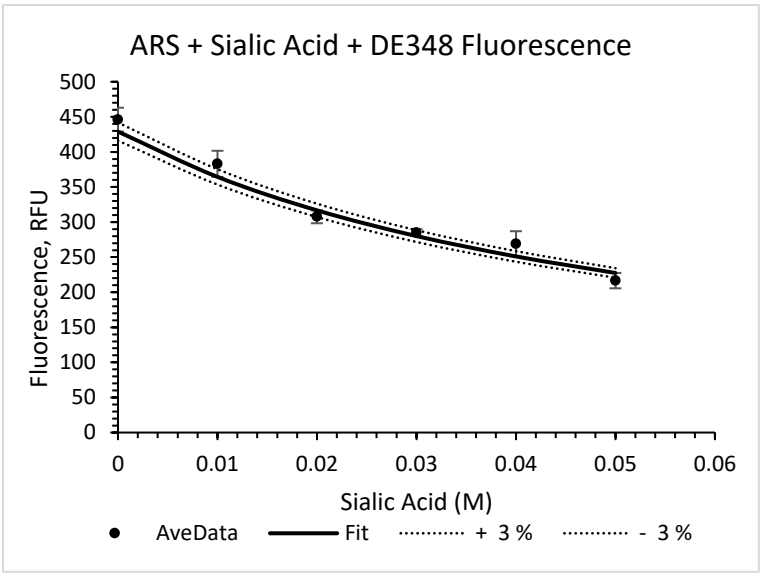

Plot of fluorescence changes of ARS-DE348 complex with increasing concentration of sialic acid. ARS (0.1 mM), DE348 (10 mM), sialic acid (0-0.1 M), HEPES buffer (100 mM, pH 7.4). (K_a was calculated to be 17.7 ± 3.8 M^{-1}). Value is the average of duplicate runs. Dotted lines represent 3% error.

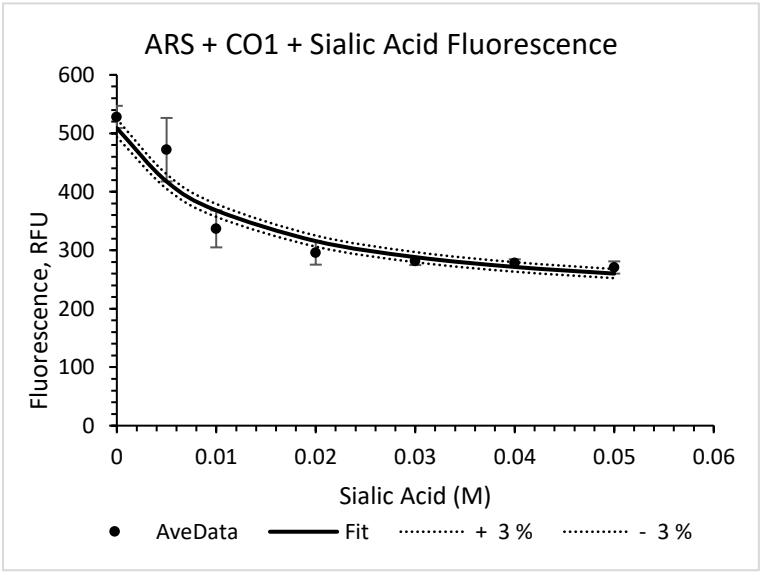

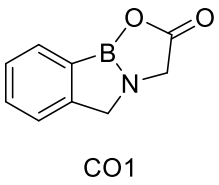

CO1

Plot of fluorescence changes of ARS-CO1 complex with increasing concentration of sialic acid. ARS (0.1 mM), CO1 (10 mM), sialic acid (0-0.1 M), HEPES buffer (100 mM, pH 7.4). (K_a was calculated to be 84.3 ± 12.5 M^{-1}). Value is the average of duplicate runs. Dotted lines represent 3% error.

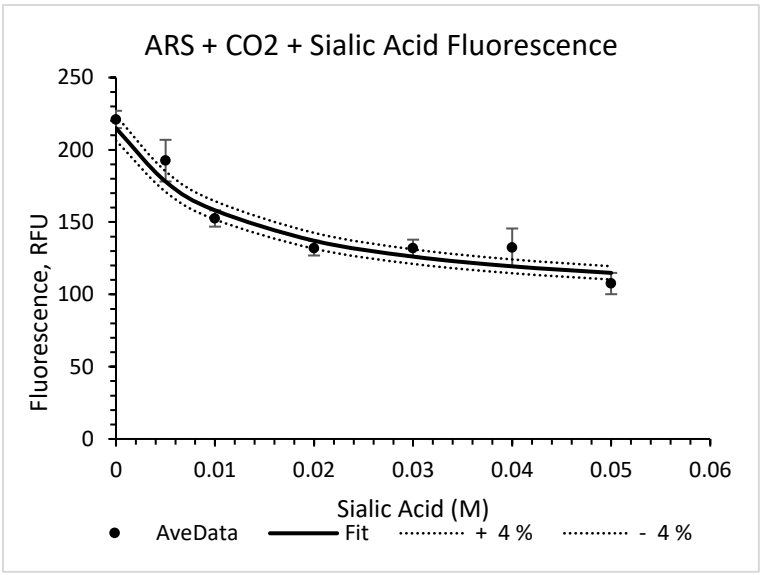

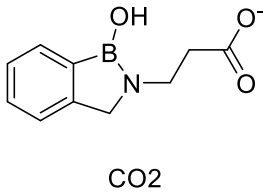

CO2

Plot of fluorescence changes of ARS-CO2 complex with increasing concentration of sialic acid. ARS (0.1 mM), CO2 (10 mM), sialic acid (0-0.1 M), HEPES buffer (100 mM, pH 7.4). (K_a was calculated to be 85.1 ± 3.9 M^{-1}). Value is the average of duplicate runs. Dotted lines represent 4% error.

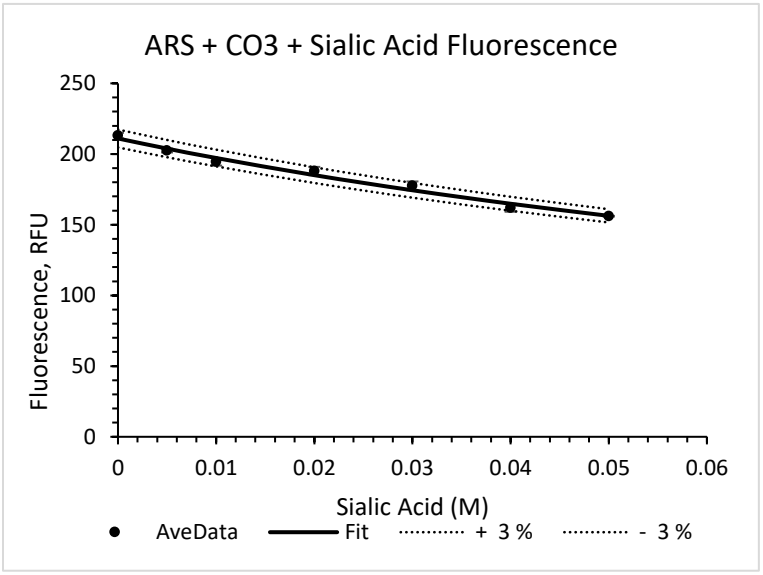

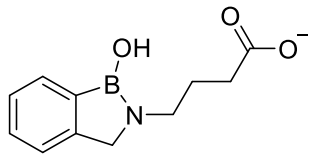

CO3

Plot of fluorescence changes of ARS-CO3 complex with increasing concentration of sialic acid. ARS (0.1 mM), CO3 (10 mM), sialic acid (0-0.1 M), HEPES buffer (100 mM, pH 7.4). (K_a was calculated to be 7.0 ± 0.22 M^{-1}). Value is the average of duplicate runs. Dotted lines represent 3% error.

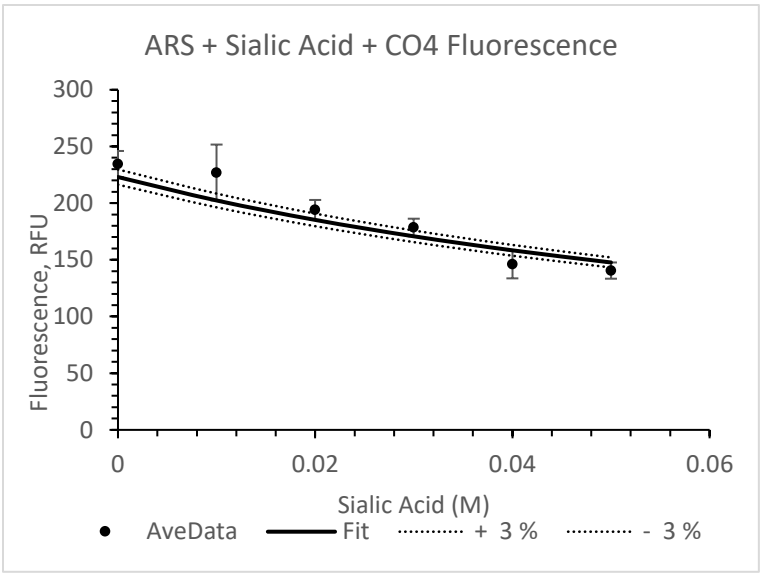

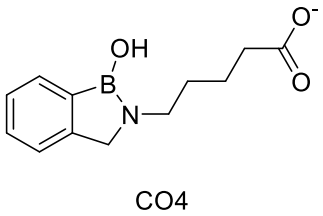

CO4

Plot of fluorescence changes of ARS-CO4 complex with increasing concentration of sialic acid. ARS (0.1 mM), CO4 (10 mM), sialic acid (0-0.1 M), HEPES buffer (100 mM, pH 7.4). (K_a was calculated to be 10.2 ± 5.7 M^{-1}). Value is the average of duplicate runs. Dotted lines represent 3% error.

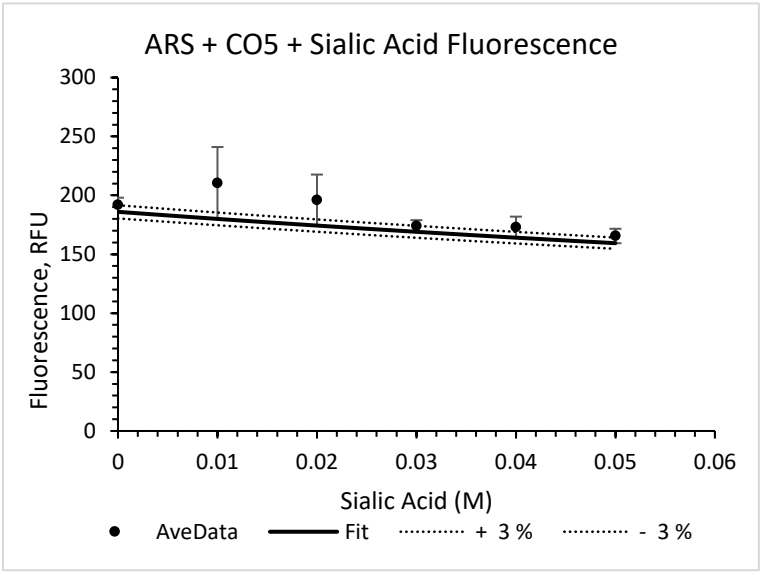

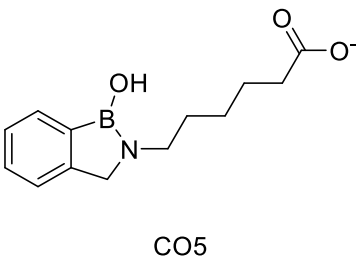

CO5

Plot of fluorescence changes of ARS-CO5 complex with increasing concentration of sialic acid. ARS (0.1 mM), CO5 (10 mM), sialic acid (0-0.1 M), HEPES buffer (100 mM, pH 7.4). (K_a was calculated to be 3.3 ± 8.9 M^{-1}). Value is the average of duplicate runs. Dotted lines represent 3% error.

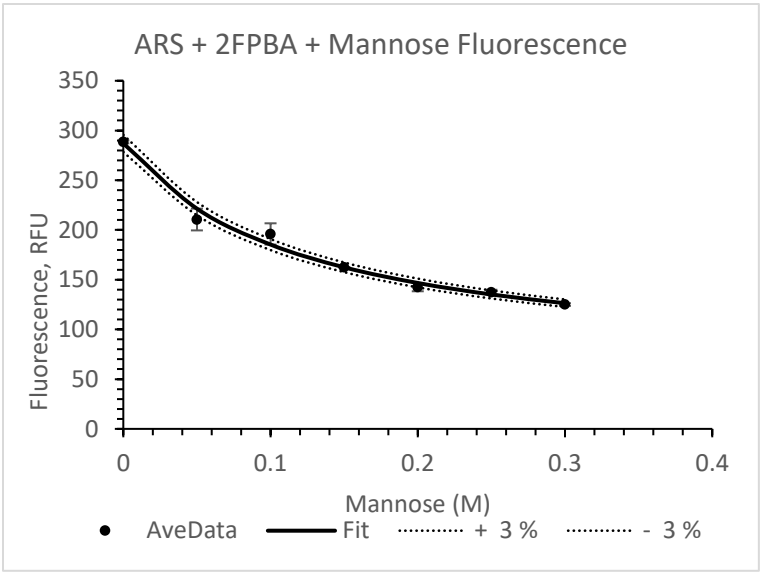

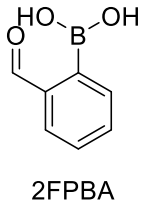

2FPBA

Plot of fluorescence changes of ARS-2FPBA complex with increasing concentration of mannose. ARS (0.1 mM), 2FPBA (10 mM), mannose (0-0.1 M), HEPES buffer (100 mM, pH 7.4). (K_a was calculated to be 8.1 ± 1.3 M^{-1}). Value is the average of duplicate runs. Dotted lines represent 3% error.

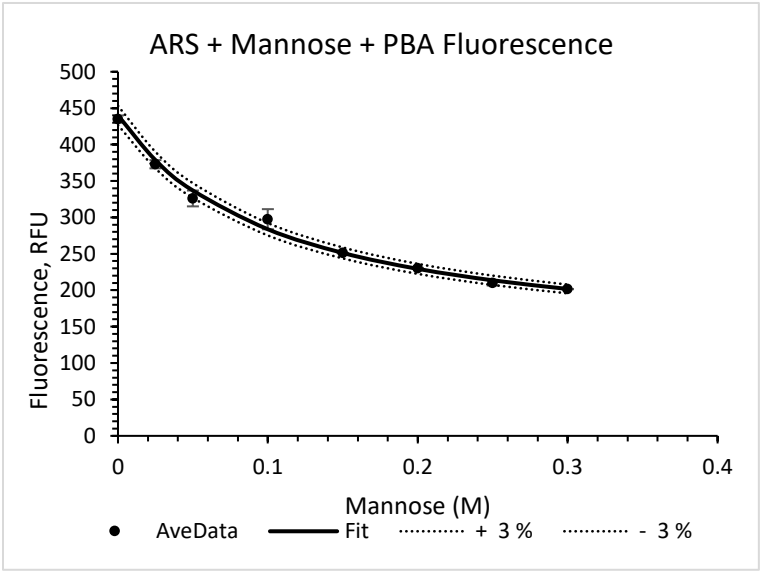

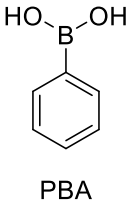

PBA

Plot of fluorescence changes of ARS-PBA complex with increasing concentration of mannose. ARS (0.1 mM), PBA (10 mM), mannose (0-0.1 M), HEPES buffer (100 mM, pH 7.4). (K_a was calculated to be 9.4 ± 1.2 M^{-1}). Value is the average of duplicate runs. Dotted lines represent 3% error.

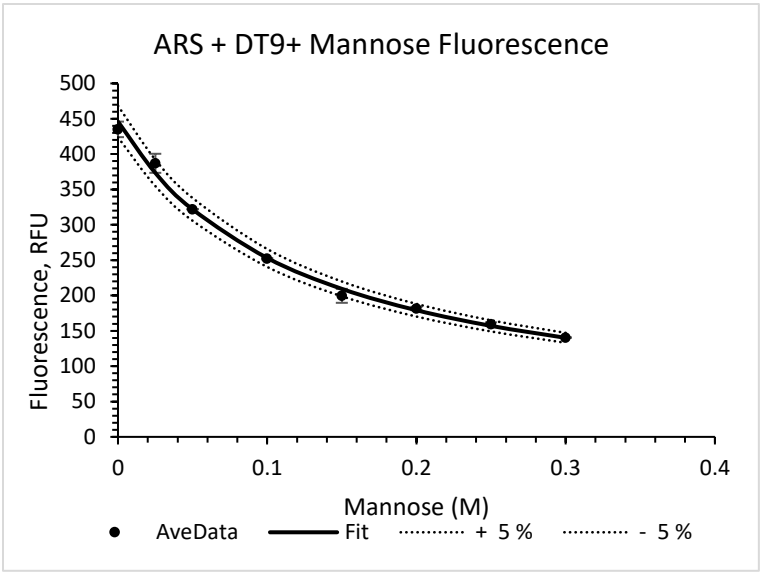

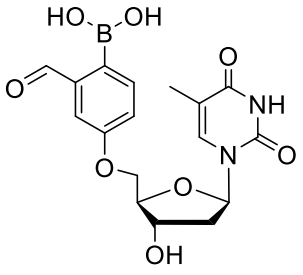

DT9

Plot of fluorescence changes of ARS-DT9 complex with increasing concentration of mannose. ARS (0.1 mM), DT9 (10 mM), mannose (0-0.1 M), HEPES buffer (100 mM, pH 7.4). (K_a was calculated to be 8.1 ± 1.3 M^{-1}). Value is the average of duplicate runs. Dotted lines represent 5% error.

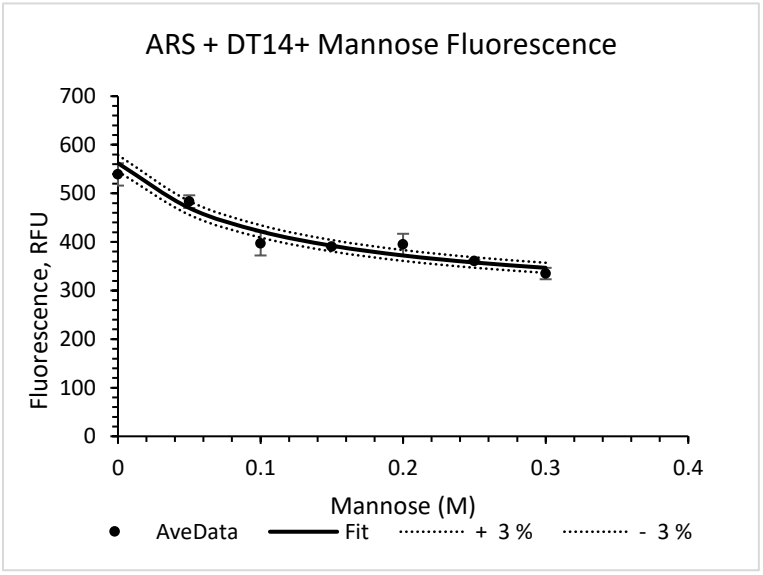

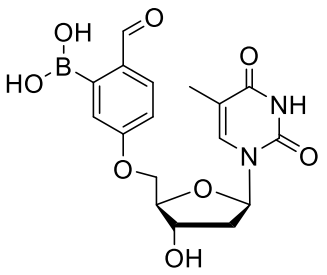

DT14

Plot of fluorescence changes of ARS-DT14 complex with increasing concentration of mannose. ARS (0.1 mM), DT14 (10 mM), mannose (0-0.1 M), HEPES buffer (100 mM, pH 7.4). (K_a was calculated to be 9.1 ± 4.5 M^{-1}). Value is the average of duplicate runs. Dotted lines represent 3% error.

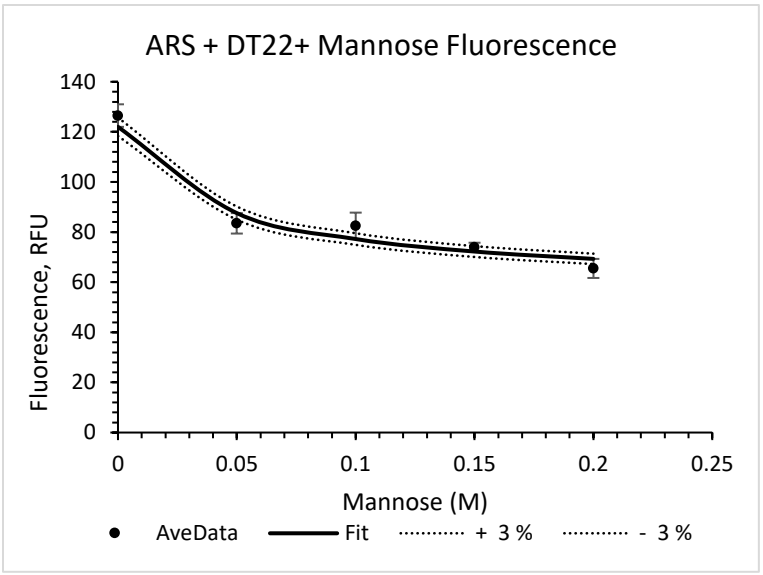

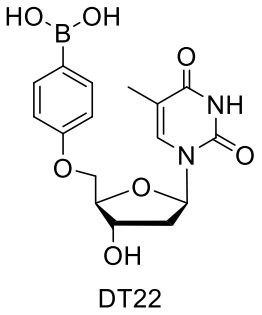

DT22

Plot of fluorescence changes of ARS-DT22 complex with increasing concentration of mannose. ARS (0.1 mM), DT22 (10 mM), mannose (0-0.1 M), HEPES buffer (100 mM, pH 7.4). (K_a was calculated to be 23.2 ± 0.97 M^{-1}). Value is the average of duplicate runs. Dotted lines represent 3% error.

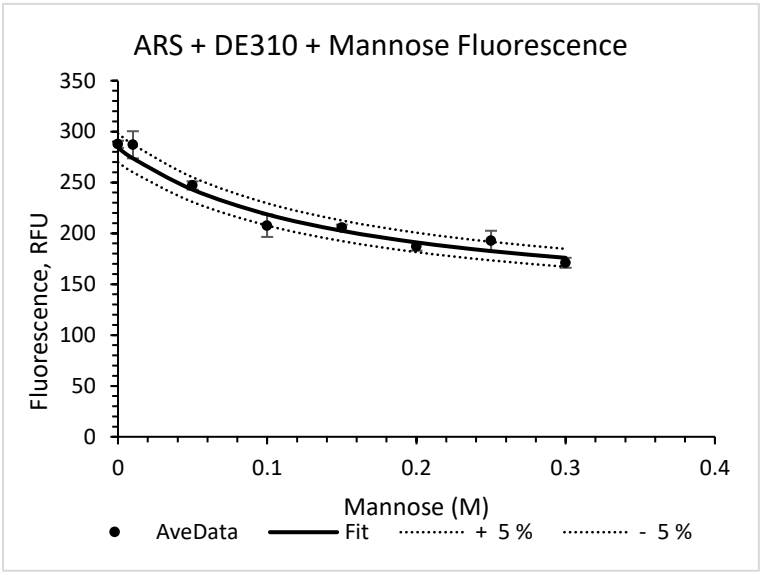

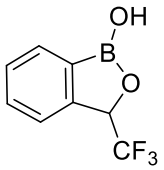

DE310

Plot of fluorescence changes of ARS-DE310 complex with increasing concentration of mannose. ARS (0.1 mM), DE310 (10 mM), mannose (0-0.1 M), HEPES buffer (100 mM, pH 7.4). (K_a was calculated to be 6.8 ± 2.1 M^{-1}). Value is the average of duplicate runs. Dotted lines represent 5% error.

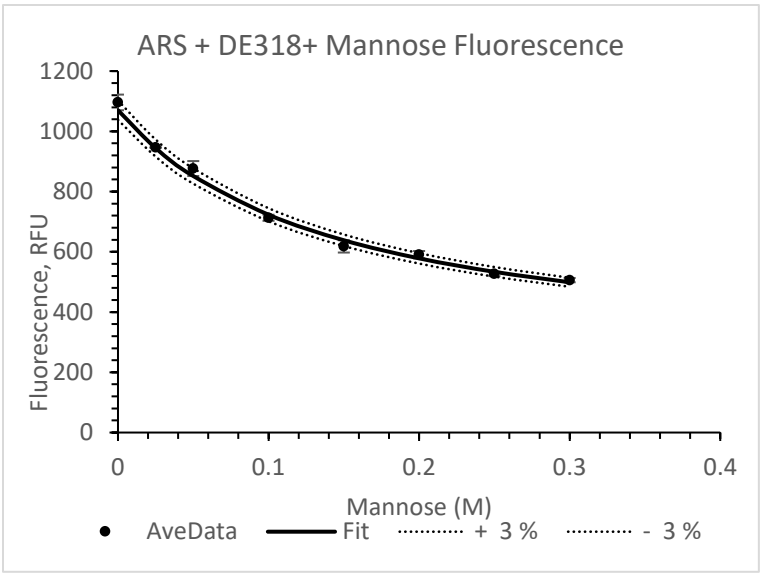

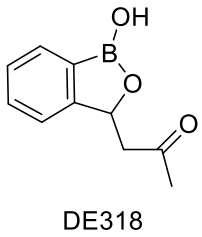

DE318

Plot of fluorescence changes of ARS-DE318 complex with increasing concentration of mannose. ARS (0.1 mM), DE318 (10 mM), mannose (0-0.1 M), HEPES buffer (100 mM, pH 7.4). (K_a was calculated to be 6.9 ± 1.6 M^{-1}). Value is the average of duplicate runs. Dotted lines represent 3% error.

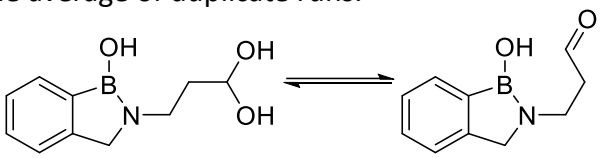

DE321

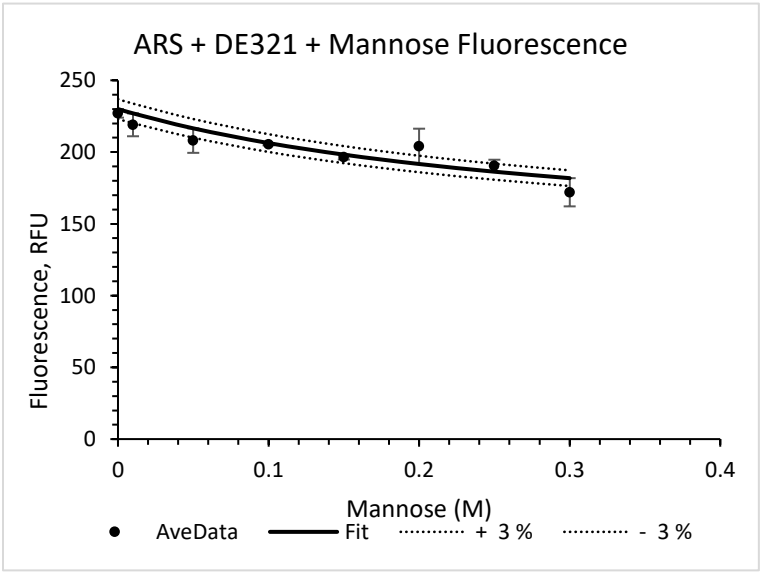

Plot of fluorescence changes of ARS-DE321 complex with increasing concentration of mannose. ARS (0.1 mM), DE321 (10 mM), mannose (0-0.1 M), HEPES buffer (100 mM, pH 7.4). (K_a was calculated to be 3.1 ± 2.1 M^{-1}). Value is the average of duplicate runs. Dotted lines represent 3% error.

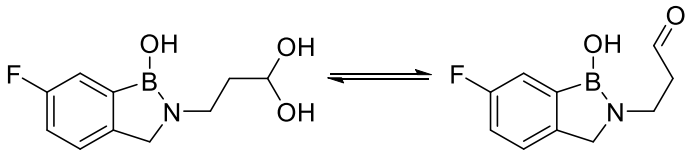

DE342

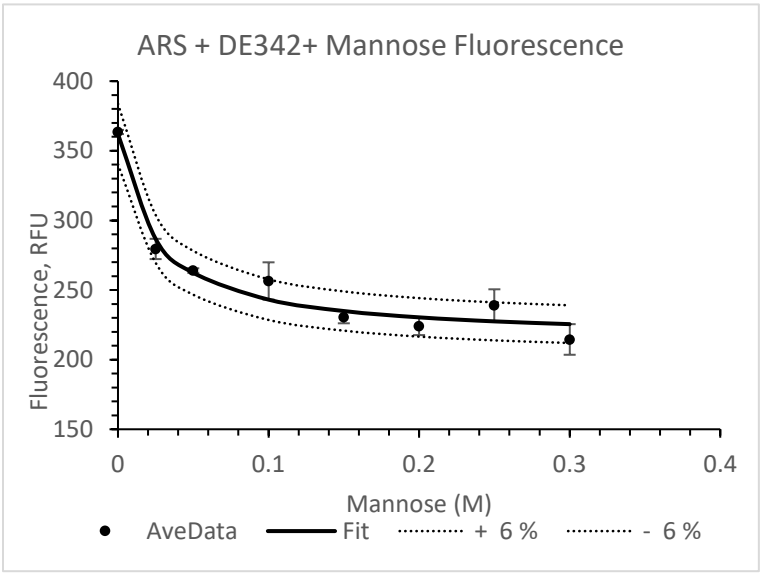

Plot of fluorescence changes of ARS-DE342 complex with increasing concentration of mannose. ARS (0.1 mM), DE342 (10 mM), mannose (0-0.1 M), HEPES buffer (100 mM, pH 7.4). (K_a was calculated to be 41.6 ± 2.3 M^{-1}). Value is the average of duplicate runs. Dotted lines represent 6% error.

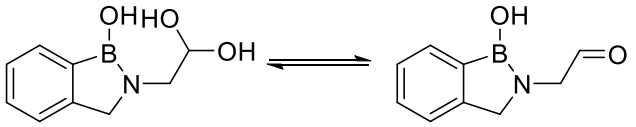

DE343

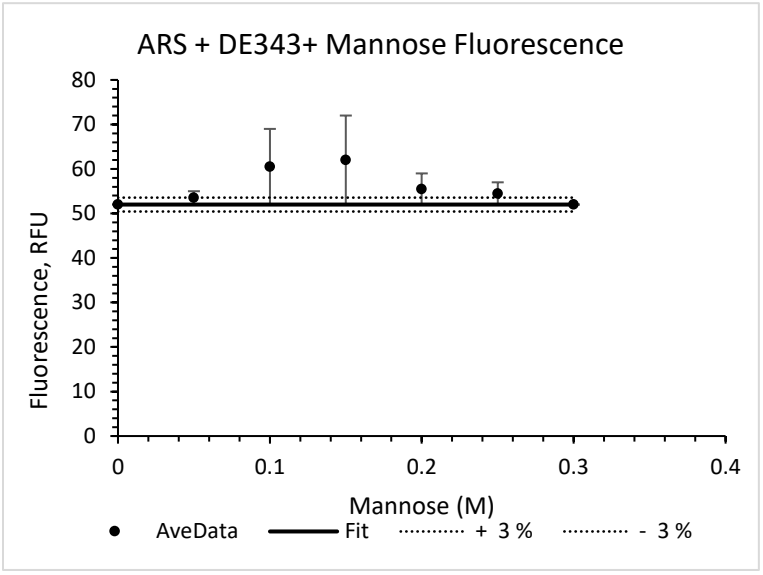

Plot of fluorescence changes of ARS-DE343 complex with increasing concentration of mannose. ARS (0.1 mM), DE343 (10 mM), mannose (0-0.1 M), HEPES buffer (100 mM, pH 7.4). (K_a was calculated to be 0.0 ± 3.7 M^{-1}). Value is the average of duplicate runs. Dotted lines represent 3% error.

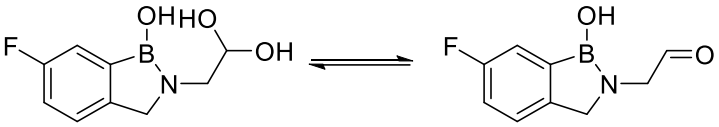

DE344

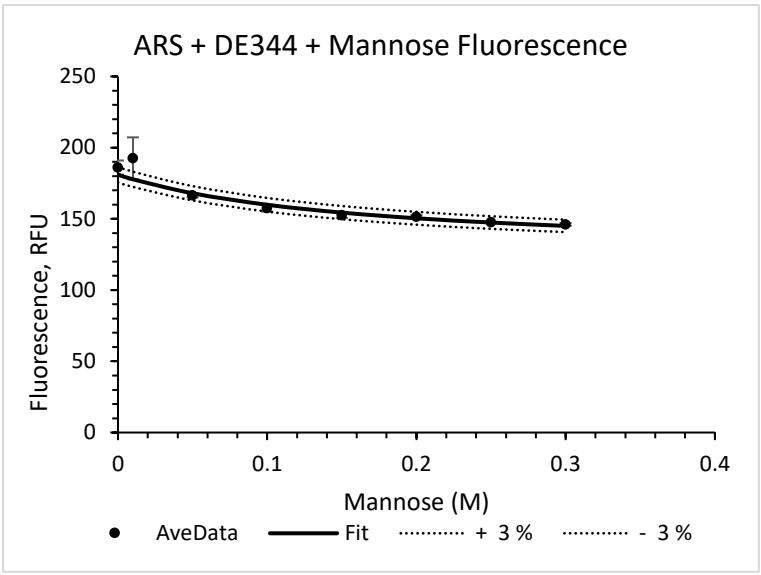

Plot of fluorescence changes of ARS-DE344 complex with increasing concentration of mannose. ARS (0.1 mM), DE344 (10 mM), mannose (0-0.1 M), HEPES buffer (100 mM, pH 7.4). (K_a was calculated to be 6.1 ± 1.4 M^{-1}). Value is the average of duplicate runs. Dotted lines represent 3% error.

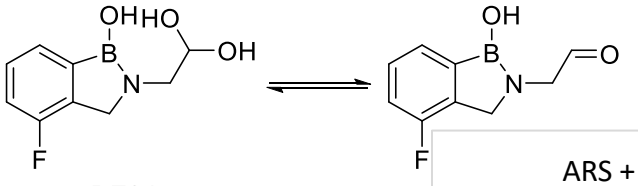

DE347

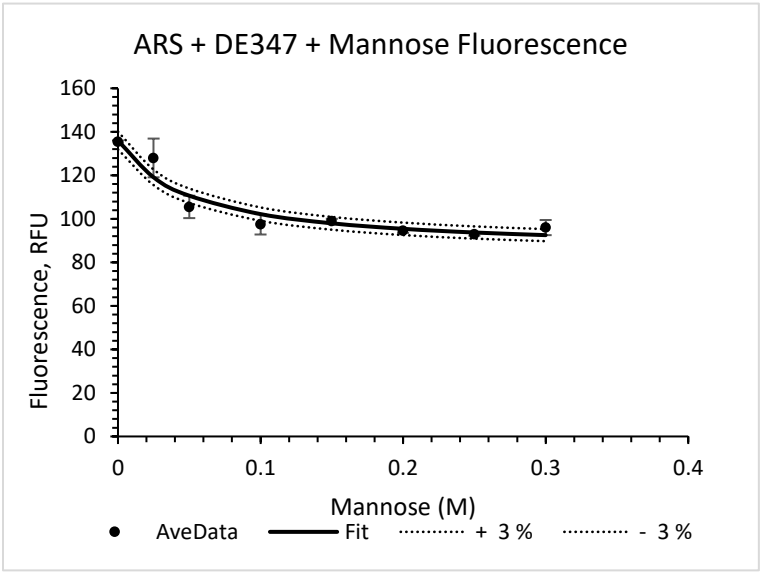

Plot of fluorescence changes of ARS-DE347 complex with increasing concentration of mannose. ARS (0.1 mM), DE347 (10 mM), mannose (0-0.1 M), HEPES buffer (100 mM, pH 7.4). (K_a was calculated to be 19.9 ± 1.3 M^{-1}). Value is the average of duplicate runs. Dotted lines represent 3% error.

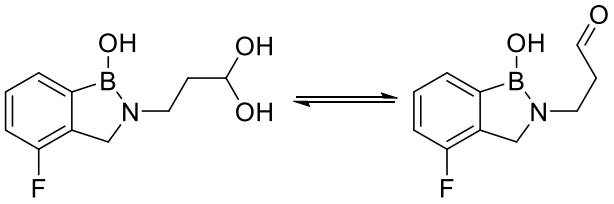

DE348

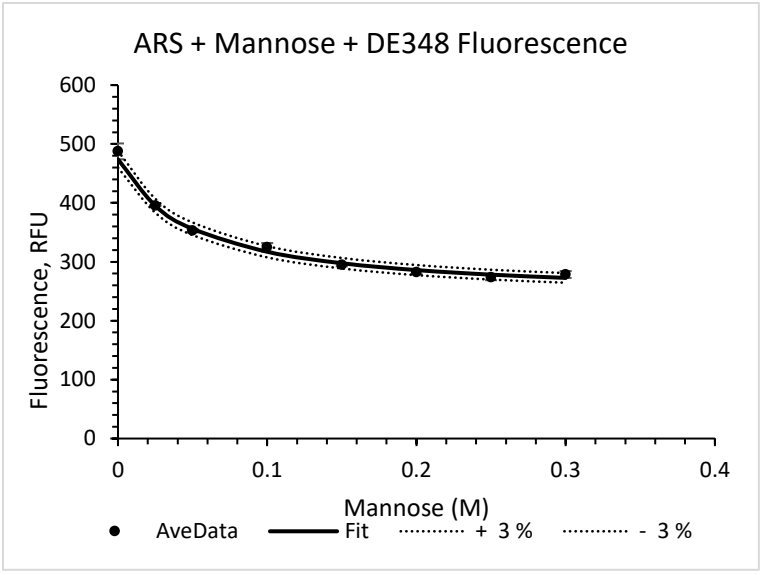

Plot of fluorescence changes of ARS-DE348 complex with increasing concentration of mannose. ARS (0.1 mM), DE348 (10 mM), mannose (0-0.1 M), HEPES buffer (100 mM, pH 7.4). (K_a was calculated to be 20.2 ± 0.85 M^{-1}). Value is the average of duplicate runs. Dotted lines represent 3% error.

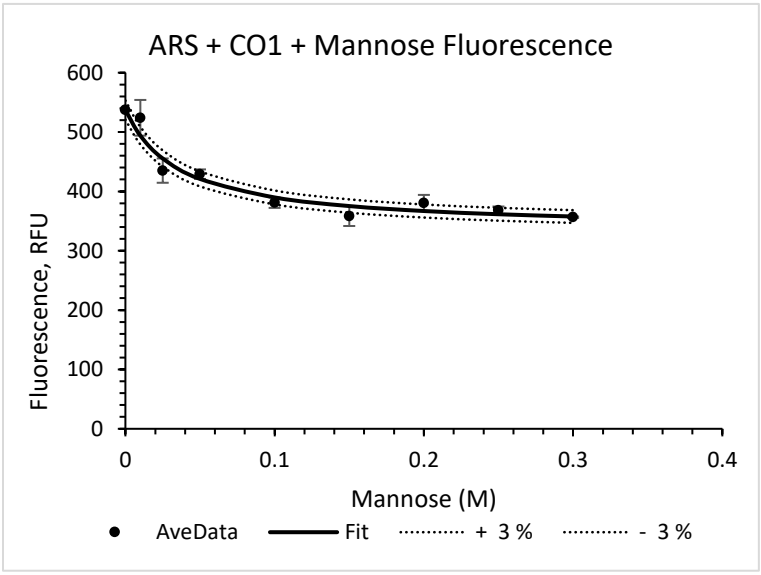

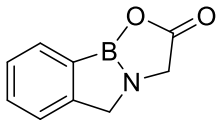

CO1

Plot of fluorescence changes of ARS-CO1 complex with increasing concentration of mannose. ARS (0.1 mM), CO1 (10 mM), mannose (0-0.1 M), HEPES buffer (100 mM, pH 7.4). (K_a was calculated to be 27.2 ± 4.5 M^{-1}). Value is the average of duplicate runs. Dotted lines represent 3% error.

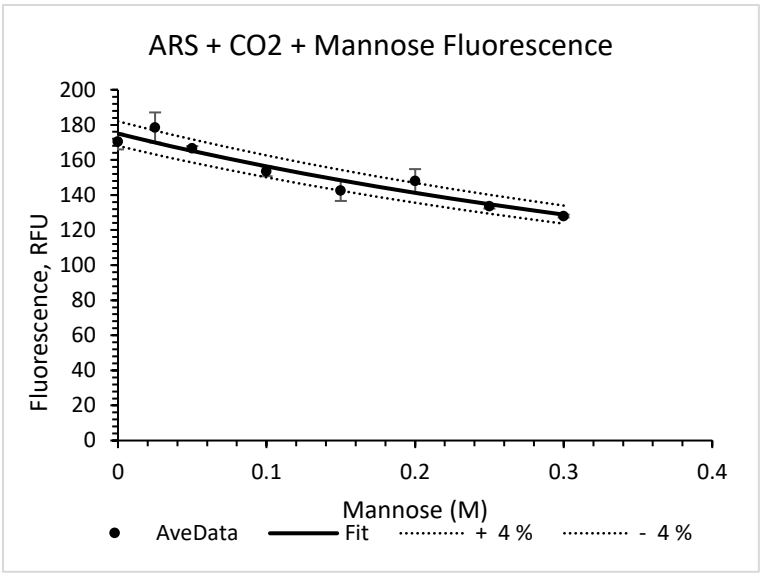

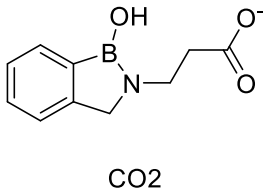

Plot of fluorescence changes of ARS-CO2 complex with increasing concentration of mannose. ARS (0.1 mM), CO2 (10 mM), mannose (0-0.1 M), HEPES buffer (100 mM, pH 7.4). (K_a was calculated to be 1.2 ± 1.2 M^{-1}). Value is the average of duplicate runs. Dotted lines represent 4% error.

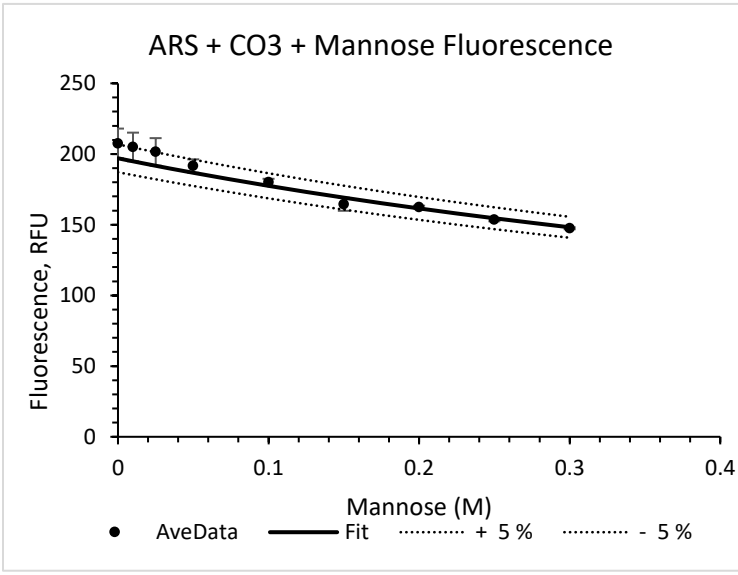

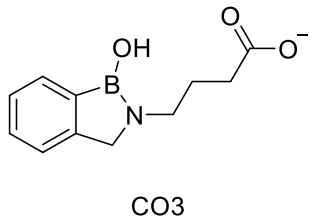

Plot of fluorescence changes of ARS-CO3 complex with increasing concentration of mannose. ARS (0.1 mM), CO3 (10 mM), mannose (0-0.1 M), HEPES buffer (100 mM, pH 7.4). (K_a was calculated to be 1.1 ± 1.8 M^{-1}). Value is the average of duplicate runs. Dotted lines represent 5% error.

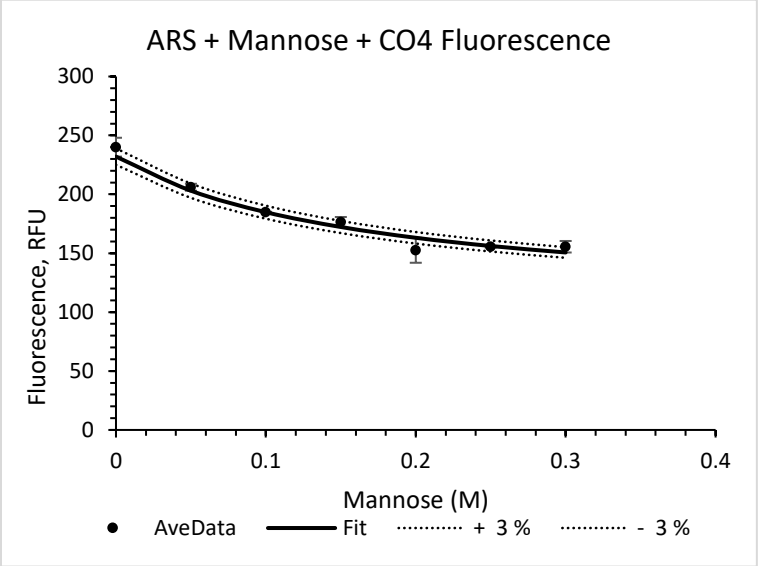

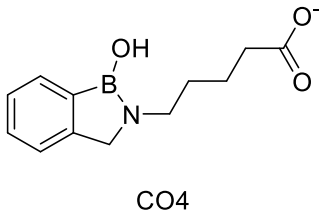

CO4

Plot of fluorescence changes of ARS-CO4 complex with increasing concentration of mannose. ARS (0.1 mM), CO4 (10 mM), mannose (0-0.1 M), HEPES buffer (100 mM, pH 7.4). (K_a was calculated to be 5.8 ± 1.3 M^{-1}). Value is the average of duplicate runs. Dotted lines represent 3% error.

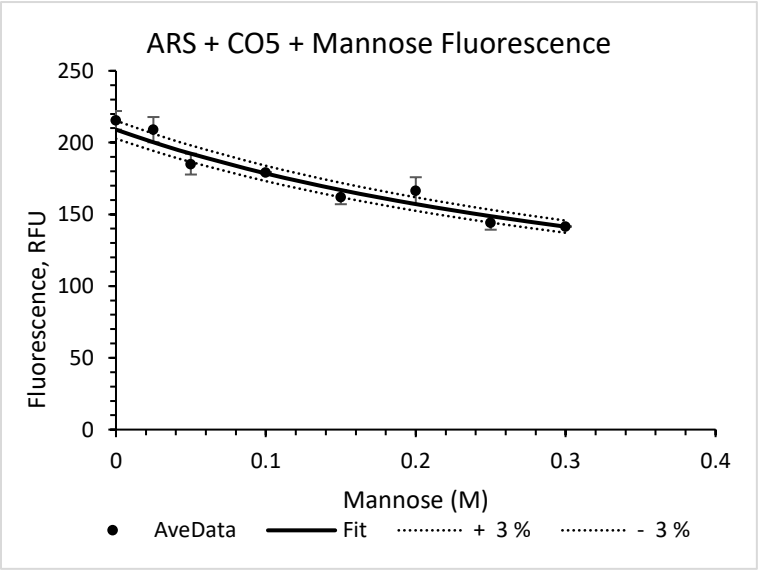

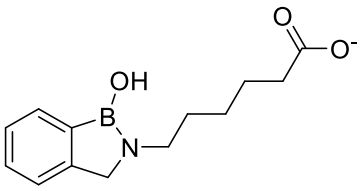

CO5

Plot of fluorescence changes of ARS-CO5 complex with increasing concentration of mannose. ARS (0.1 mM), CO5 (10 mM), mannose (0-0.1 M), HEPES buffer (100 mM, pH 7.4). (K_a was calculated to be 2.1 ± 1.7 M^{-1}). Value is the average of duplicate runs. Dotted lines represent 3% error.

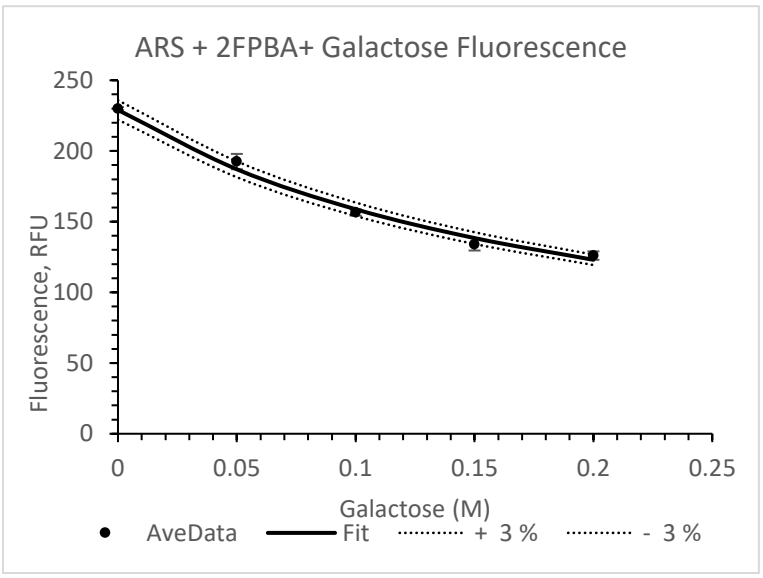

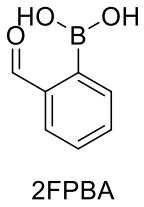

2FPBA

Plot of fluorescence changes of ARS-2FPBA complex with increasing concentration of galactose. ARS (0.1 mM), 2FPBA (10 mM), galactose (0-0.1 M), HEPES buffer (100 mM, pH 7.4). (K_a was calculated to be 4.8 ± 0.41 M^{-1}). Value is the average of duplicate runs. Dotted lines represent 3% error.

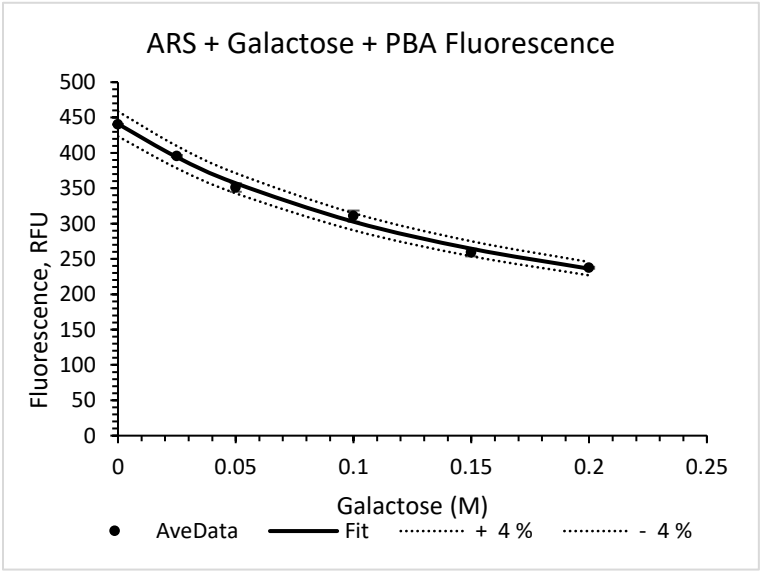

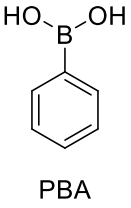

PBA

Plot of fluorescence changes of ARS-PBA complex with increasing concentration of galactose. ARS (0.1 mM), PBA (10 mM), galactose (0-0.1 M), HEPES buffer (100 mM, pH 7.4). (K_a was calculated to be 5.4 ± 0.43 M^{-1}). Value is the average of duplicate runs. Dotted lines represent 4% error.

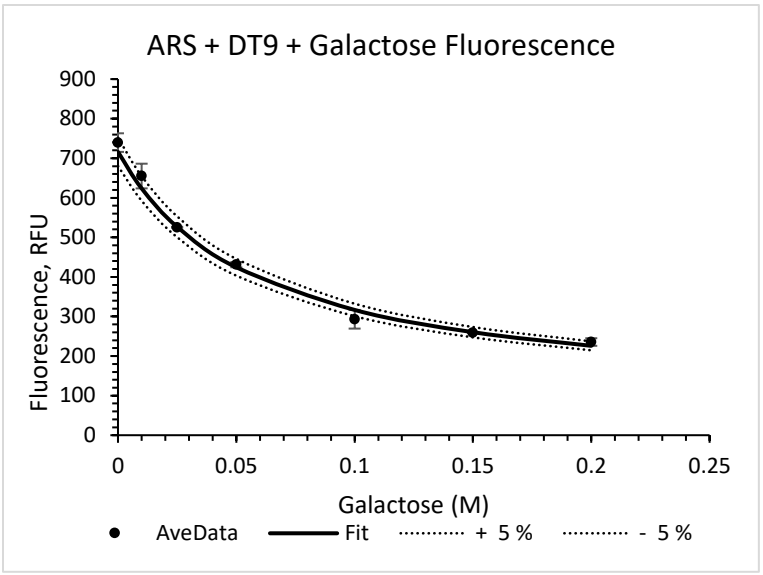

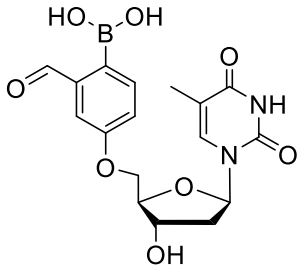

DT9

Plot of fluorescence changes of ARS-DT9 complex with increasing concentration of galactose. ARS (0.1 mM), DT9 (10 mM), galactose (0-0.1 M), HEPES buffer (100 mM, pH 7.4). (K_a was calculated to be 17.1 ± 4.6 M^{-1}). Value is the average of duplicate runs. Dotted lines represent 5% error.

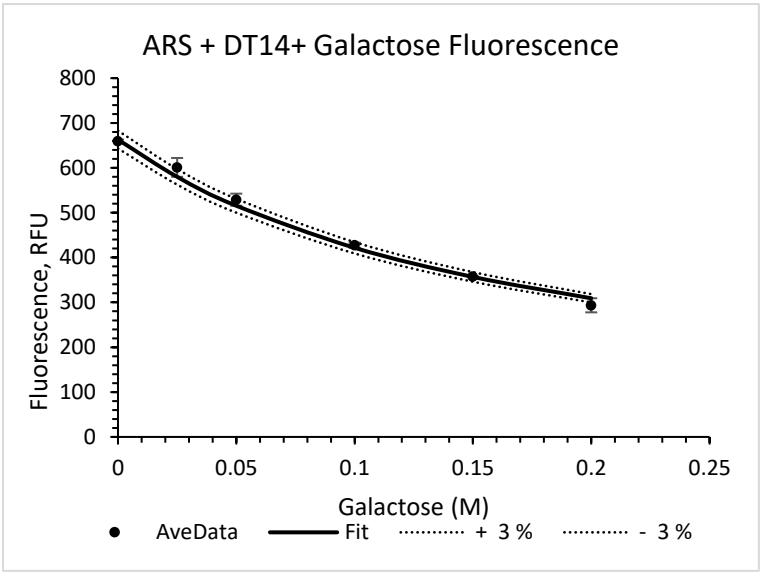

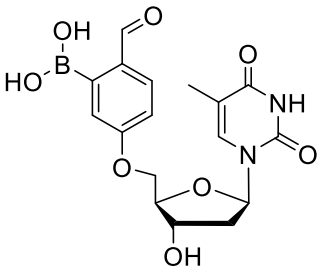

DT14

Plot of fluorescence changes of ARS-DT14 complex with increasing concentration of galactose. ARS (0.1 mM), DT14 (10 mM), galactose (0-0.1 M), HEPES buffer (100 mM, pH 7.4). (K_a was calculated to be 5.7 ± 2.0 M^{-1}). Value is the average of duplicate runs. Dotted lines represent 3% error.

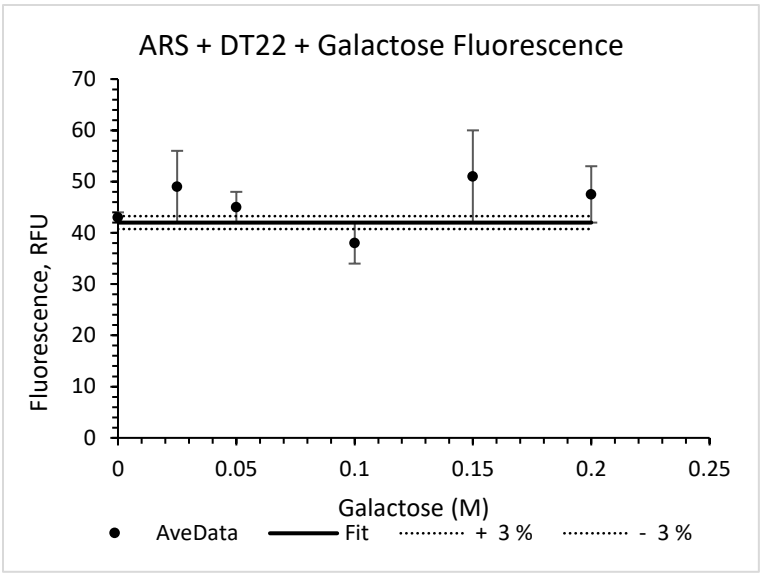

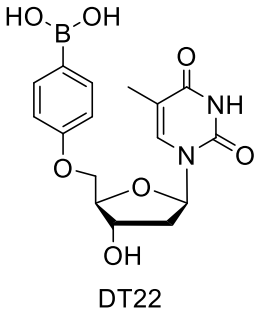

DT22

Plot of fluorescence changes of ARS-DT22 complex with increasing concentration of galactose. ARS (0.1 mM), DT22 (10 mM), galactose (0-0.1 M), HEPES buffer (100 mM, pH 7.4). (K_a was calculated to be 0.0 ± 4.4 M^{-1}). Value is the average of duplicate runs. Dotted lines represent 3% error.

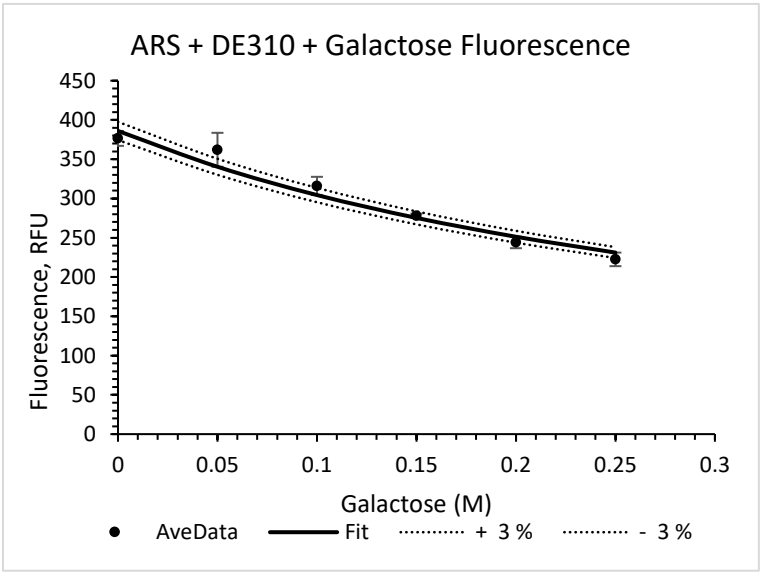

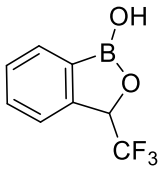

DE310

Plot of fluorescence changes of ARS-DE310 complex with increasing concentration of galactose. ARS (0.1 mM), DE310 (10 mM), galactose (0-0.1 M), HEPES buffer (100 mM, pH 7.4). (K_a was calculated to be 2.7 ± 2.6 M^{-1}). Value is the average of duplicate runs. Dotted lines represent 3% error.

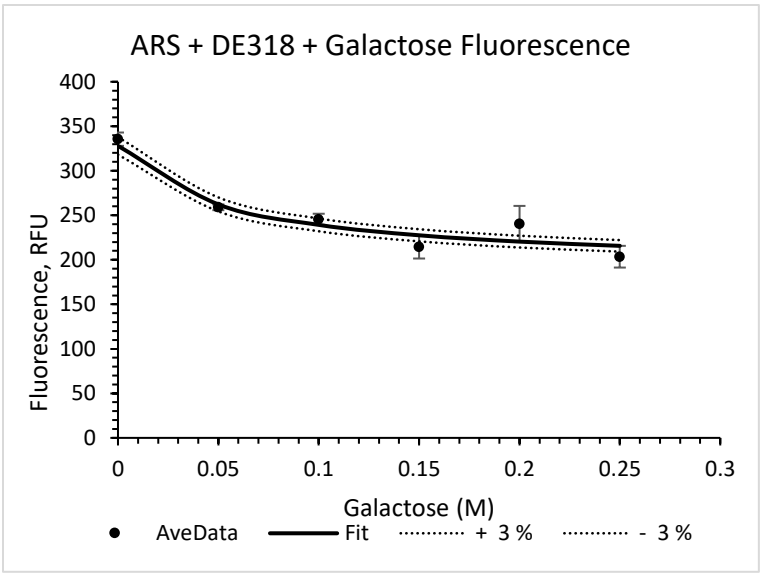

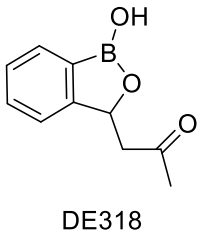

DE318

Plot of fluorescence changes of ARS-DE318 complex with increasing concentration of galactose. ARS (0.1 mM), DE318 (10 mM), galactose (0-0.1 M), HEPES buffer (100 mM, pH 7.4). (K_a was calculated to be 18.6 ± 3.6 M^{-1}). Value is the average of duplicate runs. Dotted lines represent 3% error.

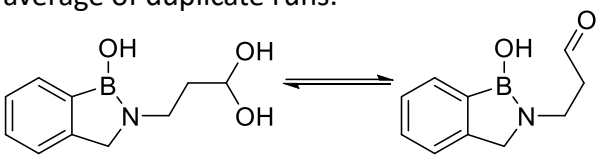

DE321

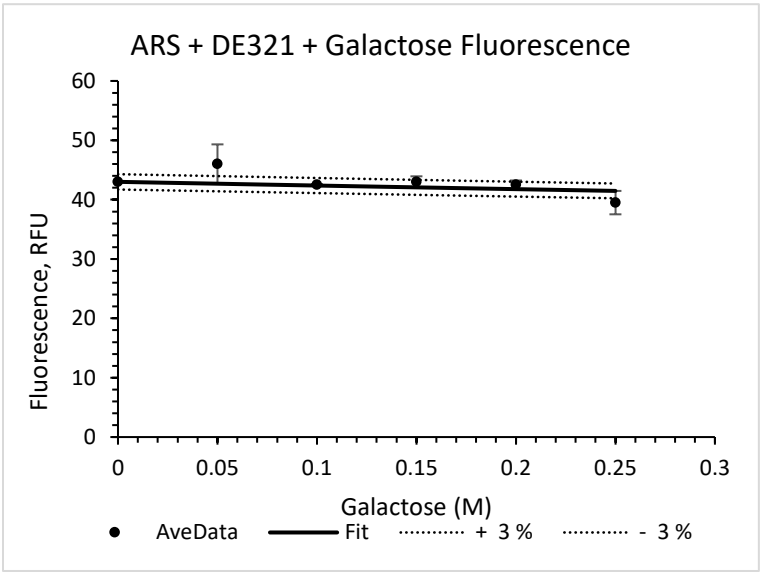

Plot of fluorescence changes of ARS-DE321 complex with increasing concentration of galactose. ARS (0.1 mM), DE321 (10 mM), galactose (0-0.1 M), HEPES buffer (100 mM, pH 7.4). (K_a was calculated to be 0.15 ± 0.38 M^{-1}). Value is the average of duplicate runs. Dotted lines represent 3% error.

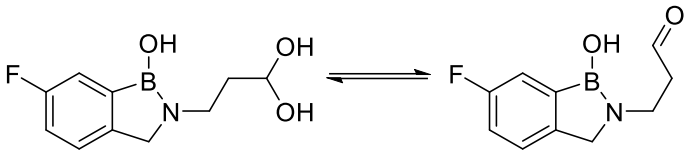

DE342

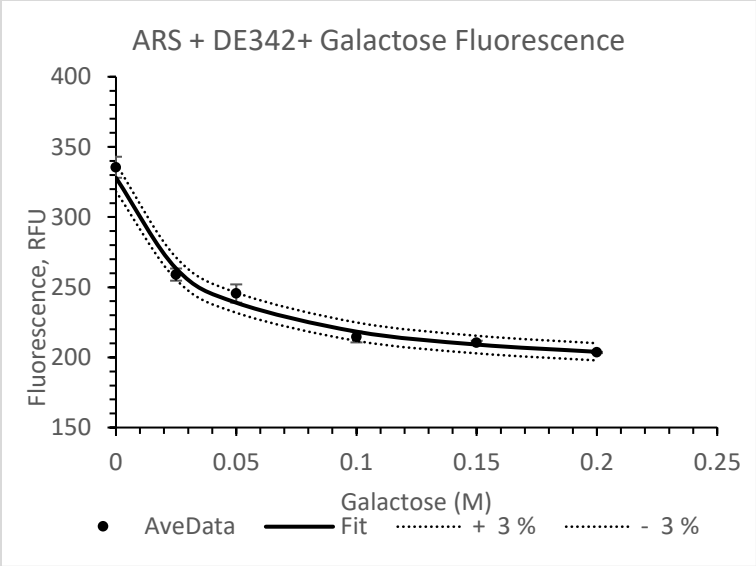

Plot of fluorescence changes of ARS-DE342 complex with increasing concentration of galactose. ARS (0.1 mM), DE342 (10 mM), galactose (0-0.1 M), HEPES buffer (100 mM, pH 7.4). (K_a was calculated to be 33.1 ± 0.49 M^{-1}). Value is the average of duplicate runs. Dotted lines represent 3% error.

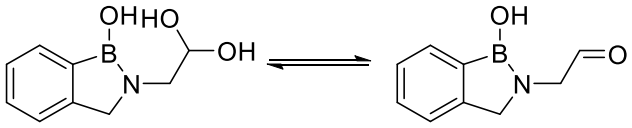

DE343

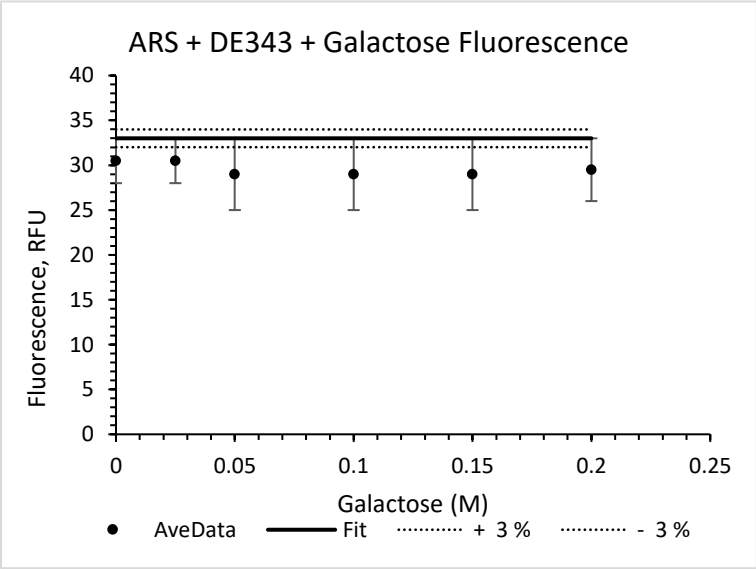

Plot of fluorescence changes of ARS-DE343 complex with increasing concentration of galactose. ARS (0.1 mM), DE343 (10 mM), galactose (0-0.1 M), HEPES buffer (100 mM, pH 7.4). (K_a was calculated to be 0.0 ± 2.2 M^{-1}). Value is the average of duplicate runs. Dotted lines represent 3% error.

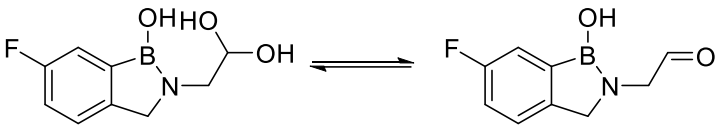

DE344

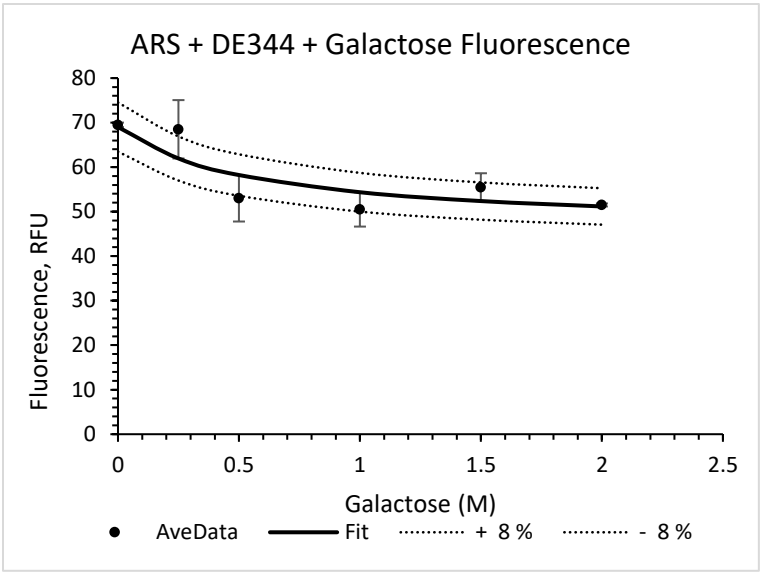

Plot of fluorescence changes of ARS-DE344 complex with increasing concentration of galactose. ARS (0.1 mM), DE344 (10 mM), galactose (0-0.1 M), HEPES buffer (100 mM, pH 7.4). (K_a was calculated to be 1.8 ± 1.6 M^{-1}). Value is the average of duplicate runs. Dotted lines represent 8% error.

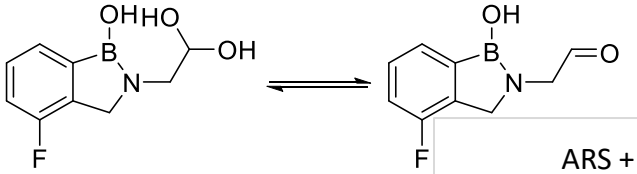

DE347

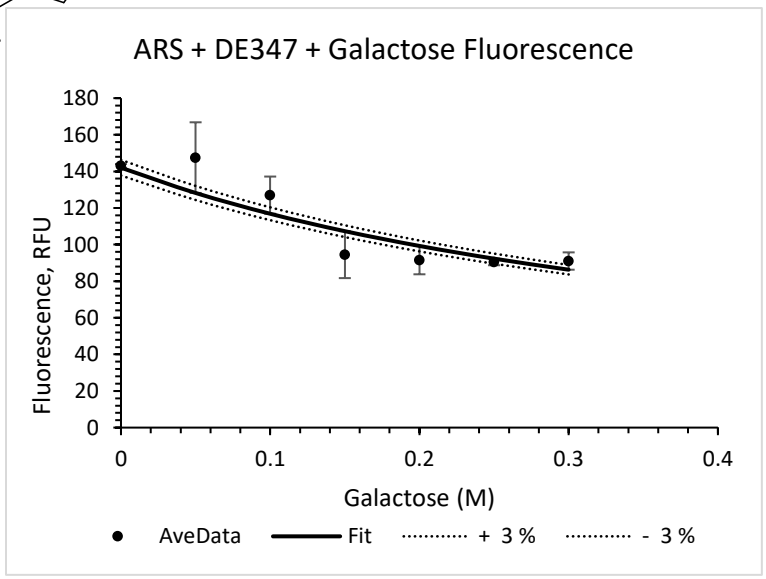

Plot of fluorescence changes of ARS-DE347 complex with increasing concentration of galactose. ARS (0.1 mM), DE347 (10 mM), galactose (0-0.1 M), HEPES buffer (100 mM, pH 7.4). (K_a was calculated to be 2.2 ± 6.2 M^{-1}). Value is the average of duplicate runs. Dotted lines represent 3% error.

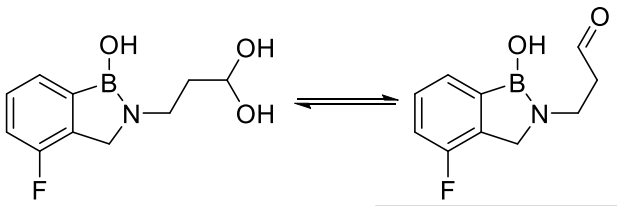

DE348

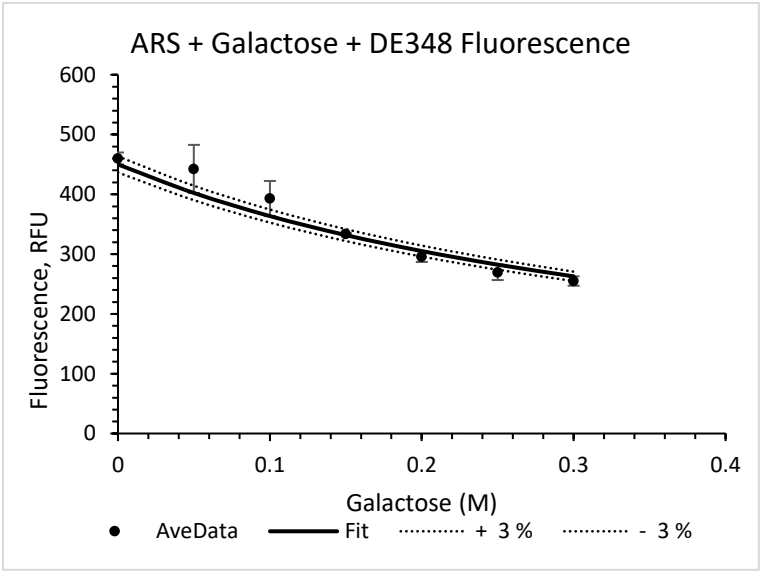

Plot of fluorescence changes of ARS-DE348 complex with increasing concentration of galactose. ARS (0.1 mM), DE348 (10 mM), galactose (0-0.1 M), HEPES buffer (100 mM, pH 7.4). (K_a was calculated to be 2.4 ± 7.7 M^{-1}). Value is the average of duplicate runs. Dotted lines represent 3% error.

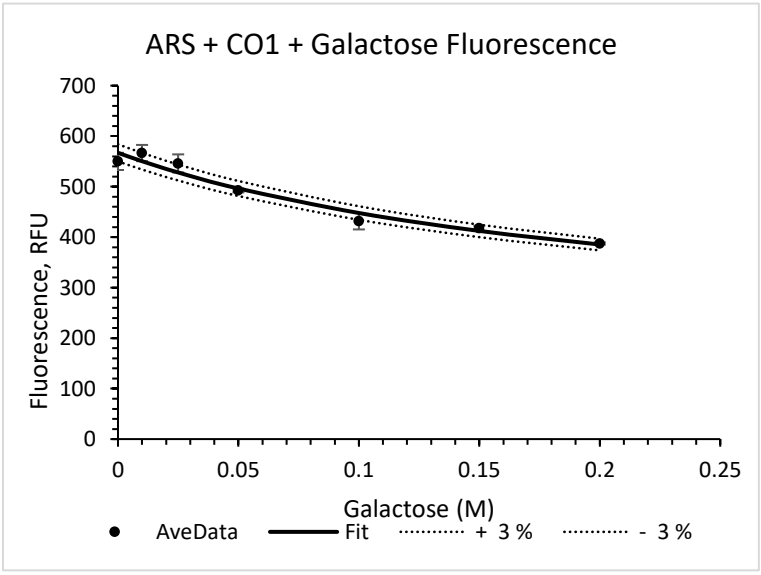

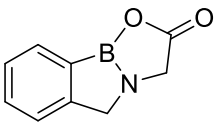

CO1

Plot of fluorescence changes of ARS-CO1 complex with increasing concentration of galactose. ARS (0.1 mM), CO1 (10 mM), galactose (0-0.1 M), HEPES buffer (100 mM, pH 7.4). (K_a was calculated to be 4.5 ± 2.3 M^{-1}). Value is the average of duplicate runs. Dotted lines represent 3% error.

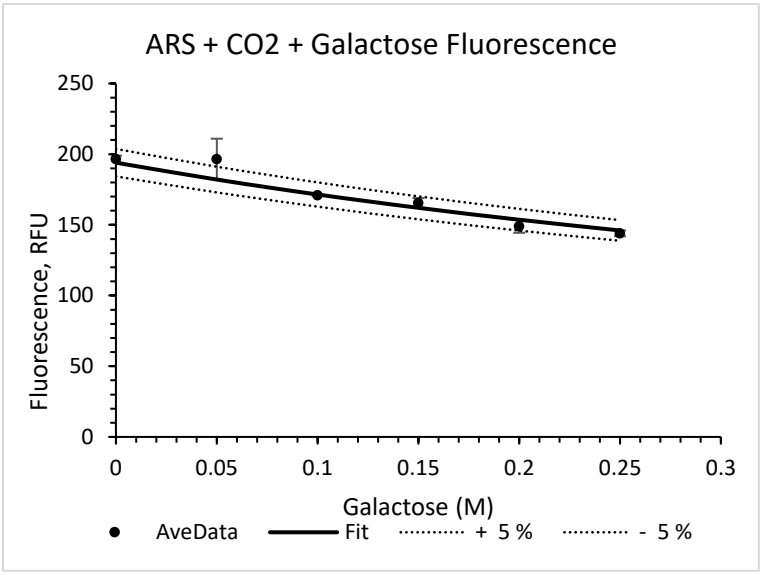

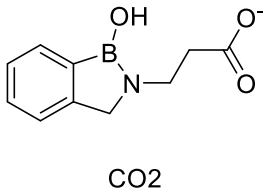

CO2

Plot of fluorescence changes of ARS-CO2 complex with increasing concentration of galactose. ARS (0.1 mM), CO2 (10 mM), galactose (0-0.1 M), HEPES buffer (100 mM, pH 7.4). (K_a was calculated to be 1.3 ± 1.4 M^{-1}). Value is the average of duplicate runs. Dotted lines represent 5% error.

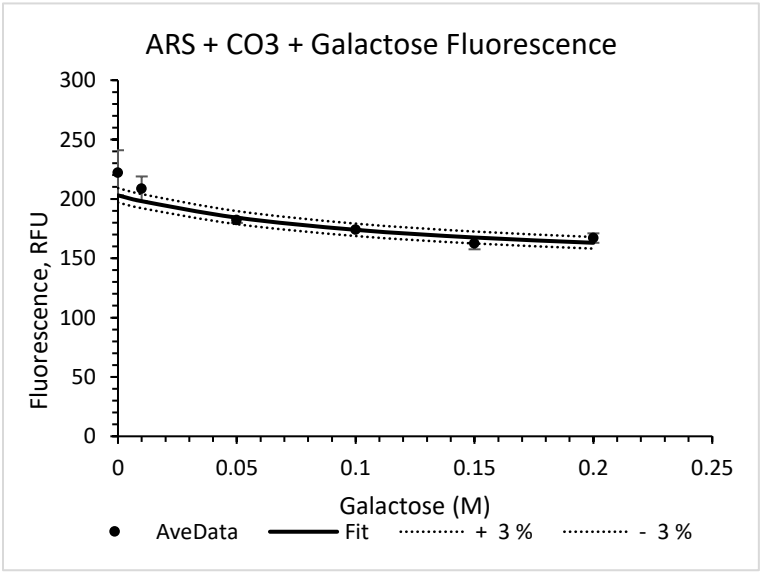

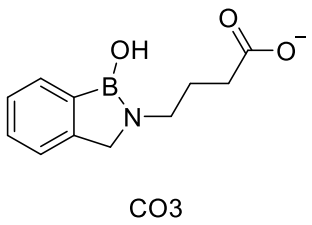

CO3

Plot of fluorescence changes of ARS-CO3 complex with increasing concentration of galactose. ARS (0.1 mM), CO3 (10 mM), galactose (0-0.1 M), HEPES buffer (100 mM, pH 7.4). (K_a was calculated to be 3.3 ± 1.6 M^{-1}). Value is the average of duplicate runs. Dotted lines represent 3% error.

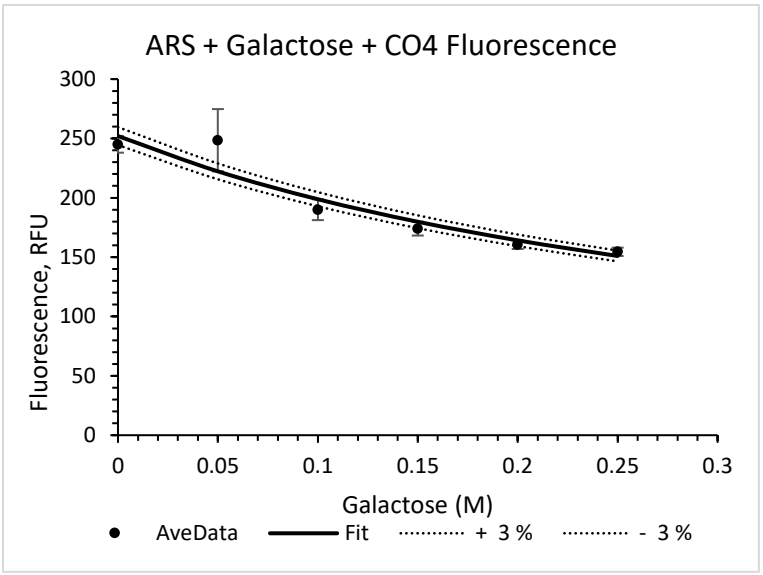

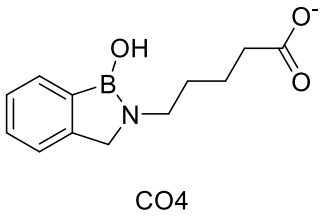

CO4

Plot of fluorescence changes of ARS-CO4 complex with increasing concentration of galactose. ARS (0.1 mM), CO4 (10 mM), galactose (0-0.1 M), HEPES buffer (100 mM, pH 7.4). (K_a was calculated to be 2.7 ± 4.0 M^{-1}). Value is the average of duplicate runs. Dotted lines represent 3% error.

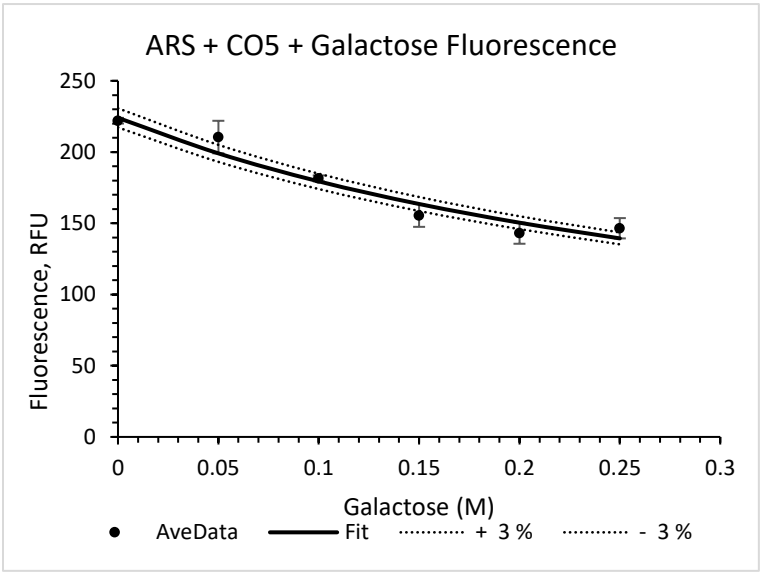

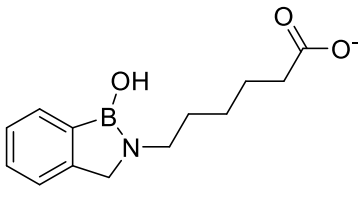

CO5

Plot of fluorescence changes of ARS-CO5 complex with increasing concentration of galactose. ARS (0.1 mM), CO5 (10 mM), galactose (0-0.1 M), HEPES buffer (100 mM, pH 7.4). (K_a was calculated to be 2.7 ± 1.8 M^{-1}). Value is the average of duplicate runs. Dotted lines represent 3% error.

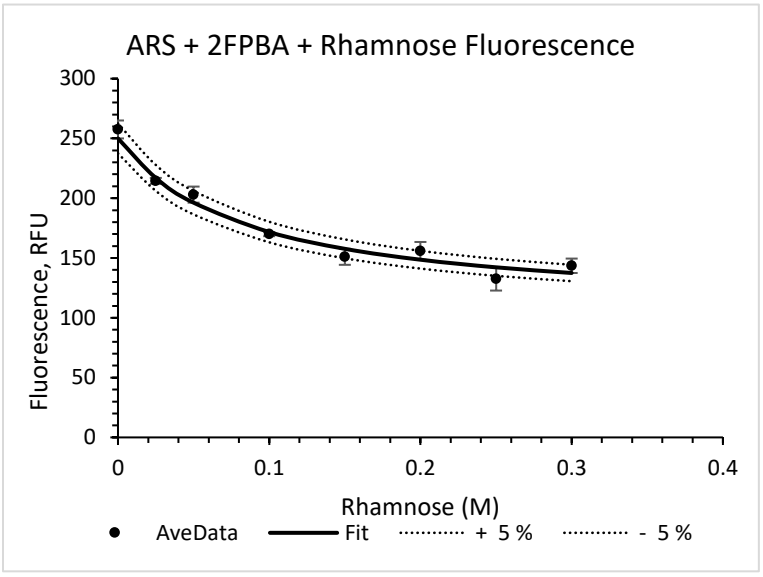

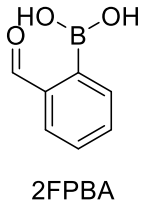

2FPBA

Plot of fluorescence changes of ARS-2FPBA complex with increasing concentration of rhamnose. ARS (0.1 mM), 2FPBA (10 mM), rhamnose (0-0.1 M), HEPES buffer (100 mM, pH 7.4). (K_a was calculated to be 11.9 ± 2.1 M^{-1}). Value is the average of duplicate runs. Dotted lines represent 5% error.

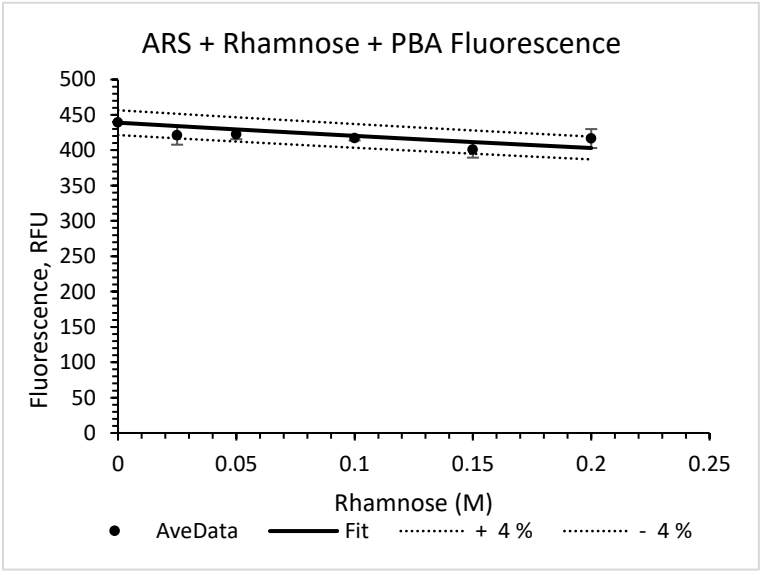

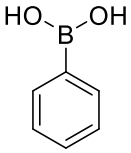

PBA

Plot of fluorescence changes of ARS-PBA complex with increasing concentration of rhamnose. ARS (0.1 mM), PBA (10 mM), rhamnose (0-0.1 M), HEPES buffer (100 mM, pH 7.4). (K_a was calculated to be 0.45 ± 1.3 M^{-1}). Value is the average of duplicate runs. Dotted lines represent 4% error.

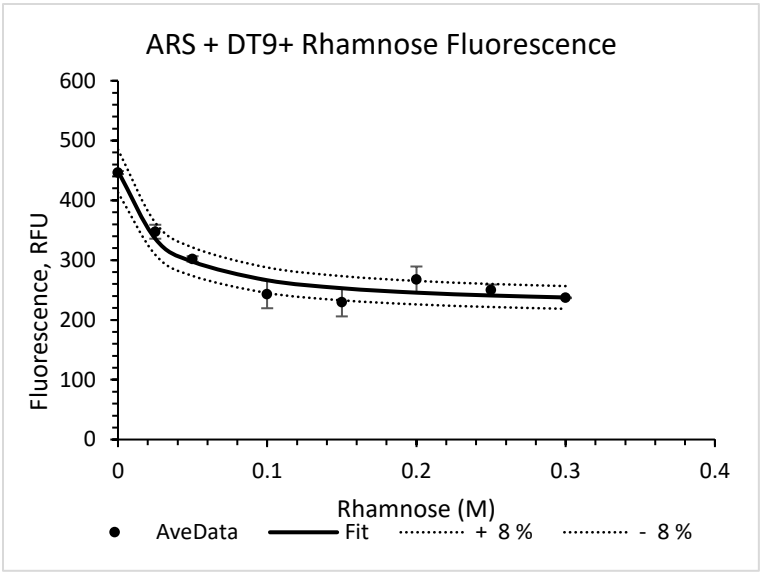

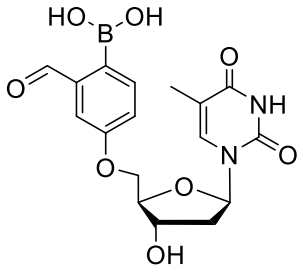

DT9

Plot of fluorescence changes of ARS-DT9 complex with increasing concentration of rhamnose. ARS (0.1 mM), DT9 (10 mM), rhamnose (0-0.1 M), HEPES buffer (100 mM, pH 7.4). (K_a was calculated to be 39.9 ± 7.0 M^{-1}). Value is the average of duplicate runs. Dotted lines represent 8% error.

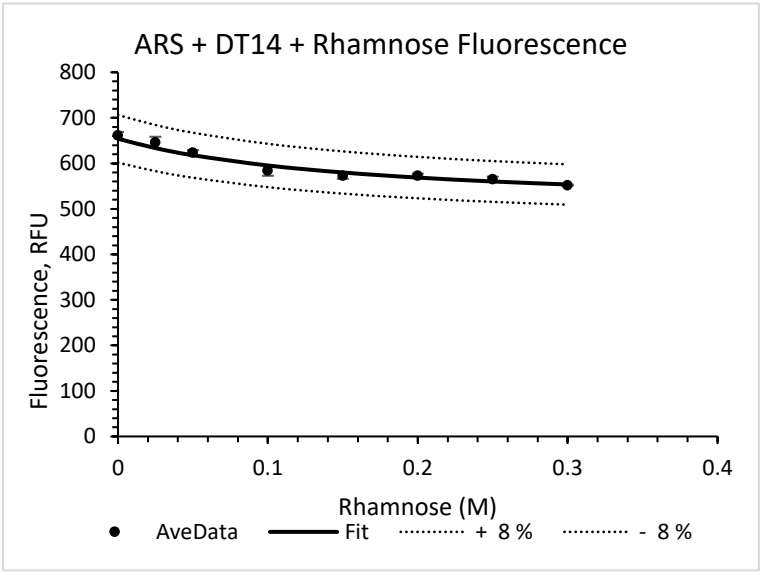

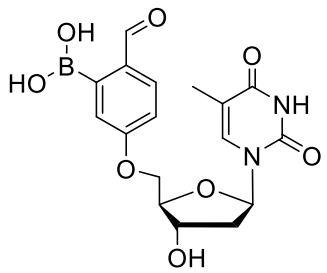

DT14

Plot of fluorescence changes of ARS-DT14 complex with increasing concentration of rhamnose. ARS (0.1 mM), DT14 (10 mM), rhamnose (0-0.1 M), HEPES buffer (100 mM, pH 7.4). (K_a was calculated to be 6.0 ± 0.77 M^{-1}). Value is the average of duplicate runs. Dotted lines represent 8% error.

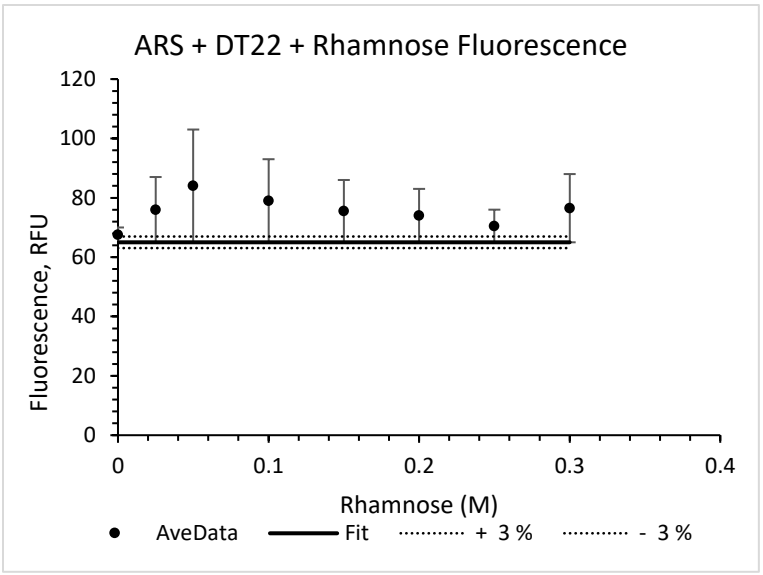

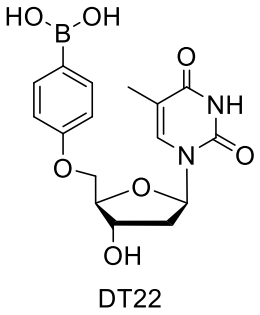

DT22

Plot of fluorescence changes of ARS-DT22 complex with increasing concentration of rhamnose. ARS (0.1 mM), DT22 (10 mM), rhamnose (0-0.1 M), HEPES buffer (100 mM, pH 7.4). (K_a was calculated to be 0.0 ± 16 M^{-1}). Value is the average of duplicate runs. Dotted lines represent 3% error.

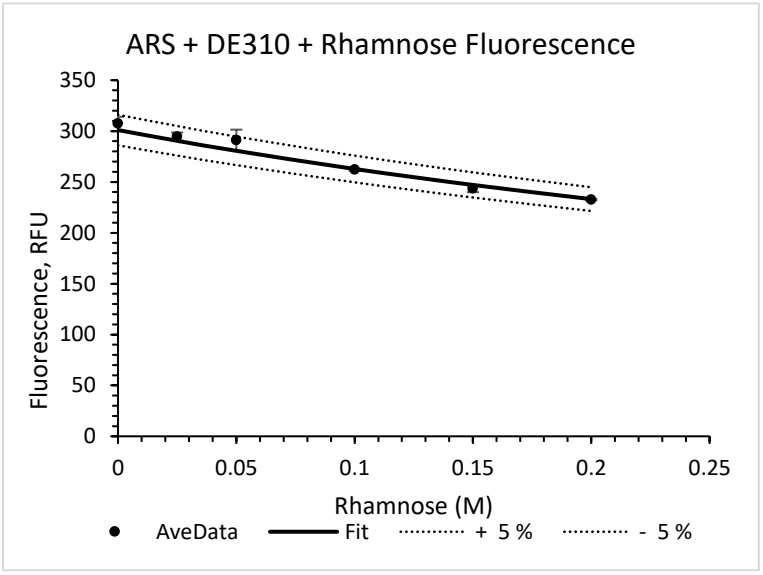

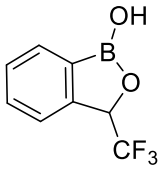

DE310

Plot of fluorescence changes of ARS-DE310 complex with increasing concentration of rhamnose. ARS (0.1 mM), DE310 (10 mM), rhamnose (0-0.1 M), HEPES buffer (100 mM, pH 7.4). (K_a was calculated to be 1.5 ± 0.64 M^{-1}). Value is the average of duplicate runs. Dotted lines represent 5% error.

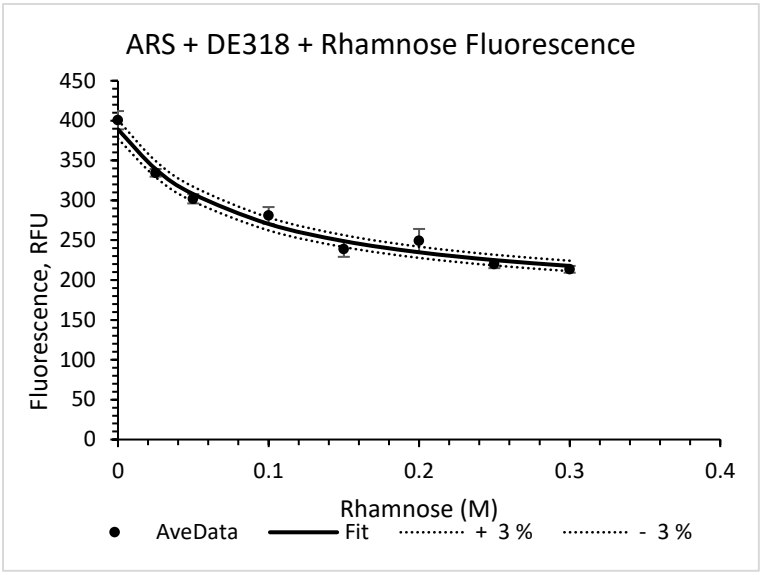

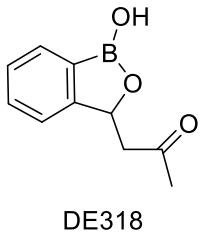

DE318

Plot of fluorescence changes of ARS-DE318 complex with increasing concentration of rhamnose. ARS (0.1 mM), DE318 (10 mM), rhamnose (0-0.1 M), HEPES buffer (100 mM, pH 7.4). (K_a was calculated to be 11.7 ± 2.4 M^{-1}). Value is the average of duplicate runs. Dotted lines represent 3% error.

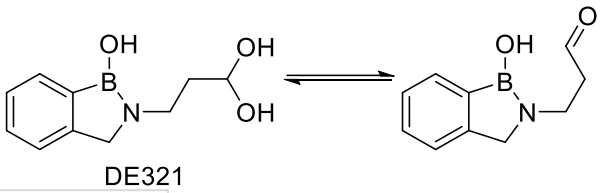

DE321

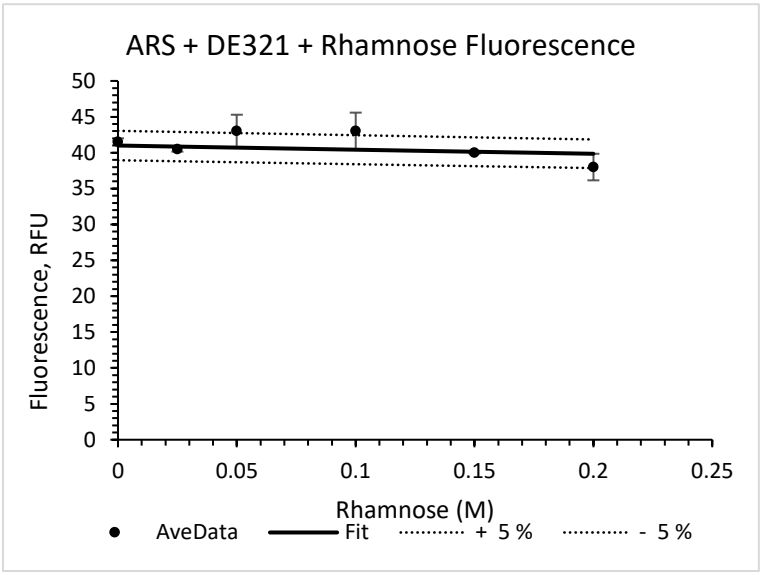

Plot of fluorescence changes of ARS-DE321 complex with increasing concentration of rhamnose. ARS (0.1 mM), DE321 (10 mM), rhamnose (0-0.1 M), HEPES buffer (100 mM, pH 7.4). (K_a was calculated to be 0.14 ± 0.39 M^{-1}). Value is the average of duplicate runs. Dotted lines represent 5% error.

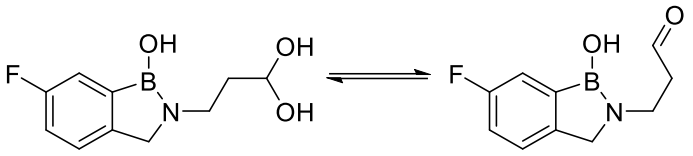

DE342

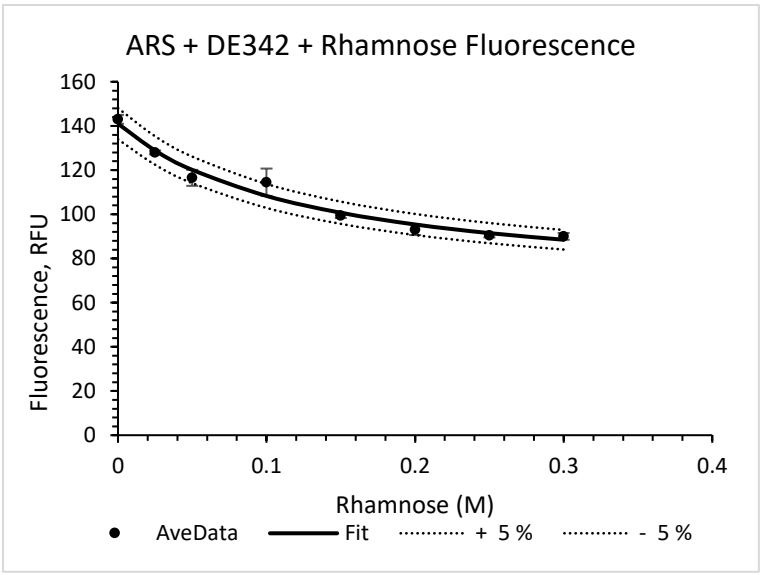

Plot of fluorescence changes of ARS-DE342 complex with increasing concentration of rhamnose. ARS (0.1 mM), DE342 (10 mM), rhamnose (0-0.1 M), HEPES buffer (100 mM, pH 7.4). (K_a was calculated to be 7.6 ± 0.61 M^{-1}). Value is the average of duplicate runs. Dotted lines represent 5% error.

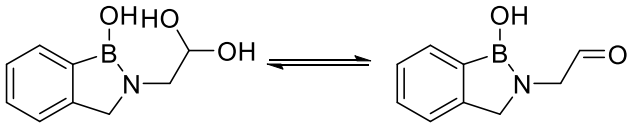

DE343

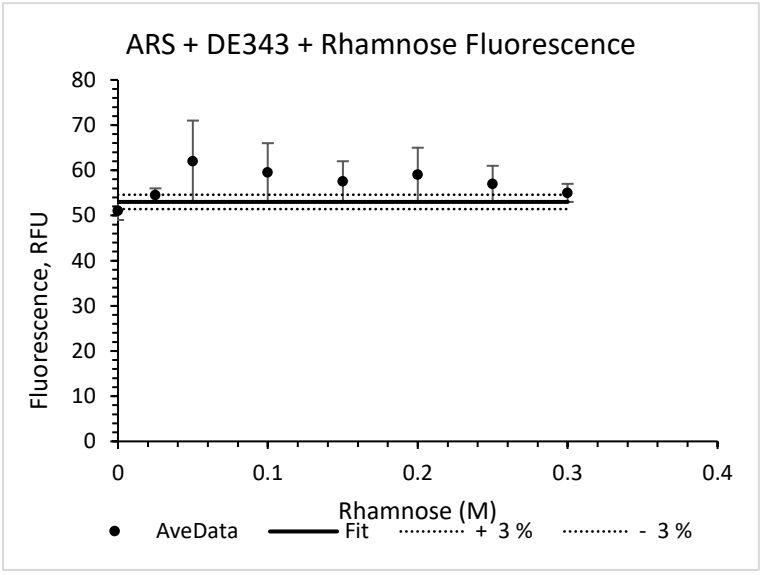

Plot of fluorescence changes of ARS-DE343 complex with increasing concentration of rhamnose. ARS (0.1 mM), DE343 (10 mM), rhamnose (0-0.1 M), HEPES buffer (100 mM, pH 7.4). (K_a was calculated to be 0.0 ± 3.9 M^{-1}). Value is the average of duplicate runs. Dotted lines represent 3% error.

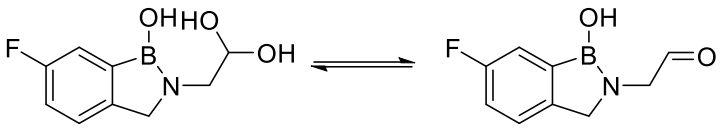

DE344

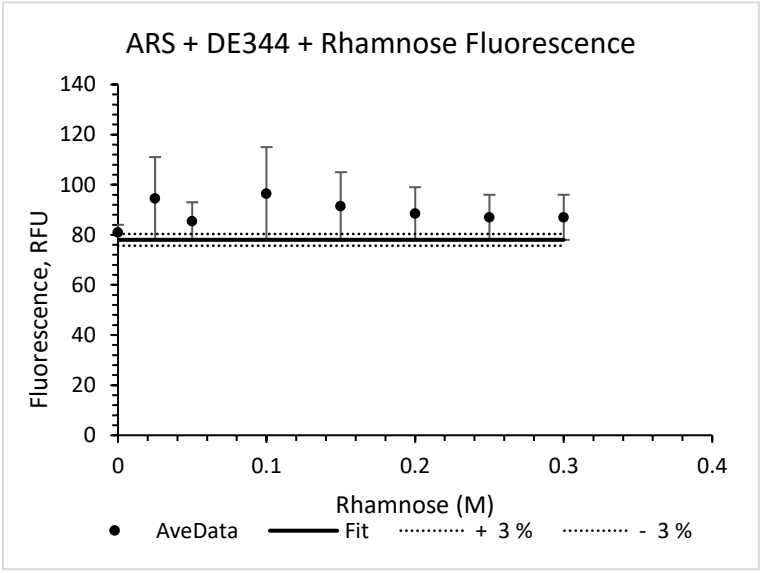

Plot of fluorescence changes of ARS-DE344 complex with increasing concentration of rhamnose. ARS (0.1 mM), DE344 (10 mM), rhamnose (0-0.1 M), HEPES buffer (100 mM, pH 7.4). (K_a was calculated to be 0.0 ± 15 M^{-1}). Value is the average of duplicate runs. Dotted lines represent 3% error.

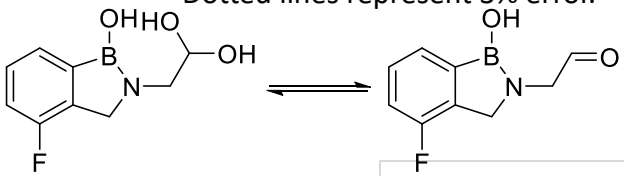

DE347

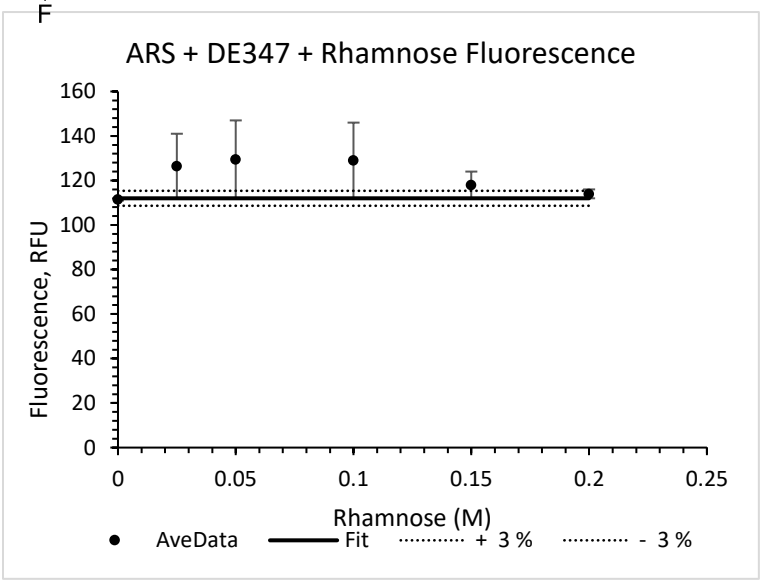

Plot of fluorescence changes of ARS-DE347 complex with increasing concentration of rhamnose. ARS (0.1 mM), DE347 (10 mM), rhamnose (0-0.1 M), HEPES buffer (100 mM, pH 7.4). (K_a was calculated to be 0.0 ± 7.6 M^{-1}). Value is the average of duplicate runs. Dotted lines represent 3% error.

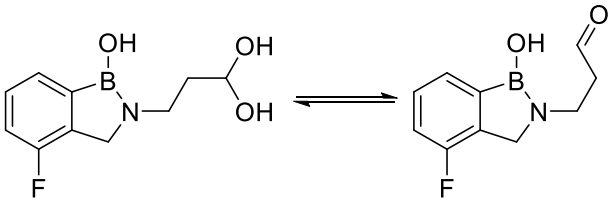

DE348

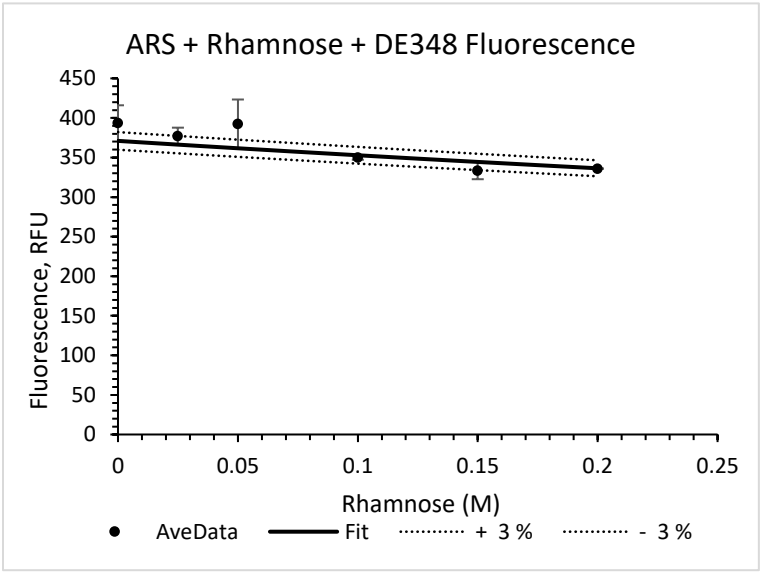

Plot of fluorescence changes of ARS-DE348 complex with increasing concentration of rhamnose. ARS (0.1 mM), DE348 (10 mM), rhamnose (0-0.1 M), HEPES buffer (100 mM, pH 7.4). (K_a was calculated to be 0.51 ± 4.7 M^{-1}). Value is the average of duplicate runs. Dotted lines represent 3% error.

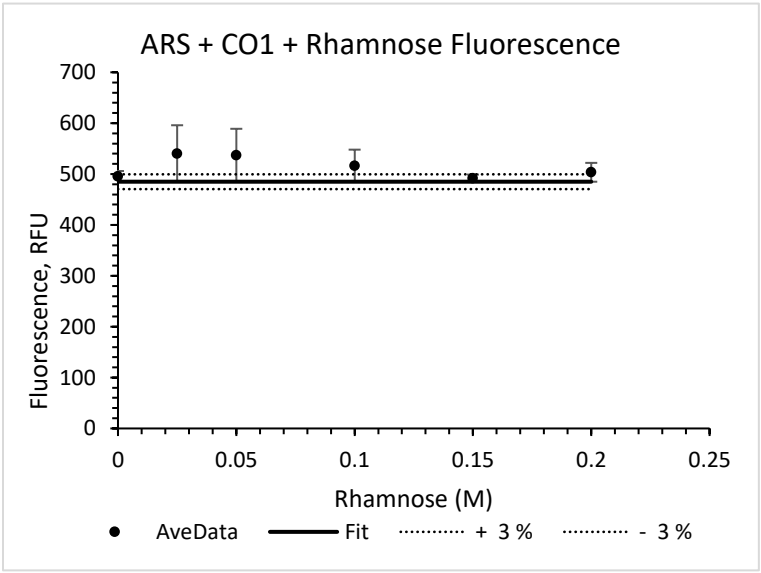

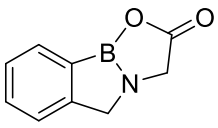

CO1

Plot of fluorescence changes of ARS-CO1 complex with increasing concentration of rhamnose. ARS (0.1 mM), CO1 (10 mM), rhamnose (0-0.1 M), HEPES buffer (100 mM, pH 7.4). (K_a was calculated to be 0.0 ± 15 M^{-1}). Value is the average of duplicate runs. Dotted lines represent 3% error.

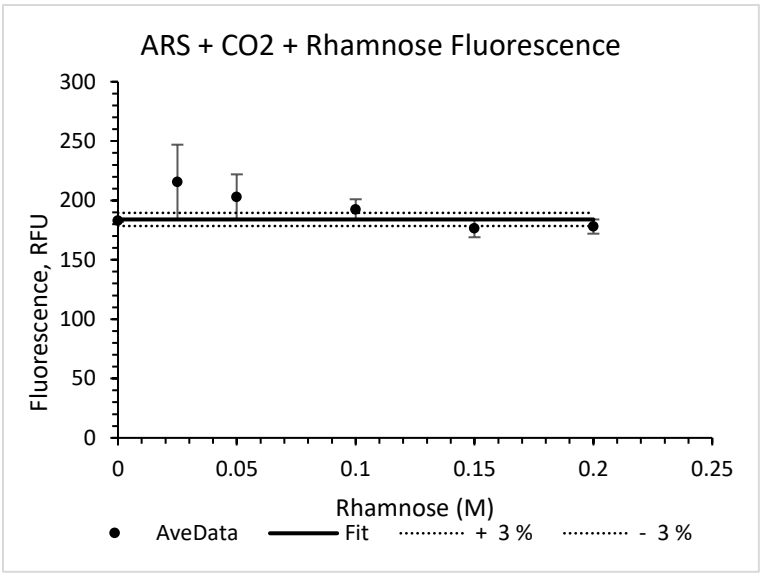

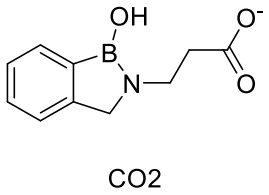

CO2

Plot of fluorescence changes of ARS-CO2 complex with increasing concentration of rhamnose. ARS (0.1 mM), CO2 (10 mM), rhamnose (0-0.1 M), HEPES buffer (100 mM, pH 7.4). (K_a was calculated to be 0.0 ± 8.3 M^{-1}). Value is the average of duplicate runs. Dotted lines represent 3% error.

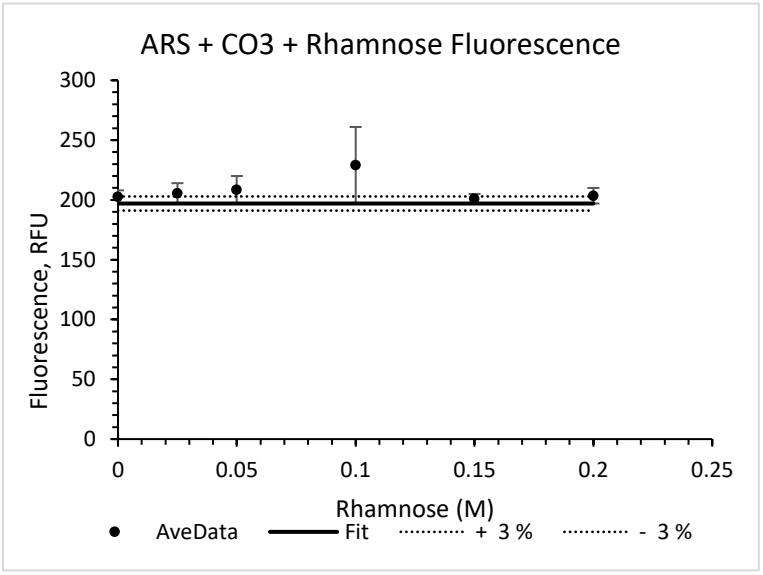

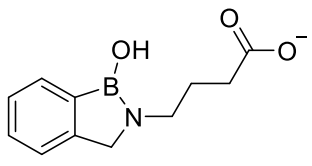

CO3

Plot of fluorescence changes of ARS-CO3 complex with increasing concentration of rhamnose. ARS (0.1 mM), CO3 (10 mM), rhamnose (0-0.1 M), HEPES buffer (100 mM, pH 7.4). (K_a was calculated to be 0.0 ± 6.7 M^{-1}). Value is the average of duplicate runs. Dotted lines represent 3% error.

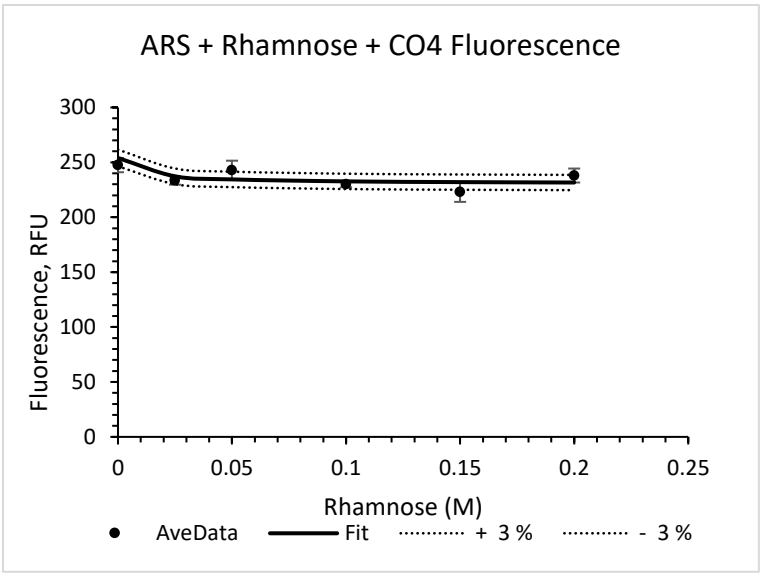

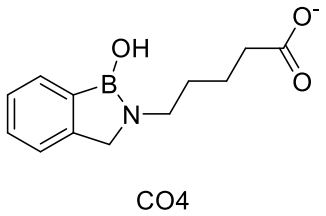

CO4

Plot of fluorescence changes of ARS-CO4 complex with increasing concentration of rhamnose. ARS (0.1 mM), CO4 (10 mM), rhamnose (0-0.1 M), HEPES buffer (100 mM, pH 7.4). (K_a was calculated to be 0.0 ± 1.1 M^{-1}). Value is the average of duplicate runs. Dotted lines represent 3% error.

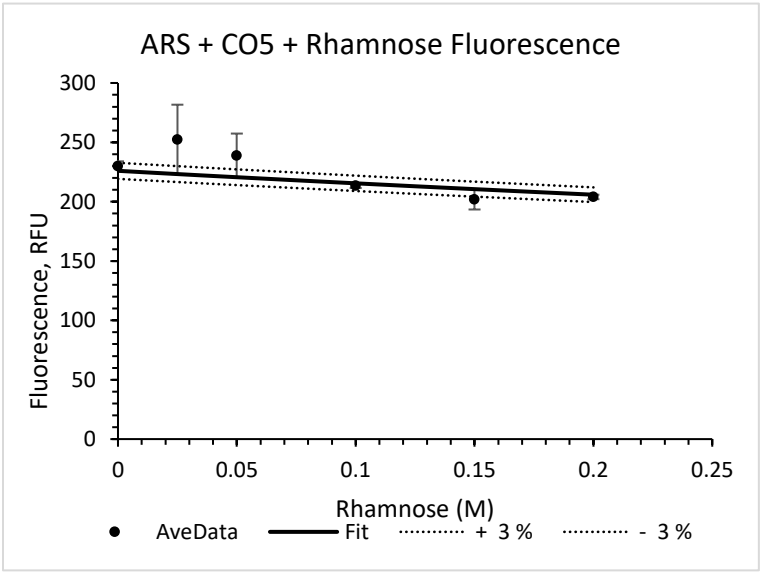

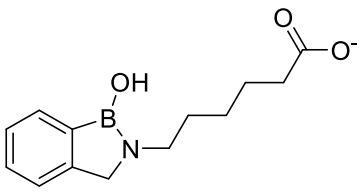

CO5

Plot of fluorescence changes of ARS-CO5 complex with increasing concentration of rhamnose. ARS (0.1 mM), CO5 (10 mM), rhamnose (0-0.1 M), HEPES buffer (100 mM, pH 7.4). (K_a was calculated to be 0.5 ± 5.8 M^{-1}). Value is the average of duplicate runs. Dotted lines represent 3% error.

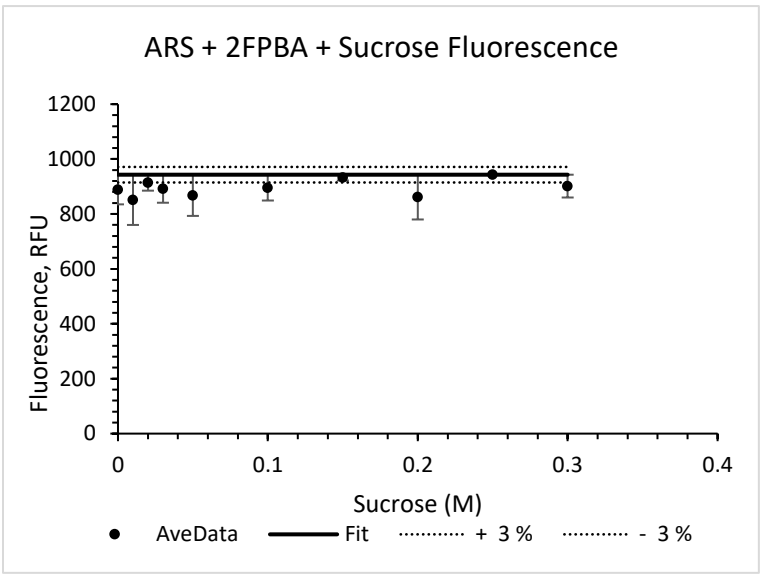

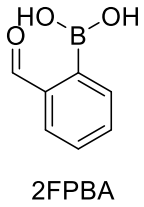

Plot of fluorescence changes of ARS-2FPBA complex with increasing concentration of sucrose. ARS (0.1 mM), 2FPBA (10 mM), sucrose (0-0.1 M), HEPES buffer (100 mM, pH 7.4). (K_a was calculated to be 0.0 ± 33 M^{-1}). Value is the average of duplicate runs. Dotted lines represent 3% error.

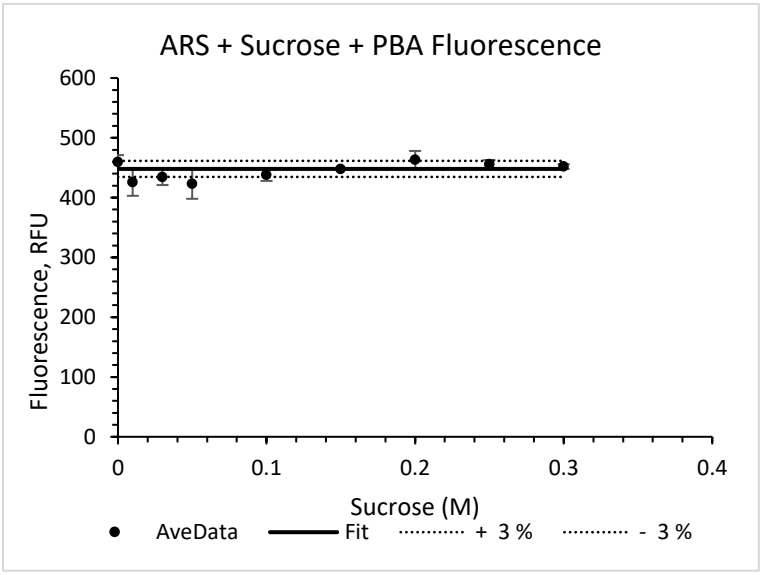

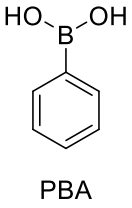

Plot of fluorescence changes of ARS-PBA complex with increasing concentration of sucrose. ARS (0.1 mM), PBA (10 mM), sucrose (0-0.1 M), HEPES buffer (100 mM, pH 7.4). (K_a was calculated to be 0.0 ± 4.1 M^{-1}). Value is the average of duplicate runs. Dotted lines represent 3% error.

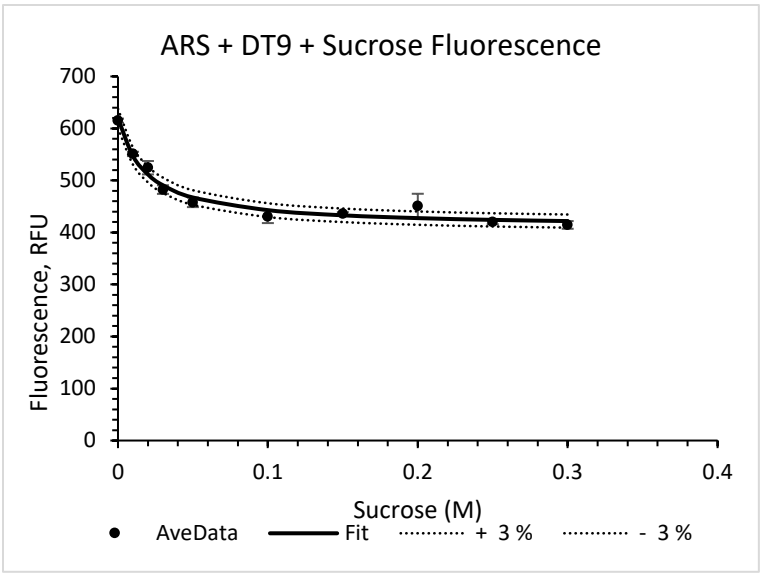

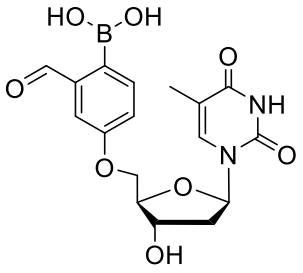

DT9

Plot of fluorescence changes of ARS-DT9 complex with increasing concentration of sucrose. ARS (0.1 mM), DT9 (10 mM), sucrose (0-0.1 M), HEPES buffer (100 mM, pH 7.4). (K_a was calculated to be 52.5 ± 2.5 M^{-1}). Value is the average of duplicate runs. Dotted lines represent 3% error.

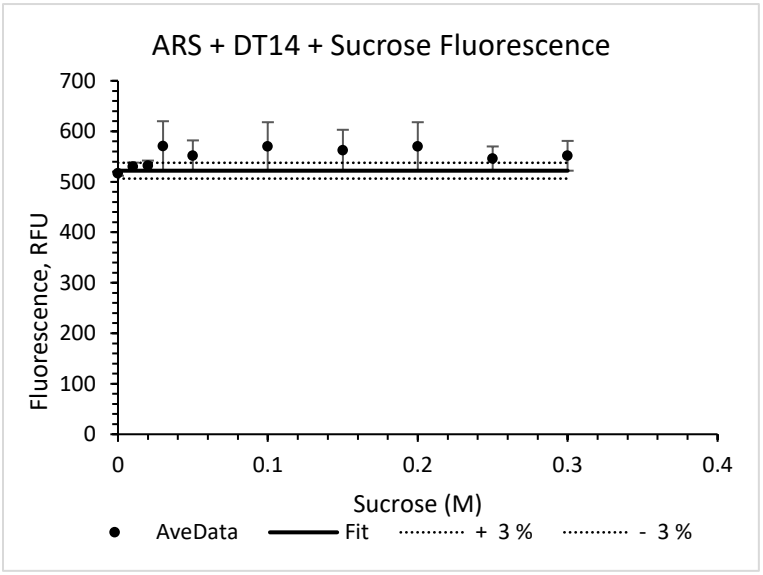

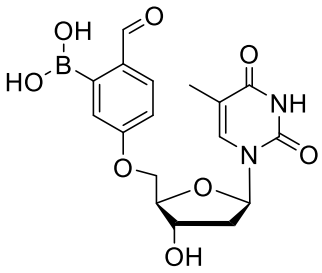

DT14

Plot of fluorescence changes of ARS-DT14 complex with increasing concentration of sucrose. ARS (0.1 mM), DT14 (10 mM), sucrose (0-0.1 M), HEPES buffer (100 mM, pH 7.4). (K_a was calculated to be 0.0 ± 21 M^{-1}). Value is the average of duplicate runs. Dotted lines represent 3% error.

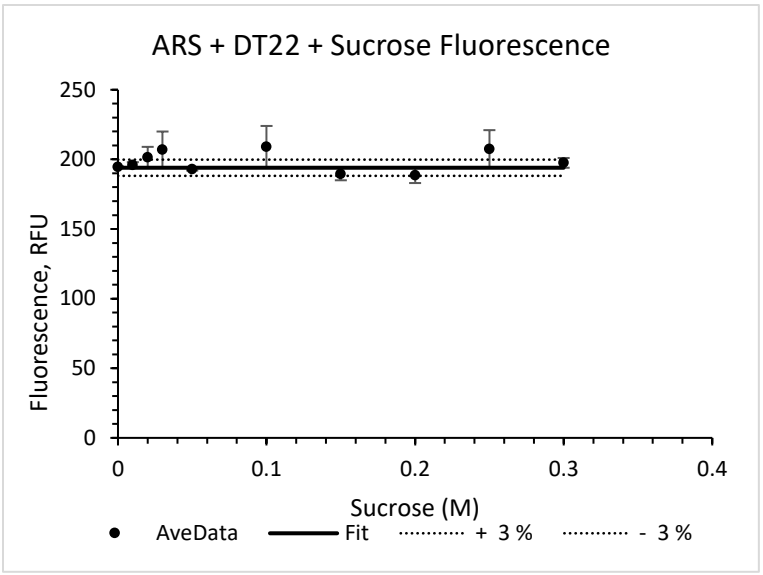

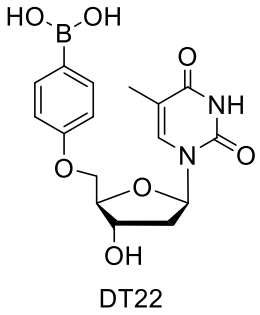

DT22

Plot of fluorescence changes of ARS-DT22 complex with increasing concentration of sucrose. ARS (0.1 mM), DT22 (10 mM), sucrose (0-0.1 M), HEPES buffer (100 mM, pH 7.4). (K_a was calculated to be 0.0 ± 3.6 M^{-1}). Value is the average of duplicate runs. Dotted lines represent 3% error.

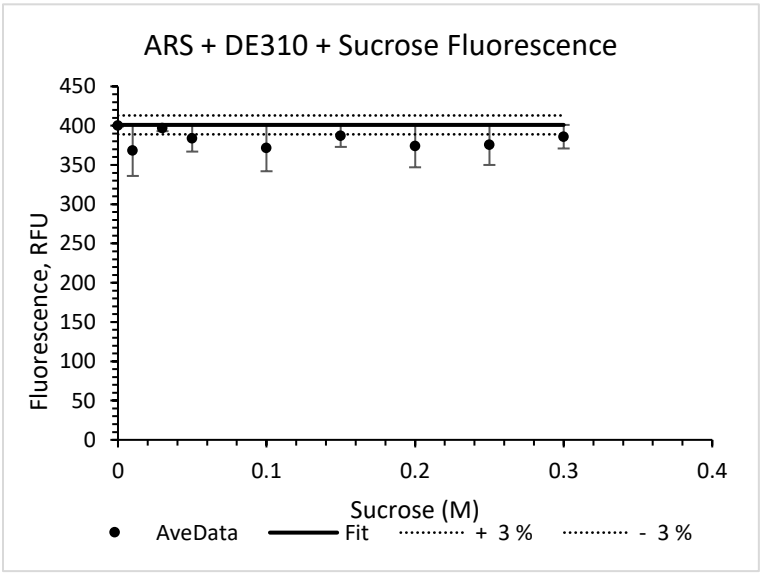

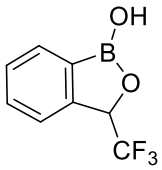

DE310

Plot of fluorescence changes of ARS-DE310 complex with increasing concentration of sucrose. ARS (0.1 mM), DE310 (10 mM), sucrose (0-0.1 M), HEPES buffer (100 mM, pH 7.4). (K_a was calculated to be 0.0 ± 10 M^{-1}). Value is the average of duplicate runs. Dotted lines represent 3% error.

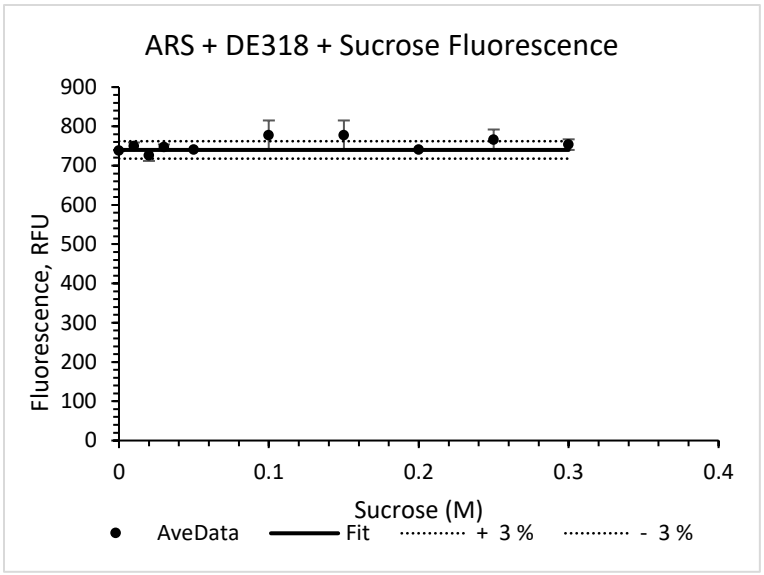

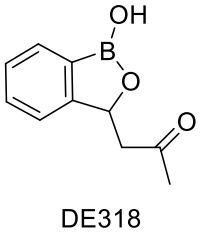

DE318

Plot of fluorescence changes of ARS-DE318 complex with increasing concentration of sucrose. ARS (0.1 mM), DE318 (10 mM), sucrose (0-0.1 M), HEPES buffer (100 mM, pH 7.4). (K_a was calculated to be 0.0 ± 5.4 M^{-1}). Value is the average of duplicate runs. Dotted lines represent 3% error.

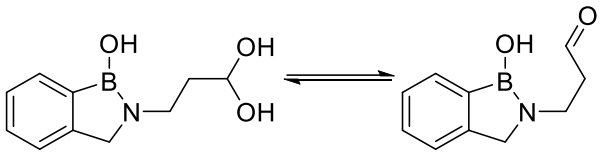

DE321

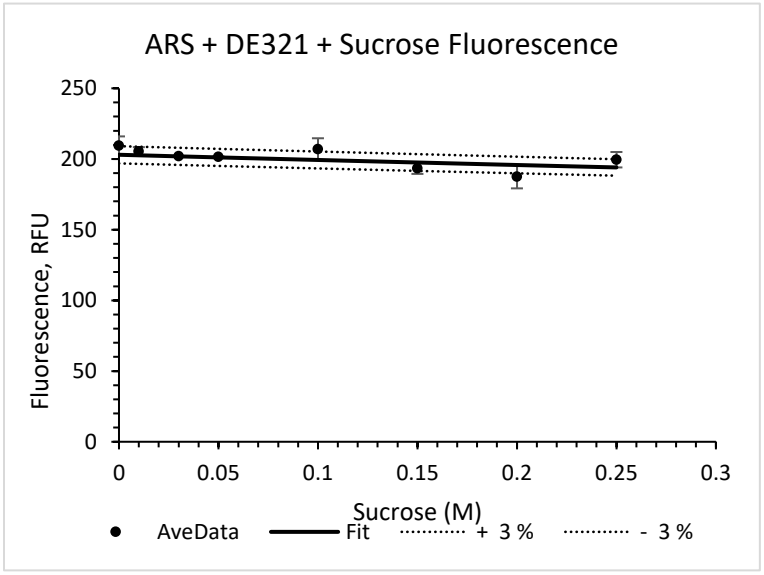

Plot of fluorescence changes of ARS-DE321 complex with increasing concentration of sucrose. ARS (0.1 mM), DE321 (10 mM), sucrose (0-0.1 M), HEPES buffer (100 mM, pH 7.4). (K_a was calculated to be 0.2 ± 1.1 M^{-1}). Value is the average of duplicate runs. Dotted lines represent 3% error.

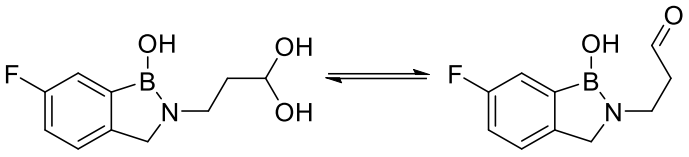

DE342

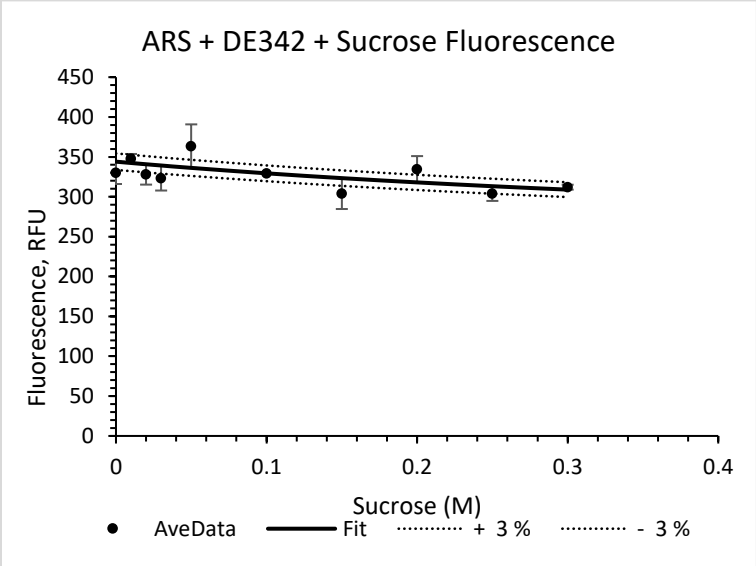

Plot of fluorescence changes of ARS-DE342 complex with increasing concentration of sucrose. ARS (0.1 mM), DE342 (10 mM), sucrose (0-0.1 M), HEPES buffer (100 mM, pH 7.4). (K_a was calculated to be 1.4 ± 6.4 M^{-1}). Value is the average of duplicate runs. Dotted lines represent 3% error.

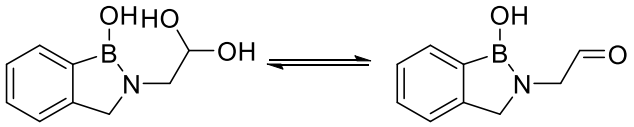

DE343

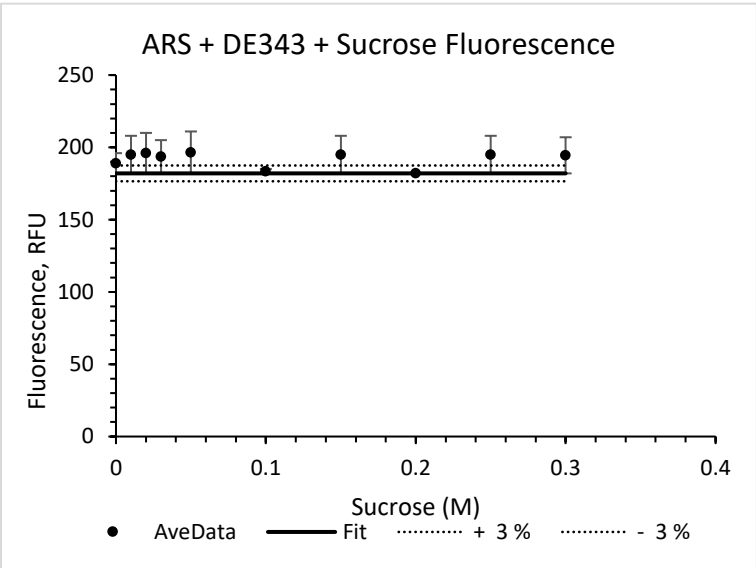

Plot of fluorescence changes of ARS-DE343 complex with increasing concentration of sucrose. ARS (0.1 mM), DE343 (10 mM), sucrose (0-0.1 M), HEPES buffer (100 mM, pH 7.4). (K_a was calculated to be 0.0 ± 6.9 M^{-1}). Value is the average of duplicate runs. Dotted lines represent 3% error.

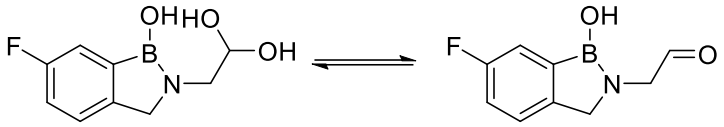

DE344

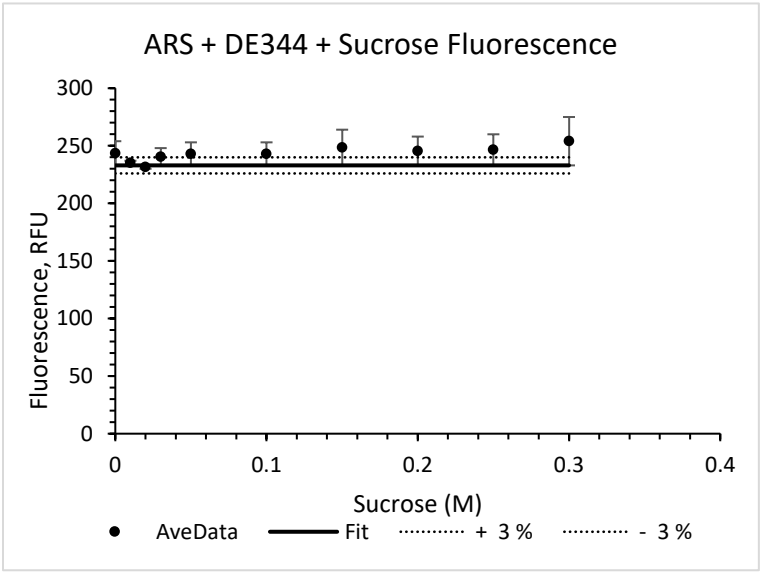

Plot of fluorescence changes of ARS-DE344 complex with increasing concentration of sucrose. ARS (0.1 mM), DE344 (10 mM), sucrose (0-0.1 M), HEPES buffer (100 mM, pH 7.4). (K_a was calculated to be 0.0 ± 5.9 M^{-1}). Value is the average of duplicate runs. Dotted lines represent 3% error.

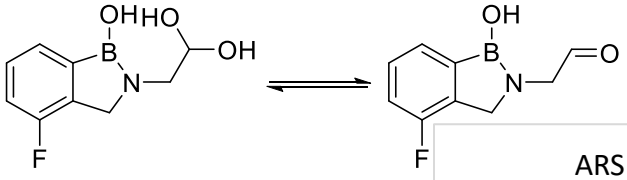

DE347

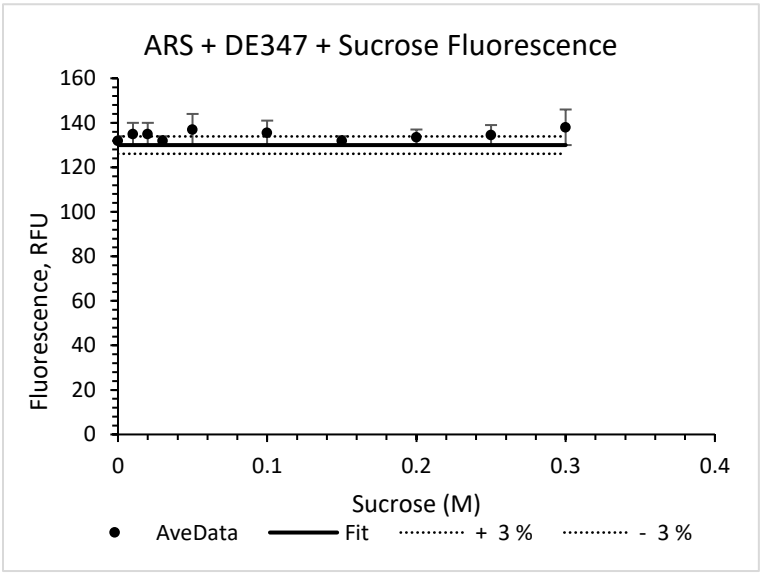

Plot of fluorescence changes of ARS-DE347 complex with increasing concentration of sucrose. ARS (0.1 mM), DE347 (10 mM), sucrose (0-0.1 M), HEPES buffer (100 mM, pH 7.4). (K_a was calculated to be 0.0 ± 1.8 M^{-1}). Value is the average of duplicate runs. Dotted lines represent 3% error.

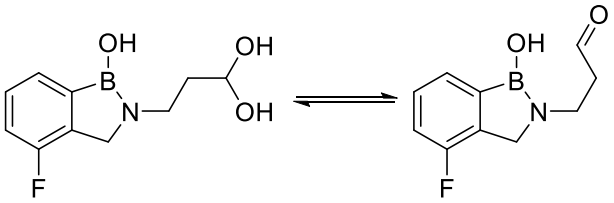

DE348

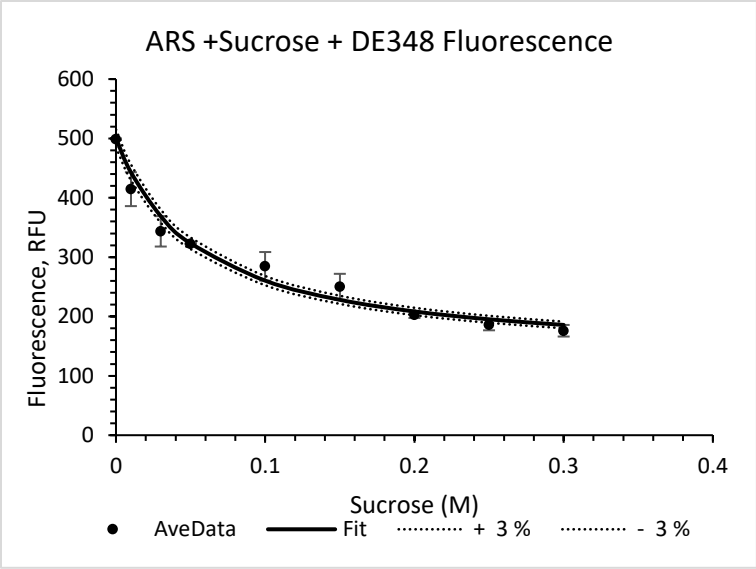

Plot of fluorescence changes of ARS-DE348 complex with increasing concentration of sucrose. ARS (0.1 mM), DE348 (10 mM), sucrose (0-0.1 M), HEPES buffer (100 mM, pH 7.4). (K_a was calculated to be 18.1 ± 9.1 M^{-1}). Value is the average of duplicate runs. Dotted lines represent 3% error.

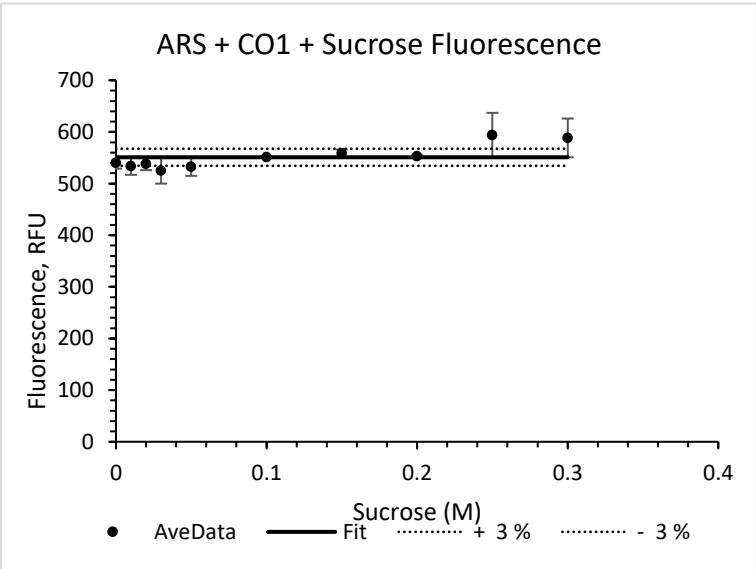

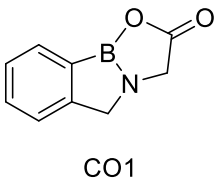

CO1

Plot of fluorescence changes of ARS-CO1 complex with increasing concentration of sucrose. ARS (0.1 mM), CO1 (10 mM), sucrose (0-0.1 M), HEPES buffer (100 mM, pH 7.4). (K_a was calculated to be 0.0 ± 8.8 M^{-1}). Value is the average of duplicate runs. Dotted lines represent 3% error.

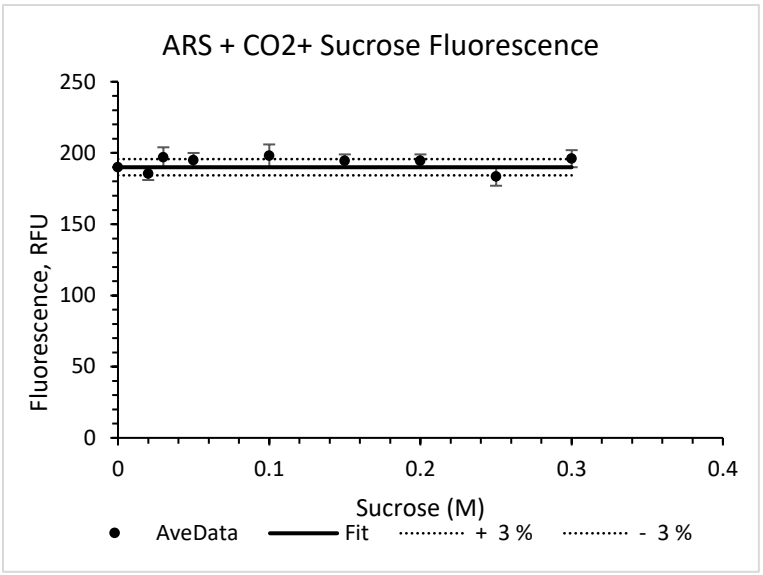

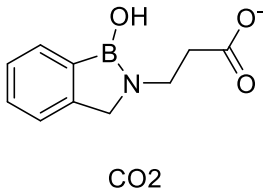

CO2

Plot of fluorescence changes of ARS-CO2 complex with increasing concentration of sucrose. ARS (0.1 mM), CO2 (10 mM), sucrose (0-0.1 M), HEPES buffer (100 mM, pH 7.4). (K_a was calculated to be 0.0 ± 1.5 M^{-1}). Value is the average of duplicate runs. Dotted lines represent 3% error.

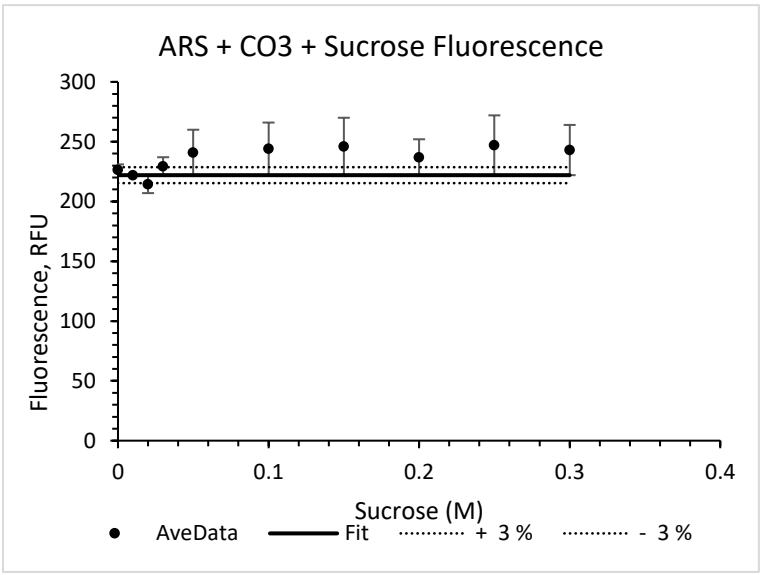

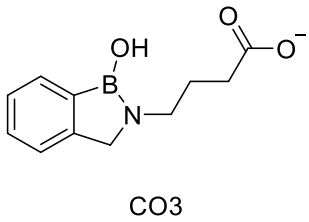

CO3

Plot of fluorescence changes of ARS-CO3 complex with increasing concentration of sucrose. ARS (0.1 mM), CO3 (10 mM), sucrose (0-0.1 M), HEPES buffer (100 mM, pH 7.4). (K_a was calculated to be 0.0 ± 13 M^{-1}). Value is the average of duplicate runs. Dotted lines represent 3% error.

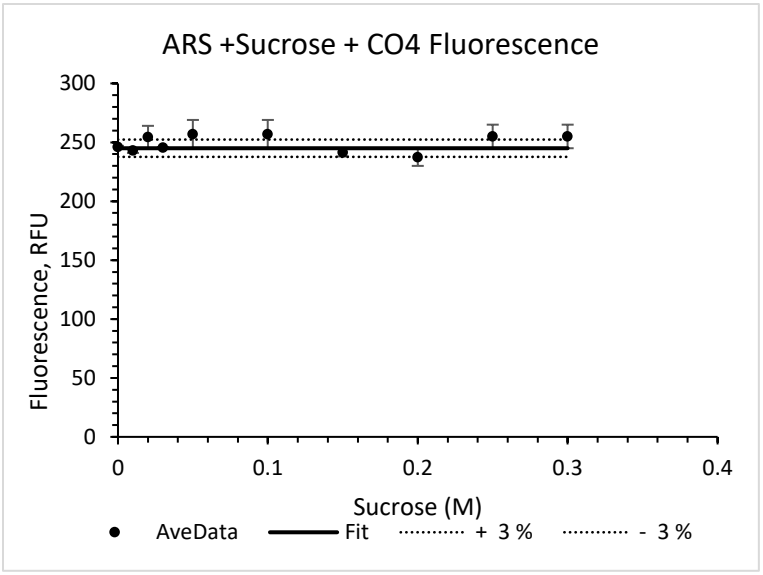

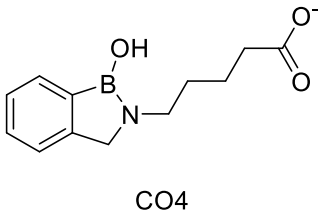

CO4

Plot of fluorescence changes of ARS-CO4 complex with increasing concentration of sucrose. ARS (0.1 mM), CO4 (10 mM), sucrose (0-0.1 M), HEPES buffer (100 mM, pH 7.4). (K_a was calculated to be 0.0 ± 2.7 M^{-1}). Value is the average of duplicate runs. Dotted lines represent 3% error.

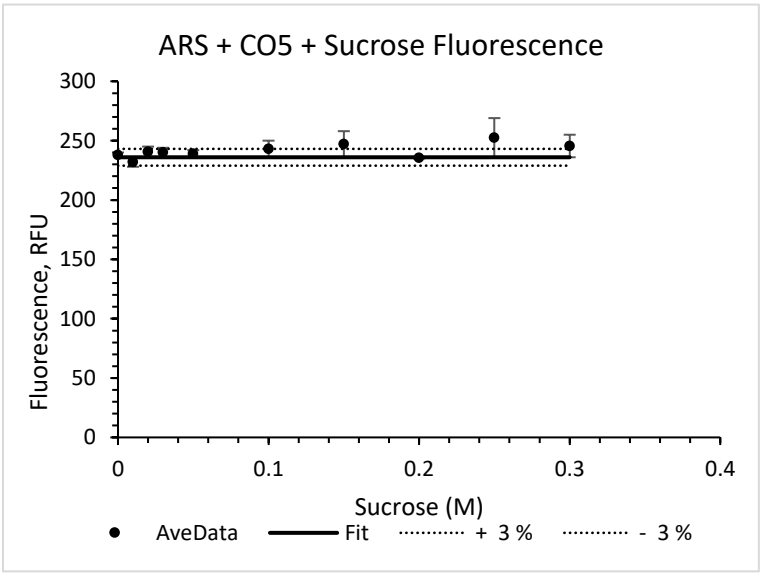

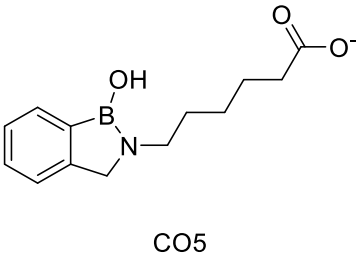

CO5

Plot of fluorescence changes of ARS-CO5 complex with increasing concentration of sucrose. ARS (0.1 mM), CO5 (10 mM), sucrose (0-0.1 M), HEPES buffer (100 mM, pH 7.4). (K_a was calculated to be 0.0 ± 2.5 M^{-1}). Value is the average of duplicate runs. Dotted lines represent 3% error.

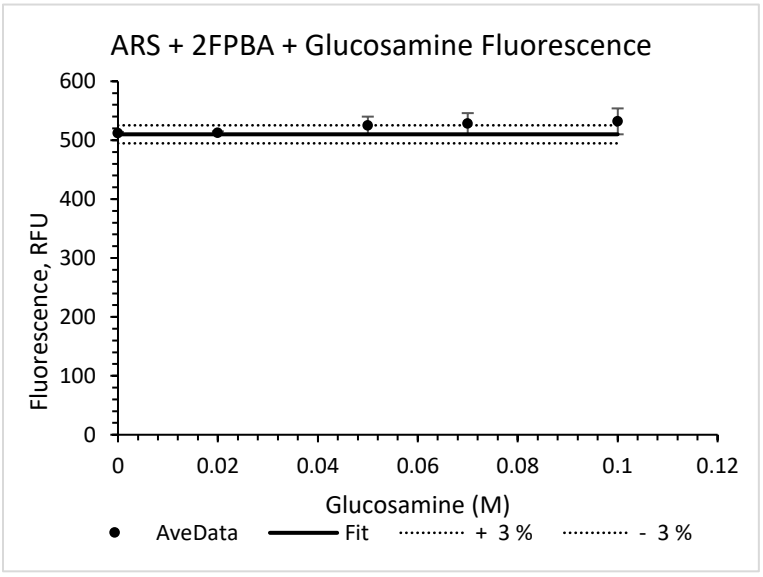

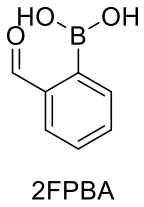

2FPBA

Plot of fluorescence changes of ARS-2FPBA complex with increasing concentration of glucosamine. ARS (0.1 mM), 2FPBA (10 mM), glucosamine (0-0.1 M), HEPES buffer (100 mM, pH 7.4). (K_a was calculated to be 0.0 ± 2.0 M^{-1}). Value is the average of duplicate runs. Dotted lines represent 3% error.

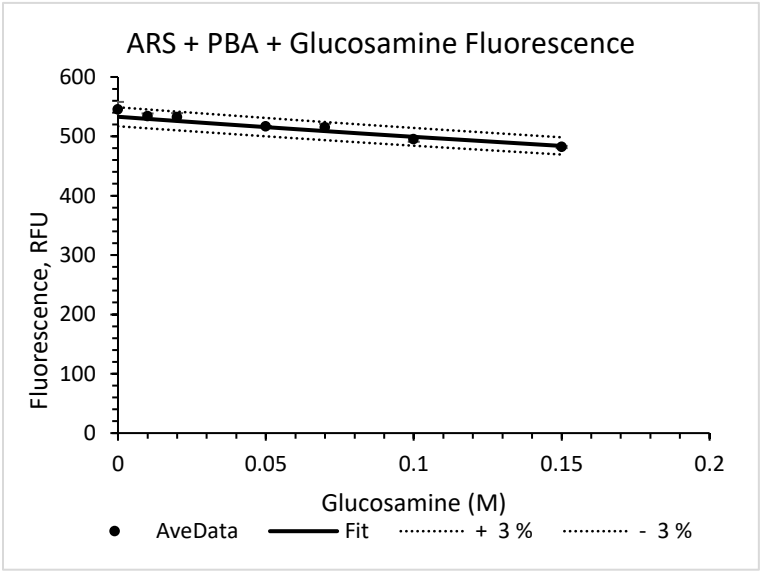

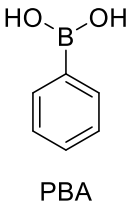

PBA

Plot of fluorescence changes of ARS-PBA complex with increasing concentration of glucosamine. ARS (0.1 mM), PBA (10 mM), glucosamine (0-0.1 M), HEPES buffer (100 mM, pH 7.4). (K_a was calculated to be 0.67 ± 0.53 M^{-1}). Value is the average of duplicate runs. Dotted lines represent 3% error.

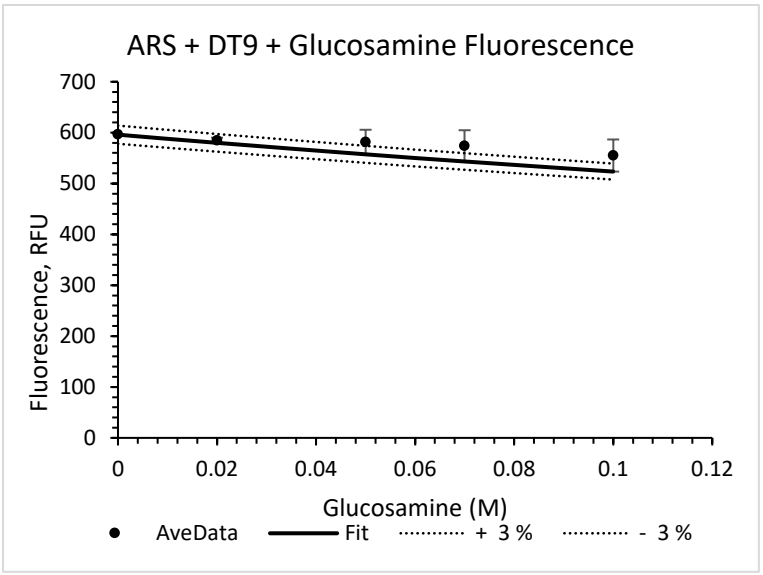

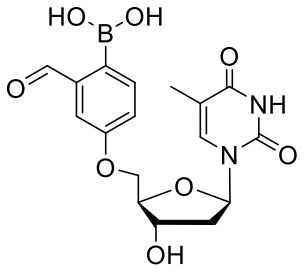

DT9

Plot of fluorescence changes of ARS-DT9 complex with increasing concentration of glucosamine. ARS (0.1 mM), DT9 (10 mM), glucosamine (0-0.1 M), HEPES buffer (100 mM, pH 7.4). (K_a was calculated to be 1.4 ± 4.7 M^{-1}). Value is the average of duplicate runs. Dotted lines represent 3% error.

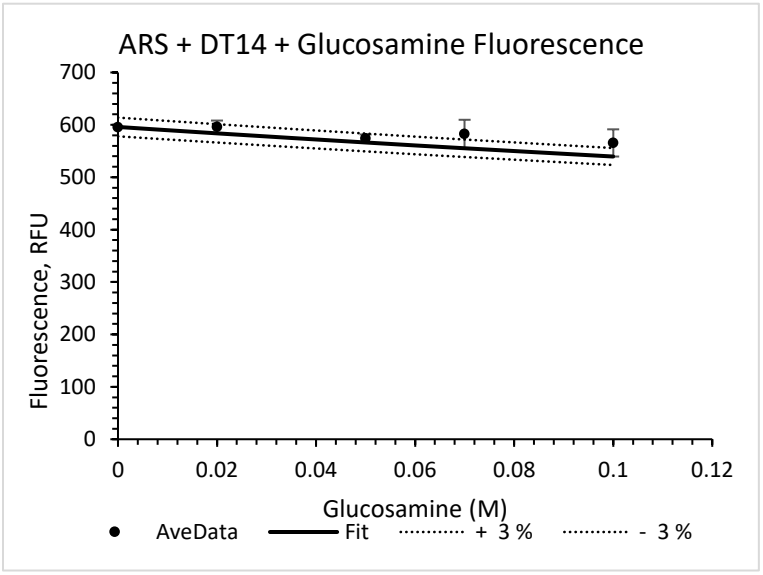

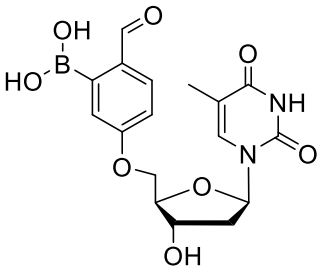

DT14

Plot of fluorescence changes of ARS-DT14 complex with increasing concentration of glucosamine. ARS (0.1 mM), DT14 (10 mM), glucosamine (0-0.1 M), HEPES buffer (100 mM, pH 7.4). (K_a was calculated to be 1.0 ± 2.9 M^{-1}). Value is the average of duplicate runs. Dotted lines represent 3% error.

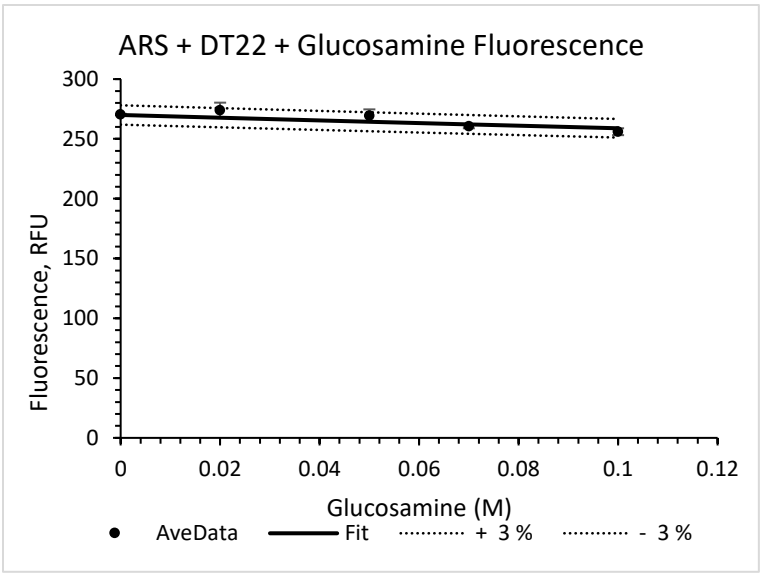

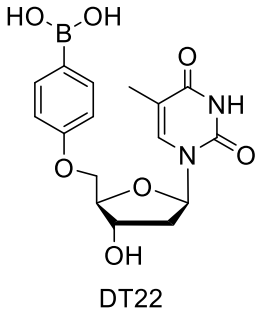

DT22

Plot of fluorescence changes of ARS-DT22 complex with increasing concentration of glucosamine. ARS (0.1 mM), DT22 (10 mM), glucosamine (0-0.1 M), HEPES buffer (100 mM, pH 7.4). (K_a was calculated to be 0.43 ± 0.23 M^{-1}). Value is the average of duplicate runs. Dotted lines represent 3% error.

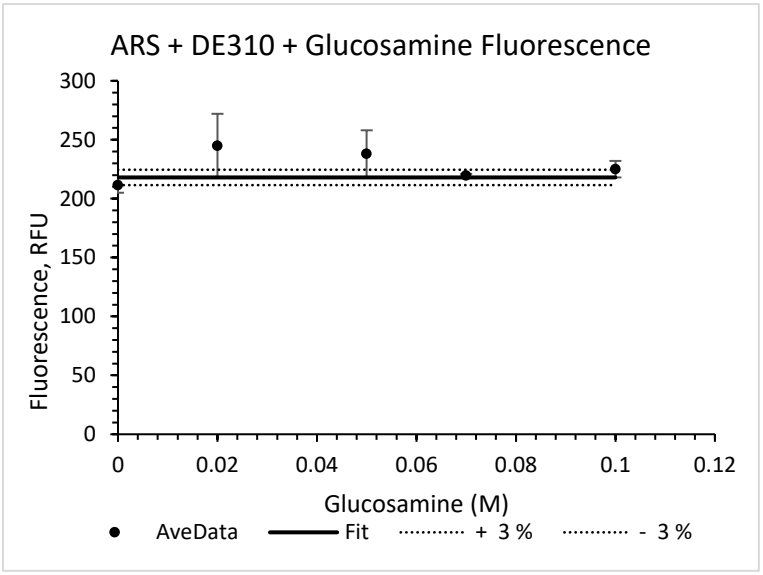

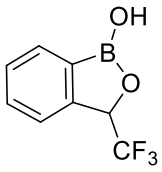

DE310

Plot of fluorescence changes of ARS-DE310 complex with increasing concentration of glucosamine. ARS (0.1 mM), DE310 (10 mM), glucosamine (0-0.1 M), HEPES buffer (100 mM, pH 7.4). (K_a was calculated to be 0.0 ± 5.6 M^{-1}). Value is the average of duplicate runs. Dotted lines represent 3% error.

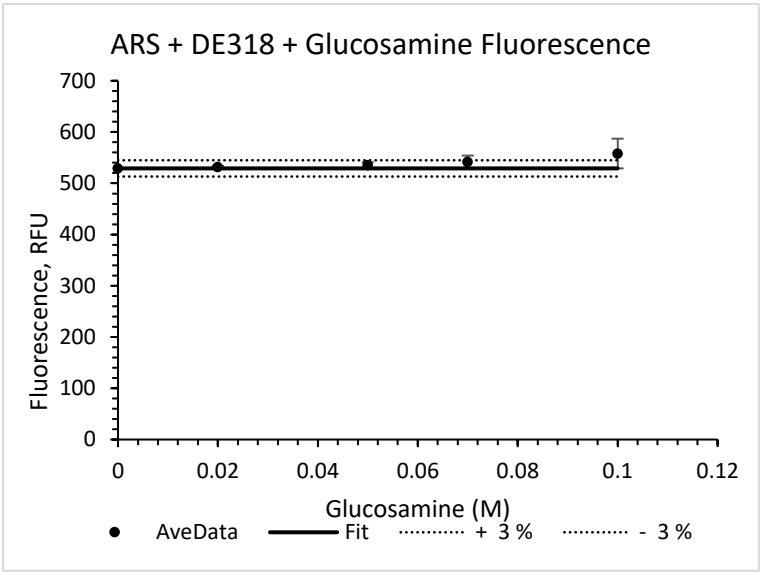

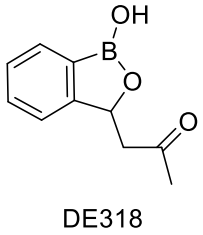

DE318

Plot of fluorescence changes of ARS-DE318 complex with increasing concentration of glucosamine. ARS (0.1 mM), DE318 (10 mM), glucosamine (0-0.1 M), HEPES buffer (100 mM, pH 7.4). (K_a was calculated to be 0.0 ± 1.9 M^{-1}). Value is the average of duplicate runs. Dotted lines represent 3% error.

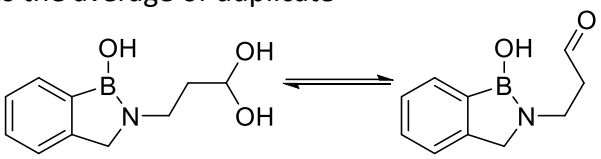

DE321

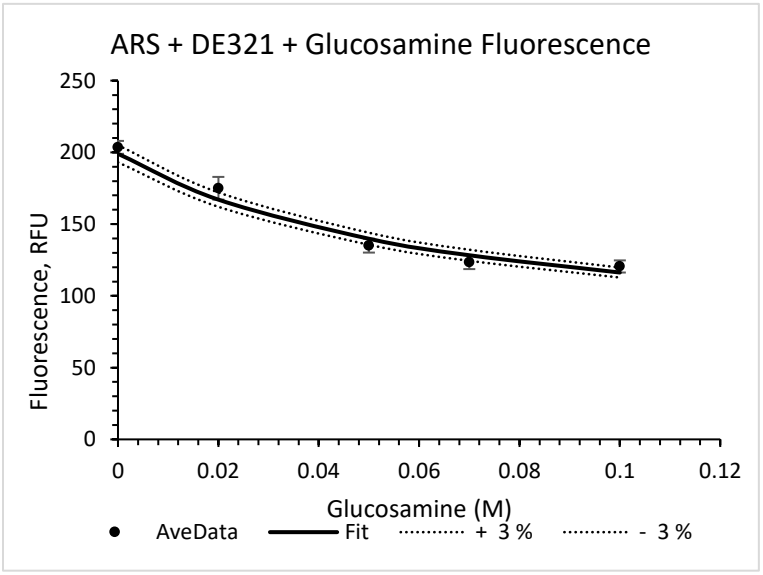

Plot of fluorescence changes of ARS-DE321 complex with increasing concentration of glucosamine. ARS (0.1 mM), DE321 (10 mM), glucosamine (0-0.1 M), HEPES buffer (100 mM, pH 7.4). (K_a was calculated to be 15.1 ± 0.98 M^{-1}). Value is the average of duplicate runs. Dotted lines represent 3% error.

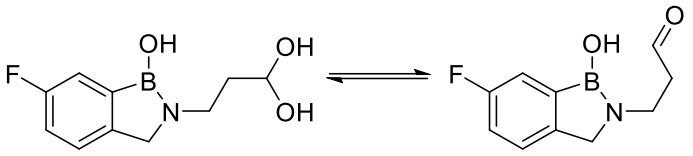

DE342

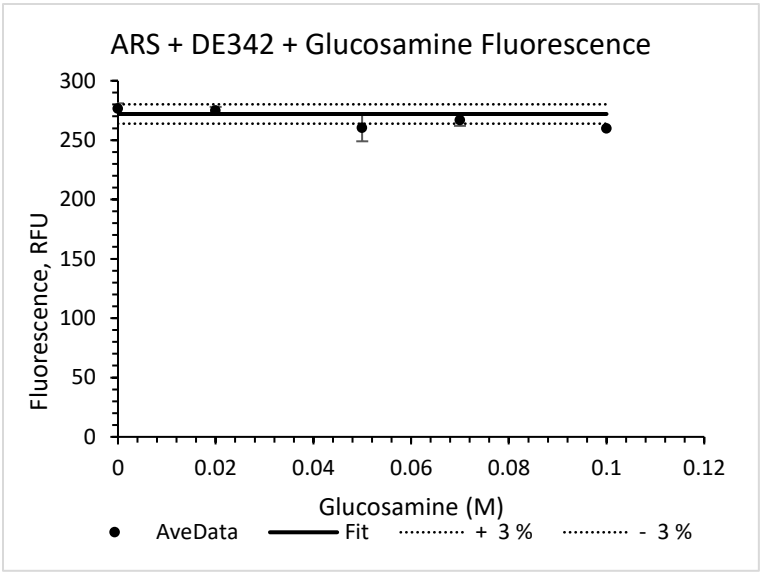

Plot of fluorescence changes of ARS-DE342 complex with increasing concentration of glucosamine. ARS (0.1 mM), DE342 (10 mM), glucosamine (0-0.1 M), HEPES buffer (100 mM, pH 7.4). (K_a was calculated to be 0.0 ± 0.69 M^{-1}). Value is the average of duplicate runs. Dotted lines represent 3% error.

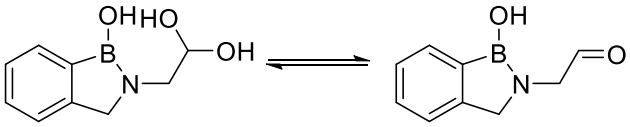

DE343

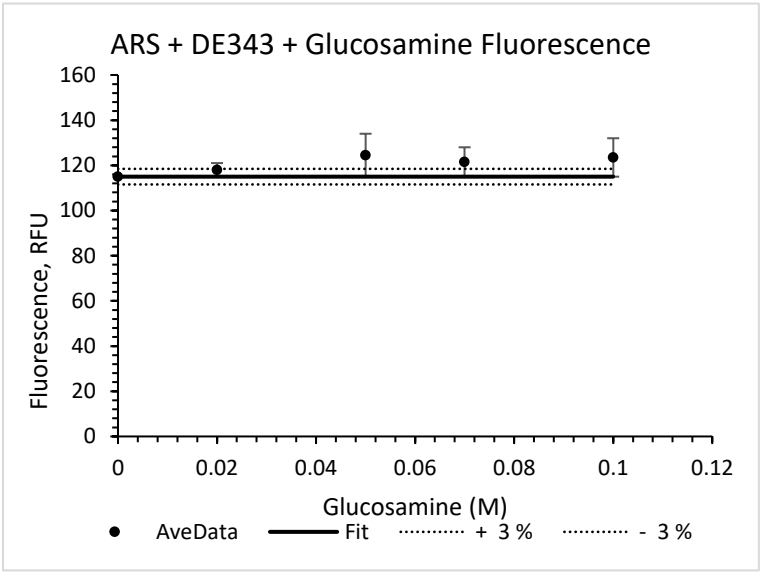

Plot of fluorescence changes of ARS-DE343 complex with increasing concentration of glucosamine. ARS (0.1 mM), DE343 (10 mM), glucosamine (0-0.1 M), HEPES buffer (100 mM, pH 7.4). (K_a was calculated to be 0.0 ± 1.9 M^{-1}). Value is the average of duplicate runs. Dotted lines represent 3% error.

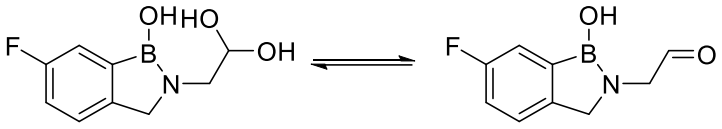

DE344

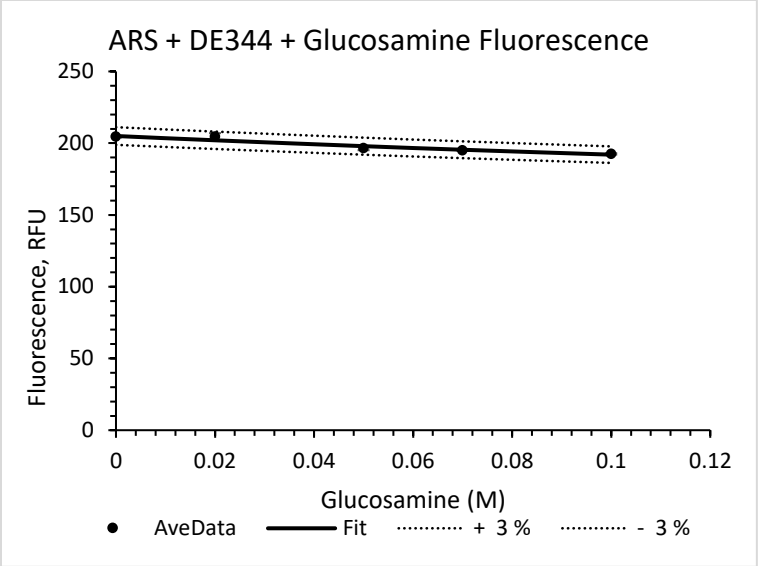

Plot of fluorescence changes of ARS-DE344 complex with increasing concentration of glucosamine. ARS (0.1 mM), DE344 (10 mM), glucosamine (0-0.1 M), HEPES buffer (100 mM, pH 7.4). (K_a was calculated to be 1.9 ± 0.044 M^{-1}). Value is the average of duplicate runs. Dotted lines represent 3% error.

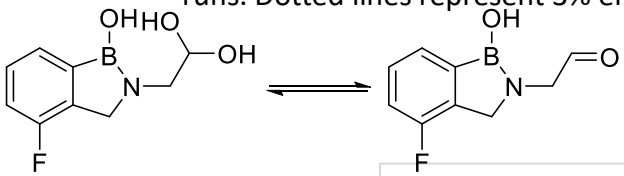

DE347

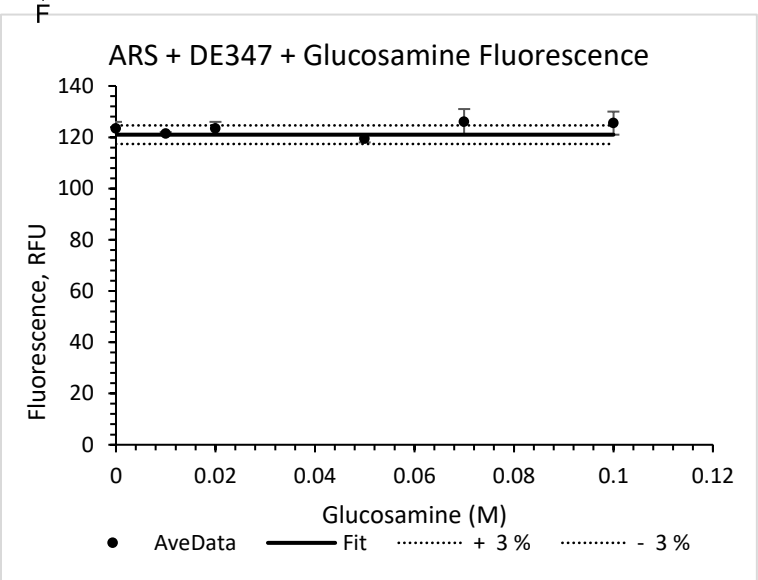

Plot of fluorescence changes of ARS-DE347 complex with increasing concentration of glucosamine. ARS (0.1 mM), DE347 (10 mM), glucosamine (0-0.1 M), HEPES buffer (100 mM, pH 7.4). (K_a was calculated to be 0.0 ± 0.49 M^{-1}). Value is the average of duplicate runs. Dotted lines represent 3% error.

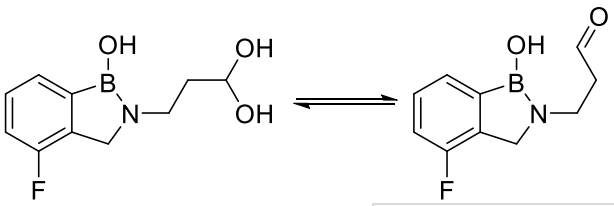

DE348

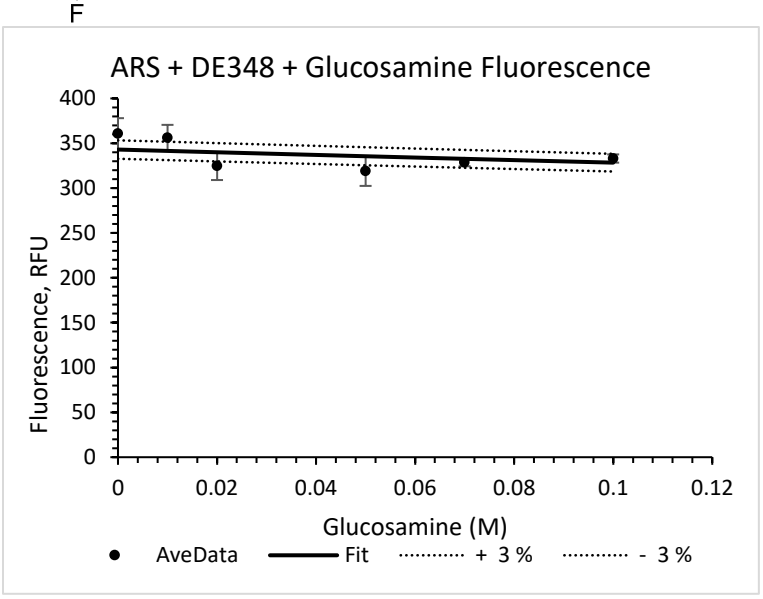

Plot of fluorescence changes of ARS-DE348 complex with increasing concentration of glucosamine. ARS (0.1 mM), DE348 (10 mM), glucosamine (0-0.1 M), HEPES buffer (100 mM, pH 7.4). (K_a was calculated to be 0.45 ± 3.1 M^{-1}). Value is the average of duplicate runs. Dotted lines represent 3% error.

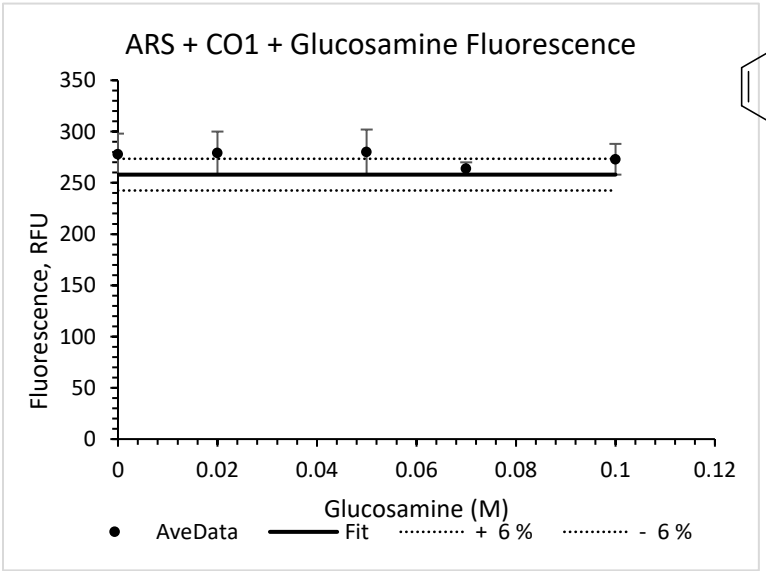

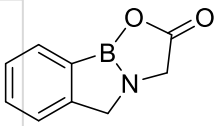

CO1

Plot of fluorescence changes of ARS-CO1 complex with increasing concentration of glucosamine. ARS (0.1 mM), CO1 (10 mM), glucosamine (0-0.1 M), HEPES buffer (100 mM, pH 7.4). (K_a was calculated to be 0.0 ± 6.1 M^{-1}). Value is the average of duplicate runs. Dotted lines represent 6% error.

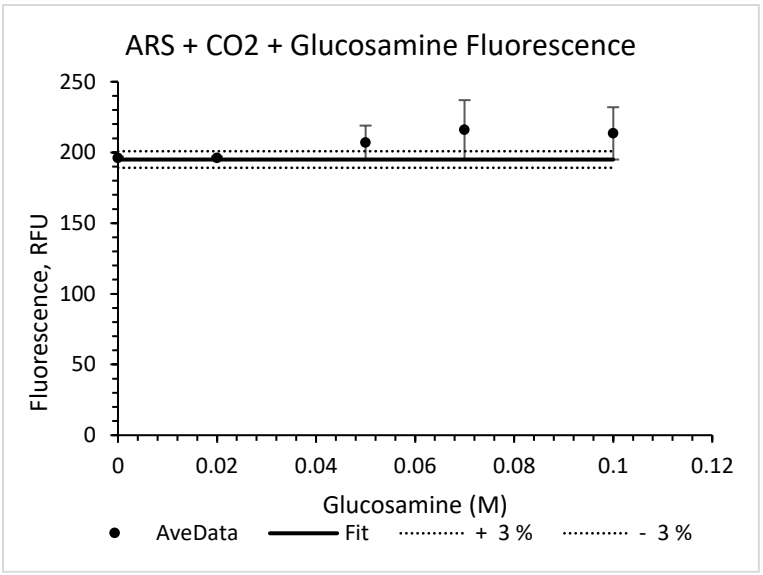

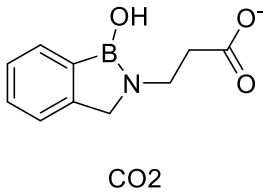

CO2

Plot of fluorescence changes of ARS-CO2 complex with increasing concentration of glucosamine. ARS (0.1 mM), CO2 (10 mM), glucosamine (0-0.1 M), HEPES buffer (100 mM, pH 7.4). (K_a was calculated to be 0.0 ± 4.8 M^{-1}). Value is the average of duplicate runs. Dotted lines represent 3% error.

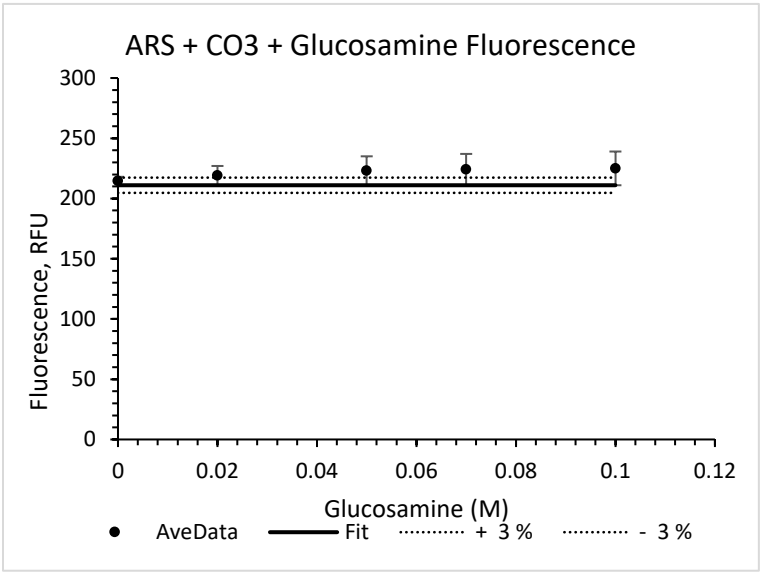

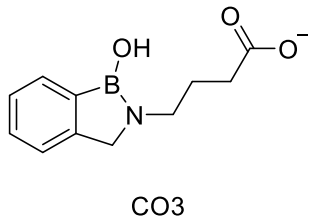

CO3

Plot of fluorescence changes of ARS-CO3 complex with increasing concentration of glucosamine. ARS (0.1 mM), CO3 (10 mM), glucosamine (0-0.1 M), HEPES buffer (100 mM, pH 7.4). (K_a was calculated to be 0.0 ± 2.8 M^{-1}). Value is the average of duplicate runs. Dotted lines represent 3% error.

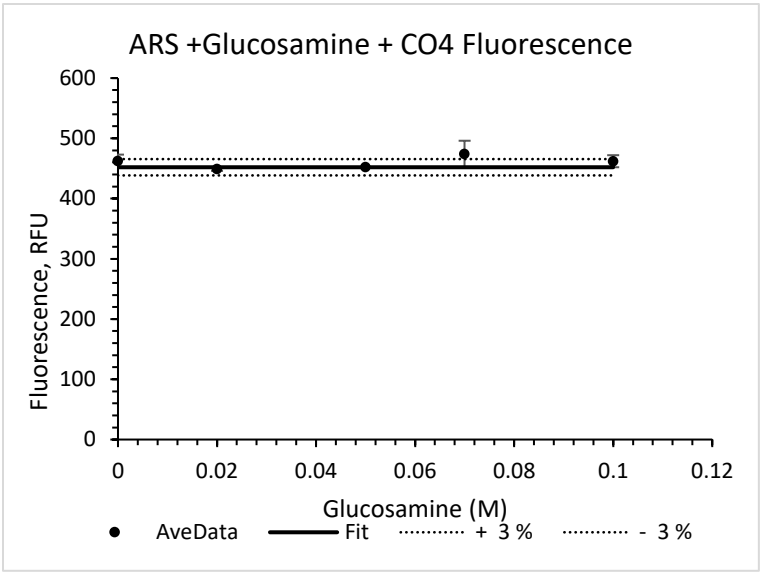

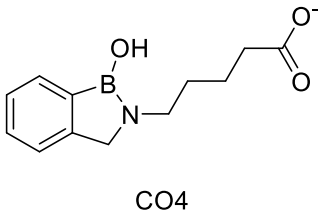

Plot of fluorescence changes of ARS-CO4 complex with increasing concentration of glucosamine. ARS (0.1 mM), CO4 (10 mM), glucosamine (0-0.1 M), HEPES buffer (100 mM, pH 7.4). (K_a was calculated to be 0.0 ± 1.6 M^{-1}). Value is the average of duplicate runs. Dotted lines represent 3% error.

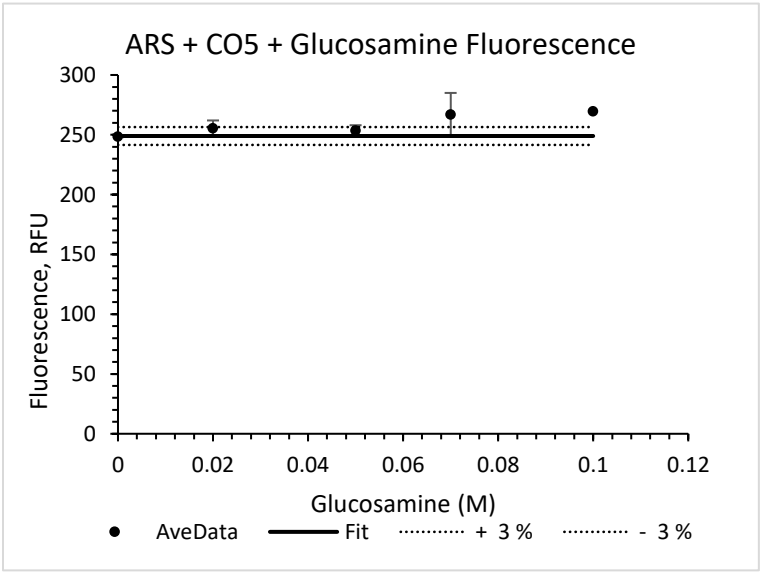

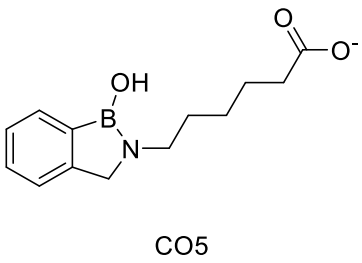

Plot of fluorescence changes of ARS-CO5 complex with increasing concentration of glucosamine. ARS (0.1 mM), CO5 (10 mM), glucosamine (0-0.1 M), HEPES buffer (100 mM, pH 7.4). (K_a was calculated to be 0.0 ± 1.6 M^{-1}). Value is the average of duplicate runs. Dotted lines represent 3% error.